ACTA CHIMICA

ACADEMIAE SCIENTIARUM HUNGARICAE

TOMUS 97 FASCICULUS 1

AKADÉMIAI KIADÓ, BUDAPEST

1978

ACTA CHIM. ACAD. SCI. HUNG. ACASA2 97 (1) 1—103 (1978)

ACTA CHIMICA

A MAGYAR TUDOMÁNYOS AKADÉMIA KÉMIAI TUDOMÁNYOK OSZTÁLYÁNAK IDEGEN NYELVŰ KÖZLEMÉNYEI

Acta Chimica is a journal for the publication of papers on all aspects of chemistry in English, German, French and Russian.

Acta Chimica is published in 4 volumes per year. Each volume consists of 4 issues of varying size.

Manuscripts should be sent to

Acta Chimica
H-1521 Budapest, Hungary

Correspondence with the editors should be sent to the same address. Manuscripts are not returned to the authors.

Subscription: $ 36.00 per volume.

Hungarian subscribers should order from Akadémiai Kiadó, 1363 Budapest, P.O. Box 24. Account No. 215 11488.

Orders from other countries are to be sent to "Kultura" Foreign Trading Company (H-1389 Budapest 62, P.O. Box 149. Account No. 218 10990) or its representatives abroad.

ACTA CHIMICA

ACADEMIAE SCIENTIARUM HUNGARICAE

TOMUS 97

AKADÉMIAI KIADÓ, BUDAPEST

1978

ACTA CHIM. ACAD. SCI. HUNG.

ACTA CHIMICA

TOMUS 97

Fasciculus 1
Fasciculus 2
Fasciculus 3
Fasciculus 4

INDEX

Acta Chimica Academiae Scientiarum Hungaricae, Tomus 97 (1), pp. 1—12 (1978)

SOME CHEMICAL REACTIONS OF THE ELECTRODE GAP AND THEIR ROLE IN SPECTROCHEMICAL ANALYSIS, XXV

THE BEHAVIOUR OF METAL OXIDES IN THE ARC IN STEADY Ar ATMOSPHERE. THE ROLE OF THE REACTIVITY OF METAL OXIDES AND THE BURNING TIME OF ARC WITH RW II AUXILIARY ELECTRODES

Z. L. SZABÓ and H. DOBOLYI-FEJÉRDY*

(Department of Inorganic and Analytical Chemistry, Eötvös L. University, Budapest
** Hungarian Optical Works, Budapest)*

Received November 15, 1976

The role of the reactivities of metal oxides was investigated on the carbon powder mixtures of 20 metal oxides. If the heat of oxidation related to one atom of bound oxygen is lower than -50 kcal, the reaction abruptly increases. This limit is in good coincidence with the heat of formation of CO_2, -48 kcal/mol. At a given electric current, the extent of reaction also depends on the amount of pure metal formed, since it transfers the heat necessary for the reaction into the bulk of sample. Particularly good chances of comparison were provided by the different oxides of the same metal with different oxidation numbers.

According to the data obtained as a function of burning time, the reaction takes place in the first few seconds when the electrode is heated to a sufficient extent. Thus the positive effect of heat of reaction on evaporation may also occur in the first period. The relative extent of heating and cooling processes is a decisive factor in controlling the temperature conditions necessary for the reaction.

Our previous paper [1] was concerned with carbon powder mixtures of five metal oxides. The results have shown that the reactivities of metal oxides must have a role, but the results were not sufficiently unambiguous. In order to study this problem in greater details, measurements were performed on 20 different metal oxides. The role of the burning time of the arc was also investigated on two selected metal oxides, the relatively unstable CuO and the very stable Al_2O_3. In both series of experiments RW II auxiliary electrodes (produced by Ringsdorff Werke GmbH) were applied, and the experiments were carried out in closed cell, under steady Ar atmosphere. The experimental method is described in detail in Part XXIII of our series [2].

The role of the reactivities of metal oxides

The metal oxides used in the investigations were as follows (in the sequence of increasing reactivity): MgO, Al_2O_3, Cr_2O_3, ZnO, SnO_2, SnO, Fe_2O_3, CdO, CoO, Sb_2O_3, Co_2O_3, PbO, Bi_2O_3, Pb_3O_4, Cu_2O, CuO, PbO_2, HgO (red and yellow

modifications), and Ag_2O. The list includes metal oxides of different constitution, such as Ag_2O, CuO, Al_2O_3, PbO_2, etc. In order to make their behaviour comparable, mixtures of identical oxygen content were prepared with carbon powder SU – 601 (produced in Czechoslovakia). The formula weight of metal oxides was divided by the number of bound oxygen atoms, and on the basis of this "equivalent weight", used as molecular weight, mixtures with a mole fraction of 0.03 of metal oxide were prepared. Carbon powder was used in large excess, in order to have practically only CO as reaction product. The basis of comparison was the heat of oxide formation; the stabilities and reactivities of metal oxides were characterized by this quantity. The heats of oxide

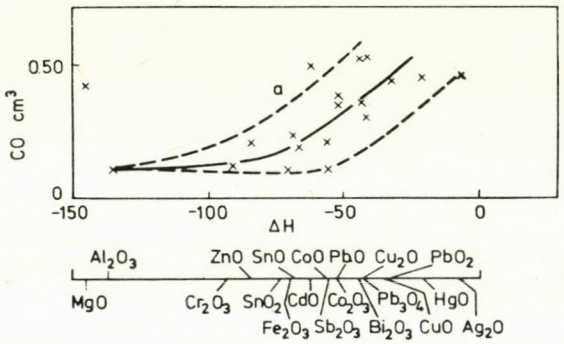

Fig. 1. CO production as a function of the reactivity of metal oxides. Anodic excitation

formation were also normalized to one oxygen, *i.e.* they were divided by the number of oxygen atoms in the formula. The above sequence of reactivities was obtained by this method. In the figures and tables of this paper ΔH denotes these normalized heats of oxide formation in kcal/mol.

Figure 1 shows the amounts of CO in cm^3, obtained with metal oxide–carbon powder mixtures filled into the boring of RW II carrier electrode. In these experiments the carrier electrode was anode, current was 7 A, burning time 10 s. Figure 2 shows the results of similar measurements with the carrier electrode as cathode. Although the amounts of CO can be seen to scatterwidely, a certain tendency can be recognized. The broken lines show the approximate limits of scattering, whereas the middle solid line shows the average tendency. The large scatter of the data must be the result of several effects. The specific weights of metal oxides appear to be important, since the data of MgO, CdO, ZnO and Bi_2O_3, which have low specific weight and thus give loose mixtures, are all higher than expected. The weight of sample filled into the boring of the electrode was also different. This effect could not be eliminated by plotting the data as the fraction of reacted material related to sample weight. Although the metal oxides were pulverized to about the same extent before preparing

the mixtures, their adherence to carbon powder and in the boring was varying. This was evident from the fact that when tapping the electrode after filling, the upper, loose layer could be removed in the form of powder in certain instances, and fell out as a small tablet in other cases. The volatilities of the metals forming the various metal oxides are greatly different, too. Both properties may affect the blow-out of the specimen from the boring of the auxiliary electrode.

Material fallen to the bottom of the cell is unable to take part in the reaction. On the other hand, material driven into the plasma, due for instance

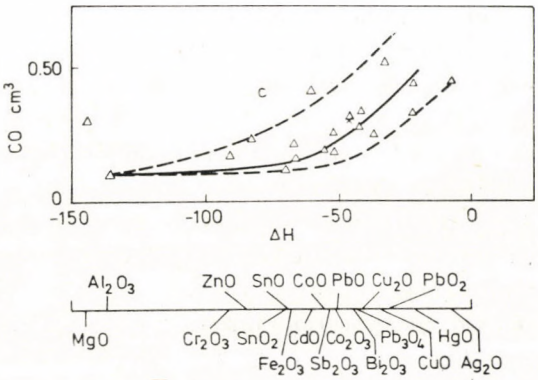

Fig. 2. CO production as a function of the reactivity of metal oxides. Cathodic excitation

to its smaller specific weight, undergoes plasma reactions instead of electrode reactions, thereby increasing the measured amount of CO. Sample spilled into the plasma also decomposes and evaporates, and then, diffusing into the colder zones of the plasma, it may react with carbon vapours arising from carbon powder and the carrier electrode [3]. Metal oxides are not fully recombined, and a fraction of the oxygen atoms formed by dissociation reacts with carbon to yield CO in the colder zones of the plasma. Of course, material may also arrive into the plasma by direct evaporation and dissociation, in addition to spilling, for this is the basis of the arc excitation of materials in spectral analysis. This is, however, of importance in the case of volatile substances only.

The amount of material missing from the boring of the electrode after arcing was measured in all experiments, and it was compared to the loss of sample calculated from the volume of CO evolved. Indeed, the largest differences between these values were found in cases when CO production was increased. However, relatively favourable results were obtained for CuO + C mixture already mentioned [2] and, among others, for Al_2O_3 + C mixture.

It is worth observing that even with stable oxides (Al_2O_3, Cr_2O_3) about 0.1 cm^3 of CO could be measured. This proves again that in the burning spot

of the arc on the electrode of very high temperature, where the heat is transferred from the arc to the electrode, spontaneous decomposition and further, plasma and vapour phase reactions must be taken into account. Consequently, there is a separate reaction zone in the upper layer of the electrode where, owing to the high temperature, the metal oxides decompose irrespectively of their properties. Below this zone, there is a second, larger but colder reaction zone also depending on the current of the arc, with downward decreasing temperature. Less stable metal oxides decompose and react in this zone. They can be found in the rising, right hand side of the curves.

The middle curves of the figures, representing the average, start to bend upwards at a heat of ca. -50 kcal/mol. This may have two reasons. On one hand, the heating (7 A) and cooling properties (heat conduction of RW II carbon, carbon powder, and thermal radiation) of the electrode may be such that the temperature of the reaction zone promotes the thermal decomposition of metal oxides with lower heats of formation, *i.e.* of the less stable ones. This is, however, impossible since the temperature of the complete bulk of RW II cathodes is much lower than that of anodes [4], and still the bending points of the curves obtained with different electrode polarities are at the same location. The other reason can be sought in the behaviour of the other reaction partner, carbon. The oxidation of carbon into CO yields -25 kcal/mol, whereas a direct oxidation into CO_2 produces ca. -48 kcal/mol pro one oxygen atom. This is in good agreement with the mentioned value of -50 kcal/mol where the curves start to bend upwards. This fact recalls the problem of CO_2 formation. Although in such excess of carbon powder practically no CO_2 could be measured in the case of CoO [2], with more reactive metal oxides, among others, the following parallel reactions should be taken into account:

$$MeO + C = Me + CO$$

$$2MeO + C = 2Me + CO_2$$

$$MeO + CO = Me + CO_2 \text{ and}$$

$$CO_2 + C = 2CO$$

To investigate these reactions, mixtures with varying amounts of carbon powder were measured under steady and flowing Ar atmosphere. These measurements will be discussed in subsequent papers.

Five of the 20 types of metal oxides deserve further discussion. The role of reactivity is well illustrated by the behaviour of the three oxides of lead: PbO, Pb_3O_4 and PbO_2. The results are shown in Table I. Labels *a* and *c* in the heading of the table indicate the polarity of the carrier electrode during arcing.

Table I

Comparison of the three types of lead oxide

a – anodic, *c* – cathodic excitation

Metal oxide	ΔH kcal/mol	CO cm³		Sample weight, g	Missing amount, g	
		a	*c*		*a*	*c*
PbO	– 52	0.28	0.18	0.0290	0.0023	0.0055
Pb_3O_4	– 44	0.36	0.28	0.0286	0.0030	0.0054
PbO_2	– 33	0.44	0.51	0.0277	0.0020	0.0056

Table II

Comparison of the two types of cobalt oxide

a – anodic, *c* – cathodic excitation

Metal oxide	ΔH kcal/mol	CO cm³		Sample weight, g	Missing amount, g	
		a	*c*		*a*	*c*
CoO	– 57	0.21	0.13	0.0231	0.0019	0.0017
Co_2O_3	– 52	0.35	0.26	0.0215	0.0011	0.0004

The heats of formation (ΔH) of these oxides pro one bound oxygen atom decrease in the above sequence, and so increase their reactivities. Since the three oxides contain the same metal, there may be no substantial difference between the evaporation rates and heat conductivities of the specimens. The adherence of the powders must also be approximately the same since the material missing from the boring of the electrode after arcing is practically the same for the three lead oxides, save for the variation with the polarity of the carrier electrode. In this case the volume of CO produced in the arc strictly follow the reactivity series with both anodic and cathodic excitation. This is even more characteristic if it is taken into account that the specific weights of mixtures containing the same amounts of bound oxygen are slightly different, and thus the sample weights decrease in the above sequence. Presumably, this fact somewhat decreases the possibility of reaction, and counteracts the role of reactivity. And still, the measured volume of CO clearly follow the sequence of reactivities. However, it reflects the stronger evaporation of lead, particularly from the cathode, that more material is lost from the boring after arcing than in the case of anodic excitation.

A similar state of affairs can be observed in the other two interesting cases, *i.e.* with CoO and Co_2O_3 (Table II) and with SnO and SnO_2 (Table III). Like in the case of lead, the comparison of these data is more justified and successful than that of the oxides of different metals.

Table III

Comparison of the two types of tin oxide

a – anodic, *c* – cathodic excitation

Metal oxide	ΔH kcal/mol	CO cm³		Sample weight, g	Missing amount, g	
		a	*c*		*a*	*c*
SnO_2	−71	0.10	0.12	0.0238	0.0006	0.0018
SnO	−69	0.24	0.21	0.0232	0.0009	0.0020

Table IV

Comparison of the two types of copper oxide

a – anodic, *c* – cathodic excitation

Metal oxide	ΔH kcal/mol	CO cm³		Sample weight, g	Missing amount, g	
		a	*c*		*a*	*c*
Cu_2O	−41	0.53	0.34	0.0270	0.0050	0.0063
CuO	−38	0.28	0.20	0.0251	0.0008	0.0021

The fourth and fifth cases already show contradictions.

The relative volumes of CO measured for CuO and Cu_2O are opposite to the expectations (Table IV). The reasons can be found in the high reactivities of copper oxides and the good heat conductivity of metal copper formed in these reactions. In the strong reaction large amount of copper metal is formed which, owing to its low volatility and high heat conductance, also transfers heat to the lower parts of the boring. Of the two mixtures, in the case of Cu_2O a double amount of good heat conductor copper is formed; the volume of CO evolved is also nearly twofold than in the case of CuO, although their oxygen content is the same. This also seems to be proved by a further experiment in which a diluted Cu_2O + C mixture was used which contained 1.72 % by weight of bound oxygen and the same amount of copper as the mixture of CuO. In this case 0.32 cm³ of CO was measured with anodic and 0.24 cm³ with cathodic excitation. These results are nearly the same as the ones obtained with the above mixture of CuO containing the same amount of copper. Consequently, the amount of pure metal formed in the reaction also has an important role in controlling the temperature of the boring of the carrier electrode. In the increased reaction, in the case of Cu_2O, the material loss from the boring of the electrode which can be observed upon the effect of the arc also increases substantially.

The carbon powder mixtures of HgO of red and yellow crystal modifications also show odd behaviour. Here the metal content of the mixture is the

Table V

Comparison of red and yellow HgO

a – anodic, *c* – cathodic excitation

HgO	CO cm^3		Sample weight, g	Missing amount, g	
	a	*c*		*a*	*c*
Red	0.48	0.35	0.0312	0.0262	0.0158
Yellow	0.45	0.32	0.0326	0.0223	0.0155

same in quantity, but on the basis of their crystal structure the red modification is known to be more stable. The results are shown in Table V. The difference in the two cases is small, but in a repeated measurement the same could be observed. In all probability, the reason may be the high volatility of mercury and the different adherences and spillings of the powders of the two types of oxides. Mercury metal formed in the reaction is very volatile, and carries the unreacted mixtures of different adherences to different extents. For that matter, this is also indicated by the very high losses from the boring of the carrier electrode.

Of the poorly reactive materials, the behaviour of Al_2O_3 (and Cr_2O_3) was found to be very favourable. This reacts to only a very small extent, and the material missing from the boring of the electrode after arcing is very little, only 0.0007 and 0.0006 g with anodic and cathodic excitation, respectively. This is ca. 3 % of the material filled into the boring, which also contains, of course, the evaporated, not only the spilled material. The reaction may run here only in the zone of the burning spot of the arc, therefore it is a very promising model material for the comparison of the behaviour of reactive CuO. Therefore, in the followings, the reactions of mixtures CuO + C and Al_2O_3 + C were studied.

The role of the burning time of arc

These investigations were carried out with CuO + C mixtures of 0.03 metal oxide mole fraction, at a current of 7 A. The measured volume of CO as a function of burning time is shown in Fig. 3. The reaction increases linearly with burning time, and the anodic values are again higher than the cathodic ones owing to the higher extent of glowing. The simultaneous change in the amount of material lost from the boring of the carrier electrode can be seen in Fig. 4. The measured data denoted with solid line show nearly linear relationship, but they are obviously higher than the expected consumption of material (broken line) calculated from the amounts of CO produced. The

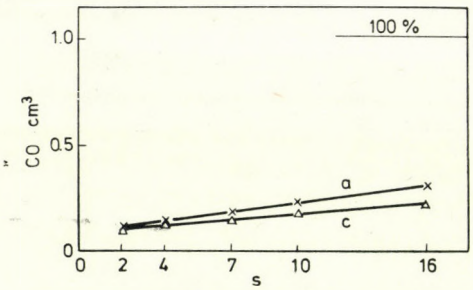

Fig. 3. CO production as a function of the burning time of arc. CuO + C mixture, 7 A; *a* – anodic, *c* – cathodic excitation

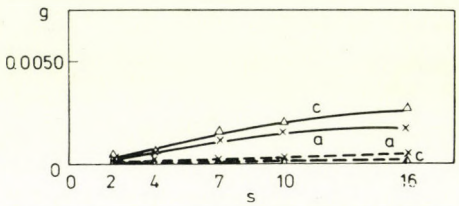

Fig. 4. The amount of material consumed from the boring of the electrode as a function of burning time. CuO + C mixture, 7 A; *a* – anodic, *c* – cathodic excitation. Solid line: measured; broken line: calculated values

difference is due to the spilling of sample. Of the measured values, however, the results obtained with cathodic excitation are higher than the anodic ones. This has been observed several times. The excitation source, as given previously [2], is a.c. polarized arc, *i.e.* in fact a pulsing d.c. Its pumping effect also causes spilling in the sample, mainly with cathodic excitation, since in this case the processes take place in the upper zone of the filling. The temperature of the burning spot of the arc is higher on the cathode [5] and, probably, this is also decisive in the spilling of material.

In parallel with the gas analytical measurements, spectra were also taken. Figure 5 shows the intensity of atom line Cu 282.4 nm ($I_{Cu\ I}$) as a function of the burning time of arc. As has been done before [6], the change in this intensity was regarded proportional with the change in the evaporation of the oxide. The curves are of saturation character. The intensities are fairly low owing to the relatively low current and the Ar atmosphere.

As a comparison, the change of the reaction with the burning time of arc was also determined with an arc of 18 A. The curves obtained from the measured volume of CO are shown in Fig. 6. These curves also show saturation character, closely approaching the 100 % line corresponding to the possible complete reaction, indicating that with higher current and longer burning time the complete bulk of sample starts to glow and react. The line intensities of the spectrum (Fig. 7 $I_{Cu\ I}$; atom line Cu 282.4 nm) also show saturation as a func-

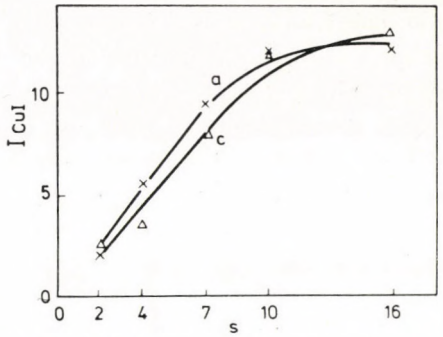

Fig. 5. The intensity of atom line Cu 282.4 nm as a function of burning time, 7 A; *a* – anodic, *c* – cathodic excitation

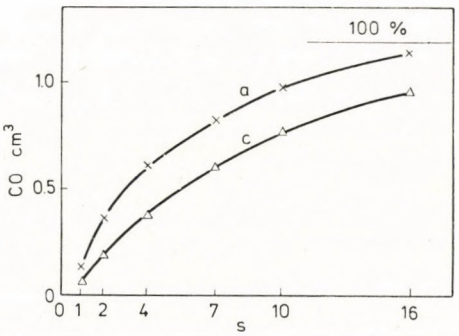

Fig. 6. CO production as a function of the burning time of arc. CuO + C mixture, 18 A; *a* – anodic, *c* – cathodic excitation

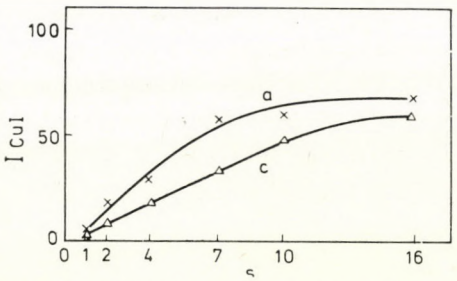

Fig. 7. The intensity of atom line Cu 282.4 nm as a function of burning time, 18 A; *a* – anodic, *c* – cathodic excitation

tion of time. The fact that saturation curves are obtained for both 7 A and 18 A indicates that the ratio of the heating and cooling of electrode is shifted in time. The temperature of the electrode does not increase proportionally with time since at higher temperatures the electrode is cooled more strongly owing to the higher temperature gradient [14]. The effect of the heat of reac-

tion on the data of the spectrum must also be stronger in the first period. The reaction zone coincides with the evaporation zone of the arc only in the first period of excitation. As the reaction proceeds in time, it moves downwards in the filling of the electrode, away from the evaporation zone of the arc, *i.e.* from the burning spot. The heat of reaction evolved far from the upper layers does not heat the upper layer proportionally. With higher currents this effect is enhanced by the fact that the reaction rate is also higher in the first period, as shown by gas analytical measurements. These facts give rise to the saturation character of intensity curves. Complete saturation can, of course, not be achieved since metallic copper formed in the reaction evaporates longer during arcing, and the intensities are integrated on the photographic plate.

To check the above considerations, measurements were also performed with Al_2O_3 + C mixtures as a function of burning time. Owing to the expected small reaction the current applied was 18 A. The results of gas analysis are shown in Fig. 8. The production of CO increases linearly with time, but it reaches 0.3 cm^3 only after 16 s with the carrier electrode as anode, which volume corresponds to only 30 % of the complete reaction calculated from the weight of sample in the boring of the electrode. In contrast, CuO produced 1.14 cm^3 of CO under the same conditions (18 A, 16 s) which corresponds to 96 % of the complete reaction calculated from the weight of the sample. This is even more characteristic if it is considered that in the case of Al_2O_3 + C mixture the amount of material missing from the boring after arcing is very low (Fig. 9), as pointed out in the end of the previous section.

The results of spectroscopic measurements can be seen in Fig. 10. The intensities of atom line Al 305.0 nm, strongly expanded vertically in the figure, also show saturation curves as a function of burning time. This supports the change of temperature conditions in time, arising from the heating and cooling of electrode, and its role in the evaporation of sample. According to the results of gas analysis, chemical reactions and their effects should hardly be taken

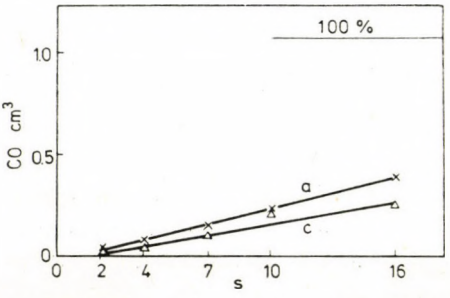

Fig. 8. CO production as a function of the burning time of arc. Al_2O_3 + C mixture, 18 A; *a* – anodic, *c* – cathodic excitation

into account here, and thus the intensity curves reflect the change of evaporation in time nearly independently of the chemical reactions. It also turns out that at these high currents, in the considerations pertaining to copper, too, it is primarily these reaction-independent heating and cooling processes that play the main role. Chemical reactions only modify the results in the same direction.

The spectrum character curves related to the mean plasma temperature ($\Delta Y_{Cu\ 237.0/282.4}$, 7 A: Fig. 11, 18 A: Fig. 12; $\Delta Y_{Al\ 281.6/305.0}$, 18 A: Fig. 13) similarly show that in the first period of burning time there are more substantial changes in the composition of the plasma, owing presumably to the initial strong increase in temperature and evaporation.

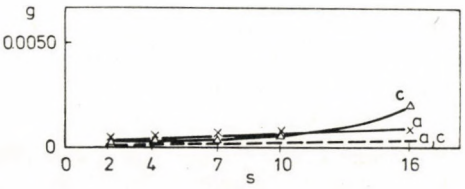

Fig. 9. The amount of material consumed from the boring of electrode as a function of burning time. Al_2O_3 + C mixture, 18 A; *a* – anodic, *c* – cathodic excitation. Solid line: measured, broken line: calculated values

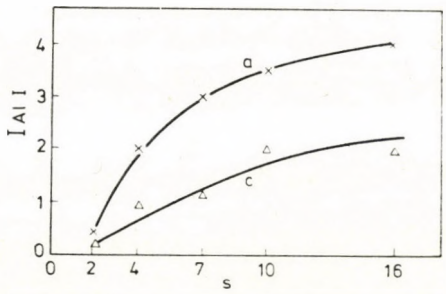

Fig. 10. The intensity of atom line Al 305.0 nm as a function of burning time, 18 A; *a* – anodic, *c* – cathodic excitation

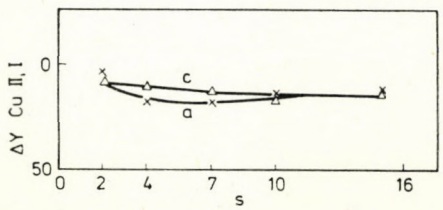

Fig. 11. The change of spectrum character ($\Delta Y_{Cu\ 237.0/282.4}$) with time. CuO + C mixture, 7 A; anodic, *c* – cathodic excitation

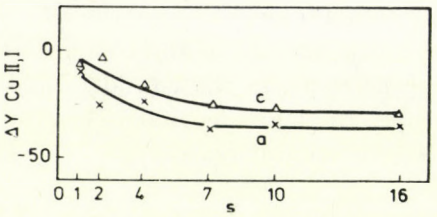

Fig. 12. The change of spectrum character ($\Delta Y_{Cu\ 237.0/282.4}$) with time. CuO + C mixture, 18 A; *a* – anodic, *c* – cathodic excitation

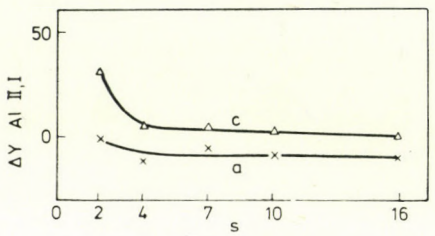

Fig. 13. The change of spectrum character ($\Delta Y_{Al\ 281.6/305.0}$) with time. Al_2O_3 mixture, 18 A; *a* – anodic, *c* – cathodic excitation

REFERENCES

[1] SZABÓ, Z. L., DOBOLYI-FEJÉRDY, H.: Acta Chim. Acad. Sci. Hung. **96,** 201 (1978)
[2] SZABÓ, Z. L., DOBOLYI-FEJÉRDY, H.: Acta Chim. Acad. Sci. Hung. **96,** 189 (1978)
[3] SZABÓ, Z. L., PÖPPL, L.: Acta Chim. (Budapest), **77,** 125 (1973)
[4] PÖPPL, L., SZABÓ, Z. L.: Acta Chim. (Budapest), **79,** 27 (1973)
[5] ZALESSZKIJ, A. M.: The Electric Arc. Műszaki Könyvkiadó, Budapest, 1968
[6] SZABÓ, Z. L., TÓTH, I.: Spectrochim. Acta, **23/B,** 107 (1972)

Zoltán László SZABÓ, H-1088 Budapest, Múzeum krt. 4/b,
Hajna DOBOLYI-FEJÉRDY, H-1126 Budapest, Csörsz u. 35–43.

Acta Chimica Academiae Scientiarum Hungaricae, Tomus 97 (1), pp. 13—25 (1978)

SOME CHEMICAL REACTIONS OF THE ELECTRODE GAP AND THEIR ROLE IN SPECTROCHEMICAL ANALYSIS, XXVI

THE BEHAVIOUR OF METAL OXIDES IN THE ARC IN STEADY Ar ATMOSPHERE. THE ROLE OF THE METAL OXIDE–CARBON POWDER RATIO WITH RW II AUXILIARY ELECTRODES

Z. L. SZABÓ and H. DOBOLYI-FEJÉRDY*

(Department of Inorganic and Analytical Chemistry, Eötvös L. University, Budapest
** Hungarian Optical Works, Budapest)*

Received November 15, 1976

When arcing carbon powder mixtures of chemically more active metal oxides, CO and CO_2 are formed in parallel reactions. Their amounts are the highest when the ratio of carbon and oxygen bound in the metal oxide is about 1 : 1. The powder specimen investigated is heated by the heat of reaction, but cooled by the pure metal formed simultaneously in the boring of the electrode, owing to its good heat conductivity. The state of the plasma is affected substantially by the carbon oxides reaching the plasma, depending on their quantity. The line intensities of the spectrum are determined by the result of these three processes.

Previous papers [1—3] of this series were concerned with the behaviour of the carbon powder mixtures of some metal oxides in the arc. The spectrum line intensities and the amounts of CO formed in the reaction were measured as a function of the current of the arc, the quality of the metal oxides and the burning time of the arc. In these experiments, large excess of carbon was applied in order to eliminate the formation of CO_2. Nevertheless, some data have indicated that CO_2 may also from in the reaction. This paper deals with the role of the ratio of metal oxide and carbon powder, in steady Ar atmosphere, with RW II carrier electodes. The experimental apparatus and method have already been described in Ref. [1]

Results and discussion

The gas analytical results [1] obtained in the preliminary experiments with the mixtures containing various amounts of CoO in carbon have shown that the higher the amount of metal oxide in the mixture the stronger the reaction. However, the measurements encompassed only the CoO + C w/w ratios up to 1 : 1, corresponding to a metal oxide mole fraction of 0.14. Already at this ratio, a slight retardation could be observed in the curves. Considering the possibilities, we were forced to conclude that we had measured the first,

rising section of a maximum curve. The curve should have a maximum at a 1 : 1 molar ratio of metal oxide and carbon, provided that one mole of metal oxide contains one oxygen atom, since this is the optimum ratio for CO formation. In the following experiments mixtures of CuO and C, considered as favourable model [3], have been used, and the results were plotted as a function of the mole fraction of CuO found in them. However, the calculations have also shown that up to the molar ratio 1 : 1 the expectable reaction is directly proportional to the number of moles filled into the boring of the electrode, and not to the mole fraction. Therefore, in the following studies the measured values were plotted against the number of moles actually measured into the boring of the electrode. In the first, left-hand sections of the curves the reaction is determined by the number of moles of metal oxide, whereas with a metal oxide content higher than 50 ml % its extent depends on the otherwise decreasing amount of carbon powder in the mixture held by the boring of the electrode. Therefore, in the following figures we have shown the mole numbers for the mixture of CuO and C powder, calculated on the basis of the amounts measured into the boring of the carrier electrode; in the left-hand sides the CuO mole numbers are increasing from left to right, and in the right-hand sides of the figures the number of C moles are increasing from right to left. Figure 1 shows the *calculated* values of the possible maximum reaction from the specimen, depending on its minor component, *i.e.* the amount of CO that would evolve if at the given sample weight the complete amount of metal oxide, or, in the right-hand section of the curve, the complete amount of carbon reacted. "Sample weight" is stressed since the higher the CuO content of the specimen, the greater, though there is no linear relationship, the specific weight of the mixture. Therefore, the same boring of the electrode (in size) will hold increasingly more amounts of sample (in weight).

In the above manner, a regular, equilateral triangle is obtained in the figure, the upper peak of which is at the molar ratio 1 : 1, where the two scales of the abscissa also meet. This, on the basis of the given sample weight, means 5.25×10^{-4} mol of CuO and C, respectively.

Figure 2. shows the *experimental* results obtained with a current of 7 A and burning time of 10 s. The mixtures were filled into the lower RW II carbon carrier electrode, and were arced against a counterelectrode of the same material. The specimen was excited by an a.c. polarized arc ignited at the maximum of voltage. With the carrier electrode connected as *anode* (curve *a*), the experimental results give a curve very similar to the calculated one, but rounded at the peak. The *cathodic* results (curve *c*) are much lower, and thus give a flatter maximum. However, the higher anodic results are also much below the calculated values. In the anodic case, the measured points were first connected with two straight lines corresponding to the two sides of the triangle, taking the position of the three points in the neighbourhood of the

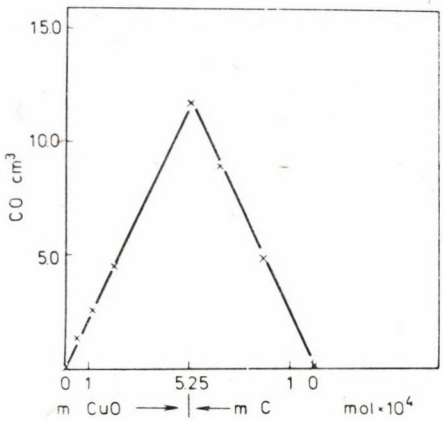

Fig. 1. The maximum possible reaction calculated from the weight of CuO + C mixture

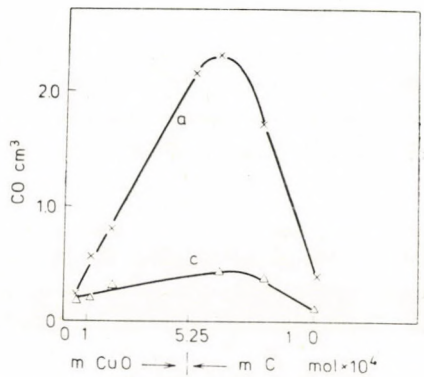

Fig. 2. Measured amount of CO as a function of the composition of CuO + C mixtures. 7 A, 10 s; *a* – anodic, *c* – cathodic excitation

peak as the scatter of the data. However, by taking into account the complete set of experimental data it could be seen that in every similar measurement (*e.g.* under flowing atmosphere, too) the three upper experimental points appear in the given locations. The mixtures consumed during the experiments were prepared again and with these the same types of curves were obtained. It could be excluded therefore that there was some mistake in the preparation of mixtures or in the weight measurements.

The locatinos of the maxima are shifted well observably towards the metal oxide contents higher than the molar ratio 1 : 1. This can also be attributed, in part, to the fact that the carrier electrode is carbon, too, which, although to a smaller extent, more precisely to an extent increasing with a decrease in the ratio of carbon powder in the mixture, also takes part in the

reaction. This is also indicated by a well measurable reaction obtained with pure CuO, *i.e.* at a "zero" mole fraction of C.

The higher values obtained with the carrier electrode connected as anode are, in agreement with the previous observations, obvious. The head of the anode glows up under arcing to observably higher extent than the cathode, and even after switching off the arc it still glows, unlike the cathode. Consequently, the stronger reaction is evident in this case.

An increase in the amount of CuO in the boring of the electrode produces an increasingly stronger oxidising system. It could therefore be expected that the oxidation of carbon proceeds further, to the formation of CO_2. Figure 3 shows the respective results. The curves of CO_2 obtained by the effect of arc are similar in run to those of CO. In the *anodic* case (curve *a*), according to the three upper points, the maximum appears again at a metal oxide concentration slightly higher than the molar ratio 1 : 1, and the cathodic curve (*c*) is similarly flatter. The maximum of the latter is shifted towards somewhat even higher metal oxide ratios. One could also observe the "delay" in the values obtained with anodic excitation at low copper oxide content, owing to the stronger reducing conditions caused by the large excess of carbon powder. It follows from the above that the two reactions, the formation of CO and CO_2, are in close correlation. From the positions of the maxima, which lie between the molar ratios 1 : 1 and 1 : 2, favouring the formation of the two types of the carbon oxides, it follows that the two reactions run in parallel and compete in using the oxidant CuO. This also explains the round tips of the peaks of the two curves.

For studying the electrode surface reactions of carbon electrodes, the measured volume ratios of CO and CO_2 could be well utilized to characterize the redox properties of the system [4]. In the cited work streaming atmosphere was used, in which the possibility of interconversion between CO and CO_2 during the diffusion through plasma zones of different temperatures was eliminated by the high flow rate of the gas, *i.e.* this reaction was "freezed in". Therefore, the CO_2/CO ratio characterized here the actual situation present in the vicinity of the electrode. Our present experiments were carried out in closed cell, in steady Ar atmosphere. Nevertheless, mainly for the sake of comparison with later experiments under flowing atmosphere, we have plotted the volume ratios CO_2/CO calculated from the measured volumes of CO_2 and CO as a function of the composition of the mixture. The results are shown in Fig. 4.

Due to the fluctuation of the points of the original curves (Figs 2 and 3), the mean values obtained with the carrier electrode as *cathode* produced a wavy curve. When the ratio CO_2/CO is calculated from the smoothed curves of CO_2 and CO production (Figs 2 and 3), the ratio curve becomes straight and shows rising character. Consequently, with increasing metal oxide ratio

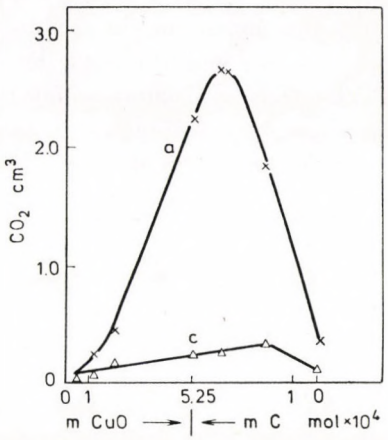

Fig. 3. Measured amount of CO_2 as a function of the composition of CuO + C mixtures. 7 A, 10 s; *a* – anodic, *c* – cathodic excitation

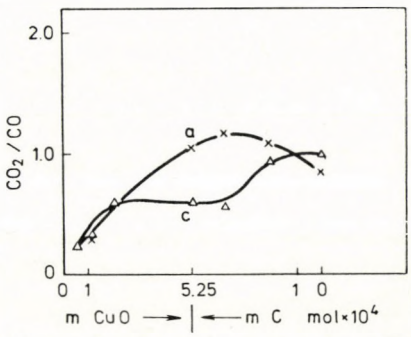

Fig. 4. Volume ratio CO_2/CO as a function of the composition of CuO + C mixtures. 7 A, 10 s; *a* – anodic, *c* – cathodic excitation

in powder mixtures, the ratio CO_2/CO indicates the increasing oxidation conditions even in steady atmosphere. The curve obtained with the carrier electrode as *anode* passes a maximum, with the CO_2/CO ratios calculated either from the experimental points or from the smoothed curves. The rising character of the curve indicates the increasing oxidation conditions in this case, too. However, this anodic curve runs above the cathodic one, since the temperature conditions occurring in the anode are probably in favour of CO_2 production. From a comparison of Fig. 2 and 3 pertaining to CO_2 and CO, respectively, it turns out that the previously delayed CO_2 production at the maximum already exceeds the volume of CO produced. After the maximum, although the amount of oxidant CuO increases further in the system, the amounts of both carbon oxides show decreasing tendency. The decrease is faster for CO_2, and thus the curve of the ratio CO_2/CO bends back. However, the reason for the more rapid decrease in CO_2 formation requires explanation. According

to our assumptions, the phenomenon should be explained again by the heating and cooling conditions, *i.e.* thermal conditions of the electrode, already mentioned several times [3]. The thermal decomposition of the increasing copper oxide content requires increasingly more energy, which is less and less compensated by the heat of reaction which decreases owing to the decreasing carbon content. Thus, the reaction zone of the temperature advantageous for CO_2 formation decreases. At the same time, the effect of the chemical reaction on the site of CO formation of higher temperature [5] is smaller, and thus the amount of CO decreases less abruptly, remaining proportional with the change in the composition of the mixture.

From the measured amounts of CO and CO_2 we have calculated the amount of metal oxide consumed in the reactions yielding the above products, as a percentage of sample weight filled into the boring of the electrode, and these results were summed. The values Σ % obtained are given in Fig. 5 as a function of the composition of powder mixture. As can be seen, the total reaction per cent gives again a maximum curve in the case of anodic excitation whereas the cathodic results decrease, first to a greater extent then at a lower rate. This must also be in relation with the above, since the same data were used in a different way. In the case of anodic excitation a further excess of oxidation takes place owing to the greater heat of reaction evolved in the stronger reaction, and this causes the maximum. On the other hand, in the colder cathode the reaction is weaker, and the cooling effect of pure metal formed in increasing quantities dominates; this accounts for the monotonously decreasing values. It can be seen that even in the case of the strongest reaction, it is below 50 % of the theoretically possible maximum reaction under the given excitation conditions. It can therefore be excluded that the reactions are controlled by the consumption of the material in the boring of the electrode, and that this phenomenon affects the correct interpretation. This is also proved by Fig. 6, which shows the loss of sample under the effect of arc. The solid line corresponds to the measured data, whereas the broken line indicates the total losses calculated from the amounts of the two carbon oxides formed here, *i.e.* leaving the system in gas form. The two curves run close to one another both with anodic (*a*) and with cathodic (*c*) excitation, *i.e.* the spilling of sample should hardly be taken into account.

In parallel with the gas analytical measurements, spectra were also taken. Figure 7 shows the intensity of atom line Cu 282.4 nm ($I_{Cu\ I}$) as a function of the composition of mixture. Like in our previous considerations, this was taken proportional to the evaporation of the sample. The measured points in the figure are joined by broken lines, and the solid line shows the mean curve. Curve *c* shows the decrease of *cathodic* results with increasing CuO content. Consequently, although the amount of copper increases in the sample, the rate of evaporation and excitation decreases. In the evaporation of sample

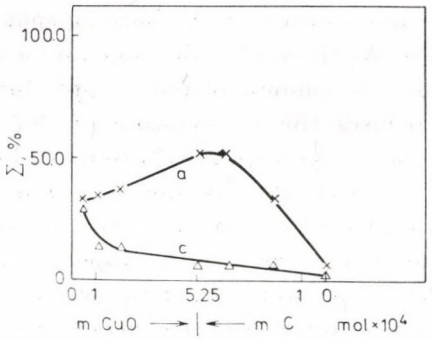

Fig. 5. The cumulated percentage evaluation of the two reactions. CuO + C mixtures, 7 A, 10 s; *a* – anodic, *c* – cathodic excitation

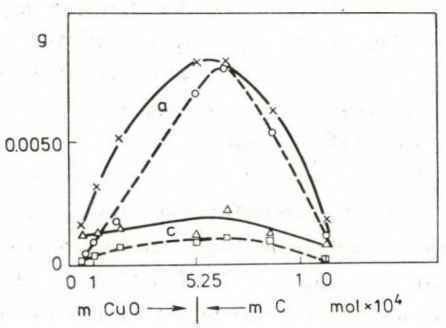

Fig. 6. The amount of material consumed from the boring of the electrode as a function of the composition of CuO + C mixtures. 7 A, 10 s; *a* – anodic, *c* – cathodic excitation

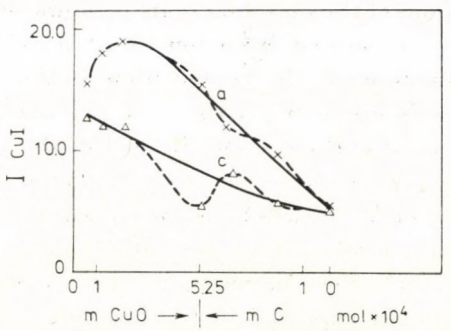

Fig. 7. The change of the intensity of atom line Cu 282.4 nm with the composition of the mixture. 7 A, 10 s; *a* – anodic, *c* – cathodic excitation

the most important role is played by the temperature of the burning spot of the arc on the surface of electrode. This depends on the melting and boiling points of the material of the electrode, in the case of carbon on its sublimation temperature. The boiling point of copper is 2336 °C, whereas the sublimation temperature of carbon is in the range of 3600–4000 °C. For mixtures with

low CuO content, the temperature of the burning spot is determined by the large excess of carbon. As, however, the amount of CuO increases in the boring of the electrode, the amount of pure copper formed in the reduction also increases. This reduces the temperature of the burning spot, which, although the copper content increases, leads to much lower line intensities in the spectrum. Curve *a*, obtained from the measurements using the carrier electrode as *anode* runs above the cathodic curve. Although with pure copper electrode under Ar atmosphere, the cathode evaporates more strongly, causing stronger lines [6], the temperature of amorphous carbon carrier electrodes and of carbon powder mixtures filled into them is higher when connected as anode [5]. Owing to the greater reaction in the warmer electrode, the heat of reaction and the evaporation of the sample are higher than in the cathode. Therefore, the line intensities also increase. The first, rising section of the anodic curve indicates the role of the increasing copper content, as well as of the chemical reaction and the heat evolved in it. However, this effect is overcompensated later by the temperature decreasing effect of the resulting pure copper already discussed with the cathodic curve.

In our opinion, the waviness of the curves drawn with broken lines is due to the fluctuation of experimental data only. The high fluctuation of intensity data is widely known, and this is the reason for always using intensity ratios in quantitative analysis. The fluctuation of experimental points can not always be eliminated to a sufficient extent even by using the mean values of several parallel measurements.

In addition to the rate of evaporation, the composition of the sample also affects the conditions of the plasma. Figure 8 shows the change of the spectrum character ($\Delta Y_{II,\,I}$), formed from ion line Cu 237.0 nm and atom line Cu 282.4 nm, as a function of the composition of the powder mixture. The change of the values is opposite to those of gas analytical measurements. The higher the amount of carbon oxides formed in the reaction in the closed cell, the lower the data of spectrum character, and *vice versa*. As is known [7], the noble gas character of Ar ensures higher plasma temperatures in the investigation of metals, and increases line intensities, particularly with cathodic excitation. Probably this effect increases the first cathodic values, thereby suppressing the maximum expected in the beginning of the cathodic curve previously shown in Fig. 7. The increasing amount of carbon oxides decreases this noble gas character of the gas atmosphere, and the $\Delta Y_{II,\,I}$ values related to the mean temperature of the plasma decrease simultaneously. The effect of the relatively large proportions of carbon oxides in the gas atmosphere is stronger than that of the change in the evaporation rate of copper. The minima of the spectrum character curves coincide with the maxima of the carbon oxide curves instead of those of the intensity curve of copper. The evaporation of copper is weak, however, the percentage changes in this evaporation may

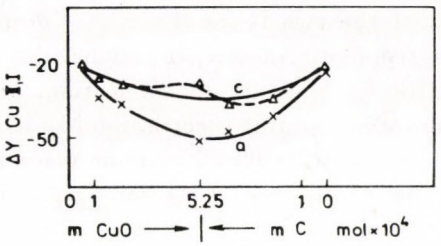

Fig. 8. The change of spectrum character ($\Delta Y_{Cu\ 237.0/282.4}$) with the composition of the mixture. 7 A, 10 s; *a* – anodic, *c* – cathodic excitation

Table I

Comparison of the fluctuations of gas analytical and spectral data

+: agreement, 0: no tendency recognized, –: opposite changes

Exication	Mole fraction of copper oxide													
	1.0		0.75		0.60		0.50		0.13		0.07		0.03	
	CO	CO_2	CO	CO_2	CO	CO_2	CO	CO_2	CO	CO_2	CO	CO_2	CO	CO_2
Anodic	0	+	+	+	0	+	0	0	+	0	0	+	+	+
Cathodic	+	+	+	0	+	–	–	–	+	+	0	+	–	–

be very high, and thus the line intensities of copper may undergo substantial changes. In our case, however, owing to their low amounts, they may hardly play any role in the properties of the plasma in comparison with the effect of carbon oxides.

We wished to discover a further relationship between the extent of chemical reactions and the line intensities measured simultaneously. For this reason, the *directions* of the fluctuations of the data obtained with gas analytical and spectroscopic methods were compared. The parallel CO and CO_2 results belonging to the single measured points were arranged into increasing sequence. The corresponding line intensities measured simultaneously with the individual, parallel gas analytical measurements were written beside these values. We have compared the directions of the fluctuations obtained in the two measurement types. The CO_2 and CO quantities obtained with the anodic and cathodic excitation of seven mixtures with different compositions give 28 sets of data. The results of comparison are shown in Table I. If the directions of the fluctuations of the two measurements are the same, a "+" mark, if no tendency is observable in the data, a "0" mark, and if the two tendencies are opposite, "–" mark is given in table. According to the table, of the 28 cases there were 15 positive, 8 neutral and only 5 negative cases. Consequently, in the majority of cases the reaction, *i.e.* gas evolution, increases with the evaporation and excitation of the sample. In the neutral and negative cases apparently

the individual errors of the two types of methods dominate and disturb the expected complete agreement. Namely, it can be observed that "$-$" marks appear exclusively in the case of cathodic excitation. And, generally, cathodic excitation produces more fluctuating spectra, too [8]. It is also worth observing that the worse agreement can be found at mole fraction 0.5, where the fluctuation of gas analytical results is also the strongest. Nevertheless, the correlation holds in broad generality. Consequently, either the reaction, increased for unknown reason, increases both evaporation and line intensities, or the extent of both processes increases for some common reason.

For the sake of comparison, various carbon powder mixtures of Al_2O_3 were also investigated. The mixtures were prepared in a manner that the formula weight of Al_2O_3 was divided by three, *i.e.* by the number of oxygen atoms bound in it, and thus not the molecular weight but the oxygen equivalent weight [3] was taken into account. "m 1/3 Al_2O_3" on the horizontal axes of the following figures denotes the oxygen equivalents obtained this way and filled into the boring of the carrier electrode. The reaction calculated for the maximum amount of CO possible on the basis of the sample weights in the boring gives, of course, an equilateral triangle also here as a function of mole numbers, or in the case of Al_2O_3 oxygen equivalents, the peak of which is at a 1 : 1 oxygen atom–carbon atom ratio, with a value of exactly 10.0 cm^3 in our case. The measured values are shown in Fig. 9. The maximum of the very flat curve is in the expected location, at 1 : 1 mole (or oxygen equivalent) ratio of Al_2O_3 and C. The low values are, of course, due to the high stability of Al_2O_3. Direct reduction with carbon can not be taken into account here. Although the "head" of the electrode glows up, like in the above cases, it is only the very little material evaporated and decomposed at the temperature of the burning spot of the arc and perhaps in its immediate neighbourhood that reacts by diffusing into colder areas. Since aluminium metal is not formed in the boring, there is no resulting cooling effect. It is worth noting that also in this case the mutual relationship of the anodic (*a*) and cathodic (*c*) curves is determined by the electrode heated better as anode, which indicates that the zone of the reaction is larger than the zone of evaporation. Consequently, some material might also decompose and react in the immediate neighbourhood of the burning spot.

Owing to the low reactivity, only the mixtures with higher oxygen content produce CO_2 in amounts of $0.05-0.07$ cm^3 exceeding the experimental errors. The percentage of reaction, too, related to the weight of the sample, could be calculated from the resulting CO only. The change of this quantity is shown in Fig. 10. In a tenfold ordinate expansion with respect to the curve of CuO for the sake of better orientation, the descending character of the curves is well observably similar to the curve of CuO obtained with cathodic excitation. (As we determined later, a 3.5-fold expansion produces almost coinciding

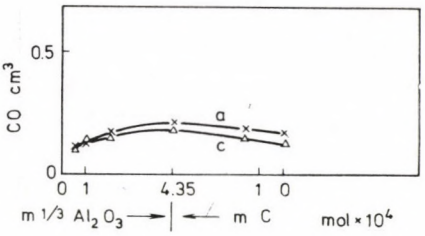

Fig. 9. Measured amounts of CO as a function of the composition of Al_2O_3 + C mixtures. 7 A, 10 s; *a* – anodic, *c* – cathodic excitation

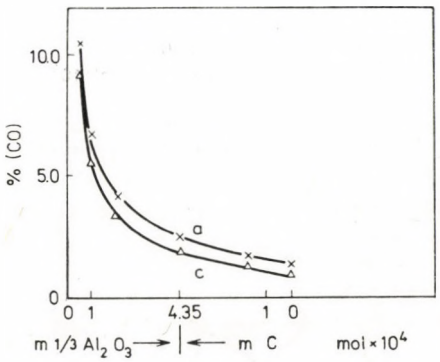

Fig. 10. The percentage evaluation of CO producing reaction with Al_2O_3 + C mixtures. 7 A, 10 s; *a* – anodic, *c* – cathodic excitation

curves.) In the cathodic excitation of CuO + C mixtures, too, only a little reaction occurred, thus its effect could be neglected approximately. In this case, however, the role of the resulting copper metal of poor volatility is played by hardly decomposing and poor heat conductor Al_2O_3. The maximum obtained with the anodic excitation of CuO powder mixtures, which is caused by the reaction, is obviously absent in the anodic excitation of practically non-reacting Al_2O_3 mixtures.

The intensity curves of aluminium (Fig. 11, $I_{Al\,305.0}$), well indicate the noble gas character of Ar. In this case higher line intensities were obtained with cathodic excitation, but the maximum character of the curves was also observable. The maxima are again located at 1 : 1 molar ratio, and they do not shift forwards, like with copper, since the extent of reaction is insufficient to promote evaporation through its heat of reaction, and no pure metal is formed in the boring of the electrode which would exert cooling effect. The maximum character in this case is due to the fact that the evaporation of the sample and the properties of the plasma are controlled first by the increasing aluminium content of the sample, and in the later phases by the decreasing temperature of the burning spot of the arc owing to the lower carbon content. Since

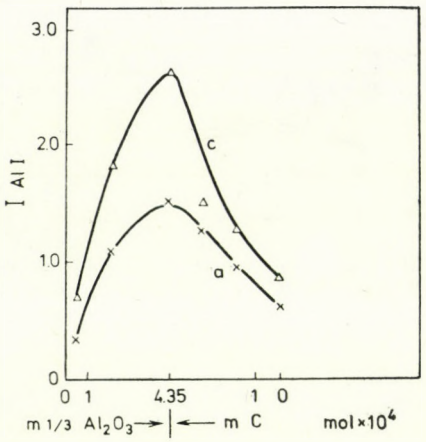

Fig. 11. The change of the intensity of atom line Al 305.0 nm with the composition of the mixture. 7 A, 10 s; *a* – anodic, *c* – cathodic excitation

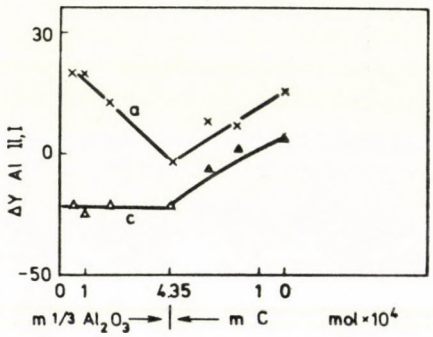

Fig. 12. The change of spectrum character ($\Delta Y_{\mathrm{Al}\,281.6/305.0}$) with the composition of the mixture. 7 A, 10 s; *a* – anodic, *c* – cathodic excitation

no pure metal is formed, the descent of the second part of the curve is smaller than in the case of CuO.

The changes in the character of plasma are shown by the spectrum character curves ($\Delta Y_{\mathrm{II,\,I}}$) given in Fig. 12, calculated from the intensity ratios of ion line Al 281.6 nm and atom line Al 305.0 nm. Their shapes and positions are opposite to those of the intensity curves. Now the changes in the plasma are due to changes in the evaporation of aluminium only, which, being the most easily ionized component, increases or decreases the mean temperature of the plasma according to its decreasing or increasing amount. The plasma is not affected by the carbon oxides formed in the reaction, since their amount is practically negligible.

The above comparisons indicate that the statements on CuO mixtures, regarding their strong reactions, are correct. The heat of reaction evolved

increases the temperature of the filling, and the pure metal formed in the boring of the electrode in the reaction acts as cooling medium, depending on its amount. Gaseous reaction products, when formed in larger quantities, may have a stronger influence on the temperature of the plasma than the metal vapour formed from the sample. The line intensities of the spectrum are ultimately determined by the result of these three processes. Consequently, in the case of chemically more active metal oxides, a type of chemical matrix effect must also be taken into account in spectrochemical analysis.

REFERENCES

[1] SZABÓ, Z. L., DOBOLYI-FEJÉRDY, H.: Acta Chim. Acad. Sci. Hung. **96,** 189 (1978)
[2] SZABÓ, Z. L., DOBOLYI-FEJÉRDY, H.: Acta Chim. Acad. Sci. Hung. **96,** 201 (1978)
[3] SZABÓ, Z. L., DOBOLYI-FEJÉRDY, H.: Acta Chim. Acad. Sci. Hung. **97,** 1 (1978)
[4] SZABÓ, Z. L.: Spectrochim. Acta, **29/B,** 231 (1974)
[5] PÖPPL, L., SZABÓ, Z. L.: Acta Chim. (Budapest) **79,** 27 (1973)
[6] SZABÓ, Z. L.: Acta Chim. (Budapest), **85,** 13 (1975)
[7] SZABÓ, Z. L., TÓTH, I.: Spectrochim. Acta, **27/B,** 107 (1972)
[8] TÖRÖK, T., SZAKÁCS, O., SZABÓ, Z. L.: Magy. Kém. Folyóirat **66,** 487 (1960)

Zoltán László SZABÓ, H-1088 Budapest, Múzeum krt. 4/b,
Hajna DOBOLYI-FEJÉRDY, H-1126 Budapest, Csörsz u. 35–43.

Acta Chimica Academiae Scientiarum Hungaricae, Tomus 97 (1), pp. 27—33 (1978)

SOME CHEMICAL REACTIONS OF THE ELECTRODE GAP AND THEIR ROLE IN SPECTROCHEMICAL ANALYSIS, XXVII

BEHAVIOUR OF METAL OXIDES IN THE ARC IN A FLOWING Ar ATMOSPHERE. ROLE OF THE FLOW RATE OF THE GAS ATMOSPHERE WITH RW II AUXILIARY ELECTRODES

Z. L. SZABÓ

(Department of Inorganic and Analytical Chemistry, Eötvös L. University, Budapest)

H. DOBOLYI-FEJÉRDY

(Hungarian Optical Works, Budapest)

Received January 24, 1977

On the study of a CuO + C mixture, the amount of CO_2 produced in the arc increases, and that of CO decreases, as a result of the passage of an Ar gas flow. The flowing gas removes the oxides of carbon from the site of their interconversion, and therefore the possibility of the reaction $CO_2 + C = 2\ CO$ decreases. This reaction takes place in the main in the plasma phase. The oxides of carbon are predominantly formed in the reaction of the constituents of the powder mixture in the boring of the carrier electrode. The flowing gas slightly increases the possibility of the sum of the reactions, and the spectral line intensities, too, are changed mainly on anodic excitation.

In preceding parts of this series, in which we dealt with the behaviour metal oxides [1—4], we reported on experiments in a stationary Ar atmosphere. In practical spectral analysis, however, as opposed to closed-cell experiments in a stationary atmosphere, measurements in partly or fully open gas cells, *i.e.* in a flowing gas atmosphere, are generally favoured [5]. In closed cells the electrode exchange and the complete or at least uniform flushing-out of the cell is difficult. Accordingly, use of the other two types is preferred, although these require a higher gas consumption in order for the air to be kept away from the arc to a satisfactory extent. At the same time the flowing gas atmosphere has a number of favourable features. In many cases it is advantageous that it cools the electrodes or the plasma. More significant than this is the fact that the gas atmosphere is almost identical in the various examinations, for the flowing gas carries aways the bulk of the gaseous reaction products and the possibly depleted gas atmosphere. Thus, it ensures a constantly fresh gas atmosphere. However, this means only approximately identical conditions. In the plasma and in the environment of the electrodes, even in the case of a flowing gas atmosphere, a large role is played by diffusional gas exchange, the rate of which is finite [6]. When a gas producing or gas consuming reaction is possible therefore, because of the relatively slow gas exchange

the gaseous reaction partner formed or consumed nevertheless makes its effect felt.

For the above reasons our further experiments were carried out in a flowing Ar atmosphere. An account of these investigations will be given in the present and following parts of this series. In the experiments reported here, on the basis of previous experience a CuO + C powder mixture was used in which the mole fraction of CuO was 0.6, while the carbon powder was a Czechoslovak product of type SU – 601. This mixture composition ensured mildly oxidizing conditions and thus, besides CO, a well measurable quantity of CO_2 was also formed in the arc reaction. Well heating-up, amorphous carbon RW II electrodes (Ringsdorff Werke GmbH) were used as auxiliary electrodes, and the powder mixture was packed into the borings in these. The counter electrode was similarly carbon of type RW II. Measurements were made of the amounts of oxides of carbon produced as a result of the A. C.-polarized arc, and of the intensities of the copper spectral lines. A detailed description of the experimental conditions and the method can be found in a previous paper [1].

Results

An examination was first made of the effects of the rate of flow of the Ar gas atmosphere on the reaction between the constituents of the mixture and on the spectral intensities. As already mentioned in the description of the experimental conditions [1], a slight change was necessary in the experimental apparatus. Between the gas cell and the evacuated gas analysis reactor flask ensuring the flow of the gas, calibrated glass capillaries of various sizes were connected, with which the rate of flow of the gas was regulated. The average current of the arc was 7 A, and its burning time was 10 s. The amounts of CO and CO_2 thus measured are shown in Figs 1 and 2, respectively. The curves denoted by *a* demonstrate anodic excitation of the carrier electrode and the mixture packed in it, while *c* indicates its excitation as cathode. For both types of excitation the quantity of CO produced in the reaction decreases, while that of CO_2 increases with increase in the rate of flow of the gas. The increasing rate of flow of the gas atmosphere may result in a number of effects. It may cool the electrodes and the reaction zone where the gases are formed, and it can reduce the possibility of interconversion of the CO and CO_2 by removing them from the reaction zone. The cooling effect of the flowing gas is not very marked here, and can not even be detected in these curves. The second effect is manifested more strongly. On cathodic excitation of the sample, when the scatter of the measurements too is higher, the ratio of the changes in the amounts of the two oxides of carbon is not sufficiently clear-cut, but in the anodic case gas flowing at higher rates causes a decrease in the quantity

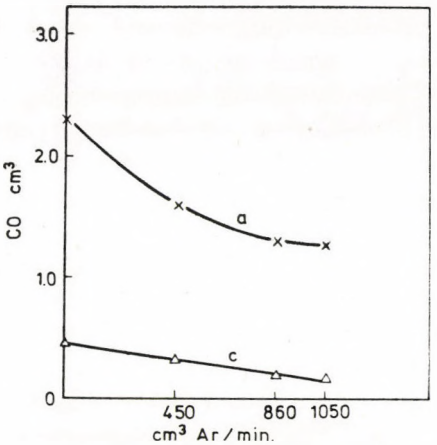

Fig. 1. Change of the amount of CO produced in the arc, as a function of the rate of flow of the Ar; *a*: anodic, *c*: cathodic excitation

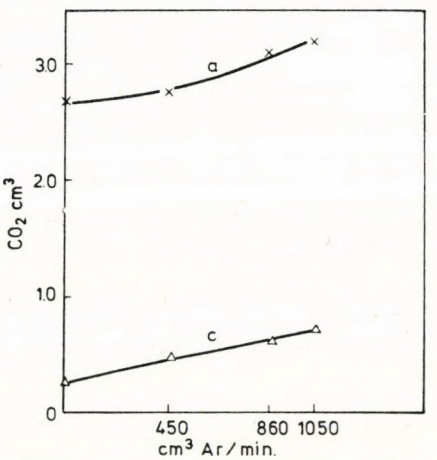

Fig. 2. Change of the amount of CO_2 produced in the arc, as a function of the rate of flow of the Ar; *a*: anodic, *c*: cathodic excitation

of CO which is exactly twice the increase in the quantity of CO_2. This confirms the reaction $CO_2 + C = 2\,CO$, in which the ratio of the produced and consumed volumes is 1 : 2. At the same time, this proves that, in the series of parallel and consecutive reactions, the final reaction determining the measurable amounts of CO and CO_2 is the above transformation between the two oxides of carbon. The curves also show that this reaction is not successfully completely frozen in the given experimental apparatus, even with the highest flow rate employed, for the data of the curves are still not constant at the given flow rates. Thus, in the otherwise previously successfully applied CO_2/CO

ratios, which will be discussed later, we could not attain values perfectly reflecting the momentary oxidation conditions. Higher flow rates could not be used, as the 600 cm^3 evacuated flask then no longer ensured the constant gas rate for 10 s. Hence, in the subsequent experiments we made do with a gas rate of 860 cm^3/min, in the knowledge that the interconversion of the two oxides of carbon could not be fully repressed.

A third effect of the passage of a gas flow is to be seen in the curves of Fig. 3. Here the overall reaction calculated from the above CO_2 and CO quantities is given as a percentage of the maximum possible reaction following from the quantities of powder mixture taken in the individual experiments (Σ %). This Figure indicates that, as the rate of flow of the gas increases, with an accompanying increase in the removal of the oxides of carbon formed, their partial pressure decreases in the environment of the reaction site, and the possibility of further reaction is increased. However, this change is of only a very slight extent. It is probable that from the reaction zone where the oxides of carbon are formed, *i.e.* the boring in the electrode, the gases pass by diffusion into the zone of transformation, from where they are carried by the gas flow.

During the burning of the arc, the quantity of material consumed from the boring in the electrode barely changes with the rate of flow of the gas, and by and large corresponds to the change in the overall reaction. Accordingly, the Figure of this is not presented separately here.

On the other hand, it is interesting to consider the dependence on the gas rate of the CO_2/CO ratio obtained from the measured volumes of CO_2 and CO (Fig. 4). The values resulting from anodic (*a*) and cathodic (*c*) excitation of the sample give intersecting curves; at higher flow rates the values relating to cathodic excitation are the larger. Both curves slope upwards, however, indicating that the possibility of reduction of CO_2 by carbon decreases if the CO_2 is rapidly removed with the gas flow. From the faster increase of the ratios obtained on cathodic excitation it may be concluded that, although these values are automatically lower than those for anodic excitation, the percentage increase of the quantity of CO_2 in the cooler cathode is more rapid than that of the larger amount in the hotter anode. If the phenomenon is examined in the opposite direction, *i.e.* if we turn from a flowing to a stationary atmosphere, this means that we do not remove the oxides of carbon from the zone of their interconversion. It may then be stated that a proportionally larger percentage of the otherwise lower amount of CO_2 is reduced on cathodic excitation than in the anodic case. This may be explained in two ways, for the transformation $CO_2 + C = 2\ CO$ may take place at two sites. One site is the surface of the carrier electrode, when one of the reaction partners, the carbon, is the material of the incandescent solid carrier electrode. The other site is presumably the upper zone of the plasma, where the temperature is

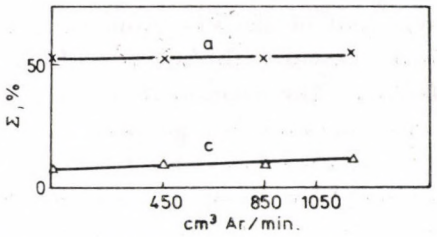

Fig. 3. Summarized percentage evaluation of the two reactions; *a*: anodic, *c*: cathodic excitation

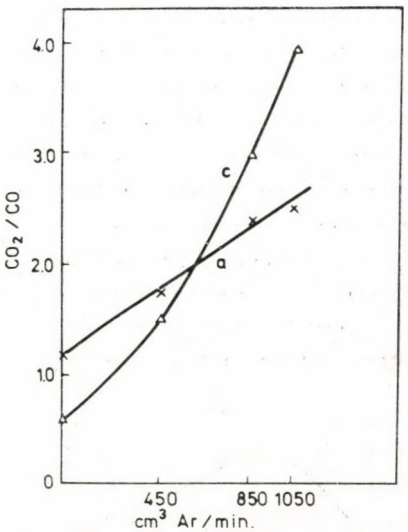

Fig. 4. Change of the ratio of the volumes of the oxides of carbon formed, as a function of the rate of flow of the Ar; *a*: anodic, *c*: cathodic excitation

suitable and where both of the reaction partners arrive. The oxidation and reduction tendencies dependent on the polarity (and current) of the electrode must be manifested in the previously-studied electrode surface reaction with the material of the carrier electrode [7]. Here the reaction must take place to a higher extent on the anode, for in the given equation the carbon is the substance of the electrode, and in the reaction this undergoes oxidation. Surface oxidation of the material of the electrode is better promoted by excitation as an anode. Therefore, it is on anodic excitation, just the opposite case to that observed experimentally, that the higher relative change should be found as a result of the flowing of the gas atmosphere. Thus, the second case is the more probable, or at least that giving rise to the larger change. It is also known that more carbon is sublimed from the higher-temperature burning spot of the cathode than from the anode [8]. Accordingly, because of the larger amount of carbon available, the reaction proceeds further in the plasma phase. The

flowing gas thus removes part of the CO_2 from the plasma phase before it can react to an even greater extent with the carbon formed in the sublimation and similarly transported here. These components are therefore rapidly carried to colder zones where this reaction is less possible.

There is, however, another problem. If the Ar gas contains small amount of O_2, the direction of the changes caused by the gas flow is similar to the one discussed above. We will deal with this problem in a future paper.

The $I_{Cu\ I}$ intensity curves plotted from the measured data for the 282.4 nm atom line of Cu (Fig. 5) show that the spectral line intensities obtained with cathodic excitation of the sample scarcely vary with increase of the rate of flow of the gas. In the anodic case, however, a maximum curve was found. This may again be the resultant of two effects. Initially the intensity values increase, for the appreciable amount of CO_2 diminishing the noble gas character of the Ar is increasingly more and more effectively removed. Later, however, it is probable that the effect of the higher gas flow in cooling the plasma is manifested, or turbulence may possibly occur, because of which a larger quantity of oxides of carbon again passes into the plasma. On cathodic excitation a much smaller amount of oxides of carbon is produced, and thus these effects do not show up, or possibly they just balance each other. All this is only assumption, of course, although the curves (Fig. 6) plotted from the

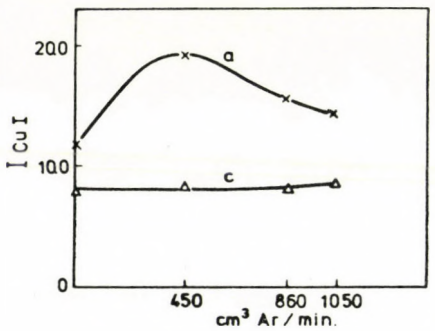

Fig. 5. Change of the intensity of the 282.4 nm atom line of Cu with the rate of flow of the Ar; *a*: anodic, *c*: cathodic excitation

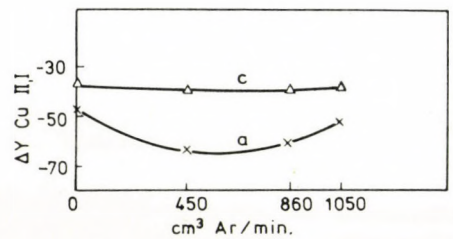

Fig. 6. Change of the spectral character ($\Delta Y_{Cu\ 237.0/282.4}$) with the rate of flow of the Ar; *a*: anodic, *c*: cathodic excitation

spectral character data (values multiplied by 100), $\Delta Y_{\text{Cu II, I}}$, formed from the 237.0 nm ion line and the 282.4 nm atom line of Cu, appear to confirm it. These curves reveal that the change of the average temperature of the plasma is just the reverse of that of the intensity values. Here, the anodic values give a minimum curve. It was demonstrated in a previous publication [4] that such a considerable change in the average temperature of the plasma may be caused by the change in composition of the plasma gases, and less so by the differences in evaporation of the copper, which otherwise is not justified at all here.

REFERENCES

[1] SZABÓ, Z. L., DOBOLYI-FEJÉRDY, H.: Acta Chim. Acad. Sci. Hung. **96,** 189 (1978)
[2] SZABÓ, Z. L., DOBOLYI-FEJÉRDY, H.: Acta Chim. Acad. Sci. Hung. **96,** 201 (1978)
[3] SZABÓ, Z. L., DOBOLYI-FEJÉRDY, H.: Acta Chim. Acad. Sci. Hung. **97,** 1 (1978)
[4] SZABÓ, Z. L., DOBOLYI-FEJÉRDY, H.: Acta Chim. Acad. Sci. Hung. **97,** 13 (1978)
[5] SZABÓ, Z. L.: Lecture at the 17th Hungarian Spectral Analysis Congress, Veszprém, 1974
[6] SZABÓ, Z. L., TÓTH, I.: Acta Chim. (Budapest), **73,** 387 (1972)
[7] SZABÓ, Z. L.: Spectrochim. Acta, **29/B,** 231 (1974)
[8] SZABÓ, Z. L., PÖPPL, L.: Acta Chim. (Budapest), **77,** 125 (1973)

Zoltán László SZABÓ, H-1088 Budapest, Múzeum krt. 4/b,
Hajna DOBOLYI-FEJÉRDY, H-1126 Budapest, Csörsz u. 35–43.

Acta Chimica Academiae Scientiarum Hungaricae, Tomus 97 (1), pp. 35–44 (1978)

MASS SPECTROMETRIC INVESTIGATION OF SOME SEMIQUINONES

M. MÁK and J. TAMÁS

(Central Research Institute of Chemistry, Hungarian Academy of Sciences, Budapest)

Received December 24, 1976

The electron-impact-induced decomposition of eight simple semiquinones has been studied in detail, using low and high resolution mass spectrometry as well as the deuterium labelling technique. The results show that the dominant fragmentation processes of these compounds are connected with the formation of ions of the more stable quinonoid structure.

In the decomposition of certain compounds examined significant *ortho*-effects and rearrangements involving methyl group migration were revealed, too.

Although the mass spectra of numerous compounds containing semiquinonoid sub-structure parts have been published (*e.g.* [1–4]), they are unsuitable for studying the correlation between the mass spectrum and the semiquinonoid skeleton, because generally it is not this structural moiety that directs the fragmentation of those molecules. Consequently, to establish the fragmentation pathways characteristic of this type of skeleton it seems to be necessary to study systematically – similarly to the case of quinones [5] – the mass spectral behaviour of simple semiquinone molecules with known structures.

In this paper the results of mass spectrometric studies of the compounds* 1 to 8 are reported.

In selecting these models it was an important consideration to establish a correlation basis for the structural elucidation of unknown compounds prepared by the oxidation of several substituted chalcones with thallium(III)-nitrate [6].

Figures 1 to 9 show the 70 eV mass spectra of the compounds studied. In order to elucidate the structures and formation pathways of the main fragment ions, observation of the metastable peaks, elemental analysis of certain ions and, in the case of **2**, partial deuterium labelling technique were used. (In Figs 1–9 arrows denote metastable supported transitions.) The mass spectra of the compounds examined show several main characteristic features. Every spectrum exhibits a molecular peak of significant abundance. The fragmentation pathways of **1** are shown in Scheme 1. As important primary frag-

* The compounds studied were synthesized by Dr. S. ANTUS.

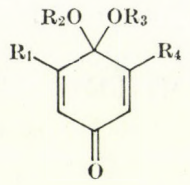

	R_1	R_2	R_3	R_4
1	H	CH_3	CH_3	H
2	OCH_3	CH_3	CH_3	OCH_3
2a	OCH_3	CD_3	CH_3	OCH_3
3	OCH_3	C_2H_5	CH_3	OCH_3
4	OCH_3	i-C_3H_7	CH_3	OCH_3
5	OCH_3	t-C_4H_9	CH_3	OCH_3
6	OCH_3	CH_3CO	CH_3	OCH_3
7	H	CH_3	$-CH_2O-$	
8	H	C_2H_5	$-CH_2O-$	

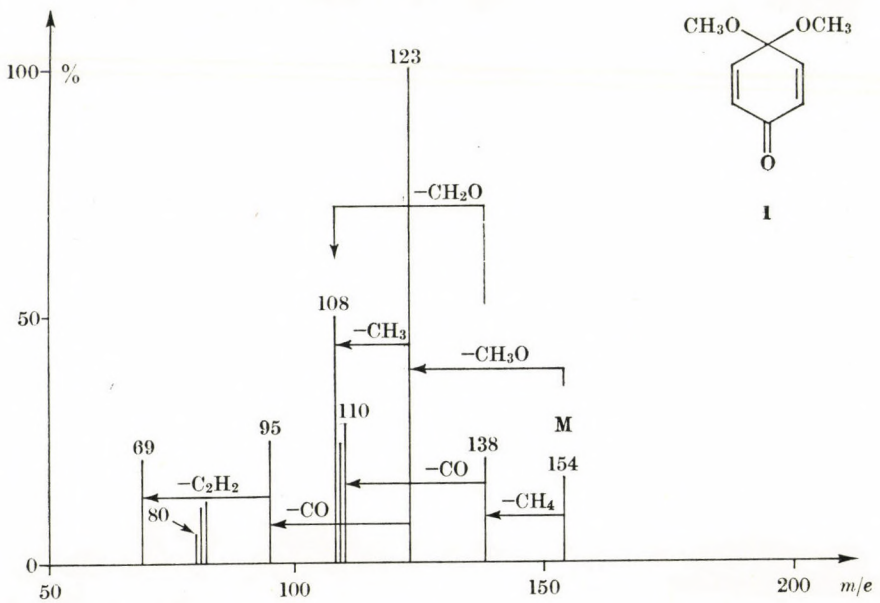

Fig. 1. The mass spectrum of 4,4-dimethoxycyclohexa-2,5-dienone (**1**)

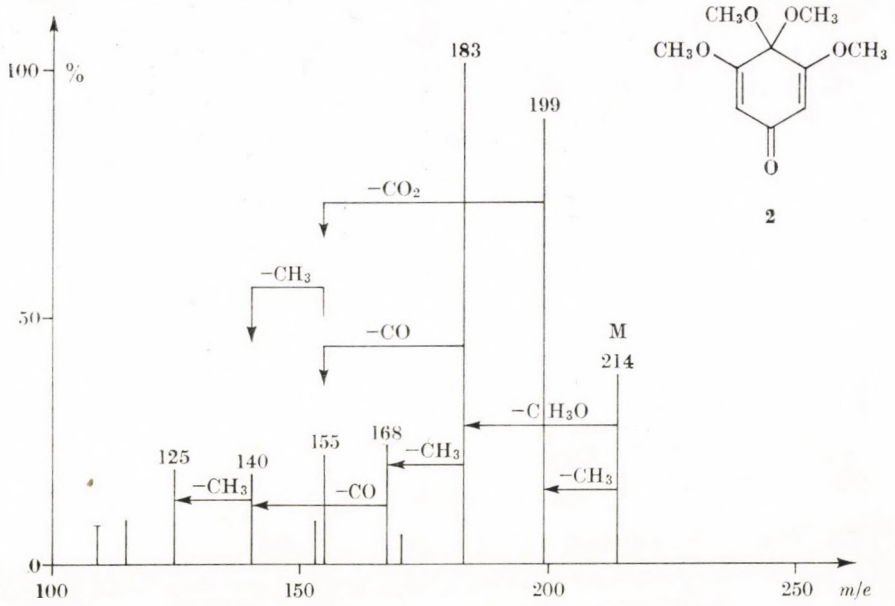

Fig. 2. The mass spectrum of 3,4,4,5-tetramethoxycyclohexa-2,5-dienone **(2)**

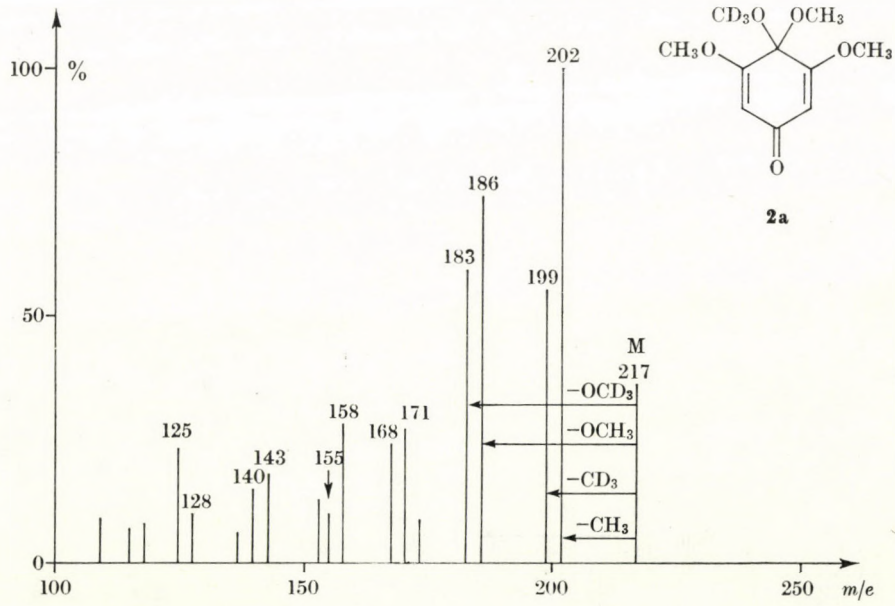

Fig. 3. The mass spectrum of 3,4,4,5-tetramethoxycyclohexa-2,5-dienone-d3 **(2a)**

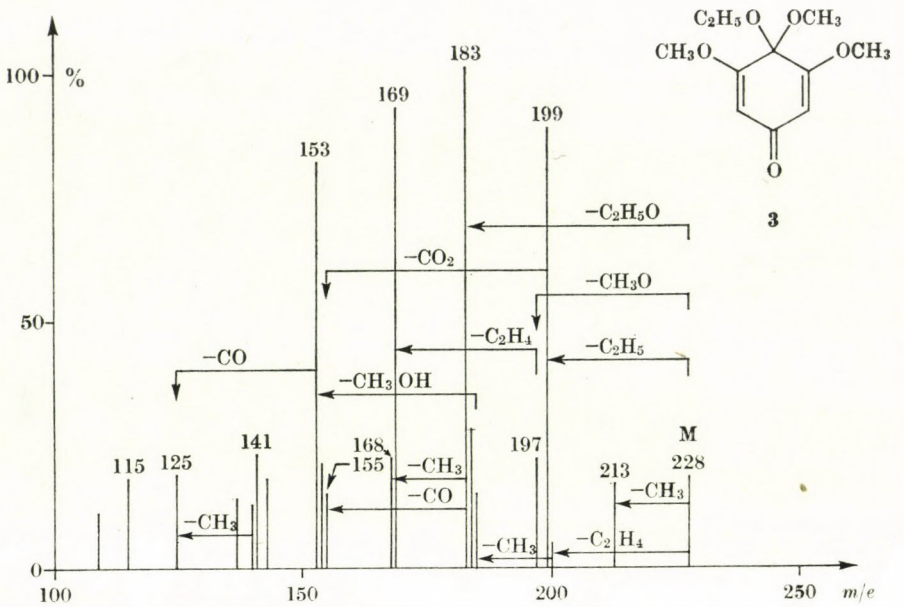

Fig. 4. The mass spectrum of 3,4,5-trimethoxy-4-ethoxycyclohexa-2,5-dienone (**3**)

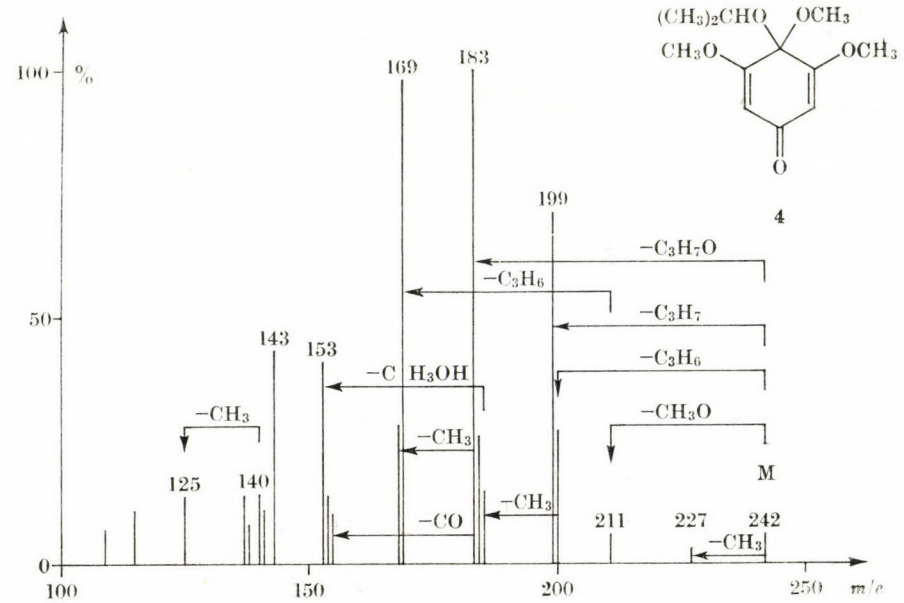

Fig. 5. The mass spectrum of 3,4,5-trimethoxy-4-isopropoxycyclohexa-2,5-dienone (**4**)

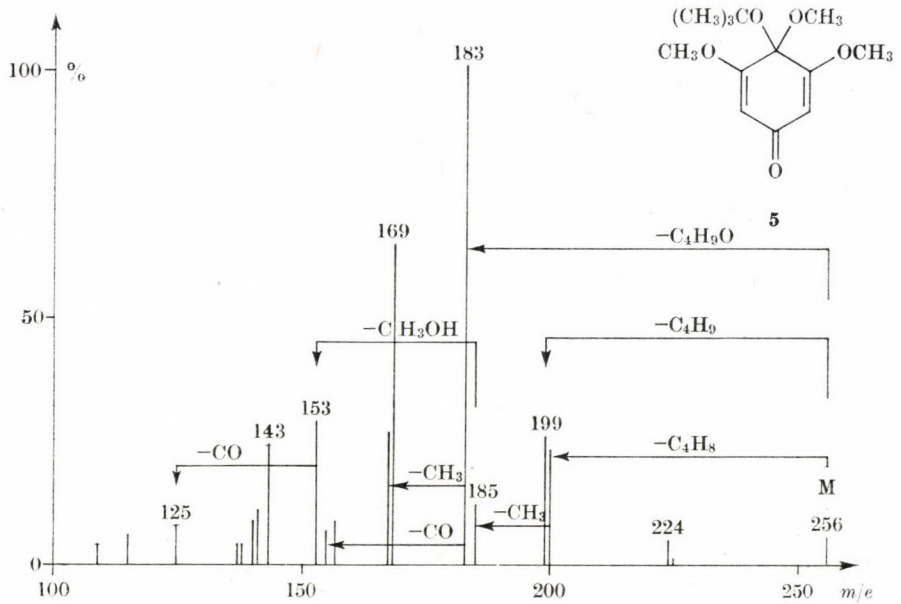

Fig. 6. The mass spectrum of 3,4,5-trimethoxy-4-isobutoxycyclohexa-2,5-dienone **(5)**

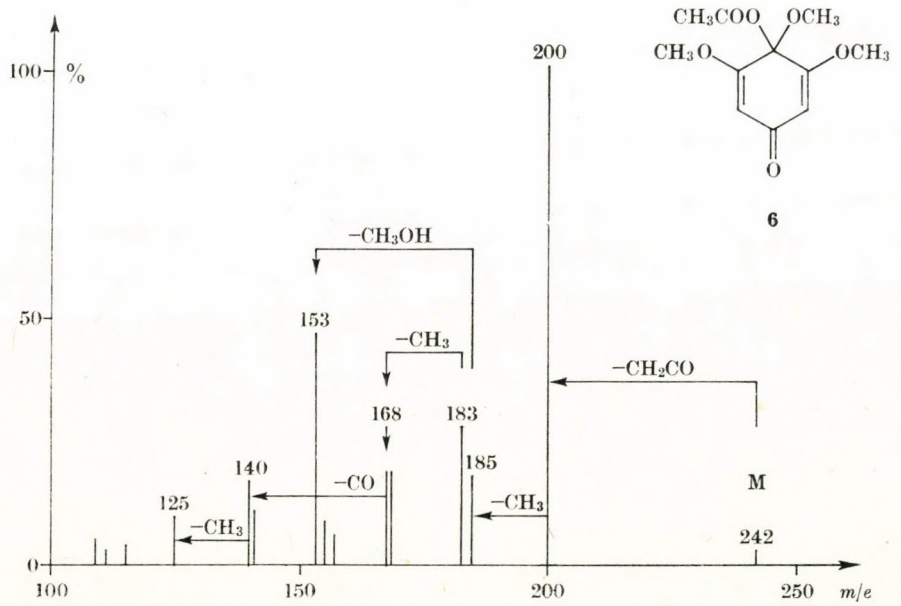

Fig. 7. The mass spectrum of 3,4,5-trimethoxy-4-acetoxycyclohexa-2,5-dienone **(6)**

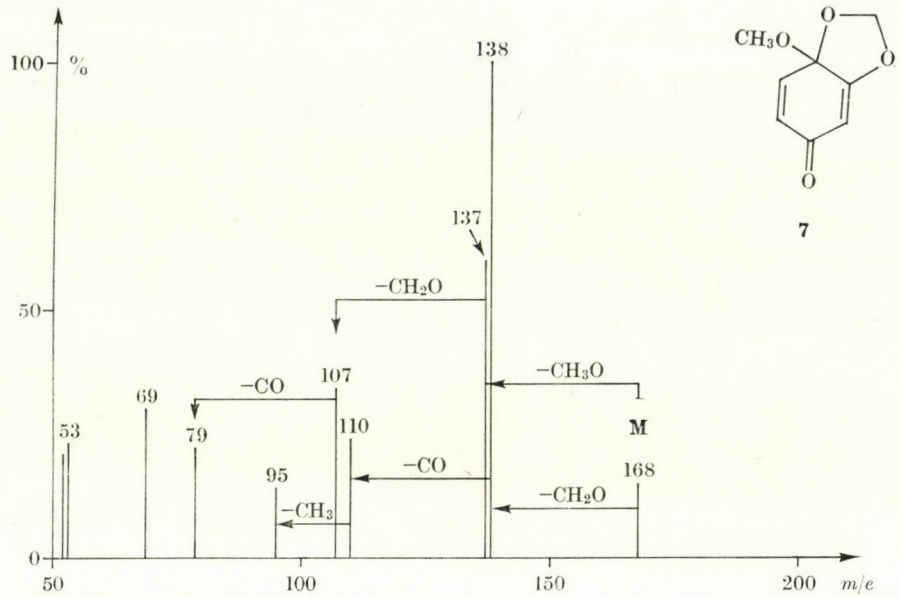

Fig. 8. The mass spectrum of 4-methoxy-3,4-methylenedioxycyclohexa-2,5-dienone (7)

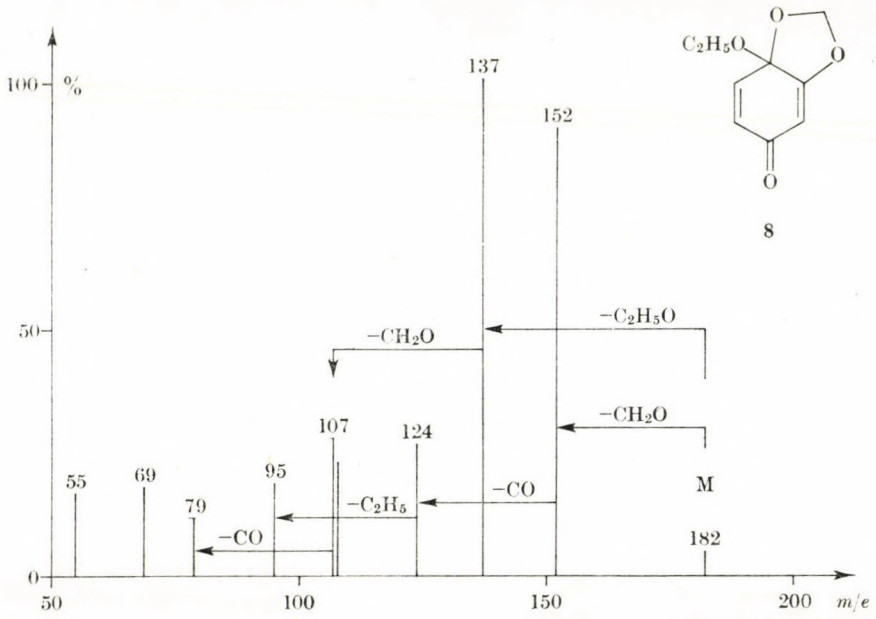

Fig. 9. The mass spectrum of 4-ethoxy-3,4-methylenedioxycyclohexa-2,5-dienone (8)

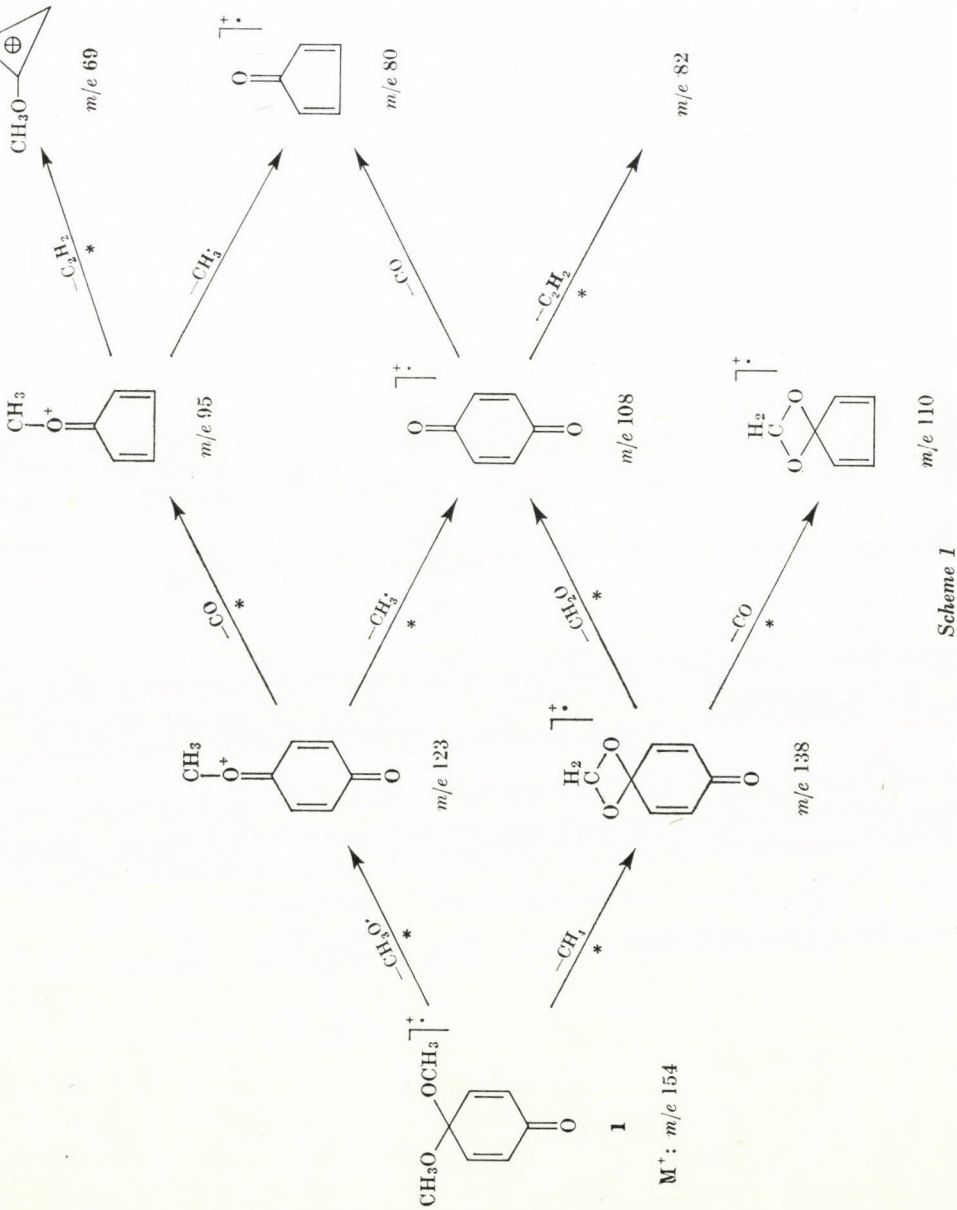

Scheme I

mentation processes the expulsion of a CH_4 molecule and the splitting off of a OCH_3 radical are observed, of which the latter route is favoured. The driving force of this process can be the formation of the stable quinonoid structure of the resulting ions (*m/e* 123). The interesting competitive route, loss of a methane molecule from the molecular ion, leads to the ion of *m/e* 138. The spirocyclic structural representation of this ion is supported by its comparatively high stability, as well as by its ability to eliminate CH_2O. It is noteworthy that CH_4 expulsion does not occur in the presence of *ortho* substituents (*cf.* the mass spectra of **2** to **6**). This effect may be due to the steric hindrance of the *o*-substituents on the spiro ring formation.

Similarly to **1**, the main primary fragmentation process of **2** is the cleavage of a methoxy group. The mass spectrum of deuterium labelled **2a** shows that only one of the geminal methoxy groups can be eliminated *via* this process. The resulting ion of quinonoid structure (*m/e* 183) can subsequently lose a methyl radical or/and a CO molecule. The results of the examination of the deuterium labelled compound (**2a**) indicate that the detachment of a methyl radical from the geminal *ortho*-methoxy groups – neglecting the isotope effects* – occurs twice more frequently than from the neighbouring *ortho*-methoxy groups. (The easy cleavage of a methyl radical from aromatic compounds bearing several methoxy substituents in the aromatic ring is a well-known phenomenon [7].)

As a consequence of the two types of methyl group detachments, the $M-CH_3$ ions observed at *m/e* 199 in the mass spectrum of **2** have to consist of a mixture of two different structures. A part of these ions is capable to eliminate a CO_2 molecule subsequently; this process must involve a methyl group rearrangement. From the ionic abundances and from the isotopic shifts of the metastables in the mass spectrum of **2a** we conclude that this CO_2 elimination is significant only for the $M-CH_3$ ions which lost a methyl radical from a geminal methoxy group.

The fragmentation of **3**–**6** is quite similar to that of **2a**. A common fragmentation pattern for these compounds are shown in Scheme 2. The importance of certain routes of decomposition presented in the Scheme is considerably altered by varying R^2. It can be seen from the ionic abundances (Fig. 2 to Fig. 7) that the detachment of $^{\bullet}R^2$ or $R^2O^{\bullet}$ radicals instead of $CH_3^{\bullet}$ or $CH_3O^{\bullet}$, respectively, become more pronounced when the size of R^2 is increasing. This phenomenon is attributed to the different stabilities of the neutral fragments lost. For **3** to **6** ($R^2 > CH_3$) elimination of an R^2-H molecule from the molecular ions also takes place. In the case of **6** this process involving H migration (a ketene expulsion) completely suppresses the homo-

* The neglect of the kinetic isotope effect is justified by the observation that the abundance ratios of metastable peaks and that of normal ions corresponding to the processes 217 → 202 and 217 → 199 are the same in case of **2a**.

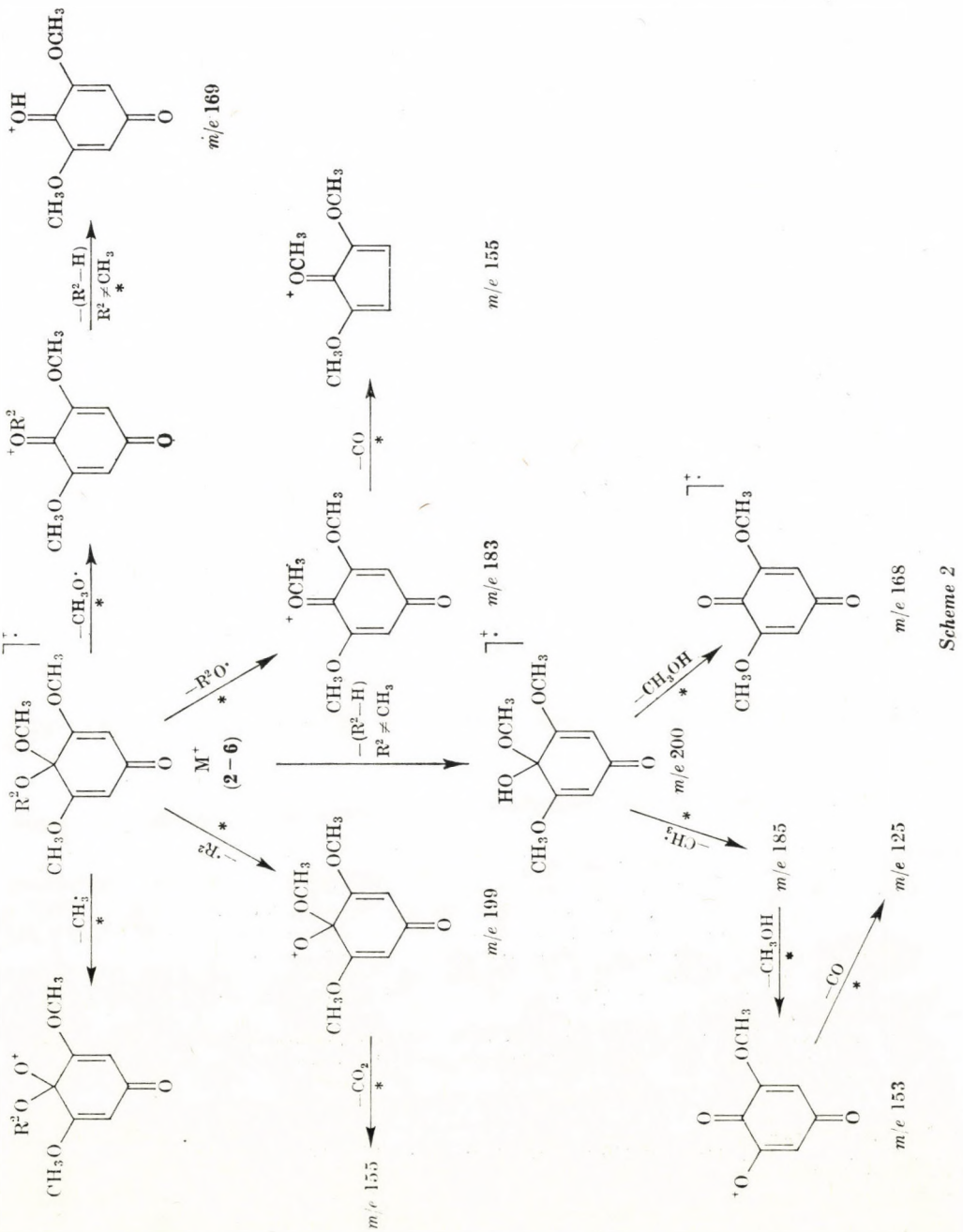

Scheme 2

lytic detachment of R^2. The ions of *m/e* 200 formed in these rearrangement processes can eliminate a methanol molecule subsequently or following the loss of a methyl group.

In the cases of **7** and **8** one of the main fragmentation pathways is the loss of the $R^2O^{\cdot}$ radical from the molecular ions. Elimination of a formaldehyde molecule from the methylenedioxy group as a competing or a subsequent process is also very significant. The abundance ratio of the $M-R^2O$ and $M-CH_2O$ ions obtained depends on the stability of R^2 (*cf.* Figs 8 and 9). Contrary to the *m/e* 199 ions of **2**–**6**, the $M-CH_2O$ ions of **7** and **8** cannot expulse a CO_2 molecule, supporting the assumption that the oxygen atom of the formaldehyde formed has been detached from the geminal position.

Finally, it can be concluded from the decomposition pathways observed for **1** to **8** that the main route of the electron-impact-induced fragmentation of these simple semiquinones involves cessation of the semiquinonoid structure giving rise to the formation of ions with the more stable quinonoid skeleton.

Experimental

Mass spectra were obtained by an AEI MS-902 double focusing mass spectrometer with an electron energy of 70 eV and a source temperature of 120 °C. The samples were introduced using a direct insertion probe. Exact mass measurements were carried out with an accuracy of ±2 ppm of the theoretical values. Metastable ions occurring in the first field free region were collected by altering the ESA voltage.

*

The authors thank Dr. S. ANTUS for putting the compounds studied at their disposa

REFERENCES

[1] PORTER, Q. N., BALDAS, J.: Mass Spectrometry of Heterocyclic Compounds, p. 102. Wiley-Interscience, New York 1971
[2] SMITH, H. E., SMITH, R. G.: Org. Mass. Spectrom., **7**, 1019 (1973)
[3] KUTNEY, J. P., SANCHEZ, I. H., YEE, T. H.: Org. Mass Spectrom., **8**, 129 (1974)
[4] MARTIN, N. H., ROSENTHAL, D., JEFFS, P. W.: Org. Mass Spectrom., **11**, 1 (1976)
[5] BUDZIKIEWICZ, H., DJERASSI, C., WILLIAMS, D. H.: Mass Spectrometry of Organic Compounds, p. 527. Holden-Day, San Francisco 1967
[6] MCKILLOP, A., PERRY, D. H., EDWARDS, M., ANTUS, S., FARKAS, L., NÓGRÁDY, M.: J. Org. Chem., **41**, 282 (1976)
[7] BUDZIKIEWICZ, H., DJERASSI, C., WILLIAMS, D. H.: Interpretation of Mass Spectra of Organic Compounds, p. 174–181. Holden-Day, San Francisco 1964

Marianna MÁK
József TAMÁS } H-1088 Budapest, Puskin u. 11–13.

Acta Chimica Academiae Scientiarum Hungaricae, Tomus 97 (1), pp. 45—49 (1978)

THE EFFECT OF IONIC STRENGTH ON THE STABILITY OUTER SPHERE COMPLEXES

L. ILCHEVA* and M. T. BECK

(Institute of Physical Chemistry, Kossuth L. University, and
** Department of Analytical Chemistry, Technical University, Sofia, Bulgaria)*

Received February 8, 1977

The stability constants of the outer sphere complexes of two inert complexes [tris(dipyridyl)-cobalt(III)] and [tris(phenanthroline)-cobalt(III)] with thiocyanate and iodide ions were determined at different ionic strengths. Potassium fluoride proved to be a suitable inert salt. The stability constant changes according to a minimum curve as a function of the ionic strength. This can be explained by the change of the activity coefficients with the ion concentration.

The determination of stability constants of outer sphere complexes raises several theoretical questions. The stability of most of these complexes is rather low, thus fairly high concentrations of the ligand are needed in order to achieve a sufficiently great conversion, consequently experiments must be carried out at rather high ionic strengths. However, to keep the ionic strength constant, the principle of constant ionic media generally applied in studies of complex equilibria cannot be made use of here [1] since ions (nitrate, perchlorate) which form complexes of but low stability are rightly expected to tend to form outer sphere complexes, and these are primarily, perhaps exclusively, results of electrostatic interactions. Several studies point towards outer sphere complexes of perchlorate ions being formed; stability constants for several species of ions have been determined. From the point of view of our studies here we consider the notable interaction of hexamine-cobalt(III) [2, 3], and of tris(phenanthroline)-iron(II) [4] complexes with perchlorate ions especially significant. In the course of our work we found that in the determination of the stability constants of the outer sphere complexes of [tris(phenanthroline)-cobalt(III)]-, and of [tris(dipyridyl)-cobalt(III)]-complexes, potassium fluoride is suitable for the maintenance of a medium of constant ionic strength because fluoride ions do not form outer sphere complexes with the ions mentioned.

Experimental

Substances. [Tris(dipyridyl)-cobalt(III)]-perchlorate, $Co(dipy)_3(ClO_4)_3 \cdot 3\,H_2O$ was prepared as described by BURSTALL and NYHOLM [5]; also the phenanthroline complex was synthesized in this way, with the necessary alterations. All the other reagents used were analytical grade commercial products.

Instruments. A Beckman B type spectrophotometer was used; this was fitted with a thermostated holder for the cuvettes which were kept at 22 ± 0.2 °C.

Results and discussion

At several suitable wave lengths the variation of the light absorption of the solutions was determined; stability constants, and molar absorptions were calculated graphically, by using a linearized equation.

$$ML_3^{3+} + X^- = ML_3X^{2+} \tag{1}$$

represents an outer sphere type complex; the equilibrium constant of its formation is

$$K = \frac{[ML_3, X^{2+}]}{[ML_3^{3+}]\,[X^-]} \tag{2}$$

where M stands for the metal ion with three positive charges, L for the electrically neutral, bidentate ligand bound in the inner sphere, and X for an anion with one negative charge, bound in the outer sphere.

Provided the absorption by X^-, respectively by its salt, is negligible at the wave length of the measurements then the absorption of the solution is

$$A = \varepsilon_i\,[ML_3^{3+}] + \varepsilon_0[ML_3, X^{2+}] \tag{3}$$

where ε_i is the molar absorption of ML_3, and ε_0 that of the ML_3, X^{2+} complex. When the materials balance

$$T_M = [ML_3^{3+}] + \varepsilon_0\,[ML_3, X^{2+}] \tag{4}$$

is taken into account,

$$A = \varepsilon_i\left(T_M - [ML_3, X^{2+}]\right) + \varepsilon_0[ML_3, X^{2+}]$$

ε_i can be determined by separate experiment. If for the value of $\varepsilon_i T_M$ we write A′, and if we consider that $[X^-]$ is approximately the same as the total concentration of X^-

$$T_X = [X^-] + [ML_3, X^{2+}] \sim [X^-]$$

then it follows that

$$\Delta A = A - A' = (\varepsilon_0 - \varepsilon_i)\,[ML_3, X^{2+}] = \Delta\varepsilon\,[ML_3, X^{2+}] \tag{5}$$

Rearrangement of (5) gives the following equation

$$\frac{T_M\,T_X}{\Delta A} = \frac{T_X}{\Delta\varepsilon} + \frac{1}{K\Delta\varepsilon} \tag{6}$$

When the left hand term of this equation is plotted as a function of T_X a straight line is obtained from, its slope and intersection K, and $\Delta\varepsilon$, or ε_0 can be calculated.

With sodium perchlorate used for maintaining permanent ionic strength, $\frac{T_M T_X}{\Delta A}$ drawn as a function of the concentration of the ligand will not yield a straight line. This suggests that perchlorate ions form outer sphere complexes with the inert complexes studied. Practically no change in the light absorption of the inert complex is caused by fluoride ions. This in itself does not prove that fluoride ions do not associate with the inert complexes here studied. However, when potassium fluoride instead of potassium chloride was applied

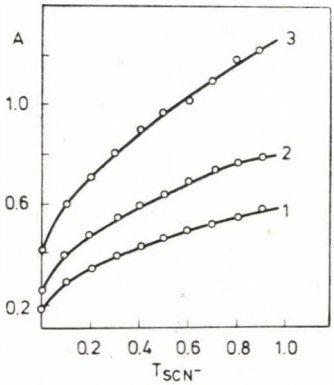

Fig. 1. Change of the light absorption of the tris(dipyridyl)-cobalt(III) complex in function of the thiocyanate ion concentration $I = 2.5$ (potassium fluoride) $T_{complex}$ $5 \cdot 10^{-4}$ mole · · dm^{-3}; width 1 cm; $t = 22$ °C. Curve 1, $\lambda = 400$ nm; Curve 2, $\lambda = 390$ nm; Curve 3, $\lambda = 380$ nm

for the maintenance of constant ionic strength, for the stability constant of ion pairs $Co(dipy)_3$, SCN^{2+} a considerably, higher value was obtained: this suggested that fluoride ions associated with the cobalt(III)-complexes in but a slight extent if at all, thus were suitably applied when the effect of ionic strength on the stability of outer sphere complexes was tested. As examples, Figures 1, and 2 show results for the $Co(dipy)_3^{3+}$ and SCN^- system at an ionic strength of one mole. Further data, very great in number, will not be printed but are made available to those who might be interested in them. Table I presents stability constants noted for various systems. Here we see that the stability constant of the ion pair $Co(dipy)_3$, SCN^{2+} has an extreme value when plotted as a function of ionic strength.

The results demand explanation from two points of view. On the one hand it is not obvious why fluoride ions should not form ion pairs with the complex ion that carries three positive charges; based on simple electrostatics the contrary is to be expected. On the other hand the question arises why the stability constant exhibits a minimum when plotted against the concentration of potassium fluoride. We think the high degree of hydratation of the fluoride ion furnishes the answer to both these questions. Owing to its small size,

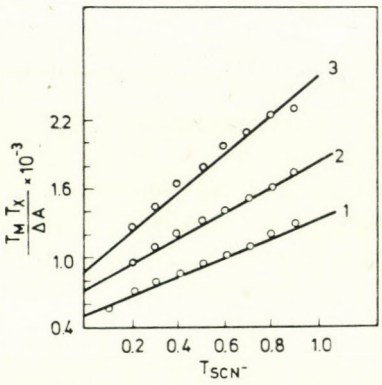

Fig. 2. Evaluation of data in Fig. 1 $\frac{T_M T_X}{A}$ as a function of the thiocyanate concentration at three different wave lengths

fluoride ion is very strongly hydrated, thus formation of an outer sphere type complex presupposes the removal of water molecules from a rather stable hydrate sheath. The high degree of hydratation of the fluoride ion, outstandingly high among single-charged anions is exhibited in the mean activity coefficient which passes through a minimumm as a function of the concentration.

Of course, the stability constants summarized in Table I are thermodynamic constants valid for the given medium. Their relationship to the stability constant K° referred to pure water as the standard state can be written as

$$K^\circ = K \frac{y_{2+}}{y_{3+}\, y_-} = K\, Y \tag{7}$$

where y_{3+}, y_{2+}, and y_- stand for the molar activity coefficients, referred to pure water as the standard state, of the corresponding ionic species. With a supposed distance of 7.5 Å between the ionic centres, and based upon the considerations of Bjerrum, we obtained 17 for K°. It is a good approximation when the activity coefficient of the thiocyanate is taken as being the same as

Table I

Complex	Medium	K
$Co(dipy)_3$, SCN^{2+}	KCl + KSCN = 1 mole · dm^{-3}	1.0±0.1
$Co(dipy)_3$, SCN^{2+}	KF + KSCN = 1 mole · dm^{-3}	1.7±0.1
$Co(dipy)_3$, SCN^{2+}	KF + KSCN = 2.5 mole · dm^{-3}	1.0±0.1
$Co(dipy)_3$, SCN^{2+}	KF + KSCN = 4.0 mole · dm^{-3}	1.2±0.1
$Co(dipy)_3$, SCN^{2+}	KF + KSCN = 6 mole · dm^{-3}	2.3±0.1
$Co(dipy)_3$, I^{2+}	KF + KI = 1 mole · dm^{-3}	1.5±0.1
$Co(phen)_3$, I^{2+}	KF + KI = 1 mole · dm^{-3}	1.7±0.1

the mean activity coefficient of potassium fluoride:

$$K^\circ = K \frac{y_{2+}}{y_{3+}\, y_\pm} \tag{8}$$

consequently if $y_\pm$ is known [6] the approximate value of the quotient of the activity coefficients of the outer sphere complex with two positive charges and that of the inert complex ion with three positive charges can be calculated (Table II). These figures do not seem to be unrealistic though it would not be correct to accept this treatment as being a quantitative one. However, it seems that the change in stability constants by varying the concentration of potassium fluoride can be explained qualitatively.

Table II

I	1	2.5	4	6
K	1.73	1.00	1.25	2.30
$\frac{K^\circ}{K}$	9.8	18	13.6	7.4
$\frac{y_{2+}}{y_{3+}}$	6.4	12.0	11.2	7.4

Finally we wish to remark that while potassium fluoride hardly affects the light absorption of the inert complex, or does not affect it at all, the molar light absorption of an outer sphere complex significantly changes as a function of the ionic strength and does so according to an extreme value at each of the wave lengths selected. Further it is worth mentioning in this context that earlier observations showed that fluoride ions had hardly any effect on the molar light absorption of the stable tetracyanonickelate(II)-complex, where as it proved highly effective [7] in the case of the less stable pentacyanonickelate(II). Furthere investigations are needed to reveal whether it is generally true that when ionic strength is varied by the use of ions not likely to form complexes, molar light absorption will change the greater the lower the stability of the complex ion.

REFERENCES

[1] Beck, M. T.: Coord. Chem. Rev., **3,** 91 (1968)
[2] Heck, L.: Inorg. Nucl. Chem. Letters, **7,** 701 (1971)
[3] Mironov, V. R., Ljubomirova, K. N., Razgulin, G. K.: Zh. Phys. Chim., **44,** 416 (1970)
[4] Margerum, D. W., Banks, C. V.: Anal. Chem., **26,** 200 (1954)
[5] Burstall, F. H., Nyholm, R. S.: J. Chem., Soc. **1952,** 3577
[6] Harned, H. S., Owen, B. B.: The Physical Chemistry of Electrolytic Solutions, p. 563; Reinhold, 1950.
[7] Beck, M. T., Bjerrum, J.: Acta Chem. Scand., **16,** 2050 (1962)

L. Ilcheva, Dep. of Anal. Chem. Techn. University Sofia, Bulgaria
Mihály T. Beck, KLTE H-4010 Debrecen, P. O. Box 7.

Acta Chimica Academiae Scientiarum Hungaricae, Tomus 97 (1), pp. 51—55 (1978)

APPLICATION OF THE PARAMETER METHOD TO VIBRATION SPECIES OF ORDER THREE EMPLOYING ISOTOPIC FREQUENCIES

E SPECIES FORCE CONSTANTS OF CH_3F

C. Egbert CHELLAM and G. ARULDHAS*

(Department of Physics, College of Engineering, Trivandrum and

** Department of Physics, University of Kerala, Kariavattam India)*

Received March 10, 1977

The parameter method has been applied to the calculation of force constants of methyl fluoride (E species of order three). Three fundamental frequencies, two zetas and one isotopic frequency have been used as input data. Two sets of force constants were obtained. Of these, the one which reproduces the other isotopic frequencies exactly has been chosen as the relevant set.

Introduction

The parameter method has been applied for calculating the force constants of polyatomic molecules in several publications [1—7]. Generally, in these methods frequencies, Coriolis coupling constants (zetas) and vibrational amplitudes have been used as input data. Frequencies of the molecule after isotopic substitution have been used as input data only in second order cases [3]. This paper introduces the use of isotopic frequencies in the third order case.

Theory of the method

The normal frequencies of a polyatomic molecule are related to the force constants by the matrix equations

$$GFL = L\Lambda \tag{1}$$

$$\tilde{L}FL = \Lambda \tag{2}$$

$$L\tilde{L} = G \tag{3}$$

where the symbols have their usual meanings [8]. Assuming that on isotopic substitution in the molecule, the F elements are unchanged, while, G, L and Λ change by small amounts, it has been shown [9] that

$$\text{diag}\,[L^{-1}(\Delta G)\tilde{L}^{-1}\Lambda] = \text{diag}\,[\Delta\Lambda] \tag{4}$$

It follows that

$$[L^{-1}\,(\Delta G)\,\tilde{L}^{-1}]_{ll} = (\Delta\lambda_l)/\lambda_l \tag{5}$$

In the parametric approach,

$$L = TA \tag{6}$$

where T is a lower triangular matrix, such that $T\,\tilde{T} = G$, and

$$A = A_{45}\,A_{46}\,A_{56} \tag{7}$$

in which A_{ij} are orthogonal matrices involving the angular parameter Φ_{ij} [1, 6]. By virtue of Eqs (7) and (6), Eq. (5) becomes

$$[\tilde{A}_{56}\,\tilde{A}_{46}\,\tilde{A}_{45}\,T^{-1}\,(\Delta G)\,\tilde{T}^{-1}\,A_{45}\,A_{46}\,A_{56}]_{ll} = (\Delta\lambda_l)/\lambda_l \tag{8}$$

where $l = 4, 5, 6$ in the case under analysis. Introducing $T^{-1}\,(\Delta G)\,\tilde{T}^{-1} = K$, one obtains

$$[\tilde{A}_{56}\,\tilde{A}_{46}\,\tilde{A}_{45}\,K\,A_{45}\,A_{46}\,A_{56}]_{ll} = (\Delta\lambda_l)/\lambda_l \tag{9}$$

Writing

$$\tilde{A}_{45}\,KA_{45} = K^* \tag{10}$$

Eq. (9) becomes

$$[\tilde{A}_{56}\,\tilde{A}_{46}\,\overset{*}{K}\,A_{46}\,A_{56}]_{ll} = (\Delta\lambda_l)/\lambda_l \tag{11}$$

Expressing A_{46} and A_{56} in terms of Φ_{46} and Φ_{56}, Eq. (11) gives

$$\overset{*}{K}_{44}\cos^2\Phi_{46} + \overset{*}{K}_{66}\sin^2\Phi_{46} + 2\overset{*}{K}_{46}\cos\Phi_{46}\sin\Phi_{46} = (\Delta\lambda_4)/\lambda_4 \tag{12}$$

$$\begin{aligned}&\overset{*}{K}_{44}\sin^2\Phi_{46}\sin^2\Phi_{56} + \overset{*}{K}_{55}\cos^2\Phi_{56} + \overset{*}{K}_{66}\cos^2\Phi_{46}\sin^2\Phi_{56} - \\ &- 2(\overset{*}{K}_{45}\sin\Phi_{46}\sin\Phi_{56}\cos\Phi_{56} + \overset{*}{K}_{46}\sin\Phi_{46}\cos\Phi_{46}\sin^2\Phi_{56} - \\ &- \overset{*}{K}_{56}\cos\Phi_{46}\sin\Phi_{56}\cos\Phi_{56}) = (\Delta\lambda_5)/\lambda_5\end{aligned} \tag{13}$$

$$\begin{aligned}&\overset{*}{K}_{44}\sin^2\Phi_{46}\cos^2\Phi_{56} + \overset{*}{K}_{55}\sin^2\Phi_{56} + \overset{*}{K}_{66}\cos^2\Phi_{46}\cos^2\Phi_{56} + \\ &+ 2(\overset{*}{K}_{45}\sin\Phi_{46}\sin\Phi_{56}\cos\Phi_{56} - \overset{*}{K}_{46}\sin\Phi_{46}\cos^2\Phi_{46}\cos^2\Phi_{56} - \\ &- \overset{*}{K}_{56}\cos\Phi_{46}\sin\Phi_{56}\cos\Phi_{56}) = (\Delta\lambda_6)/\lambda_6\end{aligned} \tag{14}$$

Equations (12), (13) and (14) make it possible to introduce the isotopic frequencies as additional data.

Application to methyl fluoride

The methyl fluoride molecule (CH_3F) belongs to the C_{3v} point group. It has 9 fundamental frequencies $3A_1 + 3E$. Of these, the $3E$ vibrations are the subject of this paper. The expressions for the G matrix elements, the data with regard to the geometry of the molecule and the experimental values of the frequencies, etc., are taken from Ref. [10].

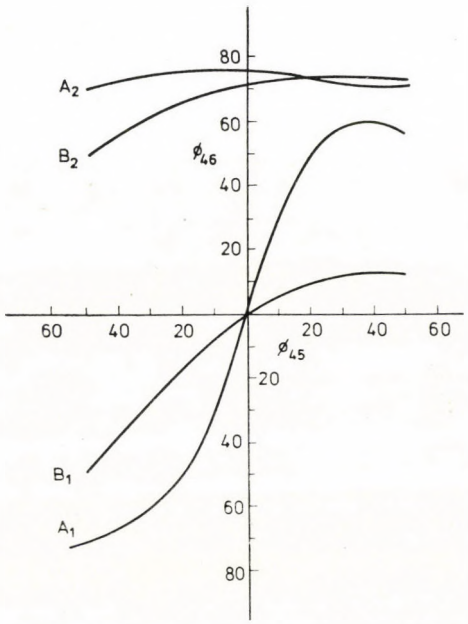

Fig. 1. Variation of Φ_{46} against Φ_{45}. Curves $A1$ and $A2$ show the values of Φ_{46} which fit the Coriolis coupling constant ζ_4. Curves $B1$ and $B2$ show the values of Φ_{46} which fit the isotopic frequency ν_4. Point of intersection of $A2$ and $B2$ is irrelevant as it lies outside the TÖRÖK limits. The point of intersection of $A1$ and $B1$ denotes the values of Φ_{45} and Φ_{46} consistent with both ζ_4 and ν_4

The actual method is as follows. For different values of Φ_{45} from $-45°$ to $+45°$ (TÖRÖK limits) [11], the values of Φ_{46} to fit ζ_4 are calculated using the relation given as Eq. (14) in Ref. [6]. Of the two values of Φ_{46} for each Φ_{45}, one lies outside the TÖRÖK limits. The variations of the two values of Φ_{46} with Φ_{45} are shown as curves A1 and A2 in Fig. 1. Also, the values of Φ_{46} to fit $(\Delta\lambda_4)/\lambda_4$ are calculated using Eq. (12). Again, there are two sets of Φ of which one set is entirely outside the TÖRÖK limits. The variations of the two values of Φ_{46} with Φ_{45} are shown as curves B1 and B2 in Fig. 1. The points of intersection of the curves give two combinations of Φ_{45} and Φ_{46} that would fit both ζ_4 and $(\Delta\lambda_4)/\lambda_4$. Out of the two points of intersection, the one lying outside the TÖRÖK limits is ignored and the other is taken as the relevant one.

The exact point of intersection found by magnifying the computation in its neighbourhood is $\Phi_{45} = -0.465°$, $\Phi_{46} = -0.445°$. The corresponding value of Φ_{56} is calculated using ζ_5 and Eq. (15) of Ref. [6]. Two values are obtained for Φ_{56}. Using each value, the matrix L is found by applying Eqs (7) and (6), and then F is calculated by Eq. (2). Each value of Φ_{56} gives a set of force constants.

In order to eliminate the irrelevant set, the isotopic frequencies are calculated using the two sets. Naturally, both sets reproduce the first frequency ν_4 of the isotopically substituted molecule. But, only one set reproduces all the frequencies satisfactorily, while the other does not, though the individual F elements are not appreciably different.

The relevant force constants (mdyn/Å) for the molecule are

$$F_{44} = 5.36 \qquad F_{55} = 0.40$$
$$F_{45} = -0.09 \qquad F_{56} = -0.05$$
$$F_{46} = 0.06 \qquad F_{66} = 0.76$$

For the sake of confirmation, the molecule CD_3F was taken as the original molecule and CH_3F as the isotopically substituted molecule, following the same procedure.

The force constants obtained are

$$F_{44} = 5.40 \qquad F_{55} = 0.43$$
$$F_{45} = -0.11 \qquad F_{56} = 0.05$$
$$F_{46} = 0.15 \qquad F_{66} = 0.85$$

The close agreement confirms the validity of the method. The slight deviations are due to the fact that the mass of the D atom is twice that of the H atom.

Thus, the parameter method can be successfully applied to vibrational problems of order three by incorporating isotopic frequencies as additional data.

*

The authors are grateful to Dr. T. R. ANANTHAKRISHNAN and Dr. C. P. GIRIJAVALLABHAN for the useful suggestions given by them during informal discussions on this topic.

REFERENCES

[1] TÖRÖK, F., PULAY, P.: J. Mol. Struct., **3,** 1 (1969)
[2] ANANTHAKRISHNAN, T. R., ARULDAS, G.: J. Mol. Struct., **13,** 163 (1972)
[3] ANANTHAKRISHNAN, T. R., GIRIJAVALLABHAN, C. P., ARULDHAS, G.: J. Mol. Struct., **16,** 149 (1973)

[4] ANANTHAKRISHNAN, T. R., ARULDHAS, G.: J. Mol. Struct., **42,** 311 (1973)
[5] RAMASWAMY, K., CHANDRASEKARAN, V.: Acta Phys. Polon., A, **48,** 105 (1975)
[6] ANANTHAKRISHNAN, T. R., ARULDHAS, G.: J. Mol. Struct., **26,** 1 (1975)
[7] ANANTHAKRISHNAN, T. R.: Current Sci., **45,** 754 (1976)
[8] WILSON, E. B., DECIUS, J. C., CROSS, P. C.: Molecular Vibrations, McGraw-Hill, New York 1955
[9] JORDANOV, B.: J. Mol. Struct., **13,** 21 (1972)
[10] ALDOUS, J., MILLS, I. M.: Spectrochim. Acta **18,** 1073 (1962)
[11] TÖRÖK, F.: Acta Chim. Acad. Sci. Hung., **52,** 205 (1967)

C. Egbert CHELLAN } Department of Phys. College of Engineering
Trivandrum 695016 India,
G. ARULDHAS } Department of Phys. University of Kerala,
Kariavattam 695581 India.

Acta Chimica Academiae Scientiarum Hungaricae, Tomus 97 (1), pp. 57–60 (1978)

FORMATION CONSTANTS OF Y(III), Pr(III), Nd(III), Sm(III), Gd(III) AND Dy(III) COMPLEXES OF 2-BENZIMIDAZOLETHIOL

(SHORT COMMUNICATION)

S. A. A. ZAIDI and V. ISLAM

(Inorganic Division Department of Chemistry, Aligarh Muslim University, Aligarh, India)

Received March 10, 1977

In revised form July 14, 1977

The formation of 1 : 1 complexes between Y(III), Pr(III), Nd(III), Sm(III) Gd(III) and Dy(III) ions and 2-benzimidazolethiol has been shown potentiometrically. The metal–ligand stability constants (log K_1) and proton ligand stability constants (log K_2^H) have been determined by the pH-titration technique at 30 °C and 0.1 *M* ionic strength.

Introduction

2-Benzimidazolethiol is an industrially important compound. Its certain metal salts have been used as heat stabilizers for polyamides [1]. Its lead complex is used in the photoconductive layers of electrophotographic plates [2]. The adducts of 2-benzimidazolethiol with tin(II) and (IV) and antimony(III) halides have also been reported [3]. Rhodium and iridium complexes have been isolated and the determination of palladium using this ligand has also been done [5]. The Ru(III) complex has been studied spectrophotometrically [6]. There are, however, no data in the literature on the interaction of this ligand with the rare earth ions. We now report the stability constants of such complexes in 50 vol. % aqueous ethanol, determined potentiometrically, as in case of Bismuthiol I [7].

Materials and methods

Anhydrous rare earth chlorides were dissolved in perchloric acid of desired normality to prevent the hydrolysis of these ions. 2-Benzimidazolethiol (m. p. 295 °C, Fluka, A. G.) was dissolved in ethanol. The sodium hydroxide(BDH) and perchloric acid (E. Merck) solutions were prepared in conductivity water and standardized by usual methods [8]. 1.0 *M* $NaClO_4$ (Riedel) solution was prepared in bidistilled water.

Apparatus. For pH determination, an ELICO LI-10 pH-meter with ± 0.05 accuracy was employed in combination with glass calomel electrodes calibrated with the help of standard buffers. An inert atmosphere was maintained by bubbling oxygen and carbon dioxide free nitrogen gas trough the solutions.

Results and discussion

Proton–ligand stability constants

2-Benzimidazolethiol (**I**) is a derivative of 1-H-benzimidazole (**II**); it contains two types of protons N – H and S – H. At low pH, the acid ligand curve lies slightly above the pure acid curve presumably due to the protonation of the N – H group in the acid–ligand system (Fig. 1). The acid–ligand curve overlaps with the pure acid curve between B = (5.0 – 8.5), but deviates at B = 8.8. The lowest value of $\bar{n}_A$, 1.085, was observed at B = 11.8 and the highest value of $\bar{n}_A$, 2.0 at B = 8.5, which indicates that only one proton is released, presumably from the N – H group. The proton–ligand formation curve has been obtained by plotting $\bar{n}_A$ against B (Fig. 2).

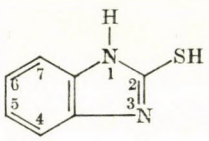

I

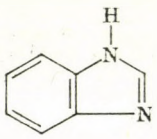

II

Thus only log K_2^H was obtained by the half integral method and pointwise calculations, also extended to the aqueous ethanol system [7].

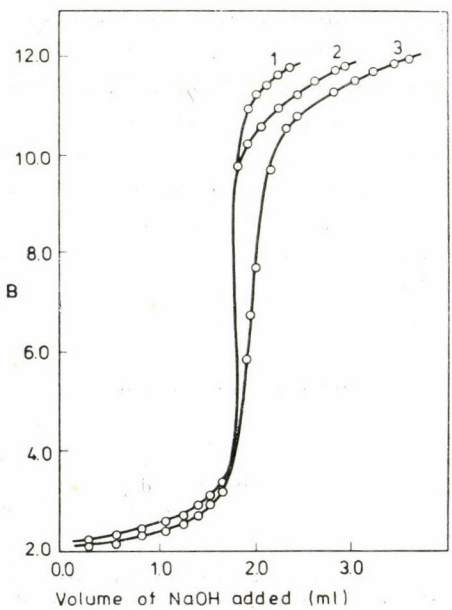

Fig. 1

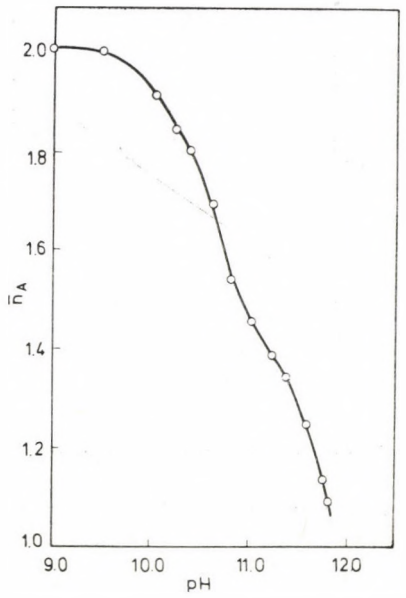

Fig. 2,

Table I

Stability constants at 30 °C ± 0.1 and μ = 0.10 M

Stability constant	log K_2^H	log K_1		
		Y(III)	Pr(III)	Nd(III)
Half integral method	10.80	7.20±0.05	7.10±0.025	7.10±0.05
Pointwise calculation	10.92	7.21±0.05	7.15±0.025	7.21±0.05
Average	10.86	7.205±0.05	7.125±0.025	7.155±0.05
Standard deviation	±0.005 ($1.3<\bar{n}_A<1.9$)	±0.025 ($0.2<\bar{n}<0.8$)	±0.0066 ($0.3<\bar{n}<0.6$)	±0.078 ($0.3<\bar{n}<0.6$)

Stability constant	log K_2^H	log K_1		
		Sm(III)	Gd(III)	Dy(III)
Half integral method	10.80	7.30±0.05	7.35±0.05	7.05±0.025
Pointwise calculation	10.92	7.38±0.05	7.30±0.05	7.09±0.025
Average	10.86	7.34±0.05	7.325±0.05	7.07±0.025
Standard deviation	±0.005 ($1.3<\bar{n}_A<1.9$)	±0.062 ($0.3<\bar{n}<0.8$)	±0.0089 ($0.3<\bar{n}<0.9$)	±0.13 ($0.3<\bar{n}<0.6$)

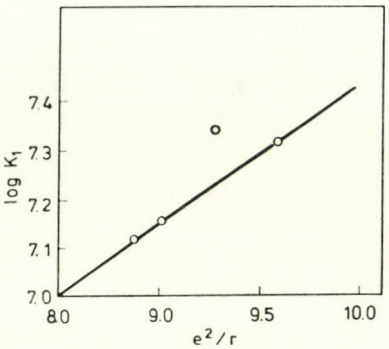

Fig. 3,

Metal–ligand stability constants

To eliminate the possibility of the hydrolysis of the rare earth ion and the presence of polynuclear species, we worked at low pH (up to B = 6.5) in dilute solutions.

The complexation reaction between lanthanide(III) ions and the reagent was obvious by the considerable deviation of the metal–ligand titration curve from the reagent curve along the volume a α is (Fig. 1).

The increase in the $\bar{n}$ values was continuous from B = 3.0 to B = 6.5 in all cases. The maximum $\bar{n}$ value in all the cases was greater than 0.5, indicating 1 : 1 complex formation. The $\bar{n}$ value changed abruptly beyond B = 6.5, due to the hydrolysis of the metal ion, therefore $\bar{n}$ values were considered only up to B = 6.5.

The pL values were calculated at various $\bar{n}$ values and log K_1 was obtained by the half integral method and by pointwise calculations. These log K_1 values plotted against e^2/r (Fig. 3) show a roughly linear increase with e^2/r, suggesting that the metal–ligand bonds have some ionic character.

*

The authors thank Prof. W. RAHMAN, Head, Department of Chemistry, for providing all the necessary research facilities. One of us (V. I.) thanks the C. S. I. R., New Delhi, for financial assistance.

REFERENCES

[1] ZIMMER, H. J.: C. A. **63,** 10136a (1965)
[2] KOSCHE, H.: C. A. **71,** 66076b (1969)
[3] OUCHI, A., TAKEUCHI, T., TAMINAGA, I.: C. A. **73,** 115913z (1970)
[4] LOMAKINA, L. N., ALIMARIN, I. P.: C. A. **66,** 101220q (1967)
[5] LOMAKENA, L. N., ALIMARIN, I. P.: C. A. **66,** 8075g (1967)
[6] PILIPENKO, A. T., SEREDA, I. P., SEMENYUK, E. P.: C. A. **74,** 49366j (1971)
[7] ZAIDI, S. A. A., ISLAM, V.: Indian J. Chem. **15A,** 155 (1977)
[8] VOGEL, A. I.: A Text Book of Quantitative Inorganic Analysis, pp. 690, 708, Longmans London 1961

S. A. A. ZAIDI
V. ISLAM
Inorganic Division, Department of Chemistry; Aligarh Muslim Univ. Aligarh-202001; India.

Acta Chimica Academiae Scientiarum Hungaricae, Tomus 97 (1), pp. 61–67 (1978)

GRAVIMETRIC STUDY OF *n*-BUTANE ADSORPTION ON Ni-BLACK CATALYST

A. SÁRKÁNY and P. TÉTÉNYI

(Institute of the Isotopes of the Hungarian Academy of Sciences)

Received August 2, 1977

Adsorption of *n*-butane and *n*-butane : hydrogen mixtures has been investigated gravimetrically on Ni black catalyst in temperature range of 20 – 200 °C. In addition to physisorption different chemisorption forms are discernible: chemisorption of *n*-butane leads to formation of dissociatively adsorbed butane, to its fragments above 88 °C and to a form of low reactivity towards hydrogen. Comparison of the rate of hydrogenolysis to the rate of hydrogenation of the chemisorbed substrate permits to suggest that the last form acts as poison for hydrogenolysis.

Transformation of saturated hydrocarbons on Ni catalysts has been extensively investigated from both kinetic and mechanism point of view [1–7]. Different reaction routes such as deuterium exchange and hydrogenolysis have been explained by assuming "weakly" and "strongly" bonded intermediates [6] on the surface the former being dehydrogenated to a lesser extent [5] than the latter one. On Ni catalyst multiply dehydrogenated species are easily formed resulting in "deep" fragmentation [6–7] of the hydrocarbon molecules and in poisoning of the surface by carbonaceous deposits. Our recent paper deals with adsorption of *n*-butane on Ni black catalyst. In order to obtain a deeper insight into the nature of the chemisorbed substrate adsorption of hydrogen: *n*-butane mixtures and the reactivity of the chemisorbed substrate with H_2 are investigated. Adsorption data can then be compared with quantity of adsorption that appears during deuterium exchange or hydrogenolysis.

Experimental

Adsorption measurements were performed by means of a Sartorius electrobalance (Type 4102) connected to a vacuum and gas handling system. Ni sample was heated by stabilized A. C.; the heating wires were placed directly on the hang-down tubes. Temperature of the sample was recorded close to the sample holders. The microbalance was tested in loaded state using Ni plates with the same weight as the catalyst itself in static as well as in flow measurements with hydrogen, *n*-butane and their mixtures in the temperature range of 20 – 200 °C. The bouyancy effects were recorded and tabulated. Ni black catalyst was prepared from $Ni(OH)_2$ *in situ*. Details of preparation have been described elsewhere [8]. In adsorption measurements 0.3 g sample was used. The specific surface area of the Ni sample used is 6.2 $m^2\ g^{-1}$ as measured by the BET/N_2 method. Gases (hydrogen and *n*-butane) were passed through

BASF-11 contact and then through a column filled with molecular sieve. *n*-Butane contained 0.02 mol % 2-methylpropane.

Adsorption measurements were performed in the temperature range of 20 – 200 °C. Before each measurement Ni catalyst was hydrogenated at 350 °C for 30 min and then evacuated for $8 - 9 \cdot 10^{-5}$ torr and finally cooled to the temperature of the experiment. In some cases after hydrogenation the sample was purged in He, at 350 °C for 30 min.

Data on *n*-butane hydrogenolysis were measured in an atmospheric flow reactor. *n*-Butane and hydrogen were mixed with helium and passed downflow through the catalyst bed consisting of 0.2 g Ni diluted carefully with 0.3 g silica sand. By adjustment of the helium and hydrogen flow rate the partial pressure of hydrogen was varied. Flow rate of *n*-butane was 29.5 ml min^{-1}. The total gas flow was maintained at 450 ml min^{-1} throughout. Rate measurements were performed at low conversion levels up to 10 %. The effluents were analysed by Packard 427 gas chromatograph. Conversion α was calculated from the balance equation, $\alpha = 100 \sum_{i=1}^{3}{}' iC_i / \sum_{i=1}^{4}{}' iC_i$. where C_i denotes molar concentration of a hydrocarbon with *i*-carbon atoms. The reaction rate was calculated to unit surface area, $r_A = 10^{-2} \alpha F S^{-1}$, where F-flow-rate of the feed- and S- the surface area of the catalyst-used.

Results

Adsorption isotherms were determined between 20 and 150 °C measuring the weight of the total adsorption by varying the equilibrium pressures between 250 and 5 torr. The weight of the chemisorbed substrate (measured at $8 - 9$ 10^{-5} torr) was then substracted from the weight of the total adsorption. Experimental results are summarized in Table I, which contains the type of isotherm, the isosteric heat of adsorption and the area occupied by an adsorbed *n*-butane. The latter value was determined from $v_{m,n-\mathrm{But}}/v_{m,\mathrm{N_2}}(\mathrm{BET})$ using $\sigma_{\mathrm{N_2}} = 16.2$ Å^2 [9].

In Table II data on *n*-butane chemisorption and the effect of hydrogen on the removal of the irreversibly bonded substrates are summarized. In the second column the weight of the reversibly adsorbed substrate ($p^0_{n-\mathrm{But}} = 50$ torr) is also given. The quantity of substrate chemisorbed below 88 °C is nearly independent of temperature. The percentage surface occupation reaches $8 - 10$ % in this temperature range. Weight of the chemisorbed substrate commences to increase above 88 °C. At 152 °C the adsorption becomes time depend-

Table I

Data on reversible adsorption of n-butane

Temp. range	20 – 60 °C	60 – 120 °C
Isotherm	F	F
Heat of adsorption $-\Delta H_a$, kJ $mole^{-1}$ (v/V_m)	33.0 – 30.5 (0.05 – 0.2)	68.1 – 45.1 (0.05 – 0.15)
Surface area 10^{20} m^2/adsorbed *n*-but.	28	112

F – Freundlich

Table II

n-Butane adsorption on Ni black

Temp./°C	Amount of *n*-butane (μg m^{-2})		Remained on the surface		Hydrogenation rate	
	physisorbed ($p_{n\text{-but}}$=50 Torr)	chemisorbed (10^{-4} Torr, 0.5 hr)	after 3 min in 50 Torr H_2	after 20 min of H_2 flow (7.5 ml min^{-1})	R_0^a μg m^{-2} min^{-1}	R_{20}^b μg m^{-2} min^{-1}
24	142	35	–	–	–	–
24[c]	138	63	–	–	–	–
32	103	32	–	–	–	–
55	87	38	10	–	–	–
88	43	43	15	10	–	–
103	21	87	32	13	–	0.83
142	12	143	57	33	15	0.92
159	10	185	127	88	26	1.21
198	10	193	142	103	62	0.76
198[d]	10	187	167	147	32	0.11
203[e]	10	249	202	182	65	0.68
197[f]	10	195	183	182	--	—

a) Initial rate; b) rate measured after 20 minutes; c) after hydrogenation sample was purged in He for 0.5 hr; d) evacuated for 5 hrs; e) sample exposed to *n*-butane for 1.5 hrs; f) sample heated in the at 450 °C (during heat treatment 15 μg weight loss was observed) — not measured

Table III

Initial composition of substrates formed from chemisorbed n-butane in H_2

T °C	C_1	C_2	C_3	$4C_4/\sum_{i=1}^{3} iC_i$
142	73.2	12.7	14.1	0.13
159	87.5	11.2	1.3	0.07
198	95.0	4.9	0.1	0.03

ent. The rate of weight increase at 198 °C is nearly proportional to the square root of the partial pressure of *n*-butane; at 50 torr it reaches 8–10 μg/10 minutes. As shown in the last two columns part of the irreversibly bonded substrate was readily hydrogenated after admission of 50 torr hydrogen. After 3 minutes the system was filled up atmospheric pressure of H_2 and further weight change was recorded in stream of H_2 (7.5 ml min^{-1}). Removed hydrocarbons were trapped and their composition was checked gas chromatographically. Results are presented in Table III, which shows the composition of the gaseous products collected in the first five minutes. Further hydrogenation resulted in formation of methane only.

Table IV

Effect of hydrogen on chemisorption and hydrogenolysis of n-butane

T °C	p_{H_2} Torr	Weight of the chemisorbed substrate $\mu g\ m^{-2}$	Initial weight loss $\mu g\ m^{-2}$	Rate *n*-butane consumption, r_A $mol\ m^{-2}\ s^{-1}$	Rate of hydrogenation[c] R_0, $mol\ m^{-2}\ s^{-1}$
23	0	33	–	–	–
	5.5	10	–	–	–
	20[b]	0	–	–	–
88	0	57	–	–	–
	4.5	10	10	–	–
	53	10	10	–	–
198	0	197	–	$1.10 \cdot 10^{-9}$	$6.12 \cdot 10^{-9}$[a]
	7.5	137	89[a]	$5.15 \cdot 10^{-8}$	$6.12 \cdot 10^{-9}$[a]
	22.5	83	57[a]	$1.33 \cdot 10^{-7}$	$3.43 \cdot 10^{-9}$[a]
	55.0	24	10	$5.12 \cdot 10^{-7}$	$6.70 \cdot 10^{-9}$
	163.0	20	14	$1.17 \cdot 10^{-6}$	$0.97 \cdot 10^{-9}$
	232.0	25	15	$1.38 \cdot 10^{-6}$	$1.02 \cdot 10^{-9}$
	515.0	20	5	$5.63 \cdot 10^{-7}$	$1.38 \cdot 10^{-9}$

[a] Measured after 5 minutes after having closed the hydrocarbon stream, otherwise initial weight loss; [b] $p_{HC} = 200$ Torr, otherwise 50 Torr; [c] it has been assumed that H/C ratio is two and methane is the only product of hydrogenation — not measured

Measurements at 198 °C revealed, that the increase of the weight of the chemisorbed substrate in course of time resulted also in raise of the weight of non-reacting substrate. Evacuation of the sample after adsorption influences also the reactivity of the adsorbed substrate probably owing to further dissociation of C–H bonds.

The effect of hydrogen on chemisorption of *n*-butane was investigated at 23, 88 and 189 °C. Results are depicted in Table IV together with rate measurements on *n*-butane hydrogenolysis. As can be seen from the results, presence of hydrogen strongly influences irreversible adsorption. At 189 °C the adsorption is time dependent: weight as well as conversion is measured after 30 minutes. Turning of the hydrocarbon stream, 5 – 15 μg of the substrate was removable immediately. In the last column rate of the further weight decrease is given.

Discussion

In agreement with earlier investigations [10] data on *n*-butane adsorption reveal different adsorption forms. The reversible adsorption below 60 °C can be ascribed to physisorption. This conclusion is based on the heat of adsorption

and on the surface area occupied by an adsorbed *n*-butane, which is close to the van der Waals area of the molecule [9]. In temperature range between 60 and 100 °C part of the adsorbed substrate is still removable by evacuation but the isosteric heat of adsorption at low coverages (0.05 – 0.1) is several times greater than the heat of condensation. Above 140 °C the reversibility of *n*-butane adsorption is ceased. (The weight decrease during evacuation at 189 °C probably corresponds to further dissociation of C–H bonds and to self-hydrogenation of the chemisorbed substrate.)

The chemisorbed substrate formed below 88 °C consist of *n*-butane. Chemisorption proceedes probably through displacement of chemisorbed hydrogen, since the remaining pressure of hydrogen is 10^{-4} Torr in the balance. The *n*-butane coverage is low and corresponds to 6 – 7 adsorbed molecules per 100 metal atom. The quantity of chemisorbed substrate increases continuously with rising temperature that may point to the non-uniformity of the surface being induced by presence of hydrogen, impurities and by the different activities of edges, corners etc. Above 152 °C the quantity of the chemisorbed substrate does depend on time. This process is analogous to the high temperature deposition of carbon discussed by several authors [11 – 13]. The temperature dependence of deposition rate (steady rate) gives an apparent activation energy of 34 ± 3 kcal mol^{-1} for *n*-butane as measured by temperature jump method between 250 and 350 °C.

Experiments concerning the removal of chemisorbed substrate prove that it consists of different chemisorption forms. As shown by hydrogenation results one part is rapidly hydrogenated and consists of *n*-butane as well as of its fragments above 88 °C. The initial rate of hydrogenation of the chemisorbed substrate at 190 °C is 60 $\mu g\ min^{-1}\ m^{-2}$. This value assuming that only methane is formed and the substrate consist of (CH_2) units corresponds to a hydrogenation rate of 7.13 10^{-8} mol $m^{-2}\ sec^{-1}$. This value is an upper limit of the hydrogenation rate; in case of *n*-butane desorption it would be 1.78 10^{-8} mol $m^{-2}\ sec^{-1}$. The apparent activation energy of hydrogenation is 12 ± 4 kcal mol^{-1}, as measured in temperature range of 142 – 200 °C. This value is lower than reported for hydrogenation of carbon deposited from benzene or propene above 500 °C, where it reaches 67 [12] and 32 [14] kcal mol^{-1}, respectively. After removal of 60 % of the substrate (within 15 minutes) the hydrogenation rate 0.76 $\mu g\ min^{-1}\ m^{-2}$ at 190 °C *i.e.* the rate of methane formation is 10.2 10^{-9} mol $m^{-2}\ sec^{-1}$. This value does agree with chromatographic results.

The quantity of the slowly reacting substrate is strongly influenced by the evacuation time as well as by further heat treatment at elevated temperatures in vacuum. Analysis of exhaust gas indicated that methane is the only detectable product. The slowly reacting substrate might consist of superficial carbide (Ni_3C) or superficial carbon atom [15], that might transform into metal or form graphite, wich is then highly unreactive towards hydrogen [16].

Presence of hydrogen as shown by results in Table IV influences the chemisorption of butane to a large extent. The retarding effect decreases with increasing temperature in agreement with kinetic investigations on deuterium exchange [17] and hydrogenolysis [5 – 7]. The quantity of chemisorbed substrate decreases markedly with increasing pressure of hydrogen. Corresponding rate measurements on hydrogenolysis at 198 °C show that the rate of *n*-butane consumption as a function of hydrogen pressure can be characterized by a broad vulcano shaped curve. The decrease of reaction rate at low H_2/*n*-butane ratios can be ascribed to the poisoning of the surface by the slowly reactive substrate *i.e.* to the decrease of the number of working active sites. Percentage of unblocked surface atoms can be calculated by assuming that the quantity of the chemisorbed substrate measured at zero partial pressure of hydrogen corresponds to the full coverage of the surface atoms. The sharp decrease of the reaction rate (apparently it is very sensitive for the quantity of the remaining substrate) is in agreement with previous suggestions according to which hydrogenolysis involves multiply dehydrogenated surface species [18, 19].

The "apparent" poisoning of the reaction rate at high hydrogen to butane ratios can be explained by assuming competition between hydrogen and *n*-butane for the adsorption sites. The competition results in a lower probability of hydrocarbon finding an unoccupied Ni site.

The quantity of the chemisorbed substrate measured under conditions of "normal" hydrogenolysis is small. The measured 5 – 15 μg weight loss recorded after turning off the hydrocarbon stream probably corresponds to the weight of the surface complex being responsible for hydrogenolysis, since the rate of hydrogenation of the remaining part is not commensurable with the rate of the hydrogenolysis. It can be stated for this reason, that the surface coverage for hydrocarbon is low, consequently the reaction proceeds only on a small fraction of the surface. This observation may underline the importance of sites having low co-ordination [19] (*e.g.* edges or B_5 sites [20]) in promoting hydrogenolysis.

To sum up, the chemisorption measurements reveal above 88 °C different chemisorption forms, although they are not sharply separable from each other. This may be the consequence of the extensive dissociation of C–H bonds that may explain almost simultaneous formation of dissociative chemisorbed butane, its fragments and of slowly reactive carbon deposits. It can be noted that this phenomenon is in agreement with kinetic measurements, since on Ni black deuterium exchange, hydrogenolysis and poisoning are unseparable from each other [21].

REFERENCES

[1] ANDERSON, J. R., MACDONALD, R. J., SHIMOYAMA, Y.: J. Cat., **20,** 147 (1971)
[2] KIKUCHI, E., MORITA, Y.: J. Cat., **15,** 217 (1969)
[3] CARTER, J. L., CUSUMANO, J. A., SINFELT, J. H.: J. Phys. Chem., **70,** 2257 (1966)
[4] GUCZI, L., TÉTÉNYI, P.: Ann. N. Y. Acad. Sci., **213,** 173 (1973); **70,** 2257 (1966)
[5] GUCZI, L., GUDKOV, B. S., TÉTÉNYI, P.: J. Cat., **24,** 187 (1972)
[6] GUCZI, L., SÁRKÁNY, A., TÉTÉNYI, P.: Proc. 5th Congr. Catalysis, Vol. 2., p. 1122
[7] SÁRKÁNY, A., GUCZI, L., TÉTÉNYI, P.: Acta Chim. (Budapest) **84,** 245 (1975)
[8] TÉTÉNYI, P., BABERNICS, L., GUCZI, L., SCHACHTER, K.: Acta Chim. Acad. Sci. Hung., **40,** 387 (1964)
[9] MCCLELLUN, A. L., HARNSBERGER, H. F.: J. Coll. Int. Sci., **23,** 577 (1967)
[10] BABERNICS, L., GUCZI, L., SÁRKÁNY, A., TÉTÉNYI, P.: Proc. 6th Congr. Catalysis, A36
[11] LOBO, L. S., TRIMM, D. L., FIGUEIREDO, J. L.: Proc. 5th Congr. Catalysis, Vol. 2., p. 1125
[12] NISHIYAMA, Y., TAMAI, Y.: Carbon, **14,** 13 (1976)
[13] NISHIYAMA, Y., TAMAI, Y.: J. Cat., **45,** 1 (1976)
[14] FIGUEIREDO, J. L., TRIMM, D. L.: J. Cat., **40,** 154 (1975)
[15] WENTRCEK, P. R., WOOD, B. J., WISE, H.: J. Cat., **43,** 363 (1976)
[16] BREISACHER, P., MARX, P. C.: J. Amer. Chem. Soc., **85,** 3518 (1963)
[17] GUCZI, L., SÁRKÁNY, A., TÉTÉNYI, P.: Comm. Dept. Chem. Bulgarian Acad. Sci., **6,** 349 (1973)
[18] KEMBALL, C.: Proc. 4th Congr. Catalysis (Hung. Acad. Sci. Budapest, 1971) Vol. 1., p. 424
[19] BOND, G. C.: Proc. Symp. Mechanismus of Hydrocarbon Reactions (Hung. Acad. Sci. 1975) p. 49
[20] VAN HARDEVELD, R., HARTOG, F.: Surface Sci., **15,** 189 (1969)
[21] GUCZI, L., SÁRKÁNY, A., TÉTÉNYI, P.: J. C. S. Faraday Trans., I. **70,** 1971 (1974)

Antal SÁRKÁNY
Pál TÉTÉNYI
H-1525 Budapest.

Acta Chimica Academiae Scientiarum Hungaricae, Tomus 97 (1), pp. 69–75 (1978)

CLEAVAGE OF THE HETEROCYCLIC RING OF ISOFLAVONOIDS BY NUCLEOPHILIC REAGENTS, V

REACTION OF ISOFLAVONE WITH HYDROXYLAMINE AND ITS RING TRANSFORMATION INTO 4-HYDROXY-3-PHENYLCOUMARIN

V. Szabó, J. Borda and L. Losonczi

(Institute of Applied Chemistry, Kossuth Lajos University, Debrecen)

Received November 4, 1976

Isoflavone reacts with hydroxylamine between pH 4 and 11, at a rate increasing with the pH, to yield 4-phenyl-5-(2'-hydroxyphenyl)-isoxazole (**1**). It follows from the structure of the product that the nucleophilic reagent attacks on the C-2 atom and cleavage of the γ-pyrone ring of isoflavone occurs. Under such conditions, isoflavone does not show the usual carbonyl reaction with hydroxylamine.

Compound **I** is very stable in acid media, however, cleavage of the isoxazole ring takes place in strongly alkaline solutions to give 2-(2'-hydroxybenzoyl)phenylacetic nitrile (**V**). This conversion confirms both the structure of **I** and the direction of the conversion of isoflavone.

Compound **V** is in ring–chain tautomeric equilibrium with 4-hydroxy-3-phenylcoumarin imine (**VIII**), depending on the pH. Compound **VIII** can be converted into 4-hydroxy-3-phenylcoumarin (**IX**) when refluxed in acid solution. In this way a ring transformation of chromone to 4-hydroxycoumarin has been achieved with the sequence: isoflavone → **I** → **V** → **VIII** → **IX**.

Introduction

Although the carbonyl reactions of flavones (2-phenylchromones) have been discussed in several papers [1–5], it is interesting to note that reactions of isoflavones (3-phenylchromones) with nitrogen containing nucleophilic reagents have not been treated yet.

Isoflavone has a basicity lower than that of chromone and flavone [6], while the sensitivity of its C–2 atom towards nucleophilic reagents is significant [7, 8]. Therefore, on treatment with nucleophilic reagents, isoflavone may give the usual carbonyl reactions, as well as cleavage of the γ-pyrone ring may occur with the formation of pyrazole, isoxazole, or even dioxime derivatives.

Results and discussion

Isoflavone was allowed to react with hydroxylamine under widely varied conditions, in order to determine the optimum yield and various possible directions of reactivity; however, the same main product was always obtained

up to pH 11. A compound with positive $FeCl_3$ reaction was also formed in small amounts; this was probably the dioxime, but its presence caused no difficulty in isolating the main product.

Table I shows that the yield was slightly, and the reaction time significantly, dependent on the concentrations of hydroxide ion and the nucleophilic agent in the solution. The reaction rate increases up to about pH 11; however, above this value the reaction is not unambiguous owing to the sensitivity of the reaction product to alkali, as well as because of the degradation of the γ-pyrone ring of isoflavone [7, 8]. A compound producing a deep violet reaction with $FeCl_3$ (not identical with the compound supposed to be the dioxime) and 2-hydroxydeoxybenzoin oxime were formed.

A multicomponent reaction product was obtained with hydroxylamine hydrochloride in hot pyridine, and similarly, with hydroxylamine base in absolute ethanol.

The main product in the above reactions was a white crystalline compound containing one nitrogen atom and one hydroxyl group which could be acetylated. The ferric chloride reaction was negative.

In view of the reactivity of the isoflavone molecule on the carbonyl group and the possibility of attack on the C–2 atom under conditions leading to an isoxazole, the formation of three compounds with different structures can be assumed, depending on whether the nucleophilic attack occurs on the C–2 or C–4 atom.

Table I

Reaction of isoflavone with hydroxylamine under various conditions

Solvent	pH	Temp., °C	Reaction time, hrs	Yield, %	M. p., °C
1. EtOH : H_2O = 80 : 20	~1*	80	~24	0	–
2. EtOH : H_2O = 80 : 20	6.0	80	7.0	75	161–164
3. EtOH : H_2O = 80 : 20	7.0	80	2.5	90	161–164
4. EtOH : H_2O = 80 : 20	8.0	80	1.5	93	161–164
5. Dioxan : H_2O = 60 : 40	9.3	30	~20	85	161–164
6. Dioxan : H_2O = 60 : 40	10.8	30	1.5	85	161–164
7. EtOH : H_2O = 90 : 10	~11	20	6.0	92	161–164
8. Absolute EtOH	–	20	~24	90	155–160**
9. Absolute EtOH	–	20	~12	60	159–161**
10. Pyridine	–	115	1.5	80	150–160**

Reagent: NH_2–OH·HCl (3 moles excess) + 2–4: acetate–alkali; 5–6: phosphate–acetate buffers; 8: NaOEt titrated to the equivalence point, 9: the same, with NaOEt excess; 2–7: raw product chromatographically pure.

* Acid catalysis (HCl); ** three-component raw product

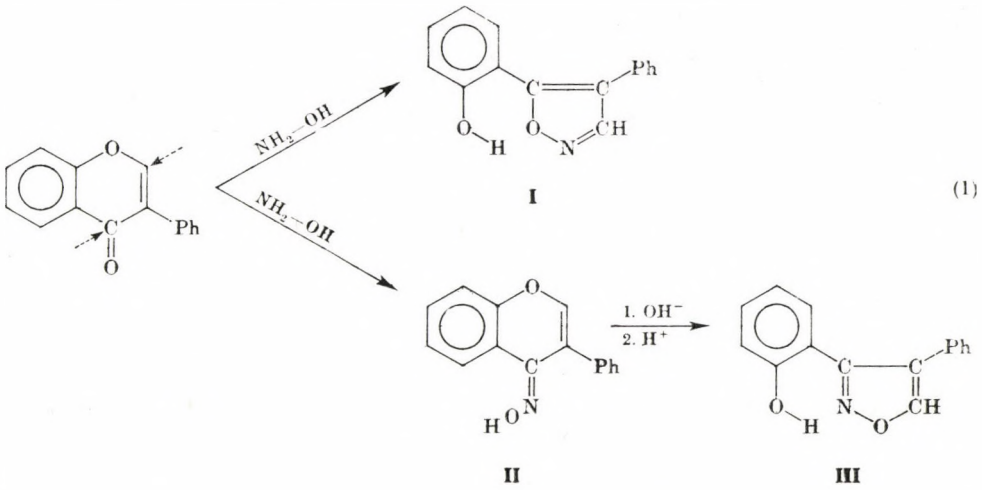

(1)

Since spectroscopic methods did not provide unambiguous evidence for compounds **I**, **II** or **III**, hydrolysis of the product with aqueous acid or alkali was attempted.

The compound obtained in the above reaction suffers no change even when treated with $5M$ hydrochloric acid in aqueous ethanol. This high stability makes structure **II** improbable, since isoflavone oxime (**II**) would undergo hydrolysis to isoflavone under such conditions.

In alkaline medium the compound suffers a change, as shown by the spectra in Fig. 1.

This conversion is reversible up to a certain pH, however, it becomes irreversible in strongly alkaline solution (about $1.25M$ aqueous alcoholic

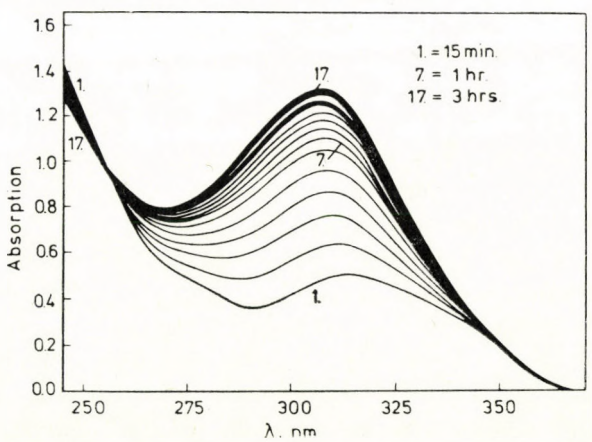

Fig. 1. Changes in the spectrum of 4-phenyl-5-(2'-hydroxyphenyl)isoxazole in $1M$ sodium hydroxide solution

alkali), and after acidifying the alkaline solution, the white crystalline compound (m.p. 98–100 °C) giving the dark violet $FeCl_3$ reaction mentioned above is obtained. The reaction is fast (30 min) and unambiguous; the yield is nearly 100 %. The compound is soluble in alkaline solutions and, according to elemental analysis, it contains one nitrogen atom. The NMR spectrum of the product, kept in darkness at 0 °C, shows a signal at 11.75 ppm which disappears on the effect of D_2O and can be assigned to the proton of a phenolic hydroxyl group in chelate bond. In the IR spectrum an intense nitrile band is found at 2270 cm^{-1}, and the band at 1640 cm^{-1} indicates the presence of a ketonic carbonyl.

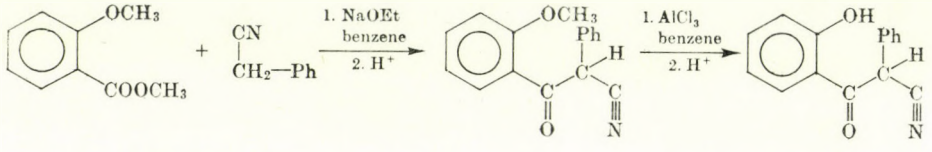

IV **V**

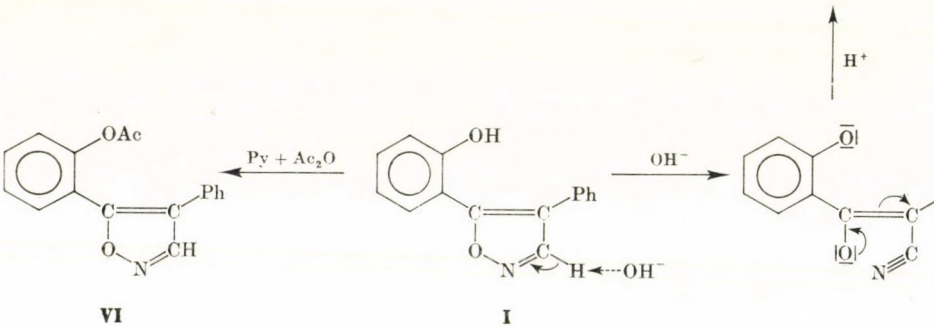

VI **I**

On the basis of the above analytical data it was supposed that this product of the alkaline conversion was 2-(2'-hydroxybenzoyl)phenylacetic nitrile (**V**). The synthesis of **V** was effected in order to confirm this assumption.

The procedure suggested by KAWASE [9] was modified to prepare 2 (2'-methoxybenzoyl)phenylacetic nitrile (**IV**), and this was demethylated to **V** with an excess of $AlCl_3$ in hot absolute benzene.

The formation of 3-phenyl-4-hydroxycoumarin imine (**VIII**) [10] was not observed during demethylation, probably owing to the relatively low temperature used and the higher stability of the $AlCl_3$ complex of the nitrile under such conditions. Compound **V** was obtained from **IV** in almost 100 % yield. The properties of the synthetic compound **V** were identical in all respects with those of the product prepared by the alkaline conversion. However, under such conditions it is only **I**, *i.e.* 4-phenyl-5-(2'-hydroxyphenyl)isoxazole, which can yield **V**.

The reaction of hydroxylamine and isoflavone starts with the nucleophilic attack on C–2 under the given reaction conditions, and the aldoxime **VII** is formed, which yields the isoxazole **I** in a rapid cyclization step. On the basis of the results given in Table I, the probability of an attack on C–4 and thus the formation of the normal oxime (**II**) or the isoxazole **III** is very small in the case of isoflavone, in contrast with the experiences with flavone [11].

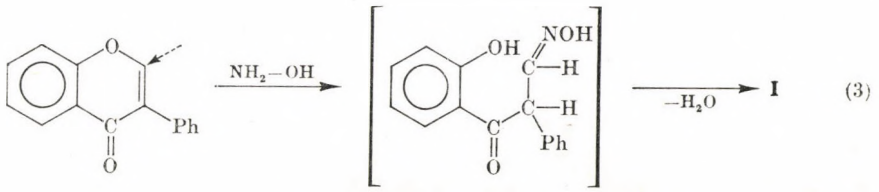

VII

Compound **V** is unstable and is converted **VIII** by treatment with acids or dilute bases. **VIII** and **V** are in the relationship of ring–chain tautomerism since **VIII** can be converted to **V** in rather concentrated (about 2.5*M*) alkali solutions.

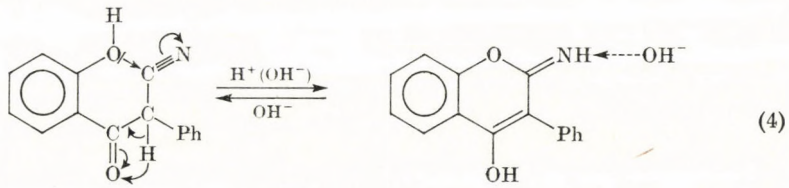

V **VIII**

Since **VIII** yields 4-hydroxy-3-phenylcoumarin (**IX**) when refluxed in acid aqueous solution [10], the present work has achieved the transformation of the chromone ring into the 4-hydroxycoumarin ring, according to the following reaction series:

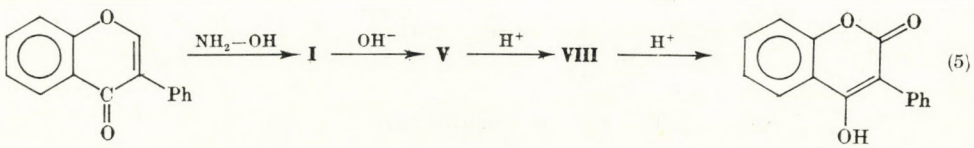

IX

*

The authors' thanks are due to Miss E. THEISZ for her valuable help in the experimental work.

Experimental

The UV spectra were recorded with a Unicam SP 800 instrument in ethanol; IR spectra were obtained with a Unicam SP-200G instrument in KBr pellets; the NMR spectra were determined with a JEOL instrument.

The reactions were monitored by the TLC technique on DC-Alurolle Silicagel 254 (Merck) layers. The developing mixture was benzene–ethanol (95 : 5). M. p.'s are uncorrected.

4-Phenyl-5-(2'-hydroxyphenyl)isoxazole (I)

Hydroxylamine hydrochloride (2.0 g; 30.0 mmoles) was dissolved in 2.5*M* sodium hydroxide (5 cm^3), and the pH of the solution was adjusted to 11. Isoflavone (2.22 g; 10.0 mmoles) was suspended in ethanol (50 cm^3) and added to the above aqueous solution of hydroxylamine. The yellow reaction mixture, in which isoflavone slowly dissolved, was allowed to stand at room temperature for 6 hrs. The solution was then acidified with hydrochloric acid (pH $\sim$ 5) and evaporated to dryness. The product was crystallized from aqueous ethanol to obtain 2.19 g (91.9 %) of **I**, m. p. 163 – 166 °C.

$C_{15}H_{11}NO_2$. Calcd. C 75.9; H 4.63; N 5.90. Found C 75.1; H 4.80; N 5.84 %.

UV: λ_{max} (log ε) 228 (4.28), 263 nm (4.03).

IR (KBr): 970 (N – O), 1620 (C = N), 3420 cm^{-1} (OH).

NMR (DMSO-d_6): 9.0 (s, 1H, C_3 – H), 10.1 ppm (s, 1H, OH; exchangeable with D_2O).

Acetate of I (VI)

Compound **I** (0.6 g; 2.5 mmoles) was allowed to stand in a mixture of acetic anhydride (1.17 cm^3; 12.5 mmoles) and absolute pyridine (0.60 cm^3; 7.5 mmoles) at room temperature for 1 day. The reaction mixture was then poured into ice-water, and the product which separated was crystallized from ethanol (0.60 g; 85.7 %), m. p. 104 – 106 °C.

$C_{17}H_{13}NO_3$. Calcd. N 5.00. Found N 4.97 %.

UV: λ_{max} (log ε) 270 nm (4.03).

IR: 1190, 1370 (C – CH_3), 1630 (C = N), 1765 cm^{-1} (C = O).

NMR ($CDCl_3$): 1.98 (s, 3H, CH_3), 8.48 ppm (s, 1H, C_3 – H).

2-(2'-Methoxybenzoyl)phenylacetic nitrile (IV)

Sodium metal (2.3 g) was dissolved in a mixture of anhydrous benzene (20 cm^3) and anhydrous ethanol (20 cm^3). Ethanol was removed from the sodium ethoxide suspension by means of distillation (the volume was kept meanwhile about constant by the addition of anhydrous benzene). Phenylacetic nitrile (5.8 g; 50.0 mmoles) and 2-methoxybenzoic acid methyl ester (8.0 g; 50.0 mmoles) were added and the solution was maintained at 90 – 95 °C while the alcohol formed evaporated from the reaction mixture. After treatment for 4 hrs, the mixture was poured into water (200 cm^3). The organic phase was extracted with water, the aqueous phase was re-extracted with ether, and the combined aqueous phases were acidified with sulfuric acid (pH = 2 – 3). The milky emulsion was cooled, whereupon a white crystalline substance separated, which was recrystallized from ethanol (10.5 g; 87.5 %), m. p. 109 – 110 °C (lit [9],. m. p. 108 – 109 °C).

IR: 1680 (C = O), 2270 (C≡N), 3050 cm^{-1} (CH).

NMR ($CDCl_3$): 3.86 (s, 3H, OCH_3), 5.82 ppm (s, 1H, C_2 – H).

2-(2'-Hydroxybenzoyl)phenylacetic nitrile (V)

(a) Compound **I** (0.60 g; 2.53 mmoles) was dissolved in a mixture of ethanol (10 cm^3) and 2.5*M* sodium hydroxide (10 cm^3). The homogeneous yellow solution was allowed to stand at room temperature for 1hr, acidified with hydrochlorid acid, and the alcohol was removed. The substance which separated was filtered off, washed until free from acid and crystallized from 80 % aqueous ethanol (0.53 g; 88.3 %); m. p. 98 – 100 °C.

$C_{15}H_{11}NO_2$. Calcd. N 5.90. Found N 5.84 %.

UV: λ_{max} (log ε) 262 nm (4.00).

IR: 1640 (C=O), 2270 (C≡N), 3050 (CH), 3250 cm^{-1} (OH).
NMR ($CDCl_3$): 5.05 (s, 1H, C_2-H), 11.75 ppm (s, 1H, OH).

(b) Compound **IV** (1.0 g; 4.0 mmoles) was dissolved in anhydrous benzene (5 cm^3) and anhydrous $AlCl_3$ (2.0 g; 15.0 mmoles) was added to the solution. The mixture was refluxed for 30 – 40 min, with vigorous stirring. The complex which separated was decomposed with 0.1*M* hydrochloric acid under cooling in ice-water ($t < 5$ °C, pH = 2 – 3). After the separation of the phases, the aqueous phase was extracted with benzene. The combined benzene solutions were dried, clarified and evaporated to dryness in vacuum. The remaining oil was shaken with petroleum ether and aceply cooled. The product separated in the form of white crystals (0.80 g; 84.0 %), m. p. 98 – 99 °C.

(c) Compound **VIII** (0.237 g; 1.0 mmole) was dissolved in ethanol (3 cm^3) and 5*M* sodium hydroxide (3 cm^3) was added to it. The yellow solution was allowed to stand at room temperature for 15 min, then acidified with hydrochloric acid, with cooling. The semi-solid substance which separated was rubbed with water and crystallized from 80 % aqueous ethanol (0.185 g; 78.0 %); m. p. 97 – 99 °C.

No m. p. depression was observed in admixtures of the compounds prepared according to *(a)*, *(b)* and *(c)*. The mixed m. p.'s were between 97 and 99 °C.

The elemental analyses of the compounds synthesized according to *(b)* and *(c)* were identical with those of the product described under *(a)*.

4-Hydroxy-3-phenylcoumarin imine (VIII)

Compound **V** (0.237 g; 1.0 mmole) was refluxed in a mixture of ethanol (3 cm^3) and conc. hydrochloric acid (2 drops) for 15 min. Some of the ethanol was evaporated, the white product was washed with water until free from acid, and crystallized from ethanol to obtain 0.21 g (88.6 %) of **VIII**, m. p. 224 – 226 °C (lit. [10] m. p. 219 – 220 °C).

IR: 1610 (C=C), 1645 (C=N), 3240 (NH), 3380 cm^{-1} (OH).

REFERENCES

[1] Mozingo, R., Adkins, H.: J. Am. Chem. Soc., **60,** 675 (1938)
[2] Baker, W., Harborne, J. B., Ollis, W. D.: J. Chem. Soc., **1952,** 1303
[3] Rákosi, M., Tőkés, A., Bognár, R.: Acta Univ. Debr., **8,** 33 (1962)
[4] Farkas, I., Costisella, B., Rákosi, M., Gross, H., Bognár, R.: Chem. Ber., **102,** 1333 (1969)
[5] Kállay, F.: Kémiai Közl., **42,** 213 (1973)
[6] Tolmacsev, A. I., Sulesko, L. M., Kiszilenko, A. A.: Zhurn. Obsch. Him., **35,** 1707 (1965)
[7] Szabó, V., Zsuga, M.: Acta Chim. (Budapest) **85,** 179 (1975)
[8] Szabó, V., Zsuga, M.: Acta Chim. (Budapest) **88,** 27 (1976)
[9] Kawase, Y.: Bull. Chem. Soc. Japan **31,** 390 (1958)
[10] Kawase, Y.: Bull. Chem. Soc. Japan **31,** 440 (1958)
[11] Basinski, W., Jerzmanowska, Z.: Roczn. Chem. **50,** 1067 (1976)

Vince Szabó
Jenő Borda
Lajos Losonczi
H-4010 Debrecen 10.

Acta Chimica Academiae Scientiarum Hungaricae, Tomus 97 (1), pp. 77–83 (1978)

OXAZEPINES AND THIAZEPINES, IV*

SYNTHESIS OF 2,3-DIHYDRO-2-PNEHYL-1,4-BENZOXAZEPINE DERIVATIVES

A. LÉVAI and R. BOGNÁR

(Institute of Organic Chemistry, Kossuth L. University, Debrecen)

Received February 9, 1977

The Schmidt reaction of flavanones gave 2,3-dihydro-2-phenyl-1,4-benzoxazepin-5(4H)-ones (**V–VIII**) which afforded the corresponding thiones (**IX–XII**) on treatment with P_2S_5. From compound **V**, N-acyl and N-alkyl derivatives (**XIII–XIX**) were also prepared.

According to KRAPCHO and TURK [2] the Schmidt reaction of flavanone (**I**) gives 2,3-dihydro-2-phenyl-1,5-benzoxazepin-4(5H)-one. Later the reaction was reinvestigated by LOCKHART, and MISITI and RIMATORI [3,4] who, on the basis of chemical degradation and spectroscopic evidences, found that the compound described by KRAPCHO and TURK [2] was in fact 2,3-dihydro-2-phenyl-1,4-benzoxazepin-5(4H)-one (**V**). 2,3-Dihydro-2-phenyl-1,4-benzoxazepin-5(4H)-one was also prepared by MISITI *et al.* [5] *via* the Schmidt reaction of 2'-hydroxychalcone. MISITI and RIMATORI [6] prepared 2,3-dihydro-2-phenyl-1,4-benzoxazepin-5(4H)-ones as major products from 6-methyl-, 6-nitro- and 8-nitroflavanone as well. Thus, the reaction took place mainly with alkyl migration. In the course of our work on the synthesis of oxazepines, the Schmidt reaction of some substituted flavanones (**II–IV**) has also been investigated.

From compounds **II**, **III** and **IV** the corresponding 2,3-dihydro-2-phenyl-1,4-benzoxazepin-5(4H)-ones (**VI–VIII**) were obtained. Their structure was unequivocally proved by comparison of their IR and ^{1}H-NMR spectra with those of authentic 2,3-dihydro-2-phenyl-1,4-benzoxazepin-5(4H)-one (**V**) [3, 4].

Thus in the Schmidt reaction of flavanones, alkyl migration leads to the formation of 2,3-dihydro-2-phenyl-1,4-benzoxazepin-5(4H)-ones. The assumed mechanism of the reaction can be illustrated as follows (Scheme I):

The conjugate acid of the ketone produces a protonated azidohydrin with hydrazoic acid, which loses water to form an iminodiazonium ion. Theoretically the iminodiazonium ion can exist in *syn* (*Z*) or *anti* (*E*) form. Concerning the Schmidt reaction of ketones it was found by SMITH and ANTONIADES [7]

* For Part III, see Ref. [1].

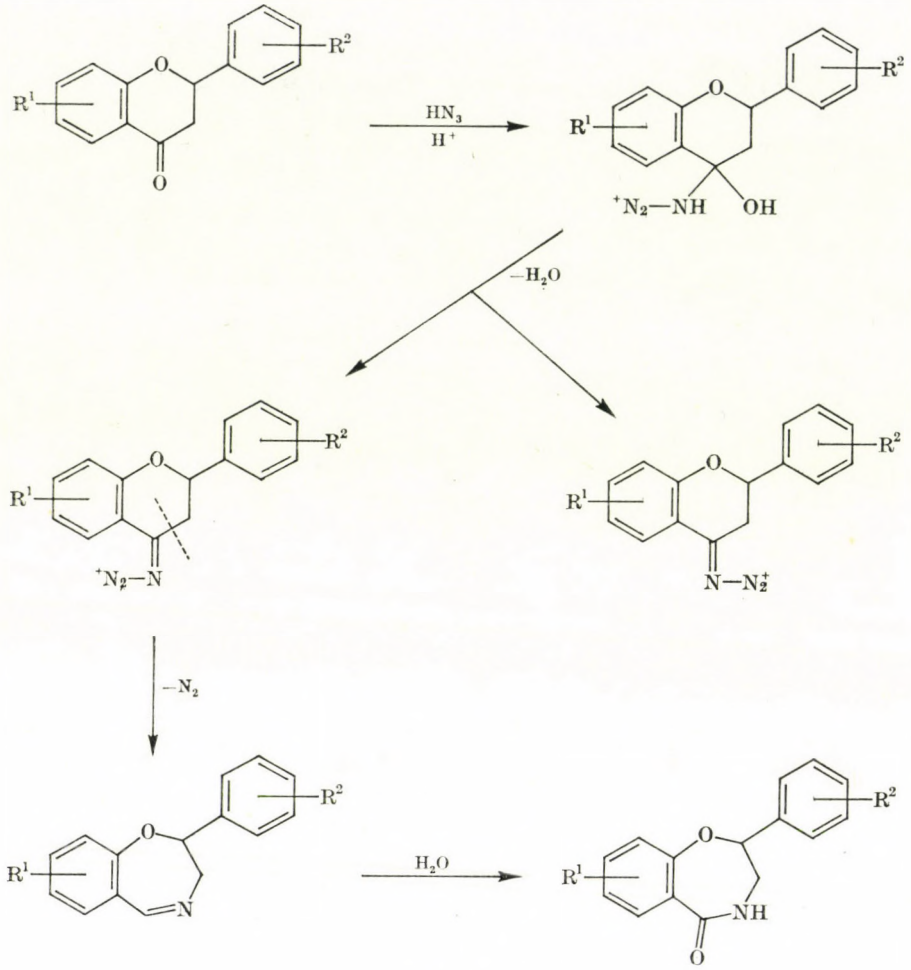

Scheme I

that rearranement occurs at this stage by migration of the group *anti* to the diazonium nitrogens. In the case of flavanones this is the CH_2 group if the iminodiazonium ion has the *anti* configuration with $-N_2^+$ directed away from the C−2 atom. Since alkyl migration was observed for all the flavanones investigated so far, it is a reasonable assumption that the iminodiazonium ion obtained from them exists in the *anti* form, which in turn leads to alkyl migration. Alkyl migration followed by nitrogen elimination gives a carbonium ion, which produces the corresponding 2,3-dihydro-2-phenyl-1,4-benzoxazepin-5(4H)-one on hydration.

The structure of the iminodiazonium ion is quite similar to that of flavanone hydrazone, the stable isomer of which was found *anti* by KÁLLAY

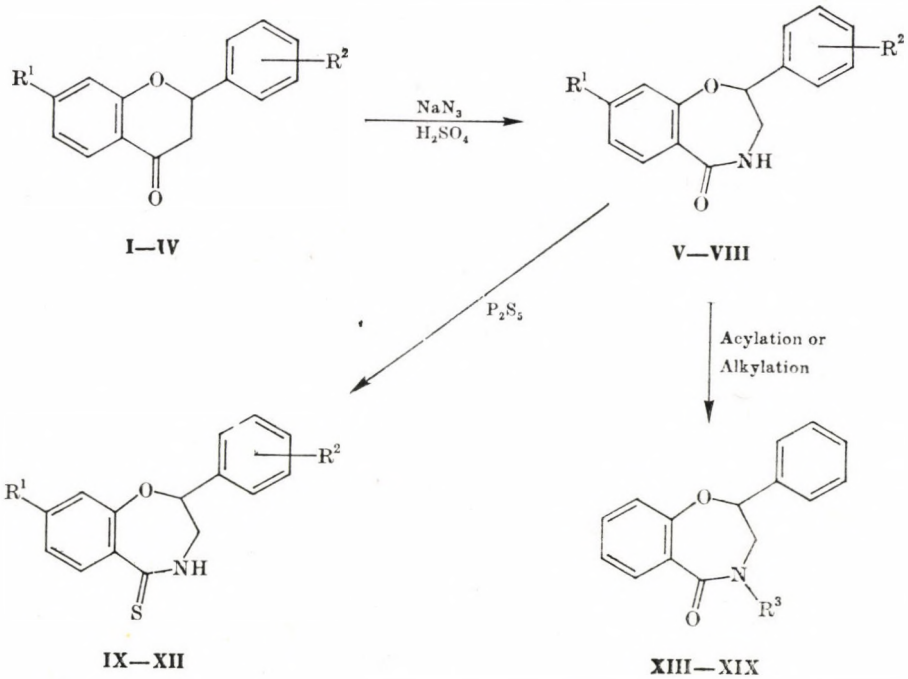

I, V, IX: $R^1 = R^2 = H$
II, VI, X: $R^1 = H$, $R^2 = 3\text{-}OCH_3$
III, VII, XI: $R^1 = OCH_3$, $R^2 = H$
IV, VIII, XII: $R^1 = OCH_3$, $R^2 = Cl$
XIII: $R^3 = CO_2CH_3$ **XVII:** $R^3 = CH_2CO_2H$
XIV: $R^3 = CO_2C_2H_5$ **XVIII:** $R^3 = (CH_2)_2CO_2H$
XV: $R^3 = COCH_2Cl$ **XIX:** $R^3 = CH_2CO_2C_2H_5$
XVI: $R^3 = COC_6H_5$

Scheme II

Table I

Spectral data

IR		^{1}H– NMR (δppm)			
ν_{CO} [cm^{-1}]		NH*	Aromatic	–CH–Ar	$-CH_2-$
V	1600	8.64	7.38 – 8.30m	5.73q	3.76m
VI	1660	7.88	6.58 – 7.60m	5.22q	3.44m
VII	1650	8.52	6.85 – 8.24m	5.68q	3.75m
VIII	1660	8.48	6.88 – 8.24m	5.66q	3.76m

* The NH signal is extinguished by D_2O

et al. [8]. This comparison might be an indirect proof of the *anti* configuration of the iminodiazonium ion.

For the preparation of 2,3-dihydro-2-phenyl-1,4-benzoxazepin-5(4H)-thiones (**IX – XII**), 2,3-dihydro-2-phenyl-1,4-benzoxazepin-5(4H)-ones, (**V – VIII**) were allowed to react with P_2S_5 under the reaction conditions described in the literature [9, 10].

Among the benzoxazepine there are compounds having various pharmacological, *i.e.* analgetic, antiphlogistic, spasmolytic, antihistaminic, cataleptic, sedative, anticonvulsive, antinarcosis, etc., activities [11 – 16]. One of the aims of the present study was the synthesis of novel, biologically active benzoxazepines, which we intended to accomplish by the preparation of some N-substituted derivatives. To obtain N-acylated derivatives **XIII – XVI** we acylated 2,3-dihydro-2-phenyl-1,4-benzoxazepin-5(4H)-one (**V**) with methyl or ethyl chloroformate and chloroacetyl or benzoyl chloride. Compound **V** was also allowed to react with iodoacetic acid or β-propiolactone to yield N-acetic acid (**XVII**) or N-propionic acid (**XVIII**) derivatives. Substance **XVII** gave an ethyl ester (**XIX**) on esterification with ethanol.

Experimental

M. p.'s are uncorrected.

The IR spectra were taken in KBr pellets on an UNICAM SP 200 G instrument. The ^{1}H-NMR spectra were recorded with a JEOL MH 100 instrument in deuterochloroform (internal standard TMS, $\delta = 0$ ppm), at room temperature.

The flavanones used as starting materials were prepared by known procedures [17 – 19].

2,3-Dihydro-2-phenyl-1,4-benzoxazepin-5(4H)-ones (V—VIII)

Concentrated sulfuric acid (2 ml) was added portionwise to the stirred and cooled mixture of flavanone (**I – IV**) (2 g), sodium azide (1.0 g) and glacial acetic acid (8 ml). The mixture was stirred for further 2 hrs at 45 – 50 °C and then poured into water. The precipitated material was filtered off, washed free of acid, and crystallized from methanol to yield compounds **V – VIII** (Tables I and II).

2,3-Dihydro-2-phenyl-1,4-benzoxazepin-5(4H)-thiones (IX— XII)

2,3-Dihydro-2-phenyl-1,4-benzoxazepin-5(4H)-one (**V – VIII**) (2 mmoles) and P_2S_5 (3 mmoles) were refluxed for 1.5 hr in dry pyridine (10 ml). The mixture was poured into water and acidified with dilute hydrochloric acid. The residue was filtered off, washed free of acid, and crystallized from methanol to afford a yellow crystalline substance (**IX – XII**) (Table II).

2,3-Dihydro-2-phenyl-4-methoxycarbonyl-1,4-benzoxazepin-5(4H)-one (XIII)

(a) 2,3-Dihydro-2-phenyl-1,4-benzoxazepin-5(4H)-one (**V**) (2.4 g) and methyl chloroformate (5 ml) were dissolved in dry acetone (100 ml), and refluxed for 5 hrs in the presence of K_2CO_3 (10 g). The inorganic salt was filtered off, the solvent evaporated in vacuum, and the residue crystallized from methanol to yield a white crystalline material (1.7 g; 56.6 %), m. p. 113 – 114 °C.

(b) Methyl chloroformate (5 ml) was added portionwise to the stirred and cooled suspension of compound **V** (2.4 g) and sodamide (2 g) in anhydrous toluene (100 ml). The mixture

Table II

Analytical and physical data of the compounds prepared

	M. p. (°C)	Yield (%)	Overall formula	Molecular weight	Analysis (%)							
					Calculated				Found			
					C	H	N	S	C	H	N	S
VI	119 – 120	33.3	$C_{16}H_{15}O_3N$	269.28	71.35	5.61	5.20	–	71.59	5.58	5.26	–
VII	131 – 132	42.8	$C_{16}H_{15}O_3N$	269.28	71.35	5.61	5.20	–	71.31	5.56	5.31	–
VIII	154 – 155	38.0	$C_{16}H_{14}O_3NCl$	303.72	63.36	4.62	4.62	–	63.64	4.72	4.66	–
IX	174 – 175	62.0	$C_{15}H_{13}ONS$	255.25	70.56	5.09	–	12.54	70.38	5.08	–	12.50
X	134 – 135	71.4	$C_{16}H_{15}O_2NS$	285.34	67.34	5.29	–	11.23	67.54	5.37	–	11.15
XI	158 – 159	49.5	$C_{16}H_{15}O_2NS$	285.34	67.34	5.29	–	11.23	67.47	5.27	–	11.10
XII	135 – 136	48.3	$C_{16}H_{14}O_2NSCl$	319.72	60.08	4.37	–	10.03	60.01	4.48	–	9.97
XIII	113 – 114	*	$C_{17}H_{15}O_4N$	297.29	68.68	5.05	4.71	–	68.83	5.10	4.82	–
XIV	97 – 98	*	$C_{18}H_{17}O_4N$	311.32	69.45	5.46	4.50	–	69.24	5.36	4.42	–
XV	108 – 109	32.2	$C_{17}H_{14}O_3NCl$	315.73	64.76	4.44	4.44	–	65.30	4.42	4.52	–
XVI	158 – 159	23.3	$C_{22}H_{17}O_3N$	343.36	76.96	4.95	4.08	–	77.01	5.04	4.12	–
XVII	172 – 173	*	$C_{17}H_{15}O_4N$	297.29	68.68	5.05	4.71	–	67.79	5.07	4.82	–
XVIII	164 – 165	32.2	$C_{18}H_{17}O_4N$	311.32	69.45	5.46	4.50	–	69.75	5.59	4.39	–
XIX	111 – 112	73.4	$C_{19}H_{19}O_4N$	325.34	70.15	5.84	4.30	–	69.92	5.81	4.40	–

* Yield is given in the experimental section

was stirred for further 8 hrs at room temperature, the precipitated inorganic salt filtered off, the solvent evaporated in vacuum and the residue crystallized from methanol to afford compound **XIII** (1.8 g; 60.0 %), m. p. 113 – 114 °C.

2,3-Dihydro-2-phenyl-4-ethoxycarbonyl-1,4-benzoxazepin-5(4H)-one (XIV)

Under the conditions applied in the preparation of **XIII**, the treatment of **V** (1.0 g) with ethyl chloroformate (2 ml) yielded compound **XIV** *(a)* (0.9 g; 69.2 %) *(b)* (0.8 g; 61.5 %), m. p. 97 – 98 °C.

Compounds **XV** and **XVI** were prepared according to method *(a)*, using chloroacetyl chloride and benzoyl chloride as acylating agents.

2,3-Dihydro-2-phenyl-4-carboxymethyl-1,4-benzoxazepin-5(4H)-one (XVII)

(a) Iodoacetic acid (1.0 g) in anhydrous toluene (30 ml) was added dropwise to the stirred and cooled suspension of compound **V** (1.0 g) and sodamide (1.0 g) in anhydrous toluene (20 ml). The mixture was stirred for 20 hrs then poured into water. The two phases were separated, the aqueous solution acidified with dilute hydrochloric acid, the precipitated material filtered off, washed free of acid, and crystallized from methanol to yield a white crystalline product (1.0 g; 83.0 %), m. p. 172 – 173 °C.

(b) Compound **V** (2.4 g) and sodium hydride (1.0 g) were dissolved in dry dimethyl formamide (70 ml). Iodoacetic acid (3.0 g) in dry dimethyl formamide (30 ml) was added dropwise to the stirred and cooled solution. The mixture was stirred for 14 hrs, poured onto crushed ice, then worked up as described for the aqueous solution under *(a)* to yield compound **XVII** (1.8 g; 60.0 %), m. p. 172 – 173 °C.

2,3-Dihydro-2-phenyl-4-(2-carboxyethyl)-1,4-benzoxazepin-5(4H)-one (XVIII)

Under the conditions (method *b*) applied in the preparation of **XVII**, the treatment of **V** (2.4 g) with β-propiolactone (2.0 ml) gave a white crystalline product (Table II).

2,3-Dihydro-2-phenyl-4-(carbethoxy methyl)-1,4-benzoxazepin-5(4H)-one (XIX)

Compound **XVII** (1.0 g) was refluxed for 7 hrs in a mixture of anhydrous ethanol (50 ml) and concentrated sulfuric acid (1 ml). The solution was poured onto crushed ice, the residue filtered off, washed free of acid and crystallized from ethanol to afford a white crystalline product (Table II).

The products prepared in different ways (*a* and *b*) gave no m. p. depression in admixture.

*

Thanks are due to Drs S. Szabó and L. Szilágyi for recording the spectra and help in the interpretation; to Mrs E. Hajnal for her technical assistance and to the staff of the Analytical Laboratory for the microanalyses. The present study was sponsored by the Hungarian Academy of Sciences, which is gratefully acknowledged.

REFERENCES

[1] Lévai, A., Bognár, R.: Acta Chim. (Budapest) **92,** 415 (1977)
[2] Krapcho, J., Turk, Ch. F.: J. Med. Chem., **9,** 191 (1966)
[3] Lockhart, I. M.: Chem. Ind. (London) 1844 (1968)
[4] Misiti, D., Rimatori, V.: Tetrahedron Letters **947** (1970)
[5] Misiti, D.: Ann. Ist. Super. Sanità **9,** 174 (1973); Cacchi, S., Palmieri, G., Misiti, D.: J. C. S. Perkin I 2371 (1976)
[6] Misiti, D., Rimatori, V.: Ann. Ist. Super. Sanità **9,** 150 (1973)
[7] Smith, P. A. S., Antoniades, E. P.: Tetrahedron **9,** 210 (1960)
[8] Kállay, F., Janzsó, G., Koczor, I.: Tetrahedron **21,** 19, 3037 (1965)

[9] BHALERAO, U. T., THYAGARAJAN, G.: Indian J. Chem., **6,** 176 (1968)
[10] THYAGARAJAN, G., BHALERAO, U. T., NASEEM, S., SUBRAMANIAN, V. S.: Indian J. Chem., **6,** 625 (1968)
[11] KRAPCHO, J., TURK, CH. F.: U. S. Pat. 3 309 361 (1967); C. A. **68,** 2930 (1968)
[12] BERNSTEIN, J.: U. S. Pat. 3 341 521 (1967); C. A. **68,** 95875 (1968)
[13] SCHINDLER, W., BLATTNER, H.: Swiss Pat. 481 128 (1969); C. A. **72,** 90543 (1970)
[14] SCHENKER, K.: Swiss Pat. 505 850 (1971); C. A. **75,** 98600 (1971)
[15] WAEFELAER, A.: Ger. Offen. 2 100 654 (1971); C. A. **75,** 129856 (1971)
[16] WAEFELAER, A.: Ger. Offen. 2 116 222 (1971); C. A. **76,** 25321 (1972)
[17] LÖWENBEIN, A.: Ber. **57,** 1515 (1924)
[18] HATTORI, S.: Bull. Chem. Soc. Japan **2,** 171 (1927)
[19] PELTER, A., BRADSHAW, J., WARREN, R. F.: Phytochem. **10,** 835 (1971)

Albert LÉVAI
Rezső BOGNÁR } H-4010 Debrecen.

Acta Chimica Academiae Scientiarum Hungaricae, Tomus 97 (1), pp. 85—89 (1978)

PROBLEMS OF 2-ETHYLANTHRAQUINONE HYDROGENATION

B. Losonczi, Á. Lengyel-Mészáros, M. Novák-Kiss, J. Morgós and J. Petró

(Department of Organic Chemical Technology, Technical University, Budapest)

Received April 13, 1977

In the reduction of 2-ethylanthraquinone the reaction stops after a hydrogen consumption of 3 moles H_2 per mole of substrate. The product is 2-ethyl-5,6,7,8-tetrahydroanthrahydroquinone. The ethyl group is protruding from the plane formed by the aromatic rings, and hinders the aromatic ring carrying the alkyl group in getting sufficiently near to the surface of the catalyst to undergo hydrogenation.

Introduction

The industrial importance of manufacturing hydrogen peroxide on 2-ethylanthraquinone basis can be characterized by the sole fact that in 1974 49 % of the world production was made by this method.

The process is the following:

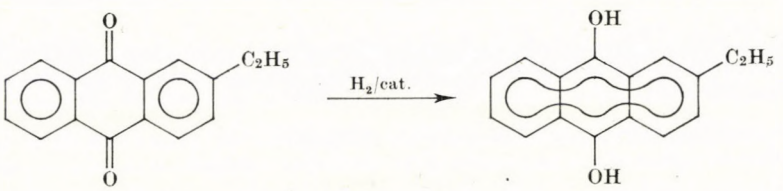

I **II**

$$\mathbf{II} \xrightarrow{O_2\ (air)} \mathbf{I} + H_2O_2.$$

The substrate is dissolved in a usually two-component solvent, in which the apolar quinone and the polar hydroquinone forms are both soluble (in about 20 % (w/w)). Hydrogenation is carried out in the presence of Raney nickel or palladium-charcoal catalyst, but it can also be effected using boride catalysts [1]. The solvents commonly used are listed in Table I (1—6). After hydrogenation the catalyst is filtered off, and the solution of **II** is oxidized by blowing air through it. Hydrogen peroxide is then extracted from the organic solution with water, and the solution of **I** is recirculated for further use.

Table I

Solvents used in the experiments

No.	Solvent	Volumetric ratio
1	Benzene–octanol	3 : 2
2	Benzene–ethanol	1 : 1
3	Dimethylformamide–octanol	5 : 1
4	Benzene–2-methylcyclohexanol	3 : 2
5	Tetraline–cyclohexanol	1 : 1
6	Dibutyl phthalate	
7	Butyl acetate	
8	Isobutyl acetate	
9	Amyl acetate	
10	Isoamyl acetate	

In the literature we can find very scanty information on the theoretical aspects of the process; however, the number of relevant patents is about 150. Most of them point out that the selectivity of the catalyst is a very important factor in the proper reduction of the aromatic ring system. At the same time, several patents mention that not only **I**, but also the eutectic mixture formed with its 5,6,7,8-tetrahydro derivative can be used.

Our investigations aimed at elucidating, as far as possible, the inconsistency of these statements.

Our experiments were carried out in the solvents listed in Table I. The experimental methods have been described in one of our earlier communications [2].

Experimental

In our first experiments the number of moles of H_2 absorbed by each mole of 2-ethylanthraquinone was investigated. The results are summarized in Table II when using $5 \cdot 10^{-3}$ mole of substrate, for the saturation of the total ring system 672.3 ml of H_2 would be required in addition to the 112.05 ml calculated for the quinone–hydroquinone conversion. However, hydrogen uptake stopped after the absorption of 320 – 345 ml. This means that besides the hydrogen needed for the quinone–hydroquinone conversion, about 2 moles of H_2 are consumed per mole of substrate. Accordingly, only one member of the ring system is saturated. Thus in the course of the reaction one of the following compounds, or their mixture, must be formed:

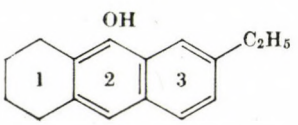

III

5,6,7,8-Tetrahydro-2-ethylanthrahydroquinone

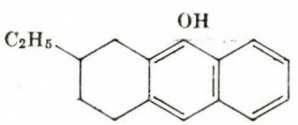

IV

1,2,3,4-Tetrahydro-2-ethylanthrahydroquinone

Table II

Total hydrogen uptake of 2-ethylanthraquinone in the hydrogenation of the aromatic ring system in different solvents

Reaction mixture: 40 ml of solvent; 1.18 g ($5 \cdot 10^{-3}$ mole) of 2-ethylanthraquinone; 1 ml of catalyst

Temperature: 25 °C

Solvent	H_2 consumption mole/mole of substrate
1	3.09
2	2.88
3	3.00
4	2.79
5	2.95
6	3.18
7	3.21
8	2.86
9	3.07
10	3.01

Table III

Oxygen uptake and H_2O_2 yield in the oxidation of 2-ethyltetrahydroanthrahydroquinone in different solvents

Solvent	O_2 consumption (mole · 10^{-3})	H_2O_2 yield (mole · 10^{-3})
1	4.85	4.93
2	5.20	5.11
3	5.01	4.95
4	4.88	4.97
5	5.15	5.15
6	5.05	5.10
7	4.97	4.95
8	4.88	4.90
9	5.23	5.20
10	5.07	5.05

On oxidizing the reaction mixtures, oxygen consumption and the yield of H_2O_2 were quantitative within the experimental errors (Table III), and better than in the case of substrate **I** [7]. However, recovery of the hydrogen peroxide was very difficult, because in the aqueous extraction of the reaction mixture an emulsion stable for 8 – 24 hours was formed.

The product of ring hydrogenation was identified. From reaction mixture in benzene-ethanol, the solvent was evaporated after oxidation and extraction. The crystals obtained were dissolved in a fivefold quantity of ethanol and precipitated from the solution with the same quantity of water. The product was isolated as yellow crystals, with a melting range of 162 – 165 °C. On the basis of data in the literature [3] and by comparison with an authentic sample

(BDH), the substance corresponds to the compound of structural formula **III**. Mixed melting points are listed in Table IV.

Table IV

Comparison of 2-ethyl-5,6,7,8-tetrahydroanthraquinone isolated from the experiments, with an authentic sample (BDH) on the basis of mixed m. p.

Own product, %	0	25	50	75	100
BDH product, %	100	75	50	25	—
M. p., °C	164 165	163 165	163 165	162 165	162 165

In hydrogenation experiments of the BDH product, H_2 uptake ceased after a consumption of 1 mole H_2 per mole of substrate. Further on, during the oxidation of this reaction mixture, in H_2O_2 production and extraction the same behaviour was observed as in the oxidation of the ring hydrogenated product formed in our experiments.

Discussion

Our investigations have shown that in the reduction of the aromatic ring system of 2-ethylanthraquinone the reaction stops after a hydrogen uptake of 3 moles per mole of substrate. The product is 2-ethyl-5,6,7,8-tetrahydroanthrahydroquinone.

The explanation of the phenomenon is, in our opinion, the following: the delocalization energy of anthracene is 5.314β; that of naphthalene is 3.683β (β has for aromatic compounds a value between -16 and -20 kcal/mole) [4, 5]. The conversion of the anthracene ring system into a ring system of naphthalenic character results in a compound of more stable structure (1.631β). The aromatic character of the latter is now so strong that it cannot be hydrogenated under the given conditions. Naturally, this would not yet exclude the possibility of the formation of compound **IV**.

If we construct the correctly proportionated molecular model, (made by the Research Institute for Organic Chemical Industry, Budapest) of the 2-ethylanthraquinone and the corresponding hydroquinone molecules, it can be seen (Figs 1 – 6) that the ethyl group is protruding from the plane of the aromatic rings and its rotation is partly hindered. Presumably, this hinders the ring carrying the alkyl group in getting sufficiently near to the catalyst surface to undergo hydrogenation. We suggest that this is the reason why the ring marked with 3 in structural formula **III** remains unchanged during hydrogenation.

Since, contrary to **II**, hydrogen peroxide is practically quantitatively formed from **III**, this would be a suitable substrate for the method. Its use is, however, prevented by its emulgating effect observed during the extraction

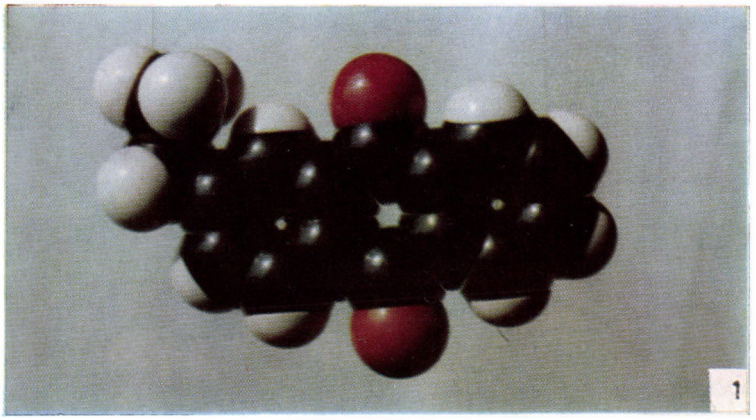

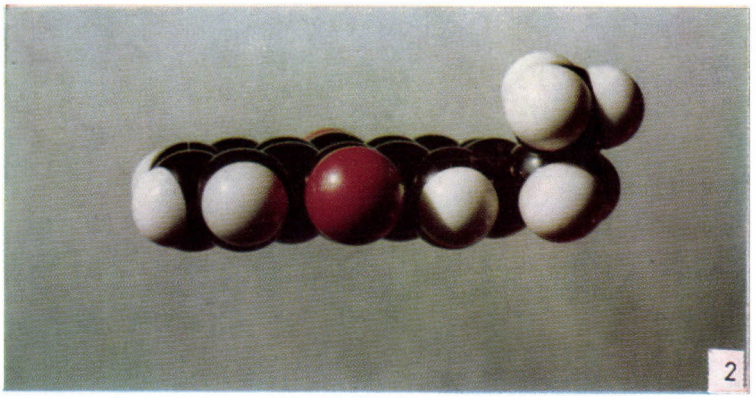

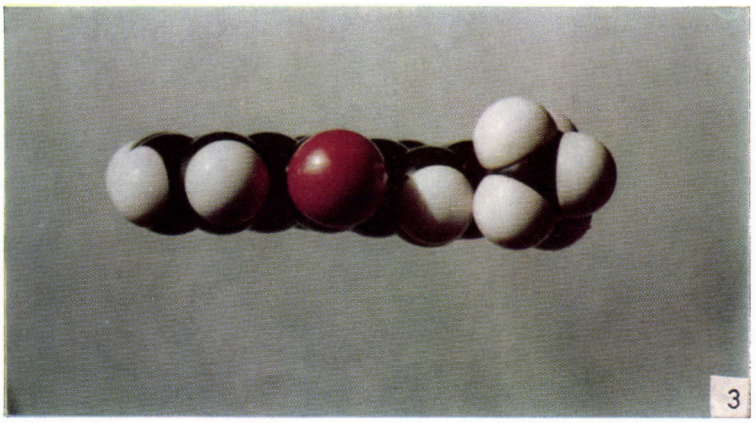

Figs 1 – 3. Molecular model of 2-ethylanthraquinone

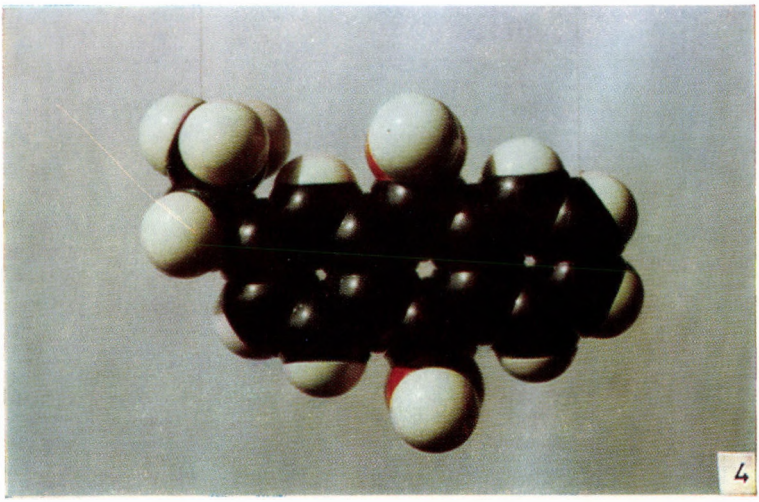

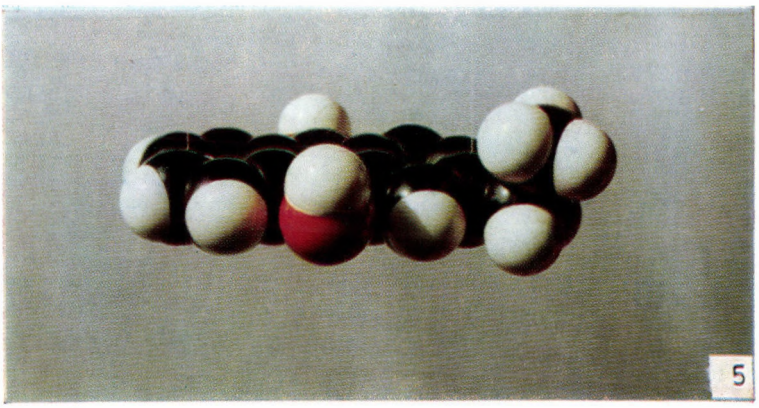

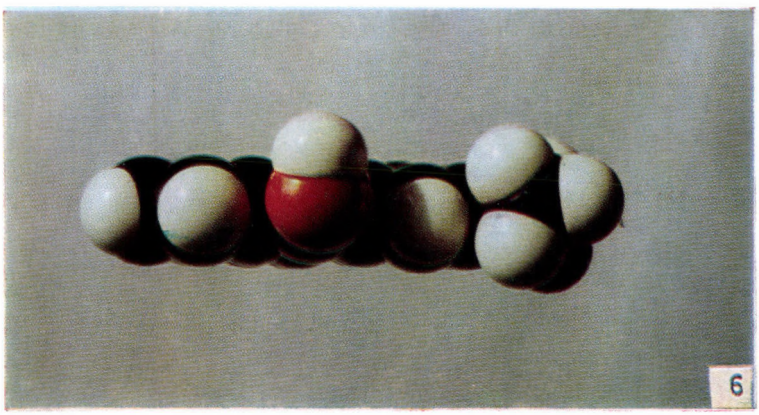

Figs 4 – 6. Molecular model of 2-ethylanthrahydroquinone

of the product. Using a mixture of eutectic composition of **I** and 2-ethyl-5,6,7,8-tetrahydroanthraquinone-9,10, this effect was not observed and the yield of hydrogen peroxide was improved by 8—10 % compared with substrate **I**.

REFERENCES

[1] Losonczi, B., Lengyel-Mészáros, A., Morgós, J.: In the press
[2] Csűrös, Z., Petró, J., Morgós, J., Losonczi, B.: Magyar Kémikusok Lapja 211 (1971)
[3] Dissent, V. E.: Zhurn. Obshch. Him., **29,** 1370 (1959)
[4] Michaelis, F. J.: J. Am. Chem. Soc., **60,** 1678 (1938)
[5] Szántay, Cs.: Elméleti Szerves Kémia, p. 132. Műszaki Könyvkiadó, Budapest 1971

Acta Chimica Academiae Scientiarum Hungaricae, Tomus 97 (1), pp. 91–103 (1978)

SOME PROPIONIC ACIDS AND DERIVATIVES, SUBSTITUTED IN POSITION 2 WITH HETEROCYCLIC GROUPS

J. NYITRAI, GY. DOMÁNY,* GY. SIMIG, J. FETTER, K. ZAUER and K. LEMPERT

(Department of Organic Chemistry, Technical University, Budapest, and Research Group for Alkaloid Chemistry of the Hungarian Academy of Sciences, Budapest)

Received July 4, 1977

A series of ethyl propionates, substituted in position 2 with non-aromatic *as*-triazine (**1a – g**, **2a – c**), aromatic *as*-triazine (**8a – h**), aromatic imidazole (**10a**, **10c**, **10e**, **12c**) and aromatic 1,2,3-thiadiazole rings (**13a**), propionamides, substituted in position 2 with aromatic imidazole rings (**12a**, **12d**, **12f**, **12h**), and of propionic acids, substituted in position 2 with aromatic imidazole (**10b**, **10d**, **10f**, **12b**, **12e**, **12g**, **12i**) and aromatic 1,2,3-thiadiazole rings (**13b**), have been synthesized. Condensation of diethyl 2-methyl-3-oxosuccinate with all benzamidrazones studied gave two isomeric *as*-triazinone derivatives each (**1e** and **2a**, **1f** and **2b**, **1g** and **2c**, respectively), furnishing thereby the first examples for the formation of isomeric *as*-triazinones in condensations of α-oxo-esters with amidrazones. While the non-aromatic *as*-triazine rings of compounds **1d – 1g** were aromatized by various methods to yield compounds **8a – h**, all attempts to convert the non-aromatic *as*-triazine rings of compounds **2a – c** into aromatic ones failed. Significant anti-inflammatory activities were observed for compounds **1f** and **12g** · HCl.

Certain *p*-substituted phenylacetic and 2-phenylpropionic acids have been known for their anti-inflammatory properties [1]. A search through the literature revealed that the inflammatory activity is retained when the phenyl groups of the above compounds are replaced by hetaryl groups (see *e.g.* Refs [2 – 7]). In the hope that compounds of enhanced activity would be obtained, we have synthesized a series of propionic acids and their derivatives, substituted in position 2 by *as*-triazine, imidazole and 1,2,3-thiadiazole rings.

A. *as-Triazine derivatives***

The ethyl 2-(2,5-dihydro-5-oxo-*as*-triazin-6-yl)propionates **1a** [**9**, 10], **1e**, **1f** and **1g** were obtained by allowing to react diethyl 2-methyl-3-oxosuccinate with thiosemicarbazide or the appropriate benzamidrazone. Whereas a single compound (**1a**) resulted (in agreement with the literature) from the reaction with thiosemicarbazide, the isomeric ethyl 2-(1,6-dihydro-6-oxo-*as*-triazin-5-yl)-propionates **2a – c** were obtained, in addition to compounds **1e – g**, from the condensations with the benzamidrazones.

* Chinoin Pharmaceutical Company Research Fellow, 1973 – 75. Present address: Chinoin Pharmaceutical Company, Budapest.

** This part of the present paper is considered as Part XX of the series *as*-Triazines and Condensed Derivatives. For Part XIX and a preliminary communication on the present studies, see Ref. [8].

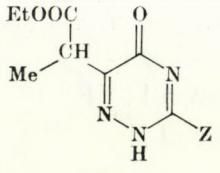

1

	Z
a	−SH*
b	−SMe
c	−NH−CH_2CH_2OH
d	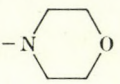
e	−Ph
f	−C_6H_4Cl-*p*
g	−C_6H_4OMe-*p*
h	−NH_2

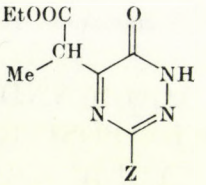

2

	Z
a	−Ph
b	−C_6H_4Cl-*p*
c	−C_6H_4OMe-*p*

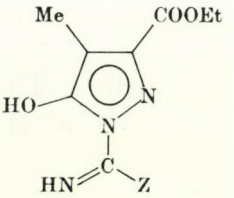

3

	Z
a	Ar
b	NH_2

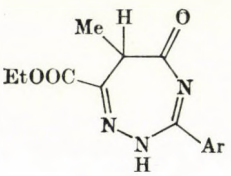

4

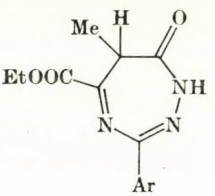

5

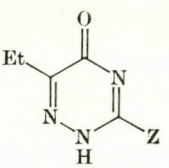

6

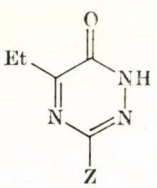

7

	Z
a	−Ph
b	−C_6H_4Cl-*p*
c	−C_6H_4OMe-*p*

The structures of the pairs of isomeric compounds follow (1) from the NMR spectra which, in all cases, exhibit 3H doublets around δ 1.4 and 1H quadruplets at about 4.0 ppm,** establishing the presence of a **MeCHCOOEt** group and ruling out the alternative type **3a** structures for *both* isomers;*** (2) from their alkaline hydrolysis followed by decarboxylation to yield products

* This compound actuallv exists as the 3(4*H*)-thioxo tautomer

** The 1H quadruplets are difficult to recognize in the case of the *p*-methoxyphenyl derivatives **1g** and **2c**.

*** Condensation of diethyl 2-methyl-3-oxosuccinate with aminoguanidine furnishes **3b** in addition to **1h** [9, 10].

whose NMR spectra exhibit typical *C*-ethyl signal patterns and to which, therefore, the isomeric structures **6a – c** and **7a – c**, respectively, had to be assigned, the type **4** and **5** structures being thereby ruled out for the original condensation products; and (3) from the mass spectra of the isomeric chloro derivatives **1f** and **2b** which both have abundant M – 101 peaks establishing thereby the presence of MeCHCOOEt groups in both isomers.

Structures **1e – 1g** and **2a – 2c**, respectively, were assigned to the higher and lower melting members of the pairs of isometric compounds resulting from the condensations with benzamidrazones on the basis of the IR spectra of their de-ethoxycarbonylation products whose highest frequency band in the double bond region appeared at about 1610 and 1660 cm^{-1}, respectively, which permitted the unequivocal assignment of the cross-conjugated type **6** and conjugated type **7** structures to the de-ethoxycarbonylation products of the higher and lower melting condensation products, respectively. In agreement herewith, the *two* highest frequency bands in the double bond region of the higher and lower melting isomers of the original condensation products appear at about 1745 and 1610, and at about 1745 and 1670 cm^{-1}, respectively.

This is the first case that isomeric *as*-triazinones have been isolated from the reaction of amidrazones and α-keto acids or their esters, *cf.* Refs [11 – 13].

Methylation of compound **1a** furnished the *S*-methyl derivative **1b** which was subsequently aminolyzed with the appropriate amines to furnish compounds **1c** and **1d.**

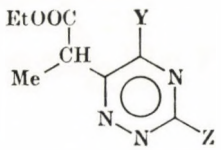

8

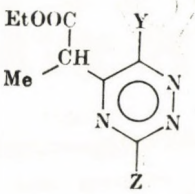

9

	Z	Y
a	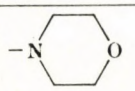	–OMe
b	–Ph	–OMe
c	$-C_6H_4Cl$-*p*	–OMe
d	$-C_6H_4OMe$-*p*	–OMe
e	–Ph	–Cl
f	$-C_6H_4Cl$-*p*	–Cl
g	–Ph	$-NEt_2$
h	$-C_6H_4Cl$-*p*	$-NEt_2$

The 2-(*as*-triazinyl)propionic acid derivatives **8a – 8d** containing *aromatic* triazine rings were obtained by treating compounds **1d – 1g** with diazomethane. According to TLC, at most traces of isomeric products were formed under the conditions applied.

Alternatively, compounds **1e** and **1f** were treated consecutively with phosphoryl chloride and diethylamine to yield the diethylamino derivatives **8g** and **8h**. In the *p*-chlorophenyl series, the intermediate **8f** was also isolated. No attempts were made to isolate the corresponding intermediate **8e** of the phenyl series.

All our attempts at converting the isomeric *as*-triazinone derivatives **2a – 2c** by either of the above methods into type **9** products containing an aromatic *as*-triazine ring, failed.

B. 2-(1- *and* 2-*Imidazolyl)propionic acid derivatives*

The ethyl 2-(4,5-diaryl-1-imidazolyl)propionates **10a**, **10c** and **10e** were obtained by allowing to react the appropriate 4,5-diarylimidazole with ethyl 2-bromopropionate. Acid-catalyzed hydrolysis of the latter furnished the corresponding free acids **10b**, **10d** and **10f**, respectively. According to their IR spectra, the latter do exist in the crystalline state in the zwitterionic forms.

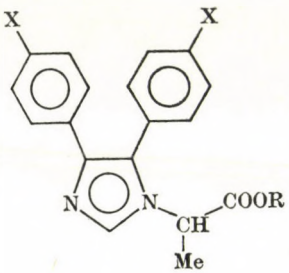

10

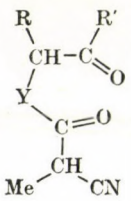

11

	X	R
a	H	Et
b	H	H
c	Cl	Et
d	Cl	H
e	MeO	Et
f	MeO	H

	R	R'	Y
a	Ph–	Ph–	O
b	Ph–	Ph–	NH
c	*p*-ClC_6H_4–	*p*-ClC_6H_4–	NH
d	*p*-$MeOC_6H_4$–	*p*-$MeOC_6H_4$–	NH
e	Me–	*p*-MeC_6H_4–	NH

Several methods were tested for the preparation of 2-(4,5-diphenyl-2--imidazolyl)propionamide **12a**, and thermal cyclization of desyl 2-cyanopro-

pionate (**11a**) or 2-cyano-*N*-desylpropionamide (**11b**) in the presence of *in situ* prepared formamide and ammonium acetate/acetic acid, respectively, proved to be the best. It is noteworthy that cyclization is accompanied by hydration of the nitrile group in both cases. Acid-catalyzed hydrolysis of the amide **10a** furnished the acid **10b**, and esterification of the of the latter gave the compound **10c**.

The 2-cyano-*N*-(2-oxoalkyl)propionamide route proved suitable for the preparation of the 2-[4,5-di(*p*-chlorophenyl)-2-imidazolyl]- (**12e**), 2-[4,5-di-(*p*-methoxyphenyl)-2-imidazolyl]- (**12g**) and 2-[4-methyl-5-(*p*-tolyl)imidazolyl]-propionic acids (**12i**) (in form of their hydrochlorides) as well.

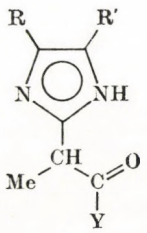

12

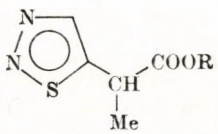

13

	R	R'	Y
a	Ph–	Ph–	$-NH_2$
b	Ph–	Ph–	–OH
c	Ph–	Ph–	–OEt
d	*p*-ClC_6H_4–	*p*-ClC_6H_4–	$-NH_2$
e	*p*-ClC_6H_4–	*p*-ClC_6H_4–	–OH
f	*p*-$MeOC_6H_4$–	*p*-$MeOC_6H_4$–	$-NH_2$
g	*p*-$MeOC_6H_4$–	*p*-$MeOC_6H_4$–	–OH
h	Me–	*p*-MeC_6H_4–	$-NH_2$
i	Me–	*p*-MeC_6H_4–	–OH

	R
a	Et
b	H

C. 2-*(1,2,3-Thiadiazol-5-yl)propionic acid derivatives*

The ethyl ester **13a** was obtained by allowing to react ethyl 2-(ethoxythiocarbonyl)propionate with diazomethane. Alkaline hydrolysis furnished the free acid **13b**.

Biological screening results

Compounds **1c**–**1g**, **2a**, **2b**, **8a**–**8d**, **8f**–**8h**, **10b**, **10d**, **10f**, **12b**, **12e**·HCl **12g**·HCl and **12i**·HCl were tested for their anti-inflammatory activities in

rats. Significant activity was observed only with compounds **1f** and **12g** · HCl. Neither of the latter displayed analgesic effects, nor were they able to potentiate the activity of narcotics.

Experimental

IR, UV and 60 MHz NMR spectra were obtained with Spectromom 2000 (Hungarian Optical Works, Budapest) and Perkin – Elmer 421 IR-, Unicam SP-700 UV- and Perkin – Elmer R-12 NMR spectrometers, respectively. TMS was used as internal standard for the NMR spectra taken in $CDCl_3$ and CCl_4, and the DMSO-d_5 signal (δ = 2.50 ppm) was used as the reference signal for the spectra taken in DMSO-d_6.

Ethyl 2-(5-oxo-3-thioxo-2,3,4,5-tetrahydro-*as*-triazin-6-yl)propionate (1a)

A mixture of diethyl 2-methyl-3-oxosuccinate [14] (30.3 g; 0.15 mole), thiosemicarbazide (13.65 g; 0.15 mole) and ethanol (200 ml) was refluxed until a homogeneous solution resulted (about 5 hrs). A solution of metallic sodium (3.55 g; 0.15 mole) in ethanol (100 ml) was added, and refluxing was continued for another hr. The solvent was evaporated in vacuum, the residue taken up in water (300 ml) and, with cooling in ice–water, slightly acidified (pH = = 6) to obtain 30.6 g (89 %) of the title compound, m. p. 155 – 156 °C (water), lit. [10] m. p. 144 °C.

$C_8H_{11}N_3O_3S$ (229.3). Calcd. C 41.91; H 4.84; N 18.33; S 13.99. Found C 41.64; H 4.87 N 17.97; S 13.67 %.

IR (KBr): 1720 and 1700 cm^{-1}.

Ethyl 2-(3-aryl-2,5-dihydro-5-oxo-*as*-triazin-6-yl)propionates (1e—1g) and ethyl 2-(3-aryl-1,6-dihydro-6-oxo-*as*-triazin-5-yl)propionates (2a—c)

(a) A mixture of benzamidrazone (8.2 g; 61 mmoles), obtained according to the procedure described for the *p*-chloro derivative [12], diethyl 2-methyl-3-oxosuccinate [14] (12.3 g; 61 mmoles) and 2-propanol (55 ml) was stirred until a clear solution resulted, and subsequently refluxed for 1 hr. The crystalline product **A** (2.75 g) consisting mainly of a mixture of compounds **1e** and **2a**, which separated on cooling, was refluxed for 15 min with benzene (50 ml) to give 2.25 g (14 %) of **1e** as the insoluble residue, m. p. 217 – 218 °C (*i*-PrOH).

$C_{14}H_{15}N_3O_3$ (273.3). Calcd. C 61.63; H 5.53; N 15.37. Found C 61.26; H 5.64; N 15.08 %.

UV (EtOH): 244 (4.38).

IR (KBr): 1740, 1605 cm^{-1}.

NMR (DMSO-d_6): δ 1.25, t, + 4.10, qu, COOEt; 1.40, d, + 3.90, qu, Me-CH<; 7.65, m, 3H, + 8.15 ppm, m, 2H, Ph.

The filtrate of fraction **A** was concentrated to about one third of its original volume to give another crystalline product (5 g). The latter was dissolved in hot methanol (50 ml); on cooling, 1.1 g of a crystalline mixture consisting mainly of compounds **1e** and **2a** separated. The methanolic filtrate was treated with water to obtain another crop of crystals which was recrystallized from benzene to yield 1.65 g (10 %) of **2a**, m. p. 138 – 139 °C (benzene or CCl_4).

$C_{14}H_{15}N_3O_3$ (273.3). Calcd. C 61.53; H 5.53; N 15.37. Found C 61.28; H 5.72; N 15.26 %.

UV (EtOH): 2.15 (3.98), sh; 262 (4.27).

IR (KBr): 1740, 1660 cm^{-1}.

NMR (DMSO-d_6): δ 1.10, t, + 4.05, qu, COOEt; 1.45, d, + 4.10, qu, Me – CH<; 7.5, m, 3H, + 8.1 ppm, m, 2H, Ph.

From the benzene filtrate of **2a** further 0.5 g of a crystalline mixture of products was recovered.

No efforts were made to separate the components of the crystalline mixtures by chromatography.

(b) A mixture of *p*-chlorobenzamidrazone [12] (3.8 g; 22.5 mmoles), diethyl 2-methyl-3-oxosuccinate [14] (4.7 g; 23.2 mmoles) and 2-propanol (15 ml) was stirred for 24 hrs at room temperature and subsequently kept overnight in a refrigerator. The crystalline product was collected and the filtrate evaporated to about one third of its original volume to give a second

crystalline crop. Chromatographic work-up (130 g Kieselgel 40, Merck, für die Säulenchromatographie, Korngrösse 0.063 – 0.200 mm, 70 – 230 mesh ASTM; solvent: benzene–ethyl acetate, 9 : 1 → 7 : 3) of the combined crystalline products (3.35 g) furnished 1.05 g (15 %) of compound **2b**, m. p. 176 – 177 °C (EtOH), and 1.25 g (18 %) of compound **1f**, m. p. 206 °C (EtOAc), in decreasing order of their R_f values.

$C_{14}H_{14}ClN_3O_3$ (307.3). Calcd. C 54.64; H 4.58; Cl 11.52; N 13.65. Compound **1f**: Found C 54.46; H 4.53; Cl 11.73; N 13.43 %. Compound **2b**: Found C 54.50; H 5.17; Cl 11.77; N 13.50 %.

UV (EtOH): Compound **1f**: 250 (4.34); compound **2b**: 211 (4.12), sh; 267 (4.33).

IR (KBr): Compound **1f**: 1745, 1620; compound **2b**: 1750, 1675 cm^{-1}.

NMR, **1f** (DMSO-d_6): δ 1.10, t, + 4.10, qu, COOEt; 1.40, d, + 3.90, qu, Me-CH<; 7.65 + 8.15, A_2B_2, *p*-ClC_6H_4. – **2b** ($CDCl_3$): 1.25, t, +4.25, qu, COOEt; 1.65, d, +4.35, qu, Me-CH<; 7.50 + 8.15 ppm, A_2B_2, *p*-ClC_6H_4.

(c) A mixture of *p*-methoxybenzamidrazone (11.8 g; 71.5 mmoles), obtained according to the procedure described for the *p*-chloro analogue [12], diethyl 2-methyl-3-oxosuccinate [14] (14.5 g; 71.8 mmoles) and 2-propanol (100 ml) was stirred for 8 hrs at room temperature, then allowed to stand for 2 days and finally refluxed for 6 hrs to obtain 14.4 g of a crystalline product. Chromatographic work-up by 4 g portions of the latter (120 g Kieselgel 40, Merck, as above; solvent: as above) furnished a total of 5.8 g (27 %) of compound **2c**, m. p. 167 – 168 °C (EtOH), and 5.0 g (23 %) of compound **1g**, m. p. 192 – 193 °C (dioxane), in decreasing order of their R_f values.

$C_{15}H_{17}N_3O_4$ (303.3). Calcd. C 59.39; H 5.65; N 13.85. Compound **1g**: Found C 59.51; H 5.71; N 13.68 %. Compound **2c**: Found C 59.21; H 5.78; N 14.16 %.

UV (EtOH): Compound **1g**: 214 (4.15), sh; 258 (4.22), sh; 283 (4.31); compound **2c**: 210 (4.13), sh; 281 (4.38).

IR (KBr): Compound **1g**: 1740, 1610; compound **2c**: 1725, 1650 cm^{-1}.

NMR (DMSO-d_6), **1g**: δ 1.15, t, + 4.10, qu, COOEt; 1.40, d, **Me**-CH<; 3.85, s, MeO; 7.15 + 8.10, A_2B_2, *p*-$MeOC_6H_4$; **2c**: 1.10, t, + 4.15, qu, COOEt; 1.45, d, **Me**-CH<; 3.80, s, MeO; 7.10 + 8.10 ppm, A_2B_2, *p*-$MeOC_6H_4$.

De-ethoxycarbonylation of compounds 1e—1g and 2a—2c

(a) Compound **1e** (2.0 g; 7.3 mmoles) was stirred for 1 hr with 10 % aqueous sodium hydroxide (10 ml) at room temperature. The solution was neutralized with 20 % aqueous hydrogen chloride (pH = 7) and the resulting crystalline product (1.05 g) refluxed for 30 min with nitromethane (0.5 ml) to yield 0.52 g (35 %) of compound **6a**, m. p. 185 °C (nitromethane).

$C_{11}H_{11}N_3O$ (201.2). Calcd. C 65.65; H 5.51; N 20.88. Found C 65.42; H 5.21; N 21.01 %.

UV (EtOH): 244 (4.28).

IR (KBr): 1620 cm^{-1}.

NMR (DMSO-d_6): δ 1.10, t, + 2.65, qu, Et; 7.7, m, 3H, + 8.2 ppm, m, 2H, Ph.

(b) Compound **1f** (0.3 g; 1 mmole) was stirred for 1 hr with 1*N* NaOH (5 ml) at room temperature. The insoluble impurities were filtered off; the filtrate was acidified with conc. aqueous hydrogen chloride and the resulting crystalline product refluxed for 1 hr with nitromethane (3 ml) to yield 0.20 g (87 %) of compound **6b**, m. p. 285 – 286 °C (DMF).

$C_{11}H_{10}ClN_3O$ (235.7). Calcd. Cl 15.05; N 17.83. Found Cl 15.11; N 17.86 %.

UV (EtOH): 251 (4.26).

IR (KBr): 1605 cm^{-1}.

(c) Compound **1g** (1.5 g; 5 mmoles) was stirred for 1 hr with 10 % aqueous NaOH solution (10 ml) at room temperature. Acidification with conc. hydrochloric acid furnished 1.1 g of a crude product which was recrystallized from dioxane to yield 0.55 g (48 %) of compound **6c**, m. p. 248 – 250 °C (dioxane).

$C_{12}H_{13}N_3O_2$ (231.2). Calcd. C 62.32; H 5.67; N 18.17. Found C 62.43; H 5.92; N 18.04 %.

UV (EtOH): 215 (4.21) sh-like; 281 (4.37).

IR (KBr): 1600 cm^{-1}.

NMR (DMSO-d_6): δ 1.10, t, + 2.65, qu, Et; 7.15 + 8.10 ppm, A_2B_2, *p*-$MeOC_6H_4$.

(d) De-ethoxycarbonylation of compounds **2a** – **2c** was carried out essentially according to the method described under *(b)*, using the following amounts of reactants and applying the following conditions:

Starting compound **2a** (0.5 g; 1.8 mmole), 1*N* NaOH 5 ml, stirring for 30 min; nitromethane 3 ml, refluxing for 1 hr; yield 0.25 g (68 %) of compound **7a**, m. p. 180 – 181 °C (EtOH).

$C_{11}H_{11}N_3O$ (201.2). Calcd. C 65.65; H 5.51; N 20.88. Found C 65.49; H 5.44; N 20.75 %.

UV (EtOH): 213 (4.01), sh; 262 (4.27).

IR (KBr): 1660 cm^{-1}.

NMR (DMSO-d_6): δ 1.25, t, + 2.85, qu, Et; 7.4, m, 3H, + 8.0 ppm, m, 2H, Ph.

Starting compound **2b** (0.4 g; 1.3 mmole), 1*N* NaOH 5 ml, stirring for 4 hrs; nitromethane 3 ml, refluxing for 20 min; yield 0.18 g (59 %) of compound **7b**, m. p. 193 – 194 °C (EtOH).

$C_{11}H_{10}ClN_3O$ (235.7). Calcd. C 56.06; H 4.28; Cl 15.05; N 17.83. Found C 56.12; H 4.36; Cl 15.35; N 17.65 %.

UV (EtOH): 267 (4.26).

IR (KBr): 1670 cm^{-1}.

NMR (DMSO-d_6): δ 1.20, t, + 2.80, qu, Et; 7.45 + 8.05 ppm, A_2B_2, *p*-ClC_6H_4.

Starting compound **2c** (0.5 g; 1.6 mmole), 1*N* NaOH 10 ml, stirring for 15 min; nitromethane 10 ml, refluxing for 1 hr; yield 0.25 g (66 %) of compound **7c**, m. p. 204 – 205 °C (EtOH).

$C_{12}H_{12}N_3O_2$ (231.2). Calcd. C 62.32; H 5.67; N 18.17. Found C 62.39; H 5.63; N 18.26 %.

UV (EtOH): 209 (4.23), sh; 281 (4.55).

IR (KBr): 1650 cm^{-1}.

NMR (DMSO-d_6): δ 1.15, t, + 2.80, qu, Et; 7.0 + 8.0 ppm, A_2B_2, *p*-$MeOC_6H_4$.

Ethyl 2-(3-methylthio-5-oxo-2,5-dihydro-*as*-triazin-6-yl)-propionate (1b)

Metallic sodium (2.3 g; 0.1 mole) and, subsequently, compound **1a** (22.9 g; 0.1 mole) were dissolved in ethanol (200 ml). Methyl iodide (6.9 ml; 0.11 mmole) was added, and the mixture allowed to stand for 15 min at room temperature and then refluxed for another 15 min. The solvent was evaporated in vacuum and the residue triturated with water to yield 24.0 g (99 %) of the title compound, m. p. 166 °C (EtOAc).

$C_9H_{13}N_3O_3S$ (243.3). Calcd. C 44.44; H 5.38; S 13.18. Found C 44.47; H 5.31; S 12.98 %.

IR (KBr): 1730 and 1630 cm^{-1}.

Ethyl 2-[3-(2-hydroxyethylamino)-5-oxo-2,5-dihydro-*as*-triazin-6-yl]propionate (1c)

A mixture of compound **1b** (2.43 g; 10 mmoles), 2-aminoethanol (0.60 ml; 10 mmoles) and anhydrous anisole (10 ml) was refluxed for 4 hrs to obtain 1.20 g (47 %) of the title compound, m. p. 179 °C (nitromethane).

$C_{10}H_{16}N_4O_4$ (256.3). Calcd. C 46.87; H 6.29; N 21.87. Found C 46.60; H 6.51; N 21.12 %.

IR (KBr): 1720 and 1620 cm^{-1}.

Ethyl 2-(3-morpholino-5-oxo-2,5-dihydro-*as*-triazin-6-yl)-propionate (1d)

A mixture of compound **1b** (2.43 g; 10 mmoles), morpholine (0.87 ml; 10 mmoles) and anhydrous anisole (10 ml) was refluxed for 3 hrs. Light petroleum (50 ml) was added after cooling, to obtain 2.10 g (74 %) of the title compound, m. p. 165 °C (EtOAc).

$C_{12}H_{18}N_4O_4$ (282.3). Calcd. C 51.06; H 6.42; N 19.86. Found C 51.07; H 6.46; N 19.91 %.

IR (KBr): 1745 and 1600 cm^{-1}.

NMR ($CDCl_3$): δ 1.25, t, + 4.20, qu, COOEt; 1.45, d, **Me**-CH<; 3.75 ppm, bs, 8H, morpholino group.

Ethyl 2-(5-methoxy-3-subst.-*as*-triazin-6-yl)propionate (8a—d)

Compounds **1d** – **1g** (10 – 20 mmoles) were stirred with excess ethereal diazomethane solution at room temperature until, according to TLC, they had been completely used up (1 – 3 hrs). Acetic acid was added to decompose the excess of the reagent. The resulting mixtures were evaporated to dryness, the residues chromatographed through columns of silica (solvent: benzene–EtOAc, 4 : 1) and the oily products crystallized from light petroleum.

Compound **8a**, 35 % yield, m. p. 68 °C.

$C_{13}H_{20}N_4O_4$ (296.3). Calcd. C 52.69; H 6.80; N 18.91. Found C 52.63; H 7.02; N 18.65 %.

IR (KBr): 1730 cm^{-1}.

NMR (CCl_4): δ 1.20, t, + 4.10, qu, COOEt; 1.45, d, **Me**-CH<; 3.75, s, 8H, morpholino group; 4.93 ppm, s, MeO.

Compound **8b**, 40 % yield, m. p. 72 °C.

$C_{15}H_{17}N_3O_3$ (287.3). Calcd. C 62.70; H 5.96; N 14.63. Found C 62.97; H 6.10; N 14.47 %.

UV (EtOH): 256 (4.15); 274 (4.08).

IR (KBr): 1735 cm^{-1}.

NMR (CCl_4): δ 1.25, t, + 4.15, qu, COOEt, 1.65, d, **Me**-CH<; 4.15, s, MeO; 7.45, m, 3H, + 8.45 ppm, m, 2H, Ph.

Compound **8c**, 57 % yield, m. p. 84 – 85 °C.

$C_{15}H_{16}ClN_3O_3$ (321.8). Calcd. C 55.99; H 5.01; Cl 11.01; N 13.06. Found C 55.90; H 5.44; Cl 11.49; N 13.00 %.

UV (EtOH): 263 (4.21); 278 (4.21).

IR (KBr): 1720 cm^{-1}.

NMR (CCl_4): δ 1.25, t, +4.20, qu, COOEt; 1.65, d, **Me**-CH<; 7.55 + 8.55 ppm, A_2B_2, *p*-ClC_6H_4.

Compound **8d**, 46 % yield, m. p. 65 – 66 °C.

$C_{16}H_{19}N_3O_4$ (317.4). Calcd. C 60.56; H 6.03; N 13.24. Found C 60.67; H 5.96; N 13.01 %.

UV (EtOH): 217 (4.22); 289 (4.32).

IR (KBr): 1720 cm^{-1}.

NMR ($CDCl_3$): δ 1.20, t, + 4.20, qu, COOEt; 1.7, d, **Me**-CH<; 3.9, s, + 4.15, s, two MeO's: 7.05 + 8.55 ppm, A_2B_2, *p*-$MeOC_6H_4$.

The yields of the oily products obtained after chromatography (which were pure according to TLC) amounted to about 80 – 90 %. In spite of the considerable losses during crystallization, no attempts were made to optimize the conditions of recovery of the products.

Ethyl 2-[5-chloro-3-(p-chlorophenyl)-*as*-triazin-6-yl]-propionic acid (8f)

Compound **1f** (1.2 g; 3.9 mmoles) was refluxed for 3 hrs with phosphoryl chloride (15 ml) and the excess reagent evaporated in vacuum. The oily residue was taken up in benzene (30 ml), the solution washed with water, dried ($MgSO_4$) and evaporated to dryness in vacuum to yield an oily product which was crystallized from gasoline to obtain 0.85 g (67 %) of the title compound, m. p. 83 – 84 °C (gasoline).

$C_{14}H_{13}Cl_2N_3O_2$ (326.2). Calcd. C 51.55; H 4.02; Cl 21.74; N 12.89. Found C 51.92; H 4.01; Cl 21.76; N 12.70 %.

UV (EtOH): 210 (4.11), sh: 270 (4.37).

IR (KBr): 1745 cm^{-1}.

NMR ($CDCl_3$): δ 1.30, t, +4.30, qu, COOEt; 1.80, d, + 4.50, qu, Me-CH<; 7.7 + 8.7 ppm, A_2B_2, *p*-ClC_6H_4.

Ethyl 2-(3-aryl-5-diethylamino-*as*-triazin-6-yl)propionates (8g, 8h)

(a) Compound **1e** (2.0 g; 7.8 mmoles) was refluxed for 3 hrs with phosphoryl chloride (15 ml), and the mixture evaporated to dryness in vacuum. The residue was triturated with ether and water (20 ml, each) and the aqueous layer extracted with two portions of ether (10 ml, each). The combined ethereal solutions were dried ($MgSO_4$) and treated with charcoal. Diethylamine (2 ml; 20 mmoles) was added and the mixture stirred for 4 hrs at room temperature. After extraction with two portions of water (20 ml, each) and drying ($MgSO_4$), the solvent was evaporated and the oily residue crystallized from gasoline to yield 1.15 g (45 %) of compound **8g**, m. p. 90 – 91 °C (gasoline).

$C_{18}H_{24}N_4O_2$ (328.40). Calcd. C 65.83; H 7.37; N 17.06. Found C 65.52; H 7.04; N 17.29 %.

UV (EtOH): 254 (4.39).

IR (KBr): 1735 cm^{-1}.

NMR ($CDCl_3$): δ 1.20, t, + 4.25, qu, COOEt; 1.35, t, + 3.70, qu, NEt_2; 1.7, d, **Me**-CH<; 7.5, m, 3H, + 8.55 ppm, m, 2H, Ph.

(b) Compound **1f** was treated with phosphoryl chloride as described for the preparation of compound **8f**. The crude compound **8f**, obtained after evaporation of its benzene solution in vacuum, was boiled up with gasoline (30 ml). The insoluble impurities were filtered off and the filtrate treated with charcoal and evaporated to dryness. The residue was dissolved in anhydrous ether and stirred for 4 hrs with diethylamine (1.2 ml; 11.7 mmoles) at room temperature. The mixture was evaporated to dryness, the residue triturated with water and the crystalline product recrystallized from aqueous ethanol and subsequently from gasoline to yield 0.82 g (58 %) of compound **8h**, m. p. 106 – 107 °C (gasoline).

$C_{18}H_{23}ClN_4O_2$ (362.9). Calcd. C 59.58; H 6.39; Cl 9.77; N 15.44. Found C 59.36; H 6.20; Cl 9.92; N 15.00 %.

IR (KBr): 1740 cm^{-1}.

NMR ($CDCl_3$): δ 1.25, m, 9H; + 3.65, m, 4H, + 4.20, m, 2H, NEt_2 + COOEt; 1.65, d, **Me**-CH<; 7.40 + 8.35 ppm, A_2B_2, *p*-ClC_6H_4.

Ethyl 2-(4,5-diaryl-1-imidazolyl)propionates (10a, 10c, 10e)

Metallic sodium (2.1 mmoles) and, subsequently, the appropriate 4,5-diarylimidazole [15 – 17] (2.0 mmoles) were dissolved in EtOH (10 ml). The mixtures were evaporated to dryness in vacuum and the resulting sodium salts dissolved in anhydrous DMF (10 ml). Ethyl 2-bromopropionate (2.1 mmoles) was added and the mixtures stirred at room temperature until, according to TLC, the reactions were complete (3 – 5 hrs). The solvents were evaporated in vacuum. Water (10 ml) was added and the resulting emulsions were extracted with ether. The crystalline residues of the ether solutions were recrystallized from tetrahydrofurane–light petroleum.

Compound **10a**, 62.5 % yield, m. p. 106°C.
$C_{20}H_{20}N_2O_2$ (320.4). Calcd. C 74.97; H 6.29; N 8.75. Found C 74.92; H 6.27; N 8.68 %.
IR (KBr): 1750 cm^{-1}.
Compound **10c**, 65 % yield, m. p. 133 °C.
$C_{20}H_{18}Cl_2N_2O_2$ (389.3). Calcd. C 61.70; H 4.66; N 7.20. Found C 61.74; H 4.49; N 7.34 %.
IR (KBr): 1750 cm^{-1}.
Compound **10e**, 58 % yield, m. p. 108 °C.
$C_{22}H_{24}N_2O_4$ (380.43). Calcd. C 69.45; H 6.36; N 7.37. Found C 69.20; H 6.45; N 7.53 %.
IR (KBr): 1760/1740 cm^{-1}, d.

2-(4,5-Diaryl-1-imidazolyl)propionic acids (10b, 10d, 10f)

Mixtures of the above esters (1 mmole), water (15 ml) and conc. aqueous hydrogen chloride (1.5 ml) were refluxed until hydrolysis was complete (2 hrs). The resulting solutions were neutralized (pH = 7) with 10 % aqueous Na_2CO_3 solution, with continuous stirring and ice-cooling, to yield the colourless crystals of the title compounds which were recrystallized from butanol.

Compound **10b**, 88 % yield, m. p. 285 °C.
$C_{18}H_{16}N_2O_2$ (292.3). Calcd. C 73.96; H 5.52; N 9.58. Found C 73.81; H 5.82; N 9.54 %.
NMR (DMSO-d_6): δ 1.6, d, **Me**-CH<; 7.0 – 7.6, m, Ph's; 8.0 ppm, s, 2-H.
Compound **10d**, 82 % yield, m. p. 245 – 246 °C.
$C_{18}H_{14}Cl_2N_2O_2$ (361.2). Calcd. C 59.85; H 3.91; Cl 19.63; N 7.76 Found C 60.10; H 4.15; Cl 19.98; N 7.62 %.
Compound **10f**, 73 % yield, m. p. 240 – 242 °C.
$C_{20}H_{20}N_2O_4$ (352.4). Calcd. C 68.17; H 5.72; N 7.95. Found C 67.92; H 6.06; N 8.15 %.

2-Cyano-*N*-desylpropionamides (11b—11c)

(a) Anhydrous pyridine (6 ml) was added, with stirring, to a mixture of desylammonium chloride (4.0 g; 16.2 mmoles), 2-cyanopropionyl chloride [18] (2 ml; 21 mmoles) and anhydrous dioxane (50 ml). After the evolution of heat had ceased, the mixture was heated to its b. p., kept for about 5 min at this temperature, stirred for another 2 hrs without further heating, allowed to stand overnight and evaporated to dryness in vacuum. Water (20 ml) and dilute aqueous hydrochloric acid were added (pH = 1) to obtain a gummy product which, when boiled up with a small amount of ethanol, became crystalline. The title compound (2.50 g; 53 %) thus obtained had m. p. 137 °C (aqueous MeOH).
$C_{18}H_{16}N_2O_2$ (292.3). Calcd. C 73.96; H 5.52; N 9.58. Found C 73.62; H 5.31; N 9.50 %.
IR (KBr): 3300, 1660 cm^{-1}.
(b) The *p,p'*-dichloro derivative was similarly prepared starting with *p,p'*-dichlorodesylammonium chloride [19, 20] (5.2 g; 16.4 mmoles). The oily residue, obtained after evaporation of the reaction mixture to dryness in vacuum, was treated with water (30 ml) and kept in a refrigerator, whereupon it gradually solidified to yield 3.9 g (65.7 %) of compound **11c**, m. p. 157 – 158 °C.
$C_{18}H_{14}Cl_2N_2O_2$ (361.23). Calcd. Cl 19.63. Found Cl 19.20 %.
IR (KBr): 3300, 1680, 1650 cm^{-1}.
This product proved, without recrystallization, sufficiently pure for conversion into **12d**.

2-Cyano-*N*-[1-(1-*p*-methylbenzoyl)ethyl]propionamide (11e)

This compound was obtained, starting with 1-(*p*-methylbenzoyl)ethylammonium chloride (7.30 g; 36.5 mmoles), 2-cyanopropionyl chloride (4 ml; 41 mmoles), anhydrous dioxane

(60 ml) and anhydrous pyridine (10 ml), in the same way as described for compound **11b**. The residue obtained after evaporation of the reaction mixture to dryness, gradually solidified when treated with water and scratched, to yield 4.70 g (53 %) of crude **11e**, m. p. 132 °C, which was subjected to cyclization to **12h** and hydrolysis to **12i** without further purification (see below).

2-(4,5-Diaryl-2-imidazolyl)propionamides (12a, 12d)

(a) A mixture of freshly recrystallized dry benzoin (8.0 g; 37 mmoles) and 2-cyanopropionyl chloride [18] (9.60 g; 82 mmoles) was heated for 1 hr at 60 – 80 °C and for 30 min at 105 °C to yield gradually a clear melt of the intermediate **11a**.

In the meantime 99 % formic acid (20 ml) was neutralized with $(NH_4)_2CO_3$ (40 g), and the mixture gradually heated to 160 °C. At this point compound **11a** was added; the flask, in which the latter was prepared, was rinsed with formamide (20 ml) and the solution added to the reaction mixture, which was then heated for 3 hrs at 170 – 180 °C. (All temperatures given were measured inside the reaction mixtures.) After cooling, ethanol (80 ml) was added and the mixture refluxed for 1 hr to yield 5.50 g (50 %) of the crystals of compound **12a**, m. p. 289 – 290 °C (EtOH).

$C_{18}H_{17}N_3O$ (291.4). Calcd. C 74.21; H 5.88; N 14.42. Found C 74.07; H 5.77; N 14.61 %.

IR (KBr): 3300, 3050, 1670 cm^{-1}.

(b) A mixture of 2-cyano-*N*-desylpropionamide (**11b**) (1.35 g; 4.5 mmoles), ammonium acetate (4 g) and acetic acid (15 ml) was refluxed for 2 hrs, evaporated to dryness and boiled up with water (15 ml) to yield 1.10 g (81.5 %) of a crystalline product, m. p. 280 °C (d) which, according to its mixed m. p. and IR spectrum, was identical with the product obtained as described under *(a)* and which was used without further purification.

(c) A mixture of crude 2-cyano-*N*-(*p*,*p*'-dichlorodesyl)propionamide (**11c**) (3.5 g; 9.7 mmoles), ammonium acetate (10 g) and acetic acid (30 ml) was refluxed for 2 hrs and concentrated to about half its original volume. Water (50 ml) was added to precipitate a gummy product which became crystalline when the mixture was heated for a short time to its b. p. Compound **12d** (3.1 g; 89 %) was obtained with m. p. 230 – 231 °C (EtOH).

$C_{18}H_{15}Cl_2N_3O$ (360.25). Calcd. N 11.66. Found N 11.76 %.

IR (KBr): 3350 (sh), 3000, 1660 cm^{-1}.

2-(4,5-Disubstituted-2-imidazolyl)propionic acids (12b, 12e, 12g, 12i)

(a) A mixture of the amide **12a** (2.3 g; 8.0 mmoles), conc. hydrochloric acid (10 ml) and water (25 ml) was refluxed for 30 min. (A thick paste of crystalline **10a** · HCl was formed after about 10 min.) The hydrochloride (2.2 g; 83 %, m. p. 160 °C) was filtered off, taken up in water and treated with $(NH_4)_2CO_3$ to adjust pH = 6. The crystalline product was filtered off and rapidly recrystallized from a mixture of ethanol (80 ml) and water (110 ml) to obtain 1.60 g (66 %) of compound **12b**, m. p. 217 – 218 °C.

$C_{18}H_{16}N_2 \cdot \frac{1}{2} H_2O$ (301.35). Calcd. C 71.74; H 5.69; N 9.30. Found C 71.26; H 5.71; N 9.67 %.

IR (KBr): 1750 cm^{-1}.

(b) A mixture of the amide **12d** (2.0 g; 56 mmoles), acetic acid (35 ml) and conc. hydrochloric acid (15 ml) was refluxed for 1 hr. Water (10 ml) was added, and refluxing was continued for another 30 min to obtain 1.90 (86 %) of compound **12e** · HCl, m. p. 264 – 265 °C (after reprecipitation of its solution in acetic acid with conc. hydrochloric acid).

$C_{18}H_{14}Cl_2N_2O_2 \cdot HCl$ (397.7). Calcd. Cl 26.74; N 7.04. Found Cl 26.56; N 6.92 %.

IR (KBr): 1760 cm^{-1}.

(c) Compound **11d** was prepared, starting with *p*,*p*'-dimethoxydesylammonium chloride [20] (5.0 g; 16.2 mmoles), similarly to the synthesis of compound **11b** described above. The gummy product, obtained after evaporation of the reaction mixture to dryness in vacuum and addition of water, was separated, the aqueous layer extracted with two portions of chloroform (10 ml, each) and the gummy product was dissolved in the combined chloroform solutions. The solution was dried over $MgSO_4$, the solvent evaporated and the residue (crude **11d**) refluxed for 90 min with a mixture of ammonium acetate (10 g) and acetic acid (30 ml). The resulting yellow solution of compound **12f** was concentrated to about 15 ml; water (20 ml) and conc. hydrochloric acid (30 ml) were added. The mixture was refluxed for 20 min and kept overnight in a refrigerator to yield 3.30 g (52.5 %) of compound **12g** · HCl, m. p. 221 – 222 °C (after reprecipitation from its solution in acetic acid with conc. HCl).

$C_{20}H_{20}N_2O_4 \cdot HCl$ (388.9). Calcd. C 61.78; H 5.44; Cl 9.12; N 7.20. Found C 61.99; H 5.59; Cl 9.59; N 7.58 %.

IR (KBr): 1760 cm^{-1}.

(d) The crude compound **11e** (4.40 g; 18 mmoles), obtained as described above, was refluxed for 1 hr with a mixture of ammonium acetate (7 g) and acetic acid (30 ml). The resulting solution of compound **12h** was concentrated to about one half its original volume. Water (40 ml) and conc. hydrochloric acid (10 ml) were added, the resulting clear solution was refluxed for 1 hr and concentrated to about 15 ml in vacuum. Conc. HCl (20 ml) was added and the mixture heated to its b. p. From the clear solution a mixture of compound **12i** · HCl and ammonium chloride separated on cooling. Recrystallization from water furnished 2.8 g (56 %) of the title compound, m. p. 175 – 176 °C (dried over P_2O_5 at 80 °C in vacuum).

$C_{14}H_{16}N_2O_2 \cdot HCl$ (280.8). Calcd. Cl 12.63; N 9.97. Found Cl 12.55; N 9.54 %.

IR (KBr): 1740 cm^{-1}.

The salt is extremely hygroscopic.

Ethyl 2-(4,5-diphenyl-2-imidazolyl)propionate (12c)

The ester, m. p. 167 °C, was obtained from the acid **12b** according to the usual esterification procedure (EtOH, HCl).

$C_{20}H_{20}N_2O_2$ (320.38). Calcd. C 74.97; H 6.29. Found C 74.73; H 6.69 %.

The same product was obtained when the *anhydrous* acid (**12b**) was recrystallized from ethanol.

Ethyl 2-(ethoxythiocarbonyl)propionate

Dry hydrogen chloride (23 g; 0.63 moles) was introduced, with ice-cooling, into a mixture of ethyl 2-cyanopropionate (Fluka) (68.4 g; 0.59 mole) and anhydrous ethanol (38 ml; 0.66 mole). The mixture was kept for 2 hrs in an ice-bath and for 16 hrs at room temperature to obtain a thick crystalline paste which was diluted with anhydrous ether (150 ml), filtered, washed with anhydrous ether (150 ml) and dried over P_2O_5 and KOH in vacuum to yield 86 g (76 %) of the imidate hydrochloride, m. p. 90 – 93 °C.

This product was added, with cooling, to anhydrous pyridine (160 ml). Dry hydrogen sulfide was introduced for 5 hrs into the suspension with cooling. The mixture was allowed to stand 20 hrs at room temperature and treated with a mixture of ice (400 g), conc. hydrochloric acid (200 ml) and ether (150 ml). The aqueous layer was extracted with two portions of ether (100 ml, each). The combined ethereal layers were washed with water (two portions, 25 ml each), dried ($MgSO_4$) and worked up by fractional distillation to obtain 71 g (91 %) of the title compound, b. p. 76 – 77 °C/3 torr, 70 °C/2 torr; n_D^{23} 1.4617.

$C_8H_{14}O_3S$ (190.3). Calcd. C 50.52; H 7.42; S 16.82. Found C 50.55; H 7.62; S 16.40 %.

IR (KBr): 1750 cm^{-1}.

NMR (CCl_4): δ 1.25, t, 1.4, t, + 4.15, qu, 4.55, qu, two EtO's; 1.5,d, +3.7 ppm, qu, Me-CH<.

Ethyl 2-(1,2,3-thiadiazol-5-yl)propionate (13a)

An ethereal diazomethane solution (120 ml), freshly prepared from *N*-methyl-*N*-nitroso-*p*-toluenesulfonamide (20 g; 94 mmoles), was added with ice-cooling to an anhydrous methanolic solution (80 ml) of ethyl 2-(ethoxythiocarbonyl)propionate (8.0 g; 42 mmoles). The mixture was kept for 6 hrs in an ice-bath and for 15 hrs at room temperature and worked up by fractional distillation in vacuum. After a fore-run of 2.2 g (28 %) of unchanged ethyl 2-(ethoxythiocarbonyl)propionate, b. p. 70 – 71 °C/2 torr, 3.7 g (47 %) of the title compound, b. p. 101 – 104 °C/1 torr was obtained.

A second distillation furnished a pure product b. p. 88 °C/0.5 torr.

$C_7H_{10}N_2O_2S$ (186.2). Calcd. C 45.16; H 5.41. Found C 45.80; H 5.64 %.

IR (KBr): 1740 cm^{-1}.

2-(1,2,3-Thiadiazolyl)propionic acid (13b)

The above ester (3 g; 16 mmoles) was treated at room temperature with a solution (20 ml) of sodium hydroxide (30 mmoles) in methanol. After 30 min the solution was evaporated to dryness in vacuum below 37 °C, the oily residue dissolved in water (15 ml) and the aqueous

solution extracted with ether. The aqueous solution was acidified with 6*N* HCl (6 ml) and extracted with ethyl acetate (40 ml, in three portions). The ethyl acetate solution was evaporated to dryness in vacuum below 37 °C to yield an orange oil which, on scratching, furnished 2.3 g (93 %) of the crystals of the title compound in almost pure form. Further purification was effected by sublimation at 1 torr and 120 °C (bath temperature); m. p. 105 – 106 °C.

$C_5H_6N_2O_2S$ (158.2). Calcd. C 37.98; H 3.82, N 17.72. Found C 38.12; H 4.23; N 17.32 %.

IR (KBr): 1705 cm^{-1}.

NMR ($CDCl_3$): δ 1.7, d, +4.3, qu, Me-CH<; 8.5, bs, COOH; 8.65 ppm, s, 4-H.

*

The authors are indebted to Mrs. I. BALOGH-BATTA and staff for the microanalyses, to Dr. P. KOLONITS and staff for the IR and NMR, to Mrs. I. BALOGH-BATTA for the UV, to Mrs. J. HEGEDÜS-VAJDA for the mass spectra and to Chinoin Pharmaceutical Company for the biological screening and for financial support.

REFERENCES

[1] ADAMS, S. S., COBB, R., in Progress in Medicinal Chemistry (Edited by G. P. Ellis and G. B. West), Vol. 5, Butterworths, p. 93. London, 1967
[2] HEPWORTH, W., THOMPSON, W. TH. (Imperiai Chem. Industries Ltd.): Brit 1,121,922 (July 31, 1968); Chem. Abstr. **69,** P 77274z (1968); Brit. Amended 1,121,922 (Aug. 14, 1969); Chem. Abstr. **75,** P 151831w (1971)
[3] BROWN, K., NEWBERRY, R. A.: Brit. 1,373,352 (April 28, 1971); Chem. Abstr. **82,** 112056x (1975)
[4] RAINER, G., RIEDEL, R., KLEMM, K. (Byk-Gulden Lomberg Chem. Fabrik G. m. b. H.): Ger. Offen. 1,946, 370 (April 22, 1971); Chem. Abstr. **75,** 49072n (1971)
[5] ABIGUENTE, E., ARENA, F., DECAPRARIIS, P., PARENTE, L.: Farm. Ed. Sci. **30,** 915 (1975)
[6] DUNNEL, D. W., EVANS, D., HICKS, T. A.: J. Med. Chem. **18,** 1158 (1975)
[7] KATO, Y., ARINA, N., NISHIMINE, H.: J. Pharm. Soc. Japan **96,** 819 (1976)
[8] DOMÁNY, GY., NYITRAI, J., SIMIG, GY., LEMPERT, K.: Tetrahedron Letters **1977,** 1393
[9] GARSIDE, S., HARTLEY, D., LUNTS, L. H. C., OXFORD, A. W. (Allen and Hanburys Ltd.): Ger. Offen. 2,255,172 (May 24, 1973; Brit. Appl. 53750/71, Nov. 19, 1971); Chem. Abstr. **79,** 53376q (1973)
[10] MAUDET, D., GRANET, R., PIEKARSKI, S.: Bull. soc. chim. France **1975,** 2696
[11] UCHYTILOVÁ, V., FIEDLER, P., PRYSTAŠ, M., GUT, J.: Coll. Czechoslov. Chem. Commun. **36,** 1955 (1971)
[12] TAYLOR, E. C., MARTIN, S. F.: J. Org. Chem. **37,** 3958 (1972)
[13] BRUGGER, M., WAMHOFF, H., KORTE, F.: Liebigs Ann. Chem. **758,** 173 (1972)
[14] COX, R. F. B., MCELVAIN, S. M.: Org. Synth., Coll. Vol. II, p. 272. John Wiley and Sons, Inc., New York, London, 1943
[15] BREDERECK, H., THEILIG, G.: Chem. Ber. **86,** 88 (1953)
[16] BREDERECK, H., GOMPPER, R., MAYER, D.: Chem. Ber. **92,** 338 (1959)
[17] NOVELLI, A.: Anales asoc. quím. argentina **27,** 161 (1939); Chem. Abstr. **34,** 1660[1] (1940)
[18] SHEVCHENKO, V. I., KORNUTA, P. P., KURSANOV, A. V.: Zh. Obshch. Khim. **35,** 1598 (1965)
[19] HATCH, M. J., CRAM, D. J.: J. Am. Chem. Soc. **75,** 38 (1953)
[20] DREFAHL, G., HARTMANN, M.: Liebigs Ann. Chem. **589,** 82 (1954)

József NYITRAI, H-1111 Budapest, Gellért tér 4.
György DOMÁNY, H-1045 Budapest, Tó u. 1 – 5.
Gyula SIMIG
József FETTER
Károly ZAUER
Károly LEMPERT
H-1111 Budapest, Gellért tér 4.

INDEX

ANALYTICAL CHEMISTRY

PHYSICAL AND INORGANIC CHAMISTRY

ORGANIC CHEMISTRY

Printed in Hungary

A kiadásért felel az Akadémiai Kiadó igazgatója. Műszaki szerkesztő: Zacsik Annamária

A kézirat nyomdába érkezett: 1978. I. 19. — Terjedelem: 9,45 (A/5) ív, 65 ábra (6 színes)

78.5408 Akadémiai Nyomda, Budapest — Felelős vezető: Bernát György

ACTA CHIMICA

ТОМ 97 – ВЫП. 1

РЕЗЮМЕ

Некоторые химические реакции в электродной щели и их роль в спектрохимическом анализе, XXV

Поведение окислов металлов в дуге с неподвижной атмосферой аргона. Роль реактивности окислов металлов и времени горения дуги в случае подсобных электродов RW II

З. Л. САБО и Х. ДОБОЛИНЕ-ФЕЙЕРДИ

Роль реакционной способности окислов металлов была обнаружена в измерениях, проведенных с углеродными порошковыми смесями двадцати различных окислов металлов. Для теплот образования окислов, отнесенных на один атом кислорода, меньших — 50 ккал, наблюдается скачок в скорости реакции. Это значение сравнимо с теплотой образования CO_2, равной — 48 ккал/моль. При данной сила тока степень протекания реакции зависит от количества чистого металла, образующегося в реакции, т. к. именно последний является передатчиком тепла во внутрь материала. Особенно хорошо можно сравнивать различные окисли одного металла переменной валентности.

Согласно данным измерений, снятых в зависимости от времени горения, реакция протекает — в зависимости от силы тока — в некоторые первые секунды, когда электрод достаточно разогревается. Таким образом, эффект усиления испарения за счет теплоты реакции проявляется на первой стадии. Важнейшим фактором в установлении температурных условий, необходимых для протекания реакции, является отношение скоростей процессов нагрева и охлаждения.

Некоторые химические реакции в электродной щели и их роль в спектрохимическом анализе, XXVI

Поведение окислов металлов в дуге с неподвижной атмосферой аргона. Роль отношения окисла металла к угольному порошку в случае подсобных электродов RW II

З. Л. САБО и Э. ДОБОЛИНЕ-ФЕЙЕРДИ

В углеродных порошковых смесях химически более активных окислов металлов под влиянием дуги образуются CO и CO_2 параллельных реакциях. Их количество является наибольшим при атомном отношении углерода и кислорода, связанного в окисле металла, равном 1 : 1. Тепло; выделяющееся в реакции, нагревает, а чистый металл, одновременно образующийся в каналях электрода, охлаждает исследуемый порошковый образец вслед-

ствие теплопередачи. В зависимости от количества окислов углерода, попадающих в плазму, значительно изменяется само состояние плазмы. Результат этих трех процессов определяет интенсивность спектральных линий.

Некоторые химические реакции в электродной щели и их роль в спектрохимическом анализе, XXVII

Поведение окислов металлов в дуге с атмосферой проточного аргона. Роль скорости потока газа в случае подхобных электродов RW II

З. Л. САБО и Х. ДОБОЛИ-ФЕЙЕРДИ

При исследовании смеси CuO + C было найдено, что за счет протока аргона в газовой атмосфере увеличивается количество CO_2, образующегося в дуге, и уменьшается количество CO. Проточный газ удаляет окислы углерода с мест взаимных превращений, поэтому уменьшается вероятность реакции $CO_2 + C$-2 CO. Эта реакция, в основном протекает в плазмовой фазе. Основная часть окислов углерода образуется в каналах электродов-носителей в реакции компонентов порошковой смеси. Проточный газ слегка увеличивает возможности всех протекающих реакций и особенно при анодном возбуждении изменяет интенсивность спектральных линий.

Масс-спектрометрические исследования некоторых семихинонов

П. МАК и Й. ТАМАШ

Была исследована фрагментация 8 простых семихинонов под влиянием электронной бомбардировки с помощью масс-спектрометрии с высоком и низким разрешением. Было установлено, что наиболее часто процессы разложения приводят к переходу от семихиноидальной структуры к наиболее стабильной хиноидальной структуре.

В фрагментации отдельных соединений наблюдается значительный орто-эффект, а также была обнаружена миграция метильной группы.

Влияние ионной силы на стабильность комплексов типа внешней сферы

Л. ИЛЬЧЕВА и М. БЕК

Стабильность комплексно типа внешней сферы для трис-(дипиридил)кобальта(III) и трис(фенантролин)кобальта(III) с тиоцианатными и иодидными ионами была определена в зависимости от ионной силы. Фтористый калий оказался подходящим инертным электролитом. Константа стабильности изменяется в зависимости от ионной силы согласно кривой с минимумом. Это можно интерпретировать на основе изменения коэффициентов активности с ионной силой.

Применение параметрического метода к колеблющимися частицам третьего порядка, используя изотопные параметры

Силовые постоянные частиц E для CH_3F

С. Е. ХЕЛАМ и Г. АРУЛДАС

Параметрический метод был использован для расчета силовых постоянных фтористого метила (частицы E третьего порядка). Три фундаментальные — две дзета и одна изотопная — частоты были использованы в качестве исходных данных. Было получено два набора силовых постоянных. Один из них, который точно воспроизводит другие изотопные частоты, был выбран как истинный набор.

Гравиметрическое исследование адсорбции н-бутана на катализаторе Ni-черни

А. ШАРКАНЬ и П. ТЕТЕНИ

Адсорбция н-бутана и смесей и-бутана с водородом была исследована гравиметрических на катализаторе Ni-черни в интервале температур 20–200°С. Помимо физической адсорбции;были обнаружены различные формы хемосорбции: хемосорбция н-бутана, приводящая к образованию дисоциативно адсорбированного н-бутана, к его фрагментам выше 88°С, а также к форме с низкой реакционной способностью по отношению к водороду. Сравнение скорости гидрогенолиза со скоростью гидрирования хемосорбированного субстрата позволяет заключить, что последняя форма имеет эффект отравителя гидрогенолиза.

Расщепление гетероциклического кольца изофлавоноидов с помощью нуклеофильных реагентов, V

Реакция изофлавона с гидроксиламином и трансформация кольца в 4-гидрокси-3-фенилкумарин

В. САБО, Й. БОРДА и Л. ЛОШОНЦИ

Описывается реакция изофлавона с гидросиамином и трансформация кольца.

При взаимодействии изофлавона с гидроксиламином в интервале pH от 4 до 11, с возрастающей скорость образуется 4-фенил-5-(2'-гидроксифенил)-изоксанол (I). Т. о., нуклеофильный реагент атакует атом C_2 и γ-пироновое кольцо изофлавона раскрывается. В этих условиях изофлавон не дает нормальной карбонильной реакции с гидроксиламином.

Соединение 1 весьма стабильно в кислой среде, а в щелочной среде изоксазольное кольцо раскрывается и образуется нитрил 2-(2'-гидроксибензоил)- фенилуксусной кислоты (V). Это превращение подтверждает как структуру соединения I, так и направлени превращения изофлавона.

Соединение V, в зависимости от pH, находится в таутомерном равновесии кольцоцель с 4-гидрокси-3-фенилкумаринимином (VIII). Соединение VIII, за счет кислого кипячения, может быть превращено в 4-гидрокси-3-фенилкумарин (IX). С помощью этой ступени была осуществлена трансформация хромон → 4-гидроксикумарин по пути изофлавон → → I → V → VIII → IX.

Оксазепины и тиазепины, IV

Синтез производных 2,3-дигидро-2-фенил-1,4-оксазепина

А. ЛЕВАИ и Р. БОГНАР

Из флавонов по реакции Шмидта были получены 2,3-дигидро-2-фенил-1,4-бензоксазепин-5(4*H*)-оны (V–VIII), которые при обработке их P_2S_5 дают соответствующие тионы (IX–XII). Из соединения V были приготовлены его N-ацилированные и N-алкилированные производные (XIII–XIX).

Проблемы гидрирования 2-этилантрахинона

Б. ЛОШОНЦИ, А. ЛЕНДЬЕЛ-МЕСАРОШ, М. НОВАК-КИШ, И. МОРГОШ и И. ПЕТРО

Экспериментально было обнаружено, что при восстановлении 2-этилантрохинона реакция остановливается после расхода водорода, равного 3 молям на моль субстрата. Продуктом реакции является 2-этил-5,6,7,8-тетрагидроантрахинон. Этильная группа

«возвычается» из плоскости ароматических колец и, таким образом, экранирует ароматическое кольцо, содержащее алильную группу, препятствуя последнему в достаточном приближении к поверхности катализатора, и тем самым гидрированию последнего.

Пропионовая кислота и ее производные, замещенные некоторыми гетероциклическими группами в положении 2

Й. НИТРАИ, ДЬ. ДОМАНИ, ДЬ. ШИМИГ, Й. ФЕТТЕР, У. ЦАУЭР и К. ЛЕМПЕРТ

Был синтезирован ряд этилпропионатов, замещенных в положении 2 неароматическими *асим*-триазиновым (*1a—1g*, *2a—2c*), ароматическим *асим*-триазиновым (*8a—8h*), ароматическим имидазольным (*10a*, *10c*, *10e*, *12c*) и ароматическим 1,2,3-тиадиазольным (*13a*) кольцами, ряд пропионамидов, замещенных в положении 2 ароматическими имидазольным кольцом (*12a*, *12d*, *12f*, *12h*), а также ряд пропионовых кислот, замещенных в положении 2 ароматическим имидазольным (*10b*, *10d*, *10f*, *12b*, *12e*, *12g*, *12i*) и ароматическим 1,2,3-тиадиазольным *(13b)* кольпами. Конденсация диэтил 2-метил-3- оксосукцината со всеми полученными бензамидразонами приводит к образованию двух изомерных производных *асим*-триазинона (*1e* и *2a*, *1f* и *2b*, а также *1g* и *2c*); это первые наблюдаемые случаи, когда при конденсации α-оксоэфиров и амидразонов образуются два изомера *асим*-триазинона. Неароматические *асим*-триазиновые кольца соединений *1d—1g* ароматизировали различными методами (с образованием промежуточных соединений *8a—8h*), а *асим*-триазиновое кольцо соединений *2a—2c* не удалось ароматизировать. Соединения *1f* и *12g*. HCl обладают значительным противоопухольным эффектом.

SYNTHESIS of PROSTAGLANDINS

By Cs. Szántay and L. Novák

Recent Developments in the Chemistry of Natural Carbon Compounds, Vol. 8.

The prostaglandins, this new family of naturally occuring fatty acids, are a most exciting group of extraordinary potent biologically active compounds to appear on the medical scientific scene during the past decade. Within the diverse biological effects of prostaglandins the control of uterin contraction and labor induction are most promising.

Now to meet the need for both an up-to-date monograph and comprehensive survey of new experimental methods, this book – first in this field – has centered on the synthesis of prostaglandins and prostaglandin analogs. It is designed to instruct and direct a practising organic chemist in the choise of design new compounds and experimental techniques.

In English – Approx. 80 pages – 17 × 25 cm – Cloth

ISBN 963 05 0702 I (of the whole series)

ISBN 963 05 1303 X (of the 8th volume)

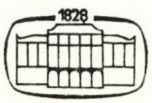

Akadémiai Kiadó

Publishing House of the Hungarian Academy of Sciences

Budapest

Distributors: KULTÚRA, H-1389 Budapest, P.O.B. 149

Les Acta Chimica paraissent en français, allemand, anglais et russe et publient des mémoires du domaine des sciences chimiques.

Les Acta Chimica sont publiés sous forme de fascicules. Quatre fascicules seront réunis en un volume (4 volumes par an).

On est prié d'envoyer les manuscrits destinés à la rédaction à l'adresse suivante:

Acta Chimica
H-1521 Budapest, Hongrie

Toute correspondance doit être envoyée à cette même adresse.

La rédaction ne rend pas de manuscript.

Le prix de l'abonnement: $ 36,00 par volume.

Abonnement en Hongrie à l'Akadémiai Kiadó (1363 Budapest, P. O. B. 24, C. C. B. 215 11488), à l'étranger à l'Entreprise du Commerce Extérieur «Kultura» (H-1389 Budapest 62, P. O. B. 149 Compte-courant No. 218 10990) ou chez représentants à l'étranger.

Die Acta Chimica veröffentlichen Abhandlungen aus dem Bereich der chemischen Wissenschaften in deutscher, englischer, französischer und russischer Sprache.

Die Acta Chimica erscheinen in Heften wechselnden Umfanges. Vier Hefte bilden einen Band. Jährlich erscheinen 4 Bände.

Die zur Veröffentlichung bestimmten Manuskripte sind an folgende Adresse zu senden:

Acta Chimica
H-1521 Budapest, Ungarn

An die gleiche Anschrift ist jede für die Redaktion bestimmte Korrespondenz zu richten.

Manuskripte werden nicht zurückerstattet.

Abonnementspreis pro Band: $ 36,00.

Bestellbar für das Inland bei Akadémiai Kiadó (1363 Budapest, Postfach 24, Bankkonto Nr. 215 11488), für das Ausland bei »Kultura« Außenhandelsunternehmen (H-1389 Budapest 62, P. O. B. 149. Bankkonto Nr. 218 10990) oder seinen Auslandsvertretungen.

«Acta Chimica» издают статьи по химии на русском, английском, французском и немецком языках.

«Acta Chimica» выходит отдельными выпусками разного объекта, 4 выпуска составляют один тдм и за год выходят 4 тома.

Предназначенные для публикации рукописи следует направлять по адресу:

Acta Chimica
H-1521 Budapest, BHP

Всякую корреспонденцию в редакцию направляйте по этому же адресу.

Редакция рукописей не возвращает.

Подписная цена — $ 36,00 за том.

Отечественные подписчики направляйте свои заявки по адресу Издательства Академии Наук (1363 Budapest, P. O. B. 24, Текущий счет 215 11488), а иностранные подписчики через организацию по внешней торговле «Kultura» (H-1389 Budapest 62, P. O. B. 149. Текущий счет 218 10990) или через ее заграничные представительства и уполномеченных.

Reviews of the Hungarian Academy of Sciences are obtainable at the following addresses:

AUSTRALIA
C.B.D. LIBRARY AND SUBSCRIPTION SERVICE, Box 4886, G.P.O., *Sydney N.S.W. 2001*
COSMOS BOOKSHOP, 135 Ackland Street, *St. Kilda (Melbourne), Victoria 3182*

AUSTRIA
GLOBUS, Höchstädtplatz 3, *1200 Wien XX*

BELGIUM
OFFICE INTERNATIONAL DE LIBRAIRIE, 30 Avenue Marnix, *1050 Bruxelles*
LIBRAIRE DU MONDE ENTIER, 162 Rue du Midi, *1000 Bruxelles*

BULGARIA
HEMUS, Bu.var Ruszki 6, *Sofia*

CANADA
PANNONIA BOOKS, P.O. Box 1017, Postal Station "B", *Toronto, Ontario M5T 2T8*

CHINA
CNPICOR, Periodical Department, P.O. Box 50, *Peking*

CZECHOSLOVAKIA
MAD'ARSKÁ KULTURA, Národní třida 22 *115 66 Praha*
PNS DOVOZ TISKU, Vinohradská 46, *Praha 2*
PNS DOVOZ TLAČE, *Bratislava 2*

DENMARK
EJNAR MUNKSGAARD, Norregade 6, *1165 Copenhagen*

FINLAND
AKATEEMINEN KIRJAKAUPPA, P.O. Box 128, *SF-00101 Helsinki 10*

FRANCE
EUROPERIODIQUES S. A. 31 Avenue de Versailles, *78170 La Celle St. Cloud*
LIBRAIRIE LAVOISIER, 11 rue Lavoisier, *75008 Paris*
OFFICE INTERNATIONAL DE DOCUMENTATION ET LIBRAIRIE, 48 rue Gay-Lussac *75240 Paris Cedex 05*

GERMAN DEMOCRATIC REPUBLIC
HAUS DER UNGARISCHEN KULTUR, Karl Liebknecht-Strasse 9, *DDR-102 Berlin*
DEUTSCHE POST ZEITUNGSVERTRIEBSAMT, Strasse der Pariser Kommüne 3—4, *DDR-104 Berlin*

GERMAN FEDERAL REPUBLIC
KUNST UND WISSEN ERICH BIEBER, Postfach 46, *7000 Stuttgart 1*

GREAT BRITAIN
BLACKWELL'S PERIODICALS DIVISION, Hythe Bridge Street, *Oxford OX1 2ET*
BUMPUS, HALDANE AND MAXWELL LTD., Cowper Works, *Olney, Bucks MK46 4BN*
COLLET'S HOLDINGS LTD., Denington Estate, *Wellingborough, Northants NN8 2QT*
W.M. DAWSON AND SONS LTD., Cannon House, *Folkes-one, Kent CT19 5EE*
H. K. LEWIS AND CO., 146 Gower Street, *London WC1E 6BS*

GREECE
KOSTARAKIS BROTHERS, International Booksellers, 2 Hippokratous Street *Athens-143*

HOLLAND
MEULENHOFF-BRUNA B.V., Beulingstraat 2, *Amsterdam*
MARTINUS NIJHOFF B.V., Lange Voorhout 9—11, *Den Haag*
SWETS SUBSCRIPTION SERVICE, 347b Heereweg *Lisse*

INDIA
ALLIED PUBLISHING PRIVATE LTD., 13/14 Asaf Ali Road, *New Delhi 110001*
150 B-6 Mount Road, *Madras 600002*
INTERNATIONAL BOOK HOUSE PVT. LTD., Madame Cama Road, *Bombay 400039*
THE STATE TRADING CORPORATION OF INDIA LTD., Books Import Division, Chandralok 36 Janpath, *New Delhi 110001*

ITALY
EUGENIO CARLUCCI, P.O. Box 252, *70100 Bari*
INTERSCIENTIA, Via Mazzé 28, *10149 Torino*
LIBRERIA COMMISSIONARIA SANSONI, Via Lamarmora 35, *50121 Firenze*
SANTO VANASIA, Via M. Macchi 58, *20124 Milano*
D. E. A., Via Lima 28, *00198 Roma*

JAPAN
KINOKUNIYA BOOK-STORE CO. LTD., 17-7 Shinjuku-ku 3 chome, Shinjuku-ku, *Tokyo 160-91*
MARUZEN COMPANY LTD., Book Department, P.O. Box 5056 Tokyo International, *Tokyo 100-31*
NAUKA LTD., IMPORT DEPARTMENT, 2-30-19 Minami Ikebukuro, Toshima-ku *Tokyo 171*

KOREA
CHULPANMUL, *Phenjan*

NORWAY
TANUM-CAMMERMEYER, Karl Johansgatan 41—43, *1000 Oslo*

POLAND
WĘGIERSÓI INSTYTUT KULTURY, Marszałkowska 80, *Warszawa*
CKP I W ul. Towarowa 28 *00-958 Warsaw*

ROMANIA
D. E. P., *Bucureşti*
ROMLIBRI Str. Biserica Amzei 7, *Bucureşti*

SOVIET UNION
SOJUZPETCHATJ — IMPORT, *Moscow*
and the post offices in each town
MEZHDUNARODNAYA KNIGA, *Moscow G-200*

SPAIN
DIAZ DE SANTOS, Lagasca 95, *Madrid 3*

SWEDEN
ALMQVIST AND WIKSELL, Gamla Brogatan 26, *101 20 Stockholm*
GUMPERTS UNIVERSITETSBOKHANDEL AB, Box 436 *401 25 Göteborg 1*

SWITZERLAND
KARGER LIBRI AG, Petersgraben 41, *4011 Basel*

USA
EBSCO SUBSCRIPTION SERVICES, P.O. Box 1943, *Birmingham, Alabama 35201*
F. W. FAXON COMPANY, INC., 15 Southwest Park, *Westwood, Mass, 02090*
THE MOORE-COTTRELL SUBSCRIPTION AGENCIES, *North Cohoc-on, N. Y. 14868*
READ-MORE PUBLICATIONS, INC., 140 Cedar Street, *New York, N. .Y. 10006*
STECHERT-MACMILLAN, INC., 7250 Westfield Avenue, *Pennsauken* N.J. 08110

VIETNAM
XUNHASABA, 42, Hai Ba Trung, *Hanoi*

YUGOSLAVIA
JUGOSLAVENSKA KNJIGA, Terazije 27, *Beograd*
FORUM, Vojvode Mišiča 1, *21000 Novi Sad*

10. VII. 1978 HU ISSN 0001—5407 Index: 26.007

ACTA CHIMICA

ACADEMIAE SCIENTIARUM HUNGARICAE

TOMUS 97 FASCICULUS 2

AKADÉMIAI KIADÓ, BUDAPEST

1978

ACTA CHIM. ACAD. SCI. HUNG. ACASA2 97 (2) 105—253 (1978)

ACTA CHIMICA

A MAGYAR TUDOMÁNYOS AKADÉMIA KÉMIAI TUDOMÁNYOK OSZTÁLYÁNAK IDEGEN NYELVŰ KÖZLEMÉNYEI

Acta Chimica is a journal for the publication of papers on all aspects of chemistry, in the English, German, French and Russian languages.

Acta Chimica is published in 4 volumes per year. Each volume consists of 4 issues of varying size.

Manuscripts should be sent to

Acta Chimica
H-1521 Budapest, Hungary

Correspondence with the Editors should be sent to the same address. Manuscripts are not returned to the Authors.

Subscription rate $ 36.00 per volume.

Hungarian subscribers should order from Akadémiai Kiadó, 1363 Budapest, P.O. Box 24. Account No. 215 11488.

Orders from other countries are to be sent to "Kultúra" Foreign Trade Company (H-1389 Budapest 62, P.O. Box 149. Account No. 218 10990) or to its representatives abroad.

Acta Chimica Academiae Scientiarum Hungaricae, Tomus 97 (2), pp. 105–110 (1978)

EINE VARIANTE DER EXTRAKTIONSFOTOMETRISCHEN ZIRKONBESTIMMUNG MIT ARSENAZO III

V. K. AKIMOV, L. T. GVELESIANI, A. I. BUSEV und P. NENNING

(Lomonossov-Universität Moskau und Karl-Marx-Universität Leipzig)

Eingegangen am 23 November, 1976

Zirkon wird aus schwefelsaurer Lösung nach Zugabe von KSCN und Antipyrin mit Dichloräthan extrahiert. Nach der Reextraktion wird das Zirkon als Arsenazokomplex spektrofotometrisch bestimmt.

Pyrazolonderivate werden häufig zur gravimetrischen, extraktionsfotometrischen Bestimmung und zur extraktiven Abtrennung einer Vielzahl Elemente verwendet [1, 2], denn sie bilden ziemlich stabile acidokomplexe Anionen. Untersucht wurde schon die Komplexbildung des Zirkons mit Diantipyrilmethan und seinen Homologen in Chlorid-, Jodid-, Rhodanid- und Nitratsystemen sowie die Extraktion der sich bildenden Komplexe [3–9].

Aktuelle Bedeutung hat die Ausarbeitung einfacher Methoden der Elementbestimmung, darunter des Zirkons, nach ihrer extraktiven Abtrennung von anderen Elementen. Unter diesem Gesichtspunkt wird die Möglichkeit einer fotometrischen Bestimmung des Zirkons unter Verwendung von Arsenazo III nach Extraktion des Zr als Rhodanidkomplex mit Pyrazolonderivaten untersucht. Arsenazo III wird ausgewählt, weil es das empfindlichste Zirkonreagenz ist. Die Extraktion der Komplexe des Zirkonrhodanids mit verschiedenen Pyrazolonderivaten wird zwecks Auswahl optimaler Extraktionsbedingungen detaillierter untersucht.

Experimenteller Teil

Reagenzien und Geräte. Antipyrin der Reinheit DAB, Diantipyrilmethan p. a., Diantipyrilmethylmethan p. a., Diantipyrilpropylmethan p. a., Diantipyrilphenylmethan p. a. werden verwendet. Zum Herstellen einer Zirkonlösung wird $ZrOCl_2$ in 2 *M* HCl gelöst und mit HCl auf 1 l aufgefüllt. Titerbestimmung gravimetrisch nach Hydroxidfällung als $ZrOCl_2$. Gehalt der Lösung 1 mg/ml Zr. Zur Untersuchung der Zirkonextraktion verwenden wir eine Lösung, die das

Isotop Zr^{97} in einer Konzentration von 1 mg/l enthält. Gemessen wird am Spektrofotometer SF-4 A, am UMF-1500 M, mit dem Zähler PP-16.

Extraktion des Zirkonrhodanidkomplexes. Als Einflußgrößen auf die Extrahierbarkeit des Zirkons werden die Art des Lösungsmittels und des Reagenzes sowie die Konzentration an Säure, an Reagenz und an Rhodanidionen untersucht. Zunächst wird 1 ml Zirkonlösung, die das Isotop Zr^{97} enthält, in einen Kolben gegeben, H_2SO_4 und KSCN zugegeben und mit Wasser auf 10 ml aufgefüllt. Die Lösung wird 1 min mit 10 ml einer Lösung eines Pyrazolonderivates in einem entsprechenden Lösungsmittel (z. B. Butanol, Dichloräthan) geschüttelt. Nach der Phasentrennung wird von jeder Phase 1 ml entnommen und die β-Aktivität gemessen. Die so ermittelten Verteilungskoeffizienten (E) und % Extraktion (R) sind in Tabelle I dargestellt. Zur Extraktion der Komplexe des Zirkonrhodanids mit Pyrazolonderivaten ist Dichloräthan besonders geeignet, als Komplexbildner sind Antipyrin (Ant), Diantipyrilmethylmethan (DAMM) und Diantipyrilpropylmethan (DAPM) zu bevorzugen.

Tabelle I

Extraktion der Zirkonrhodanidkomplexe mit Pyrazolonderivaten unter Verwendung von Butanol und Dichloräthan

Reagenz	Extraktionsmittel			
	C_4H_9OH		$Cl-CH_2-CH_2-Cl$	
	E	R %	E	R %
Antipyrin	0,57	36,0	86,0	98,8
Diantipyrilmethan	0,6	37,5	1,2	54,5
Diantipyrilmethylmethan	3,3	76,7	8,9	90,0
Diantipyrilpropylmethan	1,1	52,6	1,5	60,0
Diantipyrilphenylmethan	0,4	28,5	–	–

Der Einfluß der H_2SO_4- und der KSCN- sowie der Reagenzkonzentration auf die Extraktion des Zr wird am Beispiel der Extraktion des besonders stabilen Zirkon-DAPM-rhodanidkomplexes mit Butanol ermittelt. Es zeigt sich (Abb. 1–3), daß Konzentrationen von 1,5 *M* KSCN, 0,2–0,3 *N* H_2SO_4 und ein 50–75-facher Reagenzüberschuß optimal sind.

Aus den experimentellen Ergebnissen folgt: von den Pyrazolonderivaten ist Antipyrin besonders geeignet, von den organischen Lösungsmitteln Dichloräthan (R = 98,8 %). Der entstehende Rhodanidkomplex des Zirkons mit Antipyrin ist weniger beständig als der Zirkon-Arsenazo-Komplex und kann

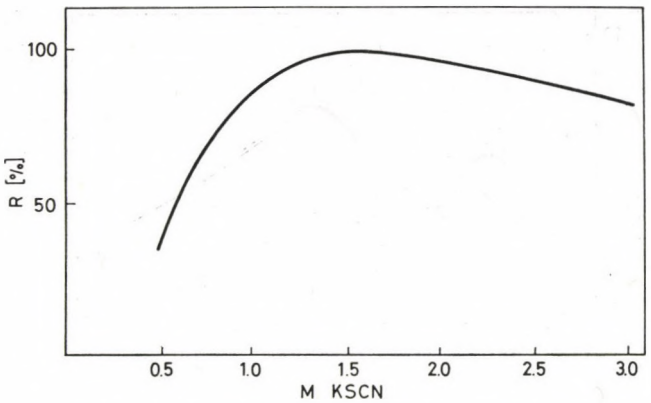

Abb. 1. Einfluß der H_2SO_4-Konzentration auf die Zirkonextraktion mit Butanol (1 *M* KSCN, 50-facher Überschuß Diantipyrilpropylmethan)

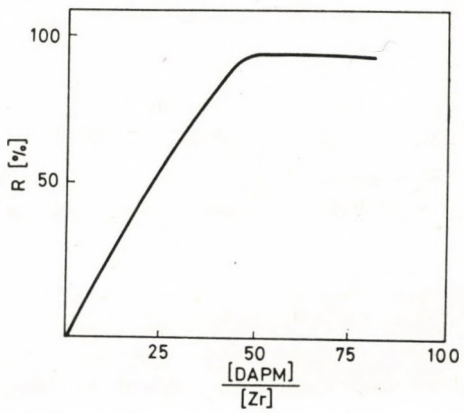

Abb. 2. Einfluß der KSCN-Konzentration auf die Zirkonextraktion mit Butanol (0,3 *N* H_2SO_4, 50-facher Überschuß Diantipyrilpropylmethan)

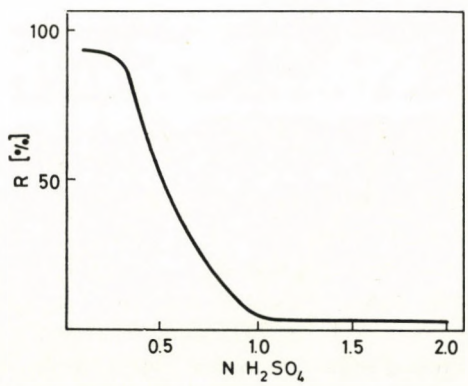

Abb. 3. Einfluß des Diantipyrilpropylmethanüberschusses auf die Zirkonextraktion mit Butanol (0,3 *N* H_2SO_4, 1,5 *M* KSCN)

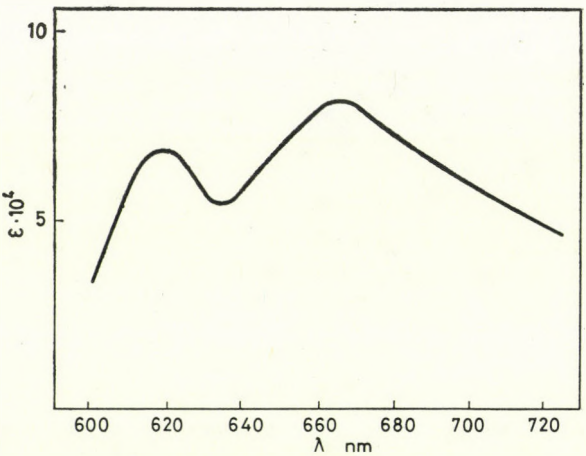

Abb. 4. Absorptionsspektrum des Zirkonkomplexes mit Arsenazo III

leicht in diesen übergeführt werden. So ist eine extraktionsfotometrische Zirkonbestimmung mit Arsenazo möglich. Das Spektrum des sich bildenden Komplexes hat ein Maximum bei $\lambda = 665$ nm, $\varepsilon = 8{,}0 \cdot 10^4 \pm 0{,}1 \cdot 10^4$). (Abb. 4). Das Lambert–Beersche Gesetz gilt für 0,1–0,5 μg/ml Zr.

Arbeitsvorschrift. Ein aliquoter Teil einer Lösung mit einem Zirkongehalt von von 5,0–20,0 μg Zr wird in einen Scheidetrichter gegeben, 1 ml 1,5 *M* H_2SO_4 und 5 ml 30 %ige KSCN-Lösung zugesetzt und mit Wasser auf 10 ml verdünnt. 10 ml einer 1,5 %igen Antipyrinlösung in Dichloräthan werden zugefügt und es wird ca 1 min geschüttelt. Nach der Phasentrennung wird die organische Phase mit 10 ml Wasser ausgeschüttelt. Die wäßrige Phase wird in einen 50-ml-Maßkolben überführt. Jetzt wird die organische Phase mit 20 ml conc. HCl ausgeschüttelt, diese wird mit der wäßrigen Phase vereinigt. Zur erhaltenen Lösung werden 4 ml 0,05 %ige Arsenazo-III-Lösung gegeben und mit conc. HCl aufgefüllt. Die Extinktion wird nach 20–30 min am Spektrofotometer SF-4 A bei $\lambda_{max} = 665$ nm in einer 1-cm-Küvette gegen ein Leerprobe gemessen.

Statistische Werte ($\alpha = 0{,}95$; $n = 5$): arithmetisches Mittel $\bar{x} = 19{,}0$; mittlere quadratische Abweichung vom arithmetischen Mittel $S = 0{,}35$; Vertrauensintervall $\varepsilon = 0{,}43$; Variationskoeffizient $V = 1{,}86$ %.

Die Bestimmung von 0,1–0,5 μg/ml Zr wird nicht gestört von Alkalimetallen und von Seltenen Erden, von anderen Elementen nicht bis zu den in Tabelle II angegebenen Konzentrationen. Hf stört. – Die extraktionsfotometrische Variante der Zirkonbestimmung mit Arsenazo III ist – wie die Tabelle zeigt – selektiver als die in der Literatur beschriebene direktfotometrische Bestimmung.

Tabelle II

Zirkonbestimmung in Anwesenheit von Fremdionen (eingesetzt: 20,0 µg Zr)

Fremdion	Verhältnis Zr : Fremdion	Fehler in %	Fremdion	Verhältnis Zr : Fremdion	Fehler in %
Cu	1 : 35	0,0	As(V)	1 : 3	−11,0
Mn(II)	1 : 40	0,0	Cd	1 : 10	0,0
Ti(IV)	1 : 10	−11,0	Pb	1 : 1	−11,0
Th	1 : 10	0,0	Co	1 : 200	0,0
Al	1 : 35	+5,0	Cr(VI)	1 : 10	−11,0
U(VI)	1 : 1	0,0	Zn	1 : 35	0,0
V(V)	1 : 10	−11,0	Ni	1 : 35	0,0
Fe(III)	1 : 20	−5,0			
Mo(VI)	1 : 10	+2,0			

Die oben beschriebene Methode wurde erprobt an Zirkonbestimmungen in Aluminium- und Magnesiumlegierungen. Dazu wird eine Einwaage von 0,1 − 0,25 g Legierung in 10 − 15 ml 6 *M* HCl gelöst, in einen 50-ml-Kolben überführt, aufgefüllt und wie beschrieben verfahren. Die Ergebnisse zeigt Tabelle III.

Tabelle III

Zirkonbestimmung in Al–Mg-Legierungen (Standards für die Spektralanalyse)

Bezeichnung der Legierung	Zirkongehalt in %	Zirkon gefunden in %	Relativer Fehler in%
121	0,084	0,086	+2,3
122	0,040	0,039	−2,5
123	0,015	0,016	+6,2
124	0,030	0,028	−7,1
125	0,032	0,030	−6,6
126	0,028	0,031	+9,6
101	0,79	0,74	−6,7
102	0,54	0,50	−8,0

LITERATUR

[1] Akimov, V. K., Busev, A. I.: J. analit. chim. (russ.) **26,** 964 (1971)
[2] Busev, A. I., Akimov, V. K., Gusev, S. I.: Uspechi chimii **34,** 565 (1965)
[3] Babko, A. K., Schtokalo, M. I.: J. anorg. chem. (russ.) **8,** 1088 (1963)
[4] Babko, A. K., Schtokalo, M. I.: Ukrain. chim. J. (russ.) **28,** 293 (1962)
[5] Babko, A. K., Schtokalo, M. I.: Die Metallindikator-Methode zur Untersuchung von Komplexen in Lösung (russ.) Kiev, Verlag Nauka 1969

[6] SCHTOKALO, M. I., ČERNUCHA, T. S.: Hochschulnachr., Chemie und chem. Technologie (russ.) **15,** 670 (1972)
[7] PETROV, B. I.: Diantipyrilmethan und seine Homologe als analytische Reagenzien, Perm, Wiss. Ber. der Univ. Perm, **324,** 140 (1974)
[8] ZHIVOPISTSEV, V. P., PETROV, B. I.: SIBIRJAKOV, N. F.: Wiss. Ber. der Univ. Perm, **207,** 144 (1970)
[9] PETROV, B. I., ZHIVOPISTSEV, V. P., MAKHNEV, J. A.: J. analit. chim. **28,** 505 (1973)

V. K. AKIMOV
L. T. GVELESIANI
A. I. BUSEV
Lomonossov-Universität Moskau,

Peter NENNING
Karl-Marx-Universität Leipzig, Sektion Chemie,
701 Leipzig Liebigstr. 18. DDR.

Acta Chimica Academiae Scientiarum Hungaricae, Tomus 97 (2), pp. 111—123 (1978)

SOME CHEMICAL REACTIONS OF THE ELECTRODE GAP AND THEIR ROLE IN SPECTROCHEMICAL ANALYSIS, XXVIII

BEHAVIOUR OF METAL OXIDES IN THE ARC IN A FLOWING Ar ATMOSPHERE. ROLES OF THE BURNING TIME AND THE CURRENT OF THE ARC WITH RW II AUXILIARY ELECTRODES

Z. L. SZABÓ

(Department of Inorganic and Analytical Chemistry, Eötvös L. University, Budapest)

H. DOBOLYI-FEJÉRDY

(Hungarian Optical Works, Budapest)

Received January 24, 1977

The study of a CuO + C powder mixture shows that the quantity of oxides of carbon produced in the arc increase with increases in either the burning time or the current of the arc. The ratios of the heating and cooling rates of the electrodes are different in the two cases, however, and therefore the rates of formation of oxides of carbon are also different. This can be well compared if the electric work of the arc in the two cases is plotted versus the product of the time and current. As the reaction proceeds in time, an increasing quantity of metallic copper is formed in the boring of the carrier electrode, and this inhibits further reaction by sealing in the lower layers of the mixture. Accordingly, the proportion of evaporation also decreases in time. From the change of the ratio of the volumes of CO_2 to CO formed it emerged that those oxidation and reduction tendencies of electric origin which control electrode-surface reactions between the gas atmosphere and the material of the electrode are not manifested in the reactions within the material of the electrode.

We earlier studied the reactions occurring in a CuO + C powder mixture as a function of the rate of flow of the Ar gas atmosphere [1]. It was found that this leads to changes in the ratio of the amounts of CO_2 and CO formed during the burning of the arc. The momentary values representing the formation of oxides of carbon are better approximated to by the values measured in a flowing atmosphere, for the flowing gas inhibits interconversion of the two oxides of carbon. For further study of the reactions and their effects, two series of experiments were carried out with RW II carbon auxiliary electrodes, their borings filled with a CuO + C mixture. In one series the burning time of the arc was varied, and in the other the current. The mole fraction of CuO in the CuO + C mixture was 0.6. In this case both oxides of carbon were formed in well-measurable amounts. An A.C. polarized arc initiated at the potential maximum was used. The rate of flow of Ar was 860 cm^3/min. Measurements were made of the changes in the amounts of CO and CO_2 formed as a result of the arc [2], and in the intensities of the spectral lines of the copper. Details of the method were reported earlier [3].

Role of the burning time of the arc

The experiments were carried out with a current of 7 A and the burning time of the arc was varied between 2 and 15 s. Figure 1 shows that the amount of CO formed as a result of the arc increases in accordance with expectations in time on excitation of the sample as either anode (curve *a*) or cathode (curve *c*). The curve relating to cathodic excitation inclines slowly upwards. It appears that on cathodic excitation in the case of a current of 7 A the carrier electrode begins to heat up better only around 15 s, and clearly remains colder

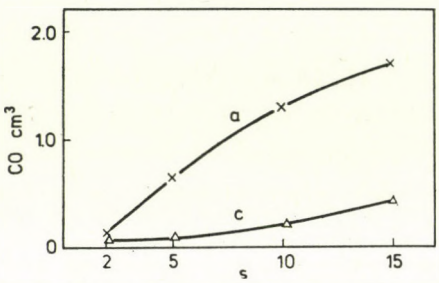

Fig. 1. Change in the quantity of CO produced with the burning time of the arc; 7 A. *a*: anodic, *c*: cathodic excitation

throughout than that connected as anode. As discussed previously, the cathodic curve is always situated below the anodic one. At the same time, the curve obtained with anodic excitation inclines weakly downwards, indicating that the reaction is already inhibited by something when the arc burns for a longer time. The differences from linearity are not large, however, which shows that the site of formation of CO is in the vicinity of the almost constant, high-temperature site of the burning spot of the arc.

Figure 2 illustrates the changes in the volume of CO_2 measured. The values relating to excitation of the sample as cathode (*c*) give a weakly upwards inclining curve, similarly as for CO. At the same time, the curve obtained with anodic excitation (*a*) begins flatly, similarly to the cathodic one, but it suddenly becomes steep and then exhibits a saturation value. It appears that on anodic excitation with a current of 7 A, about 3—4 s is necessary for the larger amount of powder mixture packed into the carrier electrode to heat up sufficiently for the reaction. When this occurs, the bulk of the CO_2 is produced in a fairly brief period (4—8 s). On cathodic excitation, the heating-up of the electrode is delayed longer.

Figure 3 shows the sum (Σ %) of the amounts of material reacted in the two reactions, as a percentage of the theoretically possible maximum reaction, calculated from the quantity of material measured in the boring of the carrier electrode. The Figure reveals that the inclinations of the anodic CO_2 and CO

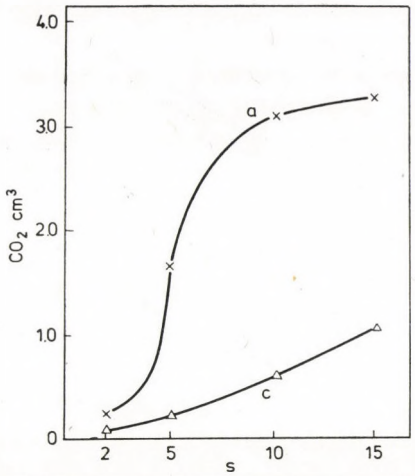

Fig. 2. Change in the quantity of CO_2 produced with the burning time of the arc; 7 A. *a*: anodic, *c*: cathodic excitation

curves to saturation can not be caused by the complete exhaustion of the material from the boring of the electrode, for the value calculated in the above manner does not attain 60 %, even when the arc burns for 15 s. The curves of Fig. 4 indicate that the spilling out of the substance from the boring in the electrode as a result of the arc can occur to only a very slight extent, for there is fairly good agreement between the curves plotted from the measured values of the substance missing from the boring in the electrode after the burning of the arc (continuous line) and from the values calculated from the quantities of oxides of carbon departing (dashed line). The only possibility, therefore, is that the metallic copper formed in the reaction occurring to a certain depth of the boring seals off the lower layers from further reaction. This given depth clearly depends among others on the current of the arc. That part of the carrier

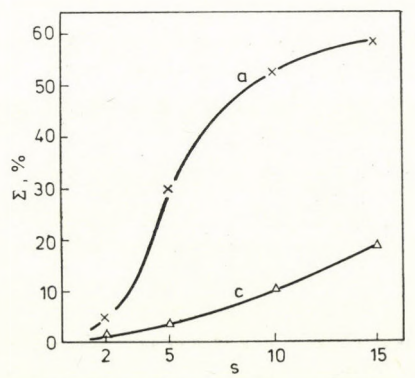

Fig. 3. Combined percentage evaluation of the reactions producing the two oxides of carbon; 7 A. *a*: anodic, *c*: cathodic excitation

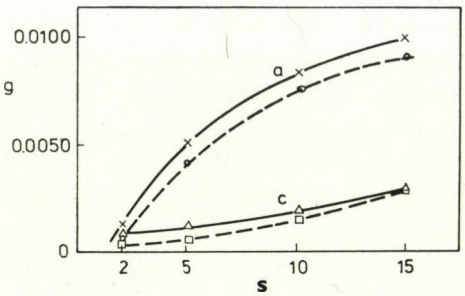

Fig. 4. Change in the quantity of material consumed from the boring of the electrode with the burning time of the arc; 7 A. *a*: anodic, *c*: cathodic excitation. Continuous line: measured values; dashed line; calculated values

electrode including the boring was broken up after the burning of the arc, and it was found that powder mixture did in fact still remain under the metallic copper globule formed, even when the arc had burned for 15 s.

Figure 5 depicts the volume ratios CO_2/CO formed from the above quantities of CO_2 and CO, as a function of the burning time of the arc. The intersecting curves reflect the different temperature conditions developing when the sample is excited under the two types of polarity, and depending on the polarity of the carrier electrode. The change here can hardly be in the oxidizing ability of the system, but only in the rate of increase of temperature of the electrodes. This is indicated by the fact that the maximum in the curve obtained with cathodic excitation can develop only later in time, since the temperature of the cathode rises more slowly. The RW II carbon cathode is always colder than the anode of the same material [4]. The decrease after the maxima, however, shows that the CO is formed in the vicinity of the burning spot of the arc in the upper layer of the electrode, while the CO_2 is produced

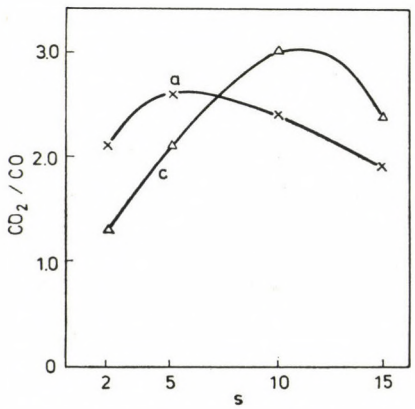

Fig. 5. Change in the volume ratio CO_2/CO with the burning time of the arc; 7 A. *a*: anodic, *c*: cathodic excitation

in the inside of the boring, in the bulkier, but less incandescent mixture. This lower layer is sealed off by the metallic copper formed in the reaction, and therefore the CO_2/CO ratios decrease after a longer time. The oxides of carbon thus have separate zones of formation, the boundaries of which naturally overlap.

The change in time in the intensity ($I_{Cu\ I}$, Cu 282.4 nm) of the previously used atom line of copper is shown in Fig. 6. The change in this value was earlier taken to be proportional to the change in the evaporation of the sample. The two curves obtained with the different electrode polarities of necessity

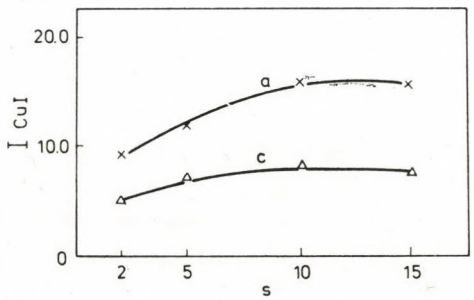

Fig. 6. Change in the intensity of the Cu 282.4 nm atom line with the burning time of the arc; 7 A. *a*: anodic, *c*: cathodic excitation

both rise, but not proportionally with time. The formation of metallic copper and the cooling effect of this in the upper layers of the mixture initially proceed in time as discussed earlier [5] compared to the charge which is still richer in carbon powder.

The data of the spectral character curves ($\Delta Y_{Cu\ II,\ I}$, Cu 237.0/282.4, values multiplied by 100) connected with the average temperature of the plasma scarcely vary in time (Fig. 7). Because of the more extensive reaction occurring in the anode, here too the change is greater in the gas atmosphere. Since a larger amount of oxides of carbon is formed and more copper evaporates, the anodic curve exhibits a lower average plasma temperature than the cathodic one.

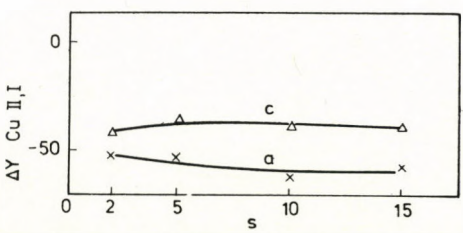

Fig. 7. Change in the spectral character ($\Delta Y_{Cu\ 237.0/282.4}$) with the burning time of the arc; 7 A. *a*: anodic, *c*: cathodic excitation

For the further study of the rate of transfer of the heat necessary for the reaction and of the resulting temperature and reaction conditions, experiments were also carried out in which the arc was left to burn for only 4 s, and the electrodes were then allowed to cool completely. During this time the cell too was flushed with pure Ar, and the oxides of carbon formed during the 4 s were measured. Next, without dismounting the cell, the arc was again burned for 4 s at the cooled electrodes, and the oxides of carbon formed in the second period were similarly measured. This procedure was repeated a further three times. Thus, all five measurement stages were obtained with a given electrode charge, but always with cooled electrodes. The five experimental points obtained from these were used to plot curves. From Fig. 8, which depicts

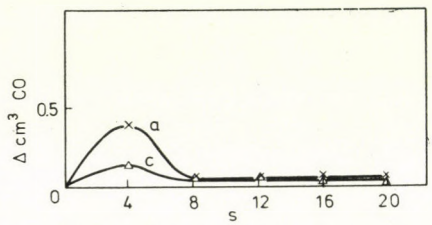

Fig. 8. Change in the quantity of CO produced with the intermittent burning time of the arc; 7 A. *a*: anodic, *c*: cathodic excitation

the change in time of the amount of CO produced intermittently in this way, it turns out that with intermittent burning of the arc a more substantial reaction can be reckoned with only in the first 4 s stage. In the first cooling period the entire electrode and the metallic copper formed in the upper layer of the charge packed into the electrode cool down to such an extent that only a very slight reaction is possible in the second burning period. This is repeated in the subsequent measurement stages. Figure 9 shows the analogous results for the CO_2 produced. Thus, the copper which forms in the reaction and then cools down seals off the lower layers of the mixture. A further burning of the arc for 4 s after the cooling down is not sufficient for these lower layers to be reheated satisfactorily. Accordingly, the metallic copper formed in the boring of the carrier electrode also has such sealing-in and cooling effects on con-

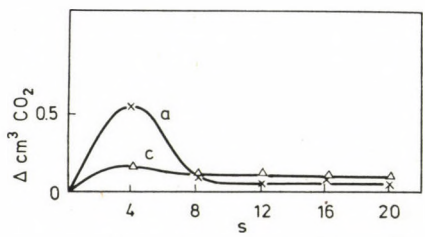

Fig. 9. Change in the quantity of CO_2 produced with the intermittent burning time of the arc; 7 A. *a*: anodic, *c*: cathodic excitation

tinuous excitation, since the processes observed on continuous excitation have been separated in time and accentuated in the experiments presented here. The fact that the curves relating to CO also have a maximum in the first period indicates that the reaction zone of formation of CO in the vicinity of the burning spot of the arc similarly moves slowly downwards in the packed charge as time passes. This is to be expected, for the material in the upper layer is consumed by reaction at the beginning of excitation.

The role of the chemical reactions is evident from the spectral line intensity curves ($I_{Cu\,I}$, Cu 282.4 nm) in Fig. 10, which were likewise obtained by such intermittent burning of the arc. The larger quantity of reaction heat liberated

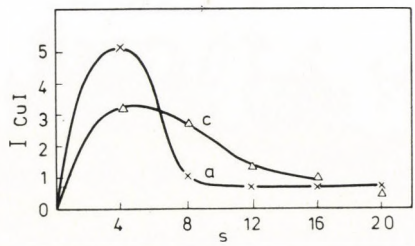

Fig. 10. Change in the intensity of the Cu 282.4 nm atomic line with the intermittent burning time of the arc; 7 A. *a*: anodic, *c*: cathodic excitation

in the more extensive reaction in the case of anodic excitation increases the evaporation of the sample to a greater extent, and also the intensities of the spectral lines, and the maximum of this curve occurs earlier than that of the cathodic curve. Because of the colder electrodes on cathodic excitation, the reaction automatically takes place to a lower extent, and the sealing layer formed from the metallic copper can form in the required thickness only more slowly and later. The intensity curve obtained with the intermittent cathodic excitation therefore exhibits a lower, but more drawn out maximum than in the anodic case.

On the intermittent burning of the arc, the change in the ratio of the part data naturally shows up in the development of the spectral character ($\Delta Y_{Cu\,II,\,I}$, Cu 237.0/282.4, values multiplied by 100) (Fig. 11). These curves

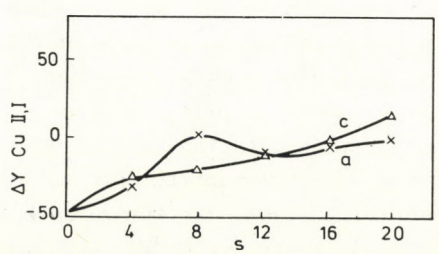

Fig. 11. Change in the spectral character ($\Delta Y_{Cu\,237.0/282.4}$) with the intermittent burning time of the arc; 7 A. *a*: anodic, *c*: cathodic excitation

are characterized by their tendency to rise, which shows ever smaller changes in the composition of the plasma as time passes. In the later stages the metal vapour undergoes excitation in an Ar atmosphere poorer in oxides of carbon, and there is less evaporated copper too. Thus, the average temperature of the plasma is increasingly higher. The slowly thickening metallic copper sealing layer likewise exerts an ever larger cooling effect, and the evaporation of the copper also diminishes in the later stages. On intermittent burning of the arc, therefore, only in the first stage do we obtain the low value of $\Delta Y_{Cu\,II,\,I}$ = ca. -50 which develops in the case of continuous burning; because of the constant reaction and the higher evaporation, this value remains throughout on continuous burning of the arc.

At any event, the above results show that the arc burning time of 10 s was a fortunate selection for the examinations. At the moderate current applied the greater part of the examined reactions and thus their effects too appear in this period. It is worth comparing this with the fact that in the case of 7 A the average current of the arc jumps ca. 0.5 A after 7–8 s, when the effect of the reaction already ceases. This period of time corresponds well to the end of the steeply rising section of the CO_2 curve observed on anodic excitation. The same was experienced in other examinations with higher currents, but earlier. Thus, in the case of an average current of 18 A, for example, a lower current of ca. 16 A was observed only in the first 2–3 s because of the faster heating and reaction, and this then jumped to a value of 18 A. The reaction and its effect therefore appear at the beginning of burning of the arc. It follows from this that, on quantitative spectral analysis of substances of this type, if it appears profitable and is not otherwise disadvantageous, in order to avoid the possible disturbing effects of the chemical reactions it is worth using a pre-arcing time and carrying out measurements only in the later stages.

Role of the current

We have already dealt with the role of the current in a stationary Ar atmosphere [6]. For further study of the question, measurements were also carried out in a flowing Ar atmosphere, in part for the sake of comparison with the results obtained with RW 0 carbon auxiliary electrodes, which will be reported later. Compared to the experiments in a stationary atmosphere, there were two further differences. In the present paper we deal only with the behaviour of the CuO + C powder mixture; in order that the CO_2 formed should also be well measurable, the mole fraction of CuO in the mixture packed into the borings in the RW II carrier electrodes was 0.6. However, the arc was similarly burned for 10 s.

Figures 12 and 13 show the changes in the amounts of CO and CO_2, respectively, formed by the arc, as functions of the average current of the arc. Here too in both cases the greater reaction was observed with the sample connected as anode (curve *a*), rather than with cathodic excitation (curve *c*), because of the stronger heating-up of the anode. At higher currents the curves showing the CO production exhibit saturation more weakly; in the case of the

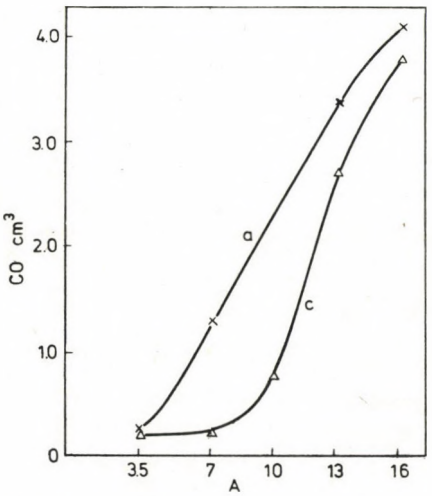

Fig. 12. Change in the quantity of CO produced with the current 10 s; *a*: anodic, *c*: cathodic excitation

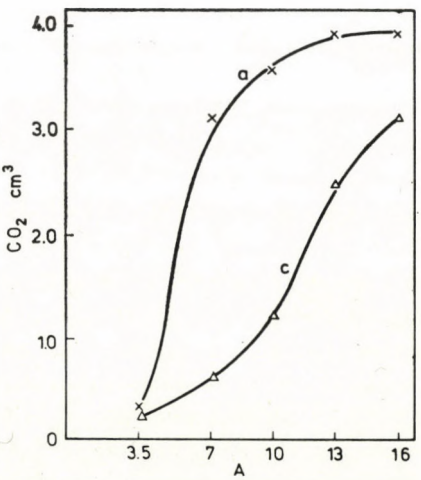

Fig. 13. Change in the quantity of CO_2 produced with the current 10 s; *a*: anodic, *c*: cathodic excitation

CO_2 curves the saturation is more marked. The great similarity to the curve obtained by the change of the burning time of the arc, presented in Fig. 2, is particularly striking for the curve obtained by anodic excitation of the sample and depicting the change of the quantity of CO_2. The electric work of the arc is given by the product of the arc voltage, the current and the burning time. Assuming identical arc voltage and turning to time×current plots, the curves of the current dependence and the burning time dependence can also be compared directly [7]. The result of the comparison is evidence of what a large role is played by the ratio of the heating and cooling rates of the electrodes in the chemical side-processes of the arc. The continuous line and the dashed line in Fig. 14 show the changes in the volume of CO_2 obtained

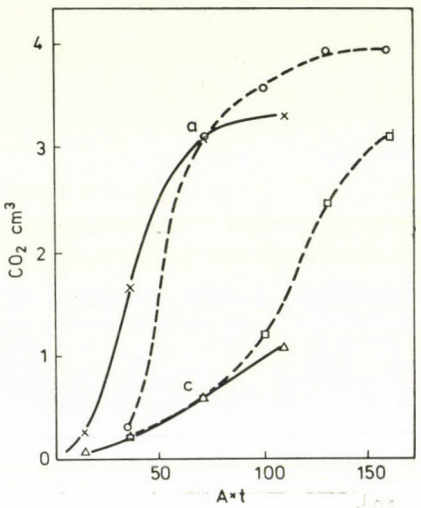

Fig. 14. Change in the quantity of CO_2 obtained with the same electric work. Continuous line: burning time dependence; dashed line: current strength dependence; *a*: anodic, *c*: cathodic excitation

by varying the burning time of the arc and the current respectively, but with the same electric work. It can be clearly seen from the Figure that initially on changing of the burning time the curve obtained by anodic excitation of the sample for a shorter time (2 – 5 s) but with a larger current (7 A) rises more rapidly than that obtained on the change of the current with excitation of the same work and polarity, but with a lower current and more protracted in time. Thus, in the case of the more concentrated transfer of the electric energy fed into the arc gap, the electrode heats up more rapidly and the material packed into the boring in the electrode also undergoes more reaction. However, the higher values accordingly exhibit an inverse proportion, since on burning of the 7 A arc for 15 s, for example, there is more time for cooling

of the electrode than during the burning of the 10 A arc for the shorter time of 10 s, even though the electric work is almost the same. Naturally, the two curves intersect each other at the common value of 7 A and 10 s. In the colder cathode this effect begins to appear only at higher electric work values, because the two curves coincide completely up to a value of the product $I \times t$ of ca. 70.

The situation is the same in the case of the CO production too, and therefore it is unnecessary to present this Figure. Similarly not shown is the current dependence of the sum (Σ %) of the percentage reactions calculated from the two types of oxidation reaction of carbon and referred to the maximum possible reaction of the quantity of mixture packed into the boring of the carrier electrode.

Figure 15 depicts the change of the volume ratio CO_2/CO, calculated from the measured quantities of CO_2 and CO, as a function of the current strength. The first half of these curves likewise resembles the complete curves obtained by change of the burning time of the arc (see Fig. 5), but naturally,

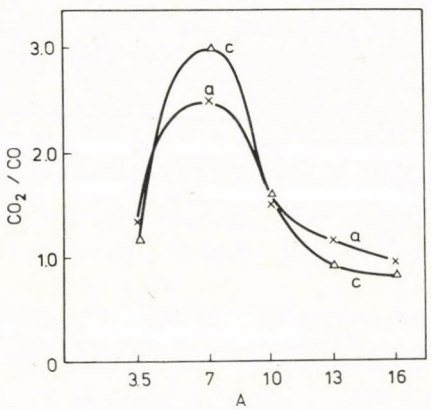

Fig. 15. Change in the volume ratio CO_2/CO with the current 10 s; *a*: anodic, *c*: cathodic excitation

because of the two different scales, here there is compression in the horizontal direction. Due to the use of a gas flow, the CO_2/CO ratios already approximate to the values corresponding to the instantaneous actual oxidation conditions, for the flowing gas prevents the later interconversion of the two oxides of carbon to a considerable extent. Thus, it can be accepted as realistic that the individual ratio values decrease with increase of the current above 7 A. It may therefore be stated that, in the reactions within the material of the electrode, there is no, or scarcely any manifestation of those oxidation and reduction tendencies [8] which show up in the electrode-surface reactions, depend on the polarities of the electrodes, and are not thermal, but exclusively electric in

origin. With increase of the current these tendencies increase proportionally, and because of them the reaction at the anode should shift in the direction of the oxidation of the material of the electrode, in the present case the formation of CO_2. At the same time, at the cathode a change should occur in the direction of reduction, or in the direction of the decrease of oxidation, which in our case would shift the CO_2/CO ratio in favour of the formation of CO. It can be seen from the curves that there are no such changes here. The CO_2/CO ratio mainly varies for thermal reasons, independently of whether the electric work of the arc is varied with the current or with the burning time, which does not influence the oxidation conditions. This is also proof that the electrode-surface reactions take place in a different way from those within the material of the electrode.

Figure 16 illustrates the intensity curves of the copper ($I_{Cu\,I}$, 282.4 nm atom line), obtained by changing the current and Fig. 17 the formation of the spectral character ($\Delta Y_{Cu\,II,\,I}$, Cu 237.0/282.4, values multiplied by 100), without any further explanation. These curves will be required in one of our later publications, for a comparison with the results of experiments carried out with RW 0 carbon carrier electrodes of a graphitic nature.

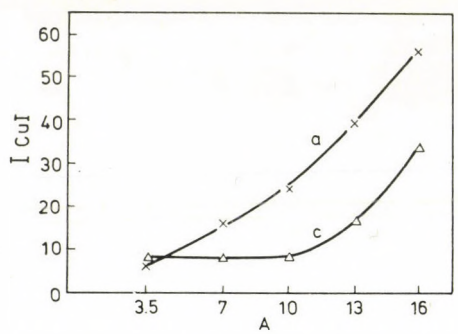

Fig. 16. Change in the intensity of the Cu 282.4 nm atom line with the current 10 s; *a*: anodic, *c*: cathodic excitation

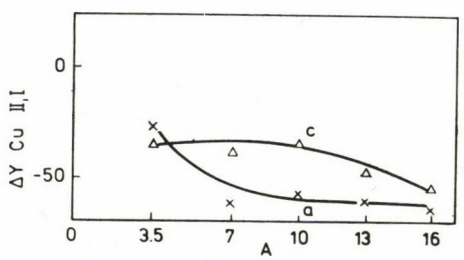

Fig. 17. Change in the spectral character ($\Delta Y_{Cu\,237.0/282.4}$) with the current 10 s; *a*: anodic, *c*: cathodic excitation

REFERENCES

[1] SZABÓ, Z. L., DOBOLYI-FEJÉRDY, H.: Acta Chim. Acad. Sci. Hung. **97,** 27 (1978)
[2] SZABÓ, Z. L., TÓTH, I.: Acta Chim. (Budapest) **73,** 363 (1972)
[3] SZABÓ, Z. L., DOBOLYI-FEJÉRDY, H.: Acta Chim. Acad. Sci. Hung. **96,** 189 (1978)
[4] PÖPPL, L., SZABÓ, Z. L.: Acta Chim. (Budapest) **79,** 27 (1973)
[5] SZABÓ, Z. L., DOBOLYI-FEJÉRDY, H.: Acta Chim. Acad. Sci. Hung. **97,** 19 (1978)
[6] SZABÓ, Z. L., DOBOLYI-FEJÉRDY, H.: Acta Chim. Acad. Sci. Hung. **96,** 201 (1978)
[7] SZABÓ, Z. L., PÖPPL, L.: Acta Chim. (Budapest) **77,** 353 (1973)
[8] SZABÓ, Z. L.: Spectrochim. Acta, **29/B,** 231 (1974)

Zoltán László SZABÓ, H-1088 Budapest, Múzeum krt. 4/b,
Hajna DOBOLYI-FEJÉRDY, H-1126 Budapest, Csörsz u. 35–43.

Acta Chimica Academiae Scientiarum Hungaricae, Tomus 97 (2), pp. 125—136 (1978)

SOME CHEMICAL REACTIONS OF THE ELECTRODE GAP AND THEIR ROLE IN SPECTROCHEMICAL ANALYSIS, XXIX

BEHAVIOUR OF METAL OXIDES IN THE ARC IN A FLOWING Ar ATMOSPHERE. ROLE OF THE RATIO OF METAL OXIDE AND CARBON POWDER WITH RW II AUXILIARY ELECTRODES

Z. L. SZABÓ

(Department of Inorganic and Analytical Chemistry, Eötvös L. University, Budapest)

H. DOBOLYI-FEJÉRDY

(Hungarian Optical Works, Budapest)

Received January 24, 1977

Experiments carried out previously in a stationary Ar atmosphere with the change of the ratio of metal oxide and carbon powder were repeated in a flowing Ar atmosphere. In agreement with the earlier results, maximum reaction was obtained when the molar ratio of metal oxide and carbon powder lay between the values of 1 : 1 and 2 : 1, optimum for the formation of CO and CO_2. The two reactions therefore proceed in parallel. From the change in the intensities of the spectral lines, the general finding was made that in the absence of chemical reactions the cathodic excitation gives a more intense spectrum. On the other hand, if a chemical reaction accompanied by heat evolution can occur in the zone of evaporation, then the anodic excitation is the more intense.

In an earlier part of this series [1] an account was given of the role of the ratio of metal oxide and carbon powder in the reactions, and their effects on the spectra when a stationary Ar atmosphere was used. When a flowing atmosphere was employed, however, it turned out that for study of the reactions and their effects it is advantageous if the gaseous reaction products formed are removed from the environment of the arc with a flowing atmosphere [2]. The possibility of interconversion of the reaction products in side reactions then decreases, and the amounts of oxides of carbon measured better reflect the momentarily developed reaction conditions. The measurements made with a stationary atmosphere were therefore repeated, but now in Ar flowing at a rate of 860 cm^3/min. The oxides of carbon formed as a result of the arc and the simultaneously arising spectral line intensities were measured with CuO + C and Al_2O_3 + C mixtures of various compositions packed into the borings in RW II "ventilating" carrier electrodes [3]. The carbon powder in the mixtures was a Czechoslovak product of type SU—601. In the examinations an A. C. polarized arc ignited at a potential maximum and burning for 10 s with a current of 7 A was used. The detailed experimental procedure was described earlier [3].

Results and discussion

Experiments were first made with carbon powder and the very reactive CuO mixed in various proportions. In accordance with previous experience [1], the horizontal axis is numbered in two directions: On the left-hand side of the Figures the number of moles of CuO in the mixture packed into the boring increases from left to right up to a mole ratio of 1 : 1, while on the right-hand side of the Figures the number of moles of carbon powder increases from right to left. The reason for this is that the production of carbon monoxide is regulated by the constituent present in lower amount in the mixture: the amount of CO produced theoretically increases linearly with the quantity of this component up to a mole ratio of 1 : 1. This is shown by the continuous line relating to CO in Fig. 1. The isosceles triangle shape was obtained by calculating from

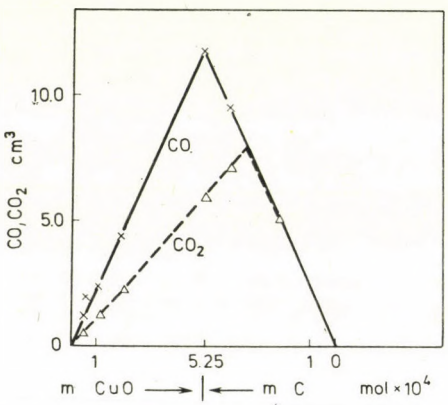

Fig. 1. Maximum possible reaction calculated for the CuO + C mixtures taken

the amount of substance packed into the borings in the carrier electrodes how much CO would be formed if the CuO or the C were to react completely as a result of the arc and if CO were the only product of the reaction. The dashed line relating to CO_2 similarly shows the values calculated on the assumption that only CO_2 would be formed in the arc. The peak of the distorted triangle shaped plot is naturally at a C : CuO mole ratio of 1 : 2 in accordance with the composition of CO_2.

Figures 2 and 3 show the quantities of CO and CO_2 measured experimentally as functions of the composition of the mixture. If these curves are compared with those obtained in a stationary Ar atmosphere (Figs 2 and 3 in [1]), a slight difference can be observed. One is that the flowing gas causes the position of the maximum in the curves *a* obtained with anodic excitation to shift slightly to the left. This change might be considered an experimental error if the shift to the left of the maximum in the curves *c* obtained with

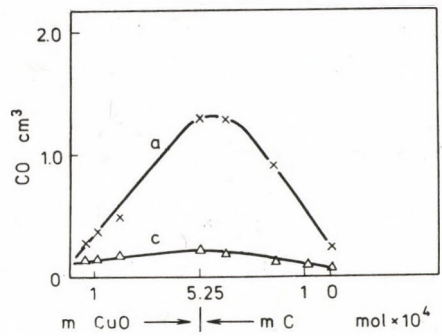

Fig. 2. Measured quantities of CO as a function of the composition of the CuO + C mixture; *a*: anodic, *c*: cathodic excitation

cathodic excitation were not so pronounced that it strongly suggests that it is so in the anodic case too. Here too, however, the positions of the maxima lie between the mole ratio mixture compositions of 1 : 1 and 1 : 2 which are optimum for the formation of CO and CO_2. This corresponds to the addition of the curves of Fig. 1 to each ofter. The upper break-points of the resulting curve are rounded off, however, for the two reactions are not independent of one another: the carbon is a reactant common to both. The two reactions therefore proceed in parallel, at different sites to a certain extent [4], but they nevertheless compete for utilization of the material necessary for the reaction.

The change in the ratio CO_2/CO formed from the measured volumes of CO_2 and CO can be seen in Fig. 4 as a function of the composition of the powder mixture. With increasing oxidant contents of the mixture, *i.e.* with increasing

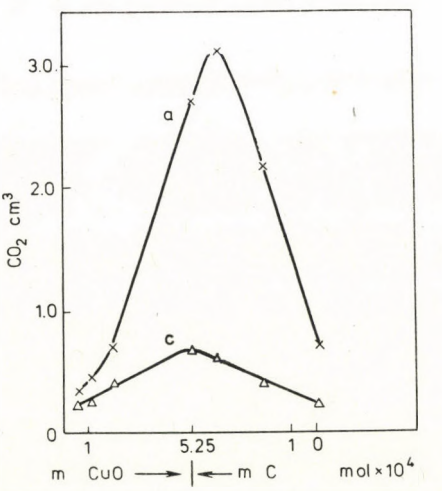

Fig. 3. Measured quantities of CO_2 as a function of the composition of the CuO + C mixture; *a*: anodic, *c*: cathodic excitation

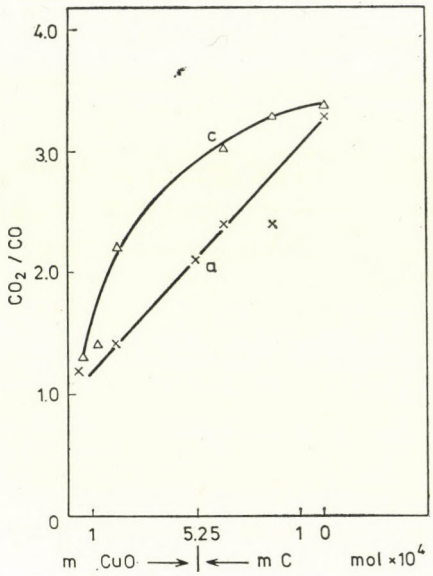

Fig. 4. Change of the volume ratio CO_2/CO with the composition of the CuO + C mixture: *a*: anodic, *c*: cathodic excitation

amounts of CuO, the curves obtained with excitation with both types of polarity rise markedly, indicating the shift of the oxidation-reduction conditions in the direction of oxidation. Here, however, the curve relating to cathodic excitation is situated higher in comparison to the anodic one in a manner characteristic of the relatively low current and the flowing Ar atmosphere. In accordance with the findings connected with the role of the flow rate [2], as a result of the flowing gas the CO_2/CO ratios increase compared to those observed in a stationary atmosphere, in favour of the formation of CO_2.

The calculated and summed CO_2 and CO results (Σ %) as percentages of the maximum theoretically possible reaction, based on the amounts of powder mixture packed into the boring in the electrode, are shown in Fig. 5. The effect of the flowing of the gas atmosphere naturally appears in these too. The course of the curve obtained with carrier electrodes connected as cathode is very similar to that relating to the stationary atmosphere. However, the curve obtained with anodic excitation, which produces more oxides of carbon, shows more clear-cut conditions than found with a stationary atmosphere. Here too the basic course of the combined reactions, evaluated percentagewise, is an asymptotically falling one, but in the anodic case this is associated with a maximum due to the increased reaction. The falling character of the curves could be well explained by the fact [1] that with the decrease of the proportion of carbon powder, *i.e.* with increasing CuO content, the electrode temperature developing during the burning of the arc is increasingly lower. The curve

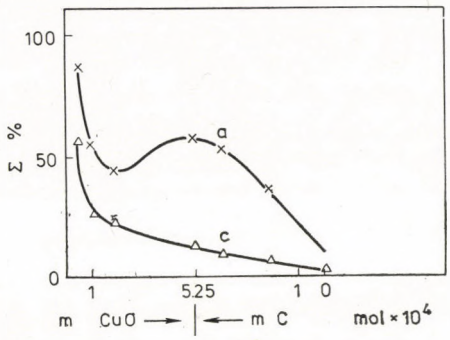

Fig. 5. Combined percentage evaluation of the two reactions. CuO + C mixtures; *a*: anodic, *c*: cathodic excitation

obtained with cathodic excitation, which has a simpler course, is very reminiscent of the intensity vs. rotation rate curves obtained with rotated metallic aluminium electrodes [5]. There the burning of the arc at ever colder sites and the decreasing extent of evaporation and reaction resulted from the increasing rate of rotation of the cylindrical aluminium electrode, while here they are caused by the change in the composition of the mixture and hence by the metallic copper formed in ever greater amount. It has been seen that there is a very close connection between the evaporation and excitation in the arc and the exothermic chemical reaction [6], and thus the decisive role of the heating and cooling conditions is proved here too.

The change in intensity of the 282.4 nm atom line of Cu ($I_{Cu\ I}$), with which the change in the evaporation of the sample is usually characterized, is likewise similar to that obtained with a stationary atmosphere (Fig. 6), except that the absolute values of the experimental points comprising the curve are larger. With the increasing CuO content of the sample and the accompanying increasing reaction, here too initially there is an increase in the quantity of metal evaporated and excited, but later the effect in the opposite direction of the physical properties of the powder charge, which differ more and more from those of carbon, far exceeds the effect of this increase. The intensities increase compared to those observed in the stationary atmosphere mainly at the beginning of the curve. This shows that the effect of the gas flow in cooling the electrode does not play a substantial role here. It appears more essential than this that the gases formed are removed from the environment of the electrode and the plasma. There may thus be a slight increase in the reaction and also in its effect enhancing the evaporation. At the same time, there may be a significant increase in the proportion of excitation of the metal vapour too, because of the changes in the composition of the plasma. The curves connecting the experimental points with dashed lines in the Figure reveal the greater fluctuation of the intensity data.

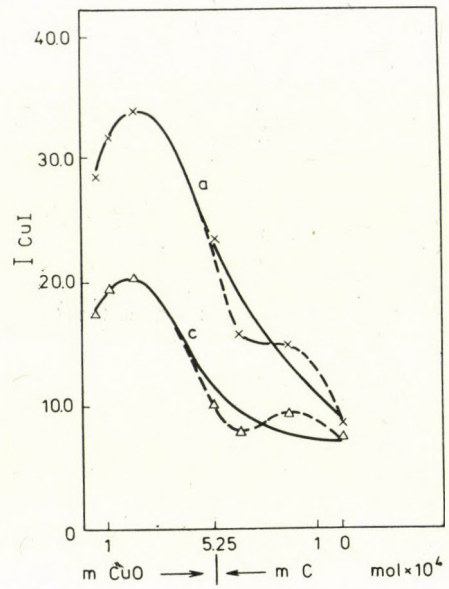

Fig. 6. Change in intensity of the Cu 282.4 nm atom line with the composition of the mixture; *a*: anodic, *c*: cathodic excitation

The variations in the evaporation and hence the average plasma temperature are also indicated by the spectral character curves ($\Delta Y_{\mathrm{Cu\ II,\ I}}$) (Fig. 7), constructed from the ratios of the intensities (multiplied by 100) of the Cu 237.0 nm ion line and the previous atom line. The minima of these curves are similarly shifted to the first half of the curves, *i.e.* to where the evaporation and the plasma cooling effect of the metal vapour are the highest.

For comparison, measurements were also made with powder mixtures of Al_2O_3 + C in various proportions, with the same excitation parameters as previously. As earlier [2], these mixtures were prepared by dividing the formula weight of Al_2O_3 by three, the number of oxygen atoms in it, and mixing the Al_2O_3 with the carbon powder on this basis. In effect, therefore, the number

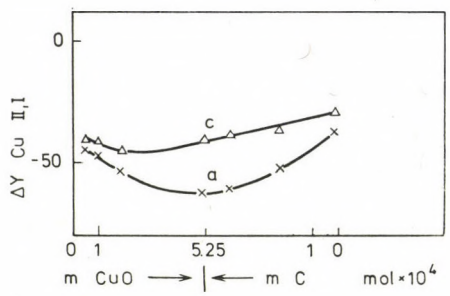

Fig. 7. Change of the spectral character ($\Delta Y_{\mathrm{Cu\ 237.0/282.4}}$) with the composition of the mixture; *a*: anodic, *c*: cathodic excitation

of moles of Al_2O_3 taken in the boring in the carrier electrode was calculated as oxygen equivalents. The "m 1/3 Al_2O_3" on the horizontal axis of the subsequent Figures means these oxygen equivalents. Naturally, very small amounts of oxides of carbon were obtained in the gas-producing reactions. The quantity of CO_2 measured varies with the amount of metal oxide according to a mild minimum curve (Fig. 8), while the curves for CO exhibit a mild maximum (Fig. 9). The shapes of these latter curves by and large correspond to those of the similar curves obtained with a stationary Ar atmosphere, but the flowing of the gas leads to a decrease of about 50 % in the measured amounts of CO. At the same time, the amounts of CO_2 increase to well-measurable

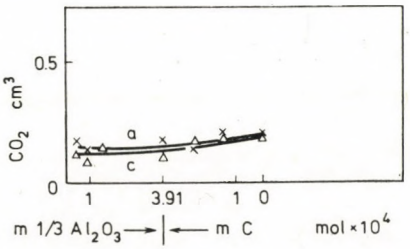

Fig. 8. Measured quantities of CO_2 as a function of the composition of the Al_2O_3 + C mixture; *a*: anodic, *c*: cathodic excitation

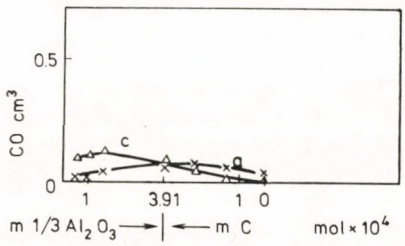

Fig. 9. Measured quantities of CO as a function of the composition of the Al_2O_3 + C mixture; *a*: anodic, *c*: cathodic excitation

quantities. These changes agree in tendency with those discussed earlier in connection with CuO + C powder mixtures. Here the second reaction zone [4], the bulk of the electrode filling, in which a larger quantity of the CO_2 would be formed, does not develop in the lower parts of the boring in the carrier electrode, and thus the Al_2O_3 decomposes only in the burning spot of the arc and its immediate vicinity. The oxygen then released may react with the evaporated carbon in the colder plasma zones, giving CO_2 and CO in parallel. The flow of the gas has scarcely any effect on the temperature of the burning spot of the arc. It is proved, therefore, that in the case of the CuO + C mixtures too the increase in the CO_2/CO ratio as a consequence of the flowing of the gas is caused by plasma processes, and more concretely by the reaction $CO_2 + C =$

= 2 CO. However, the opposite shapes of the CO and CO_2 curves mean the decrease of the temperature of the burning spot with the composition of the mixture, but at the same time an ever larger amount of reactive oxygen formed by decomposition.

When the measured oxides of carbon are plotted together as percentages of the maximum possible reaction calculated from the amount of mixture packed into the boring of the electrode (Σ %), asymptotically-falling curves are obtained here too (Fig. 10). These did not give additional information, but they did support our earlier conceptions with new data.

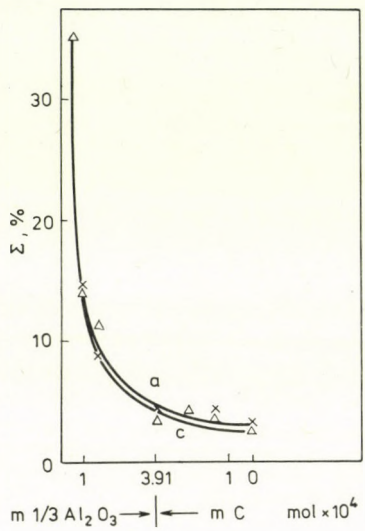

Fig. 10. Percentage evaluation of the two reactions. Al_2O_3 + C mixtures; *a*: anodic, *c*: cathodic excitation

The change in intensity of the Al 305.0 nm atom line ($I_{Al\,I}$) as a function of the composition of the powder mixture is presented in Fig. 11. In the absence of chemical reactions, or because of their insignificance, here too the curve obtained with cathodic excitation displays higher spectral line intensities than in the anodic case, similarly as was found in the study of pure metals in an inactive atmosphere [7, 8]. In general, therefore, it may be said that if an exothermic reaction takes place in the zone of evaporation or its vicinity, no matter whether this be an electrode-surface reaction [9] or a reaction within the substance of the electrode, as a consequence the evaporation will increase. As this effect is the larger on anodic excitation in the case of pure metals or powder mixtures packed into the boring in an RW II carrier electrode, the anodic excitation gives a spectrum of higher intensity than in the cathodic case. If there is no such reaction, excitation of the sample as cathode is the more intense [10].

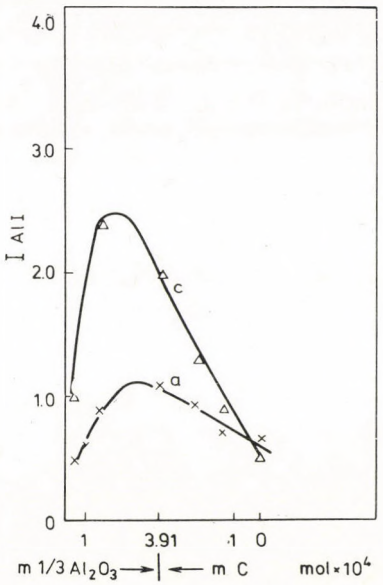

Fig. 11. Change in intensity of the Al 305.0 nm atom line with the composition of the mixture; *a*: anodic, *c*: cathodic excitation

A study was also made of how the change in the evaporation and excitation conditions affects the intensity of a spectral line of different excitation energy, but similarly of atom origin. The change in intensity of the Al 308.2 nm atom line as a function of the composition of the Al_2O_3 + C powder mixture is shown in Fig. 12. The excitation potential of this line is only 4.02 eV, whereas that of the previously used Al 305.0 nm line is 7.65 eV. The courses of the two curves are by and large the same, but the magnitudes of the measured values differ. Thus, with both curves it is possible to follow the tendency to change of the evaporation of the sample, although the ratio of the intensities of the two lines varies to a certain extent with the composition of the mixture. It is important to state this, as in certain subsequent experiments the intensity of the spectrum of the aluminium was so small that only the more intense Al 308.2 nm line could be measured.

Compared to those obtained in the experiments with a stationary atmosphere [1], the maxima in the curves presented in both latter Figures occur earlier, towards lower metal oxide contents. A role may be played here by the fact that the flowing gas also removes the metal vapour from the cell, and hence it can not accumulate there.

The spectral character curves formed with the given Al 281.6 nm ion line referred to the Al 305.0 nm and Al 308.2 nm atom lines are shown in Figs 13 and 14, respectively (values multiplied by 100). While the values referred to the Al 305.0 nm line give the expected curves containing a minimum, those

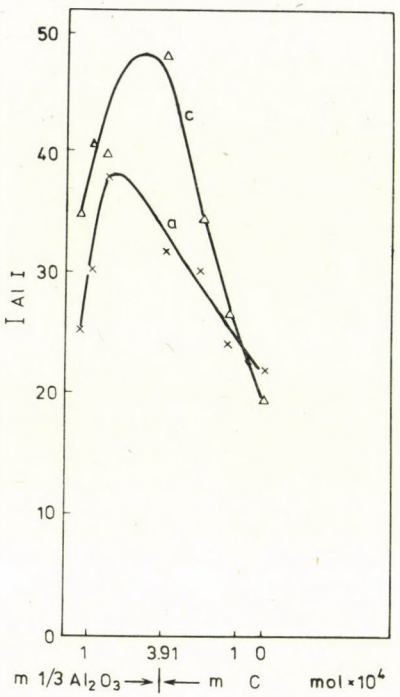

Fig. 12. Change in intensity of the Al 308.2 nm atom line with the composition of the mixture; *a*: anodic, *c*: cathodic excitation

referred to the Al 308.2 nm line give virtually straight lines; the latter at most slightly rise and do not show faithfully the expected change in the plasma conditions. Here too, therefore, it proved necessary to deal carefully with the change in the spectral character, for although this is correlated with the average temperature of the plasma, it is often not proportional to it.

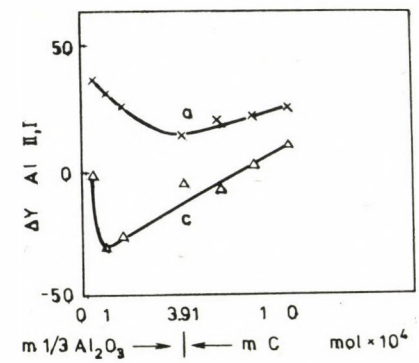

Fig. 13. Change of the spectral character ($\Delta Y_{Al\,281.6/305.0}$) with the composition of the mixture; *a*: anodic, *c*: cathodic excitation

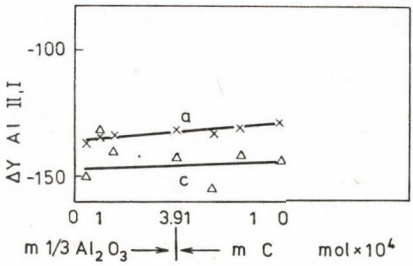

Fig. 14. Change of the spectral character ($\Delta Y_{Al\,281.6/308.2}$) with the composition of the mixture; *a*: anodic, *c*: cathodic excitation

Similarly as for the stationary Ar atmosphere, the trends in the fluctuations of the spectral-analysis data and the gas-analysis data characteristic of the chemical reactions in the case of CuO + C mixtures were compared when a flowing Ar atmosphere was used. As done previously [1], the parallel gas analysis results relating to the individual experimental points were arranged in increasing sequence and the spectral line intensities measured in the same experiments were written beside them. When the quantities of CO and CO_2 evolved were measured on anodic and cathodic excitation of the sample, with 7 different powder compositions, 28 data series pairs were obtained. An inspection was next made of the number of cases in which the spectral line intensities unambiguously increase together with the gas-analysis values. Agreement was denoted by the symbol "+"; the symbol "0" was given if the tendency between the two types of fluctuation could not be discerned; and the symbol "−" was given when the spectral line intensities varied in exactly the opposite manner in comparison to the gas-analysis results. The results are listed in Table 1. As regards the 28 data series examined, in 15 cases here the changes

Table I

Comparison of the fluctuation trends of the gas-analysis and spectral data

+: agreement; 0: no discernible tendency; −: opposite changes

Excitation	Mole fraction of CuO													
	1.0		0.75		0.60		0.50		0.13		0.07		0.03	
	CO	CO_2	CO	CO_2	CO	CO_2	CO	CO_2	CO	CO_2	CO	CO_2	CO	CO_2
Anodic	+	+	+	−	+	+	0	0	+	0	+	0	+	+
Cathodic	−	+	0	+	0	+	+	−	0	0	0	+	+	0

were in the same direction, in 10 cases there was no clear-cut connection, and in only 3 cases were the changes in opposite directions. On average, therefore,

the correlation of the chemical reactions and the spectral line intensities can be observed in a flowing gas atmosphere too.

REFERENCES

[1] SZABÓ, Z. L., DOBOLYI-FEJÉRDY, H.: Acta Chim. Acad. Sci. Hung. **97,** 13 (1978)
[2] SZABÓ, Z. L., DOBOLYI-FEJÉRDY, H.: Acta Chim. Acad. Sci. Hung. **97,** 27 (1978)
[3] SZABÓ, Z. L., DOBOLYI-FEJÉRDY, H.: Acta Chim. Acad. Sci. Hung. **96,** 189 (1978)
[4] SZABÓ, Z. L., DOBOLYI-FEJÉRDY, H.: Acta Chim. Acad. Sci. Hung. **97,** 111 (1978) in press
[5] SZABÓ, Z. L., SZAKÁCS, O.: Acta Chim. (Budapest), **73,** 143 (1972)
[6] SZABÓ, Z. L., DOBOLYI-FEJÉRDY, H.: Acta Chim. Acad. Sci. Hung. **96,** 201 (1978)
[7] SZABÓ, Z. L., TÓTH, I.: Spectrochim. Acta, **27/B,** 107 (1972)
[8] SZABÓ, Z. L.: Acta Chim. (Budapest), **85,** 13 (1975)
[9] SZABÓ, Z. L.: Spectrochim. Acta, **29/B,** 231 (1974)
[10] ANDERMAN, G., KEMP, J. W.: ASTM Techn. Pub. 259 (1959)

Zoltán László SZABÓ, H-1088 Budapest, Múzeum krt. 4/b,
Hajna DOBOLYI-FEJÉRDY, H-1126 Budapest, Csörsz ut. 35–43.

Acta Chimica Academiae Scientiarum Hungaricae, Tomus 97 (2), pp. 137—145 (1978)

SOME CHEMICAL REACTIONS OF THE ELECTRODE GAP AND THEIR ROLE IN SPECTROCHEMICAL ANALYSIS, XXX

BEHAVIOUR OF METAL OXIDES IN THE ARC IN A FLOWING Ar ATMOSPHERE. ROLE OF THE REACTIVITY OF THE METAL OXIDE WITH RW II AUXILIARY ELECTRODES

Z. L. SZABÓ

(Department of Inorganic and Analytical Chemistry, Eötvös L. University, Budapest)

H. DOBOLYI-FEJÉRDY

(Hungarian Optical Works, Budapest)

Received January 24, 1977

The roles of the reactivities of metal oxides in mixtures with carbon powder displayed both in their reactions and in the effects of the reactions on the results of spectral analysis. In the case of the more reactive metal oxides the difference between the heat of oxidation of the carbon and the heat of decomposition of the metal oxide is liberated as a result of the burning of the arc, and heats up the mixture further. Because of this, the reaction itself is enhanced and the spectral line intensities also increase. From the results of the examinations conclusions could be drawn with regard to the reactions occurring, to their sequence and to their location.

We have already dealt with the roles of the reactivities of metal oxides in their mixtures with carbon powder, in the reaction producing CO in the arc in a stationary Ar atmosphere [1]. This role was also displayed in the examined reactions in a flowing Ar atmosphere, when mixtures of CuO or Al_2O_3 in various proportions with carbon powder were compared in behaviour [2]. From the results of reactivity examinations in a stationary Ar atmosphere it emerged that the formation of CO_2 plays a decisive role in the reactions, although there only the quantities of CO formed as a result of the arc were measured as a function of the ractivities of the metal oxides. In a study of the behaviours of 20 different metal oxides, it was found that more CO is formed as a consequence of the arc if the heat of formation of the metal oxide referred to one atom of bound oxygen (characteristic of its stability and hence of its reactivity) is less than ca. -50 kcal/mole, *i.e.* if the metal oxides are less stable compounds than CO_2. The heat of formation of CO_2 referred to one atom of bound oxygen, -48 kcal/mole, agrees fairly well with the above value, and thus carbon is able to extract oxygen from less stable metal oxides. The measured CO quantities also began to increase more rapidly around this value. However, the CO values did not give a single definite curve as a function of the heats of formation of the metal oxides. The CO volumes measured with mixtures of the various metal oxides with carbon exhibited an appreciable scatter, and the above con-

clusion could be drawn only on the basis of the course of the curve connecting the average values. The cause of the large fluctuation of the values was considered to be that with the individual metal oxide and carbon powder mixtures the burning of the arc led to the material packed into the boring in the carrier electrode being ejected to different extents. Material falling to the bottom of the gas cell did not take part in the reaction, while that which was sprayed into the plasma resulted in more CO being produced than expected in the plasma reaction. Accordingly, here experiments were made only with those metal oxides which got spilt to merely a very slight extent from the boring as a consequence of the arc. A flowing Ar atmosphere (860 cm^3/min) was used, for experience had shown that the momentarily prevailing reaction conditions could be better approximated to with this [3]. We also wished to measure not only the amount of CO formed, but that of CO_2 too, and the changes in intensity of the spectral lines could be followed when oxides of a given metal, but of different compositions, and therefore different reactivities, were compared. The best model for this appeared to be the three oxides of lead [1]. The heat of oxide formation referred to one atom of bound oxygen were taken as the basis of comparison of the different metal oxides with one another. These values were obtained by dividing the heats of molecular oxide formation by the numbers of bound oxygen atoms in the respective compounds. An A. C. polarized arc ignited at the potential maximum, and burning for 10 s with an average current of 7 A, was used, with the well-heating, RW II amorphous carbon electrodes produced by Ringsdorff Werke GmbH as auxiliary electrodes. The detailed working procedure was described earlier [4].

Results and discussion

With all metal oxides the examinations were carried out with two different mole fractions of metal oxide calculated from the oxygen equivalents. In one the mole fraction was 0.15, *i.e.* a mixture ensuring more reducing conditions because of the greater carbon powder excess; in the other it was 0.6, *i.e.* a mildly oxidizing system. In accordance with previous practices, the carbon powder used in the mixtures was of type SU – 601 produced by Elektrokarbon Topolčany (Czechoslovakia). We first dealt with mixtures of carbon powder with the three lead oxides, PbO, Pb_3O_4 and PbO_2, which also give good results in a stationary Ar atmosphere [1]. Referred to one atom of bound oxygen, the reactivities of these increase in the above sequence: −52.5, −43.7 and −33.1 kcal/oxygen equivalent (ΔH in the Figures).

Figure 1 shows the change of the amounts of CO produced in the arc as functions of these heats of oxide formation, ΔH. The Figure contains 4 curves: mixtures with lead oxide oxygen equivalents n = 0.15 and n = 0.6

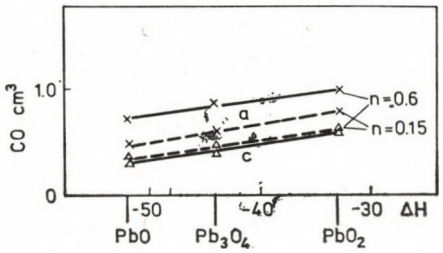

Fig. 1. Change of the quantity of CO produced as a function of the reactivity of the lead oxide. with metal oxide mixtures of two mole fractions; *a*: anodic, *c*: cathodic excitation

and with the carrier electrodes connected as anode (*a*) and cathode (*c*). All 4 curves rise linearly with decreasing stability of the lead oxides, *i.e.* with their increasing reactivity. It is worth noting that the two curves obtained with the two mixing proportions, but in both cases with cathodic excitation of the samples, coincide within the limits of experimental error. In the cathodc carrier electrode, which remains cold in the arc with its relatively low average current of 7 A, only the temperature of the immediate environment of the burning spot of the arc is high enough for the reaction producing CO to proceed. The size of this zone probably increases a little if the mixture with a metal oxide equivalent of 0.15, *i.e.* richer in carbon powder, is used. This is why the curve measured with this mixture may give just as high values as those obtained with cathodic excitation in the case of an oxygen equivalent of 0.6. The greater amount of the poorly thermally conducting carbon powder results in a higher burning spot temperature, and the heat is localized to a slightly larger area.

As has already been seen several times, on excitation of the sample as anode a larger bulk of the carrier electrode and the material filled in it is heated up. Hence, the CO production too is higher than that obtained with cathodic excitation. There is also an increase in the lower, second reaction zone [5], in which a large part of the CO_2 is formed. The zones of formation of the two oxides of carbon probably overlap, as the decrease of temperature downwards in the carrier electrode is continuous. All this must lead to an influence on the CO production too. On anodic examination of the sample, a substantial difference shows up in the CO production, in favour of the mixture with an oxygen equivalent of 0.6 (*i.e.* richer in metal oxide), which provides the more oxidizing conditions, compared to that with an equivalent of 0.15. This strongly suggests that part of the previously discussed [2, 3] reaction involving the CO_2 formed, $CO_2 + C = 2\ CO$, takes place in the boring in the carrier electrode. Earlier, it could be confirmed only that this reaction, or part of it, occurs at the colder sites of the plasma. However, if more CO_2 is formed on anodic excitation, its reduction to CO by the carbon powder also increases.

Figure 2 illustrates the amounts of CO_2 produced in the arc as functions of the ΔH values relating to the three lead oxides. The comparatively lower-temperature zone of formation of CO_2 is more readily influenced by the conditions. More substantial differences were found here in the four cases examined. The curves obtained with the powder mixtures with a metal oxide equivalent of 0.15 rise much more flatly than those obtained with the mixtures richer in metal oxide, and are almost linear, similarly to the CO curves. Because of the more oxidizing conditions ensured by the larger metal oxide content, the curves obtained with mixtures with an oxygen equivalent of 0.6 are situ-

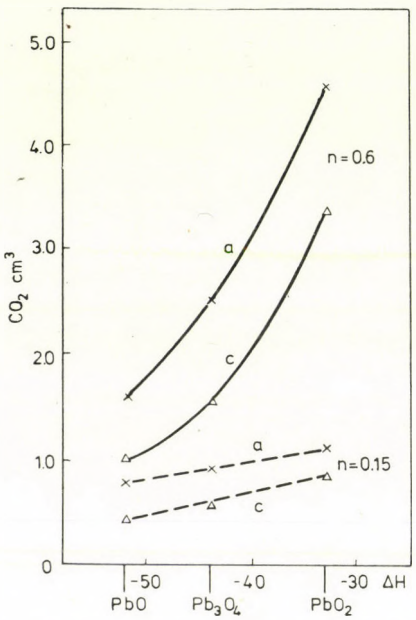

Fig. 2. Change of the quantity of CO_2 produced as a function of the reactivity of the lead oxide, with metal oxide mixtures of two mole fractions; *a*: anodic, *c*: cathodic excitation

ated higher and curve upwards steeply. It seems that the greater carbon powder excess considerably represses the reaction by ensuring more reducing conditions. If the question is examined from another aspect, the steep upwards inclination of the curves is regarded as proving that the greater amount of heat of reaction liberated in the more extensive reaction is more effective in heating up the carrier electrode and the material filled in it, whereby the latter is stimulated to further reaction. This change therefore affects more strongly a larger mass of the sample, the second reaction zone situated more deeply in the boring in the electrode, where the bulk of the CO_2 is formed. This is why the curves illustrating the CO_2 production are steeper here.

It is also worth noting that both Figures show that the curves obtained with anodic and cathodic excitation of the sample are parallel to one another for the mixtures with the two different oxygen equivalents. This is again an indication that the heating and cooling conditions, depending exclusively on the polarity of the electrodes, are decisive in these reactions. A role cannot be played here by those oxidation and reduction tendencies depending on the polarity of the electrodes and the current, which regulate the electrode-surface reactions. The other controlling factor is the reactivity of the system.

All the above is supported by the CO_2/CO volume ratios formed from these amounts of CO_2 and CO. The two curve pairs in Fig. 3 indicate that the oxidation conditions of the system vary strongly and unambiguously with the reactivity in mixtures with a metal oxide oxygen equivalent of 0.6. As regards the mixtures with an oxygen equivalent of 0.15, the role of the reactivities of the metal oxides in the reaction shows up better in the part data presented in Figs 1 and 2.

The effect of the heat of reaction liberated is also to be seen in the intensities of the spectra. Figure 4 shows the change in intensity of the Pb 324.0 nm atom line as a function of ΔH for the mixtures of the two compositions. As done earlier, the change in intensity of the atom line of the main component of the sample was taken as proportional to the change in the evaporation of the sample. In the case of the mixtures with a metal oxide mole fraction of 0.15 the intensity curves ($I_{Pb\,I}$) drawn from the three experimental points corresponding to the three lead oxides are initially horizontal, and then begin to rise slightly. With mixtures with a mole fraction of 0.6, the intensity curves obtained initially fall, and then rise. These are very characteristic for, because

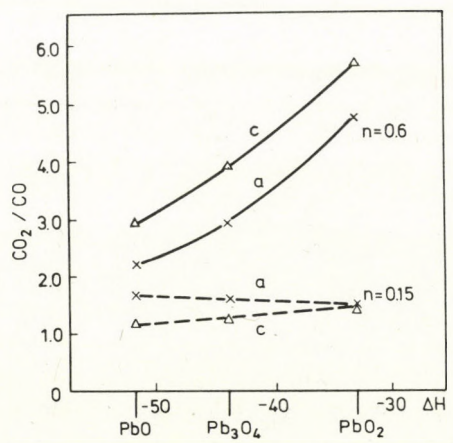

Fig. 3. Change of the CO_2/CO volume ratios as a function of the reactivity of the lead oxide, with metal oxide mixtures of two mole fractions; *a*: anodic, *c*: cathodic excitation

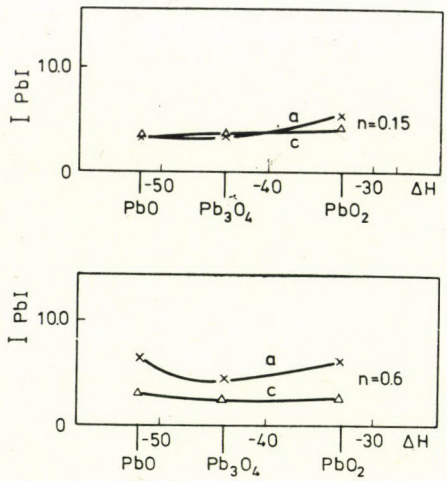

Fig. 4. Change of the intensity of the Pb 324.0 nm atomic line as a function of the reactivity of the lead oxide, with metal oxide mixtures of two mole fractions; *a*: anodic, *c*: cathodic excitation

of the different equivalent weights of the lead oxides referred to one atom of bound oxygen, the amounts of the mixtures that can be packed into the boring in the carrier electrode decrease in the increasing sequence of their reactivity series; indeed, in addition their percentage lead contents also do so. Overall, therefore, there is a decrease in the amount of lead used in the experiments. These data are presented in Table I. From the higher heat of reaction with increasing reactivity, therefore, the proportion of evaporation of the sample also increases.

Table I

Data on lead oxide mixtures taken

Mixture	Sample taken					
	$n = 0.15$			$n = 0.6$		
	Mixture g	Pb %	Pb g	Mixture g	Pb %	Pb g
PbO + C	0.0435	68.3	0.0297	0.0692	89.7	0.0620
Pb_3O_4 + C	0.0406	61.8	0.0251	0.0692	86.7	0.0600
PbO_2 + C	0.0390	51.9	0.0202	0.0674	81.2	0.0547

Subsequently, measurements were made with mixtures of carbon powder with a total of eight metal oxides. An attempt was made to compare the results of these as functions of the heats of oxide formation ΔH referred to one atom of bound oxygen. In order of increasing reactivity, the eight metal oxides

examined were the following: Al_2O_3, Cr_2O_3, SnO_2, SnO, PbO, Pb_3O_4, CuO and PbO_2. One reason for the selection of these was that they should include unreactive, moderately reactive and very reactive oxides. Another aspect of the selection, as mentioned earlier, was that these oxides were those which got spilt to only a very slight extent from the boring of the carrier electrode as a result of the arc in similar experiments in a stationary Ar atmosphere [1]. Figure 5 shows the volumes of CO and CO_2 measured with a mixture with a metal oxide oxygen equivalent of 0.15, and the CO_2/CO volumetric ratios formed from the two, as functions of ΔH. Figure 6 depicts the corresponding data for a metal oxide oxygen equivalent of 0.6. The role of the reactivities of the metal oxides in the reactions can be well observed in both Figures. Similarly to the CO curves obtained with a stationary Ar atmosphere, the curves illustrating the quantities of CO and CO_2 produced begin to rise more markedly at a heat of formation of about -50 kcal/mole. This change is always larger for CO_2 than for CO, and is particularly large with mixtures with a mole fraction of 0.6. It must be true, therefore, that the reactivity has a greater effect primarily on the CO_2 production, in agreement with what was observed on comparison of the behaviours of the three oxides of lead. If this is compared with the fact that the change in slope of the curves occurs in the vicinity of the heat of formation of CO_2 referred to one atom of bound oxygen (-48 kcal/mole), it may be states that for the more reactive metal oxides the decisive reaction is $2\,MO + C = 2\,M + CO_2$. This is connected to the CO-producing

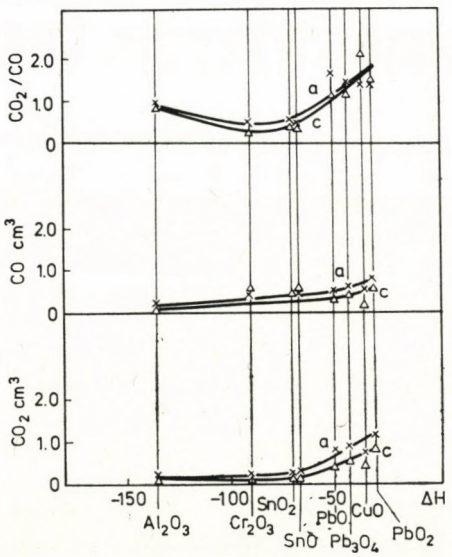

Fig. 5. Change of the gas analysis results as a function of the reactivity of the metal oxide. $n = 0.15$; *a*: anodic, *c*: cathodic excitation

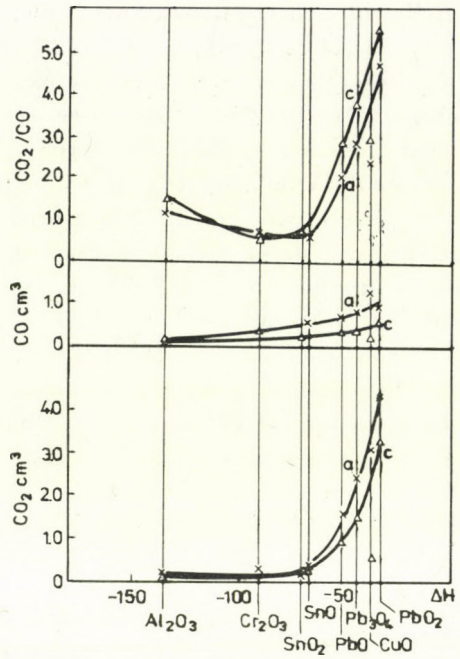

Fig. 6. Change of the gas analysis results as a function of the reactivity of the metal oxide. $n = 0.6$; *a*: anodic, *c*: cathodic excitation

reaction, probably in that part of the CO_2 evolved decomposes at the higher-temperature sites, even in the boring in the electrode, according to the reaction $CO_2 + C = 2\ CO$. At these higher-temperature sites in the upper layers of the carrier electrode, however, CO is formed directly too, in accordance with the reaction $MO + C = M + CO$ [5]. In the case of the more labile metal oxides, their simple thermal decomposition may also be reckoned with. The oxygen atoms formed in the reaction $MO = M + O$ may similarly react with the carbon. Finally, our earlier measurements [3] indicated that part of the CO_2 formed may react in the colder zones of the plasma with the carbon vapour arriving there by sublimation, according to the reaction $CO_2 + C = 2\ CO$. This latter reaction could be repressed to a large extent by the flowing of the gas atmosphere. Overall, this series of reactions gives quantities of CO and CO_2 measurable by gas analysis methods. A significant amount of heat of reaction is liberated in the reaction if the decomposition heat required by the metal oxide is less than the heat evolved on the oxidation of carbon. The difference of the two appears as excess energy in the arc. The difference of the heat of reaction released causes further heating and reaction mainly in the zone of formation of CO_2, and this influences the evaporation of the sample too. As a result of an arc of a given current, the evaporation is always more extensive from hotter electrodes [6]. Naturally, the spectral line intensities

also increase in parallel with the evaporation. At the same time, the oxides of carbon formed during the reaction may change the composition of the plasma [2], which may affect the excitation processes. We shall deal with this latter question later.

REFERENCES

[1] SZABÓ, Z. L., DOBOLYI-FEJÉRDY, H.: Acta Chim. Acad. Sci. Hung. **97,** 1 (1978)
[2] SZABÓ, Z. L., DOBOLYI-FEJÉRDY, H.: Acta Chim. Acad. Sci. Hung. **97,** 125 (1978)
[3] SZABÓ, Z. L., DOBOLYI-FEJÉRDY, H.: Acta Chim. Acad. Sci. Hung. **97,** 27 (1978)
[4] SZABÓ, Z. L., DOBOLYI-FEJÉRDY, H.: Acta Chim. Acad. Sci. Hung. **96,** 199 (1978)
[5] SZABÓ, Z. L., DOBOLYI-FEJÉRDY, H.: Acta Chim. Acad. Sci. Hung. **97,** 111 (1978)
[6] SZABÓ, Z. L., SZAKÁCS, O.: Acta Chim. (Budapest) **73,** 143 (1972)

Zoltán László SZABÓ, H-1088 Budapest, Múzeum krt. 4/b,
Hajna DOBOLYI-FEJÉRDY, H-1126 Budapest, Csörsz u. 35–43.

Acta Chimica Academiae Scientiarum Hungaricae, Tomus 97 (2), pp. 147—157 (1978)

MODEL REALIZATION OF THE IDEAL POLYMETHINE STATE BY SOLVENT-INDUCED CHANGES IN THE ELECTRONIC STRUCTURE OF SOLVATOCHROMIC DYES*

S. DÄHNE and K.-D. NOLTE

(Central Institute of Optics and Spectroscopy of the Academy of Sciences of the GDR, Berlin-Adlershof, GDR)

Received October 11, 1976

The states intermediate between the non-polar and the polar valence structure of a meropolymethine are simulated on the basis of the MO theory by superposing a reaction field of increasing polarity over the molecule. The symmetrical state through which the molecule passes has all the typical features of the ideal polymethine state, such as a minimum $N \rightarrow V_1$ transition energy corresponding to the valence bond theoretical findings of FÖRSTER, a maximum transition probability, a maximum π-electron density alternation and a minimum alternation of π-bond orders both in the ground state and, to a lesser degree, in the first excited singlet state. On light absorption in the $N \rightarrow V_1$ transition the π-electron densities are extremely reversed in the ideal polymethine state whilst the changes in the π-bond orders are minimal.

Introduction

According to FÖRSTER's derivation of 1939 [2] based on the valence bond (VB) theory, the transition energy of the longest wave length absorption

1a **1c**

1b

$n = 0, 1, 2 \ldots$

X, X′ = atoms of elements of groups IV, V or VI of the periodic table

* Communication No. 17 on problems of solvatochromism; Comm. No. 16, *cf.* [1]

band of solvatochromic dyes (**1**), $X \neq X'$, is at a minimum when the two polyenic valence structures **1a** and **1c** contribute to the same extent to the mesomeric state **1b**. For decades this finding had been regarded as one of the main supports of the resonance theory without any specific differences having been recognized between the resonance of chain-like conjugated compounds and cyclically conjugated aromatics. It was as late as 1966 when we showed [3, 4] that the mesomeric state (**1b**) of highly symmetrical polymethine cyanines ($X = X' = NR_2^{1/2\oplus}$) has unique features which bear no comparison to those of the aromatic state. This has led to the concept of an ideal polymethine state [3]. Typical features of this state are high resonance (delocalization) energies comparable to those found in aromatics, identical π-bond orders, and strongly alternating π-electron densities along the polymethine chain in the ground state. Excitation by light causes a maximum alteration of the π-electron density distribution at the individual atomic centres and a minimum change in the geometry of the molecules in respect to the π-bond orders. Connected herewith is the very deep colour of substances in the nearly ideal polymethine state as compared with conjugated aromatics or polyenes of comparable molecular size, that is maximum transition probabilities corresponding to maximum oscillator strengths along with relatively long wave length light absorption [3, 4, 5].

At first these unique properties were derived empirically for symmetrical polymethines (**1**), $X = X'$, based on the HMO formalism by systematically varying the Coulomb integral values of the terminal chain atoms, with all the other parameters remaining constant. This will yield the afore-mentioned extremes if the Coulomb integral value is approximately that of a nitrogen atom. In the meantime FABIAN and HARTMANN have shown [6, 7, 8] that the ideal polymethine state is a necessary consequence of the HMO theory, just like Hückel derived the idea for the aromatic state some 40 years ago.

Whereas in the past models simulating the ideal polymethine state have always been applied to symmetrical molecules (**1**; $X = X'$), the formalism of a solvatochromic perturbation of a molecule by a reaction field as developed within the framework of a microstructural model of solvatochromism [9] enables one to study by MO methods the properties of a molecular system whose electronic structure changes from the asymmetrical and nonpolar, polyenic state (**1a**, $X \neq X'$) towards the likewise asymmetrical but polar, polyenic state (**1c**, $X \neq X'$), passing in the course of it through state **1b**, which is symmetrical and polymethinic in terms of its π-electron distribution.

Properties of the model

When deriving the microstructural model of solvatochromism, the electric potential distribution at the surface of the molecule is calculated from the "real" charge distribution at the atomic centres of a molecule [9]. In the particular case of the pentamethinemerocyanine **1**, $n = 2$, $X = NR_2$, $X' = 0$, under study the VESCF-LCAO-MO wave functions [9, 10] have been used. In a solvent continuum the solute molecule creates a solvent reaction field φ^{LM} which is commensurate in size with the calculated potential at the surface of the molecule. The action of the solvent field on the molecule is included as the perturbation term H' in the Hamiltonian of a MO calculation using PPP wave functions:

$$H = H_0^{core} + H' \quad \text{where} \quad H' = \lambda \cdot \varphi^{LM}$$

The only parameter arbitrarily adjusted in the model is the absolute size of the perturbation term H' which for the test calculations of the microstructural model of solvatochromism [9] was selected to yield a largely symmetrical π-electron distribution in the pentamethine merocyanine at maximum perturbation ($\lambda = 1$), that is, a polymethinic structure **1b** is realized.

It is, however, not easy to estimate an exactly symmetrical structure. Taking the pentamethine merocyanine molecule **1**, $n = 2$, $X = NR_2$, $X' = 0$, as an example and looking only at the integral values of the hetero atoms, we find that both atoms have identical core integral values, as shown in Fig. 1, at $\lambda = 0.9$ in the reaction field of the ground state N and at $\lambda = 0.47$ in the reaction field of the first excited singlet state V_1. This does not apply to the methine carbon atoms, whose integral values, owing to the dipolar nature the molecule are changed in a reverse manner [9], meaning that the π-electron distribution at the methine atoms will become increasingly asymmetrical as the solvent reaction field increases. The effect, however is small compared with the relatively large changes at the hetero atoms. It can be roughly estimated that the ideal symmetrization of the molecules in the ground state N will occur at about $\lambda = 1$, and in the first excited singlet state V_1 at about $\lambda = 0.5$.

To study all the intermediate states between the valence structures **1a** → **1c**, explained at the beginning, one would have to increase the strength of the solvent interaction above the symmetrical state **1b**. As can be estimated by extrapolation of the hetero atom integral values for the reaction field in the ground state N with reference to Fig. 1, the polar state **1c** which is analogous to **1a** would hypothetically be reached at a value of λ of 1.8. The parametrization of this state corresponds, however, in principle with that in the reaction field of the first excited singlet state V_1 at a λ-value of 0.9 (*cf.* Fig. 1). That means, using the calculations in the reaction field of the first excited singlet state between $\lambda = 0$ and $\lambda = 1$, it is possible to completely simulate the transition from the nonpolar structure **1a** to the polar structure **1c**, the symmetrical polymethine state **1b** being reached at $\lambda \sim 0.5$.

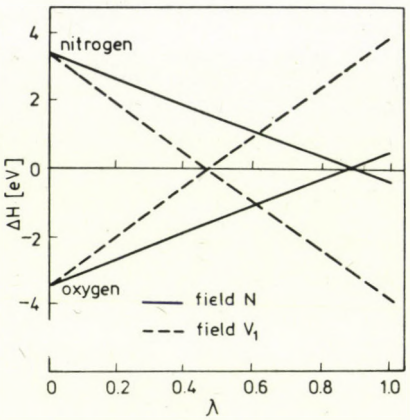

Fig. 1. Differences between the two terminal hetero atom core integral values ΔH of the pentamethine merocyanine *1* ($n = 2$, X = NR_2, X′ = 0) as a function of the solvent polarity parameter λ; solid lines: reaction field in the ground state N; dotted lines: reaction field in the first excited singlet state V_1

The reason for this behaviour is obviously that the dipole moment of the pentamethine merocyanine molecule increases from 5.8 debye to 11.8 debye, that is by a factor of 2, when the molecule in the solvent-free state ($\lambda = 0$, structure **1a**) is excited by light [9]. Thereby an electronic structure close to the mesomeric state **1b** is realized in the V_1 state already in nonpolar solvents. Interaction between this semipolar structure and the reaction field in the excited state will then yield the highly polar structure **1c** more rapidly than it is possible in the reaction field of the ground state. In accordance herewith, the perturbation parameter H' of the Hamiltonian shows a response which in the excited state is at all atomic centres greater by a factor of about 2 than in the ground state [9].

With the exception of investigating the solvent dependence of the fluorescence band, it has not been possible so far to provide evidence of the properties predicted for solvatochromic dyes in the reaction field of the excited state. It is also to be emphasized that the information gained from the model carries — in addition to the greatly simplified approximations used for determining the reaction field [9] — all the indeterminacies which are well known to occur when the PPP formalism is used to describe the features of the V_1 state. The solvent dependence of the chemical shifts in the NMR spectra of negatively solvatochromic dyes [11, 12] is a first indication, however, confirming the solvent-induced changes in the electronic structure in the direction mentioned. By virtue of their special molecular structure, these dyes have a relatively strong polar structure between **1b** and **1c**, which exists without solvent interaction already in the ground state, and continues to change towards **1c** as the polarity of the solvent increases.

Results

The behaviour of the energy of the ground state N and of the first excited singlet state V_1, as well as the behaviour of the $N \rightarrow V_1$ transition energy and oscillator strength in the reaction field of the first excited singlet state of the pentamethine merocyanine **1**, $n = 2$, $X = NR_2$, $X' = 0$, have already beeen described in [9] (*cf.* Figs 9 and 10 in [9]). Whereas the energies of the N and V_1 states in the reaction field of the ground state fall off relatively continuously with rising solvent polarity, there are broad maxima at λ values between 0.3 and 0.6 in the solvent field of the first excited singlet state, with the maximum in the ground state, in particular, being very pronounced. This accounts for the pronounced minimum at a λ value around 0.55 when calculating the transition energy within the field of the excited state which is responsible for fluorescence emission. This confirms FÖRSTER's qualitative consideration based on the VB theory [2] according to which the transition energy of a chain-like, mesomeric system (**1**) has a minimum in the symmetrical state (**1b**). Parallel to this minimum the oscillator strength in the solvent reaction field of the excited state shows [9] a clear maximum at $\lambda = 0.6$. Hence the MO calculations demonstrate convincingly that the deepest colour, that is a maximum transition probability in conjunction with a minimum transition energy is to be found in a molecule whose π-electron distribution is approximately symmetrical, such as in **1b**.

By contrast to the simple VB considerations, the LCAO-MO model used by us enables moreover more far-reaching conclusions to be drawn concerning the changes occurring in the electronic structure. The behaviour of the π-electron densities in the solvent reaction field of the first excited singlet state is illustrated in Fig. 2. Like in the reaction field of the ground state [9], the molecules in the ground state exhibit a pronounced π-electron density alternation along the polymethine chain, which is reversed in the excited state (indicated in Fig. 2 by dotted arrows between the ground and excited state). Here, too, the solvent interaction effect is greater in the ground state than in the excited state of the molecule, with a clear minimum of the π-electron densities in the ground state at the methine atoms 1, 3 and 5, and a clear maximum at the methine atoms 2 and 4 in the λ-range between 0.4 and 0.7, that is near the symmetrical structure **1b**.

Particularly striking is the behaviour of the π-bond orders in the field of the first excited singlet state shown in Fig. 3. The π-bond orders in the ground state corresponding to structure **1a** alternate very strongly in the solvent-free state ($\lambda = 0$). As the polarity of the solvent increases the alternation disappears. At λ values between 0.5 and 0.6 the highly symmetrical structure **1b** is realized. If the solvent interaction is increased still further, i.e. at λ values of about 1.0, this structure changes into structure **1c** as the bond alter-

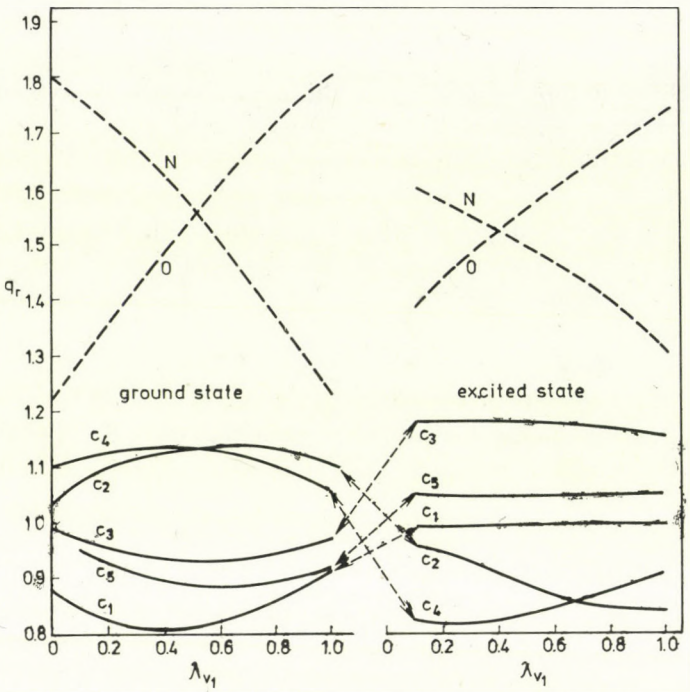

Fig. 2. Dependence of the π-electron densities q_r of the pentamethine merocyanine 1 ($n = 2$, $X = NR_2$, $X' = 0$) on the solvent polarity parameter λ in the reaction field of the first excited singlet state V_1. The methine atoms are indexed beginning at the oxygen end. Left: molecule in the ground state N; right: molecule in the first excited singlet state V_1

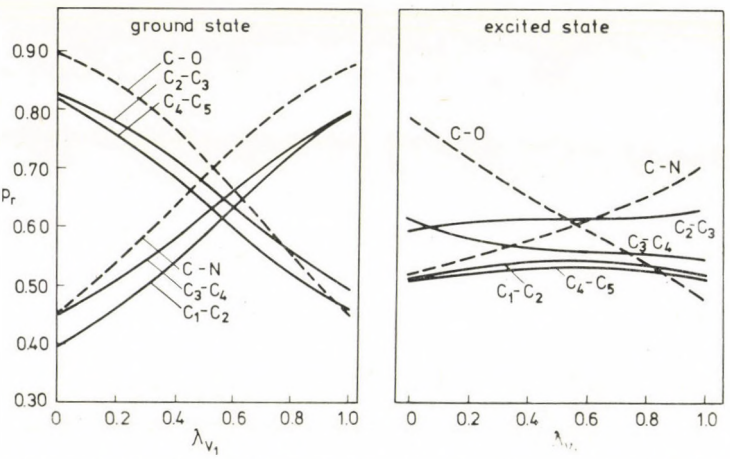

Fig. 3. Dependence of the π-bond orders p_r of the pentamethine merocyanine 1 ($n = 2$, $X = NR_2$, $X' = 0$) on the solvent polarity parameter λ in the reaction field of the first excited singlet state V_1. The methine atoms are indexed beginning at the oxygen end. Left: molecule in the ground state N; right: molecule in the first excited singlet state V_1

nation is reversed. Here again there is a considerably lower degree of solvent dependence in the excited state V_1.

The solvent dependence of the π-electron densities and π-bond orders can be illustrated even better by looking at the differences in the values of adjacent centres r, s, and by determining the arithmetic averages of the absolute values of this differences. For estimating the degree of alternation of the π-bond orders p it holds:

$$\overline{\Delta p_{r,s}} = \frac{1}{2n+3} \sum_{1}^{2n+3} |p_r - p_s| \qquad n = \text{index according to formula } \mathbf{1}.$$

To calculate the π-electron density alternation in a similar way is problematic insofar as the π-electron densities at the terminal hetero atoms of the polymethine chain are substantially higher than at the methine atoms. Consequently, they enter the calculations with a greater weight. For this reason the averages of the absolute values of the differences between the π-electron densities of adjacent centres r, s were calculated for all atoms, as well as for the methine atoms alone. The results are, however, in principle identical. It holds that

$$\bar{q}_{r,s} = \frac{1}{2n+3} \sum_{1}^{2n+3} |q_r - q_s| \qquad \text{for all atoms according to formula } \mathbf{1}$$

and

$$\bar{q}_{r,s} = \frac{1}{2n+1} \sum_{1}^{2n+1} |q_r - q_s| \qquad \text{for the methine atoms.}$$

Figure 4 shows the results in the solvent reaction field of the first excited singlet state. The π-electron density alternation in the ground state has maximum at $\lambda = 0.6$ and the π-bond order alternation in the ground state shows a pronounced minimum at $\lambda = 0.55$. But even in the excited state we still discern minor extremes around $\lambda = 0.5$, which are hardly visible in Figs 2 and 3. As a result, one achieves in addition to the ideal bond length equalization, as it is known from the VB theory, a maximum π-electron density alternation in the ground state, and also, to a lesser degree, in the first excited singlet state, this being unique features of the ideal polymethine state **1b**.

Maximum charge transfer and minimum changes on light absorption in geometry with respect to the π-bond orders* have been derived as further

* The qualification "with respect to the π-bond orders" is necessary since the bond angles are likely to undergo a maximum change [13]. This follows from the fact which KULPE *et al.* [14] established experimentally, i.e. that hybridization (and hence, the bond angle) depends on the π-electron density at the methine atoms which undergo a maximum change on light absorption, as shown by the present calculations.

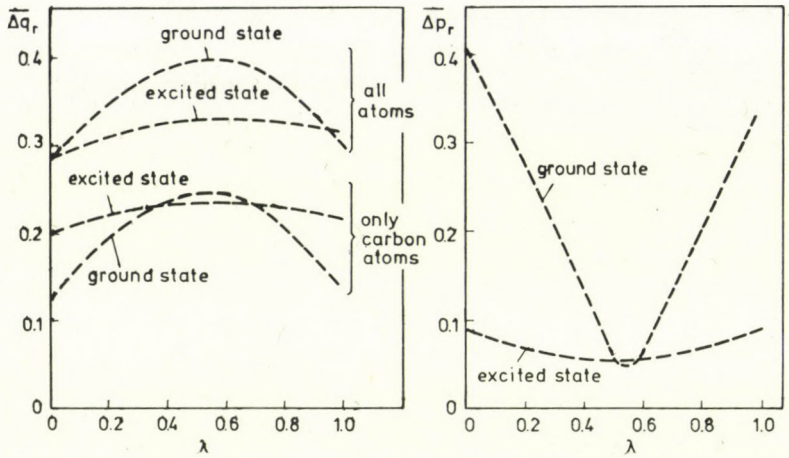

Fig. 4. Alternation of the π-electron densities $\overline{\Delta q_r}$ (left) and π-bond orders $\overline{\Delta p_r}$ (right) of the pentamethine merocyanine 1 ($n = 2$, X = NR_2, X′ = 0) *versus* solvent parameter λ in the reaction field of the first excited singlet state V_1

fundamental features of the ideal polymethine state [4, 7]. They are defined as follows:

$$\Sigma \mid \Delta q \mid_{N \to V_1} = \sum_{1}^{2n+3} \mid q_{r(N)} \mid - \mid q_{r(V_1)} \mid$$

$$\Sigma \mid \Delta p \mid_{N \to V_{1(\text{total})}} = \sum_{1}^{2n+3} \mid p_{r,s(N)} \mid - \mid p_{r,s(V_1)} \mid$$

To calculate bond contraction, only those bond orders were taken into account which decrease on light absorption and, analogously, for expansion only those which enlarge on light absorption.

In the case of studies on symmetrical polymethines in previous papers [4, 13] the intra molecular charge transfer could be compared with the behaviour of standing waves whose maxima and minima vary without causing any change in the C_{2v}-symmetry of the π-electron distribution along the longitudinal axis of the molecule. This definition of an intramolecular charge transfer which is localized at the individual atomic centres differs fundamentally from the earlier approach which goes back to NAGAKURA [15,16], according to which shifting of the charge from a residual part R of the molecule towards a substituent S and *vice versa* is the only condition essential to a charge transfer. The present considerations of the model enable us to compare the two approaches. On the one hand, the dipole moment increases in both the ground state and on light absorption with growing solvent interaction of the molecules **1**, X = NR_2, X′ = 0, that is, during the transformation of **1a** *via* **1b** to **1c**, charge is being transferred from the nitrogen atom to the oxygen atom, in the sense of NAGAKURA. But the π-electron densities, on the other hand, also change in different ways at all atomic centres both with rising solvent interaction and on light absorption in the sense of the above definition, meaning that in the molecules under consideration the two mechanisms of intramolecular charge transfer overlap each other.

The behaviour of the intramolecular charge transfer and the changes in geometry on light absorption in the sense of the polymethine concept is illus-

trated in Fig. 5 for both the solvent reaction field in the ground state and in the first excited singlet state. The charge transfer on light absorption has a peak at $\lambda = 0.7$ in the reaction field of the ground state and at $\lambda = 0.35$ in the reaction field of the excited state. The total change in geometry on light absorption shows a minimum at $\lambda = 0.9$ and at $\lambda = 0.5$ in the reaction field of the ground state and the excited state, respectively. This holds both for the total change in geometry and for the expansion and contraction of the bonds. An interesting feature is that the bonds cease contracting in the ideal polymethine state, *viz.* at $\lambda = 1.0$ for the field N and at $\lambda = 0.5$ for the field V_1. All in all, unique properties result again near the symmetrical, ideal polymethine state, even though the maximum of the intramolecular charge transfer has shifted to somewhat lower values of λ.

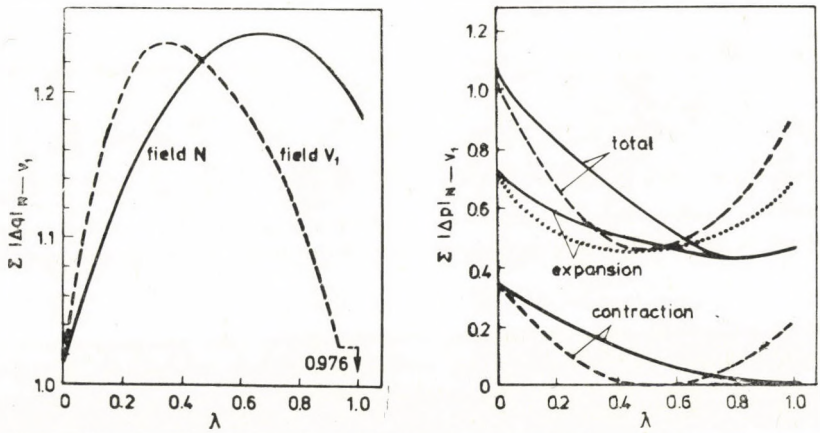

Fig. 5. Intramolecular change transfer at all atomic centres (left) and change of π-bond orders (right) on light absorption in the pentamethine merocyanine 1 ($n = 2$, X = NR_2, X′ = 0) *versus* solvent parameter λ. Solid lines: in the reaction field of the ground state N; dotted lines: in the reaction field of the first excited singlet state V_1

The charge transfer as defined by NAGAKURA [15, 16], on the other hand, shows an altogether different behaviour regardless of whether one considers the amino group as substituent S of a polyenal R, or the carbonyl group as substituent S of a dieneamine R. Figure 6 illustrates, for both examples, the charge transfer from substituent S to residue R as a function of solvent polarity for both the reaction field in the ground state and in the excited state. The result as opposed to the behaviour of the π-electron densities depicted in Fig. 4 is a steady increase in charge transfer with rising solvent polarity. This is in agreement with the increase in the dipole moments where no extremes were observed [9]. Consequently, NAGAKURA's approach of charge transfer fails to cover essential features of the changes occurring in the molecular structure of a molecule. The electron shift along the molecule's longitudinal

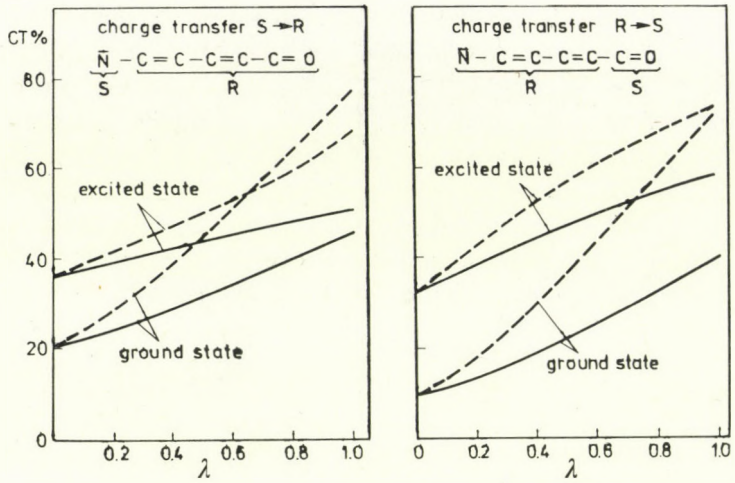

Fig. 6. Intramolecular charge transfer in the sense of NAGAKURA [15,16] as a function of the solvent parameter λ when the molecule is separated into different parts R and S. The different combinations are indicated in the top of the figure. Solid lines: in the reaction field of the ground state N; dotted lines: in the reaction field of the first excited singlet state V_1

axis is not the only point of interest when assessing the electronic structure of a solvatochromic molecule; rather it is the changes induced at all atomic centres in the electronic structure by interactions with the solvent reaction field or on light absorption which are of relevance from the point of view of a more polyenic or more polymethinic behaviour.

Conclusions

The concept of the existence of an ideal polymethine state can be hypothetically supported with the aid of the formalism of the microstructural model of solvatochromism developed by NOLTE and DÄHNE [9]. Chain-like, unsaturated molecules (**1**) which are intermediate between the polyenic valence structures **1a** and **1c** pass through a highly symmetrical state **1b**, which exhibits all the properties characteristic of the ideal polymethine state. These are [4]:

- minimum transition energy and maximum transition probability,
- maximum π-electron density alternation in the ground state and — to a lesser degree — in the first excited singlet state,
- maximum equalization of the π-bond orders in the ground state and — to a lesser extent — in the first excited singlet state,
- maximum intramolecular charge transfer at all atomic centres during the $N \rightarrow V_1$ transition,
- minimum changes in geometry with respect to the π-bond orders during the $N \rightarrow V_1$ transition.

REFERENCES

[1] NOLTE, K.-D., DÄHNE, S.: J. Prakt. Chem., **318,** 643 (1976)
[2] FÖRSTER, TH.: Z. Elektrochem., Angew. Physik. Chem., **45,** 548 (1939)
[3] DÄHNE, S., LEUPOLD, D.: Ber. Bunsenges. Physik. Chem., **70,** 618 (1966)
[4] DÄHNE, S,: Science [Washington], **199,** 1163 (1978)
[5] DÄHNE, S., RADEGLIA, R.: Tetrahedron, **27,** 3673 (1971)
[6] FABIAN, J., HARTMANN, H.: J. Signalaufzeichnungsmaterialien, **2,** 457 (1974)
[7] FABIAN, J., HARTMANN, H.: Theoret. Chim. Acta [Berl.], **36,** 351 (1975)
[8] FABIAN, J., HARTMANN, H.: J. Molec. Structure, **27,** 67 (1975)
[9] NOLTE, K.-D., DÄHNE, S.: Adv. Molec. Relax. Processes, **10,** 299 (1977)
[10] NOLTE, K.-D., DÄHNE, S.: J. Prakt. Chem. **318,** 993 (1976)
[11] BENSON, H. G., MURRELL, J. N.: J. Chem. Soc., Faraday Trans. II, **68,** 137 (1972)
[12] WÄHNERT, M., DÄHNE, S.: J. Prakt. Chem., **318,** 321 (1976)
[13] DÄHNE, S., KULPE, S., NOLTE, K.-D.: RADEGLIA, R.: Photogr. Sci. Engng., **18,** 410 (1974)
[14] KULPE, S., ZEDLER, A., DÄHNE, S., NOLTE, K.-D.: J. Prakt. Chem., **315,** 865 (1973)
[15] NAGAKURA, S., TANAKA, J.: J. Chem. Physics, **22,** 236 (1954)
[16] NAGAKURA, S.: J. Chem. Physics, **23,** 1441 (1955)

Siegfried DÄHNE
Klaus-Dieter NOLTE
Zentralinstitut für Optik und Spektroskopie der Akademie der Wissenschaften der DDR 1199, Berlin-Adlershof, Rudower Chaussee 5. DDR

Acta Chimica Academiae Scientiarum Hungaricae, Tomus 97 (2), pp. 159—166 (1978)

KINETICS AND MECHANISM OF SUBSTITUTION REACTIONS OF COMPLEXES, LV SOLVATION OF $[Cr(NCS)_4(BENZYLAMINE)_2]^-$ IN ACETONE-WATER MIXTURES

J. ZSAKÓ, CS. VÁRHELYI, D. OPRESCU* and I. GĂNESCU**

(Department of Physical Chemistry, Babeş-Bolyai University, Cluj-Napoca, Romania
*** Faculty of Chemistry, University of Craiova, Romania)*

Received February 10, 1977

The solvation kinetics of $[Cr(NCS)_4(benzylamine)_2]^-$ in acetone–water mixtures has been studied. Benzylamine molecules are not substituted, only NCS^- ions are exchanged for solvent molecules. Reaction (1) is hindered by increasing acetone content, showing the importance of solvent molecules in reaction mechanism. Reaction (1) is hindered also by hydrogen ions. Rate constants of reaction (1) do not depend on the nature of the amine in ethanol–water mixture, but in acetone–water mixtures rate constants obtained for the benzylamine derivative differe essentially from the rate constants of pyridine and aniline derivatives reported earlier.

The Reinecke salt like compounds containing the complex anion $[Cr(NCS)_4A_2]^-$, where *A* stands for ammonia or an amine, are sparingly soluble in water, but readily soluble in water-organic solvent mixtures. In these solutions the complex is not stable and undergoes solvation reactions, involving the exchange of NCS^- and A for solvent molecules.

The kinetics of such solvation reactions has been studied first by ADAMSON [1] in the case of the Reinecke salt itself (*i.e.* with $A = NH_3$) in ethanol–water and methanol–water mixtures. This author has observed the practically simultaneous exchange of two NCS^- ions for solvent molecules and has reported the kinetics of this reaction not to be influenced importantly by the solvent composition.

THOMAS and HOLBA [2] have reported also the substitution of two NCS^- ions in the case of the analogous ethylenediamine complex (A_2 = en), although these authors have found a smaller rate constant for the substitution of the second ligand, than for the substitution of the first one.

In our previous papers [3—11] several Reinecke salt like complexes have been studied in ethanol–water mixtures, with A = aniline, *p*-phenetidine, *p*-toluidine, *p*-ethylaniline, *p*-anisidine, *m*-xylidine and benzylamine. Our results showed the behaviour of the complex to depend upon the nucleophilic character of the amine. If the nucleophilic character is strong, as in the case of the complexes studied by ADAMSON, THOMAS and HOLBA and if A = benzylamine, only NCS^- ions are substituted [10]. If the nucleophilic character is

weak, also the amine molecules leave the complex ion. On the basis of our experimental data [3–9] the simultaneous exchange of two NCS^- ions and the following possible reactions can be presumed:

$$[Cr(NCS)_4A_2]^- + 2R = [Cr(NCS)_2R_2A_2]^+ + 2NCS^- \quad (1)$$

$$[Cr(NCS)_2R_2A_2]^+ + 2R = [Cr(R)_4A_2]^{3+} + 2NCS^- \quad (2)$$

$$[Cr(NCS)_4A_2]^- + 2R = [Cr(NCS)_4R_2]^- + 2A \quad (3)$$

$$[Cr(NCS)_2R_2]^- + 2R = [Cr(NCS)_2R_2A_2]^+ + 2NCS^- \quad (4)$$

$$[Cr(NCS)_2R_2A_2]^+ + 2R = [Cr(R)_6]^{3+} + 2NCS^- \quad (5)$$

where R stands for a molecule of solvent.

Reactions (1) and (4) seem to follow the S_N1 mechanism, and their kinetic parameters are practically the same for all complexes mentioned above. It is not influenced neither by the composition of the solvent, nor by the presence of mineral acids if $[H^+] > 10^{-3}$.

Reactions (2) and (5) occur only in neutral solutions, they are completely hindered by mineral acids.

Reaction (3) involves the substitution of one or two amine molecules for alcohol molecules, accordingly to a second order reaction. It is accelerated by the presence of mineral acids too and its kinetic parameters depend upon the nucleophilic character of the amine.

Reactions (3), (4) and (5) have not been observed if A = benzylamine [10].

If A = pyridine, the complex is sparsely soluble even in ethanol. This is why it has been studied in acetone–water mixtures [11]. A similar study has been made with the aniline derivative also in acetone–water mixtures [12]. These studies revealed some special features of solvation in these solvent mixtures. The general behaviour of the complex resembles the behaviour of complexes with A = aromatic amine, but there are some important differences.

1. Rate constants of reaction (1) and (4) are practically the same in ethanol–water mixtures, irrespective to the solvent composition and to the nature of the amine. In acetone–water mixtures the situation is completely different. Rate constants of reaction (1) and (4) are different, they are highly influenced by the nature of the amine, by the solvent composition and by the acidity of the solution. The rate constants decrease with increasing acetone content and with increasing mineral acid content.

This is related perhaps to the aprotic character of acetone and it is in agreement with ADAMSON's presumption [1], that the mechanism of reaction (1) is not S_N1, but S_N2 FS, involving the participation of solvent molecules through their hydrogen bridges.

2. Reaction (3) seems to be of mechanism S_N2 as in alcohol–water mixtures.

Results and discussion

In the present paper the solvation of $[Cr(NCS)_4(benzylamine)_2^-]$ has been studied in aceton–water mixtures, containing 38.89, 44.44, 50 and 100 vol % acetone (for the last one no special measures have been taken to ensure anhydrous conditions). The concentration of the unchanged complex ion and of the NCS^- ions liberated have been determined as function of time.

As in ethanol–water mixtures too, no evidence of the benzylamine substitution has been obtained.

The determination of the concentration of the initial complex ion (c) allows to derive rate constants for reaction (1). A graphical plot of $\lg \frac{c_0}{c}$ versus time gives a good linearity (Fig. 1), *i.e.* the solvation process (1) is apparently a first order reaction. The rate constants obtained are presented in Table I.

The graphical plot of $\log k/T$ versus $1/T$ showed a satisfactory linearity and the activation enthalpy and activation entropy values, given in Table II, could be calculated.

As seen, the activation enthalpy is not very much influenced by the solvent composition, excepting the pure acetone solutions, where $\Delta H^{\ddagger}$ is smaller, exactly as with the pyridine derivative in acetone–water mixtures [11]

In our previous studies the comparison of concentration data concerning the unchanged complex ion and the free NCS^- ions allowed us to obtain pieces

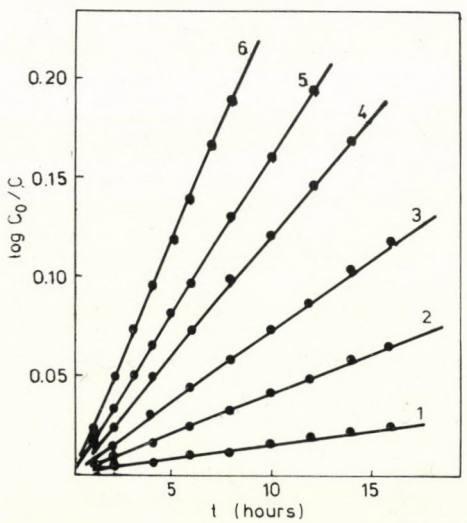

Fig. 1. Determination of the rate constant: 1 – 50 °C, 100 % ac; 2 – 50 °C, 38.9 % ac. 10^{-1} *m* $HClO_4$; 3 – 50 °C, 50 % ac; 4 – 59 °C, 38.9 % ac, 10^{-1} *m* $HClO_4$; 5 – 56 °C, 38.9 % ac; 6 – 59 °C, 44.4 % ac

Table I

First order rate constants of reaction (1) in neutral solutions
$k_1 \times 10^6$, s^{-1}

t °C	Acetone content, vol %			
	38.9	44.4	50.0	100
50	5.28	4.80	4.65	0.96
53	7.83	7.22	6.85	1.31
56	10.3	9.86	9.44	1.85
59	16.1	15.0	14.4	–

Table II

Activation parameters of reaction (1) in neutral solutions

Acetone content vol %	38.9	44.4	50.0	100
$\Delta H^{\ddagger}$, kcal/mole	25.3±1.6	26.0±1.6	26.0±1.5	22.6±0.7
$\Delta S^{\ddagger}$, e. u.	−4.7±5.1	−2.5±4.9	−2.6±4.7	−16.2±1.4

of information relatively to reaction (2). In the present paper the measurements made on the free NCS^- ions showed a finite zero time concentration, as in the case of the complexes studied earlier, but even the corrected values are very scattered and no quantitative conclusions could be drawn. At any rate, these data show reaction (2) to occur in neutral solutions, but to be hindered with increasing acetone content.

In order to study the influence of mineral acids, some runs have been performed in the presence of perchloric acid in solutions containing 38.9 vol % acetone. Rate constants derived are presented in Table III.

Table III

Influence of perchloric acid concentration on the first order rate constants of reaction (1) in solutions containing 38.9 vol % acetone
$k_1 \times 10^6$, s^{-1}

t °C	$[HClO_4]$, mole/l			
	0	10^{-3}	10^{-2}	10^{-1}
50	5.28	3.39	2.81	2.57
53	7.83	–	3.83	3.66
56	10.3	–	5.83	5.31
59	16.1	–	8.61	7.76

It is apparent that reaction (1) is sensibly hindered by hydrogen ions as with all Reinecke salt like complexes both in ethanol–water and in acetone–water mixtures. But it is worth mentioning, that rate constants decrease with increasing perchloric acid concentration up to 10^{-1} mole/l (*i.e.* in all the range investigated), exactly as with the pyridine and aniline derivatives in acetone–water mixtures [11–12]. On the other hand, in ethanol–water mixtures $[HClO_4] = 10^{-3}$ mole/l is already sufficient to hinder "basic solvolysis" and to make rate constants independent of hydrogen ion concentration.

It is interesting to compare the rate constants of reaction (1) at 50 °C with the similar constants obtained with the pyridine and aniline derivatives at the same temperature. In Tables IV and V these rate constants are given for the three derivatives in different solvent mixtures and at different acidities. Values presented for the aniline derivative have been obtained by means of interpolation by using rate constants reported earlier [12].

It is apparent that rate constants depend very much on the nature of the co-ordinated amine. In ethanol–water mixtures these rate constants have almost the same value for a large number of amines, but in acetone–water mixtures they are even not of the same order of magnitude. On the other hand

Table IV

Rate constant of reaction (1) at 50 °C in neutral solution
$k_1 \times 10^6$, s^{-1}

Influence of the solvent composition

Amine	Acetone content, vol %				Reference
	25	50	75	100	
Pyridine	–	0.94	0.44	0.31	[11]
Benzylamine	5.28*	4.65	–	0.96	this paper
Aniline	48.9	45.1	29.0**	7.54	[12]

acetone content *38.9, **90 vol %

Table V

Rate constant of reaction (1) at 50 °C
$k_1 \times 10^6$, s^{-1}

Influence of perchloric acid concentration

Amine	Acetone content vol %	$[HClO_4]$, mole/l				
		0	10^{-3}	10^{-2}	10^{-1}	Reference
Pyridine	50	0.94	0.52	0.41	0.39	[11]
Benzylamine	38.9	5.28	3.39	2.81	2.57	this paper
Aniline	25	48.9	13.2	10.8	9.75	[12]

these rate constants decrease systematically and in an important extent with increasing acetone content. In this respect one can observe a rather different behaviour in ethanol–water mixtures, where the rate constants of reaction (1) practically are not influenced by the solvent composition [10].

These phenomena show clearly the solvent molecules and their hydrogen bonds to play an important part in the mechanism of reaction (1).

As the influence of the acidity is concerned, the data presented in Table V illustrate the above statement that the rate constants are diminished by increasing acidity up to $[HClO_4] = 10^{-1}$ mole/l.

On the other hand one can see the rate constants to depend on the nature of the amine in the same extent as in neutral solutions.

Activation parameters derived from the rate constants given in Table III are presented in Table VI.

Table VI

Influence of perchloric acid concentration on the activation parameters of reaction (1) 38.9 vol % acetone

$[HClO_4]$, mole/l	0	10^{-2}	10^{-1}
$\Delta H^{\ddagger}$, kcal/mole	23.5 ± 1.6	26.5 ± 0.9	25.8 ± 0.3
$\Delta S^{\ddagger}$, e. u.	-4.7 ± 5.1	-2.3 ± 2.8	-4.5 ± 0.8

As seen, no systematic variation of the activation enthalpy can be observed. In this respect there is a fundamental difference between the behaviour of the pyridine derivative and the benzylamine one in acetone–water mixtures. In the case of the pyridine derivative the increase of the hydrogen ion concentration promotes reaction (3), requiring a higher activation enthalpy and so $\Delta H^{\ddagger}$ increases systematically. With the benzylamine derivative reaction (3) does not occur and $\Delta H^{\ddagger}$ remains practically the same.

The explanation of the rather strange behaviour of Reinecke salt like complexes in acetone–water mixtures, as compared to their behaviour in ethanol–water ones can be given in terms of ADAMSON's hypothesis concerning the mechanism of the solvation reaction (1). ADAMSON [1] presumes in the case of the Reinecke salt the formation of hydrogen bridges between the ROH type solvent molecule and the co-ordinated NH_3 and a hydrogen bridge-like interaction of the same solvent molecule and the co-ordinated NCS:

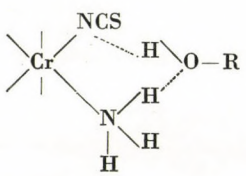

Due to the labilizing effect of this "hydrogen bridge", the NCS^- ion leaves the complex and its place will be occupied by the solvent molecule. Since acetone cannot form hydrogen bridges, decreasing of the rate constants with increasing acetone content is understandable. As the influence of the amine molecule is concerned, results presented in Tab. IV and V also support ADAMSON's presumptions, *viz.* the importance of the hydrogen bridge formation between the co-ordinated amine and the solvent molecule. The order of increasing rate constants (pyridine–benzylamine–aniline) is that of increasing tendency to hydrogen bridge formation. It is worth mentioning in this connection the behaviour of Reinecke salt like complexes in ethanol–water mixtures, where rate constants of reaction (1) are very little influenced by the nature of the co-ordinated amines. This is in disagreement with ADAMSON's hypothesis. One can presume, that in the presence of only R – OH type solvent molecules, the entering molecule is H-bridged mainly to other solvent molecules and not to the co-ordinated amine, but in acetone–water mixtures the ADAMSON mechanism becomes preponderant. The influence of perchloric acid seems also to be understandable, since protonation of the solvent molecules diminishes their tendency to give H-bridges and this is why rate constants diminish too. This effect is more important in acetone–water mixtures and practically does not appear in ethanol–water mixtures, due to the very large number of ROH type molecules able to form H-bridges.

Experimental

$NH_4[Cr(NCS)_4(benzylamine)_2] \cdot H_2O$ has been prepared as described earlier [10].

Kinetic measurements. Samples of the complex salt have been dissolved in calculated quantities of preheated acetone and diluted with preheated water to a certain volume, to obtain solutions with initial concentration of the complex of about 5×10^{-3} mole/l. The solutions were kept in an ultrathermostat. The samples taken at various times were cooled down quickly with ice and the concentration of the free NCS^- ions and that of the unchanged complex ions were determined.

Determination of NCS^-. The free NCS^- ion concentration was determined photocolorimetrically. An aqueous solution of iron(III) perchlorat (0.1 mole/l) was added in excess to the samples (1 – 2 ml solution to 0.5 – 2 ml aliquot parts diluted with dest. water to 50 ml) and the absorbance was measured, using a blue filter. The corresponding concentration values were obtained by means of a calibration curve.

Determination of the unchanged complex ion. For this purpose a precipitation reaction was used with 8-quinolinol (oxine) hydrochloride (1 mole oxine/1 in 3 *N* HCl). This salt gives a sparingly soluble product with the complex ion studied (oxine. $H[Cr(NCS)_4(benzylamine)_2]$). The precipitate was filtered through Gooch filter 1 G_4 and washed with distilled water. Than the precipitate was dissolved in methanol and the extinction of the obtained reddish violet solution was measured photocolorimetrically by means of a green filter. A calibration curve was used.

Kinetic parameters were calculated by means of the method of least squares and errors were derived on the basis of the standard deviation of the experimental points, by using $t_{0.95}$ values.

REFERENCES

[1] ADAMSON, A. W.: J. Amer. Chem. Soc. **80,** 3183 (1958)
[2] THOMAS, G., HOLBA, V.: J. Inorg. Nucl. Chem. **31,** 1749 (1969)
[3] ZSAKÓ, J., VÁRHELYI, Cs., GĂNESCU, I.: Rev. Roumaine Chim. **13,** 577 (1968)
[4] ZSAKÓ, J., VÁRHELYI, Cs., GĂNESCU, I., TURÓS, J.: Acta Chim. Acad. Sci. Hung. **61,** 167 (1969)
[5] ZSAKÓ, J., VÁRHELYI, Cs., GĂNESCU, I., ZÖLDI, L.: Monatshefte, **99,** 2235 (1968)
[6] ZSAKÓ, J.: Studia Univ. Babeș-Bolyai, Chem. **15,** 93 (1970)
[7] ZSAKÓ, J., GĂNESCU, I., VÁRHELYI, Cs., POPESCU, AL.: Rev. Chim. Minérale (Paris). **7,** 927 (1970)
[8] ZSAKÓ, J., GĂNESCU, I., VÁRHELYI, Cs., POPESCU, AL.: Z. anorg. allg. Chem. **380,** 216 (1971)
[9] ZSAKÓ, J., VOICULESCU, V., GĂNESCU, I., POPESCU, AL.: Rev. Roumaine Chim. **17,** 1977 (1972)
[10] ZSAKÓ, J., VÁRHELYI, Cs., GĂNESCU, I., OPRESCU, D.: Roczniki Chemii Ann. Soc. Chim. Polon. **48,** 1141 (1974)
[11] ZSAKÓ, J., OPRESCU, D., VÁRHELYI, Cs., GĂNESCU, I.: Zhur. neorgan. Khim. **17,** 3242 (1972)
[12] GĂNESCU, I., VOICULESCU, V., VÁRHELYI, Cs.: Monatshefte, **106,** 801 (1975)

János ZSAKÓ
Csaba VÁRHELYI
Univ. Babeș-Bolyai, Str. Arany J. 11. Cluj-Napoca, Romania,

Didina OPRESCU
Ion GĂNESCU
Facultatea de Chimie, Universitatea din Craiova, Romania.

Acta Chimica Academiae Scientiarum Hungaricae, Tomus 97 (2), pp. 167—175 (1978)

ON THE α-DIOXIMINE COMPLEXES OF TRANSITION METALS, LV

COBALT(III)-NYOXIMINE CHELATES WITH OXO ACIDS OF SULFUR

Cs. VÁRHELYI, A. BENKŐ, M. SOMAY and A. KOCH

(Faculty of Chemistry, Babeş-Bolyai University, Cluj-Napoca, Romania)

Received March 15, 1977

New complex anions of the type $[Co(Niox.H)_2XY]^{3-}$ (Niox.H_2 = 1,2-cyclohexane dione dioxime, X = Y,X ≠ Y = SO_3^{2-} and $S_2O_3^{2-}$) were obtained by means of air oxidation of Co^{2+}-nyoxime-X(Y)-mixtures or by ligand exchange reactions from the corresponding halogenoaquo non-electrolytes. Anation reactions of $[Co(Niox.H)_2(H_2O)X]^-$ with aromatic and heterocyclic amines lead to the formation of $[Co(Niox.H)_2(amine)X]^-$. 27 salts were isolated and characterized. Some structural problems were investigated by UV and IR spectral measurements. Other oxo anions of sulfur, *e.g.* SO_4^{2-} and $S_zO_6^{2-}$ ($z = 2-5$), are not suitable for these reactions due to sterical hindrances or for lack of sulfur donor atoms.

The alycyclic dioximes, like the aliphatic and aromatic ones, give a lot of dioximine chelates of cobalt(III) of various types, these later being monobasic acids ($H[Co(diox.H)_2XY]$), non-electrolytes ($[Co(diox.H)_2(amine)X]$) or bases ($[Co(diox.H)_2(amine)_2]^+$ ("diox.H" = the deprotonated dioxime molecule).

A series of 1,2-cyclopentane dione dioxime (pentoxime) and 1,2-cyclohexane dione dioxime (nyoxime) derivatives were described and characterized in our previous papers [1—4].

The aquation kinetics of some halogeno- and pseudohalogeno derivatives of the type $[Co(diox.H)_2(H_2O)X]$ and $[Co(diox.H)_2X_2]^-$ was also studied.

The very stable $Co(diox.H)_2$ ring system in the $[Co(diox.H)_2X_2]^-$ and $[Co(diox.H)_2(amine)X]$ complexes enables a great number of substitution reactions with amines, phosphines and negatively charged ligands without changing their trans geometric configuration.

From the point of view of the ligand exchange reactions — with exception of SO_3^{2-} — the oxo anions of sulfur ($S_2O_3^{2-}$, SO_4^{2-}, $S_2O_8^{2-}$ and $S_xO_6^{2-}$ (x = 2—6) were less investigated.

The SO_3^{2-}-ion enters easily in the inner co-ordination sphere of some metals of the VIII-th group.

Mononuclear cobalt(III) complexes with mono- and bidentate sulfito-ligands, as well as binuclear complexes with SO_3-bridges were described in the literature (*e.g.* $[Co(NH_3)_5(SO_3)]^+$ [10], $[Co(pn)_2(SO_3)_2]^-$ [11], $Na_3[CoNH_3)_2(SO_3)_2(NO_2)_2]$ [12], $[Co(CN)_4(SO_3)(H_2O)]^{3-}$ [13], $[Co_2(SO_3)(OH)_2(NH_3)_6]^{2+}$ [10].

Some sulfito-complexes of cobalt(III) and rhodium(III) with dimethylglyoxime, monomethylglyoxime and benzyldioxime were obtained by SYRZOVA *et al.* [14–17].

Some thiosulfato-complexes of cobalt: $[Co(NH_3)_5(S_2O_3)]^+$ [18], $[Co(CN)_5(S_2O_3)]^{4-}$ [19] were also mentioned.

The substitution reactions of $[Co(Niox.H)_2XY]$ complexes with oxo anions of sulfur were not investigated.

Table I

New complex salts of the $[Co(Niox.\ H)_2(So_3)_2]^{3-}$ *and* $[Co(Niox.H))_2(S_2O_3)_2]^{3-}$ *ions*

No.	Formula	Mol. wt. calcd.	Yield (%)	Aspect	Analysis	
					Calcd.	Found
1.	$[Co(NH_3)_6]$. $[Co(Niox.\ H)_2(SO_3)_2].14\ H_2O$	914.7	80	yellow microcryst.	Co 12.88 S 7.06 H_2O 27.56	12 60 7.30 27.10
2.	$[Co(NH_3)_5(H_2O)]$. $[Co(Niox.\ H)_2(SO_3)_2].14\ H_2O$	915.7	75	brown-yellow thin plates	Co 12.80 S 7.02 H_2O 27.54	12.55 7.12 27.20
3.	cis-$[Co(en)_2(NH_3)_2]$. $[Co(Niox.\ H)_2(SO_3)_2].8\ H_2O$	858.5	60	yellow plates	Co 13.73 NH_3 3.96 H_2O 16.79	13.75 3.80 16.40
4.	$[Co(en)_3]$. $[Co(Niox.\ H)_2(SO_3)_2].8\ H_2O$	884.6	75	yellow, short needles	Co 13.32 H_2O 16.29	13.36 16.00
5.	$[Cr(en)_3]$. $[Co(Niox.\ H)_2(SO_3)_2].5\ H_2O$	823.4	50	long, yellow prisms	Co + Cr 13.47 N 17.01 H_2O 10.94 Co + Cr	13.10 16.80 11.20
6.	$[Cr(urea)_6]$. $[Co(Niox.\ H)_2(SO_3)_2].5\ H_2O$	1003.8	70	yellow-green hexagonal cryst.	11.05 S 12.80 H_2O 8.79	11.20 12.40 8.70
7.	$[Co(NH_3)_6]$. $[Co(Niox.\ H)_2(S_2O_3)_2].10\ H_2O$	906.8	60	yellow dendrites	Co 13.00 S 14.14 H_2O 19.86	13.18 14.00 19.17
8.	$[Co(NH_3)_5(H_2O)]$. $[Co(Niox.\ H)_2(S_2O_3)_2].9\ H_2O$	889.8	50	brown-yellow rhomb. plates	Co 13.25 S 14.41 H_2O 18.22	13.45 14.60 18.67
10.	$[Co(en)_3]$. $[Co(Niox.\ H)_2(S_2O_3)_2].3\ H_2O$	858.5	60	dark yellow prisms	Co 13.73 S 14.94 H_2O 6.29	13.69 14.75 6.15
10.	$[Cr(en)_3]$. $[Co(Niox.\ H)_2(S_2O_3)_2].3\ H_2O$	851.5	55	dark yellow spears	Co + Cr 13.02 S 15.06 H_2O 6.34	12.86 15.20 6.10
11.	$[Cr(urea)_6]$. $[Co(Niox.\ H)_2(S_2O_3)_2].6\ H_2O$	1085.9	60	brown prisms	Co + Cr 10.21 S 11.81 H_2O 9.95	10.00 11.60 10.18

In the present paper the ligand exchange reactions of some $[Co(Niox.H)_2(H_2O)X]$ type complexes (X = Cl Br, I, NO_2, NCS, NCSe) with the alkaline and ammonium salts of the oxo acids of sulfur were studied from preparative point of view.

Both in sulfito- and thiosulfato complexes the central atom is directly bonded to an S donor atom [11–13, 19]. On the other hand SO_4^{2-} and $S_2O_6^{2-}$ ions have been observed not to enter in the cobalt(III) nyoximine nucleus. This means, that the presence of a sulfur donor atom is absolutely necessary.

Although in $S_xO_6^{2-}$ (x = 3, 4, 5, 6) there are sulfur donor atom, these ions do not enter in the co-ordination sphere of the cobalt(III) complexes. This is due probably to a sterical hindrance.

The classical air oxidation applied to the Co^{2+}-nyoxime-Na_2SO_3 ($Na_2S_2O_3$) mixtures yields $[Co(Niox.H)_2(SO_3)_2]^{3-}$ and $[Co(Niox.H)_2(S_2O_3)_2]^{3-}$, respectively

$$2Co^{2+} + 4Niox.H_2 + 1/2O_2 + 4SO_3^{2-} = 2[Co(Niox.H)_2(SO_3)_2]^{3-} + H_2O + 2H^+$$

$$2Co^{2+} + 4Niox.H_2 + 1/2O_2 + 4S_2O_3^{2-} = 2[Co(Niox.H)_2(S_2O_3)_2]^{3-} + H_2O + 2H^+$$

These complexes have been isolated as alkaline, ammonium and luteo salts.

The substitution reactions of $[Co(Niox.H)_2(H_2O)X]$ (X = Cl, Br, I, NCO, NCS and NCSe) with stoichiometric amounts of $(NH_4)_2SO_3$ and $(NH_4)_2S_2O_3$ lead to the formation of highly soluble $NH_4[Co(Niox.H)_2(H_2O)(SO_3)]$ and $NH_4[Co(Niox.H)_2(H_2O)(S_2O_3)]$, respectively.The co-ordinated water molecule in these compounds can be easily replaced by aromatic or heterocyclic amines.

The aromatic primary amines with pK = 9 – 13 are suitable for this purpose (aniline, alkyl-, alkoxy-anilines, chloro-, bromo-, iodo-anilines). The very weak bases, *e.g.* nitroanilines, sulfanylic- and anthranylic acids (pK = = 14–16) do not co-ordinate to cobalt. The pyridine bases (pK < 9) form also compounds of this type. The condensed heterocyclic bases (chinoleine, chinaldine, acridine, as well as α-picoline, give negative results probably because of sterical hindrance.

The anation reaction of $[Co(Niox.H)_2(SO_3)(H_2O)]^-$ with stoichiometric amounts of $Na_2S_2O_3$ gives $[Co(Niox.H)_2(SO_3)(S_2O_3)]^{3-}$ which can be characterized also by means of double decomposition reactions with luteo salts.

The substitution of water in the $[Co(Niox.H)_2(SO_3)(H_2O)]^-$ with Cl^-, Br^-, I^-, NCS^-, $NCSe^-$, NCO^- and N_3^- yields the corresponding $[Co(Niox.H)_2(SO_3)X]^{2-}$, which can be isolated as complex salts. The analogous reactions with $[Co(Niox.H)_2(S_2O_3)(H_2O)]^-$ lead to the formation of extremly highly soluble products in the common polar solvents used (H_2O, methanol, ethanol, acetone, dimethylformamide). Some complexes of the type amine.H $[Co(Niox.H)_2(S_2O_3)(amine)]$ were also isolated.

Table II

*New sulfito-(thiosulfato)-complex salts of the type amine.*H[Co(Niox.H)$_2$X(amine)] (X = SO_3^{2-} *or* $S_2O_3^{2-}$)

No.	Formula	Mol wt. calcd.	Yield (%)	Aspect	Analysis		
					Calcd.		Found
1.	pyridine.H[Co(Niox. H)$_2$–(SO_3) (pyridine)].H_2O	597.5	70	brown rhomb. plates	Co H_2O N	9.86 3.01 14.07	9.87 2.80 13.75
2.	β-picoline.H[Co(Niox.H)$_2$–(SO_3) (β-picoline)].H_2O	625.5	80	yellow hexagonal plates	Co S H_2O	9.42 5.12 2.88	9.40 5.30 3.10
3.	γ-picoline.H[Co(Niox.H)$_2$–(SO_3) (γ-picoline)].2 H_2O	643.5	60	yellow square plates	Co S H_2O	9.16 4.98 5.59	9.13 5.20 5.20
4.	*m*-toluidine.H[Co(Niox.H)$_2$–(SO_3) (*m*-toluidine)].5 H_2O	725.9	50	long yellow prisms	Co N H_2O	8.12 11.57 12.40	8.36 11.30 11.95
5.	*p*-toluidine.H[Co(Niox.H)$_2$–(SO_3) (*p*-toluidine)].5 H_2O	725.9	60	brown prisms	Co N H_2O	8.12 11.57 12.40	8.20 11.44 12.10
6.	aniline.H[Co(Niox.H)$_2$–(SO_3) (aniline)].2 H_2O	643.5	50	brown prisms	Co H_2O N	9.16 5.59 13.06	9.08 5.30 12.78
7.	NH_4[Co(Niox.H)$_2$(*p*-Cl-aniline) (SO_3)].2 H_2O	602.9	60	brown irregular cryst.	Co N H_2O	9.77 13.94 5.97	10.02 13.75 5.60
8.	NH_4[Co(Niox.H)$_2$(*p*-J-aniline) (SO_3)].H_2O	676.4	70	brown irregular cryst.	Co H_2O N	8.71 2.66 12.42	8.34 2.30 12.16
9.	NH_4[Co(Niox.H)$_2$(SO_3)–(thiourea)].H_2O	565.5	50	brown prisms	Co H_2O	10.42 3.18	10.60 3.60
10.	NH_4[Co(Niox.H)$_2$(SO_3)–(allylthiourea)]	555.5	60	brown plates	Co N	10.61 17.65	10.60 17.48
11.	*m*-xylidine.H[Co(Niox.H)$_2$–(SO_3) (*m*-xylidine)].5 H_2O	753.7	70	yellow, thin square plates	Co S H_2O	7.82 4.25 11.95	7.79 4.55 11.20
12.	Thiourea.H[Co(Niox.H)$_2$–(SO_3) (thiourea)].3 H_2O	627.6	50	yellow prisms (from acetone)	Co H_2O	9.39 8.61	9.63 8.15
13.	NH_4[Co(Niox.H)$_2$(S_2O_3)–(pyridine)].4 H_2O	622.5	30	short brown needles (from acetone)	Co H_2O N	9.46 11.57 13.50	9.91 11.45 13.35
14.	pyridine.H[Co(Niox.H)$_2$–(S_2O_3) (pyridine)].4 H_2O	684.6	35	brown prisms	Co H_2O N	8.61 10.52 12.75	8.75 10.30 12.46
15.	NH_4[Co(Niox.H)$_2$(S_2O_3)–(γ-picoline)]	564.5	30	short brown prisms	Co N	10.44 14.89	10.75 14.76

We observed that the reverse reaction, *i.e.*

$$[Co(Niox.H)_2(H_2O)X] + SO_3^{2-} = [Co(Niox.H)_2(SO_3)X]^{2-} + H_2O$$

(or with $S_2O_3^{2-}$, respectively) does not occur, only

$$[Co(Niox.H)_2(H_2O)(SO_3)]^- \ ([Co(Niox.H)_2(H_2O)(S_2O_3)]^-)$$

being formed.

This phenomenon shows the SO_3^{2-} and $S_2O_3^{2-}$ to have a greater "*trans*" effect than the halogen or pseudohalogen ions, in the mixed dioximine-cobalt(III)-chelates.

The electronic spectra of some sulfito- and thiosulfato-bis-nyoximino-cobalt(III) derivatives have been recorded in aqueous solutions.

In the electronic spectra of the complexes studied in the visible region no absorption maxima or inflexion points are observed. Therefore one can presume the ligand field transition bands to be overlapped by the first charge-transfer band. This band begins in the visible region and has its maximum at 28 – 33 kK. Generally 3 bands appear in UV region, both in the case of the SO_3- and S_2O_3-derivatives, exactly as with the analogous dimethylglyoximine complexes. As compared to the $[Co(DH)_2(SO_3)(amine)]^-$ complexes, the absorption bands of the $[Co(Niox.H)_2(SO_3)(amine)]^-$-derivatives seem to be at lower wave number. The wave number of the third band is always higher than in the case of the dimethylglyoxime derivatives, but with nyoxime it is sometimes lower than 50 kK. The mean values of the wave numbers are presented for the 3 absorption bands in Table III.

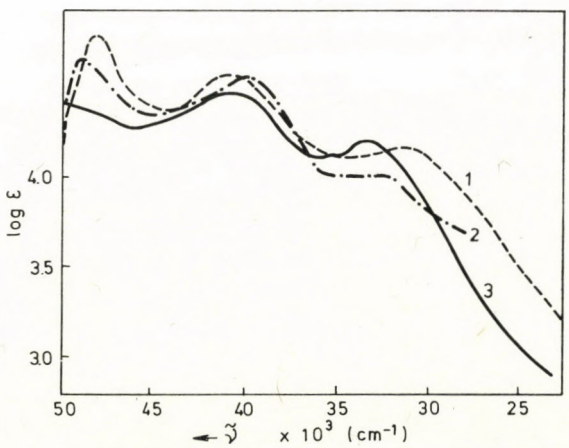

Fig. 1. Electronic spectra of some complexes of the type $NH_4[Co(Niox.H)_2(SO_3)(amine)]$: "1" $NH_4[Co(Niox.H)_2(SO_3)$ (allylthiourea)]; "2" $NH_4[Co(Niox.H)_2(SO_3)$ (*p*-J-aniline]); "3" *p*-toluidine.H$[Co(Niox.H)_2(SO_3)$ (*p*-toluidine)]

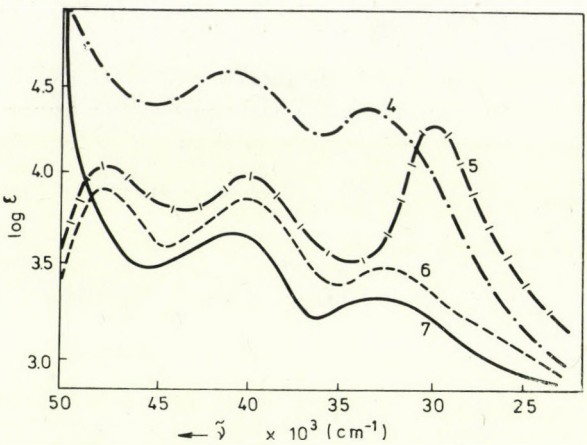

Fig. 2. Electronic spectra of some complexes of the type [Co(Niox.H)$_2$XY]: "4" γ-picoline. H[Co(Niox.H)$_2$(SO$_3$) (γ-picoline)]; "5" Na$_3$[Co(Niox.H)$_2$(S$_2$O$_3$)$_2$]; "6" NH$_4$[Co(Niox.H)$_2$(S$_2$O$_3$) (pyridine)]; "7" aniline.H[Co(Niox.H)$_2$(SO$_3$) (aniline)]

The effect of substitution of SO_3^{2-} by $S_2O_3^{2-}$ can be seen in the case of the pyridine derivative. It is apparent that the absorption bands are shifted towards the lower wave number values, exactly as with the corresponding dimethylglyoxime derivatives.

The IR spectra of the $[Co(Niox.H)_2(SO_3)_2]^{3-}$, $[Co(Niox.H)_2(SO_3)$-(amine)]$^-$, $[Co(Niox.H)_2(S_2O_3)_2]^{3-}$ and $[Co(Niox.H)_2(S_2O_3)(amine)]^-$ derivatives show the presence of strong intramolecular O−H...O hydrogen bridges (ν_{O-H}: 2350−2400 cm^{-1} (weak), δ_{O-H} 1700−1800 cm^{-1} (weak)), similarly to the analogous dimethylglyoxime derivatives. These hydrogen bridges stabilize the coplanar Co(Niox.H)$_2$ ring system, *i.e.* the "*trans*" configuration of the complexes of this type.

Table III

Mean values of the wave number of UV *absorption bands of* [Co(diox.H)$_2$XY] *type complexes*

Diox. H	X = SO_3^{2-}, Y = amine			X = Y = amine		
	wave number kK					
	a	*b*	*c*	*a*	*b*	*c*
DH	50	41.4	33.8	49.1	39.9	32.7*
Niox.H	50	40.7	33.2	–	–	–
Diph.H	48.6	37.7	31.0	49.3	38.6	31.5**

(DH$_2$ = dimethylglyoxime, Diph.H$_2$ = α-benzyldioxime, *, ** unpublished

The $\nu_{C=N}$ vibrations of the co-ordinated oxime groups have been found at 1580 – 1585 cm^{-1} (very strong). This band is situated at 1620 – 1640 cm^{-1} in the case of the free, non co-ordinated oxime.

The sulfito-ligand, like other XY_3 groups, with a pyramidale structure and a C_{3v} symmetry, has four IR and Raman active vibration frequencies: ν_1(S – O): 960 – 1010, $\nu_2(SO_2)$: 620 – 630, ν_3(S – O): 933 – 960, $\nu_4(SO_2)$ 469 – 495 cm^{-1} [20 – 22].

The thiosulfato group has also a C_{3v} symmetry with six IR and Raman active vibration frequencies: ν_1(S – S): 447, ν_2(S – O): 1004, $\nu_3(SO_2)$: 670, ν_4(S – O): 1106, $\nu_5(SO_2)$: 538 and ν_6: 339 cm^{-1} [23 – 25].

By co-ordination to metal ions through the sulfur atom, the S – O valence frequencies are shifted to higher wave number values in both cases [24 – 25]. The shift in the opposite direction is characteristic for a Me – O – S – O-co-ordination.

The IR absorption bands of the sulfito- and thiosulfato complexes investigated show that the Co – SO_3 and Co – S_2O_3-bonds are realized through the sulfur atom.

The ν_{N-H} vibrations were found at 3230 and 3080 – 3150 cm^{-1} indicating the strong covalent character of the Co – N (amine) bond in the $[Co(Niox.H)_2(SO_3)(amine)]^-$ type complexes.

The IR spectral data of some sulfito- and thiosulfato derivatives are given in Table IV.

Experimental

Preparation of $Na_3[Co(Niox.H)_2(SO_3)_2].9H_2O$. 5.0 g (20 mmole) of cobalt(II)-acetate and 5.6 g (40 mmole) of nyoxime in 150 ml diluted alcoholic solution (1 : 1) were oxidized by air bubbling for 3 – 4 hours, then 40 mmole of $Na_2SO_3 7\ H_2O$ were added and after 30 – 40 min the disulfito-salt precipitated from the filtered dark yellow solution with an excess of acetone (250 – 300 ml). Small, yellow needles. Yield: 80 %.

Analysis: Found Co 7.72, S 9.03, H_2O 21.40.

For $Na_3[Co(C_6H_9N_2O_2)_2(SO_3)_2].9\ H_2O$ (mol. wt. calcd. 732.4).

Calcd. Co 8.04, S 8.75, H_2O 22.13.

$Na_3[Co(Niox.H)_2(S_2O_3)_2]$-solution was obtained by an analogous way.

The luteo-salt of $[Co(Niox.H)_2(SO_3)_2]^{3-}$ and $[Co(Niox.H)_2(S_2O_3)_2]^{3-}$ were obtained by a double decomposition reaction from 5 – 5 mmole $Na_3[Co(Niox.H)_2(SO_3)_2]$ and $Na_3[Co(Niox.H)_2(S_2O_3)_2]$ in 50 ml solution by precipitation with 4 – 4 g $[Co(NH_3)_6]Cl_3$, $[Co(en)_3]Cl_3$, $[Cr(en)_3]Cl_3$, etc. in 100 ml aqueous solutions.

Synthesis of $[Co(Niox.H)_2(H_2O)Cl].H_2O$

23.7 g $CoCl_2.6\ H_2O$ (100 mmole) and 28.2 g nyoxime (200 mmole) in 500 ml diluted methanol (1 : 1) were oxidized by air bubbling for 6 – 8 hours. The separated brown crystalline product (trigonal prisms) was washed with water. Yield: 85 %.

Analysis: Found Co 14.13, H_2O 8.26.

For $Co(C_6H_9N_2O_2)_2(H_2O)Cl.H_2O$ (mol. wt. calcd. 412.9).

Calcd. Co 14.12, H_2O 8.36.

Table IV

Infrared absorption bands of some sulfito and thiosulfato derivatives

Characteristic frequency	1.	2.	3.	4.	5.
	wave number, cm^{-1}				
ν_{O-H}	–	–	3250 – 3550s	–	3300 – 3500m
ν_{C-H}	–	–	2980s	2980s	2970s
ν_{N-H}	–	–	2890s		3090m
			–	–	3230m
$\delta_{O-H\,..\,O}$	–	–	1730 – 1770w	1700 – 1800w	1720 – 1800 w
δ_{NH_2}	–	–			1640m
δ_{OH_2}			1650 – 1670s	1650 – 1670s	
$\nu_{C=N(nyoxim)}$	–	–	1585s	1580s	1580s
δ_{CH_2}	–	–	1460m	1450m	1460s
$\nu_{N-OH(nyoxim)}$	–	–	1240s	1240s	1240s
ν_{S-O} / $\nu_{N-O\,..\,(nyoxim)}$	920 – 1020s	1085s 1105s 1130s	1085 – 1110s	1170m	1085 – 1120s
ν_{S-O} / $\gamma_{O-H(nyoxim)}$	870 – 880s	995 – 1005s	970 – 980s	950 – 970s	960s
γ_{NH_2}	–	–	–	–	830m
δ_{SO_2}	630 – 660s	635 – 670s	630 – 635m 585 – 600m	625 – 635s 560 – 580m	630 – 650m
δ_{SO_2}	515 – 540s	540s 560s	470m 440m		470m
ν_{Co-N}	–	–	520 – 530m	520s	510 – 520s
ν_{S-S}	–	450 – 470s	–	440m 470m	–

1. $CdSO_3$, 2. BaS_2O_3, 3. $Na_3[Co(Niox.H)_2(SO_3)_2]\,.9\,H_2O$, 4. $(NH_4)_3[Co(Niox.H)_2\text{-}(S_2O_3)_2]$, 5. $NH_4[Co(Niox.H)_2(p\text{-Cl-aniline})\,(SO_3)]\,.2\,H_2O$

$NH_4[Co(Niox.H)_2(SO_3)\,(H_2O)]$ and $NH_4[Co(Niox.H)_2(S_2O_3)\,(H_2O)]$-solutions

20.5 g $[Co(Niox.H)_2(H_2O)Cl]\,.H_2O$ (50 mmole) in 200 ml water were treated with 50 mmole of $(NH_4)_2SO_3\,.H_2O$ ($(NH_4)_2S_2O_3$) in small portions. The crystalline non-electrolyte was dissolved slowly, the dark brown solution was filtered and used for substitution reactions.

Amine.H[Co(Niox.H)$_2$(SO$_3$) (amine)] and amine.H[Co(Niox.H)$_2$(S$_2$O$_3$) (amine)]

10 mmole of sulfito-aquo .. or thiosulfato-aquo-complexes in 20 – 25 ml aqueous solution were treated with a mixture of 20 mmole amine hydrochloride and amine in 5 – 10 ml ethanol. The sulfito-amine- and thiosulfato-amine derivatives were crystallized on standing for 2 – 48 hours. The obtained products were filtered, washed with ice-cooled water and dried on air.

In any cases $NH_4[Co(Niox.H)_2(SO_3)$ (amine)]-salts were obtained in the presence of $NH_4.Cl$.

Spectral investigations. The IR spectra of the complexes were recorded in KBr pellets on a UR 20 (Carl Zeiss, Jena) spectrophotometer between 400 and 4000 cm^{-1}.

Analyses. Cobalt was determined complexometrically, sulfur as $BaSO_4$, nitrogen by the micro-Dumas method. In the case of chromium derivatives the sum of the oxides (Co_3O_4 + + Cr_2O_3) was determined after an hour of heating at 900 °C.

REFERENCES

[1] VÁRHELYI, Cs., SZOTYORI, L.: Rev. Roumaine Chim. **10,** 1049 (1965)
[2] RIPAN, R., VÁRHELYI, Cs., SZOTYORI, L.: Studia Univ. Babeş-Bolyai, Chem. **12** (2), 133 (1967)
[3] ZSAKÓ, J., VÁRHELYI, Cs., KÉKEDY, E.: Acta Chim. Acad. Sci. Hung. **51,** 54 (1967)
[4] RIPAN, R., VÁRHELYI, Cs., SZOTYORI, L.: Z. anorg. allg. Chem. **357,** 149 (1968)
[5] VÁRHELYI, Cs., FINTA, Z., ZSAKÓ, J.: Z. anorg. allg. Chem. **374,** 326 (1970)
[6] VÁRHELYI, Cs., ZSAKÓ, J., FINTA, Z.: Studia Univ. Babeş-Bolyai, Chem. **15** (1), 81 (1970)
[7] VÁRHELYI, Cs., SZOTYORI, L., PÁLFI, J.: Studia Univ. Babeş-Bolyai, Chem. **16** (1), 21 (1971)
[8] FINTA, Z., ZSAKÓ, J., VÁRHELYI, Cs.: Rev. Roumaine Chim. **16** (1), 1731 (1971)
[9] VÁRHELYI, Cs., ZSAKÓ, J., FINTA, Z.: J. Inorg. Nucl. Chem. **34,** 2583 (1972)
[10] SIEBERT, H., WITTKE, G.: Z. Anorg. allg. Chem. **399,** 43 (1973)
[11] MURRAY, R. S., STRANKS, D. R., JANDELL, J. K.: J. Inorg. Chem. **9,** 751 (1970)
[12] BABAEVA, A. V., BARANOVSKI, J. V.: Zhur. neorgan. Khim. **7,** 783 (1962)
[13] TEWARI, P., GAWER, R. W., WILCOX, H. K., WILMARTH, W. K.: J. Inorg. Chem. **6,** 611 (1967)
[14] ABLOV, A. V., SYRZOVA, G. P.: Zhur. neorgan. Khim. **5,** 1221 (1960)
[15] SYRZOVA, G. P., KORLETYANU, L. N.: Zhur. neorgan. Khim. **11,** 2302 (1966); **13,** 2161 (1968)
[16] SYRZOVA, G. P., NGUEN ZUI LIUNG: Zhur. neorgan. Khim. **15,** 1027, 2722 (1970); **16,** 704 (1971)
[17] SYRZOVA, G. P., BOLGAR, T. S.: Zhur. neorgan. Khim. **17,** 455, 3015 (1972); **18,** 2706 (1973)
[18] RÂY, P.: J. Indian Chem. Soc. **4,** 330 (1927)
[19] RÂY, P., DUTT, N. K.: Z. anorg. allg. Chem. **234,** 65 (1937)
[20] NYBERG, B., BARSSON, P.: Acta Chem. Scand. **27,** 63 (1973)
[21] SIMON, A., WALDMANN, K.: Z. physik. Chem. **204,** 235 (1955)
[22] SIEBERT, H.: Z. anorg. allg. Chem. **298,** 51 (1959)
[23] DUVAL, C., LECOMTE, J.: Comptes rend. hébd. sc. Ser A., **262/B,** 1000 (1966)
[24] BERTIN, E. P., PENLAND, R. B., MIZUSHIMA, S., CURRAN, C., QUAGLIANO, J. V.: J. Amer. Chem. Soc. **81,** 3821 (1959)
[25] MILLER, E. A., WILKINS, C. H.: Anal. Chem. **24,** 1253 (1952)

Csaba VÁRHELYI
András BENKŐ
Magda SOMAY
Antal KOCH

Faculty of Chemistry, Babeş-Bolyai University, Cluj-Napoca, Romania.

Acta Chimica Academiae Scientiarum Hungaricae, Tomus 97 (2), pp. 177—185 (1978)

SIMS STUDY OF IRON-NICKEL AND IRON-CHROMIUM ALLOYS, I

INVESTIGATION OF THE SPUTTERING OF THE ALLOYS

M. RIEDEL,* T. NENADOVIĆ and B. PEROVIĆ

(Boris Kidrič Institute of Nuclear Sciences, Belgrade, Yugoslavia)

(Department of Physical Chemistry and Radiology, Eötvös L. University, Budapest)*

Received March 16, 1977

The sputtering, and secondary atomic and cluster ion emission of binary Fe-based alloys with simple phase diagrams were studied by means of a secondary ion mass spectrometer (SIMS). Series of Fe—Ni and Fe—Cr alloys in the concentration range 0—100 % were bombarded with 4 KeV Kr^+ ions. By the modification of the ion source of the SIMS and by electron-microprobe analysis of the sputtered material, simultaneous study of sputtering and secondary ion emission was possible.

The first part of this study deals with the composition dependence of the sputtering of alloys. The sputtering rate proportions of the constituents of the alloys, necessary for evaluation of ion emission studies, were determined. The relative sputtering coefficients of the alloying components are near to unity; the alloying component with lower sputtering rate sputters faster in the alloy, but the decrease of the sputtering rate of the other component could also be observed.

Introduction

Secondary ionization mass-spectrometry (SIMS) is a new method in solid-state analysis, which may be employed to advantage in cases when the depth and surface distributions of low-concentration ($c < 1$ %) components are to be determined [1—4 etc.]. The secondary ion current produced by ionic bombardment is directly proportional to the concentration; *i.e.* with appropriate calibration, and in the knowledge of the secondary ion yield (S^+) of the substance under examination, the concentration may be determined from the ion current [5]. Experimental experience has revealed that S^+ depends not only on many parameters of the apparatus (nature and energy of the primary ion, vacuum conditions), but also on the nature of the element examined, and it may depend too on the matrix and the concentration [6—9 etc.]. A knowledge of the value of the secondary ion yield in the system in question is important, therefore, with regard to the analytical work, while in general the study of the sputtering and secondary ion emission of alloys is also of theoretical importance, for it may give further information on the mechanism of interaction of high-energy ions and solids.

Most SIMS studies in this respect relate only to the range of dilute alloys; there are only sporadic experimental data on more concentrated alloys, and the few experimental data available are difficult to reconcile with the theories describing the secondary ion emission of pure metals [6–11]. Interest has recently increased in the sputtering of alloys and multicomponent systems in general [12–14]. As regards the further clarification of the details of the emission process, joint investigations of the two part-processes of secondary ion emission, *i.e.* sputtering and secondary ionization, have not been made in the overall composition range (c = 0–100 %).

Accordingly, in the present experiments a study was made in the concentration range 0–100 % on the sputtering and atomic and cluster ion emissions of binary iron alloys (iron-nickel and iron-chromium) which form solid solutions of relatively simple phase diagrams [22], and which at the same time are of practical importance. An experimental set-up was used which, in addition to mass-spectrometric analysis of the secondary ions, permitted determination of the composition of the total sputtered material (ionic and neutral) in the same experiment. Joint evaluation of the experimental results may contribute to a better understanding of the secondary ion emission process; at the same time, individual study of the single part processes may also yield useful new information as regards the phenomena accompanying the sputtering of alloys. In the present publication we report our results relating to the sputtering of these alloys, while those on the atomic [15] and cluster ion [16] emission will be published separately.

Experimental

The Fe–Ni and Fe–Cr alloys to be investigated were prepared by the co-melting of the high-purity (99.9 %) metals. The compositions of the members of the alloy sequences were 0, 20, 40, 60, 80 and 100 wt. % (±0.5 %). The surfaces of the samples, with average grain sizes of 100–200 μm, were pretreated by mechanical polishing with diamond paste.

Examinations were made with a home-constructed secondary ionization mass spectrometer, which was described in detail earlier [17, 18]. The primary Kr^+ ions with an energy of 4 KeV were focused on a 0.1 cm² surface area of the sample with an incidence angle of 45°. The primary ion current density was varied in the range $i_p = 1-20$ μA/cm². The pressure of the background gas in the vicinity of the sample was 2×10^{-6} torr; its composition was checked in the course of the measurements with a quadrupole mass spectrometer connected to the ion source for this purpose. The positive secondary ions were analyzed with a magnetic mass spectrometer; an electron multiplier was employed as a detector after an energy filter.

For determination of the composition of the sputtered material, a collector plate prepared from high-purity aluminium was placed on the first electrode of the ion optics of the SIMS (Fig. 1). Part of the sputtered material passed into the mass spectrometer through a slit in the middle of the plate; the rest could be captured on the plate, in the form of a thin layer on the substrate. After ion bombardment for various periods, an AEI electron microprobe was used to determine the composition of this material in the area indicated in Fig. 1 (at a number of points in the immediate vicinity of the slit), with an accuracy of ±1 %. This set-up permitted determination of quantities characteristic of the sputtering and the ion emission in one and the same experiment. The bombarding ion dose employed in each experiment varied in the range $D = 1-4\times10^{18}$ ion/cm².

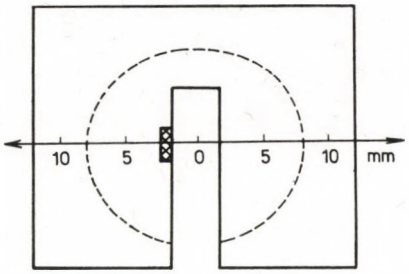

Fig. 1. Outline of collector plate for capture of sputtered material. The dashed line encloses the area of deposition of the sputtered material, and the shading shows the site of the electron microprobe measurements

Results and discussion

The sputtering coefficients (S_M) of the individual components (which means the numbers of ionic and neutral secondary particles formed on the action of the bombarding primary ions, and which are proportional to the rate of sputtering under given bombardment conditions) can be determined from the electron-microprobe measurement data [18, 19]:

$$S_M = k \,.\, a_M \frac{I_F/I_M}{D} \tag{1}$$

I_F and I_M are the measured X-ray intensities of the metal examined, in the case of the thin layer and a sufficiently thick standard, respectively. k is a constant characteristic of the microprobe; a_M is the sensitivity of detection of the metal M [20]. The numerical value of k was not established, for the sputtering rates of the individual elements can also be compared via the quantity S_M^*, which can be calculated directly from the experimental results:

$$S_M^* = a_M \frac{I_F/I_M}{D} \tag{2}$$

Instead of the sputtering coefficient, therefore, in our publications S_M^* is given in units of 10^{-19} cm^2/ion. Table I contains the experimentally determined S_M^* data measured for Fe, Ni and Cr in the pure state and as components of the alloys. It should be noted that the accuracy of measurement of these (± 20 %) is restricted by the accuracy of the ion-dose measurement; the relative sputtering coefficients (Eq. 3) could be determined with a considerably smaller error (± 5 %).

It may be stated that, as regards their sputtering rates determined in the pure state, the sequence of the metals in question agrees with the results

Table I

S values characteristic of the sputtering rates of the Fe, the Ni, the Cr and the alloys, as functions of composition*

Composition of sample (% Fe)	S* (10^{-19} cm³/ion)					
	Fe–Ni			Fe–Cr		
	Ni	Fe	alloy	Cr	Fe	alloy
0	2.6	–	2.6	1.7	–	1.7
20	3.0	3.9	3.2	1.4	1.4	1.4
40	2.1	2.4	2.2	1.7	1.7	1.7
60	2.4	2.6	2.6	2.5	2.0	2.2
80	2.9	2.8	2.8	2.3	2.0	2.0
100	–	2.5	2.5	–	2.5	2.5

obtained by LAEGRID and WEHNER [21] by bombardment with 45 keV krypton ions: $S_{Ni} > S_{Fe} > S_{Cr}$. It can further be seen that the sputtering coefficients of the individual elements depend on the composition of the alloys investigated, and differ from the sputtering rates of the pure metals.

The experiments revealed that the composition of the sputtered thin layers exhibit systematic differences from those of the alloys examined (Fig. 2, Table II). In the case of Fe–Ni samples at high Ni concentrations the sputtered material contains about 4–5 % more Fe than the bombarded alloy; for Fe–Cr samples with high Fe content the Cr concentration of the thin layer is higher to a similar extent. This phenomenon is connected with the different sputtering rates of the components of the alloy.

If the ion sputtering is regarded as a congruent process, similarly to equilibrium vaporization, then in principle, in the event of bombardment for a sufficiently long period, the composition of the sputtered thin layer must

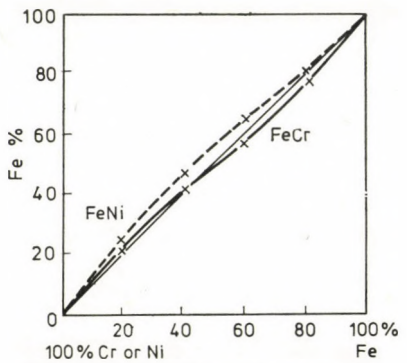

Fig. 2. Compositions of sputtered Fe–Ni and Fe–Cr thin layers as functions of the compositions of the bombarded samples

Table II

Composition of the sputtered material in the case of bombardment of Fe–Ni *and* Fe–Cr *alloys with* 4 KeV Kr^+ *ions* ($D = 1-4\times10^{18}$ *ion/cm²*)

Composition of sample (% Fe)	Composition of sputtered material (% Fe)	
	Fe–Ni	Fe–Cr
0	0	0
20	24	21
40	44	40
60	62	55
80	80	77
100	100	100

agree with the composition of the sample. For a more detailed study of the cause of the difference, we determined the relative sputtering coefficients of the constituent elements of the alloy; these can also be calculated from the S* data in accordance with Eqs (1) and (2):

$$S_{rel} = \frac{S_{M,1}}{S_{M.2}} = \frac{S^*_{M,1}}{S^*_{M,2}} \tag{3}$$

The concentration dependences of the relative sputtering coefficients (S'_{rel}) measured for Fe/Ni and Cr/Fe in the alloys are presented in Fig. 3, together with the S_{rel} data calculated from the sputtering rates of the pure metals.

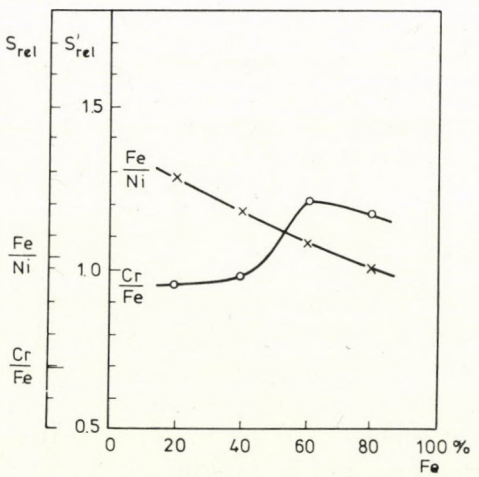

Fig. 3. Relative sputtering coefficients (S'_{rel}) of the components of the Fe–Ni and Fe–Cr alloys as functions of composition. The left-hand axis gives the values obtained (S_{rel}) on sputtering of the pure substances

(S data refer to the pure state, and S′ data to the alloys.) It may be stated that S'_{rel} for the Fe–Cr alloys is about 30–40 % larger than the ratio of the sputtering coefficients for the pure metals, and for both the Fe–Ni and the Fe–Cr alloys has a value of ~1. To a first approximation, this fact corresponds to the congruence of the sputtering, according to which

$$S'_{M,1} = S'_{M,2} \tag{4}$$

where, in general

$$S'_M \neq S_M \tag{5}$$

In addition, however, a further increase (~15–20 %) in the relative sputtering coefficient for the Fe and the Cr can also be observed in certain concentration intervals, and this excess increase results in the composition of the sputtered material differing from that of the bombarded sample.

The difference between S'_{rel} and S_{rel} in the alloyed state may be caused by both the increase and the decrease of the sputtering coefficients of the individual elements. Accordingly, by comparison of the sputtering coefficients of the individual metals, measured in the pure state and in the alloy, direct data may be obtained on this phenomenon of preferred (or possibly retarded) sputtering. Indirectly, by studying the layer developing on the surface of bombarded binary systems, this layer having a composition different from that of the bulk of the sample, a number of authors have recently demonstrated that, in the binary systems investigated, the sputtering rate of the component with the smaller sputtering coefficient increases compared to that measured in the pure state (POATE *et al.* [13]: Si in the Pt–Si system; FÄBER *et al.* [14]: Ag in Ag–Au). In our experiments the S* data were determined by measurement of the amount of sputtered material, and thus sputtering with a different rate in the alloy, and the composition dependence of this, could also be demonstrated by sputtering coefficient measurement. The ratios are more striking if the preferred sputtering factor is introduced:

$$Ps \equiv \frac{S'_M}{S_M} = \frac{S'^*_M}{S^*_M} \tag{6}$$

Table III contains the Ps values of the Fe, the Ni and the Cr in both the Fe–Ni and the Fe–Cr alloys. It may be stated that the Fe in the Fe–Ni, and the Cr in the Fe–Cr, are strongly increased at low and high Fe concentrations, respectively, the sputtering rate being even 1.5 times larger. At the same time, in the Fe–Cr alloy the decrease of the sputtering rate of the Fe occurs too. This phenomenon may be interpreted in that a cross effect arises between the components of the alloy, this being particularly marked in the Fe–Cr system. At high concentration, the Cr (the sputtering coefficient of

Table III

Ratio of sputtering coefficient of Fe, Ni, Cr *and the alloys to sputtering coefficient of pure metals* (Ps)

Alloy composition (% Fe)	Ps					
	Fe–Ni			Fe–Cr		
	Ni	Fe	alloy	Cr	Fe	alloy
0	1.0	–	1.0	1.0	–	1.0
20	1.2	1.5	1.3	0.8	0.6	0.8
40	0.8	1.0	0.9	1.0	0.7	0.8
60	1.0	1.1	1.0	1.4	0.8	1.0
80	1.1	1.1	1.1	1.4	0.8	0.9
100	–	1.0	1.0	–	1.0	1.0

which is smaller than that of the Fe in the pure state) decreases the sputtering of the Fe; at high Fe contents, on the other hand, the sputtering rate of the Cr increases (because the surface bonding energy is lowered by the action of the neighbouring Fe atoms). A similar phenomenon can also be observed for the Fe–Ni alloys, although the effect is not so pronounced because of the smaller difference in S.

In the knowledge of the alloy sputtering coefficients of the components, we determined the total sputtering coefficients of the alloy on the basis of the following expression:

$$S'^* = S_1'^* \cdot c_1 + S_2'^* \cdot c_2 \tag{7}$$

In addition, similarly by linear combination, the S* data on the pure components were used to calculate the value which would be observed if the composition did not affect the sputtering of the individual components. The quotient (Ps) of the values calculated in these two ways is characteristic of the difference from ideality of the sputtering rate of the alloy (Fig. 4). In general, in Fe–Ni alloys an increase, and in Fe–Cr alloys a decrease can be observed. On the basis of some literature data, it would be expected that the sputtering rate of a homogeneous alloy is closer to the S of the component which can be sputtered more easily, while in the case of two-phase systems the combined rate is controlled by the smaller S [12, 14, 23, 24]. The present experiments show that the Fe–Ni alloys sputter more rapidly, and the Fe–Cr alloys more slowly than the average; that is, in the case of homogeneous alloys the sputtering coefficient may either increase or decrease, depending on the substances and the concentrations.

In the whole concentration range, the alloys examined are of solid solution type. Their melting point minimum occurs at 68 wt. % Ni, and at 22 wt. %

Cr [22]. From a comparison of the sputtering coefficients of the components of the alloy and of the alloy itself with the phase diagrams of the alloys, it may be stated that the more extensive variation with concentration observed for the Fe – Cr samples is justified, if it is taken into consideration that the melting point varies with composition to a greater extent from pure Fe to pure Cr, than from pure Fe to pure Ni. At the concentration relating to the melting point minimum, where the surface bonding energy of the atoms is presumably

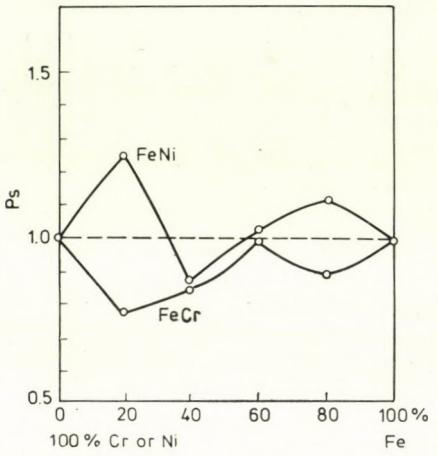

Fig. 4. Quotient (Ps) of the actual sputtering value for the Fe – Ni or Fe – Cr alloys and the value calculated from the data for the pure metals, as a function of the composition of the alloy

also at a minimum, the increase of the sputtering coefficients would be expected. Although our experiments indicate that the course of the S* values undoubtedly changes in this range, and the maximum too is strongly suggested, further experimental data in this concentration range would be necessary for a deeper clarification of the correlation.

To summarize, it may be stated that, besides the direct demonstration of preferred sputtering, our experimental results indicate that the changes in the sputtering rates of the components can not be neglected in the study of the secondary ion emission phenomena of multicomponent system: they must be taken into account in the determination of the degree of ionization of atomic and cluster ions, in the correction of the secondary ion currents of the individual components, and at times in SIMS analysis too.

*

The authors express their thanks to Dr. B. Djurić and D. Cerović (Boris Kidrič Institute) for their help in the electron-microprobe measurements.

REFERENCES

[1] ANDERSEN, C. A.: Microprobe Analysis, Wiley, New York 1973
[2] SOCHA, A. J.: Surf. Sci. **25,** 147 (1971)
[3] RIEDEL, M.: Magy. Fiz. Folyóirat **XXIII,** 539 (1975)
[4] RIEDEL, M.: Secondary Ionization Mass Spectrometry, in New Results in Chemistry (in Hungarian), Vol. 45. Akad. Kiadó, Budapest, 1979
[5] WERNER, H. W.: Vacuum **24,** 493 (1974)
[6] BESKE, H. E.: Z. Naturforsch. **22A,** 459 (1967)
[7] SCHELTEN, J.: Z. Naturforsch. **23A,** 109 (1968)
[8] LEROY, V., SERVAIS, J. P., HABRAKEN, L.: CRM Rep. (Liège) No. **35,** 69 (1973)
[9] CHEREPIN, V. T., VASILYEV, A. M.: Vtorichnaya ionno-ionnaya emissiya metalov i splavov, Naukova Dumka, Kiev, 1975
[10] RODRIGUEZ-MURCIA, H., BESKE, H. E.: Ber. der Kernforschungsanlage, Jülich, Nr. Jül. 1296 (1976)
[11] RÜDENAUER, F. G., STEIGER, W., PORTENSCLAG, R.: Microchim. Acta Suppl. **5,** 421 (1974)
[12] WEHNER, G. K.: 2. Coll. Int. de Pulverisation Cathodique, Nice, 1976
[13] POATE, J. M., BROWN, W. L., HOMER, R., AUGUSTYNIAK, W. M., MAYER, J. M., TU, K. N., VAN DER WEG, W. F.: Nucl. Inst. Meth. **132,** 345 (1976)
[14] FÄBER, W., BETS, G., BRAUN, P.: Nucl. Inst. Meth. **132,** 351 (1976)
[15] RIEDEL, M., NENADOVIĆ, T., PEROVIĆ, B.: Acta Chim. Acad. Sci. Hung. **97,** 187 (1978)
[16] RIEDEL, M., NENADOVIĆ, T., PEROVIĆ, B.: Acta Chim. Acad. Sci. Hung. **97,** 197 (1978)
[17] RIEDEL, M., PEROVIĆ, B.: Boris Kidrič Inst. Publ. No. 1331 (1975)
[18] RIEDEL, M., NENADOVIĆ, T., PEROVIĆ, B.: Boris Kidrič Inst. Publ. No. 1400 (1976)
[19] DJURIĆ, B., CEROVIĆ, D.: in Proc. of the Vth Int. Congr. on X-ray Optics and Microanal., Ed. by G. MÖLLENSTEDT and K. H. GAUKLER, Springer, 1969, p. 99
[20] BIRKS, L. S.: Electron Microprobe Microanalysis, Interscience, 1963
[21] LAEGRID, W., WEHNER, G. K.: J. Appl. Phys. **32,** 365 (1961)
[22] HANSEN, M.: Constitution of Binary Alloys, McGraw-Hill, New York 1958
[23] ANDERSON, G. S.: J. Appl. Phys. **40,** 2884 (1969)
[24] DAHLGREEN, S. D., MCCLANAHAN, E. D.: J. Appl. Phys. **43,** 1541 (1972)

Miklós RIEDEL Department of Physical Chemistry and Radiology, Eötvös L. University, H-1088 Budapest, Puskin u. 11–13.

T. NENADOVIĆ, B. PEROVIĆ Boris Kidrič Institute of Nuclear Sciences, Belgrade, Yugoslavia.

Acta Chimica Academiae Scientiarum Hungaricae, Tomus 97 (2), pp. 187–196 (1978)

SIMS STUDY OF IRON–NICKEL AND IRON–CHROMIUM ALLOYS, II

STUDY OF THE EMISSION OF MONOATOMIC SINGLY-CHARGED SECONDARY IONS AS A FUNCTION OF COMPOSITION

M. RIEDEL,* T. NENADOVIĆ and B. PEROVIĆ

(Boris Kidrič Institute of Nuclear Sciences, Belgrade, Yugoslavia)

(Department of Physical Chemistry and Radiology, Eötvös L. University, Budapest)*

Received March 16, 1977

Of the different ionic species in the secondary ion spectra of highly concentrated Fe–Ni and Fe–Cr alloys, the singly-charged monoatomic ions of the metals were studied in the present work. The experiments showed that the relative secondary ion yield displays a marked concentration dependence. By the simultaneous measurement of sputtering and ion emission, the relative degree of ionization could be calculated, which assumes an extreme value in the range of the melting point minimum of the alloy. The experimental data could be fitted to the LTE and ASI models of secondary ionization only with limited accuracy. This means that a better description of the concentration dependence of the ion emission is possible only *via* better approximations.

Introduction

It is known that in the case of SIMS analysis the secondary ion current (I^+) of some element with concentration c in a multicomponent system can be given by the following expression [1, 2]:

$$I^+ = \eta \cdot S^+ \cdot c \cdot I_p \tag{1}$$

where η is the transmission of the mass spectrometer, I_p is the primary ion current, and the secondary ion yield (S^+) is characteristic of the measure of ion emission by the individual elements. In the knowledge of the sputtering coefficient (S), giving the extent of splitting-off of atoms from solids, the degree of ionization (α^+) of the element in question can be determined (if $\alpha^+ \ll 1$):

$$\alpha^+ = S^+/S \tag{2}$$

This quantity is directly characteristic of the ionization of the atoms leaving during bombardment [2, 3], and can be calculated to a certain approximation on the basis of the secondary ionization models [4–10].

Publications to date dealing with the secondary ion emission of alloys have not devoted sufficient attention to the possibility that the sputtering

coefficient may depend on the composition of the alloy, and therefore the secondary ion current has been regarded as directly proportional to the degree of ionization [3, 11–15]. The most recent investigations, however, demonstrated that the sputtering coefficient may depend on the composition of the sample too [16–18]. In our work, therefore, we have studied the ionization of the components of the alloy by taking into account the composition dependence of the sputtering coefficient determined in the same experimental series.

Experimental

The SIMS apparatus, the characteristics of the substances examined (Fe – Ni and Fe – Cr; c = 0, 20, 40, 60, 80 and 100 %), and the means of joint determination of the sputtering coefficient and the mass spectrum were described elsewhere [19, 21]. In the course of the experiments the polished samples were bombarded for 2 hr at a current density of $i_p = 20\ \mu A/cm^2$, in order to clean the surface. Next the secondary ion mass spectrum of the sample was recorded for i_p values increasing and decreasing in the range $i_p = 2-15\ \mu A/cm^2$, at several different current densities, in the mass number interval m/e = 12 – 140. Before recording of the spectrum, the sample was bombarded at the given i_p for 20 – 30 min, during which time the spectral peaks reached constant values. This meant the stationary adsorption and desorption state of the surface of the sample [22]. The isotope abundance and the mass-dependent sensitivity of the detector of the mass spectrometer were taken into consideration in the determination of the secondary ion current of an element. Together with the recording of the secondary ion spectra, the sputtering coefficients of the components of the alloy were also determined [19].

Results and discussion

1. Concentration dependence of secondary ionization

We recorded numerous peaks of various origins in the SIMS spectrum; of these, in the present paper the peaks of the monoatomic singly-charged ions of the alloy components (Fe^+, Ni^+, Cr^+) will be dealt with, while the results connected with the cluster ions will be reported in a subsequent paper [23]. In order to avoid the effects of possible experimental and apparatus errors, we determined the ion-current values referred to iron, as a common constituent element in all alloys:

$$I^+_{rel} = \frac{I^+_M}{I^+_{Fe}} = S_{rel}(c) \cdot \alpha^+_{rel}(c) \cdot \frac{c_M}{c_{Fe}} \qquad (3)$$

where M is Ni or Cr. It follows from this relation that the $I^+_{rel} \cdot c_{Fe}$ *vs.* c_M curve is the calibration curve of the SIMS analysis [12]; it will be linear if neither the sputtering coefficient nor the degree of ionization depend on the composition. Our experimental results are presented in Fig. 1, where the numbers on the curves are the values of the primary ion-current density at which the spectra were recorded. The relative secondary ion yields S^+_{Ni}/S^+_{Fe} and S^+_{Cr}/S^+_{Fe}

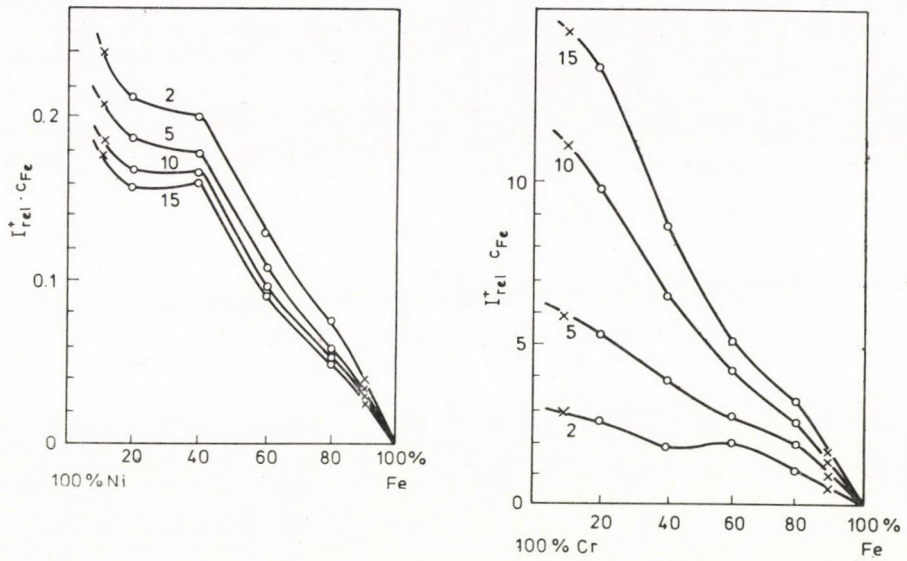

Fig. 1. Secondary ion emission of Fe – Ni (a) and Fe – Cr (b) alloys as a function of composition, expressed in ($I^{+}_{rel} \cdot c_{Fe}$). Parameter i_p = 2, 5, 10, 15 μA/cm². Values denoted by x were calculated from the inverse function

as functions of the composition are given in Table 1 for the primary ion-current densities i_p = 2 and 15 μA/cm² (the accuracy of the measurements is ±20 %). It can be seen that the slopes of the curves vary strongly in the vicinity of the alloy composition relating to the melting point minimum (68 % Ni and 22 % Cr). This phenomenon is more marked in the Fe – Ni alloys and in general at higher primary ion-current densities. The slopes of the curves, *i.e.* the relative secondary ion yields (S^{+}_{rel}), are roughly the same before and after

Table I

Relative secondary ion yields S^{+}_{Ni}/S^{+}_{Fe} *and* S^{+}_{Cr}/S^{+}_{Fe} *for the* Fe – Ni *and* Fe – Cr *alloys and the pure metals*

c_{Fe} %	S^{+}_{rel}			
	Fe – Ni i_p [μA/cm²]		Fe – Cr i_p [μA/cm²]	
	2	15	2	15
20	0.36	0.26	3.7	18.7
40	0.45	0.46	3.5	16.1
60	0.44	0.31	5.6	14.5
80	0.40	0.36	6.8	17.6
From pure metals	0.14	0.22	2.8	5.0

Table II

Relative secondary ion yields of Ni *and* Cr, *referred to* Fe, *from pure metals and alloys*

S^+_{rel}				Ref.
Ni/Fe		Cr/Fe		
from pure metal	from alloy	from pure metal	from alloy	
0.3	–	5.0	–	[20]
0.71	0.71	7.14	3.5	[13]
0.21	0.21	–	–	[11]
–	0.79	–	2.55	[12]

this range. For comparison, Table II contains relative secondary ion yield data published in the literature with regard to measurements on pure metal and dilute alloys.

In the knowledge of the sputtering coefficient determined in the same experiment [19, 21], we calculated the relative degrees of ionization of the Ni and the Cr referred to the Fe, as a function of the composition of the alloy ($\alpha^+_{rel}(c)$). The results obtained are given in Fig. 2. The relative degree of ionization was similarly calculated from the ion current measured on bombardment of the pure metals, and this is given for the two different i_p values indicated beside the right-hand axis. It can be seen that the sequence of the elements with

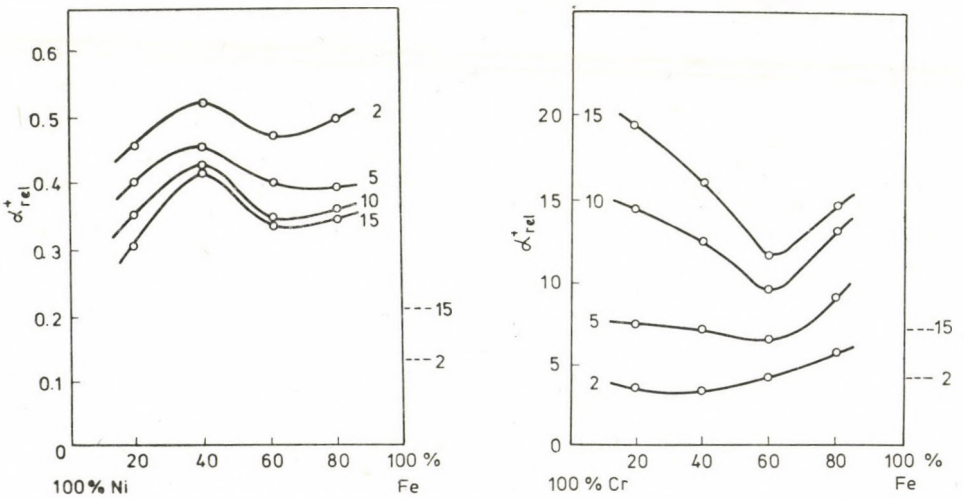

Fig. 2. Relative degree of ionization of constituent elements of Fe–Ni (a) and Fe–Cr (b) alloys as a function of concentration at various primary ion-current densities (i_p = 2, 5, 10, 15 μA/cm^2). α^+_{rel} calculated from the ion currents of the pure metals is indicated beside the right-hand axis, in the cases of i_p = 2 and 15 μA/cm^2

regard to the extent of their secondary ionization is

$$\alpha^+_{Cr} > \alpha^+_{Fe} > \alpha^+_{Ni}$$

which is the same both in the alloys and in the pure state. The strong matrix dependence of the secondary ionization was observed: the α^+_{rel} measured in the case of the alloys was about 1.5 – 3.5 times larger than the relative values of the pure metals. A similar phenomenon was described earlier by several authors for dilute alloys [13, 24]. Recently the composition dependence of the secondary ion current was observed in case of some concentrated alloys [3, 15, 37, 38].

By comparison of our results on the ionization with Fig. 3 of our earlier publication [19] and with the phase diagrams of the alloys [25], it may be stated that in the homogeneous alloys examined the secondary ionization is in a more direct connection with the structure of the alloy than the ion sputtering. The observed concentration dependence of the ion-sputtering (congruence, preferred sputtering), however, indicates that neglect of the sputtering coefficient in the experimental determination of the degree of ionization [11 – 15], or its calculation with a linear combination from the data determined on the pure elements [4], can be accepted only as first approximations.

From a comparison of the curves relating to the ion-current densities 2 and 15 μA/cm^2 it may be stated that the influence of the alloy composition on the ionization of the metals examined is the greater, the higher the density of the bombarding ion current. In the case of a higher bombarding ion current the sample surface is less covered with the adsorbing background gases [22], *i.e.* the purer the surface from which the secondary ions originate, the more strongly the effect of the structure of the alloy is manifested. Further, at a higher surface coverage α^+_{rel} becomes almost identical in the entire concentration range. As regards determination of the composition of the alloys too, this observation supports the secondary ionization mass-spectrometric practice according to which a reactive gas atmosphere is created in the environment of the sample to be studied, in the interest of attaining a higher sensitivity, a more homogeneous ion etching, etc. [26, 27].

2. Study of secondary ionization models for concentrated alloys

Numerous models have been constructed for the description of the mechanism of secondary ion emission [1, 2, 5], but most of them can not be employed because of the complex mathematical description for a broad scale of elements, or because of the lack of the necessary quantum-mechanical, electric, etc. data. At present, only the local thermal plasma equilibrium (LTE) [28] and

the adiabatic surface ionization (ASI) [6] models seem to be usable in SIMS practice. Besides their application to pure elements, a number of authors have attempted to use these models to describe the ionization of secondary particles emitted from dilute and concentrated alloys [5, 7, 14, 15, 37]. Since an appropriate approximation has not previously been reported for concentrated alloys, we have attempted to fit the above two models to our experimental data.

The LTE model assumes that plasma in thermal equilibrium develops in the close environment of the impact of the primary ions, and that in this the ratio of the ions to neutrals, and thus the degree of secondary ionization, is described by the Saha-Eggert equation (ANDERSEN and HINTHORNE) [7, 28]:

$$\alpha^+ = \frac{2Q^+}{Q^0} \frac{(2\pi\, m\, kT)^{3/2}}{h^3} e^{-(eI - eI')/kT} \cdot \frac{1}{n_e} \tag{4}$$

where Q^+ and Q^0 are the statistical probabilities of the ionic and neutral states, T is the temperature of the plasma in the original correlation, n_e is the assumed density of free electrons in the plasma, I′ is the extent of the ionization energy decrease occurring in the plasma, h is Planck's constant, and e is the electronic charge.

In our case, if the Saha-Eggert equation is written for the two component elements of an alloy, the following expression is obtained for the relative degree of ionization of the components (assuming that I′ is the same for both elements):

$$\alpha^+_{rel} = \left(\frac{Q^+}{Q^0}\right)_M \left(\frac{Q^0}{Q^+}\right)_{Fe} e^{-(eI_M - eI_{Fe})/kT} \tag{5}$$

n_e does not figure in the equation for in a given alloy, at a given primary ion-current density, it is characteristic of the whole of the plasma, and can therefore be regarded as the same for the two metals. Only one parameter to be fitted, T, remains in the expression. In the knowledge of the ionization potentials [29] and the probability weighting functions for 5000 K [30], Eq. (5) may be written in the following form:

$$\ln\left[\alpha^+_{rel} \Big/ \left(\frac{Q^+}{Q^0}\right)_M\right] = -0.430 + 9.17 \times 10^4 \cdot \frac{1}{T} - \frac{eI_M}{k} \cdot \frac{1}{T} \tag{6}$$

which is suitable for studying the possibility of fitting the model to the experimental data. In Fig. 3,

$$\ln\left[\alpha^+_{rel} \Big/ \left(\frac{Q^+}{Q^0}\right)_M\right]$$

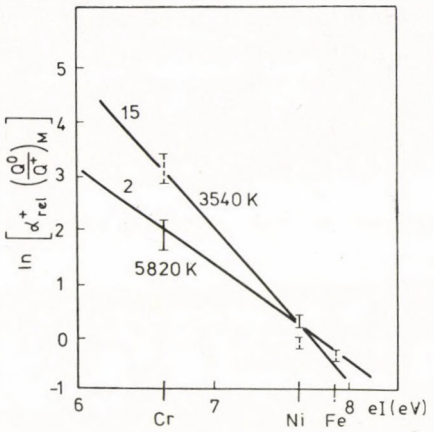

Fig. 3. Fitting of the LTE model to the experimental data measured at 2 and 15 μA/cm^2

is plotted as a function of the ionization energy of the elements at the current densities $i_p = 2$ and 15 μA/cm^2. The data determined at the various compositions were recorded at the same site; in the Figure, these are located in the range indicated by the full line at 2 μA/cm^2, and by the dotted line at 15 μA/cm^2. In the case of Fe, the function value arising from the relative value of the degree of ionization is the same for every alloy and current density.

The Figure shows the straight lines fitted by the least squares method, and the "temperature" data determined from these. The relative degree of ionization data calculated with these T values agree with the measured α^+_{rel} data within a standard deviation of ± 25 %.

The average T values obtained lie close to the results of RÜDENAUER *et al.* [14], determined on steel standards. It may be observed that T increases with increasing surface coverage. The concentration dependence of parameter T was also determined with expression (6). Particularly for the Fe–Ni alloys, T exhibits a strong change between 4000 and 10,000 K. These temperatures are not realistic physically, and the considerable change with alloy composition can not be justified either. In the range of concentrated alloys too, therefore, our results support the fact established by several other authors [1, 36] for pure metals and dilute alloys, that T can only be regarded as a parameter not possessing physical meaning if the LTE theory assuming equilibrium is applied to the fundamentally non-equilibrium ion-sputtering process [3].

On the other hand, however, the number of free electrons (n_e), the only quantity which may depend on the composition of the alloy and on the state of the surface, falls out in the formation of α^+_{rel}. In the plasma model, therefore, there is no quantity which physically too can be conceived as a function of *c*. A similar difficulty arises with the other thermal ionization models of secondary ion emission [9, 10], if one wishes to apply these to concentrated alloys.

On the basis of a quantum-mechanical description, the ASI model gives the following expression for the degree of ionization of an element [6]:

$$\alpha^{+} = \left(\frac{B}{eI - e\Phi}\right)^{2} \left[\frac{hv}{2\pi a} \frac{1}{(eI - e\Phi)}\right]^{n} \tag{7}$$

where B is the bonding energy of the surface atoms, v is the velocity of the sputtered particles, and Φ is the work function. a and n are parameters to be fitted, and the other designations are the same as in Eq. [4]. By introducing some approximations, a number of authors have attempted to extend the validity of the equation to the range of dilute alloys too (SCHROEER [5, 31], RÜDENAUAR *et al.* [4], GRIES *et al.* [32]). Because of the lack of the necessary tabulated data for concentrated alloys, it is obvious to accept the following assumptions from these.

1. The bonding energy of the surface atoms can be calculated from the sublimation heat by linear combination [4].

2. On the basis of the energy distribution of the secondary ions, it may be assumed that $n=1$ [32]; this approximation is supported by the fitting with the experimental data obtained for the pure metals [4].

3. It may be assumed further that the average velocities of atoms and ions sputtered from the same alloy are identical.

4. a was brought into correlation with the lattice constant by RÜDENAUER *et al.* [4], and with the course of the emitted particles in the surface zone by GRIES *et al.* [32]. In both approaches, a must be the same for the two components of a given sample.

On the above basis, in our case the relative degree of ionization is expressed by the following relation:

$$\alpha^{+}_{rel} = (B_{rel})^{2} \left(\frac{I_{Fe} - \Phi}{I_{M} - \Phi}\right)^{3} \tag{8}$$

The degree of ionization is therefore a function of the work function, and the dependence of this on the alloy composition and the surface coverage can be accepted as physically realistic, although there are no experimental data relating to the concentrated alloys examined. Via the above expression, the concentration dependence of Φ was determined from the measured data for α^{+}_{rel} with the aid of the sublimation heats relating to 293 K [33] (Fig. 4). It can be seen that Φ depends only slightly on c, but the influence of i_p is substantially larger. To a first approximation, this result is in agreement with the expected properties of the work function. It can be seen, however, that the calculated values of Φ, particularly for the Fe–Ni alloys, are irrealistically large, being about 4–5 eV higher than the work function for clean surfaces of pure metals

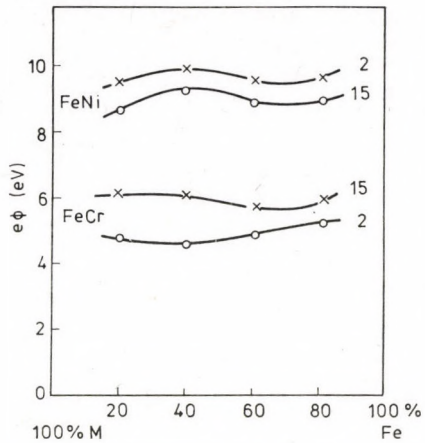

Fig. 4. Composition dependence of $e\Phi$ values calculated on the basis of the ASI model from ion emission data measured at 2 and 15 $\mu A/cm^2$

[34]. In the case of the ASI model too, therefore, it may be stated that either an appropriate concentration-dependent quantity is missing from Eq. (8), or refinement of the given approximations is necessary. The numerical values of α^+_{rel} calculated with the average value of Φ for each of the alloys agree with the experimental data within ± 30 %, which, as a measure of the fit, can be said to be satisfactory in this case too. Similar results are to be expected for quantum-mechanical models constructed on the basis of similar principles [35].

To summarize, it may be stated that in their present forms neither the LTE nor the ASI model gives a satisfactory description of the secondary ion emission of concentrated alloys. In the former T, and in the latter Φ is not sufficient for a suitable fit of the experimentally determined values. A factor is missing which would describe the dependence of the relative ionization on the alloy composition, taking into account, for example, the extreme value of α^+_{rel} observed in the vicinity of the composition relating to the melting minimum, or the change in the extent of the ion emission in the case of a phase transformation [3], *i.e.* which in general would create a connection between the characteristics of the phase diagrams and the concentration effects of the secondary ionization [3, 15]. A similar conclusion was recently reached by RODRIGUEZ-MURCIA and BESKE [15] in a study of concentrated Cu–Ni alloys.

It may be stated that both the LTE and the ASI models must be modified for a description of the secondary ion emission of concentrated alloys. It would be necessary in the former to introduce a further c-dependent variable, and in the latter to introduce suitable forms of the surface bonding energy and the work function, as possible factors, and to determine the experimental data relating to these.

REFERENCES

[1] WERNER, H. W.: Vacuum **24,** 493 (1974)
[2] RIEDEL, M.: Secondary Ionization Mass Spectrometry, in New Results in Chemistry (in Hungarian), Vol. 45. Akad. Kiadó Budapest, 1979
[3] CHEREPIN, V. T., VASILYEV, A. M.: Vtorichnaya ionno-ionnaya emissiya metalov i splavov, Naukova Dumka, Kiev, 1975
[4] RÜDENAUER, F. G., STEIGER, W., PORTESCHLAG, R.: Microchim. Acta Suppl. **5,** 421 (1974)
[5] SCHROEER, J. M.: IV. Conf. on Atomic Collisions in Solids, Amsterdam, 1975
[6] SCHROEER, J. M., RHODIN, T. M., BRADLEY, R. M.: Surf. Sci. **34,** 571 (1973)
[7] ANDERSEN, C. A., HINTHORNE, J. R.: Anal. Chem. **45,** 1421 (1973)
[8] BLAISE, G.: Rad. Effects **18,** 235 (1973)
[9] JURELA, Z.: Int. J. Mass Spectry **12,** 33 (1973)
[10] KROHN, V. E.: Int. J. Mass Spectry **22,** 43 (1976)
[11] SCHELTEN, J.: Z. Naturforsch. **23a,** 109 (1968)
[12] LEROY, V., SEVAIS, J.-P., HABRAKEN, L.: C. R. M. Rep. (Liège) No. 35, 69 (1973)
[13] BESKE, H. E.: Z. Naturforsch. **22a,** 459 (1976)
[14] RÜDENAUER, F. G., STEIGER, W., WERNER, H. W.: Surf. Sci. **54,** 553 (1976)
[15] RODRIGUEZ-MURCIA, H., BESKE, H. E.: Berichte der Kernforschungsanlage, Jülich Nr. Jül. 1292 (1976)
[16] WEHNER, G. K.: 2. Coll. Int. de Pulverisation Cathodique, Nice, 1976
[17] POATE, J. M., BROWN, W. L., HOMER, R., AUGUSTYNIAK, W. M., MAYER, J. M., TU, K. N., VAN DER WEEG, W. F.: Nucl. Inst. Meth. **132,** 345 (1976)
[18] RIEDEL, M., NENADOVIĆ, T., PEROVIĆ, B.: 2. Coll. Int. de Pulverisation Cathodique, Nice, 1976
[19] RIEDEL, M., NENADOVIĆ, T., PEROVIĆ, B.: Acta Chim. Acad. Sci. Hung. **97,** 177 (1978)
[20] BENNINGHOVEN, A.: Z. Naturforsch. **22a,** 841 (1967)
[21] RIEDEL, M., NENADOVIĆ, T., PEROVIĆ, B.: Boris Kidrič Inst. Publ. No. 1400 (1976)
[22] RÜBALKO, V. F., KOLOT, V. YA., FOGEL, YA. M.: Zh. Fiz. Khim. **43,** 955 (1969)
[23] RIEDEL, M., NENADOVIĆ, T., PEROVIĆ, B.: Acta Chim. Acad. Sci. Hung. **97,** 197 (1978)
[24] KLEMM, D. D.: Exp. Tech. Phys. **XIX,** 467 (1971)
[25] HANSEN, M.: Constitution of Binary Alloys, McGraw-Hill, New York 1958
[26] GUENOT, D.: Thesis, Orsay (1966)
[27] WERNER, H. W.: in "Developments in Applied Spectroscopy", Eds E. L. GROVE, A. J. PARKINS, Plenum Press, **7A,** 239 (1969)
[28] ANDERSEN, C. A., HINTHORNE, J.: Science **175,** 853 (1972)
[29] KIENITZ, H.: Massenspektrometrie, Vlg. Chemie GmbH, Weinheim, 1968
[30] BOUMANS, P. W. J. M.: Theory of Spectrochemical Excitation, Hilger and Watts, London, 1966
[31] SCHROEER, J. M.: Surf. Sci. **35,** 485 (1973)
[32] GRIES, W. H., RÜDENAUER, F. G.: SGAE Berichte No. 2430, Vienna, 1975
[33] MARGRAVE, J. L.: The Characterization of High Temperature Vapors, Wiley, New York, 1969
[34] MOESTA, H.: Chemisorption und Ionisation in Metall-Metall Systemen, Springer Vlg., Berlin, 1968
[35] SROUBEK, Z.: Surf. Sci. **44,** 47 (1974)
[36] WERNER, H. W., MORGAN, A. R.: 7th Int. Mass Spectr. Conf., Florence, 1976
[37] NARUSAVA, T., SATAKE, T., KOMIYA, S.: J. Vac. Sci. Technol. **13,** 514 (1976)
[38] PIVIN, J. C., ROCQUES-CARMES, C.: J. Microsc. Spectrosc. Electron. **2,** 301, (1977)

Miklós RIEDEL Department of Physical Chemistry and Radiology, Eötvös L. University, H-1088 Budapest, Puskin u. 11–13.

T. NENADOVIĆ, B. PEROVIĆ Boris Kidrič Institute of Nuclear Sciences Belgrade, Yugoslavia.

Acta Chimica Academiae Scientiarum Hungaricae, Tomus 97 (2), pp. 197–206 (1978)

SIMS STUDY OF IRON-NICKEL AND IRON-CHROMIUM ALLOYS, III

DEPENDENCE OF EMISSION OF DIATOMIC CLUSTER IONS ON ALLOY COMPOSITION

M. RIEDEL,* T. NENADOVIĆ and B. PEROVIĆ

(Boris Kidrič Institute of Nuclear Sciences, Belgrade, Yugoslavia)

(Department of Physical Chemistry and Radiology, Eötvös L. University, Budapest)*

Received March 16, 1977

Intense peaks of cluster ions consisting of identical (Fe_2^+, Ni_2^+ and Cr_2^+) and different ($FeNi^+$ and $FeCr^+$) atoms were observed in the secondary ion spectra of concentrated Fe–Ni and Fe–Cr alloys bombarded with Kr^+ ions. The formation of the cluster ions exhibits a strong concentration-dependence, and the current intensity of the cluster ions increases on increase of the primary ion-current density. The probable mechanisms of formation of the cluster ions were postulated by determination of the relative degree of ionization of the cluster ions.

Introduction

Attention has recently increased with regard to secondary cluster ions formed during the bombardment of solids; the properties and conditions of formation of these ions are connected with many theoretically important questions (stability and ionization, of molecular particles etc.) [1–4]. In addition, the cluster ions similarly play a not insignificant role in secondary ion-emission mass-spectrometric practice (spectral peak interferences [5], "characteristic spectra" [6], vacuum conditions [7], etc.). Publications dealing with cluster ions to date have dealt primarily with the energy [3, 8], angle [9] and size [1, 4, 10] distributions of clusters emitted from pure elements. Data on the connection between the cluster ions and the structure of the bombarded sample [4] are scarcely to be found, however, and the case is the same for cluster ion emission from alloys [11, 12]. In the present work, therefore, we have studied the connection of the emission of cluster secondary ions formed from Fe–Ni and Fe–Cr alloys and the composition of the alloy. Such studies will also contribute to the understanding of the mechanism of emission of cluster ions.

Experimental

Series of Fe–Ni and Fe–Cr alloys (c = 0, 20, 40, 60, 80 and 100 %) were bombarded with 4 keV Kr^+ ions in a secondary ionization mass spectrometer as described earlier [13, 14]. The mass resolution of the SIMS was $m/\Delta m \sim 100$, and thus the study of diatomic ions did not cause any difficulty. The secondary ion spectrum of every individual sample was recorded

at various primary ion-current densities ($i_p = 2-15$ μA/cm^2). The mass-dependent sensitivity of the detector of the mass spectrometer and the isotope abundances were not taken into consideration in the evaluation of the ion-current intensities .These are independent of the concentration of the sample, and in our present studies, therefore, where the concentration dependence of the emission of the individual ionic species was investigated, this neglect did not lead to an error. Simultaneously with the SIMS study, the alloy sputtering coefficients of the individual elements were also determined [13].

Results and discussion

Besides those of the monoatomic ions [15], intense peaks of the cluster ions appeared too in the secondary ion spectra; these were identified as the Fe_2^+, Ni_2^+ and Cr_2^+ (homogeneous cluster) and the $FeNi^+$ and $FeCr^+$ (heterogenous cluster) ions. In the interest of being able to compare the extents of emission of the individual ionic species, we determined the ratio of the current intensities of the cluster ions (I_{cl}^+) and the monoatomic ions (I_M^+):

$$I_{rel}^+ = \frac{I_{cl}^+}{I_M^+} \tag{1}$$

In the case of the heterogeneous ions, reference was made to Fe. Formation of the quotient in eqn. (1) reduced the influence of possible measurement errors, while at the same time the expression shows the superfluousness of taking into account the isotope. Figure 1 presents the concentration dependence of the relative ion current intensity of the Fe_2^+ and Ni_2^+ ions emitted from the Fe – Ni alloys, at various bombarding ion current densities. Figure 2 gives an analogous picture for Fe_2^+ and Cr_2^+ from Fe – Cr alloys, while Figure 3 depicts the relative

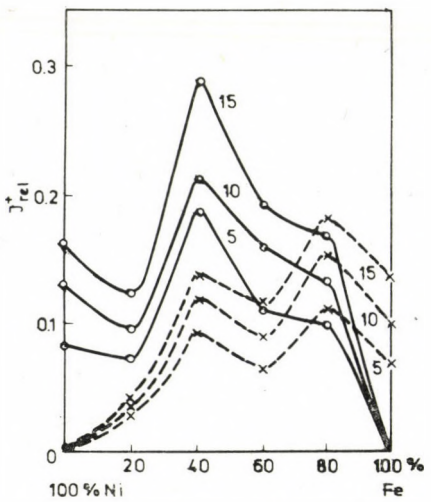

Fig. 1. Relative ion currents of Fe_2^+ and Ni_2^+ ions referred to Fe^+ and Ni^+, as functions of the concentration of the Fe – Ni alloy, at various primary ion-current densities ($i_p = 5$, 10, 15 μA/cm^2) (dashed line: Fe_2^+; continuous line: Ni_2^+)

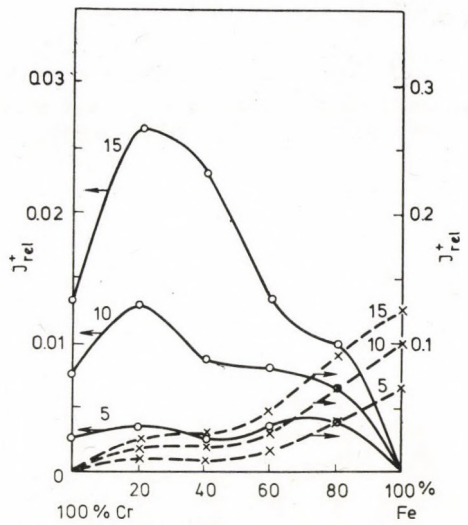

Fig. 2. Relative ion currents of Fe_2^+ and Cr_2^+ ions as functions of the concentration of the alloy, at various primary ion-current densities (i_p = 5, 10, 15 μA/cm²) (dashed line: Fe_2^+; continuous line: Cr_2^+)

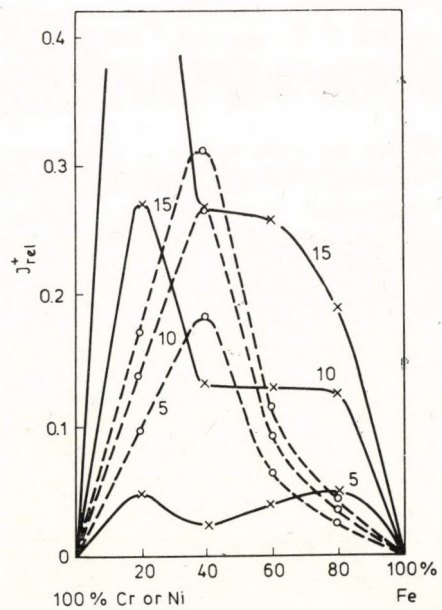

Fig. 3. Relative ion currents of $FeNi^+$ and $FeCr^+$ ions referred to Fe^+, at various primary ion-current densities (dashed line: $FeNi^+$; continuous line: $FeCr^+$)

Table I

Relative ion currents of diatomic cluster ions referred to monoatomic ions, as functions of the alloy composition ($i_p = 10\ \mu A/cm^2$)

Alloy	c_{Fe} %	I^+_{rel}		
		Fe_2^+/Fe^+	Ni_2^+/Ni^+	$FeNi^+/Fe^+$
Fe – Ni	0	0	0.13	0
	20	0.03	0.097	0.14
	40	0.12	0.21	0.27
	60	0.09	0.16	0.09
	80	0.15	0.14	0.04
	100	0.10	0	0
		Fe_2^+/Fe^+	Cr_2^+/Cr^+	$FeCr^+/Fe^+$
Fe – Cr	0	0	0.0075	0
	20	0.016	0.012	0.27
	40	0.020	0.0090	0.13
	60	0.031	0.0080	0.13
	80	0.070	0.0068	0.13
	100	0.099	0	0

ion current intensities of the heterogeneous ions. Table I lists the relative ion-current intensities of the individual diatomic cluster ion species, measured at $i_p = 10\ \mu A/cm^2$, as a function of the alloy composition (the accuracy of the measurements was ± 30 %). For comparison, Table II contains the relative ion current intensities reported in the literature for the same ions.

The amount of the cluster ions is generally 10 – 30 % of that of the monoatomic ions, with the exception of the amount of Cr_2^+ ions, which is about one

Table II

Relative ion currents of diatomic cluster ions from Fe, Ni, Cr *and* Fe – Cr *samples (literature data)*

Cluster ion	Bombarded sample	I^+_{rel}	Ref.
Fe_2^+	pure Fe	0.24	[16]
Ni_2^+	pure Ni	0.33	[17, 18]
Cr_2^+	pure Cr	0.2	[19]
Fe_2^+	Fe – Cr alloy containing 47 % Cr	0.015	[11]
Cr_2^+		0.126	
$FeCr^+$		0.045	

order of magnitude smaller. The amount of the heterogeneous cluster ions in the case of $FeCr^+$ is higher, however, attaining even 70 %. Intense cluster-ion emission such as that observed for several metals by WITTMAACK and STAUDENMAIER [2] ($I^+_{rel} > 1$) was not experienced in our systems. In addition, a considerable composition dependence too can be observed for all ionic species. The relative ion-currents of ions consisting of the same atoms increase with the alloy concentration of the element in question, whereas those of ions consisting of different atoms are the highest at medium concentrations. The effect of the current intensity of the bombarding ions is similarly marked: the relative secondary ion current increases with increasing i_p.

In the case of homogeneous binary alloys, cluster ion formation can be regarded as a second-order process. This means that the amount of cluster ion M_2^+ emitted is proportional to the square of the alloy concentration (c) of the element M. The ion current similarly depends on the sputtering coefficient ($S_{cl}(c)$) and degree of ionization ($\alpha^+_{cl}(c)$) of the diatomic system M_2:

$$I^+_{cl} = \eta \cdot S_{cl}(c) \cdot \alpha^+_{cl}(c) \cdot c^2 \cdot I_p \tag{2}$$

where I^+_{cl} is the detected current of the ions, and η is the sensitivity of the SIMS. The relative ion current can therefore be written in the following way:

$$I^+_{rel} = \frac{S_{cl}}{S_M} \frac{\alpha^+_{cl}}{\alpha^+_M} \cdot c \tag{3}$$

where S_M and α^+_M are the sputtering coefficient and degree of ionization of the monoatomic ion. The experimentally observed i_p dependence of I^+_{rel} indicates that the coverage of the surface of the sample influences the emission of the cluster secondary ions, as also follows from the data of BENNINGHOVEN [16–19] measured on pure Fe, Ni and Cr metals, and from the secondary ion emission studies by MAUL and WITTMAACK [6] on silicon.

On the basis of eqn. (3), to a first approximation the curves of Figs 1 and 2 should be linear as a function of concentration. It is obvious from the shapes of the curves, however, that the quantity of cluster ions emitted from the alloys Fe–Ni and Fe–Cr is also affected by the structure of the alloy, and further, according to Eq. (s), *via* the concentration dependence of the sputtering coefficient and the degree of ionization.

A number of conceptions have been published in the literature with regard to the mechanism of formation of cluster secondary ions in the course of ionic bombardment:

1. The cluster ion splits off the solid directly, preserving certain information about the structure of the sample [4, 20]. On leaving the surface, the cluster particle may undergo ionization. For the diatomic case this may be

written as

$$\text{metal} \rightarrow M_2 \rightarrow M_2^+$$

2. Under suitable conditions, the sputtered atoms may combine to form cluster ions (low energy, emission angle and time differences). These cluster particles may ionize because of their high internal energy [3, 8, 10]:

$$\text{metal} \rightarrow M + M \rightarrow M_2 \rightarrow M_2^+$$

3. A sputtered atom and a secondary ion combine under conditions corresponding to the previous ones:

$$\text{metal} \rightarrow M + M^+ \rightarrow M_2^+$$

4. Because of the low probability of formation of such large particles [1, 10], one may exclude the dissociation into smaller cluster ions of excited big aggregates which have broken off the solid in one:

$$\text{metal} \rightarrow M_n \rightarrow M_2^+ + M_{n-2}$$

For each mechanism the concentration dependence of the relative ion current of the cluster ions can be written by modification of Eq. (3). On the analogy of chemical reactions, it is necessary to introduce a quantity analogous to the customary collision cross-section, which expresses the probability of association of sputtered neutral and neutral (w^0) and of neutral and ionic particles (w^+); these quantities relate to particles in the free state, and are therefore concentration independent. It may be assumed further that the departure of the cluster particle in the first mechanism can be given by the same sputtering coefficient as for the atoms:

$$S_{cl} = S_M^2 \cdot w \tag{4}$$

where w is the probability of joint emission of two atomic particles. In this case, however, w may depend on the composition of the sample. In such a way, for each mechanism I_{rel}^+ is a function of the sputtering coefficient of the atoms, and of the alloy concentration of the element in question. Since the sputtering coefficients of the constituent elements of the alloy have been determined [13], the relative degree of ionization of the cluster ions referred to the monoatomic ions can be obtained from the experimentally found relative ion currents:

$$\alpha_{rel}^+ \equiv \frac{\alpha_{cl}^+}{\alpha_M^+} = \frac{I_{rel}^+}{S_M \cdot c} \tag{5}$$

In the knowledge of the experimentally found S_M^* data, to characterize the ionization of the cluster ions it is practical to determine a quantity proportional to α_{rel}^+:

$$K\alpha_{rel}^+ = \frac{I_{rel}^+}{S_M^* \cdot c} \tag{6}$$

where K contains the proportionality factor k defined previously [13]. It must be noted that, because of the arbitrarily selected units of S_M^*, the relative degree of ionization can also be obtained from Eq. (6) in arbitrary units. Thus, $K\alpha_{rel}^+$ is to be regarded as a ratio, with which the ionizations of the individual ionic species can be compared with one another and can be examined in the c, i_p dependence, but the absolute value of $K\alpha_{rel}^+$ does not mean the extent of ionization directly.

$K\alpha_{rel}^+$ can be given as follows for the processes described above:

Cluster formation mechanism	$K\alpha_{rel}^+ =$
1.	$\frac{\alpha_{Cl}^+}{\alpha_M^+} \cdot c \cdot w$
2.	$\frac{\alpha_{Cl}^+}{\alpha_M^+} \cdot c \cdot w^0$
3. a. homogeneous cluster	w^+
b. heterogeneous cluster	$\frac{\alpha_M^+}{\alpha_{Fe}^+} \cdot c \cdot w^+$

Table III gives the quantities $K\alpha_{rel}^+$ proportional to the relative degrees of ionization of the individual cluster ion species referred to the monoatomic ions, as functions of the alloy composition, at two different bombarding ion-current densities. Figures 4 and 5 present the concentrations dependence of the relative degree of ionization of the ions emitted from the Fe–Ni and Fe–Cr samples, at $i_p = 10$ $\mu A/cm^2$.

Similarly to the relative ion current, the extent of ionization of the cluster ions referred to the monoatomic ions increases with the primary ion-current density. The cluster particles emitted from the Fe–Cr alloys are particularly sensitive in this respect (*e.g.* the ionization of the $FeCr^+$ ion in the case of $i_p = 15$ $\mu A/cm^2$ is about 50–100 times the value determined at 2 $\mu A/cm^2$).

The ionization of Fe_2 emitted from Fe–Ni samples is higher than in the case of Fe–Cr samples, but in general is somewhat lower than in the case of the bombardment of pure iron. The ionization of Ni_2 and Cr_2 emitted from the alloys is substantially higher than for the pure metals.

The ionization of the cluster particles depends strongly on the composition of the alloy. From a comparison of the curves of Figs. 4 and 5 it may be stated

Table III

Relative degrees of ionization of diatomic cluster ions referred to monoatomic ions, as functions of the alloy composition, at various primary current densities (in arbitrary units)

Alloy	c_{Fe} %	$K\alpha^+_{rel}$					
		i_p [μA/cm$_2$]					
		5	10	5	10	5	10
		Fe_2^+		Ni_2^+		FeNi+	
Fe – Ni	0	0	0	0.032	0.050	0	0
	20	0.038	0.038	0.031	0.040	0.042	0.058
	40	0.094	0.13	0.15	0.17	0.14	0.21
	60	0.038	0.058	0.12	0.17	0.063	0.095
	80	0.049	0.067	0.16	0.24	0.052	0.069
	100	0.028	0.040	0	0	0	0
		Fe_2^+		Cr_2^+		FeCr+	
Fe – Cr	0	0	0	0.0016	0.0044	0	0
	20	0 036	0.057	0.0031	0.011	0.045	0.24
	40	0.015	0.029	0.0027	0.0088	0.025	0.13
	60	0.015	0.026	0.0035	0.0080	0.042	0.13
	80	0.025	0.044	0.0083	0.0148	0.11	0.28
	100	0.028	0.040	0	0	0	0

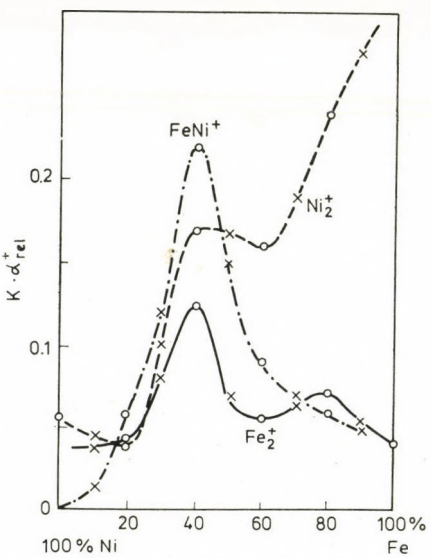

Fig. 4. Ionization of Fe_2^+, Ni_2^+ and $FeNi^+$ ions as functions of the composition of the Fe – Ni alloy. Data denoted by x are values calculated by interpolation. ($K\alpha^+_{rel}$ in arbitrary units; $i_p = 10\ \mu A/cm^2$)

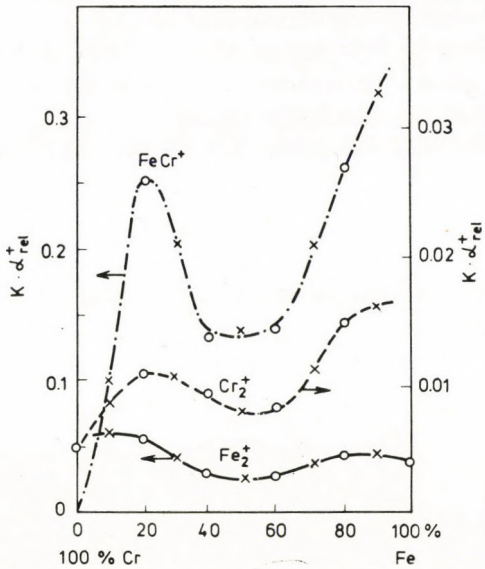

Fig. 5. Ionization of Fe_2^+, Cr_2^+ and $FeCr^+$ ions as functions of the composition of the Fe—Cr alloy. Data denoted by x are values calculated by interpolation. ($K\alpha^+_{rel}$ in arbitrary units; $i_p = 10\ \mu A/cm^2$)

that the composition and structure of the alloy have a greater influence on the extent of ionization of the cluster particles emitted than the nature of the cluster particle itself. It follows from this, however, that clarification of the electronic structures of the polyatomic aggregates is alone not sufficient to explain the mechanism of formation of the cluster ions, in contrast with the view of JOYES *et al.* [10].

The concentration dependence of the relative degree of ionization of the cluster particles permits the further conclusion that the earlier-outlined mechanism 3, according to which only the ionization of the heterogeneous particles can exhibit a c-dependence, did not contribute to the ion formation in our case. This is supported in general too by the fact that the ionic proportion of the sputtered particles is small, and thus the probability of the corresponding aggregation is also minute.

The fact that the ionization of the cluster particles depends on the surface coverage and on the structure of the sample permits the conclusion that mechanism 1, *i.e.* the direct emission of dimeric ions, is the most probable. In addition, however, process 2 is also conceivable, if it is taken into account that the ion sputtering gives rise to a large quantitity of excited neutral atoms too, which associate and lead to ionization of the cluster particles. On the other hand, under given bombardment conditions the extent of excitation of the atoms is largely controlled by the properties of the solid.

To summarize, it may be stated that the formation of cluster ions is is one of the important processes of secondary ion emission; from studies made as a function of the alloy concentration it may be assumed that this process may occur in accordance with both mechanism 1 and mechanism 2. Further more detailed examinations are necessary, however, for the elucidation of a possible closer connection with the phase diagrams of the alloys.

REFERENCES

[1] HERZOG, R. F. K., POSCHENRIEDER, W. P., SATKIEWICZ, F. G.: Rad. Effects **18,** 199 (1973)
[2] WITTMAACK, K., STAUDENMAIER, G.: Appl. Phys. Lett. **27,** 318 (1975)
[3] STAUDENMAIER, G.: Rad. Effects **13,** 87 (1973)
[4] FELDMAN, C., SATKIEWICZ, F. G.: J. Electrochem. Soc. **120,** 1111 (1973)
[5] COLBY, B. N., EVANS, C. A.: Appl. Spectroscopy **27,** 274 (1973)
[6] WERNER, H. W., GREFTE, H. A. M., VAN DER BERG: Rad. Effects **18,** 305 (1973)
[7] MAUL, J., WITTMAACK, K.: Surf. Sci. **47,** 358 (1975)
[8] KÖNNEN, G. P., TIP, A., DE VRIES, A. E.: Rad. Effects **21,** 269 (1973)
[9] STAUDENMAIER, G.: Rad. Effects **18,** 181 (1973)
[10] LELEYTER, M., JOYES, P.: Rad. Effects **18,** 105 (1973)
[11] CHEREPIN, V. T., VASILYEV, A. M.: Vtorichnaya ionno-ionnaya emissiya metalov i splavov, Naukova Dumka, Kiev, 1975
[12] RODRIGUEZ, H., BESKE, H. E.: 7th Int. Mass Spectry Conf., Florence, 1976
[13] RIEDEL, M., NENADOVIĆ, T., PEROVIĆ, B.: Acta Chim. Acad. Sci. Hung. **97.** 177 (1978)
[14] RIEDEL, M., NENADOVIĆ, T., PEROVIĆ, B.: Boris Kidrič Inst. Publ. No. 1400 (1976)
[15] RIEDEL, M., NENADOVIĆ, T., PEROVIĆ, B.: Acta Chim. Acad. Sci. Hung. **97.** 187 (1978)
[16] STUMPE, E., BENNINGHOVEN, A.: Phys. Stat. Sol. **21a,** 479 (1974)
[17] MÜLLER, A., BENNINGHOVEN, A.: Surf. Sci. **41,** 493 (1974)
[18] data of A. BENNINGHOVEN (in OECHSNER, H., GERHARD, W.: Surf. Sci. **44,** 480 (1974))
[19] BENNINGHOVEN, A., MÜLLER, A.: Surf. Sci. **39,** 416 (1973)
[20] CHUPAKIN, M. S.: Zh. Anal. Khim. **22—23,** 325 (1967)

Miklós RIEDEL Department of Physical Chemistry and Radiology
Eötvös L. University, H-1088 Budapest, Puskin u. 11—13.

T. NENADOVIĆ, B. PEROVIĆ Boris Kidrič Institute of Nuclear Sciences, Belgrade, Yugoslavia

Acta Chimica Academiae Scientiarum Hungaricae, Tomus 97 (2), pp. 207–211 (1978)

POLYATOMIC CATIONS OF LOW OXIDATION STATE TELLURIUM IN CHLOROSULPHURIC ACID

S. A. A. ZAIDI, Z. A. SIDDIQI and N. A. ANSARI

(Department of Chemistry, Inorganic Division Alligarh Muslim University, Alligarh, U. P., India)

Received September 13, 1976

In revised form April 2, 1977

Conductometric and ultraviolet visible spectroscopic studies on solutions of tellurium in chlorosulphuric acid indicate that the red colour of the solution produced in neat HSO_3Cl is due to Te_4^{2+} cation. It has also been shown that the red species Te_4^{2+} can be oxidized to the yellow species Te_4^{4+} by oxidizing agents like $K_2S_2O_8$ and TeO_2. In excess of the oxidizing agents however TeO_2 is formed.

Introduction

The formation of polyatomic cations [1–4] S_{16}^{2+}, S_8^{2+}, S_4^{2+}, Se_4^{2+}, Se_8^{2+} Te_4^{2+} and Te_4^{4+} having the elements in low oxidation states has been reported in H_2SO_4, $H_2S_2O_7$ and HSO_3F. Recently chlorosulphuric acid which is a strong ionizing solvent [5–7] and is intermediate in strength between sulphuric and fluorosulphuric acids, formation of polyatomic cations only of selenium has been reported [8] from these laboratories. It was therefore thought of interest to study the oxidation of tellurium in chlorosulphuric acid yielding polyatomic cationic species as a stable entity.

Experimental

All the materials used including the solvent chlorosulphuric acid (Riedel) were commercially pure samples excepting tellurium dioxide which was synthesized according to the established methods [9].

The design of the conductivity cell, meaning and significance of the notations γ and ω have been discussed elsewhere [5–7].

A systronics type 302-S. R. No 306 conductivity bridge thermostatted at 25 ± 0.1 °C was used for the conductance measurements and ultraviolet visible spectra of the solutions were recorded on a Beckman Model DU 2 spectrophotometer.

Results and discussion

Conductometric Evidences: Tellurium dissolves in chlorosulphuric acid producing red colour conducting solutions. The conductance of the solutions stayed constant for about twelve hours, however, the red colour gradually

changed to an orange-yellow and finally a colourless solution was obtained. On the addition of the oxidizing agents like tellurium dioxide and potassium persulphate the red colour of the solutions was immediately changed to yellow. However, with a large excess of these oxidizing agents colourless solutions were obtained. These observations therefore indicate that the coloured solutions of tellurium in chlorosulphuric acid correspond to positive oxidation states of tellurium and the yellow species are in a higher oxidation state than the red one.

The value of v *i.e.* the number of moles of SO_3Cl^- ions (responsible for conducting almost all the current in the solution) produced by each atom of tellurium is 0.60, obtained from the comparison of the specific conductance-concentration curves of the solute with that of a reference electrolyte KCl (Fig. 1). The observed value of v is consistent with the formation of the polyatomic cationic species Te_4^{2+} containing the element in low oxidation state, according to the following reaction given below

$$4Te + 4HSO_3Cl \rightarrow Te_4^{2+} + SO_2 + 2HCl + H_2SO_4 + 2SO_3Cl^- \qquad (1)$$

It has also been indicated from the conductometric studies that in HSO_3Cl the red species Te_4^{2+} can be oxidized to the yellow Te_4^{4+} by the above mentioned oxidizing agents. This may be seen from the conductometric titration of the red species with the oxidizing agents TeO_2 and $K_2S_2O_8$ shown in Figs 2 and 3, respectively. It is evident from the figures that a clear break occurs at the ratios

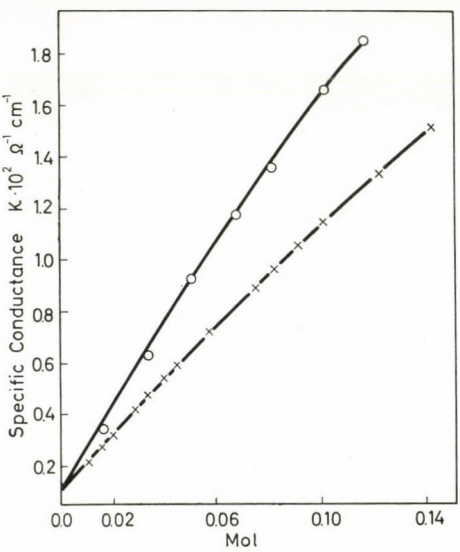

Fig. 1. Specific conductance-concentration curves of solutes in HSO_3Cl at 25 °C o Potassium chloride; × tellurium metal

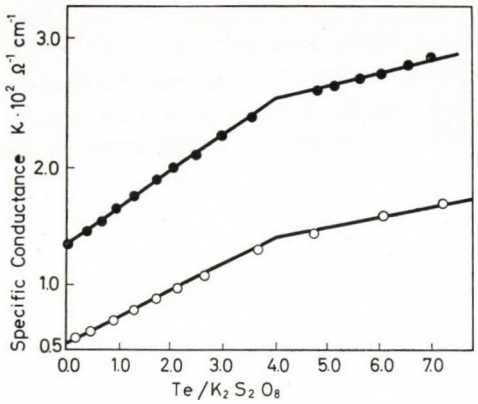

Fig. 2. Conductometric titrations of the solutions of tellurium with TeO_2 at 25 °C. ○ Concentration of Te 0.1630 w; × concentration of Te 0.1471 w

$Te/K_2S_2O_8 = 4.0$ and $TeO_2/Te = 0.16$. Tellurium dioxide oxidizes Te_4^{2+} to Te_4^{4+} and is itself reduced to Te_4^{4+} as shown below

$$6Te_4^{2+} + 4Te(IV) \rightarrow 7Te_4^{4+} \quad (2)$$

The reaction occurring in HSO_3Cl may be given as below

$$6Te_4^{2+} + 4TeO_2 + 24HSO_3Cl \rightarrow 7Te_4^{4+} + 8H_2SO_4 + 8HCl + 16SO_3Cl^- \quad (3)$$

The equation for overall reaction for the formation of Te_4^{4+} from Te in a chlorosulphuric acid solution containing TeO_2 may be obtained by combining equations (1) and (3) as

$$24Te + 4TeO_2 + 48HSO_3Cl \rightarrow 7Te_4^{4+} + 6SO_2 + 14H_2SO_4 + 20HCl + 28SO_3Cl^- \quad (4)$$

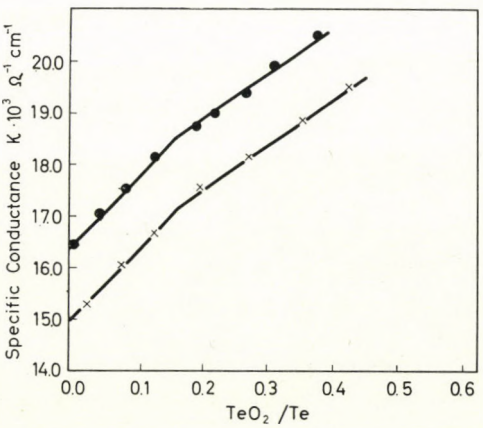

Fig. 3. Conductometric titrations of the solutions of tellurium with $K_2S_2O_8$. ○ Concentration of $K_2S_2O_8$ 0.0378 w; ⊙ concentration of $K_2S_2O_8$ 0.01687 w

At equivalence point of the formation of the yellow species Te_4^{4+} the predicted ratio $TeO_2/Te = 0.17$ is in excellent agreement with the experimentally observed value of $TeO_2/Te = 0.16$ and therefore confirms the mode of reaction represented by equation (4).

Potassium persulphate is known to be a strong oxidizing agent.

An attempt was therefore made to check the oxidation of Te_4^{2+} to Te_4^{4+} by this oxidizing agent and the reaction occurring in HSO_3Cl may be given as

$$Te_4^{2+} + K_2S_2O_8 + 4HSO_3Cl \rightarrow Te_4^{4+} + 2H_2SO_4 + 2K^+ + 4SO_3Cl^- \quad (5)$$

The overall reaction for the formation of the yellow species Te_4^{4+} in a chlorosulphuric acid solution containing $K_2S_2O_8$ may be given by adding equations (1) and (5) as given below

$$4Te + K_2S_2O_8 + 8HSO_3Cl \rightarrow Te_4^{4+} + SO_2 + \\ + 2HCl + 3H_2SO_4 + 2K^+ + 6SO_3Cl^- \quad (6)$$

The observed ratio $Te/K_2S_2O_8 = 4.0$ at the equivalence point of the formation of Te_4^{4+} is in excellent agreement with the expected value according to equation (6) therefore confirming it to be the mode of the reaction.

Spectrophotometric evidences: The absorption spectrum of the red species obtained by dissolving tellurium in cold chlorosulphuric acid has been shown in Figure 4 (Curve A). This species has an intense band centered at 550 nm and a very weak absorption having the maximum at 430 nm. A similar spectrum [4] of the red species formed by dissolving tellurium in fluorosulphuric acid has been earlier assigned to the existence of Te_4^{2+} cation.

The absorption spectrum of the orange-yellow solution in chlorosulphuric acid obtained by oxidizing the red solution with small amount of $K_2S_2O_8$ such that $Te/K_2S_2O_8 = 7.0$ has been shown in Figure 4 (Curve B). This solution has an intense band having maximum at 550 nm and two weak maxima centred at 380 and 430 nm. The absorption spectrum of the yellow species Te_4^{4+} in HSO_3F has been reported [4] to contain an intense band at 250 nm and two weak bands at around 360 and 420 nm. The intense band at 250 nm characteristic of Te_4^{4+} could not be observed in HSO_3Cl due to the solvent cut off at 280 nm. The appearance of the intense band at 550 nm characteristic of the Te_4^{2+} suggests that the solution contains a mixture of both the cationic species *i.e.* Te_4^{2+} and Te_4^{4+}. However, when the red solution was oxidized with a larger concentration of $K_2S_2O_8$ such that $Te/K_2S_2O_8 = 1.0$ only a weak band at 350 nm characteristic of the Te_4^{4+} could be observed indicating the existence of yellow species only. The colourless solutions obtained by the excess of the oxidizing agents correspond to the higher oxidation state Te(IV) presumably

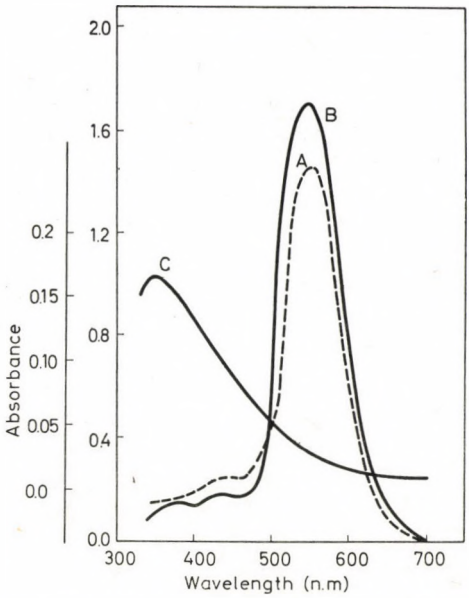

Fig. 4. Absorption spectra of the solutions of tellurium in HSO_3Cl at 25 °C. A. red species; B. orange-yellow species; C. yellow species

TeO_2. In the case of selenium also it has been reported [8] that in large excess of the oxidizing agent selenium is converted to SeO_2 which accounts for the colourless solution.

*

Prof. W. RAHMAN is thanked for providing the research facilities. One of us (N. A. A.) is grateful to Aligarh Muslim University, Aligarh for financial assistance.

REFERENCES

[1] BARR, J., GILLESPIE, R. J., KAPOOR, R., MALHOTRA, K. C.: Can. J. Chem. **46,** 149 (1968)
[2] BARR, J., GRUMP, D., GILLESPIE, R. J., KAPOOR, R., UMMAT, P. K.: Can. J. Chem. **46,** 3607 (1968)
[3] GILLESPIE, R. J., PASSMORE, J., UMMAT, P. K., VAIDYA, O. C.: Inorg. Chem. **10,** 1327 (1971)
[4] BARR, J., GILLESPIE, R. J., PEZ, G. P., UMMAT, P. K., VAIDYA, O. C.: Inorg. Chem. **10,** 362 (1971)
[5] ZAIDI, S. A. A., SIDDIQI, Z. A.: J. Inorg. Nucl. Chem. **37,** 1806 (1975)
[6] ZAIDI, S. A. A., SIDDIQI, Z. A.: J. Inorg. Nucl. Chem., **38,** 1404 (1967)
[7] ZAIDI, S. A. A., SIDDIQI, Z. A.: Acta Chimica (Budapest) **92,** 57 (1977)
[8] ZAIDI, S. A. A., SIDDIQI, Z. A., ANSARI, N. A.: Acta Chimica (Budapest) **93,** 395 (1977)
[9] Handbook of Preparative Inorganic Chemistry, Edited by G. BRAUER, Academic Press New York, Vol. 1 pp 447 (1963)

S. A. A. ZAIDI
Z. A. SIDDIQI
N. A. ANSARI
Department of Chemistry Inorganic Division Aligarh Muslim University, Aligarh-202001 U. P., India.

Acta Chimica Academiae Scientiarum Hungaricae, Tomus 97 (2), pp. 213–220 (1978)

THE CATALYTIC OXIDATION OF SORBOSE

Á. LENGYEL-MÉSZÁROS, B. LOSONCZI, J. PETRÓ and I. RUSZNÁK

(Department of Organic Chemical Technology, Technical University, Budapest)

Received April 13, 1977

The heterogeneous catalytic oxidation of sorbose has been investigated, using a specially prepared Pd/C catalyst. It has been found that a yield of about 50 % can be achieved in a 20 % (w/w) solution at 60 – 70 °C in 4 – 6 hours, and the selectivity for sorbose is 80 %. Therefore, the process appears to be suitable for industrial realization.

In manufacturing Vitamin C, one of the intermediate steps is the oxidation of sorbose to 2-ketogulonic acid (KGA), which can be effected with chemicals, catalytically, or by microbiological route [1].

In industrial processes, generally the diacetone derivative is oxidized instead of sorbose, as in this way side reactions are eliminated and the process is more economical in spite of the two additional reaction steps.

There are several descriptions and patents for the direct catalytic oxidation of sorbose [2–7], however, these have no industrial importance, because the end product is obtained in the form of a dilute solution (4–6 % (w/w)) after a long reaction time (180 hours) and in a poor yield (25–50 %).

During an investigation of the catalytic oxidation of diacetone-sorbose [8] we have developed a palladium catalyst, which is suitable for oxidation under industrial conditions. The use of this catalyst has now been investigated in the oxidation of sorbose, too.

The quantity of the products formed was investigated as a function of reaction conditions with the aim of determining the optimal parameters.

Oxidation was carried out in water, in the presence of Pd-on-charcoal catalyst, with air, in the apparatus shown in Fig. 1. The composition of the reaction mixture was determined by the conductiometric and polarographic methods developed by us earlier [9].

Effects of temperature

The composition of the reaction mixture was the following:

Sorbose	5 g
$NaHCO_3$	3.5 g
Pd/C (10 %)	1 g
Water	50 ml
Air flow rate	3 l/min/l of solution

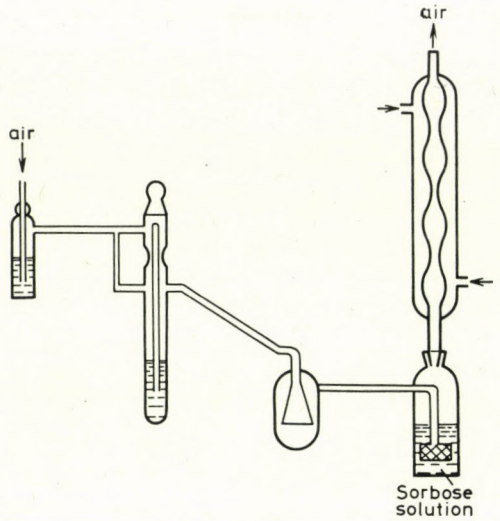

Fig. 1. Apparatus for the oxidaton of sorbose

The reaction temperature was varied between 20 and 90 °C. The results are shown in Table I and in Fig. 2.

From the data it can be seen that under the given reaction conditions the optimal temperature is 60 – 70 °C, at which a KGA production of about 50 % can be attained in 4 – 6 hours, while 80 – 82 % of the sorbose is converted into the desired product. The results of a reaction carried out under these near-optimal conditions are summarized in Fig. 3.

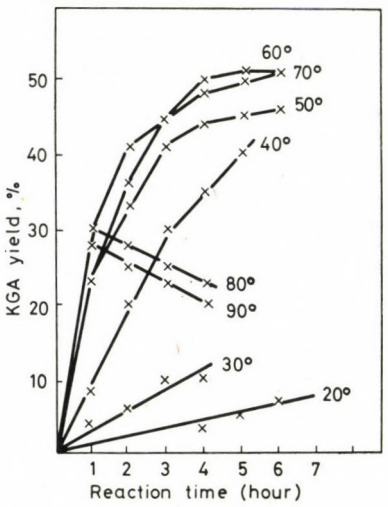

Fig. 2. Oxidation of sorbose into ketogulonic acid (KGA) at various temperatures

Table I

The effect of temperature on the composition of the reaction mixture

Temperature, °C	Time, hr.	Sorbose consumption, %	KGA yield, %	Oxalic acid + threonic acid, %	Selectivity for sorbose → KGA reaction, %
20	1	–	–	–	
	2	–	–	–	
	3	–	–	–	
	4	–	3	–	
	5	5	5	–	
	6	10	7	–	
30	1	5	4	–	
	2	8	6	–	
	3	15	10	3	
	4	17	10	4	
	5	–	–	–	
	6	–	–	–	
40	1	10	8	2	80
	2	26	20	6	77
	3	38	30	8	79
	4	44	35	8	80
	5	50	40	9	80
	6	–	–	–	–
50	1	27	23	4	85
	2	41	33	8	81
	3	50	41	9	82
	4	53	44	9	83
	5	54	45	9	83
	6	56	46	10	82
60	1	28	25	5	82
	2	45	37	8	82
	3	55	45	10	82
	4	60	50	10	83
	5	63	51	12	81
	6	–	–	–	–

Table I (continued)

Temperature, °C	Time, hr.	Sorbose consumption, %	KGA yield, %	Oxalic acid + threonic acid, %	Selectivity for sorbose → KGA reaction, %
70	1	37	30	7	81
	2	49	41	8	84
	3	54	44	9	81
	4	59	48	11	81
	5	63	50	12	79
	6	67	51	16	76
80	1	42	30	12	72
	2	60	28	32	57
	3	66	25	41	38
	4	72	23	49	32
	5	–	–	–	–
	6	–	–	–	–
90	1	47	28	19	60
	2	72	25	46	35
	3	76	23	53	30
	4	78	20	58	26
	5	–	–	–	–
	6	–	–	–	–

Effect of concentration

The concentration of the solution in which the oxidation can be carried out, is important from the technological point of view. Therefore, keeping the sorbose : $NaHCO_3$: catalyst ratio constant, the effect of the increase in sorbose concentration investigated at 70 °C.

The results are summarized in Table II and Fig. 4.

It can be seen from these data that increase of the sorbose concentration up to 20 % does not substantially affect either the reaction rate or the attainable yield. This concentration range (10 – 20 %) is already acceptable for a possible industrial process.

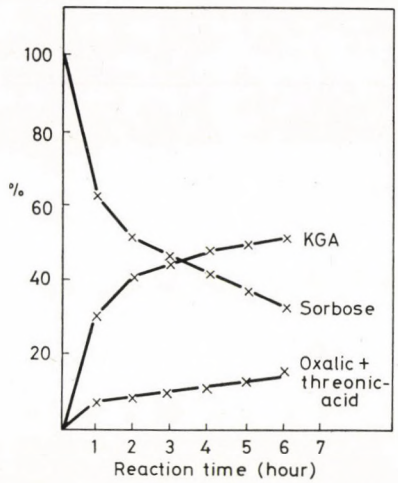

Fig. 3. Oxidation of sorbose at 70 °C

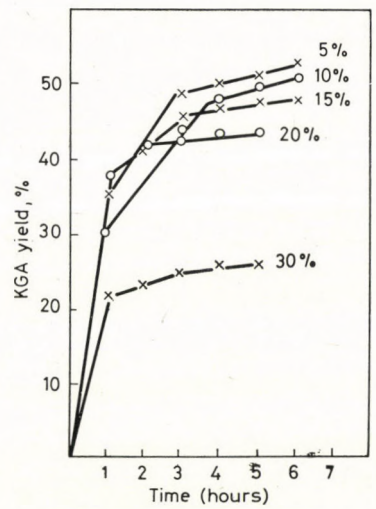

Fig. 4. Oxidation of sorbose solutions of various concentrations

Effect of the quantity and the nature of additives on the oxidation

The catalytic oxidation of sorbose into ketogulonic acid can be carried out only in mildly alkaline medium. In the literature sodiumacetate, potassium oxalate, sodium hydrogen carbonate, sodium carbonate and various sodium phosphates are mentioned as additives. We used potassium oxalate, $NaHCO_3$ and Na_2CO_3. Potassium oxalate was tried because it may suppress the for-

Table II

Oxidation of sorbose solutions of different concentrations

Concn., g/100 ml	Time, hr.	Sorbose consumption, %	KGA yield, %	Oxalic acid + threonic acid, %	Selectivity for sorbose→KGA reaction, %
5	1	41	35	7	85
	2	48	42	6	87
	3	55	49	6	89
	4	60	50	10	83
	5	63	51	12	81
	6	65	53	12	81
10	1	37	30	7	81
	2	49	41	8	84
	3	54	44	9	81
	4	59	48	11	81
	5	63	50	12	79
	6	67	51	16	76
15	1	37	38	2	95
	2	47	43	5	91
	3	52	46	6	88
	4	56	47	9	84
	5	57	48	9	84
	6	59	48	11	82
20	1	41	38	3	92
	2	49	42	6	86
	3	53	45	8	85
	4	57	46	11	81
	5	57	46	11	81
	6	–	–	–	–
25	1	39	22	17	62
	2	46	23	24	50
	3	52	25	27	48
	4	57	26	31	46
	5	57	26	–	46
	6	–	–	–	–

mation of oxalic acid and provide for a pH of 7–8. As contrary to data in the literature, practically no oxidation occurred in the presence of potassium oxalate, whether used alone or in combination with $NaHCO_3$.

It has been found that the quantity of $NaHCO_3$ should not be reduced below 1.5 molar equivalent, because when the pH of the reaction mixture decreases after a certain time below 7, the oxidation stops. If the pH of the initial mixture is increased, this increases the danger of undesired additional oxidation. Our detailed results are summarized in Table III.

Table III

Composition of the reaction mixture after 4 hrs of oxidation at 70 °C in the presence of different additives

Additive		pH at the beginning of oxidation	Sorbose consumption, %	KGA yield, %	Oxalic acid + threonic acid yield, %	Selectivity for sorbose → KGA reaction, %
Nature	Quantity molar equ.					
K oxalate	1.5	~7	–	–	–	–
K oxalate + + $NaHCO_3$	1+1	~7	–	–	–	–
$NaHCO_3$	1.0	~8	45	40	5	89
$NaHCO_3$	1.5	~8	59	48	11	81
$NaHCO_3$	2.25	~8	54	40	14	74
Na_2CO_3	1.5	~10	70	42	28	60

Effect of the quantity and Pd content of the catalyst on the oxidation

A further increase of the quantity of catalyst (sorbose: Pd/C < 5) did not increase the reaction rate. On changing the palladium content of the catalyst, it was found that the reaction rate was scarcely reduced and the lifetime of the catalyst became shorter when a catalyst of lower Pd content (*e.g.* 5 % (w/w)) was used. An increase of the palladium content did neither increase the reaction rate, nor improve the yield, and the lifetime of the catalyst was not substantially longer. Thus, the use catalysts with a palladium content of about 10 % (w/w) seems to be optimal.

REFERENCES

[1] Bayer, I., Bodánszky, I.: Gyógyszerek és gyógyszergyártás. Műszaki Könyvkiadó, Budapest 1957
[2] Heyns, K.: U. S. Pat. 21,899,778 (1940)
[3] Belg. Pat. 422,705 (1936)

[4] SHEEDEN, R. P. A., TURNER, R. B.: J. Am. Chem. Soc. **77,** 190 (1955)
[5] HEYNS, K., PAULSEN, H.: Angew. Chem. **69**, 600 (1957)
[6] MERCK, E.: Ger. Pat. 692,892 (1939)
[7] HEYNS, K.: Ann. **558,** 177 (1947)
[8] CSŰRÖS, Z., PETRÓ, J., FOGASSY, E., LENGYEL-MÉSZÁROS, A.: Hung. Pat. 162, 772 (1970)
[9] LOSONCZI, B., LENGYEL-MÉSZÁROS, A., PETRÓ, J.: In the press

Ágnes LENGYEL-MÉSZÁROS
Béla LOSONCZI
József PETRÓ
István RUSZNÁK

H-1521 Budapest

Acta Chimica Academiae Scientiarum Hungaricae, Tomus 97 (2), pp. 221–234 (1978)

ON THE MECHANISM OF ETHANE HYDROGENOLYSIS ON METAL CATALYSTS

P. TÉTÉNYI, L. GUCZI and A. SÁRKÁNY

(Institute of Isotopes of the Hungarian Academy of Sciences, Budapest)

Received April 15, 1977

Data on adsorption and H–D exchange in CH_4 and C_2H_6 were compared with hydrogenolysis on Co, Ni, Rh, Pd, Ir and Pt blacks. It was found for all catalysts that $w_{ex} > w_h$ and $E_{ex} < E_h$. The activity sequence for hydrogenolysis is Rh > Ru > Ir > Ni > Co > Pd > Pt, which considerably differs from that for exchange. A parallelism between the activity in hydrogenolysis, chemisorption and the multiple to single exchange ratio has been found with ethane.

These considerations reveal the importance of the strong interaction of hydrocarbons with the metal in the process of hydrogenolysis. However, the formation of C = M or $C(M)_2$ structures in the rate-determining step of hydrogenolysis, put forward earlier should be rejected on the basis of the comparison of respective activation energies.

The analysis of all data (exchange, chemisorption and hydrogenolysis) suggests that the rupture of the C–C bond in chemisorbed ethane is the rate-determining step. This was supported also by energy calculations.

Introduction

Several papers have been published recently on the mechanism of hydrogenolysis of hydrocarbons. Their authors have approached the problem mainly from a kinetic viewpoint. SINFELT's work is of basic importanec [1–3] because he developed further the kinetics proposed by CIMINO, BOUDART and TAYLOR [4]. A new version of the kinetics of ethane hydrogenolysis has been put forward by BOUDART [5].

Similarly to other catalytic reactions, it seems that the approach and interpretation of the mechanism from a merely kinetic viewpoint is not sufficient for final and unambiguous conclusion. This statement is supported by the wide criticism of the works mentioned [6–9]. It has been shown earlier [10, 11] that the character of the kinetic equation in itself cannot be regarded as evidence for the mechanism of a heterogeneous catalytic reaction. Later, a similar conclusion has been drawn also by BOUDART [5].

The above facts stimulated us to carry out wide, comparative studies on the adsorption of methane and ethane, on their hydrogen deuterium exchange and on ethane hydrogenolysis. These studies have been carried out

over nickel [12], platinum and cobalt [13, 14], palladium [15], ruthenium, rhodium and iridium [16] catalysts. Pure unsupported metal blacks were used as the catalysts, in contrast to the works of SINFELT, in order to avoid eventual support effects.

Data obtained as a result of these studies permit to draw generalized conclusions on the correlations between adsorption, exchange and hydrogenolysis. This allows us to make certain statements with respect to the mechanism of hydrogenolysis. It has to be remarked, however, that these conclusions are valid only for the low temperature range of hydrogenolysis (below 573 K), and further, that both exchange and hydrogenolysis were studied in considerable excess hydrogen of *i.e.* in the range of negative hydrogen exponents.

1. Comparison between exchange and hydrogenolysis

The initial step of both hydrogen–deuterium exchange and hydrogenolysis of ethane is hydrocarbon adsorption, therefore, it is reasonable to compare these metals with respect to their activity shown in exchange and hydrogenolysis. Every metal studied (except for cobalt) shows such a temperature range where hydrogen–deuterium exchange takes place in ethane but no hydrogenolysis occurs. This is illustrated by the comparison of the so-called "threshold temperatures" that is at the same time suitable for comparison of the catalytic activities of the respective metals in these processes (Table I).

Table I

Data on hydrogen–deuterium exchange in CH_4 *and* C_2H_6 *and hydrogenolysis of* C_2H_6

Catalyst	Reaction						$\left(\frac{w_{ex}}{w_h}\right) t_x$
	$CH_4 + D_2$		$C_2H_6 + D_2$		$C_2H_6 + H_2 \rightarrow 2CH_4$		
	t_t (°C)	w_{ex}	t_t (°C)	w_{ex}	t_t (°C)	w_h	
Co	310	4.34×10^{11}	–	–	269	8.73×10^{12}	–
Ni	164	2.07×10^{13}	64	3.01×10^{15}	210	2.55×10^{13}	1.38×10^{0}
Ru	103	5.25×10^{15}	39	5.66×10^{16}	126	5.25×10^{17}	6.03×10^{1}
Rh	94	2.39×10^{16}	17	5.64×10^{16}	107	1.68×10^{17}	5.39×10^{2}
Pd	151	1.93×10^{14}	67	2.88×10^{16}	297	1.27×10^{12}	5.86×10^{3}
Ir	97	1.97×10^{17}	103	7.52×10^{16}	186	1.20×10^{16}	8.21×10^{2}
Pt	95	1.54×10^{16}	37	4.99×10^{16}	321	1.85×10^{11}	3.74×10^{4}

t_t: temperature for 0.5 % $h^{-1}\,m^{-2}$ conversion; w_{ex}, w_h: rate of exchange and hydrogenolysis in mol $s^{-1}\,m^{-2}$ units, at 165 and 250 °C, respectively; $\left(\frac{w_{ex}}{w_h}\right) t_x$: ratio of ethane exchange and hydrogenolysis at $w_h = 10^{15}$ mol $s^{-1}m^{-2}$

It can be seen from the data in Table I that the rate of ethane hydrogenolysis reaches a value comparable with that of exchange only at much higher temperatures; in other words, the rate of exchange at the same temperature is much higher than that of hydrogenolysis. No direct correlation can be found between exchange and hydrogenolysis; this can be seen if the activity orders in the two reactions are compared (the activities are characterized here by the reciprocal threshold temperatures):

Exchange: Rh > Pt > Ru > Ni > Pd > Ir.

Hydrogenolysis: Rh > Ru > Ir > Ni > Co > Pd > Pt.

The corresponding activation energies also show that hydrogenolysis is a more hindered process than exchange (Table II). The activation energies for hydrogenolysis are, as a rule, two (for Pd and Pt three) times higher than those of H–D exchange in ethane.

Interesting observations can be made concerning the activation energies of methane exchange. These values are higher than the corresponding ones for ethane but do not reach those of ethane hydrogenolysis, and neither do the even higher activation energies for multiple exchange of methane, with the exception of cobalt.

Table II

Activation energies (kJ mol^{-1}) of the reactions quoted in Table I

Catalyst	E_{d_1}	E_{d_4}	E_{ex}^{m}	E_{ex}^{et}	E_h
Co	92	113	88	–	113
Ni	121	138	125	88	167
Ru	71	102	97	59	119
Rh	72	103	94	71	156
Pd	111	180	112	73	222
Ir	96	113	111	82	163
Pt	79	105	105	79	222

E_{d_1}: activation energy of CH_3D formation; E_{d_4}: activation energy calculated from CH_2D_2, CHD_3 and CD_4 formation; E_{ex}^{m}, E_{ex}^{et}: activation energy of methane and ethane exchange, calculated from the consumption of "light" hydrocarbons; E_h: activation energy of ethane hydrogenolysis

The differences in activation energy can be readily interpreted, considering the energy requirement for the rupture of various bonds, applying the method of BALANDIN [17].

The energy requirement for the rupture of the C–C bond over a metal surface is

$$Q_{CC,M} = Q_{CC} - 2Q_{CM} \quad (1)$$

where Q_{CC} denotes the energy of the C–C bond, equal to 364 kJ mol^{-1} [18];
Q_{CM} is the energy of the carbon-metal bond which is between 83 and 96 kJ mol^{-1} for the metals studied, according to spectroscopic measurements [19].

Consequently, the energy requirement for the rupture of the C–C bond varies between 170 and 200 kJ mol^{-1}, depending on the nature of the metal.

The slowest step of the exchange reaction in a saturated hydrocarbon is, in all probability, the C–H bond rupture, because the adsorption of hydrogen (and also deuterium) as well as the H_2–D_2 exchange are well-known, very rapid processes with much higher rates than H–D exchange in hydrocarbons [20, 21]. The energy requirement of C–H bond rupture is:

$$Q_{CH,M} = Q_{CH} - Q_{CM} - Q_{HM} \qquad (2)$$

Considering that the average value of Q_{CH} is 413 kJ mol^{-1} [18], and that Q_{HM} is between 266 and 280 kJ mol^{-1}, depending on the nature of the metal [19], thus $Q_{CH,M}$ should be between 37 and 64 kJ mol^{-1}, *i.e.* much below the energy requirement for the rupture of the C–C bond on metal surfaces. This explains the very considerable difference between the energies of activation of ethane exchange and hydrogenolysis.

We explain the difference between the exchange of methane and ethane by the possibility of a 1,2-interaction in the case of the latter hydrocarbon, which is more favourable from a geometrical and even more from an energetic point of view than the 1,1-interaction, being the only possibility with methane. This is demonstrated by the individual bond energies [22]:

$Q_{CH_3-H} = 435$ kJ $\qquad$ $Q_{C_2H_5-H} = 413$ kJ

$Q_{CH_2-H} = 435$ kJ $\qquad$ $Q_{C_2H_4-H} = 163$ kJ

The more favourable character of the 1.2-interaction is demonstrated also by the fact that deuterium uptake by ethane over nickel and platinum below 473 K takes place in symmetrical positions and only at higher temperatures do appear also asymmetrically deuterated species [14].

Table II shows that the formation of multiply deuterated methane is much more hindered than that of the singly exchanged CH_3D. KEMBALL interpreted [23] the higher activation energy in terms of different mechanisms for the two processes, *i.e.* by the higher energy requirement for the formation of species (I) and (II) necessary for multiple exchange:

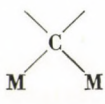

(I) and (II)

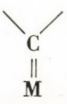

It should be noted, however, that the actual difference between E_{d_4} and E_{d_1} over various catalysts shows large variations.

To interpret these facts, it can be considered that the formation of structure I requires probably a higher energy of activation than that of structure II. This is supported by the predominantly linear adsorption of CO [24]; at the same time bridged species represent the stronger, hardly removable adsorption. The higher activation energy follows from the strained character of the bridged structure (the value of the M–C–M angles is between 123 and 132° on (100) planes and between 76 and 80° on (111) planes, depending on the atomic diameter of the metal). No unambiguous correlation can be found between the geometry, chemical nature, electronic properties of the metal and the corresponding $E_{d_4} - E_{d_1}$ values.

This is probably due to the fact that the "weight" of structures I and II is different for various metals in producing multiply deuterated hydrocarbons. Their role is determined mainly by the proportion of low Miller index planes in polycrystalline metals. Experimental data show [24] that the formation of bridged structures is more probable on (100) planes since their strain would be very high on (111) planes. The relative amount of structure I and II is also influenced by the various contents of edges and corners (*i.e.* the relative amount of low coordination number atoms) in different samples. This is supported by the fact that the structure of the adsorbed layer depends on the stepwise character of platinum single crystals [25]. We conclude that the ratio of singly and multiply deuterated species must depend considerably on the preparation and pretreatment of individual catalyst samples.

Structures I and II must play a role also in ethane hydrogenolysis since the rupture of the C–C bond of dissociatively chemisorbed ethane results necessarily in the formation of species:

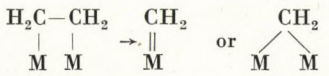

(III)

This is evidenced by the formation of multiply deuterated methane from ethane in the presence of deuterium under such conditions where no H–D exchange takes place in methane [12]. Accordingly, over those catalysts that are more active in hydrogenolysis, more extensive multiple exchange can be expected than in the case of less active metals. In order to check this suggestion, the rates of $w_{d_1 d_2}$ and $w_{d_3 - d_6}$ have been calculated on the basis of the initial product distribution of the H–D exchange of ethane. This calculation was based on the assumption that the formation of ethane containing one or two

D atoms can be attributed to "weak" interactions:

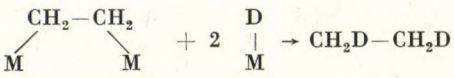

(IV)

and

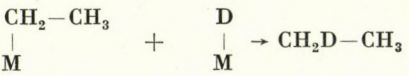

(V)

On the other hand, the precursors of multiply deuterated hydrocarbons are hydrocarbon radicals with multiple carbon–metal bonds. Data have been calculated at identical total reaction rates (10^{15} mol m^{-2} s^{-1}). The values of the ratio $w_{d_3-d_6}/w_{d_1d_2}$ for various metals are as follows

Rh	Ru	Ir	Ni	Pd	Pt
3.86	3.13	2.29	1.18	0.75	0.55

This order is fully identical with that observed for the hydrogenolysis activity. This is in agreement with KEMBALL's finding [23], who demonstrated a similar parallelism between multiple exchange of methane and the rate of butane hydrogenolysis.

2. Adsorption of methane and ethane and hydrogenolysis

Very marked differences have been found between the adsorption and especially the chemisorption properties of various metals with respect to methane and ethane adsorbates. No parallelism could be observed between the adsorptivity and hydrogenolysis activity. For example, platinum does adsorb much higher amounts than nickel, yet, it is less active in hydrogenolysis (Tables I and II [14]).

The situation is different when the irreversible adsorption of methane and ethane is compared with the hydrogenolysis activity of the corresponding metal. Typical data are shown in Table III. On the basis of this, the following order can be established with respect to the ratio of irreversible adsorption (chemisorption) of ethane within its total adsorption:

$$Rh > Ru > Ir > Co > Ni > Pd > Pt$$

This corresponds to the order of hydrogenolysis activity, again with the exception of cobalt. It should be pointed out also that the threshold temperature of chemisorption is below 195 K for the metals most active in hydro-

genolysis; cobalt and nickel with medium activities have threshold temperatures between 213 and 273 K, whereas the corresponding values for the least active Pd and Pt are between 273 and 373 K (Pt is exceptional: no methane chemisorption could be observed even at 573 K).

Table III

Data on Irreversible Adsorption of CH_4 and C_2H_6

Catalyst	t_t^0		q_{irr}/q_t		$t(\vec{°C})$
	CH_4	C_2H_6	CH_4	C_2H_6	
Co	−30	−60	0.75	0.69	290
Ni	− 6	−40	0.22	0.31	190
Ru	< −78	< −78	0.81	0.91	120
Rh	< −78	< −78	0.81	0.93	100
Pd	60	27	0.09	0.11	227
Ir	< −78	< −78	0.78	0.85	130
Pt	>300	90	–	0.90	360

t_t^0: threshold temperature (°C) for irreversible adsorption; $\frac{q_{irr}}{q_t}$: ratio of irreversibly adsorbed amount to total adsorption at 120°C; $t\ \vec{°C}$: starting temperature of the rapid increase of irreversible adsorption

The comparison of the threshold temperature of hydrogenolysis and the starting temperature of rapidly increasing chemisorption (Tables I and III) illustrate also the parallelism between chemisorptivity and hydrogenolysis activity. This parallelism shows that a tendency to strong interactions between metals and hydrocarbons is related to properties which are favourable for hydrogenolysis. This is supported also by the shift of the H–D exchange of hydrocarbons towards multiple exchange (requiring multiple, *i.e.* stronger interactions) over metals more active in hydrogenolysis.

3. Evaluation of exchange and hydrogenolysis data from mechanistic aspects

The above evidence together with that reported earlier can be summed up with respect to the hydrogenolysis mechanism as follows.

The significant differences between the rates and other kinetic parameters for exchange and hydrogenolysis (with the exception of cobalt) suggest that the rate-determining step is different in these reactions.

Several facts permit to conclude that the rate-determining step for hydrogen–deuterium exchange in methane and ethane is the dissociative

adsorption of the hydrocarbon with the rupture of one C–H bond, at least for the majority of metal catalysts. The isotope effect found for the exchange of perdeuterated hydrocarbon should be mentioned here [14]. Further evidence is provided by the lack of isotope effects in the hydrogen–deuterium and hydrogen–tritium exchange of ethane [21]. The rate-determining character of adsorption is supported also by the identical activation energies of methane and ethane adsorption and their H–D exchange over platinum. Another fact supporting this conclusion is that the adsorptivity of methane is lower on all metals than that of ethane [14–16], similarly to the higher barrier and lower rate of methane exchange as compared with that of ethane.

Since, on the other hand, hydrogenolysis has much lower rates and a higher activation energy than H–D exchange, it can be concluded that hydrocarbon adsorption is *not* rate-determining in hydrogenolysis. Neither is rate-determining the desorption of reaction products, at least when the partial pressure of hydrogen exceeds that of ethane. The desorption of hydrocarbon radicals is promoted by the increase of hydrogen partial pressure. Therefore, if desorption were rate-determining, positive hydrogen orders should be obtained. In fact, negative hydrogen exponents are found in the range of higher hydrogen pressures [12, 13, 15, 16]. This excludes desorption from the possible rate-determining steps. Cobalt is again an exception in this respect, showing a positive hydrogen order. Another evidence against rate-determining desorption is the marked difference between the rates of hydrogenolysis of different hydrocarbons even under such conditions when the reaction is strongly shifted towards methane formation.

Special experiments have demonstrated [12, 13] that the rate of ethane → methane conversion is independent of whether the process is carried out in the presence of hydrogen or deuterium. Thus, associative product desorption with hydrogen (or deuterium) uptake may not be rate-determining, which at the same time proves that hydrogen desorption does not participate in the rate-determining step, either. The same follows from the fact that the rate of hydrogen adsorption — as shown by the isotope effect studies cited — is much higher even than that of isotope exchange which, in turn, takes place more rapidly than hydrogenolysis. The much higher rate of H_2–D_2 exchange relative to that of isotope exchange in hydrocarbons is another argument against the rate-determining role of hydrogen desorption [20]. All these permit us to conclude that the rate-determining process in hydrogenolysis is the surface reaction. The much lower entropy of activation in the case of exchange as compared with hydrogenolysis also points to this assumption (Table IV).

The question is now what the rate-determining elementary step may be in the surface reaction. The formation of multiply deuterated methane from ethane in the presence of deuterium [13] evidences the existence of multiple carbon–metal bonds in hydrogenolysis. This is supported also by the

Table IV

Activation Entropies of the exchange and hydrogenolysis of C_2H_6

Catalyst	$-\Delta S$(J mol^{-1} K^{-1})	
	Exchange	Hydrogenolysis
Co	–	239
Ni	261	127
Ru	248	148
Rh	220	100
Pd	225	47
Ir	193	83
Pt	194	63

parallelism between the tendency of ethane to undergo multiple exchange and hydrogenolysis as discussed in Section 1 as well as by the correlation between the chemisorptivity of metals and their activity in hydrogenolysis (Section 2). It can be concluded, therefore, that the formation of a surface species with multiple metal–carbon bonds from an adsorbed hydrocarbon radical is important in the surface reaction. This process may take place either via the rupture of the carbon–carbon bond (Reaction III) or by dissociation of further hydrogen atom(s) from the surface radical:*

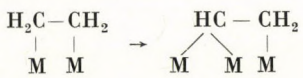

(VI)

and the carbon–carbon bond of the multiply bonded ethane breaks very rapidly:

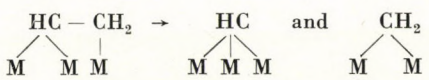

(VII)

If Reaction (VI) were rate-determining, the values of E_{d_t} and E_h ought to be very close to each other, or at least should show a close correlation. As far as apparent activation energies permit to draw reliable conclusions, it can be stated that the data shown in Table II disprove the rate-determining character of Reaction (VI), with the exception of cobalt. This follows also from the more detailed comparison of data obtained for exchange and hydrogenolysis.

Table I demonstrates that Pd and Pt, very active in exchange, are the least active catalysts in hydrogenolysis. The highest difference between the

* Multiply bonded surface complexes may have either structure (I) or (II).

activation energies of exchange and hydrogenolysis of ethane manifests itself in the case of these two metals. This renders it improbable that the catalytic activity in hydrogenolysis, similarly to exchange, would be determined by the reactivity of the metal in breaking C–H bonds. The difference E_{d_4}–E_{d_1} is only 26 kJ in the case of platinum, which is very close to the value measured for Ru and Rh, being much more active in hydrogenolysis. The E_{d_4}–E_{d_1} difference is identical in the case of nickel and iridium, latter being much more active in hydrogenolysis.

On this basis, the previous suggestion [23] that the hydrogenolysis activity is determined exclusively by the ability of the catalyst to produce structures with multiple metal–carbon bonds should be rejected. The parallelism between the *ratio* of rates of multiple and single exchange and the rate of hydrogenolysis has no decisive role in this respect, because this has been determined by relating two reaction rates at a given temperature disregarding the energies of activation.

Of course, the occurrence of Reaction (VI) cannot be excluded since this process is a precondition of the formation of multiply deuterated species, which is experimentally proven. It should rather be suggested that the surface species produced in Reaction (VI) reacts with adsorbed hydrogen and either desorbs in its original form or breaks down:

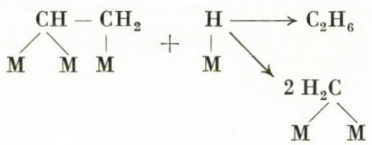

(VIII)

In can be concluded that the catalytic activity of various metals in hydrogenolysis depends on their activity in breaking both C–H and C–C bonds. The extent of activity is, however, influenced also by the tendency of formation of multiple carbon–metal bonds, as demonstrated by the parallelism between the ratio of $w_{d_3-d_6}/w_{d_1, d_2}$ and hydrogenolysis activity, and supported by the parallelism between hydrogenolysis and chemisorption tendency.

In summary, Reactions (III), (VI) and (VIII) can be combined as follows, to characterize the pathway of conversion of adsorbed ethane to give methane:

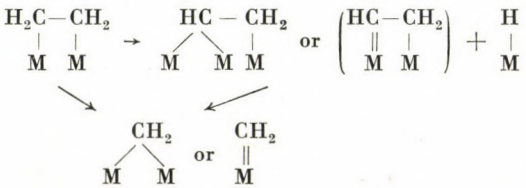

(IX)

The above considerations cannot be applied to cobalt, over which exchange is not faster than hydrogenolysis, E_h being equal to E_{d_4}.

It is possible that the reactions over cobalt are influenced by too strong product adsorption. This is also supported by the fact [14] that ethane chemisorbed at 473 K can be recovered from cobalt in the form of methane only. The situation is entirely different with platinum and nickel, where ethane chemisorbed under such conditions can be partly desorbed by treatment with hydrogen.

4. Energy barrier calculations

In order to check this concept for the mechanism of hydrogenolysis, BALANDIN's method [17] was used to calculate the energy requirement for the formation of surface complexes from the bond energy values, and the results were compared with the activation energies for exchange and hydrogenolysis.

The first step of methane exchange is process:

$$CH_4 + 2M \rightarrow CH_3M + HM$$

Following BALANDIN [17] and ELEY [26], the energy requirement of the above process can be given as

$$\Delta U_{ex} = Q_{CH_3-H} - Q_{CM} - Q_{HM} \tag{3}$$

The calculation of ΔU_{ex} has been carried out on the basis of Q_{CM} and Q_{HM} values determined earlier for similar catalysts [27]. Bond energy values used for the calculations as well as the resulting ΔU_{ex} values are given in Table V. From the latter, using BALANDIN's approximation:

$$E \approx 0.75\, \Delta U \tag{4}$$

the energy of activation can be estimated. Thus, on the basis of ΔU_{ex} values we calculated the approximate activation energy of single methane exchange ($E_{d_1}^{calc}$), assuming that adsorption is the rate-determining step of exchange. Comparison of the values thus obtained with those collected in Table II, shows that the agreement is within 10 – 20 % for the majority of the catalysts and nickel is the only metal where the difference is unacceptably high. (Here it has to be remarked that the calculated value is close to the activation energy of methane adsorption, which is 72 kJ mol^{-1} [14].) In any case, the calculations support the statement for most catalysts that the rate-determining step of the exchange is adsorption with the dissociation of one C–H bond.

Similar calculations can be carried out for ethane exchange, too, but a much higher uncertainty can be expected since no experimental data are available with respect to single exchange in ethane; the activation energies refer to the overall exchange rate, thus the comparison is not possible.

Calculations concerning ethane hydrogenolysis are of particular interest. On the above basis, the overall energy effect is written for the following reaction:

$$CH_3-CH_3 \rightarrow 2CH_2M_2 + 2HM$$

When the expression for the energy barrier is written, apart from the energy values of the bonds broken and formed, the additional fact should also be considered that the surface complex forms a multiple bond with the surface, as depicted by structure I or II. The difference between the formation of singly and multiply deuterated methane demonstrates that the latter involves a higher activation energy. The difference between the activation energies can be used to define the energy requirement of the creation of multiple surface bonds:

$$\Delta Q^{=} = \frac{3}{4}(E_{d_4} - E_{d_1}) \tag{5}$$

Data on this correction term are summarized in Table V. Its value is different for various catalysts. Since the method of preparation of the catalyst may significantly influence the ratio of singly and multiply exchanged products, it can be concluded that the E_{d_4}–E_{d_1} values depend strongly also on the preparation and pretreatment of the catalyst.

Considering the above facts, the following expression can be written for the energy barrier of the surface complex participating in hydrogenolysis according to Eq. (IX):

$$\Delta U_h = Q_{C_2H_5-H} + Q_{C_2H_4-H} + Q_{C-C} + 2\Delta Q^{=} - 2Q_{HM} - 4Q_{CM} \tag{6}$$

Table V

Energy effects (kJ mol^{-1}) *of the formation of surface complexes*

Catalyst	Q_{HMe}	Q_{CMe}	ΔU_{ex}	$E_{d_1}^{calc}$	$\Delta Q^{=}$	ΔU_h	E_h^{calc}
Co	217	100	120	90	28	162	122
Ni	253	79	105	79	23	164	123
Ru	242	92	103	77	41	170	128
Rh	242	78	111	83	41	226	170
Pd	233	87	117	88	92	310	233
Ir	256	87	94	71	23	126	95
Pt	234	82	121	91	35	214	161

Considering the bond energy values given in Section 1:

$$U_h = 940 + 2\Delta Q^{=} - 2Q_{HM} - 4Q_{CM} \qquad (7)$$

ΔU_h values calculated on the basis of Eq. (7) and E_h^{calc} values (calculated from equation (41)) are listed in Table V. On comparison of these values with those in Table II, an agreement within 20–35 % can be found between calculated and experimental data. Since the values of Q_{HM} and Q_{CM} have been determined for catalysts prepared by an analogous method but in a different batch, and since expression (4) is of an approximate character and its validity is different for various reactions or catalysts, the agreement can be regarded as sufficiently good for stating that it supports the correctness of the proposed mechanism.

The closeness of experimental and calculated values, of course, cannot be regarded as an exclusive proof for the given mechanism. This is indicated also by the example of cobalt, where the difference is about 35 %. Hydrogenolysis over cobalt involves probably a mechanism different from that discussed above, and yet the difference mentioned is about the same as in the case of ruthenium, where the rate-determining character of step (III) seems to be more probable.

Data in Table V and Eq. (6) indicate that $\Delta Q^{=}$ values contribute considerably to the energy barrier: the values of $2\Delta Q$ are about 20–50 % of the total ΔU_h values. This may explain why various authors have found hydrogenolysis to be very "structure-sensitive" [5, 28]. The method of preparation may change the activity of metal powders used here by several orders of magnitude [29]. We have pointed out the fact that the values of E_{d_4}–E_{d_1} are strongly affected by the relative amounts of various index planes, edges, corners in different samples. This, in turn, influences the ratio of linear and bridged species, which is ultimately reflected in the $\Delta Q^{=}$ correction terms and in the dependence of ΔU_h on the method of preparation.

REFERENCES

[1] SINFELT, J. H.: Catal. Rev., **3,** 175 (1969)
[2] SINFELT, J. H.: J. Catal., **27,** 468 (1972)
[3] SINFELT, J. H.: Adv. Catal., **23,** 91 (1973)
[4] CIMINO, A., BOUDART, M., TAYLOR, H. S.: J. Phys. Chem., **58,** 796 (1954)
[5] BOUDART, M.: A. I. Ch. E. Journal, **18,** 465 (1972)
[6] ANDERSON, J. R., BAKER, B. G.: Proc. Roy. Soc., **A271,** 402 (1963)
[7] SHEPHARD, F. E.: J. Catal., **14,** 148 (1969)
[8] FREEL, J., GALWEY, A. K.: J. Catal., **10,** 277 (1968)
[9] FRENNET, A., DEGAS, L., LIENARD, G., CROCG, A.: J. Catal., **35,** 18 (1974)
[10] TÉTÉNYI, P.: Acta Chim. Acad. Sci. Hung., **22,** 247 (1960)
[11] TÉTÉNYI, P., BABERNICS, L., PETHŐ, A.: Acta Chim. Acad. Sci. Hung., **28,** 375 (1961)
[12] GUCZI, L., GUDKOV, B., TÉTÉNYI, P.: J. Catal., **24,** 187 (1972)
[13] GUCZI, L., SÁRKÁNY, A., TÉTÉNYI, P.: J. Chem. Soc. Faraday Trans. I, **70,** 1971 (1974)

[14] BABERNICS, L., GUCZI, L., MATUSEK, K., SÁRKÁNY, A., TÉTÉNYI, P.: 6th Int. Congress on Catalysis, Paper A 36. London 1976
[15] SÁRKÁNY, A., GUCZI, L., TÉTÉNYI, P.: Acta Chim. Acad. Sci. Hung. **96,** 27 (1978)
[16] SÁRKÁNY, A., MATUSEK, K., TÉTÉNYI, P.: J. Chem. Soc. Faraday Trans. I, **73,** 1699 (1977)
[17] BALANDIN, A.: Adv. Catal., **19,** 1 (1969)
[18] KONDRATIEV: Atomic and Molecular Structure (in Russian). Fizmatgiz, Moscow 1959
[19] UGO, R.: Catal. Rev., **11,** 225 (1975)
[20] GUCZI, L., TÉTÉNYI, P.: Isotopenpraxis, **3,** 184 (1967)
[21] GUCZI, L., SÁRKÁNY, A., TÉTÉNYI, P.: Z. Phys. Chem. (Frankfurt), **74,** 26 (1971)
[22] KERR, J. A.: Chem. Rev., **66,** 465 (1966)
[23] KEMBALL, C.: Catal. Rev., **5,** 33 (1971)
[24] MORGAN, A., E. SOMORJAI G.: Surface Sci., **12,** 405 (1968)
[25] BLAKELY, D. W., SOMORJAI, G. A.: J. Catal., **42,** 181 (1976)
[26] MEYER, E. F., KEMBALL, C.: J. Catal., **4,** 711 (1965)
[27] TÉTÉNYI, P.: Acta Chim. Acad. Sci. Hung., **54,** 267 (1967)
[28] BOUDART, M.: Plenary lecture, 6th International Congress on Catalysis, London 1976
[29] TÉTÉNYI, P., GUCZI, L., PAÁL, Z., SÁRKÁNY, A.: Kém. Közl., **47,** 391 (1977)

Pál TÉTÉNYI
László GUCZI
Antal SÁRKÁNY

H-1525 Budapest 114, P. O. B. 77.

Acta Chimica Academiae Scientiarum Hungaricae, Tomus 97 (2), pp. 235—245 (1978)

TETRA-, TRI-, AND DI-CO-ORDINATED COMPLEXES OF SOME PYRIDINE DERIVATIVES WITH COPPER(I) PERCHLORATE

M. A. S. GOHER

(Department of Chemistry, Faculty of Science, Alexandria University, Alexandria, A. R. Egypt)

Received May 3, 1977

A series of stable tetra-, tri-, and di-co-ordinated complexes of some pyridine derivatives with copper(I) perchlorate have been prepared and characterized. The perchlorate groups are ionic in all the tetrakis, tris and some bis complexes. As indicated from the IR results, the formally di-co-ordinated complexes attain a higher co-ordination number than two through different ways depending upon the nature of the substituent group. It may be due to the formation of π-complexes, metal clusters or electron deficient bonds when the substituent is an electron releasing group. For meta-, and para-carbomethoxy or carboethoxy derivatives (i.e. electron attracting groups), the higher co-ordination number is attained through the co-ordinated perchlorates. In case of ortho-carbonyl substituted pyridines, the copper(I) ion attains the tetrahedral geometry through the coordination via the nitrogen atom and carbonyl group in the bis complexes. In the complexes studied, the apparent co-ordination number of copper(I) depends upon the steric requirements and the base strength of the ligand.

Introduction

Until recently the coordination number in copper(I) complexes was generally assumed to be two (linear) or more often four (tetrahedral) in the presence of soft donor atoms [1]. Although the number of structural determinations of copper(I) complexes is still small, a definite example of linear co-ordination is known for $[CuCl_2]^-$ anion [2], while examples of tetrahedral co-ordination are known for the monomer L_2CuX (L = PPh_3, X = a bidenta anion such as NO_3^- or BH_4^- [3]), for the dimer $[(PPh_3)_2CuN_3]_2$ [4], and for the monomer tetrakis(pyridine)copper(I) perchlorate [5, 6]. Recently tri-co-ordinated copper(I) were found in the anion $[Cu(CN)_2]^-$ [7], $[Cu(etu)_3]_2SO_4$ (etu = = ethylene thiourea) [8], and tris(2-picoline)copper(I) perchlorate [9] by means of X-ray single crystal analysis.

To provide more information on the structural types and the co-ordination numbers preferred by copper(I) with the heterocyclic nitrogen bases, the following investigation was undertaken. A prelimenary report has appeared [10]. However, during the course of this work, some of the complexes mentioned here have been reported by LEWIN *et al.* [6]. The ligands taken in this later study, were pyridine and alkyl pyridines. In our study two types of substituted pyridines have been used, namely; electron attracting substituents

e.g. ortho-, *meta-* and *para*-carbonyl derivatives, and electron releasing substituents *e.g.* mono, di- and tri-alkyl pyridines. These ligands have been chosen in order to study not only the effect of the position of the substituent in pyridine ring on the overall coordination number of copper(I), but also the effect of the nature of the substituent.

Experimental

All ligands were GLC purified, and the other chemicals were analytical gradel and commercially available.

Magnetic measurements were made by the Faraday method at room temperature. Conductivity measurements were carried out at 25 °C on 10^{-3} F solutions in chloroform and acetone under dry nitrogen with a Radiometer conductivity bridge model CDM 2e. Electronic spectra were recorded on a Unicam spectrophotometer SP 800. Reflectance spectra of the solids were measured over 220 – 1000 nm range on a VSU-1 (Zeiss, Jena) instrument with MgO as a standard and diluent. IR spectra in the regions 4000 – 400 cm^{-1} and 500 – 200 cm^{-1} were measured on a UR-20 (Zeiss, Jena) and a Perkin – Elmer 325 spectrophotometer, respectively.

Analysis

Microanalysis of C, H and N were carried out on the Perkin – Elmer 240 elemental analyzer. Copper was determined gravimetrically as CuSCN after degradation and oxidation of the complexes with boiling mixtures of concentrated H_2SO_4 and 30 % H_2O_2.

Preparation of the complexes

The complexes were generally prepared and recrystallized according to the procedure described previously [11] by mixing $CuSO_4$ solution with the ligand in question then ascorbic acid and sodium perchlorate solution are added. When more than one complex were obtained by the same ligand, an excess of the ligand and a little lower amounts were added for complexes with the highest and lowest ligand contents, respectively. Care must be taken for the intermediate complexes.

Results and discussion

The isolated complexes, their elemental analysis, and some of their physical properties together with the pK_a's of some ligands [12, 13] are given in Table I.

The use of ascorbic acid as a reducing agent for the synthesis of copper(I) complexes has enabled us to isolate a variety of the complexes in which copper(I) could be tetra-, tri- and di-co-ordinated as seen from Table I.

The stability of the isolated complexes against air oxidation depends on both the nature of the substituent group and the number of ligands per copper atom in the complex molecule. Thus those derived from ligands with electron attracting substituents in pyridine are generally more stable than those derived from ligands with electron releasing groups. On the other hand, for a series of 1 : 4, 1 : 3 and 1 : 2 complexes of the same ligand, the stability decreases in the same order.

Table I

Analytical data and some physical properties of the complexes

Complex	Color	M→L[a]	pK_a	Analysis% Found / Calcd.			
				Cu	C	H	N
$(EtIN)_4^*CuClO_4$	red	375		8.25	49.99	4.94	7.25
(767.4)[b]	orange			8.28	50.07	4.73	7.30
$(MeIN)_4CuClO_4$	red	475	3.29	8.82	46.98	3.89	7.55
(711.4)	orange			8.93	47.27	3.97	7.87
$(Py)_4CuClO_4$	canarian	420	5.30	13.08	49.92	4.14	11.62
(479.4)	yellow			13.30	50.10	4.20	11.73
$(4\text{-pic})_4CuClO_4$	light		6.10	11.54	52.10	5.10	10.17
(535.4)	brown			11.86	53.82	5.27	10.46
$(EtIN)_3CuClO_4$	yellow	420		10.22	47.23	4.62	6.88
(616.3)	crystals			10.30	46.76	4.41	6.81
$(MeIN)_3CuClO_4$	yellow	420		11.45	42.90	3.58	7.11
(574.2)	crystals			11.85	43.90	3.68	7.31
$(MeN)_3CuClO_4$	canarian	420		11.62	43.23	3.72	7.23
(574.2)	yellow			11.85	43.90	3.68	7.31
$(3\text{-Ac-py})_3CuClO_4$	canarian	420		11.76	47.36	3.95	7.80
(526)	yellow			12.07	47.92	4.00	8.00
$(EtP)_2CuClO_4$	red brown	490		13.45	41.13	4.10	6.12
(465.2)	crystal			13.65	41.30	3.90	6.02
$(MeP)_2CuClO_4$	red brown	490		14.63	38.72	3.12	6.52
(437.2)	crystals			14.53	38.54	3.23	6.40
$(2\text{-Ac-py})_2CuClO_4$	deep red	500		15.27	41.86	3.34	7.10
(405)	brown			15.67	41.51	3.45	6.90
$(2,5\text{-lut})_3CuClO_4$	very light		7.55	13.01	51.66	5.47	8.56
(484.4)	brown			13.13	52.06	5.62	8.67
$(EtIN)_2CuClO_4$	white			13.36	40.83	4.04	5.92
(465.2)				13.65	41.30	3.90	6.02
$(MeIN)_2CuClO_4$	white			14.25	38.33	3.22	6.20
(437.2)				14.53	38.54	3.23	6.40
$(EtN)_2CuClO_4$	white			13.47	41.91	3.82	5.87
(465.2)				13.65	41.30	3.90	6.02
$(4\text{-pic})_2CuClO_4$	white			17.92	43.05	4.19	8.20
(349.2)				18.19	41.26	4.04	8.02
$(2,4\text{-lut})_2CuClO_4$	white		6.80	16.58	44.56	4.87	7.56
(377.3)				16.84	44.56	4.80	7.42
$(2,5\text{-lut})_2CuClO_4$	white			16.53	44.76	4.89	7.34
(377.3)				16.84	44.56	4.80	7.42
$(2,6\text{-lut})_2CuClO_4$	white		6.72	16.53	44.16	4.88	7.39
(377.3)				16.84	44.56	4.80	7.42
$(s\text{-coll})_2CuClO_4$	white		7.63	15.87	46.97	5.58	6.80
(405.3)				15.68	47.42	5.47	6.91

* EtIN = ethyl isonicotinate, MeIN = methyl isonicotinate, Py = pyridine, 4-pic = = picoline, lut = lutidine, coll = collidine, EtN = ethyl nicotinate, MeN = methyl nicotinate, EtP = ethyl picolinate, MeP = methyl picolinate, Ac-py = acetyl pyridine; [a] λ is given in nm, from the reflectance spectra of the solids, [b] the values given are the formula weights

(i) *Magnetic properties and conductivity*

Since some copper(I) complexes have been reported [5, 6], as paramagnetic compounds with relatively high magnetic moments, the molar magnetic susceptibilities of the isolated complexes at room temperature are listed in

Table II, together with their conductivities. For all complexes the corrected magnetic susceptibilities are calculated based on the summation of the individual magnetic susceptibilities of the elements [14]. As seen from the Table, all the isolated complexes had corrected molar susceptibilities in the range $\pm 40 \times 10^6$ c.g.s. This corresponds to a magnetic moment of ± 0.3 BM. Within the experimental error, such a low susceptibility is indicative of diamagnetism as expected from the d^{10} configuration. The results given here for complexes of pyridine, 4-picoline and 2,4-lutidine are comparable with the reported data [2]. For the 1 : 2 complexes of 2,6-lutidine and sym-collidine the molar susceptibilities for our samples are much higher than those reported (see Table I). The small magnetic moments observed for some complexes could be due to the formation of some copper(II) species from air oxidation.

All the complexes behave as 1 : 1 electrolytes in acetone [15] and nitrobenzene [16]. Accordingly, in solutions, these tetrakis, tris and bis complexes

Table II

Magnetic properties and conductivities[a] of the complexes

Cation	$\chi_M^b \cdot 10^6$	$\chi_M^{corr.\,d} \cdot 10^6$	Conductivity Ω^{-1} cm^2 mole^{-1}	
			A	NB
$(EtIN)_4Cu^+$	−289	+39	137.5	28.0
$(EtIN)_3Cu^+$	−215	+37	142.0	31.0
$(EtIN)_2Cu^+$	−145	+23	132.0	29.5
$(MeIN)_4Cu^+$	−276	+16	141.0	28.0
$(MeIN)_3Cu^+$	−189	+30	137.0	29.0
$(MeIN)_2Cu^+$	−168	0.0	118.0	27.5
$(EtN)_2Cu^+$	−140	+28	126.0	28.0
$(MeN)_3Cu^+$	−240	−21	131.0	29.0
$(3\text{-Ac-py})_3Cu^+$	−234	−39	136.0	29.0
$(EtP)_2Cu^+$	−189	−21	129.0	31.0
$(MeP)_2Cu^+$	−186	−29	138.0	32.0
$(2\text{-Ac-py})_2Cu^+$	−178	−34	140.0	30.0
$(Py)_4Cu^+$	−205 (−216)[c]	+36 (+25)	130.0	29.0
$(4\text{-pic})_4Cu^+$	−245 (−269)	+38 (+14)	136.0	28.0
$(2,5\text{-lut})_3Cu^+$	−219 (−258)	+38 (+1)	134.0	27.5
$(4\text{-pic})_2Cu^+$	−169	−27	128.0	28.5
$(2,4\text{-lut})_2Cu^+$	−153 (−179)	+25 (−9)	135.0	26.5
$(2,5\text{-lut})_2Cu^+$	−148	+30	142.0	29.0
$(2,6\text{-lut})_2Cu^+$	−187 (−119)	+1 (+69)	138.0	30.0
$(s\text{-coll})_2Cu^+$	−249 (−159)	−38 (+52)	141.0	32.0

[a] The conductivities given are based on the formula weights, [b] In c.g.s. units/mole. [c] values between parenthesis are given from ref. [6], [d] corrected magnetic molar susceptibilities in c.g.s. units. A = acetone, NB = nitrobenzene

may be formulated as $(L_4Cu)^+ClO_4$, $(L_3Cu)^+ClO_4$ and $(L_2Cu)^+ClO_4$, respectively. Copper(I) ion, therefore, attains tetrahedral and trigonal geometries in the first two formulas, respectively. For the bis complexes, copper(I) ion is tetrahedrally co-ordinated when the ligand is α-carbonyl substituted pyridine (see later) and attains linear geometry for the other ligands.

(ii) *M → L charge transfer spectra*

In acetone and chloroform the spectra of the colored complexes are quite similar to those of the parent ligands in the UV and visible regions giving rise to an absorption band around 270 – 280 nm due to the $\pi - \pi^*$ transitions of the ligands.

In the reflectance spectra of the solid samples, copper(I) complexes derived from methyl and ethyl nicotinate, isonicotinate and picolinate and the corresponding acetyl derivatives (see Table I and Figure 1) *i.e.* ligands with electron attracting substituents, show an intense absorption in the visible region. These intense absorption is due to M → L charge transfer transitions from d^{10}-orbitals on copper(I) to an empty π^*-orbitals on the ligands [17]. The λ_{max} of the M → L absorption shifts to longer wave length as the number of ligands per copper atom is increased in the complex molecule for the series of the same ligand. This behaviour is reasonable, since increasing the number of ligands per copper ion leads to increasing the power of the reducing part in the complex molecule which in turn shifts the λ_{max} to longer wave length [18].

WILLIAMS [18] and KRUMHOLZ [19] pointed out that the conjugation and chelation of di-imine to Fe(II) and Cu(I) are the factors causing the M→L

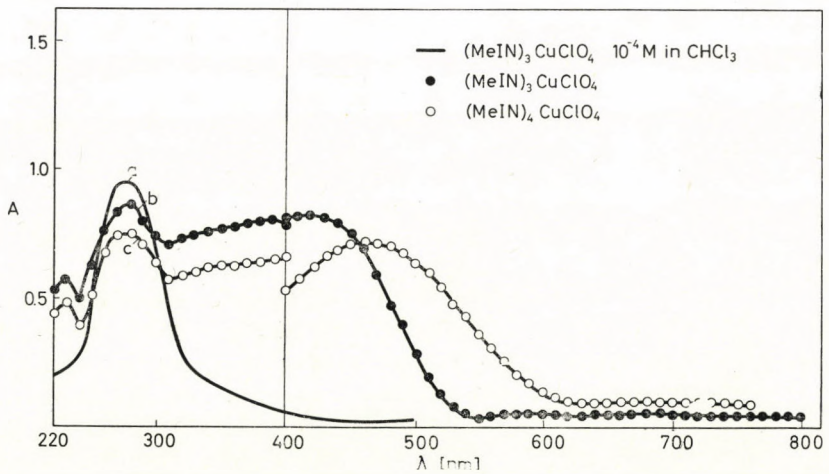

Fig. 1. a – Electronic spectrum of $(MeIN)_3CuClO_4$ (10^{-4} M) in chloroform solution, *b* – reflectance spectrum of solid $(MeIN)_3CuClO_4$; *c* – reflectance spectrum of solid $(MeIN)_4CuClO_4$

charge transfer transition. That the the α-carbonyl substituted pyridine form chelate compounds with copper(I) ion, may explain why the 1 : 2 complexes of these ligands show M → L bands at higher wave lengths than the 1 : 4 copper(I) complexes of the other carbonyl pyridine ligands *e.g.* MeN and MeIN. These latter ligands do not form chelates with the copper(I) ion.

(iii) *Infrared absorption spectra*

The IR spectra of all the isolated complexes showed that the fundamental vibration modes of the ligands are shifted to higher frequencies upon complexation as expected for nitrogen bonded ligands [20, 21]. Only for the α-carbonyl substituted pyridine ligands, the IR spectra indicate a co-ordination via the carbonyl group in addition to the heterocyclic nitrogen [22]. Since detailed analyses of the ligand spectra have been examined for related compounds [23 – 25], these spectral properties are not concerned here. Table III, therefore, contains only the vibration frequencies related to the perchlorate groups in the isolated complexes. Figure 2 shows the IR spectra of 1 : 2 and 1 : 4 copper(I) perchlorate complexes of MeIN, in the region 1200 – 600 cm^{1}. In Table IV the far IR spectral data for some complexes are collected.

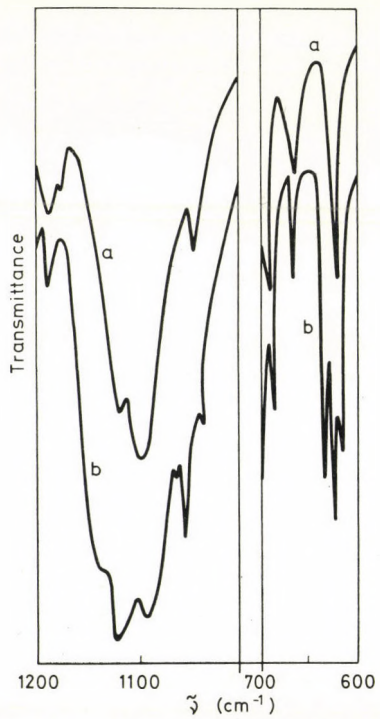

Fig. 2. IR spectra, *a* – of $(MeIN)_4CuClO_4$; *b* – of $(MeIN)_2CuClO_4$

Table III

Vibrational frequencies (cm^{-1}) of the perchlorate groups in complexes

Complex	ClO_4		
	ν_1	ν_3	ν_4
$(EtIN)_4CuClO_4$	932 w	1120 – 1090 vs	627 s
$(MeIN)_4CuClO_4$	935 sh	1110 – 1090 vs	627 s
$(Py)_4CuClO_4$	925 vw	1115 – 1090 vs	627 s
$(4\text{-pic})_4CuClO_4$	932 w	1110 – 1095 vs	627 s
$(EtIN)_3CuClO_4$	–	1115 vs	627 m
$(MeIN)_3CuClO_4$	930 w	1110 – 1085 vs	627 s
$(MeN)_3CuClO_4$	935 w	1115 – 1090 vs	627 s
$(3\text{-Ac-py})_3CuClO_4$	930 w	1110 – 1090 vs	625 s
$(2,5\text{-lut})_3CuClO_4$	932 w	1110 – 1090 vs	625 s
$(EtP)_2CuClO_4$	930 w	1115 vs	627 s
$(MeP)_2CuClO_4$	930 w	1110 – 1095 vs	627 s
$(EtIN)_2CuClO_4$	935 wm	1115 vs	635 s
		1080 vs	628 s
		1058 m	620 m
$(MeIN)_2CuClO_4$	930 wm	1120 vs	635 s
		1090 vs	625 s
		1050 m	618 m
$(EtN)_2CuClO_4$	930 m	1105 s	638 s
		1080 s	625 m
		1050 s	625 m
$(2\text{-Ac-py})_2CuClO_4$	930 w	1110 – 1095 vs	625 vs
$(4\text{-pic})_2CuClO_4$	932 w	1110 – 1095 vs	627 vs
$(2,4\text{-lut})_2CuClO_4$	932 w	1110 – 1080 vs	627 vs
$(2,5\text{-lut})_2CuClO_4$	932 w	1110 s	627 s
$(2,6\text{-lut})_2CuClO_4$	–	1115 – 1080 vs	627 vs
$(sym\text{-coll})_2CuClO_4$	–	1110 – 1090 vs	627 vs

w: weak, m: medium, s: strong, v: very,

The perchlorate group can act as an ion, monodentate and bidentate ligands, with successive lowering in symmetry. According to which the number of IR active vibrations are increased from two to six to nine modes, respectively [26, 27]. As seen from Table III, except the 1 : 2 complexes of EtN, EtIN and MeIN, the perchlorate groups act as an ion in all other complexes showing the antisymmetrical stretching ν_3 mode around 1100 cmV¹, antisymmetrical bending ν_4 mode at 627 cm^{-1} and the IR inactive ν_1 vibration

mode at 930 cm^{-1}. In the solid state, therefore, these complexes have the same formulations given above for them in solution. One of the 1 : 4 complexes; the tetrakis(pyridine)copper(I) perchlorate, has been studied by X-ray analysis, which showed the complex to consist of the tetrahedral cation $(Py)_4Cu^+$ [5]. The trigonal structure of the tris(2-picoline) copper(I) complex has been confirmed by X-ray analysis [9].

For the formally di-co-ordinated complexes of MeIN, EtIN and EtN, the vibration modes ν_3 and ν_4 split into three components for each as seen from Fig. 2. Such splitting is consistent only with bidentate perchlorate groups. Copper(I) ion in these complexes is, therefore, proposed to be four co-ordinated and adopting approximately tetrahedral geometry. This formulation differs from that proposed for these complexes in solution, and from the 1 : 2 complexes of the other ligands.

Far IR spectroscopy has been used to study substituted pyridine complexes of copper(II) halides. The absorption frequencies for the copper–nitrogen and copper–halogen bond stretching modes have been reported [28]. For copper–nitrogen, the stretching frequency was observed in the range 230 – 270 cm^{-1}, for copper—chloride it was 230 – 330 cm^{-1} and for copper–bromide the range was 190 – 260 cm^{-1}.

As seen from Table IV and in accordance with LEWIN *et al.* [6], the complexes $(Py)_4CuClO_4$ and $(4\text{-pic})_4CuClO_4$ prepared by us are transparent in the region of 200 – 375 cm^{-1}. In order to be certain that the transparency is not due to the cation $[(Py_4Cu)]^+$, we prepared a complex of the formula (Py)CuI and measured its far IR spectrum. This compound too is transparent in the region of 200 – 375 cm^{-1}. The tetrakis complexes of MeIN and EtIN showed only one band associated with the stretching copper–nitrogen vibrations. The assignment of this band as the copper–nitrogen stretching was given is accordance with the calculated and observed values which have been reported [29] for the isoelectronic zinc(II) complex of methyl isonicotinate MeIN.

For the di-co-ordinated complexes of methyl and ethyl-isonicotinate and ethyl nicotinat, two very strong bands are observed in their far IR spectra as seen from Fig. 3. These bands are twice as strong as the band associated with copper–nitrogen stretching vibrations in the spectra of these complexes. Since these two bands are not observed in the spectra of all the halo, cyano and thiocyanato complexes of variable stoichiometry derived from the same ligands [30], one could not assign them as the nitrogen–copper stretching vibrations. These two bands are, therefore, assigned as the copper–oxygen stretching frequencies. Since for the formula;

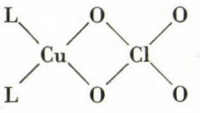

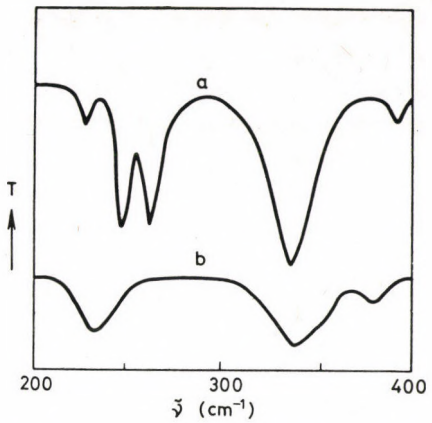

Fig. 3. Far IR spectra. *a* – of $(MeIN)_2CuClO_4$; *b* – of $(MeIN)_4CuClO_4$

two IR active copper–oxygen frequencies are expected, the appearance of these two bands in addition to at least one band associated with copper–nitrogen stretching vibrations suggested that copper(I) ion has an approximate tetrahedral geometry in these complexes. This result confirms our previous conclusion which attained from the splitting of ν_3 and ν_4 modes of the perchlorate groups. It is clear from Table IV that the position of the copper–oxygen

Table IV

Far IR *spectral data of some complexes*

Complex	ν Cu–N	ν Cu–O
$(EtIN)_4CuClO_4$	206 m	
$(MeIN)_4CuClO_4$	203 m	
$(Py)_4CuClO_4$	transparent	
$(4\text{-pic})_4CuClO_4$	transparent	
$(2,5\text{-lut})_3CuClO_4$	312 m (306)	
$(MeN)_3CuClO_4$	225 s	
$(MeIN)_2CuClO_4$	230 m	264 vs, 251 vs
$(EtIN)_2CuClO_4$	210 m	262 vs, 246 s
$(EtN)_2CuClO_4$	280 s, 240 m	348 s, 335 vs
$(2,4\text{-lut})_2CuClO_4$	315 w (315), 266 s (266)	
$(2,5\text{-lut})_2CuClO_4$	343 s, 312 s	
$(2,6\text{-lut})_2CuClO_4$	343 m (345), 259 (259)	
$(s\text{-coll})_2CuClO_4$	327 s (325), 300 s (298)	

The values between parenthesis are given from Ref. 6; m = medium, w = weak, s = = strong, v = very

frequencies is dependent upon the substituent group and more upon its position in the pyridine ring.

Our results for some of the formally di-co-ordinated complexes are in excellent agreement with those reported by LEWIN *et al.* [6]. The appearance of two bands in the copper–nitrogen region leads to the conclusion that these complexes definitely do not have local symmetry containing N–Cu–N arrangement. Such deviation from N–Cu–N arrangement may be due to a tendency to increase the co-ordination number of copper(I) ion.

(iv) *The effect of the steric requirements and base strength of the pyridine ligands on the stereochemistry of the copper(I) complexes*

The co-ordination number of the synthesized copper(I) complexes of the pyridine derivatives can be related to the steric requirements and base strength of the ligands. Thus complexation of copper(I) with pyridine or 4-substituted pyridine leads to the formation of complexes with the maximum co-ordination number of four. The *para*-substituent group on pyridine ring do not exert any effect on the co-ordination number of copper(I) though the pK_a changes from 3.26 for MeIN to 5.30 for pyridine to 6.10 for 4-picoline.

The meta-substituted pyridines, on the other hand, gave complexes with co-ordination number three for MeN and formally co-ordination number two for EtN. Since 3-picoline forms a complex with co-ordination number of four [31], so the variation in co-ordination number of copper(I) with such ligands is due to the steric requirements.

2,6-Lutidine and sym-collidine yield di-co-ordinated copper(I) complexes which is undoubtedly due to the steric hindrance of the two *ortho*-methyl groups. The copper(I) perchlorate complex of 2,5-lutidine is tri-co-ordinated, as expected from both the steric effect and pK_a. However, 2,4-lutidine which has essentially the same steric effect as 2,5-lutidine gave a di-co-ordinated copper(I) perchlorate complex, may be due to its slightly greater basicity ($\Delta pK_a = 0.25$).

REFERENCES

[1] REICHLE, W. T.: Inorg. Chim. Acta **5,** 325 (1971), and references therein.
[2] NEWTON, M. G., CAUGHMAN, H. D., TAYLOR, R. G.: Chem. Commun. **1227** (1970)
[3] LIPPARD, S. J., PALENIK, G. J.: Inorg. Chem. **10,** 1322 (1971), and ref. therein
[4] ZIOLO, R. F., GAUGHAN, A. P., DORI, C. G. P., EISENBERG, R.: Inorg. Chem. **10,** 1289 (1971)
[5] LEWIN, A. H., MICHL, R. J., GANIS, P., LEPORE, U., ANITAVILE, G.: Chem. Commun. **1400** (1971)
[6] LEWIN, A. H., COHEN, I. A., MICHL, R. J.: J. Inorg. Nucl. Chem. **36,** 1951 (1974)
[7] CROMER, D. T.: J. Phys. Chem. **61,** 1388 (1957)
[8] WEININGER, M. S., HUNT, G. W., AMMA, E. L.: Chem. Commun. **1140** (1972)
[9] LEWIN, A. H., MICHL, R. J., GANIS, P., LEPORE, U.: Chem. Commun. **661** (1972)
[10] GOHER, M. A. S., DRÁTOVSKY, M.: Naturwissenschaften **63,** 89 (1976)

[11] GOHER, M. A. S., DRÁTOVSKY, M.: Coll. Czech. Chem. Commun. 26, **40** (1975)
[12] Handbook of Chemistry and Physics, 50th ed. The Chemical Rubber Publishing Company, Cleveland 1969
[13] WONG, P. T. T., BREWER, D. G.: Can. J. Chem. **47,** 4589 (1969)
[14] DORFMAN, Y. G.: "Diamagnetism and the Chemical Bond." Edward Arnold. London, 1965
[15] AINSCOUGH, E. W., PLOWMAN, R. A.: Aust. J. Chem. **23,** 1269 (1970)
[16] FERGUSSON, J. E., HICKFORD, J.: Aust. J. Chem. **23,** 453 (1970)
[17] LEVER, A. B. P.: "Inorganic Electronic Spectroscopy", Chapter 8, page 229, Elsevier, Amsterdam 1968
[18] WILLIAMS, R. J. P.: J. Chem. Soc. **137** (1955)
[19] KRUMHOLZ, P.: J. Amer. Chem. Soc. **75,** 2163 (1953)
[20] CLARK, R. J. H., WILLIAMS, C. S.: Inorg. Chem. **4,** 350 (1965)
[21] FRANK, C. W., ROGERS, L. B.: Inorg. Chem. **5,** 615 (1966)
[22] GOHER, M. A. S., ATTIA, A.: To be published.
[23] GILL, N. S., NUTTALL, R. H., SCAIFE, D. E., SHARP, R. W. A.: J. Inorg. Nucl. Chem. **18,** 79 (1961)
[24] GILL, N. S., KINGDON, H. J.: Aust. J. Chem. **19,** 2197 (1966)
[25] GOLDSTEIN, M., MOONY, E. F., ANDERSON, A., GEBBIE, H. A.: Spectrochim. Acta **21,** 105 (1965)
[26] HATHAWAY, B. J., HOLAH, D. G., HUDSON, M.: J. Chem. Soc. **4586** (1963)
[27] NAKAMOTO, K.: "Infrared Spectra of Inorganic and Coordination Compounds." p. 170, 2nd. Edn. Wiley, London, 1970
[28] HATFIELD, W. E., WHYMAN, R.: In "Transition Metal Chemistry" (Edited by R. L. Carlin) Marcell Dekker, New York, 1969
[29] WONG, P. T. T., BREWER, D. G.: Can. J. Chem. **46,** 131 (1968)
[30] GOHER, M. A. S.: To be published
[31] DEAHNA, H. D., HARDT, H. D.: Z. Anorg. Allg. Chem. **387,** 61 (1972)

M. A. S. GOHER Department of Chemistry, Faculty of Science, Alexandria University, Alexandria, A. R. Egypt.

Acta Chimica Academiae Scientiarum Hungaricae, Tomus 97 (2), pp. 247–253 (1978)

CALCULATIONS ON THE ABSORPTION SPECTRA OF MEROCYANINES BY FEMO METHOD

Nivedita MISHRA, Lalit N. PATNAIK and M. K. ROUT*

(Department of Chemistry, Ravenshaw College, Cuttack, Orissa)

Received February 15, 1977

In revised form October 17, 1977

The absorption spectra of 24 merocyanines have been investigated by the use of Free Electron Molecular Orbital Model employing two procedures: (i) by the method developed by KUHN [J. Chem. Phys., **17**, 1198 (1949)] with appropriate modifications with respect to the box length and the number of pi-electrons and (ii) by the use of first order perturbation theory developed by us. Both methods give results that are in excellent agreement with experiment. The latter method is shown to have an additional advantage over the former in not making explicit use of any empirical parameters.

Recently we have become increasingly interested in the applicability of the simple one dimensional free electron gas model to the spectral investigation of organic dyestuffs. This model describes the pi-electron wave function of conjugated system in terms of standing sine and cosine functions. In our earlier communications [1–4], we have reported that this crude yet simple and elegant quantum mechanical scheme gives good results with respect to the prediction of the intense long wave length transitions in organic dyestuffs with a judicious choice of certain parameters involved in the FE equations.

In the present paper, we report a few more calculations on the absorption spectra of some merocyanine dyes, and suggest some improvements about the choice of the box length for this particular class of dyes. We also report here the investigation of the absorption spectra of merocyanines by the use of first order perturbation theory employing the free electron wave functions. The results are interesting for the quantitative prediction of spectra, as they do not involve any adjustable parameters.

Results and discussion

(1) *Method involving length and Vo*

(i) Although it has been customary to use the value of 1.39 A as the average bond length in the free electron calculations, we prefer to take the C–C=C length as 2.82 A (1.34 + 1.48), as in case of butadiene, since we consider that in the ground state, the merocyanines resemble the polyenes in their electronic structure. Average bond length of 1.39 A (benzene) would be more appropriate in case of symmetrical dyes, where the two extreme structures

are degenerate. By taking the merocyanines to be systems of unequal bond lengths, an elastic σ-bond framework is implicit in our calculation. The pi-electrons always tend to deform the originally equal σ-bonds in order to produce alternatingly longer and shorter ones. This trend is counteracted, however, by the need of strain energy and the increase in the interaction energy between pi-electrons. But since the change in the ground state energy on account of these parameters are almost same as that in case of the excited state [5], these terms cancel each other and presumably will have no material effect on the transition energy.

KUHN *et al.* [6] have found out the wave functions and energy levels of the polyenes on the basis of simple sine curve potential model and found that they compare quite well with those given by more refined methods, *viz.*, in which the pi-electrons are treated as electrons in a (a) one-dimensional wave-shape potential and (b) two dimensional potential trough models with nuclear charge and shielding effects. The results of all three treatments are in good agreement, and by considering the electron density distribution along the chain, each treatment leads to the same conclusion, that each single bond and each double bond in a long chain polyene must have, respectively, the same length as the single bond and the double bond in butadiene. The values of the absorption maxima given by the three models are in good agreement with the experimental values.

It is well known that the equilibrium positions of the nuclei in optically excited molecules differ from those in the ground state. Thus, for a more accurate description of the spectra, it is desirable that the change in the total length is to be incorporated in the calculations. LABHART [7] has reported the theoretical values of the changes in the bond length ($\Delta L = L^e - L^g$) on optical excitation and has shown that for singlet transitions, there is a convergence in the ΔL values. The values reported are much too small (~ 0.08 A) for $n > 10$ (as in case of di-, tetra- and hexa-methine merocyanines considered here) to have any appreciable influence on the calculations. We have, therefore, not considered such changes in the molecular dimensions in our calculations.

(ii) As in previous calculations, the free electron path is assumed to terminate one bond length beyond the end atoms [8] the extension being in keeping with the conjugated system, *i.e.*, contributing an additional 2.82 A to the geometrical length. The total length L can thus be written in a convenient mnemonic form as:

$$L = 2.82 \cdot n,$$

where $2n$ = no. of pi-electrons.

(iii) In case of dyes derived from quinoline-2, the chromophoric chain is taken to be the intermediate of the following two [3]:

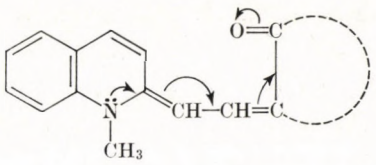

1

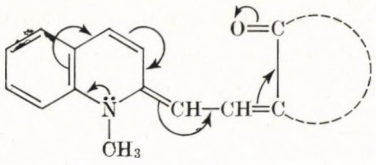

2

The absorption spectra of merocyanines may be considered similar to those of polyenes, in the sense that the lowest energy electronic transition of these dyes occur at a shorter wave length than the corresponding isoenergetic wave length derived from the parent cyanines and oxonols. In case of polyenes this has been explained in the electron gas model by introducing a periodic potential which partly localises the pi-electrons into the potential throughs at the double bonds. A satisfactory agreement between observed and calculated electronic transition energies of polyenes has been obtained [9, 10].

It is apparent from the results in Table I that there is an excellent agreement between the calculated and experimental values of the electronic transition energies of merocyanine dyes, in fact much better than one would expect from such a simple model.

The results reported in Table I have been derived from the approximate solution of the one-dimensional Schrödinger equation for a system of varying potential by an appropriate adjustment of the parameters L and V_0. Some of the recent papers have reported improved wave functions using an iterative procedure [10—13] for the calculations of the spectral properties of polyenes and cyanine type aggregates and some asymmetrical systems like corrinoids and pseudo isocyanine aggregates. The gain in the accuracy in the calculated absorption frequencies is far superseded by the mathematical complexity.

(2) *Method of perturbation*

The periodic potential (V_p) introduced by KUHN [14], which has the following form, may be taken as the perturbing component on a chosen zero order system and the changes in the energy levels due to this perturbation may be calculated by using first order perturbation theory.

$$V_p = V_0 \cos \frac{2\,n\pi x}{L} \tag{1}$$

We consider the energy levels derived from the isoenergetic wave length of the merocyanine as those corresponding to the unperturbed system. Since there are $2n$ number of pi-electrons, the ground state energy level is described by the n^{th} quantum state and the change in ε_n due to perturbation is given by,

$$\Delta\varepsilon_n = \int_0^L \varphi_n \hat{V}_p \varphi_n \, \mathrm{d}x = \frac{2V_0}{L} \int_0^L \sin \frac{2\,n\pi x}{L} \cos \frac{2\,n\pi x}{L} \, \mathrm{d}x = -\frac{V_0}{2} \tag{2}$$

Table I

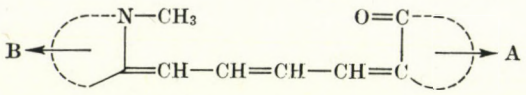

Sl. no.	Nature of *B*	Nature of *A*	V_0 kK	λ(Calc) nm	λ(Obs) nm	|λCalc−λObs| nm
1.	Quinoline-2	3-Phenyl isooxazolone	2.57	521	626	5
2.	-do-	2-Phenyl-5-oxazolone	1.98	642	640	2
3.	-do-	1-Phenyl-3-methyl pyrazolone	2.65	617	618	1
4.	-do-	Diphenyl thiobarbituric acid	2.37	628	625	2
5.	-do-	4-Hydroxy coumarin	3.28	596	592	4
6.	-do-	2-Benzyl thiothiazolone	1.64	655	650	5
7.	Quinoline-4	3-Phenyl isooxazolone	0.57	709	685	24
8.	-do-	1-Phenyl-3-methyl pyrazolone	0.33	711	692	19
9.	-do-	2-Benzyl thiothiazolone	0.17	719	685	34
10.	Benzoxazole-2	1-Phenyl-3-methyl pyrazolone	1.09	555	547	8
11.	-do-	4-Hydroxy coumarin	0.96	594	550	44
12.	-do-	2-Benzyl thiothiazolone	—	—	590	—
13.	Thiazoline-2	1-Phenyl-3-methyl pyrazolone	2.36	530	522	8
14.	-do-	Diphenyl thiobarbituric acid.	1.62	550	529	21
15.	-do-	4-Hydroxy coumarin	1.55	551	525	26
16.	-do-	5,6-Benzchroman-2,4-dione	1.50	552	535	27
17.	-do-	3-Phenyl thiohydantoin	1.26	559	505	54
18.	-do-	7,8-Benzchroman-2,4-dione	1.03	566	537	29
19.	-do-	3-Phenyl rhodanine	0.92	569	552	17
20.	-do-	4,7-Dihydroxy coumarin	3.78	544	525	19
21.	Cyclopentadienylene-triphenyl phospho-rane-2*	Indane-1,3-dione	4.83	538	565	27
22.	-do-	Diphenyl thiobarbituric acid	4.83	538	570	32
23.	-do-	3-Phenyl rhodanine	3.94	561	550	11
24.	-do-	1-Phenyl-3-methyl pyrazolone	5.74	517	550	33

* Values refer to trimethine merocyanines, already reported in Ref. [2]

Similarly, the change in the energy levels in the first excited state,

$$\Delta\varepsilon_{n+1} = \int_0^L \varphi_{n+1}\hat{V}\varphi_{n+1}\,dx = 0 \qquad (3)$$

Therefore, the net energy change from the isoenergetic transition energy (ΔE_i) due to the perturbing potential will be,

$$(\Delta\varepsilon_{n+1}) - (\Delta\varepsilon_n) = \frac{V_0}{2} \tag{4a}$$

that is,

$$\Delta E - \Delta E_i = \frac{V_0}{2} \tag{4b}$$

The results obtained by this method are given in Table II.

Table II

Dye no.*	V_0 (k. K)	λ_i nm	λCalc. nm Eq. 4(b)	λObs nm	| λObs − λCalc | nm
1.	−0.18	622.5	626	626	0
2.		640	640	640	0
3.	0.26	625	620	618	2
4.	0.36	625	626	625	1
5.	0.92	620	602	592	10
6.	1.20	665	643	650	7
7.	−0.82	672.5	691	685	6
8.	−0.10	685	687	692	5
9.	1.60	715	684	685	1
10.	2.18	570	537	547	10
11.	−0.94	555	570	550	20
12.	0.82	600	586	590	4
13.	1.90	540	514	522	8
14.	1.46	542.5	522	529	7
15.	−0.14	537	539	525	14
16.	−0.36	542.5	539	535	4
17.	3.58	577.5	523	505	18
18.	−0.54	542	550	537	13
19.	3.08	582.5	535	552	17
20.	1.4	547.5	527	525	2
21.	0.60	578.5	568	565	3
22.	0.84	578.5	565	560	5
23.	1.58	608.5	581	550	31
24.	1.50	568.5	545	550	5

* The dye numbers refer to the Sl. no. given in Table I V_0 values have been calculated by using the experimental values of the lower homologue, *i.e.* dimethin merocyanines for dyes 1 – 20 and monomethine merocyanines in case of dyes 21 – 24

The perturbation method apparently is quite straightforward and simple. The predicted wave lengths are in much better agreement with experiment, without one having to use any empirical parameters explicitly. Nevertheless the method still suffers from the disadvantage of an arbitrary choice of the zero-order system.

The perturbation affects only the highest occupied MO (φ_n) by an amount equivalent to $\frac{V_0}{2}$ leaving all other energy levels unaffected. This does not, however, create any anomaly in the energy level spacings, that is, φ_n^p is still greater than φ_{n-1}^0.

It is also possible to avoid the explicit use of L and V_0 by KUHN's method for this method in terms of the isoenergetic transition energy becomes,

$$\frac{1}{\lambda} - \frac{1}{\lambda_i} = V_0\left(1 - \frac{1}{N}\right) \tag{5}$$

($N = 2n$ = no. of pi-electrons)

This procedure yields a value of V_0, which is different from that obtained by the perturbation method by a factor of $2\left(1 - \frac{1}{N}\right)$ that is approximately by a factor of 2 for large values of N, so that both methods should yield results very close to each other, when used for the purpose of prediction (Table III).

Table III

Comparison of the absorption maxima calculated by Eqs 4(b) and 5

Dye no.	Eq. 4(b)	Eq. 5
1	626	626
2	640	640
3	620	620
4	628	626
5	603	602
6	644	643
7	691	691
8	687	687
9	683	684

*

The absorption data have been taken from the Ph. D. theses of Dr. P. B. TRIPATHY, Dr. P. C. RATH and Dr. D. C. PATI (Utkal University).

The authors are grateful to the University Grants Commission, New Delhi, India for the award of a research grant to LNP.

REFERENCES

[1] ROUT, M. K., PATNAIK, L. N.: Z. Phys. Chemie, **256,** 785 (1975)
[2] (Mrs) MISHRA, NIVEDITA, PATNAIK, L. N., ROUT, M. K.: Ind. J. Chem. **14A,** 56 (1976)
[3] PATNAIK, L. N., MISHRA, P. K., ROUT, M. K.: J. Ind. Chem. Soc., **53,** 391 (1976)
[4] BHUYAN, B., PATNAIK, L. N., ROUT, M. K.: Z. Phys. Chem. **258,** 601 (1977)
[5] LABHART, H.: J. Chem. Phys. **27,** 957 (1957)
[6] BAR, F., HUBER, W., HANDSCHIG, G., MARTIN, M., KUHN, H.: J. Chem. Phys. **32,** 470 (1960)
[7] LABHART, H.: J. Chem. Phys. **27,** 963 (1957)
[8] RUEDENBERG, K., SCHERR, C. W.: J. Chem. Phys. **21,** 1565 (1953)
[9] KUHN, H.: Chimia **2,** 11 (1948)
[10] NOLTE, H. J., BUSS, V.: Chem. Phys. Letters **19,** 395 (1973)
[11] STRATMAN, W., SEELING, F. F.: Z. Naturforsch, **422,** 998 (1967)
[13] CZIKKELY, V., FOSTERLING, H. D., KUHN, H.: Chem. Phys. Letters, **6,** 11 (1970)
[13] BUSS, V., FOSTERLING, H. D.: Tetrahedron, **29,** 3001 (1973)
[14] KUHN, H.: J. Chem. Phys. **17,** 1198 (1949)

Nivedita MISHRA
Lalit N. PATNAIK
M. K. ROUT
Ravenshaw College, Cuttack 753003 (Orissa), India.

INDEX

ANALYTICAL CHEMISTRY

PHYSICAL AND INORGANIC CHEMISTRY

Printed in Hungary

A kiadásért felel az Akadémiai Kiadó igazgatója — Műszaki szerkesztő: Zacsik Annamária

A kézirat nyomdába érkezett: 1978. I. 20. — Terjedelem: 13,65 (A/5) ív, 79 ábra

78.5412 Akadémiai Nyomda, Budapest — Felelős vezető: Bernát György

ACTA CHIMICA

ТОМ 97 – ВЫП. 2

РЕЗЮМЕ

Определение циркония путем экстракционной фотометрии с арсеназо III

В. К. АКИМОВ, Л. Т. ГВЕЛЕСИАНИ, А. И. БУСЕВ и П. НЕННИНГ

Цирконий был экстрагирован дихлорэтаном из сернокислого раствора после добавки KSCN и антипирина. После обратной экстракции цирконий определяется фоторметрически в виде его комплекса с арсеназо III.

Некоторые химические реакции в электродной щели и их роль в спектрохимическом анализе, XXVIII

Поведение окислов металлов в дуге с атмосферой проточного аргона. Роль времени горения дуги и силы тока в случае подсобных электродов RW II

З. Л. САБО и Х. ДОБОЛИ-ФЕЙЕРДИ

Исследуя порошковые смеси CuO + C, было найдено, что выход окислов углерода в дуге возрастает с увеличением времени горения и с повышением силы тока. В двух различных случаях отношение скоростей нагревания и охлаждения электродов различны, а поэтому и различаются скорости образования окислов углерода. Это особенно наглядно, если изображать для двух различных случаев электрическую работа дуги в зависимости от произведения время на силу тока. С протеканием реакции в канале электрода-носителя накапливается металлическая медь, которая препятствует дальнейшей реакции, т. к. ухудшается доступ к нижним слоям порошковой смеси. Поэтому со временем уменьшается и доля испарения. Исхода из изменения объемного отношения образующихся CO_2 и CO, можно заключить, что те окислительные и восстановительные тенденции электрического происхождения, которые направляют реакции между газовой атмосферой и материалом электрода на поверхности электрода, не справедливы для реакций внутри материала электрода.

Некоторые химические реакции в электродной щели и их роль в спектрохимическом анализе, XXIX

Поведение окислов металлов в дуге с атмосферой проточного аргона. Роль отношения окись металла/порошок углерода в случае подсобных электродов RW II

З. Л. САБО и Х. ДОБОЛИ-ФЕЙЕРДИ

Были повторены исследования с изменяемым отношением окись металла/порошок углерода с той разницей, что вместо атмосферы с неподвижным аргоном использовали атмосферу с проточным аргоном. В согласии с ранними результатами, максимальная скорость реакции была получена, когда отношение окись металла/порошок углерода находится в интервале молярных отношений 1 : 1 и 2 : 1, являющихся оптималпными для образования

CO и CO_2. Т. е., две реакции протекают параллельно. Исходя из изменения интенсивности спектральных линий, было обобщено то заключение, что в отсутствии химических реакций катодное возбуждение дает более интенсивный спектр. А если в зоне испарения потекает химическая реакция с выделением тепла, то анодное возбуждение более интенсивно.

Некоторые химические реакции в электродной щели и их роль в спектрохимическом анализе, XXX

Поведение окислов металлов в дуге с атмосферой проточного аргона. Влияние реакционной способности окислов металлов в случае подсобных электродов RW II

З. Л. САБО и Х. ДОБОЛИ-ФЕЙЕРДИ

Влияние реакционной способности окислов металлов проявляется как в реакциях в угольных порошковых смесях, так и на результатах спектрального анализа этих реакций. Под влиянием горения дуги, в случае более реактивных окислов металлов, освобождается разность между теплотой окисления углерода и теплотой разложения окисла металла, что приводит к повышенному разогреву смеси. Вследствие этого реакция ускоряется и усиливается интенсивность спектральных линий. Исходя из результатов исследований, можно делать заключения относительно протекающих реакций, их последовательности и мест протекания.

Модельная реализация идеального полиметинового состояния с помощью изменений, индуцированных растворителями в электронной структуре сольватохромных красителей

С. ДЕНЕ и К.-Д. НОЛЬТЕ

Были симулированы неполярные и полярные валентные структуры мерополиметина на основе теории МО, полагая суперпонирование реакционного поля увеличивающейся полярности на молекулу. Симметричное состояние, через которое проходит молекула, обладает всеми типичными характеристиками идеального полиметинового состояния, такими как минимум перехода энергии $N \rightarrow V_1$, соответствующий VB теоретическим заключениям Т. Фёрстера, максимум вероятности перехода, максимум чередования π-электронной плотности, чередование минимума порядка π-связи как в основном состоянии, так и в меньшей степени, в первом возбужденном синглетном состоянии. При светопоглащении, π-электронные плотности в переходах $N \rightarrow V_1$ экспремально обратны в идеальном полиметиновом состоянии, в то время как изменения в порядке π-связи минимальны.

Кинетика и механизм реакций замещения комплексов, V

Сольватация $[Cr(NCS)_4(\text{бензиламина})_2]^-$ в смесях ацетона с водой

Й. ЖАКО, Ч. ВАРХЕИ, Д. ОПРЕСКУ и И. ГОНЕСКУ

Была исследована кинетика сольватации $[Cr(NSC(_4(\text{бензиламина})_2]^-$ в смесях ацетона с водой. Молекулы бензиламина не замещены. только ионы NCS^- обменены на молекулы растворителя. Реакция (1) затрудняется с увеличением содержания ацетона указывая на важную роль молекул растворителя в механизме реакции. Реакция (1) затрудняется также ионами водорода. Константа скорости реакции (1) не зависит от природы амина в смеси этанола с водой, но в смесях ацетона с водой константы скорости, полученные для производного бензиламина, значительно отличаются от констант скоростей производных пиридина и анилина, сообщенных ранее.

О комплексах α-диоксимина с переходными металлами, V

Хелаты кобальт(III)-ниоксимина с оксокислотами серы

Ч. ВАРХЕИ, А. БЕНКЁ, М. ШОМАИ и А. КОХ

Новые комплексные анионы типа $[Co(niox.H)_2XV]^{-3}$ (где $niox.H_2$ = 1,2-циклогексан-дион - диоксим, X = У, X У = SO_3 и S_2O_3) были получены путем окисления на воздухе смесей Co^{+2}-ниоксим-X У, либо с помощью реакций лигандного обмена из соответствующих галогеноакво-неэлектролитов. Переход от акваформы $[Co(niox.H)_2-(H_2O)X]^-$ в аминоформу с помощью ароматических и гетероциклических аминов приводит 27 солей. к образованию $[Co(niox.\ H)_2(амин)X]^-$. Была изолирована и охарактеризована серия из Некоторые структурные проблемы были исследованы с помощью УФ и ИК спектральных измерений. Другие оксо-анионы серы, такие как SO_4^{-2} и S_nO_6 (n = 2—5), не пригодны для этих реакций вследствие стерических затруднений или отсутствия донорных атомов серы.

Исследование сплавов железо-никель и железо-хром с помощью МСВИ, I

Исследования в связи с ионным распылением

М. РИДЕЛЬ, Т. НЕНАДОВИЧ и Б. ПЕРОВИЧ

Ионное распыление двухкомпонентных железных сплавов с простой фазовой диаграммой, а также их атомная и комплексная ионная эмиссия были исследованы масс-спектроскопией со вторичной ионизацией (МСВИ). Сплавы Fe—Ni и Fe—Cr с интервалом концентраций 0—100% подвергались бомбардировке ионами Kr^+ с энергией 4 Кэв. Модифицированием источника ионов в МСВИ и анализом с помощью электронного микрозонда открывается возможность симультанного исследования ионного распыления и вторичной ионной эмиссии.

В первом сообщении обсуждалась зависимость распыления сплавов Fe—Ni и Fe—Cr от состава. Были определены отношения скоростей распыления, необходимые для оценки исследований вторичной ионной эмиссии, а также их зависимость от состава. Относительный коэффициент распыления компонентов сплава равен приблизительно единице; в чистом состоянии вещество с меньшим коэффициентом распыления более интенсивно распыляется в сплаве, и в тоже самое время наблюдалось уменьшение скорости распыления другого компонента.

Исследование спланов железо-никель и железо-хром с помощью МСВИ, II

Исследование эмиссии вторичных одноатомных и однозарядных ионов в зависимости от состава

М. РИДЕЛЬ, Т. НЕНАДОВИЧ и Б. ПЕРОВИЧ

Среди многочисленных ионов, появляющихся в спектре вторичных ионов высоко-концентрированных сплавов железо-никель и железо-хром, были исследованы лишь одноатомные и однозарядные ионы металлов. Согласно исследованиям, относительный выход вторичных ионов сильно зависит от концентрации. С помощью симультанного измерения распыления и ионной эмиссии была определена относительная степень ионизации, которая принимает предельное значение при составе, относящемся к минимальной точке плавления сплавов. Согласование моделей LTE и ASI, описывающих вторичную ионизацию, с экспериментальными данными было возможно лишь с ограниченной точностью. Это, в свою очередь, указывает не то, что гучшее описание концентрационной зависимости ионной эмиссии возможно лишь при лучших приближениях.

Исследование сплавов железо-никель и железо-хром с помощью МСВИ, III

Зависимость эмиссии двухатомных комплексных ионов от состава сплава

М. РИДЕЛЬ, Т. НЕНАДОВИЧ и Б. ПЕРОВИЧ

В спектре вторичных ионов концентрированных сплавов Fe—Ni и Fe—Cr, подвергнутых бомбардировке ионами Kr^+, наблюдались интенсивные пики ионов, состоящих из одинаковых (Fe_2^+, Ni_2^+, Cr_2^+) и различных атомов ($FeNi^+$, $FeCr^+$). Образование комплексных ионов сильно зависит от концентрации, а сила тока сложных ионов увеличивается при увеличении плотности тока первичных ионов. На основе определения относительной степени ионизации комплексных ионов, был построен механизм образования комплексных ионов.

Полиатомные катионы теллурия с низким валентным состоянием

С. А. А. ЗАИДИ, З. А. СИДДИКИ и Н. А. АНСАРИ

Кондуктометрические измерения и спектроскопические исследования в ультрафиолетовой в видимой областях растворов теллурия в хлористом сульфуриле указывают на то, что красный цвет раствора, приготовленного в чистом HSO_3Cl, вызван катионом Te_4^{+2}. Было также показано, что красные ионы Te_4^{+2} могут быть окислены с помощью таких окисляющих реагентов, как $K_2S_2O_8$ и TeO_2, до желтых ионов Te_4^{+4}. В присутствии избытка окисляющего реагента образуется TeO_2.

Исследование каталитического окисления сорбозы

А. ЛЕНДЬЕЛ-МЕСАРОШ, Б. ЛОШОНЦИ, Й. ПЕТРО и Й. РУСНАК

Гетерогенное каталитическое окисление сорбозы до 2-кетогулоновой кислоты было исследовано с катализатором палладий на носителе активированный уголь. Было найдено, что в 20% вес.%-ом растворе при 60—70°C за 4—6 часов был достигнут приблизительно 50%-ый выход и селективность для сорбозы равна 80%. Таким образом, этот метод может быть использован и для промышленных целей.

Механизм гидрогенолиза этана на металлических катализаторах

П. ТЕТЕНИ, Л. ГУЦИ и А. ШАРКАНЬ

Данные адсорбции и обмена H — D в CH_4 и C_2H_6 сравнивались с данными гидрогенолиза на Co, Ni, Rh, Pd, Ir и на платиновой черни.

Было найдено, что для всех изученных катализаторов $W_{ex} > W_h$, и $E_{ex} < E_h$. Последовательность по активности металнови: Rh, Ru, Ir, Ni, Co, Pd Pt, что значительно отличается от ряда наблюденной при обмене последовательности. Был найден параллелизм между активностью в гидрогенолизе, хемосорбцией и соотношением многократного к однократному обмену в этане.

Эти соображения подтверждают важность сильных взаимодействий углеводородов с металлами в процессе гидрогенолиза. Однако, положение, предложенное Кембаллом от ом что;образование структур C = Me или $C(Me)_2$ является ступенью, определяющей скорость гидрогенолиза, не подтверждается при сравнения величин энергий активации исследованных реакций.

Анализируя все данные (обмен, хемосорбция, гидрогенолиз), было заключено, что разрыв связи C—C хемосорбированного этана является ступенью, определяющей скорость процесса. Это было также подтверждено энергетическими расчетами.

Тетра-, три- и дикоординированные комплексы некоторых производных пиридина с перхлоратом меди[I]

М. А. С. ГОХЕР

Были приготовлены и охарактеризованы серии стабильных тетра-, три- и дикоординированных комплексов некоторых производных пиридина с перхлоратом меди(I). Перхлоратные группы являются ионными во всех тетракис-, трис- и бискомплексах. Согласно спектрам ик, формально дикоординированные комплексы обладают координационным числом большим, чем два. Это происходит, в зависимости от природы заместителя, различными путями: либо в результате образования π-комплексов, либо через образование металлических кластеров или электроннообедненных связей, когда заместитель представляет собой электронодонорную группу. Для мета- и пара-карбометокси- или карбоэтокси-производных (т. е. электроноакцепторных групп) более высокое координационное число достигается через координированные перхлораты. В случае ортокарбонильных пиридинов ион меди (I) принимает тетраэдрическую геометрию за счет координирования через атом азота и карбонильную группу в бискомплексе. Кажущееся координационное число меди(I) в изученных комплексах зависит от стерических условий и основности лиганда.

Расчеты абсорбционных спектров мероцианина методом FEMO

Н. МИШРА, Л. Н. ПАТНАИК и М. К. РОУТ

Абсорбционные спектры 24 мероцианинов были исследованы с помощью Модели Свободно-Электронных Молекулярных Орбиталей (FEMO), применяя две процедуры: 1) с помощью метода, разработанного Куном [J. Chem. Phys., *17*, 1198 (1949)] и с соответствующими модификациями — с учетом длины поробки и числа π-электронов и 2) используя теорию возмущения первого порядка, разработанную авторами. Оба метода дают результаты, находящиеся в превосходном согласии с экспериментом. Последний метод, помимо этого, имеет также и то преимущество по сравнению с первым, что избегает эксплицитное использование эмпирических параметров.

RECENT DEVELOMENT IN THE CHEMISRTY OF NATURAL CARBON COMPOUNDS IX.

Edited by Cs. Szántay

This volume contains three important papers relating to natural carbon compounds. — The Japanese Kenji Mori's study entitled Synthetic Chemistry of Insect Pheromones and Juvenile Hormones includes a large number of synthetic schemes and equations utilizing all the achievements of modern organic chemistry. — In the review: Composition of the Bulgarian Rose Flower Concrete; the Structure and the Biogenesis of its Components, B. Stoianova-Ivanova reaches new conclusions on the biosynthesis of natural plant waxes. — Chalcone epoxides, deemed to be important intermediates in the biosyntheses of flavonoids, are reported on by Gy. Litkei (Hungary). Investigations on the Algar-Flynn-Oyamada reaction are separately discussed and a new mechanism is put forward for interpretation.

In English — Approx. 200 pages — Cloth

ISBN 963 05 1632 2

AKADÉMIAI KIADÓ

Publishing House of the Hungarian Academy of Sciences, Budapest

Pataki, László-Zapp, Erika:

BASIC ANALYTICAL CHEMISTRY

This book consists of four comprehensive chapters. The first deals with the theoretical principles of analytical chemistry, and, beyond this, it provides solid fundamentals to chemistry in its entirety. In the second chapter qualitative analysis is treated on the basis of group reactions; instead of hundreds of reactions, detailed descriptions of 8—10 reaction types are given thereby providing a reliable survey of qualitative chemical analysis. Different quantitative methods are discussed in Chapter 3. The fourth chapter summarizes physico-chemical measuring techniques of analytical chemistry.

In English — Approx. 400 pages — 93 figures — 89 tables — Cloth

ISBN 963 05 1543 4

AKADÉMIAI KIADÓ

Publishing House of the Hungarian Academy of Sciences, Budapest

Les Acta Chimica paraissent en français, allemand, anglais et russe et publient des mémoires du domaine des sciences chimiques.

Les Acta Chimica sont publiés sous forme de fascicules. Quatre fascicules seront réunis en un volume (4 volumes par an).

On est prié d'envoyer les manuscrits destinés à la rédaction l'adresse suivante:

Acta Chimica
H-1521 Budapest, Hongrie

Toute correspondance doit être envoyée à cette même adresse.

La rédaction ne rend pas de manuscript.

Le prix de l'abonnement est de $ 36,00 par volume.

Abonnement — en Hongrie l'Akadémiai Kiadó l'Entreprise pour le Commerce Extérieur « Kultúra » (1389 H-Budapest 62, P.O.B. 149 Compte-courant No. 218 10990) ou à l'étranger chez tous les représentants ou dépositaires.

Die Acta Chimica veröffentlichen Abhandlungen aus dem Bereich der chemischen Wissenschaften in deutscher, englischer, französischer und russischer Sprache.

Die Acta Chimica erscheinen in Heften wechselnden Umfanges. Vier Hefte bilden einen Band. Jährlich erscheinen 4 Bände.

Die zur Veröffentlichung bestimmten Manuskripte sind an folgende Adresse zu senden:

Acta Chimica
H-1521 Budapest, Ungarn

An die gleiche Anschrift ist auch jede für die Redaktion bestimmte Korrespondenz zu richten.

Manuskripte werden nicht zurückerstattet.

Abonnementpreis pro Band: $ 36,00.

Bestellbar für das Inland bei Akadémiai Kiadó (1363 Budapest, Postfach 24, Bankkonto Nr. 215 11488), für das Ausland Außenhandels-Unternehmen » Kultúra « (1389 Budapest 62, P.O.B. 149. Bankkonto Nr. 218 10990) oder bei seinen Auslandsvertretungen und Kommissionären.

«Acta Chimica» издает статьи по химии на русском, французском, английском и немецком языках.

«Acta Chimica» выходит отдельными выпусками разного объема, 4 выпуска составляют один том и за год выходит 4 тома.

Предназначенные для публикации рукописи следует направлять по адресу:

Acta Chimica
H-1521 Budapest, BHP

Всякую корреспонденцию в редакцию направляйте по этому же адресу.

Редакция рукописей не возвращает.

Подписная цена — $ 36,00 за том.

Отечественные подписчики направляйте свои заявки по адресу Издательства Академии Наук (1363 Budapest, P.O.B. 24, Текущий счет 215 11488), а иностранные подписчики через организацию по3 внешней торговле «Kultúra» (H-1389 Budapest 62, P.O.B. 149. Текущий кчет 218 10990) или через ее заграничные представительства и уполномоченных.

Reviews of the Hungarian Academy of Sciences are obtainable at the following addresses:

AUSTRALIA
C.B.D. LIBRARY AND SUBSCRIPTION SERVICE, Box 4886, G.P.O., *Sydney N.S.W. 2001*
COSMOS BOOKSHOP, 135 Ackland Street, *St. Kilda (Melbourne), Victoria 3182*

AUSTRIA
GLOBUS, Höchstädtplatz 3, *1200 Wien XX*

BELGIUM
OFFICE INTERNATIONAL DE LIBRAIRIE, 30 Avenue Marnix, *1050 Bruxelles*
LIBRAIRIE DU MONDE ENTIER, 162 Rue du Midi, *1000 Bruxelles*

BULGARIA
HEMUS, Bulvar Ruszki 6, *Sofia*

CANADA
PANNONIA BOOKS, P.O. Box 1017, Postal Station "B", *Toronto, Ontario M5T 2T8*

CHINA
CNPICOR, Periodical Department, P.O. Box 50, *Peking*

CZECHOSLOVAKIA
MAD'ARSKÁ KULTURA, Národní třida 22, *115 66 Praha*
PNS DOVOZ TISKU, Vinohradská 46, *Praha 2*
PNS DOVOZ TLAČE, *Bratislava 2*

DENMARK
EJNAR MUNKSGAARD, Norregade 6, *1165 Copenhagen*

FINLAND
AKATEEMINEN KIRJAKAUPPA, P.O. Box 128, *SF-00101 Helsinki 10*

FRANCE
EUROPERIODIQUES S. A., 31 Avenue de Versailles, *78170 La Celle St.-Cloud*
LIBRAIRIE LAVOISIER, 11 rue Lavoisier, *75008 Paris*
OFFICE INTERNATIONAL DE DOCUMENTATION ET LIBRAIRIE, 38 rue Gay-Lussac, *75240 Paris Cedex 05*

GERMAN DEMOCRATIC REPUBLIC
HAUS DER UNGARISCHEN KULTUR, Karl-Liebknecht-Strasse 9, *DDR-102 Berlin*
DEUTSCHE POST, ZEITUNGSVERTRIEBSAMT, Strasse der Pariser Kommüne 3—4, *DDR-104 Berlin*

GERMAN FEDERAL REPUBLIC
KUNST UND WISSEN ERICH BIEBER, Postfach 46, *7000 Stuttgart 1*

GREAT BRITAIN
BLACKWELL'S PERIODICALS DIVISION, Hythe Bridge Street, *Oxford OX1 2ET*
BUMPUS, HALDANE AND MAXWELL LTD., Cowper Works, *Olney, Bucks MK46 4BN*
COLLET'S HOLDINGS LTD., Denington Estate, *Wellingborough, Northants NN8 2QT*
WM. DAWSON AND SONS LTD., Cannon House, *Folkestone, Kent CT19 5EE*
H. K. LEWIS AND CO., 146 Gower Street, *London WC1E 6BS*

GREECE
KOSTARAKIS BROTHERS, International Booksellers, 2 Hippokratous Street, *Athens-143*

HOLLAND
MEULENHOFF-BRUNA B.V., Beulingstraat 2, *Amsterdam*
MARTINUS NIJHOFF B.V., Lange Voorhout 9—11, *Den Haag*
SWETS SUBSCRIPTION SERVICE, 347b Heereweg, *Lisse*

INDIA
ALLIED PUBLISHING PRIVATE LTD., 13/14 Asaf Ali Road, *New Delhi 110001*
150 B-6 Mount Road, *Madras 600002*
INTERNATIONAL BOOK HOUSE PVT. LTD., Madame Cama Road, *Bombay 400039*
THE STATE TRADING CORPORATION OF INDIA LTD., Books Import Division, Chandralok, 36 Janpath, *New Delhi 110001*

ITALY
EUGENIO CARLUCCI, P.O. Box 252, *70100 Bari*
INTERSCIENTIA, Via Mazzé 28, *10149 Torino*
LIBRERIA COMMISSIONARIA SANSONI, Via Lamarmora 45, *50121 Firenze*
SANTO VANASIA, Via M. Macchi 58, *20124 Milano*
D. E. A., Via Lima 28, *00198 Roma*

JAPAN
KINOKUNIYA BOOK-STORE CO. LTD., 17-7 Shinjuku-ku 3 chome, Shinjuku-ku, *Tokyo 160-91*
MARUZEN COMPANY LTD., Book Department, P.O. Box 5056 Tokyo International, *Tokyo 100-31*
NAUKA LTD., IMPORT DEPARTMENT, 2-30-19 Minami Ikebukuro, Toshima-ku, *Tokyo 171*

KOREA
CHULPANMUL, *Phenjan*

NORWAY
TANUM-CAMMERMEYER, Karl Johansgatan 41—43, *1000 Oslo*

POLAND
WĘGIERSKI INSTYTUT KULTURY, Marszałkowska 80, *Warszawa*
CKP I W ul. Towarowa 28 *00-958 Warsaw*

ROUMANIA
D. E. P., *Bucureşti*
ROMLIBRI, Str. Biserica Amzei 7, *Bucureşti*

SOVIET UNION
SOJUZPETCHATJ — IMPORT, *Moscow*
and the post offices in each town
MEZHDUNARODNAYA KNIGA, *Moscow G-200*

SPAIN
DIAZ DE SANTOS, Lagasca 95, *Madrid 3*

SWEDEN
ALMQVIST AND WIKSELL, Gamla Brogatan 26, *101 20 Stockholm*
GUMPERTS UNIVERSITETSBOKHANDEL AB, Box 346, *401 25 Göteborg 1*

SWITZERLAND
KARGER LIBRI AG, Petersgraben 41, *4011 Basel*

USA
EBSCO SUBSCRIPTION SERVICES, P.O. Box 1943, *Birmingham, Alabama 35201*
F. W. FAXON COMPANY, INC., 15 Southwest Park, *Westwood, Mass, 02090*
THE MOORE-COTTRELL SUBSCRIPTION AGENCIES, *North Cohocton, N. Y. 14868*
READ-MORE PUBLICATIONS, INC., 140 Cedar Street, *New York, N. Y. 10006*
STECHERT-MACMILLAN, INC., 7250 Westfield Avenue, *Pennsauken N. J. 08110*

VIETNAM
XUNHASABA, 32, Hai Ba Trung, *Hanoi*

YUGOSLAVIA
JUGOSLAVENSKA KNJIGA, Terazije 27, *Beograd*
FORUM, Vojvode Mišiča 1, *21000 Novi Sad*

27. VII. 1978 HU ISSN 0001—5407 **Index: 26.007**

ACTA CHIMICA

ACADEMIAE SCIENTIARUM HUNGARICAE

TOMUS 97 FASCICULUS 3

AKADÉMIAI KIADÓ, BUDAPEST

1978

ACTA CHIM. ACAD. SCI. HUNG. ACASA2 97 (3) 255–367 (1978)

ACTA CHIMICA

A MAGYAR TUDOMÁNYOS AKADÉMIA KÉMIAI TUDOMÁNYOK OSZTÁLYÁNAK IDEGEN NYELVŰ KÖZLEMÉNYEI

Acta Chimica is a journal for the publication of papers on all aspects of chemistry in English, German, French and Russian.

Acta Chimica is published in 4 volumes per year. Each volume consists of 4 issues of varying size.

Manuscripts should be sent to

Acta Chimica
H-1521 Budapest, Hungary

Correspondence with the editors should be sent to the same address. Manuscripts are not returned to the authors.

Subscription: $ 36.00 per volume.

Hungarian subscribers should order from Akadémiai Kiadó, 1363 Budapest, P.O. Box 24. Account No. 215 11488.

Orders from other countries are to be sent to "Kultura" Foreign Trading Company (H-1389 Budapest 62, P.O. Box 149. Account No. 218 10990) or its representatives abroad.

Acta Chimica Academiae Scientiarum Hungaricae, Tomus 97 (3), pp. 255–264 (1978)

RADIOLYSIS OF AQUEOUS IRON(III)-EDTA SYSTEMS

M. WÉBER, G. FÖLDIÁK and E. KOCSIS

(Training Reactor, Technical University, Budapest)

Received September 30, 1976*

To investigate the possibility of partial substitution of stainless steel, the major construction material of nuclear power plants, by the less expensive perlitic steel, the radiolysis of the Fe^{III}–edta system has been studied, in aqueous solutions. It has been found that an equilibrium is established between the radiolyses of Fe^{III}–edta and Fe^{II}–edta. The influence of formic acid and methanol as secondary additives, as well as that of the edta complexes of alloying chromium and nickel has also been studied. The basic radiolytic process was found to be the radiolysis of water, the products of which interact with dissolved substances. There is a competition between the radiolysis products of water and the solutes.

Introduction

Heat exchange systems of power plants are made almost exclusively of stainless steel. These construction materials, however, – due to the high price of certain alloying components, such as titanium, chromium, nickel – increase capital investment costs considerably. Therefore, it would be of great economic importance if stainless could be substituted by perlitic steel in some parts of the power plant equipment. There is some indication that this is possible [1] by creating a good quality magnetite layer over the surfaces exposed to corrosion with aqueous Fe^{III}–edta solutions or by keeping the metals formed upon corrosion in solution by complexation.

In addition to fossile fuels, nuclear power plants gain more and more importance in energy production. No unambigous data are available so far as to whether the above complexation process can be used in nuclear power plants, in which the proportion of stainless steel structures is rather high, therefore, the economic importance of the problem is greater as compared with traditional power plants. In order to elucidate this technical-economical problem, it is necessary to know the behaviour of edta complexes under the effect of ionizing radiation [2].

A short literature survey as well as the initial stage of our experiments will be reported in this paper.

* In final form December 16, 1977.

1. Literature survey

Search of the literature has not revealed papers dealing with the radiation chemistry of the iron^{III}-ethylenediamine-tetraacetic-acid complex (Fe^{III}–edta) under the effect of mixed neutron-γ radiation.

The batch type experiments aimed at investigating the decomposition of Fe^{III}–edta under the effect of X-rays are bearest to our study although a few reports have appeared on γ-radiolysis with ^{137}Cs [3]. These studies have been carried out at room temperature and atmospheric pressure. Some of the experiments were performed in solutions saturated with air, others in deaerated solutions, saturated with argon.

Figure 1 shows that a linear correlation exists between the dose and the extent of decomposition of the complex at pH = 1, in the given dose range which is, however, very small compared with those encountered in radiation chemistry and reactor technique. The relatively low G-values indicate that the decomposition is not a chain reaction.

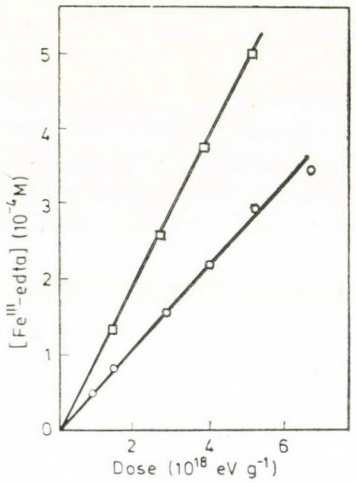

Fig. 1. Dose dependence of the radiolysis of a 3 mM Fe^{III}–edta solution containing 0.5 *M* H_2SO_4 in systems saturated with air (0) and argon (□) (Ref. [3])

The correlation between the dose and G-values has also been studied with degassed neutral $[Cr\ en_3]Cl_3 . 3.5\ H_2O$ solutions containing the complex at different initial concentrations (Fig. 2): the curves show that radiation chemical yields decrease with increasing dose as well as with increasing initial concentrations of tris(ethylenediamine)chromium(III) [4]. Thus, under the conditions met in nuclear reactors, the decomposition is relatively small.

Aqueous solutions of Fe^{III}–edta have been studied to some extent, using γ-radiation rather than X-rays (Fig. 3). The G-value increases up to about

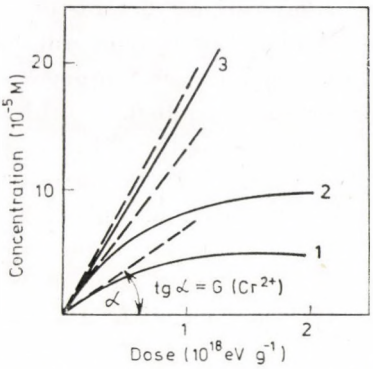

Fig. 2. G(Cr^{2+}) values as a function of the dose in solutions of [Cr en_3]Cl_3.3.5 H_2O of different concentrations; *1* : 5×10^{-3} *M*; *2*: 10^{-2} *M*; *3*: 5×10^{-2} *M* (Ref. [4])

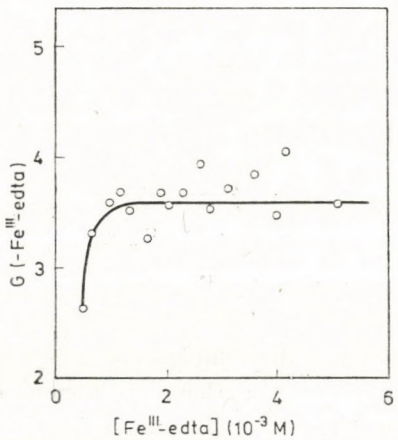

Fig. 3. The variation of G(-Fe^{III}–edta) as a function of the initial concentration of air containing aqueous solution (Ref. [3])

10^{-3} *M* in solutions saturated with air, but above this value, the initial concentration has no influence on the extent of decomposition [3]. The G(-Fe^{III}–edta) of decomposition may reach 3.50 ± 0.30 as a limiting value in solutions saturated with air; on the other hand, the analogous value in deaerated but argon-saturated solutions is 5.85 ± 0.20 molecule per 100 eV. The difference may, presumably, be attributed to the rapid reoxidation of at least a part of the product Fe^{II}–edta complex into the initial complex containing trivalent iron in the presence of water radiolysis products and oxygen. It has been shown that the majority of products are chemically stable.

In the absence of radiation edta complexes decompose at about 250 °C. No direct data have been published so far with respect to the temperature dependence of radiation chemical decomposition. However, since the process is

connected with primary decomposition reactions of water, some assumptions can be made on their basis. An increase in temperature generally (athough not always) decreases the G-values of water and aqueous solutions [5].

The effect of pH has also been studied. According to the data obtained, minima are observed in the values of both $G(H + e_{aq}^-)$ and $G(OH^\cdot)$ in neutral solutions (G = 2.7 and 2.2, respectively); the corresponding values at pH = 1 are 3.7 and 3.8, while at pH = 13, G = 3.2 and 3.2 have been found [3].

It is important from the viewpoint of nuclear reactor technique that added Fe^{2+} ions influence the radiolysis of aqueous Fe^{III}–edta solutions since they interact in a competitive manner with $OH^\cdot$ radicals formed in water radiolysis (Fig. 4).

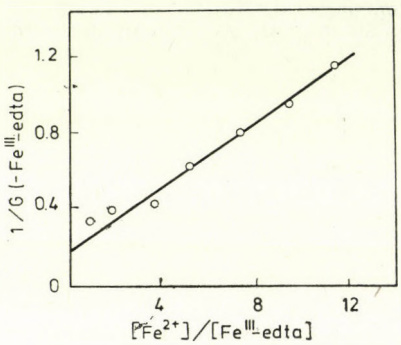

Fig. 4. Kinetic curve of the reaction of $OH^\cdot$ radicals with Fe^{2+} and Fe^{III}–edta (Ref. [4])

Some data indicate that the radiolysis of complexes can be suppressed by means of appropriate additives (methanol or formic acid which react competitively), in other words, the Fe^{III}–edta can be 'protected' by added chemicals (Table I).

Table I

Radiolysis of aqueous solutions of $[Cr\ en_3]Cl_3 .3.5\ H_2O$ *(oxygen-free, concentration:* 10^{-2} *M) in the presence of secondary additives at concentrations of 1.6 M*
(Dose: 5.2×10^{17} eV g^{-1} = 8.3 krd (From Ref. [4])

Secondary additive	None	$NaNO_3$	HCOONa	Na_2CO_3	CH_3OH
G(-[Cr en_3]Cl_3)	3.89	1.84	1.6	1.46	1.27

Presumably, the edta complexes of the alloying metals of steel (mainly Cr and Ni) decompose in a manner similar to that of the analogous Fe-complexes (Table II). Probably, the ions of alloying metals can be considered – to a first, crude approximation – as competitive factors similarly to the case of Fe^{2+} ions (Fig. 4) [3].

Table II

G-values of decomposition of metal complexonates

Complex	Oxygen		pH	Ref.
	absent	present		
Fe^{III}– edta	5.85 ± 0.20	3.50 ± 0.30	1	[3]
Co^{III}– edta	4.75 ± 0.25	2.65 ± 0.30	1	[6]
Ni^{II}edta	1.2 ± 0.1	2.1 ± 0.2	7	[7]
$[Cr\ en_3]Cl_3.3.5\ H_2O$	3.9	?	7	[4]

2. Experimental

Chemicals of p. a. and pss. grades supplied by REANAL as well as bidistilled water have been used in the experiments.

Irradiations have been carried out in the "K-120000" ^{60}Co γ-irradiation source of the Institute of Isotopes of the Hungarian Academy of Sciences with a nominal activity of 3×10^{15} Bq (80 000 Ci) [8]. The dose rate applied was, as a rule, 3.5×10^{16} eV g^{-1} s^{-1} (2 Mrd h^{-1}). The doses have been monitored by chlorobenzene dosimetry using oscillometric titration [9]. The temperature during irradiation was 30 – 35 °C.

All experiments were carried out in commercial borosilicate ampules (volume 10 cm^3, diameter 12.5 mm, wall thickness 1 mm) [10]. These have been heated to 300 – 400 °C prior to use in air, in order to oxidize or decompose any possible organic impurities.

Ampoules containing the test solutions were, in general, irradiated in an open state; in experiments for studying the effect of nitrogen and oxygen, the ampoules were closed with rubber caps and the gas was bubbled through two injection needles led through the rubber cap.

The radiation chemical decomposition of the samples was followed on a Beckman DB-GT spectrophotometer at the wavelength corresponding to the absorption maximum of Fe^{III}–edta (258 nm).

3. Results and discussion

The primary purpose of the experiments was to study the effect of various factors on the radiation chemical decomposition.

3.1. *Effects of Fe^{III}–edta concentration, dose and dose rate*

The effect of concentration has been studied at a dose of 3.1×10^{19} eV g^{-1} (0.5 Mrd). As shown by Fig. 5, the G-value of the decomposition of Fe^{III}–edta is constant above 2×10^{-3} *M* and equals $\sim$ 2.7 molecules per 100 eV.

Considering the concentrations used in caloric energetics for the cleaning of boilers (*i.e.* for producing an appropriate magnetite layer on their heat transferring surfaces) as well as the above statements [1], the studies on the influence of dose and dose rate have been carried out with a Fe^{III}–edta solution of 3.5×10^{-3} *M* concentration. Irradiations were performed in air as well as with solutions flushed with oxygen and nitrogen prior to irradiation. The

duration of irradiation was between 3 min and 10 hrs, corresponding to doses of (0.1 – 20 Mrd) $0.6-125\times10^{19}$ eV g^{-1} considering the constant dose rate of 3.5×10^{16} eV $g^{-1}s^{-1}$ (2 Mrd h^{-1}). The radiation chemical decomposition and the concentration dependence for the complex are shown in Figs 6 and 7.

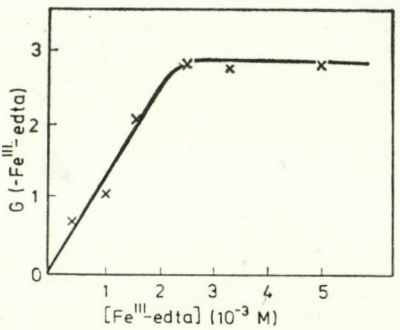

Fig. 5. Variation of G(-Fe^{III}–edta) as a function of the initial concentration of air saturated aqueous solution

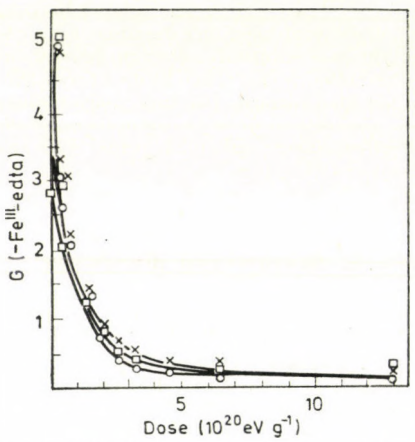

Fig. 6. Dose dependence of G(-Fe^{III}–edta) in systems containing air (□), nitrogen (x) and oxygen (o)

On comparing our data for the radiolysis of air-saturated solutions with those obtained by BHATTACHARYYA and KUNDU (who applied X-rays with doses between $3.7-7.5\times10^{18}$ eV g^{-1}, *i.e.* $6-12\times10^{4}$ rd) some differences can be observed. The above authors have found G = 3.5 as opposed to our G = 2.8, which can be attributed to the different experimental conditions although our measurements indicate that the G-value is independent of the dose rate up to 10^{16} eV $g^{-1}s^{-1}$ (0.6 Mrd h^{-1}).

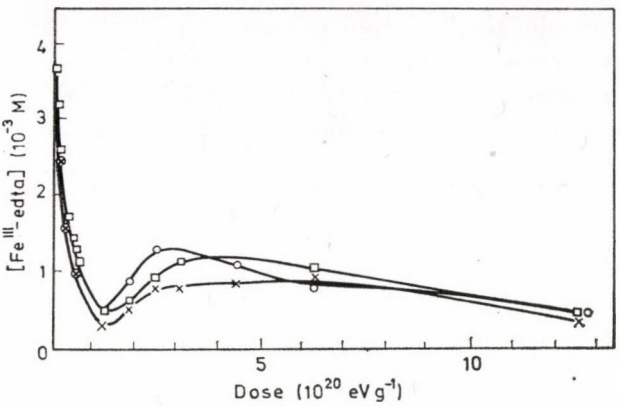

Fig. 7. Concentration of Fe^{III}–edta as a function of the dose in systems containing air (□), nitrogen (x) and oxygen (o)

It is conspicuous that the concentration vs. dose curves have local minima and maxima with all three gases (Fig. 7).

No significant differences can be observed between the radiolyses of solutions saturated with air, oxygen and nitrogen at lower doses; this presumably indicates that the overall process in this dose range is limited to the interaction of water and Fe^{III}–edta and the effect of oxygen is negligible (Fig. 6).

In the range of more intensive reoxidation, the behaviour of the system can be better characterized by the concentrations vs. dose curves (Fig. 7). According to this, reoxidation of Fe^{II}–edta is promoted by higher oxygen concentrations. As opposed to this, above doses of $5-6\times10^{20}$ eV g^{-1} (8–10 Mrd), no differences can be observed (within the limits of experimental error) for different gases above the solution.

Although no final conclusions can be drawn on the basis of the experiments carried out so far, the following working hypothesis can be put forward:

– in the radiolysis of aqueous Fe^{III}–edta solutions, the latter reacts with the radiolysis products of water (*e.g.* H) and is reduced to Fe^{II}–edta. If the G-value were independent of the dose, then a dose of 6×10^{19} eV g^{-1} ($\sim$ 1 Mrd) would decompose 1 g of Fe^{III}–edta in 1 litre of solution;

– from the beginning of irradiation, also such reactions take place which increase the concentration of Fe^{III}–edta by oxidizing Fe^{II}–edta according to a nearly exponential function. The existence of the latter processes is supported not only by the fact that the concentration of Fe^{III}–edta in aqueous solutions irradiated by doses higher than the above-mentioned 6×10^{19} eV g^{-1} ($\sim$ 1 Mrd) is significant (10^{-3} *M*), but also by the observation that this concentration is practically not affected by further irradiation, *i.e.* some kind of equilibrium is maintained between the two processes;

– in principle, the radiolysis of pure (dry) Fe^{III}–edta should also be taken into consideration but this proved to be negligibly small: in order to observe decomposition with certainty, doses of 2.5×10^{21} eV g^{-1} (40 Mrd) had to be applied; thus G(-Fe^{III}–edta) was lower than 0.01.

3.2. *Effect of secondary additives*

HART has shown that in the presence of formic acid, a fraction of Fe^{2+} ions is oxidized under the conditions of irradiation into Fe^{3+} [11]. If this effect occurs also in aqueous solutions of Fe^{III}–edta, formic acid ought to decrease the value of G(-Fe^{III}–edta). On addition of $0.002-0.1$ *M* formic acid to a 1 g l^{-1} (0.002 *M*) solution of Fe^{III}–edta, the curves depicted in Fig. 8 are obtained. It can be seen that whereas the decomposition of Fe^{III}–edta definitely decreases with increasing secondary additive concentrations at absorbed doses of 3.1×10^{19} eV g^{-1} (0.5 Mrd), slightly increasing G-values are observed at 6.2×10^{20} eV g^{-1} (10 Mrd). The latter phenomenon can, presumably, be attributed to the more rapid radiolysis of formic acid.

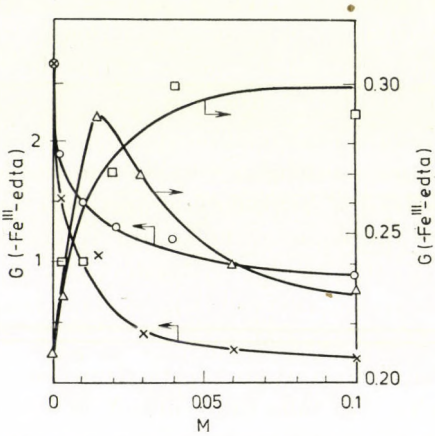

Fig. 8. Variation of G(-Fe^{III}–edta) in the presence of secondary additives

Additive	Dose	
	3.1×10^{19} eV g^{-1} = 0.5Mrd	6.2×10^{20} eV g^{-1} = 10 Mrd
Formic acid	o	□
Methanol	×	△

The effect of methanol is also shown in Fig. 8: whereas at doses of 3.1×10^{19} eV g^{-1} (0.5 Mrd) the monotonically increasing "protecting" effect of the secondary additive is apparent, the effect is not unambiguous at 6.2×10^{20} eV g^{-1} (10 Mrd) since the maximum barely exceeds the experimental error.

Without drawing far-fetched conclusions from these preliminary experiments, it can be established that the radiolysis of Fe^{III}–edta can be decreased by appropriate additives in aqueous solutions, which – if suitable systems will be developed – may improve the economics of the complexonate method.

3.3. *Effect of steel alloying elements*

If steel interacts with aqueous solutions of edta, not only iron but also the alloying metals will form edta–metal complexes. Since the only metals present in considerable amounts in stainless steel are chromium and nickel, the aqueous solutions listed in Table III were also irradiated in the presence of air. The data indicate that the presence of alloying metals decreases the G(-Fe^{III}–edta)-value since part of the radiolysis products of water reduces the Cr^{3+} and Ni^{2+} edta complexes instead to Fe^{3+} ions. As a result, competition is observed between the different metal ions.

Finally, in addition to chromium and nickel ions, the effects of formic and methanol have also been investigated in the radiolysis of Fe^{III}–edta. Preliminary experiments show that in such systems secondary additives also influence the radiolysis of the iron^{III}-edta complex.

Table III

Data on the radiolysis of Fe^{III}–edta solutions containing ions of steel alloying metals

Ratio of metal ions			Absorbed dose		Fe^{III}–edta concentration in the irradiated sample (10^{-3} *M*)	Δc Fe^{III}–edta (10^{-3} *M*)	G(–Fe^{III}– edta) (molecule per 100 eV)
Fe^{3+}	Cr^{3+}	Ni^{2+}	(10^{19} eV g^{-1})	(Mrd)			
100	–	–	3.1	0.5	2.1	1.7	2.70
80	20	–	3.1	0.5	1.8	1.0	1.56
90	–	10	3.1	0.5	1.7	1.4	2.29
70	20	10	3.1	0.5	1.3	1.1	1.78
100	–	–	62	10	1.1	2.7	0.21
80	20	–	62	10	1.0	1.8	0.15
90	–	10	62	10	0.8	2.3	0.18
70	20	10	62	10	0.6	1.8	0.15

*

The authors are indebted to Mrs. G. KEDIK (Radiation Chemistry Data Center, Notre Dame, Ind., USA) for her kind help in compiling the literature as well as to Dr. J. MINK and Mr. V. STENGER (Institute of Isotopes of the Hungarian Academy of Sciences, Budapest) for their help in the experimental work.

REFERENCES

[1] MARGULOVA, T. H.: Primenenie kompleksonov v teploenergetike. Izd. Energiya, Moscow 1973
[2] MILAYEV, A. I., TEVLIN, S. A.: At. Energ., **33,** 673 (1972)
[3] BHATTACHARYYA, S. N., KUNDU, K. P.: Int. J. Radiat. Phys. Chem., **3,** 1 (1971)
[4] NEOKLADNOVA, L. N., SILIVANCHIK, I. P., PANSEVICH, V. V.: Khim. Vys. Energ., **6,** 558 (1972)
[5] SPINKS, J. W. T., WOODS, R. J.: An Introduction to Radiation Chemistry. Wiley, New York —London—Sydney 1964
[6] MATSUURA, N., SHINOHARA, N., NISHIKAWA, M.: Bull. Chem. Soc. Japan, **41,** 1284 (1968)
[7] BHATTACHARYYA, S. N., KUNDU, K. P.: Radiat. Res., **51,** (1973)
[8] HIRLING, J., STENGER, V.: Energia és atomtechnika (in Hungarian), **22,** 446 (1969)
[9] HORVÁTH, Zs., BÁNYAI, É., FÖLDIÁK, G.: Radiochim. Acta, **13,** 150 (1970)
[10] WÉBER, M.: Thesis, Budapest 1976
[11] HART, E. I., WALSCH, P. D.: Radiation Res., **1,** 342 (1954)

Marianna WÉBER
Gábor FÖLDIÁK
Elemér KOCSIS

H-1521 Budapest.

Acta Chimica Academiae Scientiarum Hungaricae, Tomus 97 (3), pp. 265–281 (1978)

STATISTICAL APPROACH OF THE ELECTRODIC FUNCTION OF ION-SELECTIVE MEMBRANE ELECTRODES

C. LITEANU, E. HOPÎRTEAN and I. C. POPESCU

(Department of Analytical Chemistry, University of Cluj-Napoca, Cluj-Napoca, Romania)

Received January 10, 1977

The statistical treatment of the electrode function allows to estimate the following fundamental parameters: the limit value $(pc)_l$ of the linear domain, the detection limit $(\overline{pc})_d$, the determination limit $(\overline{pc})_D$ and the background concentration $(\overline{pc})_b$. The statistical estimation of the detection limit and the determination limit, by using the statistical theory of signal detection, allows the use of the electrode function in the non-linear domain, too.

Introduction

Being a component part of an analytical system, an ion-selective membrane-electrode (ISME) functions as an information system, as seen in Fig. 1.

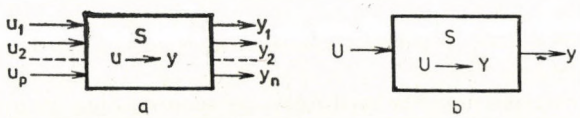

Fig. 1. Scheme of an informational system: a) separate variables; b) unified variables

Considering the transfer function, namely the correlation between the concentration of a species u_i and the corresponding signal y_k

$$y_k = f(u_i) \tag{1}$$

the total signal Y, in the case of a selectivity for a certain species i will assume the form:

$$Y = Y_0 + f(u_i) \tag{2}$$

in which Y_0, the background noise, corresponds to relation:

$$Y_0 = y_{u_1} + y_{u_2} + \ldots + y_{u_{p-1}} = f(u_1) + f(u_2) + \ldots + f(u_{p-1}) = \sum_{j=1}^{p-1} y_j \tag{3}$$

Further expression (2), *i.e.* the calibration function of an analytical system will be:

$$y = \bar{y}_0 + f(c) \tag{4}$$

where y is the analytical signal, $\bar{y}_0$ the background noise and c the concentration.

Taking into account the fact that the analytical signal is a random variable, the statistical methodology is the only efficient approach to evaluate the calibration function of an ISME:

$$E = f(pc) = E_0 + bpc \tag{5}$$

The following characteristics of the function of an ISME will be statistically treated: the limit value $(pc)_l$ of the linear domain, the detection limit $(pc)_d$, the determination limit $(pc)_D$, the background concentration $(\overline{cp})_b$ and the stability of the electrode function.

Estimating the limit value $(pc)_l$ of the linear domain [1]

Considering that the parameters of the electrode function (5) have been calculated by the least squares method, it may be admitted that the differences

$$\left| E_{\text{calc.}} - E_{\text{exp.}} \right| = \left| E_{\text{exp.}} - [E_0 + b\,(pc)_{\text{exp.}}] \right| \tag{6}$$

have a normal distribution. Accordingly, as seen in Fig. 2, the deviation from linearity will correspond to that $(pc)_l$ value for which the value $\delta_l = \left| E - [E_0 + b(pc)_l] \right|$ assumes a character of extreme value which can be eliminated based on a certain statistical criterion and considering a certain probability P.

As can be seen in Fig. 2, the δ_l value corresponds to the half-width of the confidence band limited by the two hyperbola arcs [2] in the point on the calibration straight line with the $[E_l, (pc)_l]$ coordinates. Considering now the expression of the two hyperbola arcs:

$$E = E_i \pm t_{(P,n-2)} \frac{\sqrt{SPD}\ \sqrt{S_{cc} + n\,[(pc)_i - \overline{pc}]^2}}{\sqrt{n\,(n-2)}\ \sqrt{S_{cc}}} \tag{7}$$

there results:

$$\delta_l = t_{(P,n-2)} \frac{\sqrt{SPD}\ \sqrt{S_{cc} + n\,[(pc)_l - \overline{pc}]^2}}{\sqrt{n\,(n-2)}\ \sqrt{S_{cc}}} \tag{8}$$

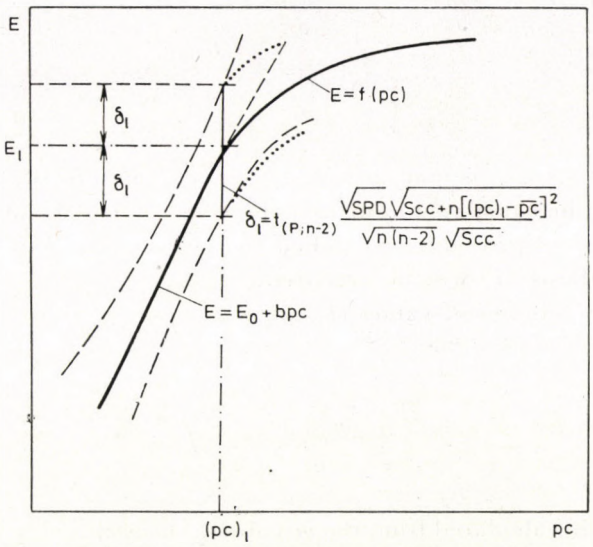

Fig. 2. Scheme of the statistical procedure for estimating the extreme value $(pc)_l$ of the linear domain [1]

In expression (7): $\overline{pc} = \left[\sum_{i-1}^{n} (pc)_i\right] \Big/ n$; $SPD = S_{yy} - bS_{cy}$;

$$S_{yy} = \sum_{i=1}^{n} E_i^2 - \left(\sum_{i=1}^{n} E_i\right)^2 \Big/ n; \quad S_{cy} = \sum_{i=1}^{n} (pc)_i E_i - \left[\sum_{i=1}^{n} (pc)_i \sum_{i=1}^{n} E_i\right] \Big/ n;$$

$$S_{cc} = \sum_{i=1}^{n} (pc)_i^2 - \left[\sum^{n} (pc)_i\right]^2 \Big/ n$$

According to Eq. (8) the estimation of the $(pc)_l$ value requires the estimation of the δ_l value. For this purpose, it is possible to use all the criteria permitting the acceptance of hypothesis $H_1 : \delta_l > \bar{\delta}$. The t criterion (Student) will be used below. Therefore, the first to be calculated are the δ values obtained from relation (6) in which the parameters of the calibration equation were calculated from n value pairs (E, pc) belonging to the linear domain.

For this purpose, the graphical representation of the (E, pc) values permits to estimate the n number of (E, pc) values having a linear correlation and which are then used to calculate the parameters of the calibration equation (5). By means of relation (6) one proceeds then to calculate the n δ values as well as the mean of δ values $(\bar{\delta})$ and standard deviation (s_δ). Further on, one verifies if the $n + 1$ experimental value belongs to the linear domain, too. For this, the value $\delta_{n+1} = |E_{n+1} - [E_0 + b(pc)_{n+1}]|$ is calculated and it is subjected to the hypothesis $H_1 : \delta_{n+1} > \bar{\delta}$, by means of the t (Student) test:

$$t = \frac{\delta_{n+1} - \bar{\delta}}{s_\delta \sqrt{\frac{n+1}{n}}} > t_{[P;\,(n+1)-2]} \tag{9}$$

If hypothesis H_1 is not accepted, the parameters of the calibration equation (5) will be calculated now from the series of $n + 1$ values (E, pc) and the above described procedure is applied to the following experimental value until the hypothesis H_1 will be accepted.

If m is the number of values (E, pc) which belong to the linear domain, the expression of δ_l will be:

$$\delta_l = \bar{\delta} + \sqrt{\frac{m+1}{m}}\, s_\delta \times t_{(P;\,m-1)} \tag{10}$$

where δ and s_δ are calculated from the m values. The $(pc)_l$ value will be estimated based on expression (8).

Considering the data listed in Table I and also Fig. 3, the linear domain has been estimated to extend up to approximately $(pc)_7 = 3.30$. From the 7 value pairs (E, pc) there results:

$$E = -72.2 + 55.7\ pc \tag{11}$$

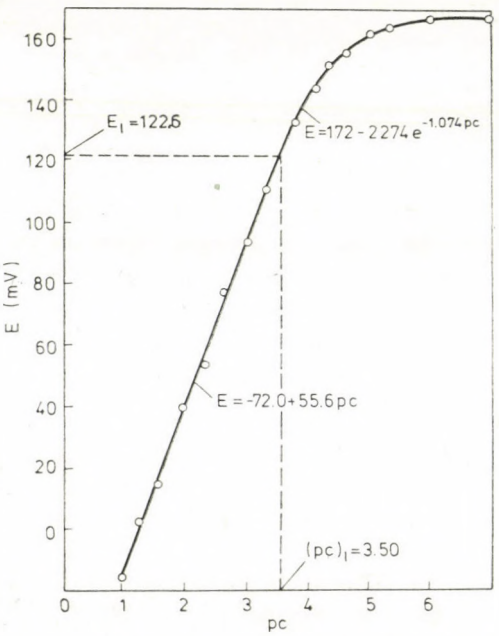

Fig. 3. Electrode function obtained by using the data from Table I

Table I

Data for the analytical electrode function (MV-85 potentiometer) obtained with a nitrate-selective membrane electrode [3]

No.	c (mol/l)	pc	E (mV)	$n = 7$	$n = 8$	$\lvert E-u\rvert / \lvert E-172\rvert$	$\log \lvert E-u\rvert / \log \lvert E-172\rvert$
1	2	3	4	5	6	7	8
1	10^{-1}	1.00	−17	0.48	0.60		
2	5.0×10^{-2}	1.30	2	2.18	1.72		
3	2.5×10^{-2}	1.60	15	1.89	1.96		
4	10^{-2}	2.00	40	0.89	0.80		
5	5.0×10^{-3}	2.30	54	1.86	1.88		
6	2.5×10^{-3}	2.60	75	2.43	2.44		
7	10^{-3}	3.00	94	0.84	0.80		
8	5.0×10^{-4}	3.30	111	0.61	0.48		
9	2.5×10^{-4}	3.60	124		4.16	48	1.681
10	10^{-4}	4.00	140			32	1.505
11	5.0×10^{-5}	4.30	151			21	1.322
12	2.5×10^{-5}	4.60	155			17	1.230
13	10^{-5}	5.00	162			10	1.000
14	5.0×10^{-6}	5.30	164			8	0.903
15	10^{-6}	6.00	167				
16	5.0×10^{-7}	6.30	166.8				
17	2.5×10^{-7}	6.60	167.2				
18	10^{-7}	7.00	167.0				

Obs. Results 1 – 14 are the mean of two measurements (±1 mV precision), approximated to upper value. Results 15 – 18 are the mean of 5 measurements

The 7δ values calculated by means of expression (6) are listed in column 5 and for them $\bar{\delta} = 1.50$ and $s_\delta = 0.62$. Since $\delta_{7+1} = 0.61 < \bar{\delta} = 1.50$ it makes no sense to consider it as an extreme value, respectively, to apply it the t test according to expression (9). Therefore, the point of co-ordinates (111, 3.30) must be included in the calculus of the parameters of the calibration equation. Thus one obtains:

$$E = -72.0 + 55.\dot{6}\ pc \qquad (12)$$

The δ values obtained on the basis of this equation are listed in column 6, and $\bar{\delta} = 1.34$ and $s_\delta = 0.72$. Since $\delta_{8+1} = 4.16$ ($E_{\text{exp}} < E_{\text{calc}}$) in agreement with expression (9) one obtains: $t = (4.16 - 1.34)/0.72\sqrt{9/8} = 3.78 > 2.37 = t_{(0.95;7)}$. In conclusion, the 9th value pair (124, 3.60) cannot be included in the calculation of the parameters of the calibration equation.

Considering $t_{(0.95;8-1)} = 2.37$ there results from expression (10), $\delta_l = 1.34 + \sqrt{9/8} \times 0.72 \times 2.37 = 3.15$ and from the 8 value pairs (E, pc) one obtains: $\overline{pc} = 2.138$; $S_{yy} = 14.3315$; $S_{cy} = 257.7$; $S_{cc} = 4.64$; $SPD = 18.9$. Since $t_{(0.95;8-2)} = 2.45$, expression (8) will have the form:

$$3.15 = 0.714 \sqrt{4.64 + 8\,[(pc)_l - 2.138]^2} \qquad (13)$$

whence $(pc)_1 = 3.50$, respectively, $c_l = 3.16 \times 10^{-4} M$ and in agreement with equation (12), $E_l = 122.6$. The results are also given in Fig. 4.

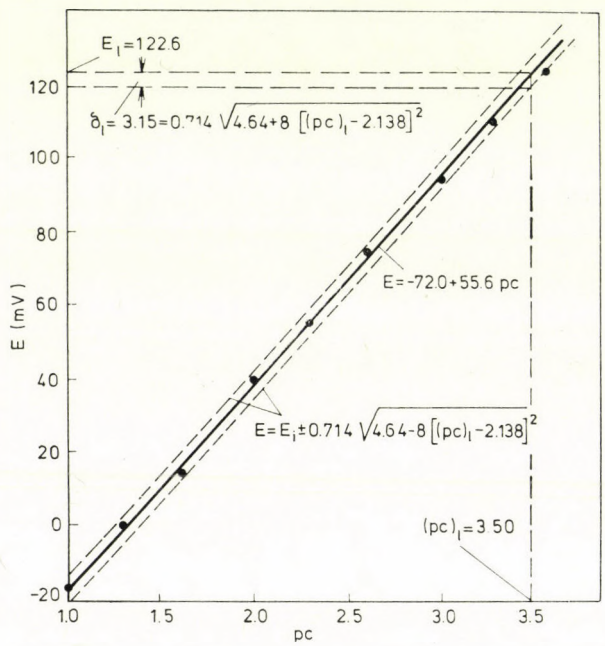

Fig. 4. Scheme of the statistical procedure for estimating the limit value $(pc)_l$ of the linear domain (data from Table I) [1]

Estimating the detection limit $(\overline{pc})_d$ [4]

To estimate this fundamental parameter, the detection limit was considered to be that *pc* value for which the *E*—*pc* correlation deviates from linearity [5] (Fig. 5a) or the value corresponding to the intersection of the prolonged linear domain with the background line [6] (Fig. 5b). It has also been suggested [7, 8] to consider as detection limit that *pc* value for which $|E_{\text{background}} - E_{\text{det.}}| =$

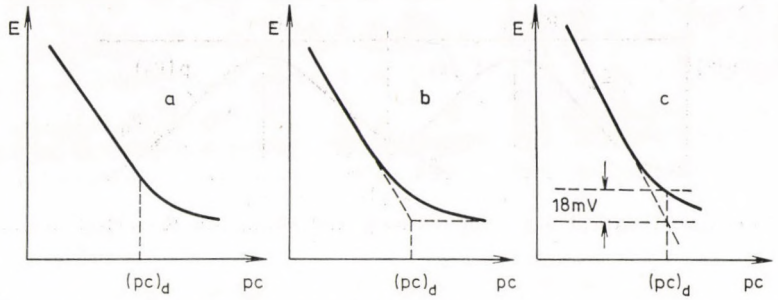

Fig. 5. Three nonstatistical approaches for ISME detection limit definition and estimation [4]

= 18 mV (Fig. 5c) which corresponds, for a monovalent ion, to the ratio $c_{\text{det.}}/c_{\text{background}} = 2$. Evidently, all these procedures for estimating the detection limit have nothing to do with the statistical theory of signal detection.

Considering the fact that the analytical signal is a random variable, it is natural to treat the problem of detection by means of the ISME potential on the basis of the statistical theory of signal detection, a theory in which the signal to background noise ratio plays the central part.

Since one of the two equiprobable alternative is eliminated in the detection process, in agreement with BRILLOUINS's formula [9] an amount of information $I_d = \log_2 P_0/P = \log_2 2/1 = 1$ bit will be obtained.

Based on such considerations, *i.e.* taking into account a certain overlapping degree of the fluctuation field of the background noise to the signal fluctuations, a correct estimation of the detection limit in the ISME case, as in fact in the case of any analytical system, must rely on a mechanism such as that presented in Fig. 6.

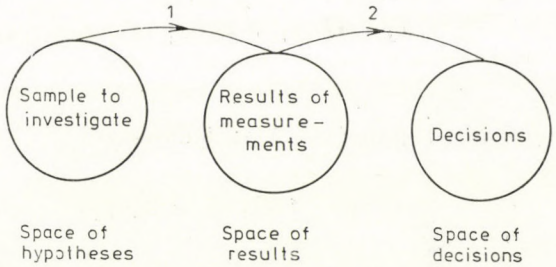

Fig. 6. Mechanism of the analytical detection process [11]

Figure 7 shows the statistical relation between the ISME signal and the background noise based on a two-step model [4, 10, 11] where for $E > (E_k)_d$ values one accepts the H_1 hypothesis, namely that the component is detected (present), hypothesis to which a false detection probability P_{10} and a true detection probability P_{11}, are associated.

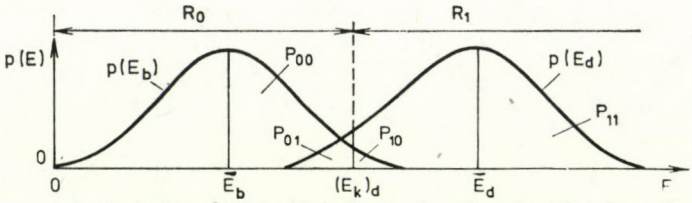

Fig. 7. Two-step statistical model for defining and estimating the detection limit [10]

Considering the expression for the false detection probability P_{10}:

$$P_{10} = \int_{(E_k)_d}^{\infty} p(E_b)dE_b \tag{14}$$

by normalization, for the $(E_k)_d$ detection level there results:

$$(E_k)_d = \bar{E}_b + (z_k)_d \, \sigma_{E_b} \tag{15}$$

in which $(z_k)_d \Rightarrow \Phi\,(z_k)_d = 0.5 - P_{10}$.

Considering the expression for the correct detection probability P_{11}:

$$P_{11} = \int_{(E_k)_d}^{\infty} p(E_d)dE_d \tag{16}$$

therefore, for the potential corresponding to the detection limit we obtain:

$$\bar{E}_d = (E_k)_d + z_d \, \sigma_{E_d} \tag{17}$$

in which $z_d \Rightarrow \Phi(z_d) = P_{11} - 0.5$.

From expressions (15) and (17) it follows:

$$\bar{E}_d = \bar{E}_b + (z_k)_d \, \sigma_{E_b} + z_d \sigma_{E_d} . \tag{18}$$

By considering the $\sigma_{E_b} \simeq \sigma_{E_d}$ approximation, for the detection signal from equation (18) one obtains:

$$\bar{E}_d = \bar{E}_b + [(z_k)_d + z_d] \, \sigma_{E_d} = \bar{E}_b + k_d \sigma_{E_d} \tag{19}$$

based on which from the calibration function (5) one obtains the $(pc)_d$ value of the detection limit.

Considering equations (15) and (17), the following relation can be written:

$$(\overline{pc})_d = f[(P_{10})_d, (P_{11})_d] \tag{20}$$

which, by analogy with the detection characteristics of a detector [12] can be termed detection characteristic of an ISME [4].

In view of estimating the detection limit, as resulted from equation (18), it is necessary on the one hand, to consider the two probabilities P_{11} and P_{10} based on which one obtains the Laplace function values $\Phi(z_k)$ and $\Phi(z_d)$, and by which we can get the z_k and z_d values by tabulation [13]. On the other hand, it is necessary to know both the mean value E_b and the standard deviation σ_{E_b} of the background as well as the standard deviation of the detection signal, σ_{E_d}.

Taking into account the fact that $\bar{E}_b \neq E_l$, to estimate the $\bar{E}_b$, σ_{E_b} and σ_{E_d} values, it is necessary to know the form of data from Table I, for values $pc > (pc)_l = 3.50$, we get:

$$E = 172 - 2274\ e^{-1.074p\cdot} \tag{21}$$

respectively:

$$\log | E - 172 | = 3.35677 - 0.4664\ pc\,. \tag{22}$$

Since for $c \leq 10^{-6}M$ the E values remain practically constant, based on the 20 value pairs (E, pc) (Table II) one obtains $\bar{E}_b = 167.0$ mV and $s_{E_b} = 0.827$.

Table II

Signal values (MV-85 potentiometer) used for the background estimation [4]

c (mol/l)	pc	E (mV)					$\bar{E}$ (mV)
10^{-6}	6.00	167	166	166	168	168	167.0
5.0×10^{-7}	6.30	166	167	166	167	167	166.8
2.5×10^{-7}	6.60	167	168	166	167	168	167.2
10^{-7}	7.00	168	166	167	166	168	167.0

Considering the true detection probability $P_{11} = 0.975$, $\Phi(z_d) = 0.975 - 0.5 = 0.475$; $z_d = 1.96$, as well as the false detection probability $P_{10} = 0.025$; $\Phi(z_k)_d = 0.5 - 0.025 = 0.475$; $(z_k)_d = 1.96$ and admitting the approximation $\sigma_{E_b} \simeq \sigma_{E_d}$, respectively $s_{E_b} \simeq s_{E_d} = 0.827$, in agreement with expression (19), there results: $\bar{E}_d = 167.8 - 3.92\times0.827 = 163.76$ mV. In conclusion, based on the calibration equation (21) the estimated value of the

detection limit will be: $(\overline{pc})'_d = 5.23$, respectively $\bar{c}'_d = 5.89 \times 10^{-6} M$. Hence, it results that the detection limit defined and estimated by the statistical theory of signal detection corresponds to a concentration of $c_l/\bar{c}'_d = 3.16 \times \times 10^{-4}/5.89 \times 10^{-6} \simeq 54$ times lower than that corresponding to the limit value of the linear domain. The result is given in Fig. 9.

Estimating the determination limit $(\overline{pc})_D$

Since in the determination process more indefiniteness is removed than in the detection process, the amount of information obtained is always $I_D > 1$ bit. In conclusion, the fluctuation field of the determination signal is again correlated to the fluctuation field of the detection signal by a two-step statistical model.

Taking into account the correlation of detection to the background noise, according to the two-step statistical model (Fig. 7), the determination limit can also be defined and estimated in the ISME case by using a four-step statistical model [14] (Fig. 8), where for $E > (E_k)_D$ values one accepts the H_1 hypothesis, namely that the signal belongs to the fluctuation field of the determination hypothesis to which a false detection probability P_{10} and a true probability P_{11} are associated.

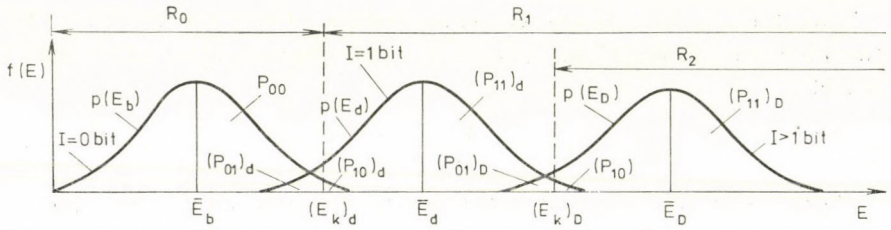

Fig. 8. Four-step statistical model for defining and estimating the determination limit [14]

Hence, considering a correct determination probability $(P_{11})_D$ and a false determination probability $(P_{10})_D$, in relation to the determination level $(E_k)_D$, proceeding in a similar manner to the detection case, one obtains:

$$\bar{E}_D = \bar{E}_d + (z_k)_D \, \sigma_{E_d} + z_D \sigma_{E_D} \tag{23}$$

an expression from which, if one considers the $\sigma_{E_d} \simeq \sigma_{E_D}$ approximation, it results:

$$\bar{E}_D = \bar{E}_d + [(z_k)_D + z_D]\sigma_{E_D} = E_d + k_D \sigma_{E_D} \tag{24}$$

From expressions (18) and (24) it follows:

$$\bar{E}_D = \bar{E}_b + k_d \sigma_{E_d} + k_D \sigma_{E_D} \tag{25}$$

so that considering the $\sigma_{E_b} \approx \sigma_{E_d} \approx \sigma_{E_D}$ approximations one obtains:

$$\bar{E}_D = \bar{E}_b + (k_d + k_D)\sigma_E \tag{26}$$

In agreement with equation (25), by analogy with the detection characteristics [12], the expression below can be written for the determination characteristics in the ISME case:

$$(\overline{pc})_D = f[(P_{10})_d, (P_{11})_d, (P_{10})_D, (P_{11})_D] \tag{27}$$

Considering $(P_{10})_D = 0.025$, $(z_k)_D = 1.96$ and $(P_{11})_D = 0.975$, $z_D = 1.96$ and since $s_{E_d} = 1.033$ and $\bar{E}'_d = 163.76$, admitting $s_{E_d} \simeq s_{E_D}$, in agreement with equation (24), $\bar{E}'_D = 159.72$ so that, based on relation (21) $(\overline{pc})'_D = 4.86$, $\bar{c}'_D = 1.38 \times 10^{-5} M$. In conclusion, the determination limit corresponds to a concentration of $c_l/\bar{c}'_D = 3.16 \times 10^{-4}/1.38 \times 10^{-5} \simeq 23$ times lower than that corresponding to the limit value of the linear domain. The result is shown in Fig. 9.

Estimating the background concentration value $(\overline{pc})_b$

This is the concentration value for which signal $E = \bar{E}_b$, and since, as was shown, $\bar{E}'_b = 167.0$ mV agreement with expression (21) one obtains $(\overline{pc})'_b = 5.70$ and $\bar{c}'_b = 2 \times 10^{-6} M$. The result is presented in Fig. 9.

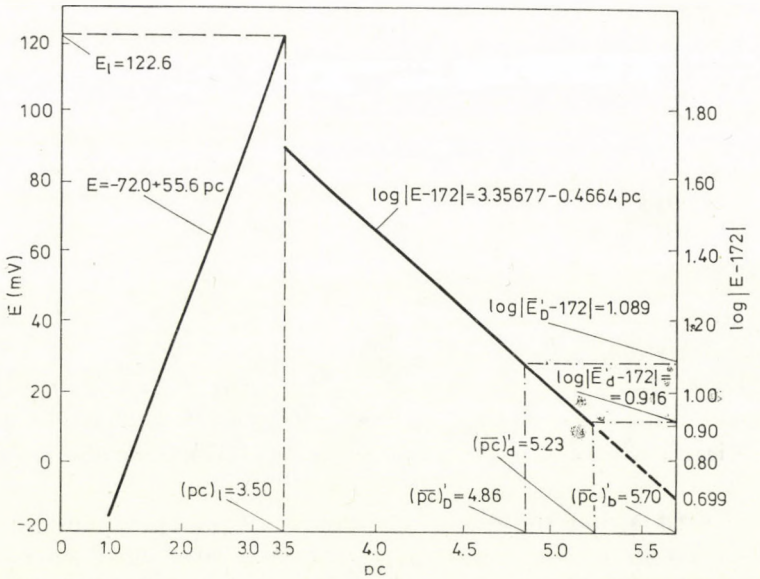

Fig. 9. Results of the statistical approach of the electrode function (data from Table I) [4]

Stability of the electrode function [15]

The functional instability of any analytical system may lead to serious analysis errors. Hence, the necessity to verify the stability in time of the parameters of the transfer function $y = f(c)$, respectively, of the calibration equation. In the case of the ISME electrode function, *i.e.* of equation (5), the stability in time will be treated by the method of serial correlation [16].

To do this, considering the value series: $y_1, y_2, \ldots, y_n$ obtained at various time intervals, the serial correlation coefficient R_h will be calculated:

$$R_h = \frac{\sum_{i=1}^{n} y_i y_{i+h} - \left(\sum_{i=1}^{n} y_i\right)^2 \Big/ n}{\sum_{i=1}^{n} y_i^2 - \left(\sum_{i=1}^{n} y_i\right)^2 \Big/ n} \tag{28}$$

in which h is the gap between the y_i values ($h = 1, 2, \ldots, n-1$).

For a sufficiently large number of E_i values normally distributed and variable, R_1 has a normal distribution [17] with parameters:

$$M(R_1) \simeq \frac{-1}{n-1} \tag{29}$$

and

$$\sigma^2_{(R_1)} \simeq \frac{n-2}{(n-1)^2} \tag{30}$$

In view of estimating the stability of the analytical system, the $R_{1(\mathrm{exp})}$ values are compared to the tabulated R values:

a) If: $R_{0.975} < R_{1(\mathrm{exp})} < R_{0.025}$, the system is stable

b) If: $R_{0.975} > R_{1(\mathrm{exp})} > R_{0.995}$ or if $R_{0.025} < R_{1(\mathrm{exp})} < R_{0.005}$, the system is of doubtful stability

c) If: $R_{1(\mathrm{exp})} < R_{0.995}$ or if $R_{1(\mathrm{exp})} > R_{0.005}$, the system is unstable.

Based on the data obtained with a liquid nitrate selective electrode [15], for the series of $i = 13$ E values, corresponding to b, one obtains $R_{1(\mathrm{exp})} = -0.225$ so that, since $R_{0.975} = -0.417 < R_{1(\mathrm{exp})} < 0.341 = R_{0.025}$, the conclusions reached is that the system is stable from the standpoint of the slope of the electrode function. This is observed in Fig. 10 c which shows that the oscillations of b values are less frequent and more reduced in amplitude.

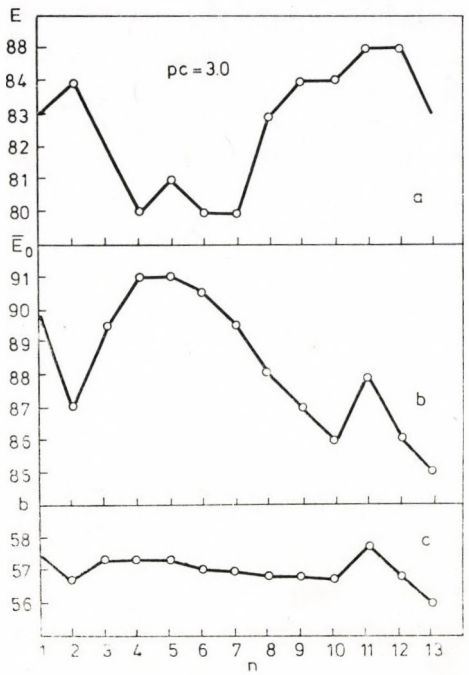

Fig. 10. Time stability of the electrode function [15]

Conclusions

The statistical treatment of the electrode function, apart from estimating the most probable values of the parameters of the calibration equation (5) by the least-squares method, is apt not only to largely extend the ISME utilization possibilities but also to permit the estimation of new functional parameters. Thus, the limit value of the linear domain, $(pc)_l$, the detection limit $(\overline{pc})_d$, the determination limit $(\overline{pc})_D$, the background concentration $(\overline{pc})_b$, the stability of the electrode function, represent the fundamental characteristics of the electrode function. The statistical estimation of the detection and the determination limit, allows the extension of the ISME utilization domain and enables an analytical use of the non-linear domain of the ISME electrode function as well. The stability of the electrode function was treated statistically by the method of serial correlation.

REFERENCES

[1] Liteanu, C., Popescu, I. C., Hopîrtean, E.: Anal. Chem., **48**, 2010 (1976)
[2] Acton, F. S.: Analysis of Straight-Line Data, J. Wiley, New York 1959, p. 34
[3] Hopîrtean, E., Stefănigă, E., Liteanu, C., Gusan, I.: Rev. Chim., **27**, 346 (1976)
[4] Liteanu, C., Hopîrtean, E., Popescu, I. C.: Anal. Chem., **48**, 2013 (1976)

[5] MOODY, C. J., THOMAS, J. D. R.: Selective Ion Sensitive Electrodes, Merrow, Watford 1971, p. 5
[6] WOODSON, J. H., LIEBHAFSKY, H. H.: Anal. Chem., **41**, 1894 (1969)
[7] FRANT, M. S.: Cron. Chim., (44), 3 (1974)
[8] IUPAC, Information Bulletin No. 43 (1975), p. 2, Recommendations for Nomenclature of Ion-Selective Electrodes
[9] BRILLOUIN, L.: Scientific Uncertainty and Information, Academic Press, New York 1964, p. 27
[10] LITEANU, C., RÎCĂ, I.: Mikrochim. Acta [Wien], 745 (1973)
[11] LITEANU, C., RÎCĂ, I.: Pure Appl. Chem., **44**, 535 (1975)
[12] LITEANU, C., RÎCĂ, I.: Mikrochim. Acta [Wien], 591 (1975)
[13] LARK, P. D., VRAVEN, B. R., BOSWORTH, R. C. L.: The Handling of Chemical Data, Pergamon Press, Oxford 1969, p. 335
[14] LITEANU, C., HOPÎRTEAN, E., RÎCĂ, I.: in press
[15] LITEANU, C., HOPÎRTEAN, E.: Z. Anal. Chem., **288**, 59 (1977)
[16] BENNET, C. A., FRANKLIN, N. L.: Statistical Analysis in Chemistry and the Chemical Industry, J. Wiley, New York 1954, p. 684
[17] ANDERSON, R. L.: Ann. Meth. Stat., **13**, 1 (1942)

C. LITEANU,
E. HOPÎRTEAN
I. C. POPESCU
Department of Analytical Chemistry, University of Cluj-Napoca
3400 Cluj-Napoca, Romania.

A comment on "Statistical approach of the electrodic function" by LITEANU

G. E. VERESS

In their paper LITEANU *et al.* [1] have studied one of the most important problems of the data processing, *i.e.* the determination of the limit value of the linear domain for electrode functions. The purpose of this note is to call attention to their disputable approach.

Using the author's notations, they introduce the calibration function of an electrode function

$$E = E_0 + b(pc)$$

and the deviations of the measured points $\{E_i, (pc)_i\}$ from the calibration function

$$\delta_i = |E_i - [E_0 + b(pc)_i]| \qquad i = 1, \ldots, N.$$

It is assumed that the points $i = 1, \ldots, n$ belong to the linear domain and based on these points we can calculate the parameters of the calibration function by means of the least squares method. Having these parameters, the deviations $\delta_1, \ldots, \delta_n$ can be calculated, and their average and standard deviation, too.

The authors disputable statement is the following: the $(n + 1)$th point belongs to the linear domain, if the hypothesis $H_1 : \delta_{n+1} > \bar{\delta}$ is rejected by means of the t (Student)-test, where the statistics t is the following:

$$t = \frac{\delta_{n+1} - \bar{\delta}}{s_\delta} \sqrt{\frac{n}{n+1}}$$

The author's approach seems to be inefficient. Namely, on the one hand, their approach is based only on the value δ_{n+1}, that is, only one on measured point, so it is very slight from the point of view of statistics, and on the other hand, their approach is not based on the fact that there is a relationship among the measured points, so it should be based on the (non-linear, monotonous) trend of the measured points.

The application of the t-test seems to be inadequate, because neglecting the problem of absolute value, the author's t-test can be regarded as a special case of a two-sample t-test, where one sample has only one element. Even if the author's t-test is admitted, one point will be approximately outlying only if the inequality

$$\frac{\delta_{n+1} - \bar{\delta}}{\bar{\delta}} > 2 \frac{s_\delta}{\bar{\delta}}$$

holds, but this occured only by very strong nonlinearity.

The purpose of this paper is not to solve the above problem, but only direct the attention on that the determination of the limit value of the linear domain which should be based on the trend of the deviations $\delta_{n+1}, \ldots, \delta_{n+k}$, where $k > 1$, so the statistical principles and approaches used for the time series analysis should be applied for solving this problem (see *e.g.* [2]).

REFERENCES

[1] Liteanu, C., Hopîrtean, E., Popescu, I. C.: Statistical Approach of the Electrodic Function of Ion-selective Membrane Electrodes, Acta Chim. Acad. Sci. Hung. **97**, 265 (1978)

[2] Ashis Sen, Srivastava, M. S.: Some One-Sided Tests for Change in Level, Technometrics, **17** (1), 61—64 (1975)

Gábor E. Veress H-1521 Budapest.

ANSWER, to the comment on the paper "Statistical processing of the electrodic function" by G. E. Veress

C. Liteanu, E. Hopîrtean, J. C. Popescu

It is the case only of the procedure for the calculation of the limit value of the linear domain, procedure which is mentioned at the bibliography [1] [C. Liteanu, I. C. Popescu, E. Hopîrtean, Anal. Chem., **48**, 2010 (1976)], paper which is annexed and which describes in detail the procedure.

a) Before to formulate the hypothesis $H_1 : \delta_{n+1} > \bar{\delta}$, one examinates the figure $E = f(pc)$; figure reveals that the linear domain is extended up to about $pc = a$. This value is not used yet to calculate the parameters of the calibration equation.

Therefore, the departure from the value δ_{n+1}, is based on the examination of the figure $E = f(pc)$, namely the point $n + 1$, is supposed to be removable, considering its graphycal position.

For example, let us consider only the first 5 pairs of points E, pc (columns 4 and 3). Using the least square method one obtains: $E = -70.77 + 54.62\ pc$, respectively: $\delta_1 = 0.85$, $\delta_2 = 1.76$, $\delta_3 = 1.62$, $\delta_4 = 1.53$, $\delta_5 = 0.86$, respectively, $\delta_6 = 3.76$ are obtained. Further on from the first five δ values results $\bar{\delta} = 1.32$ and $s_\delta = 0.436$ so that for $\delta_6 = 3.76$:

$$t = \frac{3.76 - 1.32}{0.436 \sqrt{6/5}} = 5.11 > 2.78 = t_{(0.95;4)} \text{ is obtained.}$$

So that in this case point 6 ($E = 75$ mV, $pc = 2.60$) does not belong to the statistic population of the first five points, that is, it s h o u l d b e l o n g t o t h e n o n - l i n e a r r e g i o n.

b) Starting from the first five points, let us examine now the situation of point 7 ($E = 94$ mV, $pc = 3.00$) for which according to the equation calculated for these five points: $E = 70.77 + 54.62\ pc$ and $\delta_7 = 0.91$.

We obtain:

$$t = \frac{1.32 - 0.91}{0.436 \sqrt{6/5}} = 0.86 < 2.78 = t_{(0.95;4)}$$

Consequently the point 7 belongs from the statistic point of view to the first five point groups, consequently it b e l o n g s t o t h e l i n e a r r e g i o n. Then point $n-1$, that is $7-1 = 6$, also belongs to the linear region.

In conclusion, it is necessary to examinate the figure $E = f(pc)$, before to formulate the hypothesis H_1: $\delta_{n+1} > \bar{\delta}$.

Therefore, considering the fluctuations field of the δ values from the linear domain, there is the possibility that the expression having the form (9) (V. V. NALIMOV, "Primenenie matematicheskoi statistiki pri analize veschestva", Gos. izd. fiz-mat. lit, Moskov, 1960, p. 172), namely,

$$t = \frac{\delta_i - \bar{\delta}}{s_\delta \sqrt{\frac{n+1}{n}}} t_{(P;\, n-2)}$$

to be valid for δ values from the begining of the linear domain, too. It is evident that hypothesis H_1: $\delta_{n+1} > \bar{\delta}$, that is an expression of the type (9),

to be verified successively only for δ values which result from $E-pc$ values from the linear regression domain, $E = f(pc)$, which connects with the non-linear regression range $E = f(pc)$.

Considering this situation, as well as the fact that from expressions (9) and (10) it results that always $\delta_l < \delta_{n+1}$, one considers that the procedure presented, which is based on the t-test is justified.

Concerning the inequality $\frac{\delta_{n+1} - \bar{\delta}}{\bar{\delta}} > 2\frac{s\delta}{\bar{\delta}}$, namely $\delta_{n+1} - \delta > 2s_\delta$, the value δ_{n+1}, would be "eliminable approximately", if $\delta_{n+1} > \bar{\delta} + 2s_\delta$. Since it is the case of a sampling (selection) one operates with s_δ^2 not with σ_δ^2, the value δ_{n+1}, would be eliminable approximately, based on the t distribution, therefore only if $\delta_{n+1} > \bar{\delta} + t_{[P=0.95;\,(n+1)-1]} \cdot s_\delta$.

It was considered $P = 0.95$ because for $z = 2$, $P = 0.9545$ [z = standard normal deviate: $\Phi(z) = f(P)$].

Acta Chimica Academiae Scientiarum Hungaricae, Tomus 97 (3), pp. 283–297 (1978)

STUDY OF ION-SOLVENT INTERACTIONS IN ALCOHOL–HYDROGEN CHLORIDE SYSTEMS

F. RATKOVICS and K. BARATI-DÉSI

(Department of Physical Chemistry, Chemical Industry University, Veszprém)

Received April, 10 1977

The e. m. f. of the $Pt/H_{2(gas)}/HCl$-alcohol/Hg_2Cl_2/Hg electrode system was investigated in the temperature range 20 – 40 °C. The normal potential of the alcoholic calomel electrode was determined in methanol, ethanol, 1-propanol and 1-butanol. A study was made of the concentration dependence of the mean ion activity coefficient at concentrations above the range of validity of the DEBYE – HÜCKEL theory. It was found that the deviations from this theory can be interpreted by the assumption of the strong interaction of the ions and the solvent. The interaction between the ions and the solvent increases with the increase of the molecular weight of the solvent. This phenomenon also provides an explanation for the finding that the solubility of gaseous hydrogen chloride in the alcohols increases considerably with the increase of the molecular weight of the alcohol.

In connection with investigations of alcohols and alcohol-containing liquid mixtures, we have studied the ion–solvent interaction in a higher range of ion concentrations than usual, *i.e.* considerably beyong the limits of validity of the DEBYE-HÜCKEL theory. A number of authors [1–5] have dealt with the question, approaching the problems from the aspect of the ion activity, but the data to be found in the literature mainly relate only to methanol and ethanol, and generally, to only one temperature in each case. Accordingly, we have carried out studies in systems of hydrogen chloride with methanol, ethanol, 1-propanol and *n*-butanol in the temperature range 20 – 40 °C.

Experimental

The alcohols used for the measurements were of analytical purity, and were carefully freed from water. The alcohol–hydrogen chloride mixtures were prepared in the apparatus shown in Fig. 1, by introducing dry hydrogen chloride into the alcohol. The concentration of the mixture was determined afterwards by titration with 0.1 or 0.01 *N* NaOH. Before being passed into the alcohol, the gaseous HCl was flushed out of a concentrated aqueous hydrochloric acid solution by a stream of nitrogen, purified by passage through sulfuric acid and then over silica gel, and finally, freed from water.

The alcohol–hydrogen chloride mixture prepared in this way was placed in the cell illustrated in Fig. 2, and was examined by measuring the potential difference between a $Pt/H_{2(g)}$ and a calomel electrode. The partial pressure of hydrogen was 1 atm. In every measurement the calomel electrode was filled with the electrolyte to be examined. A Radelkis type OP-205 Precision pH-meter was used for the measurements.

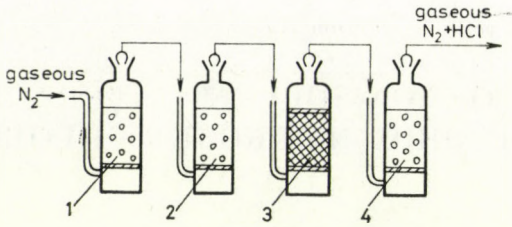

Fig. 1. Preparation of anhydrous alcohol–hydrogen chloride mixture; (1) aqueous HCl, (2) 80 % H_2SO_4, (3) silica gel, (4) anhydrous alcohol–hydrogen chloride

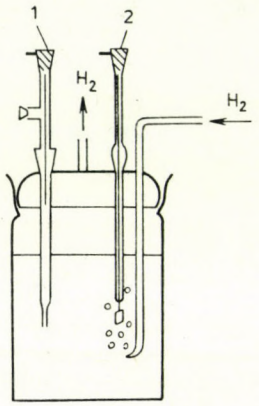

Fig. 2. The measuring cell

The measuring cell was placed in an ultrathermostat and the introduction of H_2 was begun. After the establishment of thermal equilibrium the e. m. f. was measured; then, a sample was taken from the alcohol–hydrogen chloride solution and its HCl concentration was determined by titration with 0.1 or 0.01 *N* NaOH solution. It was necessary for the analysis to be performed at the end as the prolonged bubbling of H_2 to the hydrogen electrode slightly, but perceptibly, carried off HCl from the solution.

Results

The e.m.f. of the cell was determined at 20, 25, 30 and 40 °C in mixtures of hydrogen chloride with methanol, ethanol, 1-propanol and 1-butanol. The concentration of hydrogen chloride in the examined mixtures varied from 0 to 1 *M*. The experimental results are listed in Tables I – IV.

Discussion

The diffusion potential arising between the calomel-saturated alcoholic hydrogen chloride solution and the calomel-free solution was disregarded in the evaluation of the experimental results [6]. We feel that this neglect does not affect the essence of our conclusions.

Table I

E. m. f. of the $Pt/H_{2(gas,\ 1\ atm)}$–methanol HCl (c)–calomel cell

C (mol/dm³)	E.m.f. (mV)			
	20 °C	25 °C	30 °C	40 °C
0.934	121.0	119.5	116.0	110.5
0.690	134.5	130.5	127.5	12.05
0.467	148.0	144.0	142.0	140.5
0.233	167.5	163.5	161.0	154.5
0.140	181.5	178.5	175.0	169.5
0.093	194.5	191.5	188.5	183.0
0.069	210.5	207.5	204.0	199.0
0.047	212.5	209.0	206.5	200.5
0.023	252.5	250.0	247.0	242.0
0.019	252.0	250.0	248.0	243.0
0.014	266.0	259.0	255.5	252.0
0.009	289.5	284.5	287.0	284.5
0.008	283.0	282.0	281.0	278.5
0.007	300.0	298.0	296.0	292.0
0.004	319.5	317.0	313.5	310.5
0.002	346.0	345.5	345.0	343.5
0.0008	401.0	399.5	398.5	397.0

The e. m. f. of the measuring cell is:

$$\text{e. m. f.} = E_{cal} - E_{H_2} \tag{1}$$

where, in the case of the use of gaseous H_2 at a pressure of 1 atm:

$$E_{H_2} = \frac{RT}{zF} \ln [H^+] \gamma \tag{2}$$

and

$$E_{cal} = E^\circ_{cal} - \frac{RT}{zF} \ln [Cl^-] \gamma \tag{3}$$

where the E values are the electrode potentials, E°_{cal} is the normal potential of the calomel electrode, γ is the mean ion activity coefficient, $[H^+]$ and $[Cl^-]$ are the concentrations of the ions, and RT and zF are the well-known quantities of the Nernst Law.

Assuming that, in the concentration range in question and in the given medium, hydrogen chloride is present completely in the dissociated state,

Table II

E. m. f. of the $Pt/H_{2(gas,\ 1\ atm)}$*–ethanol HCl (c)–calomel cell*

C (mol/dm³)	E.m.f. (mV)			
	20 °C	25 °C	30 °C	40 °C
0.704	111.0	108.5	106.5	101.0
0.524	113.0	111.0	106.5	101.5
0.382	117.5	115.5	113.0	108.0
0.234	139.5	137.0	134.5	128.5
0.215	131.0	128.5	126.0	121.5
0.196	144.0	142.0	139.0	133.0
0.115	174.0	171.5	169.0	165.0
0.082	150.0	148.0	145.5	142.0
0.080	156.5	155.0	153.0	148.0
0.070	183.0	179.5	177.0	170.0
0.052	180.5	179.0	175.0	170.0
0.027	169.5	193.5	189.0	183.0
0.025	194.0	192.0	190.5	185.5
0.014	212.0	211.0	208.5	204.0
0.012	215.5	213.0	210.5	204.5
0.007	249.0	247.5	244.5	239.5
0.005	250.0	247.5	246.5	241.5
0.003	264.0	262.5	261.5	257.5
0.002	292.0	289.5	286.5	282.0
0.0009	328.0	325.0	322.0	316.0

the hydrogen chloride concentration (c) of the solution will be the same as the concentration of the chloride or hydrogen ions.

$$c = [H^+] = [Cl^-]$$

Using this:

$$\text{e.m.f.} = E^{\circ}_{cal} - 2\frac{RT}{zF}\ln c\gamma \qquad (4)$$

In the range of validity of the DEBYE – HÜCKEL theory, the activity coefficient can be calculated in the knowledge of the ionic strength and the dielectric constant of the solvent. Thus, in the case of an electrolyte consisting of univalent ions, if the ionic strength is defined by the correlation

$$I = c$$

Table III

E. m. f. of the $Pt/H_{2(gas,\ 1\ atm)}$*-propanol HCl (c)–calomel cell*

C (mol/dm³)	E.m.f. (mV)			
	20 °C	25 °C	30 °C	40 °C
1.144	66.5	64.0	62.5	58.0
1.025	58.5	57.5	56.5	52.5
0.650	66.5	64.5	63.0	61.0
0.549	71.0	69.5	68.0	66.0
0.377	78.0	77.0	76.0	72.0
0.226	94.5	93.0	91.5	89.0
0.137	108.5	107.0	105.0	101.0
0.076	118.0	117.0	116.0	113.0
0.053	103.0	128.5	126.5	122.5
0.030	153.5	152.0	150.0	143.5
0.017	167.5	164.0	162.0	157.0
0.009	192.5	192.0	192.0	189.5
0.008	185.5	184.0	182.5	179.0
0.005	220.0	218.0	216.0	211.0
0.004	220.0	219.0	218.5	215.5
0.002	244.0	243.0	243.0	242.5
0.001	252.0	250.5	249.0	245.5
0.0004	315.0	313.0	311.0	306.5

the definition I = 2c is less frequent in the literature [3]), the theory leads to the relation

$$\log \gamma_D = - A\sqrt{c} \tag{5}$$

where γ_D is the mean ion activity coefficient that can be calculated from the DEBYE – HÜCKEL theory:

$$A = \frac{1.8246 \times 10^6}{(\varepsilon T)^{3/2}}$$

where ε is the dielectric constant of the solvent and T is the absolute temperature.

The actual activity coefficient may be resolved into the product of two factors. Let

$$\gamma = \gamma_D \gamma^* \tag{6}$$

Table IV

E. m. f. of the $Pt/H_{2(gas,\ 1\ atm)}$*l–1-butanol HCl (c)–calomel cell*

C (mol/dm³)	E.m.f. (mV)			
	20 °C	25 °C	30 °C	40 °C
0.640	87.0	85.0	83.5	77.0
0.380	84.0	83.0	84.5	84.5
0.260	88.5	87.0	86.0	82.5
0.200	98.0	97.0	94.0	92.0
0.160	104.0	103.0	102.5	98.5
0.130	117.0	115.0	115.0	111.0
0.096	129.0	127.5	125.5	121.0
0.070	153.5	151.0	149.5	143.0
0.060	145.0	143.0	139.5	134.5
0.040	152.0	150.5	148.0	146.5
0.022	158.0	157.0	156.5	151.5
0.021	175.5	174.5	173.0	169.0
0.017	188.0	185.5	183.5	179.5
0.013	161.5	160.0	158.0	153.0
0.009	192.0	191.0	189.0	184.0
0.008	197.0	195.5	192.5	188.0
0.006	200.0	200.5	199.5	197.0
0.004	220.0	217.0	214.5	215.5
0.002	245.5	245.5	243.0	235.0
0.0008	267.5	272.0	270.0	263.5
0.0005	294.5	299.0	310.0	303.0

where γ^* shows the deviation from the theoretical value. Utilizing this and taking logarithms to the base 10:

$$\text{e. m. f.} = E^{\circ}_{\text{cal}} - 2\frac{RT}{zF}\,2.303\left[\log c + \log \gamma^* - A\sqrt{c}\right] \tag{7}$$

It can be seen from this relation that if the e. m. f. is plotted as a function of $-(\log c - A\,.\,\sqrt{c})$, a curve is obtained which, in the range of dilute solutions for which the DEBYE–HÜCKEL theory holds, approximates to a straight line of slope 4.606 RT/zF intercepting the ordinate at the point E°.

Our results were plotted in accordance with this (Figs 3–6) and the normal potential of the calomel electrode was determined by extrapolation to the e. m. f. value relating to the abscissa value $-(\log c - A.\sqrt{c}) = 0$. The evaluation is facilitated by the fact that the slope of the straight line used for extrapolation is known to be 4.606 RT/zF. The results are given in Table 5.

Table V

E°_{cal} as a function of temperature in various alcohol–hydrogen chloride systems

Solvent	E°_{cal} (mV)			
	20 °C	25 °C	30 °C	40 °C
Methanol	25	13	9	0
Ethanol	−39	−49	−55	−64
1-Propanol	−89	−103	−107	−113
1-Butanol	−99	−108	−116	−122

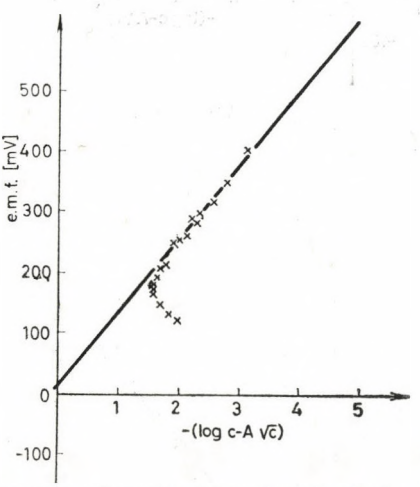

Fig. 3. Experimental results in methanol solution at 25 °C

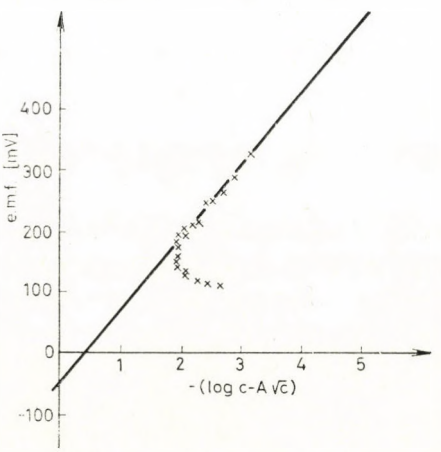

Fig. 4. Experimental results in ethanol solution at 25 °C

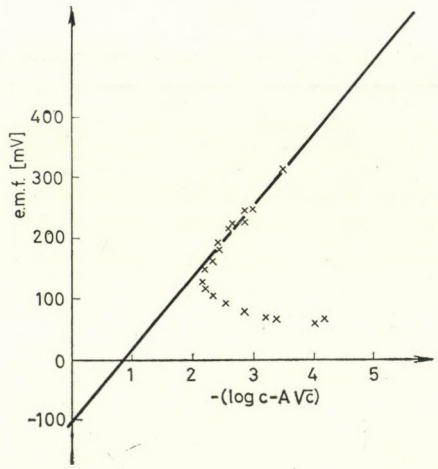

Fig. 5. Experimental results in 1-propanol solution at 25 °C

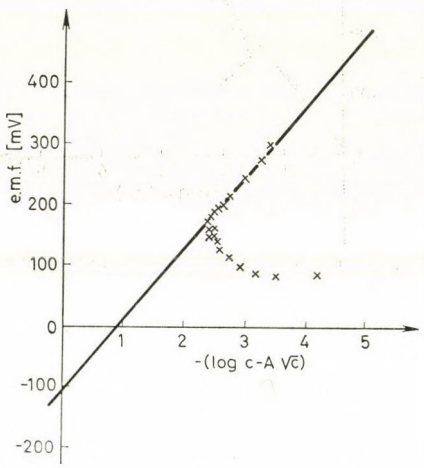

Fig. 6. Experimental results in 1-butanol solution at 25 °C

It can be seen that the normal potential of the calomel electrode depends appreciably on the nature of the solvent, and varies to only a slight extent as a function of the temperature (Fig. 7).

In the knowledge of the normal potential, we calculated some thermodynamic characteristics of the reaction $1/2\ H_{2(gas)} + 1/2\ Hg_2Cl_{2(solid)} \rightarrow \rightarrow H_{(liquid)} + HCl_{(dissolved)}$. These data are listed in Table VI.

It can be seen from the data of the Table that with the increase of the molecular weight of the solvent the absolute value of ΔS° increases slightly,

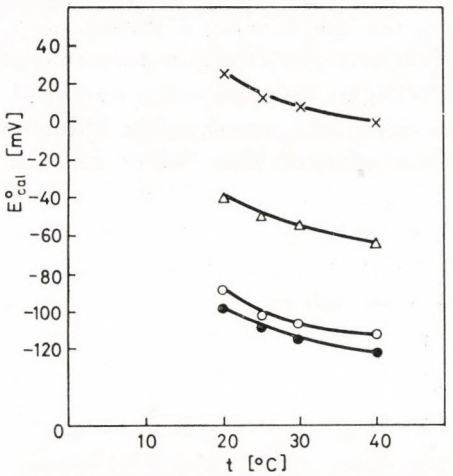

Fig. 7. Normal potential of the calomel electrode as a function of the temperature; × in methanol, △ in ethanol, ○ in 1-propanol, ● in 1-butanol

Table VI

Standard thermodynamic characteristics of the reaction $1/2\ H_{2(gas)} + 1/2\ Hg_2Cl_{2(solid)} \rightarrow Hgl_{(liquid)} + HC_{(dissolved)}$ *at 25 °C*

Solvent	$\Delta G°$		$\Delta S°$		$\Delta H°$	
	(J/mol)	(cal/mol)	(J/mol K)	(cal/mol K)	(J/mol)	(cal/mol)
Methanol	−1254.4	−299.8	−134.2	−32.1	−41246.0	−9865.6
Ethanol	4728.2	1130.0	−152.3	−36.4	−40649.9	−9717.2
1-Propanol	9939.8	2375.4	−162.6	−38.9	−38516.0	−9216.8
1-Butanol	10432.0	2490.7	−162.8	−38.9	−38082.0	−9101.5

and in every case $-T\Delta S°$ makes a positive contribution to the standard-free enthalpy of the reaction. The value of $\Delta H°$ is negative in every solvent, and its absolute value decreases to a slight extent with the increase of the molecular weight of the solvent.

Since both changes result in the increase of the standard free enthalpy, the value of $\Delta G°$ rises very rapidly with the increase in the molecular weight of the solvent. The equilibrium constant of the reaction in question is very small in the higher alcohol homologues.

The quantity γ^* in Eq. (6) deserves special attention, because it involves those effects not taken into consideration by the DEBYE–HÜCKEL theory.

Figure 8 presents the values of log γ^* measured at 25° as a function of the concentration in various systems. It can be seen that at a fixed concentration log γ is the larger, the higher the molecular weight of the solvent.

Figure 9 shows the results measured in 1-propanol as a function of the temperature. As the temperature rises, log γ^* decreases. Its value is positive everywhere in the examined cases. As concerns deviations from the ideal behaviour, therefore, in the reference system with the infinitely dilute solution regarded as ideal (asymmetric reference system), the ions form a of solution positive deviation with the alcohol.

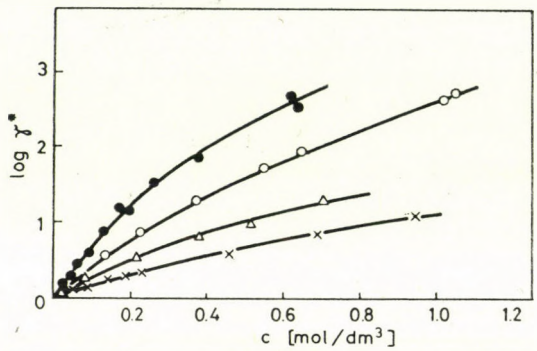

Fig. 8. log γ^* as a function of the hydrogen chloride concentration at 25 °C; × in methanol, △ in ethanol, ○ in 1-propanol, ● 1-butanol

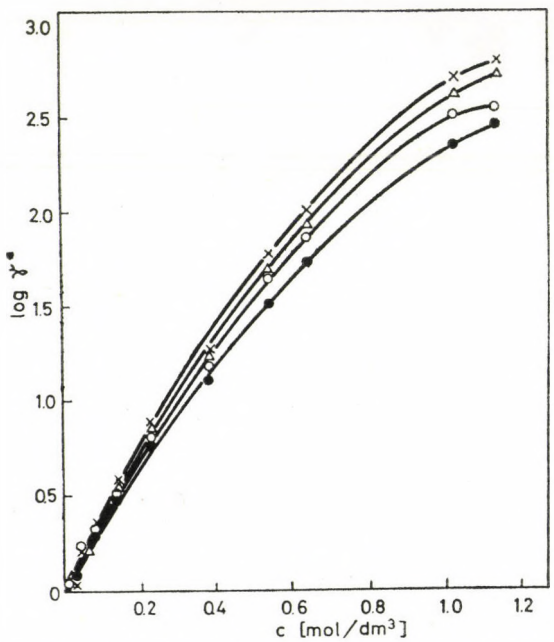

Fig. 9. log γ^* as a function of the hydrogen chloride concentration in 1-propanol; × at 20 °C, △ at 25 °C, ○ at 30 °C, ● at 40 °C

Table VII

log γ^* as a function of concentration and temperature in methanol solution

C (mol/dm³)	log γ^*			
	20 °C	25 °C	30 °C	40 °C
0.934	1.16	1.09	1.03	0.94
0.690	0.89	0.86	0.85	0.74
0.467	0.65	0.60	0.57	0.47
0.233	0.37	0.33	0.31	0.28
0.140	0.25	0.21	0.20	0.19
0.093	0.18	0.14	0.13	0.12
0.069	0.23	0.20	0.20	0.185
0.047	0.13	0.11	0.11	0.11
0.023	0.04	0.03	0.03	0.02
0.019	0.15	0.13	0.13	0.14
0.014	0.02	0.02	0.03	0.02
0.009	0.08	0.06	0.09	0.09
0.008	0.03	0.03	0.03	0.02
0.004	0.01	0.00	0.03	0.04
0.0008	0.00	0.02	0.00	0.03

The log γ^* *vs.* c data are listed in Tables VII – X. The activity coefficient γ^* takes into account the effects attributable to the mutual influence of ions arising from interactions other than those of the ionic charges (these are not taken into consideration by the DEBYE – HÜCKEL theory). It, therefore, appeared reasonable to interpret the concentration dependence of γ^* not in terms of the asymmetric activity convention used in electrochemistry, but by the symmetric activity convention used much more widely in the thermodynamic treatment of mixtures. In this latter reference system the activity coefficient of the pure component is unity, and a positive value of log γ^* means a negative deviation from ideality, for

$$\gamma^* = \frac{\gamma^\circ}{\gamma^{\circ\infty}}$$

where γ° is the activity coefficient written in accordance with the symmetric convention, while $\gamma^{\circ\infty}$ is the same in the infinitely dilute solution. Use of the symmetric activity convention has the advantage that empirical or semiempirical relations describing the dependence of $\ln \gamma^\circ$ on the concentration (mole fraction) are available in large numbers. An example is the relation $\ln \gamma^\circ = B(1 - x)^2$, which can be derived for regular mixtures, but which can also be employed as a semiempirical relation for non-regular mixtures too.

Table VIII

log γ^* as a function of concentration and temperature in ethanol solution

C (mol/dm³)	log γ^*			
	20 °C	25 °C	30 °C	40 °C
0.704	1.40	1.29	1.23	1.11
0.524	1.07	0.98	0.95	0.84
0.382	0.94	0.86	0.82	0.72
0.215	0.60	0.54	0.51	0.43
0.196	0.39	0.34	0.30	0.27
0.115	0.13	0.07	0.06	0.02
0.082	0.32	0.26	0.25	0.21
0.080	0.26	0.20	0.18	0.15
0.070	0.03	0.01	0.01	0.02
0.052	0.08	0.02	0.02	0.02
0.027	0.02	0.01	0.02	0.04
0.025	0.06	0.03	0.01	0.02
0.014	0.05	0.01	0.01	0.02
0.012	0.06	0.03	0.03	0.05
0.005	0.01	0.00	0.01	0.00
0.003	0.05	0.03	0.03	0.04
0.002	0.02	0.01	0.04	0.06
0.0009	0.06	0.05	0.00	0.01

The constant in the equation gives information on the magnitude of the intermolecular interactions, as it determines the apparent value of the exchange energy ($\triangle U^\circ$) (defined in the theory of regular mixtures) characteristic of the mixture:

$$B = \ln \gamma^{\circ\infty} = \frac{\Delta U^\circ}{RT}$$

since, in the sense of the foregoing, $\ln \gamma^* = \ln \gamma^\circ - \ln \gamma^{\circ\infty}$

$$\ln \gamma^* = B(1 - x)^2 - B$$

It can be seen that, to a first approximation, $\ln \gamma^*$ and $\ln \gamma^\circ$ are both linear functions of $(1 - x)^2$, where x is the mole fraction of the ions. Our results in this plot are presented in Fig. 10.

It can be seen in the Figure that the deviation from ideality increases considerably with the increase of the molecular weight of the solvent. According to the symmetric activity convention, the mixture displays a negative deviation

Table IX

log γ^* as a function of concentration and temperature in 1-propanol solution

C (mol/dm³)	log γ^*			
	20 °C	25 °C	30 °C	40 °C
1.144	2.79	2.74	2.55	2.47
1.025	2.71	2.63	2.52	2.36
0.650	1.98	1.94	1.87	1.73
0.549	1.76	1.73	1.66	1.52
0.377	1.26	1.27	1.19	1.10
0.226	0.88	0.86	0.83	0.77
0.137	0.55	0.56	0.53	0.48
0.076	0.35	0.36	0.33	0.31
0.053	0.21	0.22	0.23	0.22
0.030	0.05	0.05	0.05	0.06
0.017	0.06	0.05	0.05	0.06
0.009	0.08	0.08	0.10	0.04
0.008	0.06	0.05	0.10	0.06
0.001	0.03	0.03	0.02	0.10

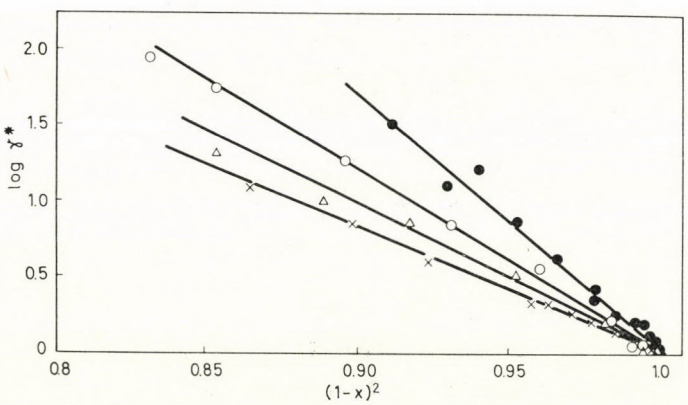

Fig. 10. log γ^* as a function of the square of the alcohol mole fraction at 25 °C; × in methanol, △ in ethanol, ○ in 1-propanol, ● in 1-butanol

from ideality. The interaction between the ions and the solvent molecules is increasingly stronger with the increase of the molecular weight of the alcohol. The value of B, characteristic of the strength of the interaction, is negative, and therefore, the exchange energy typical of the mixture is exothermic. This

phenomenon is in agreement with our experience that the solubility of gaseous hydrogen chloride in the alcohol homologues increases significantly with increase of the molecular weight of the solvent.

The B values calculated from the experimental data are given in Table XI.

Table X

log γ as a function of concentration and temperature in 1-butanol solution*

C (mol/dm³)	log γ*			
	20 °C	25 °C	30 °C	40 °C
0.640	2.58	2.50	2.38	2.20
0.620	2.71	2.69	2.56	2.33
0.380	1.89	1.83	1.70	1.49
0.260	1.68	1.52	1.41	1.29
0.200	1.20	1.09	0.99	0.89
0.170	1.23	1.21	1.11	1.00
0.130	0.89	0.87	0.78	0.69
0.096	0.63	0.61	0.56	0.46
0.070	0.32	0.31	0.25	0.21
0.060	0.45	0.43	0.39	0.35
0.040	0.26	0.25	0.19	0.17
0.022	0.21	0.20	0.14	0.12
0.017	0.10	0.08	0.14	0.13
0.008	0.00	0.01	0.00	0.00
0.006	0.10	0.09	0.07	0.06
0.004	0.03	0.00	0.04	0.04
0.002	0.00	0.01	0.00	0.05
0.0005	0.01	0.01	0.01	0.06

Table XI

Values of constant B in hydrogen chloride–alcohol systems

Alcohol	B			
	20 °C	25 °C	30 °C	40 °C
Methanol	−21.42	−19.35	−18.54	−16.81
Ethanol	−24.41	−22.34	−21.19	−19.35
1-Propanol	−28.44	−27.75	−26.60	−24.53
1-Butanol	−42.00	−40.07	−37.31	−33.62

REFERENCES

[1] ROBINSON, R. A., STOKES, R. H.: Electrolyte Solutions. Butterworth s London 1955
[2] HAASE, R.: Thermodynamik der Mischphasen. Springer Verlag. Berlin 1956
[3] ERDEY-GRÚZ T., SCHAY, G.: Theoretical Physical Chemistry, Vol. III (in Hungarian). Tankönyvkiadó, Budapest 1962
[4] HARNED, H. I., FALLON, L. D.: J. Amer. Chem. Soc., **61,** 2374 (1939)
[5] KOSKIKALLIO, J., SOUMEN, O.: Kem., **30B,** 43, 111 (1957)
[6] LENGYEL, S., GIBER, J., TAMÁS, J.: Magyar Kém. Folyóirat, **66,** 5, 161 (1960)

Ferenc RATKOVICS
Katalin BARATI-DÉSI
H-8201 Veszprém, Schönherz Z. u. 10.

Acta Chimica Academiae Scientiarum Hungaricae, Tomus 97 (3), pp. 299—311 (1978)

POTENTIAL OSCILLATIONS AT PLATINUM ELECTRODES IMMERSED INTO SOLUTIONS OF ORGANIC SUBSTANCES AND REDOX SYSTEMS

OPEN-CIRCUIT PERIODIC PHENOMENA SIMILAR TO GALVANOSTATIC POTENTIAL OSCILLATIONS DURING ELECTRO-OXIDATION

G. HORÁNYI

(Central Research Institute for Chemistry, Hungarian Academy of Sciences, Budapest)

G. INZELT and É. SZETEY

(Physical Chemistry and Radiology, Department of Eötvös L. University, Budapest)

Received April 28, 1977

It has been shown experimentally that oscillation phenomena at platinum electrodes during the galvanostatic electro-oxidation of certain organic substances can be produced also as oscillations of the rest potential of the electrode immersed into a solution containing the organic substance and a redox system. The oscillations of the rest potential were demonstrated on systems containing Ce^{4+} or Fe^{3+}, and methanol, formaldehyde, formic acid, ethylene glycol, glycolaldehyde, glyoxal or isopropanol. It has been shown that, in the potential range corresponding to the cathodic limiting diffusion current of the oxidant, the conditions provided otherwise by the galvanostat are essentially fulfilled. If the galvanostatic potential oscillations fall into this region, the oscillation of the rest potential will also take place. The galvanostatic potential oscillations were compared with the rest potential oscillations in the case of ethylene glycol.

Periodic phenomena in electrochemical processes were first observed 150 years ago [1]. Since then, the sphere of known phenomena has been considerably extended. The monograph of WOJTOWICZ [1] gives a survey on electrochemical oscillation phenomena and on attempts at their interpretation.

Essentially, these phenomena can be classed into three main groups if the behaviour and changes of the two fundamental electrochemical parameters, current (or current density) and potential are taken into consideration.

a) Galvanostatic potential oscillations.

b) Potentiostatic current oscillations.

c) Periodic changes of the rest potential in the case of open circuits.

In the first two cases, it is rather important from the point of view of the interpretation and discussion of the periodic phenomena that the properties of the external circuit may also determine the behaviour of the whole system. Therefore, in many cases periodic phenomena cannot be unequivocally assigned to processes occurring at the electrodes investigated. Numerous data

are reported in the literature on periodic potential changes during the galvanostatic electro-oxidation of various organic substances (methanol, formaldehyde, formic acid, isopropanol). On the other hand, potentiostatic current oscillations are often not even known for most of the systems investigated.

Incidentally, the question arises whether in the case of galvanostatic potential oscillations the phenomena observed are characteristic of the periodic processes at the electrode or of the whole electric system including the external circuit and the main and auxiliary electrodes.

This question could be unequivocally answered if the oscillations observed in galvanostatic investigations were produced without the external circuit used in the galvanostatic process. This seems possible, at least in principle, in consideration of the third type of oscillation discussed above.

Oscillations of the rest potential have been observed mainly in the dissolution of various metals. Oscillation of the rest potential occurs in this case as a result of periodic changes in the rate of the simultaneous anode and cathode processes.

If it is assumed that, in the course of galvanostatic electro-oxidation of organic substances at platinum electrodes, the role of the external circuit in the periodic phenomena is limited to providing for the constant flow of electrons, the external circuit can, in principle, be replaced by a redox system in the liquid phase, capable of accepting electrons at a constant rate directly from the platinum electrode. In this case, the anode process, electro-oxidation, could be coupleted with a cathode process (reduction of the redox system) without the use of an external circuit.

If the anodpe rocess shows a periodic behaviour, this must be revealed in the periodic changes of the rest potential of the platinum electrode immersed into the solution of the two reacting components.

The redox system can perform a task equivalent to that of the galvanostat only if its reduction rate does not change with the electrode potential in a rather wide potential interval. It is well known that this condition can be readily realized in the potential range corresponding to the cathodic limiting diffusion current of the redox system. As concerns practical realization, attention must be paid to the fact that the potential interval in which electro-oxidation and potential oscillations occur, should fall within the potential range corresponding to the cathodic limiting current of the redox system. This precondition limits to a certain extent the number of usable redox systems; but it was thought that, in the absence of other interfering factors, the system Ce^{4+}/Ce^{3+} may, in all cases, meet the requirements.

The present communication reports on investigations undertaken on the basis of the above considerations with the aim of producing potential oscillations at a platinum electrode immersed into the solution of various organic substances, and Ce^{4+} or Fe^{3+} ions.

Experimental

The behaviour of methanol, formaldehyde, formic acid, ethylene glycol, glyoxal, glycolaldehyde and isopropanol was studied. 1 *M* $HClO_4$ and 1 *M* H_2SO_4 were used as supporting electrolytes. Periodic phenomena were investigated on both bright and platinized Pt electrodes. The geometrical surface of the electrodes used was 10 cm^2. The roughness factor of the platinized electrodes varied between 500 and 1000. All the electrode potentials given in this paper were measured against a hydrogen electrode immersed into the supporting electrolyte.

Three-electrode cells were used in the experiments. The auxiliary electrode was a platinized platinum electrode, which was used only in polarization measurements but had no role at all in the investigation of the oscillations of the rest potential. The compartments for the reference and auxiliary electrodes were separated from the cell of the main electrode by realed ground stopcocks. The solution was stirred partly by a flow of argon, partly with a magnetic stirrer. The flow of argon simultaneously provided for an inert gas atmosphere.

A Model PS-20 (Meinsberg) potentiostat was used for the potentiostatic investigations, while the galvanostatic measurements were carried out with a galvanostat designed in this laboratory. The electrode potentials were measured and recorded with a Model EMG-1363 digital voltmeter, a Model Radelkis OP-207 recording pH-meter and a Model Zeiss GIBl recorder.

Results

Figures 1 – 8 show the potential oscillations observed in various systems. It is apparent from the figures that, as expected, oscillations of the rest potential can be produced with the aid of suitable redox systems.

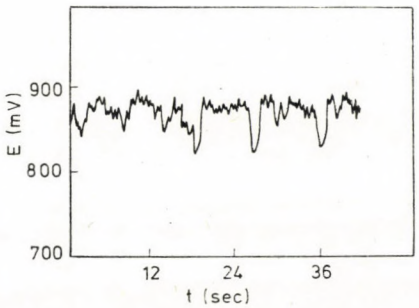

Fig. 1. Potential oscillations in the methanol–Ce^{4+} system at a bright platinum electrode. $c_{methanol} = 2$ mol/dm^3; $c_{Ce^{4+}} = 2.5 \times 10^{-3}$ mol/dm^3

When Fe^{3+} ions are used, the possibilities for the production of oscillation phenomena are considerably more limited than in the case of Ce^{4+}. This evidently follows from the fact that the standard redox potential of the Fe^{3+}/Fe^{2+} system (0.771 V) is substantially lower than that of the Ce^{4+}/Ce^{3+} system (1.61 V). Accordingly, the potential section corresponding to the cathodic limiting diffusion current does not coincide for all substances with the potential interval corresponding to potential oscillation. The fact that in certain cases potential oscillations can be realized in the presence of both Fe^{3+} and Ce^{4+}

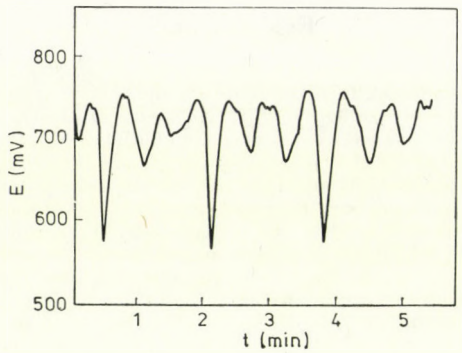

Fig. 2. Potential oscillations i n the formaldehyde–Ce^{4+} system at a bright platinum electrode. $c_{formaldehide} = 2$ mol/dm^3; $c_{Ce^{4+}} = 1.2\times10^{-4}$ mol/dm^3

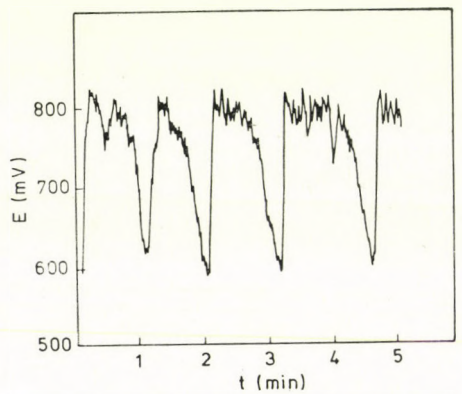

Fig. 3. Potential oscillations in the formic acid–Ce^{4+} system at a bright platinum electrode. $c_{formic\ acid} = 1$ mol/dm^3; $c_{Ce^{4+}} = 1\times10^{-4}$ mol/dm^3

ions obviously testifies that the phenomena observed are independent of the nature of the ions. Thus, the role of the ions is actually restricted to the acceptance of the electrons released during electro-oxidation.

Regrettably, certain interfering side effects must be faced also in the case of Ce^{4+} ions of otherwise advantageous properties. It is known from the literature [2] that Ce^{4+} ions react in aqueous medium also in homogeneous phase with different alcohols, aldehydes, etc. (Certain cerimetric determinations are based on this fact.)

However, the rate of these homogeneous reactions is so low under the conditions used that they do not cause substantial changes in the Ce^{4+} concentration even after prolonged periods of time although this concentration is sometimes not very high. Naturally, the concentration of Ce^{4+} is not constant even in the absence of this side-reaction, as it must decrease also on account of the reduction process at the platinum electrode. (Evidently, the same is valid for Fe^{3+} ions.)

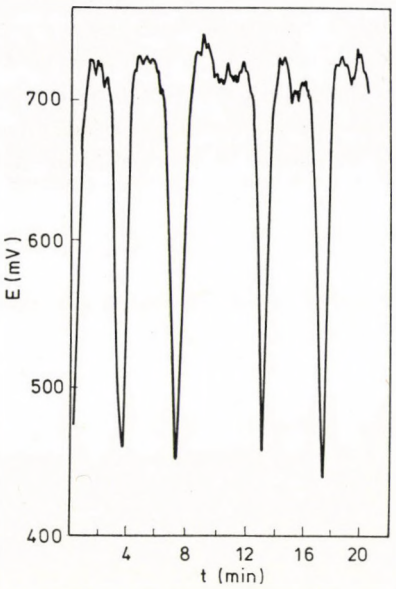

Fig. 4. Potential oscillations in the glycolaldehyde–Ce^{4+} system at a platinized platinum electrode. $c_{\text{glycolaldehyde}} = 0.5$ mol/dm³; $c_{Ce^{4+}} = 2.5 \times 10^{-2}$ mol/dm³

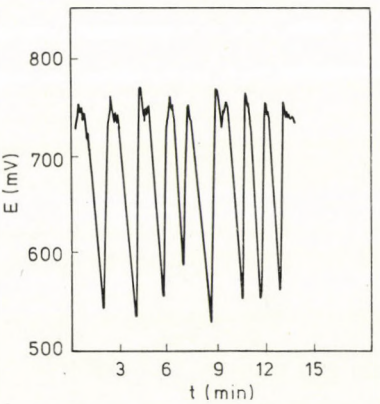

Fig. 5. Potential oscillations in the isopropanol–Ce^{4+} system at a bright platinum electrode. $c_{\text{isopropanol}} = 0.5$ mol/dm³; $c_{Ce^{4+}} = 1.5 \times 10^{-4}$ mol/dm³

In this case, the concentration of the oxidant decreases exponentially with time, because in the range of the diffusion limiting current the quantity of oxidant arriving in unit time at the electrode surface $\left(-\frac{dq}{dt}\right)$ can be expressed in the following way:

$$\frac{dq}{dt} = \frac{Ai_1}{dF} = A\,k_D\,c$$

where i_1 is the density of the limiting diffusion current, referred to the geometrical surface, A is the geometrical surface area of the electrode, k_D is the apparent rate constant of diffusion process referred to unit geometrical surface of the electrode, c is the concentration of the oxidant in the solution, n is the stoichiometric number of electrons in the equation describing the reduction (ox + ne = red), and F is the Faraday constant.

Since $\frac{q}{v} = c$, where v is the volume of the solution phase, the relationship

$$\frac{\mathrm{d}c}{\mathrm{d}t} = A \frac{k_D}{v} c$$

si valid, from which follows the relationship

$$c = c_0 e^{-A\frac{k_D}{v}t}$$

where c_0 is the initial concentration of the oxidant in the solution at time $t = 0$. Thus, the density of the limiting diffusion current changes with time according to the relationship

$$i_1 = n F k_D c_0 e^{-A\frac{k_D}{v}t}$$

The trivial statement follows unequivocally that, under given diffusion conditions, the smaller the $\frac{A}{v}$ ratio, the slower the concentration of the oxidant changes with time. However, it is important that the above relationships are valid for both bright and platinized electrodes, because only the geometrical surface plays a role in the diffusion process. Naturally, there will be a great difference in current densities referred to the "true" surface If the roughness factor of the bright electrode is denoted by v_s and of the platinized electrode by v_k, and it is assumed that the magnitude of the "true" surface has been determined in both cases by the same method (*e.g.* from the charging curves), then the current densities referred to the "true" surface in the case of identical i_1 values will be

$$i_1' = \frac{i_1}{v_s}; \qquad i_1'' = \frac{i_1}{v_k}$$

On the other hand, it follows from the above relationships that in the case of the platinized electrode, the oxidant must be applied at a concentration by $\frac{v_k}{v_s}$-times higher than in the case of the bright electrode, if identical true

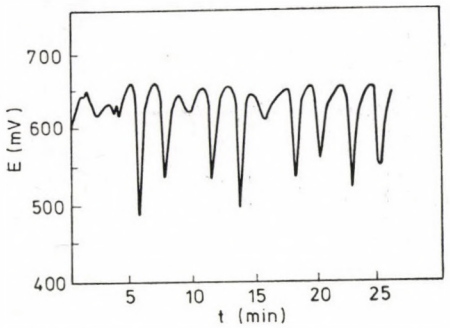

Fig. 6. Potential oscillations in the ethylene glycol–Fe^{3+} system at a platinized platinum electrode. Supporting electrolyte 1 mol/dm³ $HClO_4$; $c_{\text{ethylene glycol}} = 0.5$ mol/dm³; $c_{Fe^{3+}} = 0.05$ mol/dm³

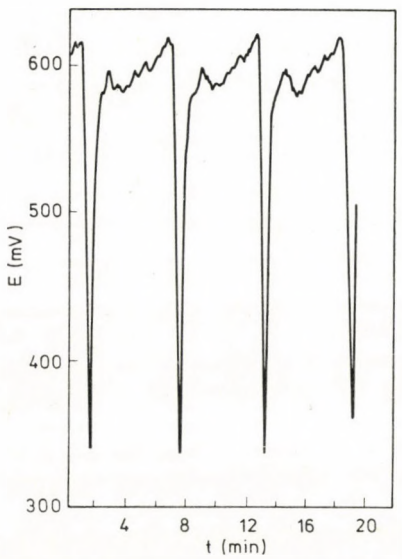

Fig. 7. Potential oscillations in the glyoxal–Fe^{3+} system at a platinized platinum electrode. Supporting electrolyte 1 mol/dm³ $HClO_4$; $c_{\text{glyoxal}} = 0.2$ mol/dm³; $c_{Fe^{3+}} = 1.2 \times 10^{-2}$ mol/dm³

current densities are to be provided (presuming that k_D is identical in both cases).

Thus, it follows from the aforesaid that, depending on the experimental conditions, the oscillation phenomena observed can be assigned to approximately steady states only in a certain time interval. This interval may sometimes be as long as 30 min or even 1 h, and within this interval potential oscillations can be conveniently observed. At the systems investigated only

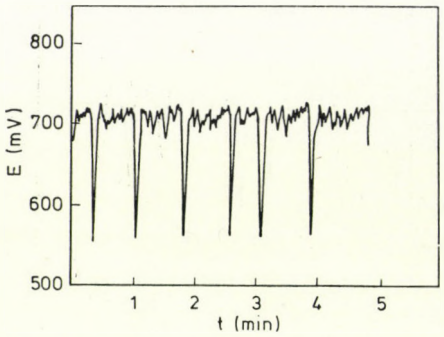

Fig. 8. Potential oscillations in the ethylene glycol–Ce^{4+} system at a bright platinum electrode. $c_{\text{ethylene glycol}} = 1$ mol/dm^3; $c_{Ce^{4+}} = 3 \times 10^{-4}$ mol/dm^3

in the case of glyoxal was the difficulty encountered that owing to the homogeneous oxidation reaction with Ce^{4+}, no oscillations permanent over a longer period could be observed. However, in this case oscillations could be produced with Fe^{3+} ions, as shown in Fig. 7. The consumption of Ce^{4+}, *i.e.* the decrease in its concentration could be visually followed through the decolouration of the solution and the change in intensity of the yellow colour of the solution. It should be mentioned that in our preliminary investigations experiments were carried out also with $Cr_2O_7^{2-}$ ions. The use of the $Cr_2O_7^{2-}/Cr^{3+}$ system had to be given up for the reason that the rate of homogeneous oxidation was too high. Not more than one or at the most two potential oscillations could be observed up to the consumption of the chromate ions, indicated also by the colour change of the solution. No redox system seems to exist for which the homogeneous oxidation reactions can be completely disregarded.

When it has been established that oscillation phenomena can be realized also in the case of open circuits in the systems discussed above, a closer inspection of the relationship between the oscillations of the rest potential and the galvanostatic potential oscillations seemed to be appropriate. Results of these investigations will be shown on the example of the electro-oxidation of ethylene glycol at a platinized platinum electrode.

Figures 9, 10, 11 and 12 show galvanostatic and Ce^{4+}-induced potential oscillations for various ethylene glycol concentrations, current densities and Ce^{4+} concentrations, respectively. Currents belonging the galvanostatic cases (I) may be correlated with the limiting rate of reduction of Ce^{4+} ions. Information on the magnitude of the limiting diffusion current (I_1) could be obtained from the potentiostatic polarization curves recorded for the system containing Ce^{4+} ions and ethylene glycol. Curves of this kind are shown in Fig. 13. From the long limiting current section belonging to the cathodic part of the polarization curve, the limiting current can be unambiguously determined. (In fact, it is sufficient for this purpose to determine the current at a single potential

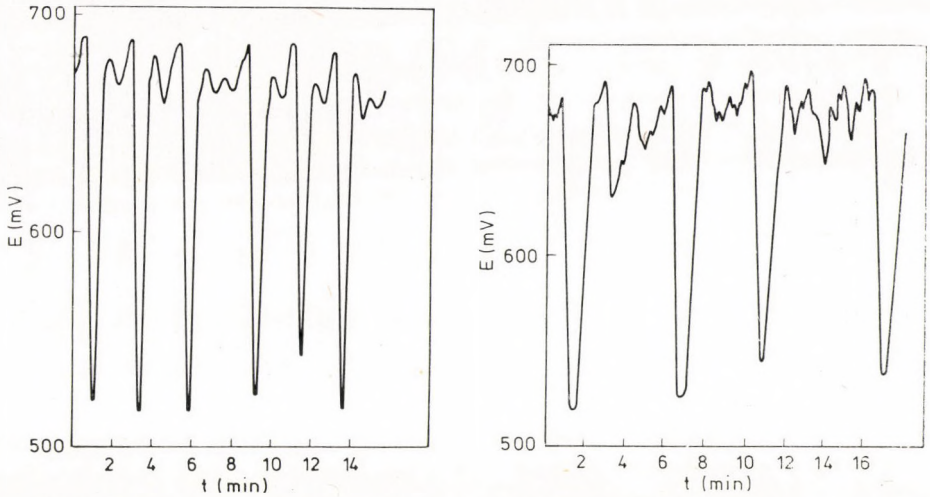

Fig. 9a. Galvanostatic potential oscillations at a platinized platinum electrode. $I = 15$ mA
9b. Rest potential oscillations with Ce^{4+}. $I_1 = 13$ mA, $c_{\text{ethylene glycol}} = 0.2$ mol/dm^3

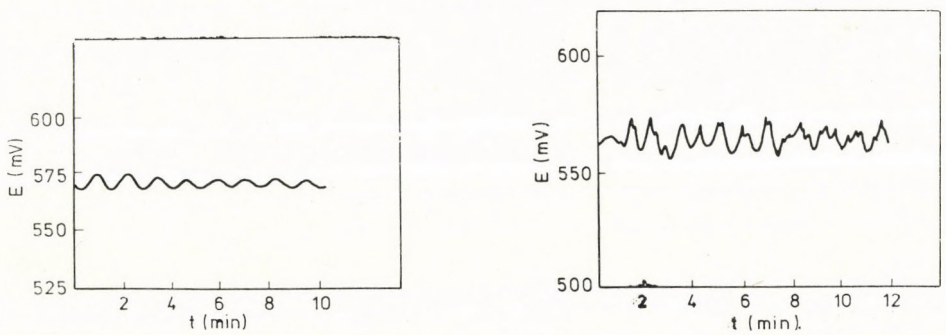

Fig. 10a. Galvanostatic potential oscillations at a platinized platinum electrode. $I = 11$ mA
10b. Oscillations of the rest potential with Ce^{4+}.
$I_1 = 10.5$ mA, $c_{\text{ethylene glycol}} = 0.4$ mol/dm^3

inside the potential range corresponding to the limiting current section.) When Fe^{3+} ions and other organic substances are used, similar polarization curves are obtained, as can be noted from Fig. 14. The similarity of oscillations produced by the galvanostatic and the redox systems at similar I and I_1 values can be clearly seen. By the increase or decrease of ethylene glycol concentration, changes of similar character are produced in the periodic phenomena in both cases. The same is relevant to changes in the galvanostatic current and the limiting diffusion current.

It has been known since long in conjunction with galvanostatic potential oscillations that under given experimental conditions oscillations do not begin

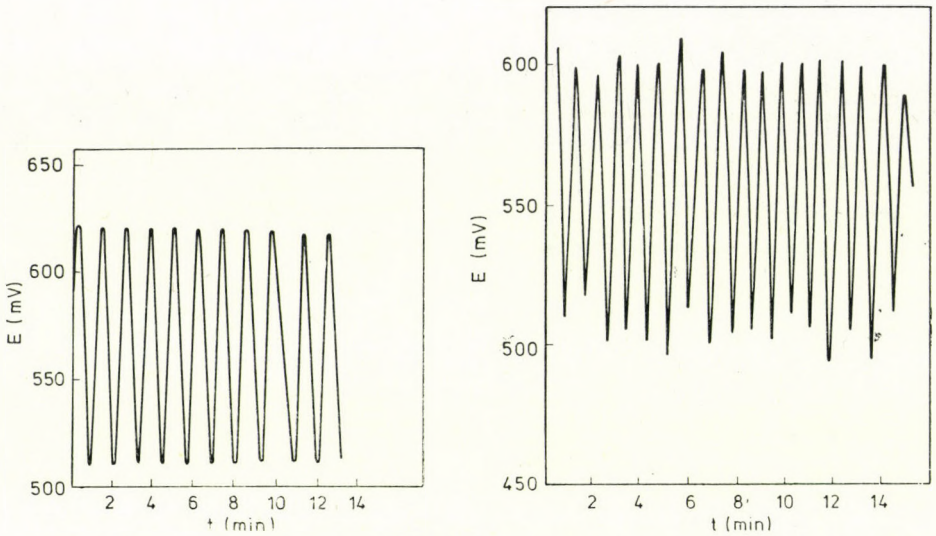

Fig. 11a. Galvanostatic potential oscillations at a platinized platinum electrode. $I = 11$ mA
11b. Oscillations of the rest potential with Ce^{4+}
$I_1 = 10.5$ mA, $c_{\text{ethylene glycol}} = 0.8$ mol/dm^3

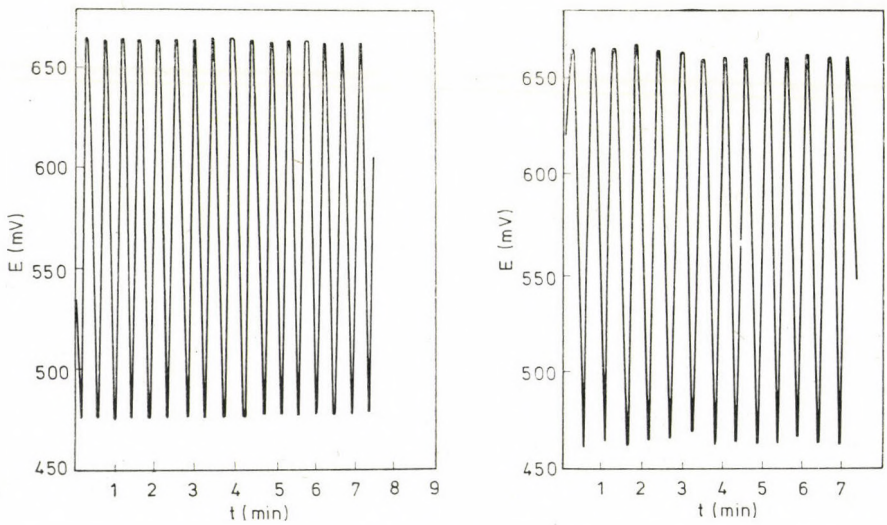

Fig. 12a. Galvanostatic potential oscillations at a platinized platinum electrode, $I = 16.5$ mA
12b. Oscillations of the rest potential with Ce^{4+}
$I_1 = 17$ mA, $c_{\text{ethylene glycol}} = 1.6$ mol/dm^3

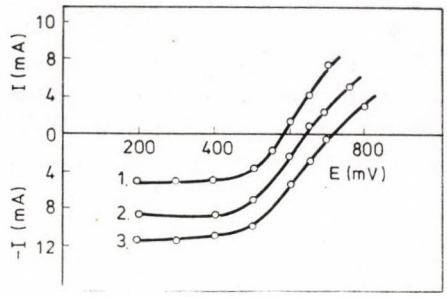

Fig. 13. Potentiostatic polarization curves of a platinized platinum electrode in the ethylene glycol–Ce^{4+} system. $c_{\text{ethylene glycol}} = 0.3$ mol/dm³; $c_{Ce^{4+}} = 0.3$ mol/dm³; $c_{Ce^{4+}} = 1\times.10^{-2}$ (1); 1.8×10^{-2} (2); 2.5×10^{-2} (3) mol/dm³

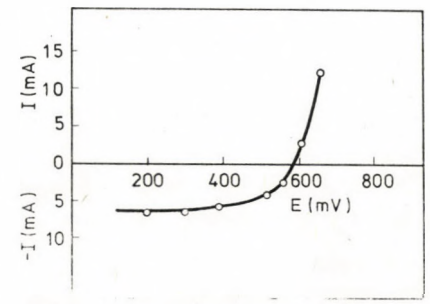

Fig. 14. Potentiostatic polarization curve of a platinized platinum electrode in the glyoxal–Fe^{3+} system. $c_{\text{glyoxal}} = 0.1$ mol/dm³; $c_{Fe^{3+}} = 5\times10^{-3}$ mol/dm³

below a certain current value and cannot be observed above a certain current. The same is true in the case of oscillations produced by redox systems with respect to the magnitude of the limiting current, so that also here a close parallelism exists between the two methods.

In view of the fact that the magnitude of the limiting diffusion current can be changed by varying the stirring intensity, a relatively convenient method is available for the changing of periodic phenomena. This procedure is essentially equivalent to the changing of current intensity in the galvanostatic method.

Conclusions

Our initial assumption that galvanostatic potential oscillations can be simulated by the oscillation of the rest potential of systems containing a redox system and an organic substance, could be proved on the basis of the experimental material presented in this paper. These observations cast doubt on the assumptions according to which, the external circuit plays a decisive role in the production of galvanostatic potential oscillations, at least in the cases investigated.

The results permit further to conclude that the number of systems in which oscillations of the "rest" potential can be produced, may be considerably increased. It is sufficient for the production of potential oscillation, if only one of the coupled cathode and anode processes reveals a periodic behaviour.

After the exclusion of the possible role of the external circuit, the question arises what processes at the electrode surface are responsible for the periodic potential oscillations. In many of the cases investigated, oscillations occur in a potential interval in which no oxide layer has yet been formed on the platinum surface, so that the phenomenon cannot be explained by oscillation models involving the assumption of an oxide layer.

It seems rather more likely that the development of oscillation phenomena should be attributed to the behaviour of the chemisorbed layer of the organic substances. Attempts have been made to take this factor into consideration in the interpretation of potential oscillations occurring in the galvanostatic electro-oxidation of isopropanol [3].

During oxidation the organic substance can participate in the following processes:

(Ia) Chemisorption, involving dehydrogenation, the rupture of bonds, possibly the splitting of the molecule and considerable charge transfer. Essentially, this is an oxidation process, too.

(Ib) Oxidation of the products of chemisorption and removal of the oxidation products from the electrode surface.

(II) Oxidation of the organic molecule yielding some definite end-product, which proceeds on free sites not involved in chemisorption (*e.g.* formation of formaldehyde or formic acid from methanol, of glycolaldehyde or glyoxal from ethylene glycol). Processes (Ia) and (Ib) are well-known from the literature [4–8]. The oxidation of chemisorbed molecules takes place only above certain potential values, so that at potentials more negative than these, the surface is virtually completely covered with chemisorbed molecules. This chemisorbed layer forms a barrier to reactions of type (II) and behaves as a passive layer. Accordingly, the oxidation of the chemisorbed layer increases the reaction rates, because it increases the number of free sites. A change in coverage with chemisorbed molecules affects therefore the rate of processes proceeding by route (II). In steady-state galvanostatic cases the current is distributed on the basis of the aforesaid between three processes:

$$I = I_a + I_1 + I_2$$

where I_a, I_1 and I_2 are the currents corresponding to chemisorption, to the oxidation of chemisorbed molecules and to the actual oxidation processes, respectively. In the steady state, all three partial currents are constant. If potential

oscillations can be observed, the charge involved in charging and discharging of the electrode must also be taken into account in the charge balance. If the capacitance of the electrode is C, then the above equation will have the following form:

$$I = I_a(E,t) + I_1(E,t) + I_2(E,t) + C\frac{dE}{dt}$$

where it is indicated that I_a, I_1 and I_2 depend on the potential (E) and on time (t), their magnitude and ratio changing as a function of time. I is naturally constant. To these equations, the equation describing the variation of the coverage by chemisorbed molecules with time must be added:

$$\frac{d\theta}{dt} = \frac{1}{p}\left(\frac{I_a}{Fn_a} - \frac{I_1}{Fn_1}\right)$$

where F is the Faraday constant, n_a and n_1 are the stoichiometric numbers of the electron in the equations describing chemisorption and oxidation of the chemisorbed molecule, and p is the amount of the chemisorbed molecules (mol) at the surface in the case of complete coverage. On the basis of various models, I_a, I_1 and I_2 can be given as a function of Θ and E. Actually, the system of differential equations obtained in this way should be analyzed to determine whether periodic solutions do exist. The selection of suitable models is the subject of further investigations.

REFERENCES

[1] WOJTOWICZ, J.: Oscillatory Behaviour in Electrochemical Systems, in Modern Aspects of Electrochemistry, Vol. 8. Plenum Press, New York 1972
[2] WELLS, C. F., HUSAIN, M.: Trans. Faraday Soc., **66,** 679, 2855 (1970); **67,** 1086 (1971) PETZOLD, W.: Die Cerimetrie. Verlag-Chemie 1955
[3] HORÁNYI, G., VÉRTES, G., KÖNIG, P.: Z. phys. Chem., **254,** 298 (1973)
[4] BREITER, W. W.: Electrochemical Processes in Fuel Cells. Springer-Verlag, Berlin 1969
[5] DAMASKIN, B. B., PETRII, O. A., BATRAKOV, V. V.: Adsorptsiya organicheskikh soedinenii na elektrodakh. Izd. Nauka, Moscow 1968
[6] GILEADI, E.: Electrosorption. Plenum Press, New York 1967
[7] PIERSMA, B. J., GILEADI, E.: The Mechanism of Electrochemical Oxidation of Organic Fuels, in Modern Aspects of Electrochemistry, Vol. 4. Plenum Press, New York 1966
[8] HORÁNYI, G.: J. Electroanal. Chem., **51,** 163 (1974)

György HORÁNYI H-1025 Budapest, Pusztaszeri út 59–67.

György INZELT
Éva SZETEY
} H-1088 Budapest, Puskin u. 11–13.

Acta Chimica Academiae Scientiarum Hungaricae, Tomus 97 (3), pp. 313–325 (1978)

ELECTROCHEMICAL BEHAVIOUR OF ETHYLENE GLYCOL AND ITS OXIDATION PRODUCTS AT THE PLATINUM ELECTRODE, I

ELECTROREDUCTION OF OXO CONTAINING BIFUNCTIONAL COMPOUNDS WITH TWO CARBON ATOMS IN ACIDIC MEDIA

G. Horányi

(Central Research Institute for Chemistry, Hungarian Academy of Sciences, Budapest)

G. Inzelt and É. Szetey

(Department of Physical Chemistry and Radiology, Eötvös L. University, Budapest)

Received May 10, 1977

It has been shown that during the oxidation of ethyleneglycol in acidic media on platinized platinum electrodes, among other products, compounds are formed which are reduced at appreciable rates at potentials slightly more positive than the potential of the equilibrium hydrogen electrode. To interpret the phenomena observed, the electrohydrogenation and the catalytic hydrogenation of the oxidation products of ethylene glycol ($HOCH_2-CHO$, $OHC-CHO$, $HOCH_2-COOH$, $OHC-COOH$, $HOOC-COOH$) at the platinized platinum electrode and on a platinum powder catalyst in an acidic medium have been investigated. Appreciable reduction rates were found only in the case of the oxo compounds. It has been shown that hydrogenation reactions can be observed only if definite experimental procedures are used. For the rate of electrohydrogenation or hydrogenation the following order has been established: $HOCH_2-CHO > OHC-CHO \gg OHC-COOH$. As a result of the electrohydrogenation or hydrogenation of glycolaldehyde and glyoxal, mainly ethane is formed, presumably *via* acetaldehyde as an intermediate.

Experimental results unequivocally show that glycolaldehyde or glyoxal, or both compounds may be formed in substantial amounts during the oxidation of ethylene glycol.

The electrochemical behaviour of ethylene glycol and its oxidation products ($HOCH_2-CHO$, $OHC-CHO$, $HOCH_2-COOH$, $OHC-COOH$, $HOOC-COOH$) at the platinum electrode has been discussed in several papers [1–18]. The papers cited deal primarily with problems of electro-oxidation and adsorption. In spite of this, with the exception of oxalic acid, little information is available on the actual route of oxidation of these compounds. Information is even more limited on the electroreduction of these compounds; indeed, on the basis of the literature the conclusion might be drawn that they are essentially not reduced at the platinum electrode. Certain doubts arise in conjunction with the justification of this latter assumption, as earlier investigations [19–21] have shown that simple aliphatic oxo compounds (acetone, methyl ethyl ketone, acetaldehyde, propionaldehyde) can be reduced in acidic media at an appreciable rate at the platinum electrode, and the respective hydrocar-

bons sometimes form a considerable part of the products obtained. Doubtless, the existence of these reactions has long escaped attention because of aging phenomena due to the strong chemisorption of the starting materials and by-products possibly formed in small amounts. Presumably, similar phenomena exist also in the case of oxo compounds derived from ethylene glycol. Starting from this assumption, the possible reduction of the oxidized derivatives of ethylene glycol will be investigated in this paper.

The elucidation of problems related to the reduction of these compounds, besides possibly extending our knowledge on their electrochemical properties, seems to be important also because during certain operations in oxidation studies, *e.g.* during cathodic regeneration, the electrode may attain potentials, at which possible reduction products may distort the results of subsequent oxidative investigations.

Experimental

1 *M* $HClO_4$ and H_2SO_4 were used as supporting electrolytes. Potentiostatic measurements were carried out with a PS-20 (Meinsberg) potentiostat. A three-electrode cell, well-known from electrochemical literature, has been used. The reference electrode was a hydrogen electrode immersed into the supporting solution. All potential values reported are referred to the potential of this electrode.

Hydrogenation experiments were carried out with platinum powder of about 10 m^2/g specific surface. A hydrogenator fitted with a thermostating jacket was used in combination with a shaker of variable oscillation number. Hydrogenations were carried out at 25 °C.

Reduction of the oxidation products of ethylene glycol

As already mentioned the route through which electro-oxidation of ethylene glycol proceeds is essentially unknown. As a working hypothesis, let us start from the following simple reaction scheme:

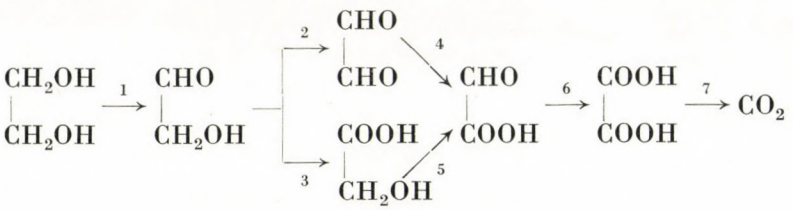

It should not be forgotten that other reaction routes are also possible. Thus, for example, by analogy to homogeneous oxidation reactions, it may be presumed that formic acid is also formed as an intermediate in the electro-oxidation of hydroxy or oxo acids, from which carbon dioxide is formed, similarly as from oxalic acid.

The electro-oxidation of ethylene glycol proceeds on the platinized platinum electrode already at moderately positive potentials at appreciable rates, as can be seen from the section of the potentiostatic polarization curve shown in Fig. 1. It is known from earlier investigations [14] that in the potential

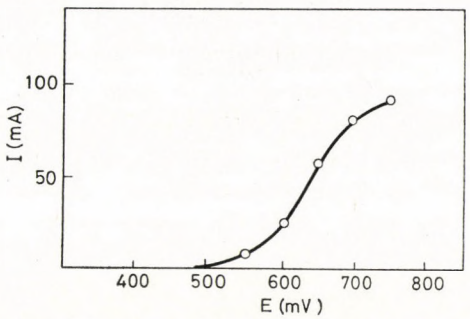

Fig. 1. Polarization curve of ethylene glycol (0.2 mol/dm³) in 1 *M* $HClO_4$ as supporting electrolyte

interval corresponding to this section oxalic acid is either not oxidized or only at a very low rate. Thus, presumably, the complete oxidation of ethylene glycol, yielding CO_2, need not be taken into consideration. When polarizing the electrode over a longer time at a given potential, between 500 and 700 mV, then rapidly decreasing the potential to 0 mV, then depending on the amount of charge having passed through the system during oxidation, a considerable cathodic current can be observed in the potential interval from 0 to 100 mV. Cathodic polarization curves observed after anodic polarization of different extents are shown in Fig. 2. This phenomenon shows that products are formed during oxidation which undergo reduction at potentials more negative than 100 mV.

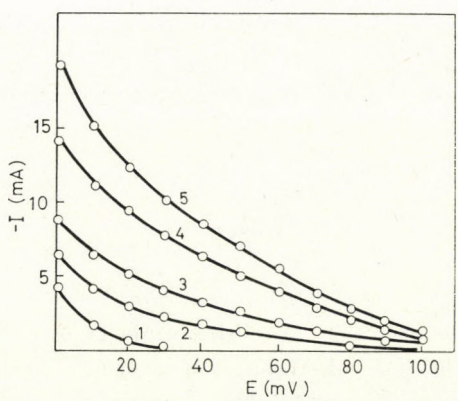

Fig. 2. Cathodic polarization curves after anodic polarization for different periods. Magnitud of charge passed during anodic polarization: 0 (1); 85 (2); 145 (3); 320 (4); 560 (5)C

It should be mentioned that in recording the cathodic polarization curves we always started from 0 mV and proceeded towards more positive potentials. In the opposite case a substantially lower current was obtained. In the determination of current values belonging to given potentials, we waited only for 3–5 min, because the current decreased with time. These problems will be discussed later on. The set of curves presented unequivocally shows that, within an identical procedure the magnitude of the cathodic current at a given potential is a function of the amount of charge having passed through the system during anodic polarization.

Since no data are available concerning the reduction of the assumed intermediates under the given experimental conditions, it seemed necessary to investigate in detail the reduction of the compounds involved in the scheme for the oxidation of ethylene glycol.

Electroreduction of the assumed intermediates

Observable cathodic processes have been encountered in the case of glycolaldehyde, glyoxal and glyoxylic acid, *i.e.* in the case of oxo compounds. Essentially, this is in agreement with the statement that neither acids nor alcohols are reduced at the platinum electrode [22]. (The reduction of oxalic acid, *e.g.*, to glycolic acid takes place at the mercury or lead electrode, at potentials considerably more negative than those investigated by us.) However, definite experimental methods are needed to make the electroreduction or electrohydrogenation of these compounds actually observable. It is known from the literature [2, 3, 9] that glycolaldehyde, glyoxal and glyoxylic acid are strongly chemisorbed on the platinum surface *via* dehydrogenation. The extent and rate of chemisorption depend on the electrode potential. At potentials more negative than 100–150 mV, the process is slow and, accordingly, at these potentials relatively low coverages by the organic substances can be observed even after rather long times. At potential values ranging from 200 to 500 mV chemisorption is rapid, the molecules already adsorbed can be removed from the electrode surface only by oxidation. At potentials around 0 mV, the products of chemisorption remain also on the electrode surface, *i.e.* they are resistant to hydrogenation or reduction. This calls attention to the fact that great care is needed in the investigation of the hydrogenation reaction. The chemisorbed layer may constitute a substantial barrier for the hydrogenation reaction to be investigated. This assumption is the more justified, because it is known to be the case in oxidation reactions [23, 24]. Consequently, chemisorption should be minimized if the reduction process is to be investigated.

Accordingly, the test substance was added to the system with the electrode adjusted in the supporting electrolyte to 0 mV or more negative potentials. Figure 3 shows the phenomena observed in the case of glycolaldehyde.

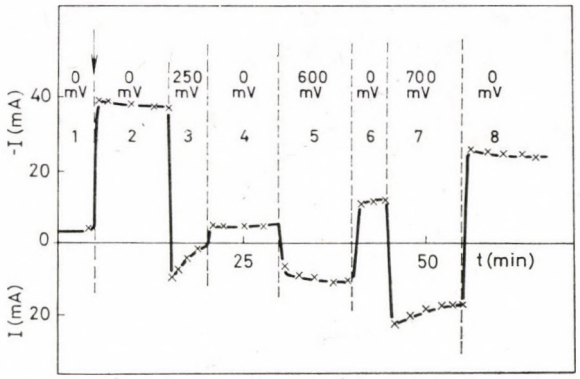

Fig. 3. Investigation of the reduction of glycolaldehyde as a function of the life-history of the electrode. For detailed explanation see text

Passing argon through the system at 0 mV, a cathodic current corresponding to hydrogen diffusion can be observed (section 1). Glycolaldehyde was added to the system at the moment indicated by an arrow. The current increased by almost an order of magnitude (section 2), which unequivocally indicates that a reduction process is taking place at a considerable rate.

To prove that the chemisorbed layer formed by dehydrogenation inhibits the reduction process, the potential of the electrode was changed to 250 mV and kept for some time at this value (section 3). In this section, chemisorption is accompanied by an anodic current decreasing in time. After this (section 4) at 0 mV, current is but slightly higher than before the addition of glycolaldehyde.

Moreover, it is known from the literature that the oxidation of chemisorbed molecules begins already at 500 – 600 mV and, following this, the oxidation of the organic substance in the solution proceed at the liberated sites. Accordingly, keeping the electrode at 600 mV (section 5) an anodic current of substantial magnitude can be observed. The decreasing coverage by chemisorbed molecules is shown by section 6, in which a perceptible cathodic current is flowing again at 0 mV, *i.e.* the reduction process takes place again.

The same is proved by sections 7 and 8. At 700 mV a greater fraction of the chemisorbed layer can be removed than at 600 mV. As a result of this, a higher cathodic current can be observed at 0 mV than before.

The reduction rate of glycolaldehyde may considerably decrease with time at a given potential. This phenomenon depends on the concentration of glycolaldehyde, as shown by Fig. 4. At low concentrations only slight "aging" is revealed. It can be concluded from this that the decrease in rate is caused either by the concentration dependent slow chemisorption of glycolaldehyde or by the chemisorption of some impurity. It seems very important that an approximately steady state can be attained rather easily at low concentrations, at

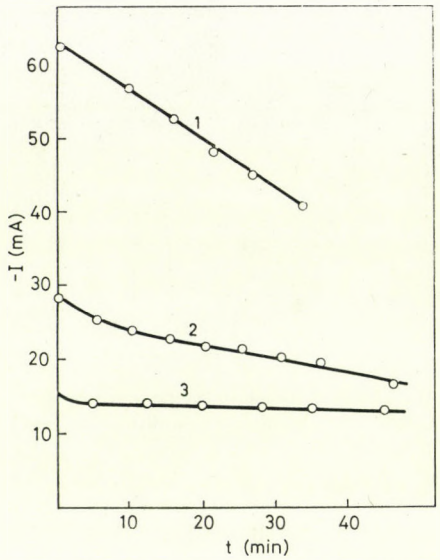

Fig. 4. Variation of the reduction rate of glycolaldehyde with time at various glycolaldehyde concentrations. (1) 6×10^{-2}; (2) 3×10^{-2}; (3) 1×10^{-2} mol/dm^3

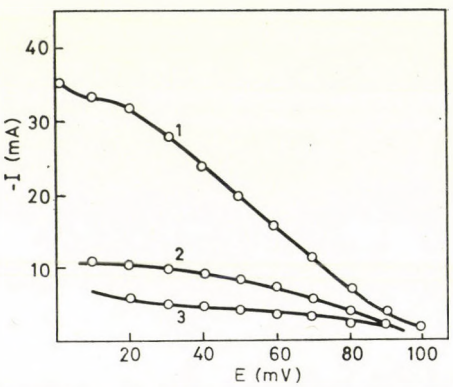

Fig. 5. Cathodic polarization curves in the presence of glycolaldehyde at 3×10^{-2} (1) and 5×10^{-3} (2) mol/dm^3 concentrations, starting from 0 mV. Curve 3 was plotted starting from 90 mV, at 5×10^{-3} mol/dm^3 concentration

least at potentials of $10-30$ mV, provided that the decrease in concentration of the solution due to the reaction need not be taken into consideration.

At the same time, difficulties are met in the recording of steady-state polarization curves, because the rate of aging (deactivation) phenomena increases too upon changing the potential in the positive direction. Starting from 0 mV, in the $0-100$ mV interval the polarization curves shown in Fig. 5 are obtained at two different concentrations (curves 1 and 2). Current values belonging to the given potentials were determined after 5 min of waiting. Proceeding in the opposite direction, substantially lower values are obtained,

as shown by curve 3, which has been recorded for the lower concentration, starting from 90 mV and proceeding in the negative direction.

In the case of glyoxal, similar phenomena have been observed, but the rate of reduction, under otherwise identical conditions, is considerably lower than in the case of glycolaldehyde. This is shown by the polarization curves in Fig. 6, recorded under identical conditions.

In the case of glyoxylic acid, the rate of reduction is very low, reduction at an appreciable rate could be observed only at relatively high concentrations. Curve 3 in Fig. 6 is the polarization curve of glyoxylic acid at a concentration 5 times higher than those of glycolaldehyde and glyoxal. The deactivation of the electrode was more marked than in the two previous cases.

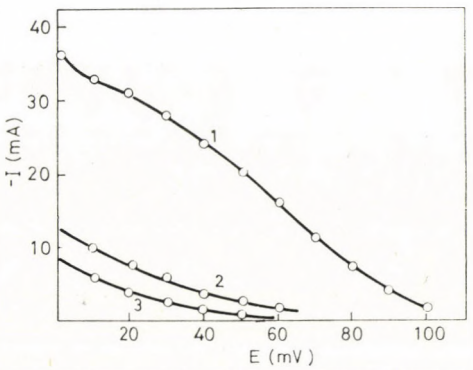

Fig. 6. Cathodic polarization curves of glycolaldehyde (1) and glyoxal (2) at 3×10^{-2} mol/dm^3 concentration, and of glyoxylic acid (3) at 1.5×10^{-1} mol/dm^3 concentration

During the reduction of glycolaldehyde and glyoxal, vigorous gas evolution is observed. Mass spectrometric analyses (for which we wish to thank Dr. K. UJSZÁSZY) have shown that the gaseous product formed is ethane, *i.e.* the oxogroup is converted into a CH_3 group according to expectations. In the case of glycolaldehyde, a few per cent of methane was also present besides ethane, its amount changing from experiment to experiment. When the volume of the gas evolved is plotted against the amount of charge passing through the system, the straight line shown in Fig. 7 is obtained. These experiments were carried out at 30 mV. For comparison, hydrogen was made to evolve from the background solution under identical conditions but at −20 mV. The ratio of the slopes of the lines is approximately H_2 : glyoxal : glycolaldehyde = 1 : 4 : 3, *i.e.* the reactions described by the overall equations

$$HOCH_2-CHO + 6H^+ + 6e \rightarrow CH_3-CH_3 + 2H_2O$$

and

$$OHC-CHO + 8H^+ + 8e \rightarrow CH_3-CH_3 + 2H_2O$$

may be assumed to occur at the electrode.

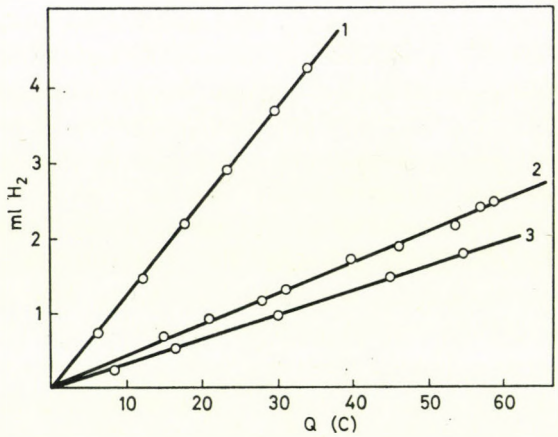

Fig. 7. Volume of gas evolved as a function of the amount of charge having passed the system. (1) H_2; (2) $HOCH_2-CHO$; (3) $OHC-CHO$

Further information relevant to the reaction products is obtained from the results of catalytic hydrogenation. In the following, these investigations will be described.

Investigation of catalytic hydrogenation

Earlier experiments [26] have shown that an investigation of direct catalytic hydrogenation may be very helpful in the study of processes during electrohydrogenation. Under similar experimental conditions, hydrogenation and electrohydrogenation are necessity equivalent to one another, *i.e.* the reactions of the organic molecule are identical in both cases so that identical products should be obtained. Thus, the hydrogenation of glycolaldehyde, glyoxal and glyoxylic acid was investigated on a platinum catalyst. Similarly as in electrohydrogenation, special care had to be observed in the realization of hydrogenation, because at a relatively high concentration of the organic substance the rate of the reaction considerably decreases. This happens also if the catalyst, before saturation with hydrogen, is in contact with the solution containing the organic substance. If the shaking of the hydrogenator is stopped when the reaction rate is still substantial, and after some time (10 – 20 min) shaking is started again, a considerably lower hydrogen uptake rate is observed or the reaction may even stop altogether. Therefore, the compound to be hydrogenated was added to a system previously saturated with hydrogen, and shaking was immediately started.

The phenomena observed can be unequivocally interpreted on the basis of findings in the investigation of electrohydrogenation. If the hydrogen supply is inadequate, the reaction proceeds at the expense of hydrogen adsorbed on the catalyst. As a result of this, the potential of the catalyst becomes

gradually more positive. The rate of chemisorption increases with increasing potential and, as has been seen, the rate of hydrogenation decreases because of increased chemisorption. Therefore, when carrying out the reaction, care should be taken to ensure a near equilibrium state in the whole system (gas–liquid boundary phase) with respect to hydrogen, to realize a state similar to that attainable in electrohydrogenation at potentials only somewhat more positive (10 – 20 mV) than 0 mV.

In Figs 8a and 8b hydrogen uptake rates are plotted against time for glyoxal and glycolaldehyde. It can be noted from curves 1 that the rate of hydrogen uptake very rapidly decreases with time. The fact that this phenomenon is not exclusively due to a decrease in the activity of the catalyst can be seen from sections 2. At the time marked by an arrow, fresh quantities of the organic substances were introduced into the system. In the case of glyoxal, this amount was the same as that initially added, while in the case of glycol-

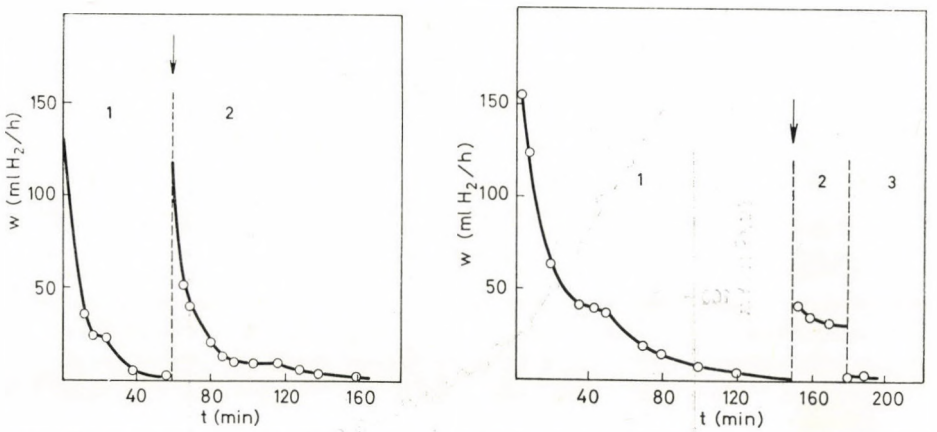

Fig. 8a. Rate of glyoxal hydrogenation as a function of time (for detailed explanation see text)
Fig. 8b. Rate of glycolaldehyde hydrogenation as a function of time (for details see text)

aldehyde, one half of the initial amount was added. The rate increase unequivocally testifies that the change of the hydrogenation rate in time observed in the first experiment is due to the change in concentration of the substance hydrogenated. When the shaking of the hydrogenator was interrupted for a brief period (15 min), *i.e.* the rate of hydrogen supply was considerably reduced, the rate of hydrogenation became virtually zero (section 3 of Fig. 8b).

In both hydrogenations, the reaction seems to be approximately of the first order along a fairly long initial section. When the rate of hydrogen uptake is plotted against the volume of hydrogen absorbed, the initial sections are linear up to rather high conversions, as can be seen from Figs 9a and 9b for glycolaldehyde and glyoxal. Following the linear section, both curves exhibit a break.

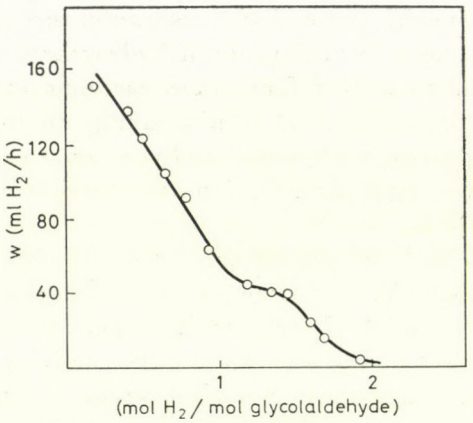

Fig. 9a. Rate of apparent hydrogen uptake as a function of the amount of hydrogen (mol) apparently taken up by 1 mol of glycolaldehyde (0.5 g Pt)

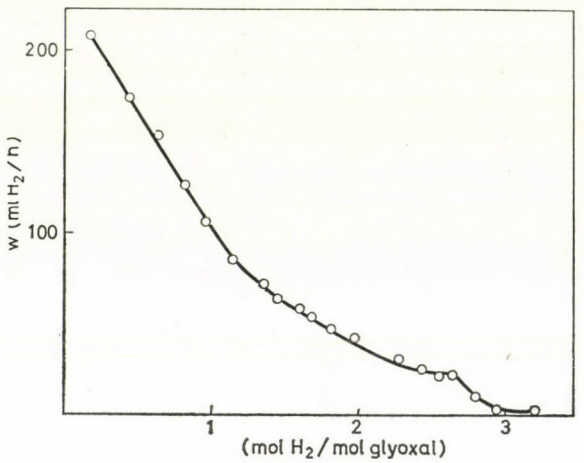

Fig. 9b. Same as in Fig. 9a, in the case of glyoxal (2.5 g Pt)

For glycolaldehyde the apparent hydrogen uptake referred to 1 mol of the organic substance, is about 2 mol whereas for glyoxal it is about 3 mol. It must be emphasized that we can speak only of apparent hydrogen uptake, because when gaseous products are formed, the actual hydrogen uptake can be calculated only is knowledge of the reactions taking place. On the other hand, we have seen in conjunction with electrohydrogenation that the formation of gaseous products must be taken into consideration.

Mass spectrometric analysis showed also in this case the formation of ethane. (Similarly as in electrohydrogenation, sometimes a few per cent of methane was also formed, particularly in the case of glycolaldehyde.)

Considering the apparent hydrogen uptake, it can be assumed that the hydrogenation reaction proceeds mainly according to the overall equations

$$HOCH_2-CHO + 3H_2 \rightarrow CH_3-CH_3 + 2H_2O$$

and

$$OHC-CHO + 4H_2 \rightarrow CH_3-CH_3 + 2H_2O.$$

Moreover, it follows that in the cases investigated the transport or the activation (dissociative adsorption) of hydrogen cannot be the rate-determining step in hydrogenation, because in this case the rate would not depend on the concentration of the organic substance.

To prove that hydrogen transport cannot be the rate-determining step, the reduction of Fe^{3+} ions has also been studied. Figure 10 shows the rate of hydrogen uptake in the complete reduction of a given amount of Fe^{3+} ions. In this case the rate of hydrogen uptake does not depend on the concentration of Fe^{3+} ions in the solution, but remains practically constant until the uptake of the required amount of hydrogen; indeed, it rather increases than decreases, and only in the short section before the termination of the reaction can a sudden drop of hydrogenation rate be observed. On the other hand, in this case the rate of hydrogen uptake is considerably higher than in the case of glycolaldehyde or glyoxal. (For comparison, the curve found for glycolaldehyde is also shown in Fig. 10 by the broken line.)

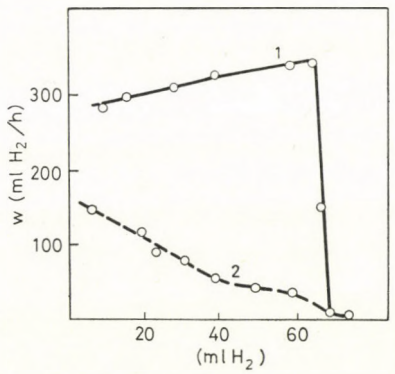

Fig. 10. Comparison of hydrogenation rates observed in the presence of Fe^{3+} ions (1) and glycolaldehyde (2), under identical experimental conditions

The maximal hydrogen uptake rate of 100 – 150 ml/h found for organic substances is also considerably lower than the rate of 350 ml/h measured in the reduction of Fe^{3+} ions, so that it can be stated with certainty that in the former cases neither the activation of hydrogen, nor the transport of hydrogen is the rate-determining step.

The rates of hydrogenation of glyoxylic acid are considerably lower than those for the other two compounds, similarly to their electrohydrogenation. 1 mol of glyoxylic acid takes up about 1 mol of hydrogen. Owing mainly to its low rate and uncertain reproducibility, this reaction has not been investigated in detail.

Discussion

The experimental results unequivocally show that the reducible product formed during the oxidation of ethylene glycol can only be an oxo compound. Of the three possible oxo compounds, glycolaldehyde, glyoxal and glyoxylic acid, only the first two show appreciable reduction currents, so that one of these or both are formed in a considerable amounts during the mild oxidation of ethylene glycol carried out at not too high potentials. As concerns the reduction of glyoxal and glycolaldehyde, from the available data it is rather difficult to draw conclusions on the mechanism of the process. The fact that ethane is formed from glyoxal is actually not suprising in view of what is known about the reduction of simple oxo compounds. In the case of glycolaldehyde, this finding is not easily understood since, beside the conversion of the CHO group, the reductive elimination of the OH group should also occur. Under the conditions investigated by us, the reduction of alcohols is not to be expected. However, the OH group of glycolaldehyde is loosened, as has been proved by the investigations of GILEADI *et al.* [25]. In the reduction of glycol aldehyde at the mercury electrode at high negative potentials, resulting pinacol, the found acetaldehyde as intermediate product.

If we assume that acetaldehyde is the first reduction product on the platinum electrode, the formation of ethane can be considered already as inevitable. Accordingly, the acetaldehyde intermediate can be assumed also in the reduction of glyoxal. However, in this case the formation of glycolaldehyde in the first step of reduction cannot be excluded. Taking all this into consideration, a possible route of the reduction of glyoxal and glycolaldehyde to ethane can be given by the following scheme:

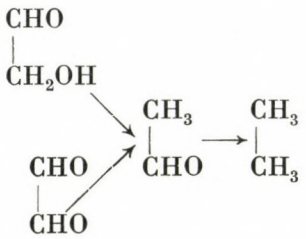

Proof of the assumed reaction route requires further investigations. However, on the basis of the experimental results reported in this paper, it can be stated with certainty that the electrohydrogenation and hydrogena-

tion of oxo containing bifunctional compounds with two carbon atoms can be realized at the platinum electrode. The electroreduction of glyoxal and glycolaldehyde serves as a further example of the fact that the conversion of the oxo group into a CH_3 group does not require the use of electrodes at which the hydrogen overvoltage is high.

REFERENCES

[1] BAGOTSKII, V. S., VASILEV, YU. B.: Electrochim. Acta, **11**, 1439 (1966)
[2] TRASATTI, S., FORMARO, L.: J. Electroanal. Chem., **17**, 343 (1968)
[3] FORMARO, L., CASTELLI, G.: J. Electroanal. Chem., **28**, 363 (1970)
[4] DANIEL-BEK, V. S., GLAZATOVA, T. N.: Zh. Prikl. Khim., **39**, 2510 (1966)
[5] BIANCHI, G., FORMARO, L., TRASATTI, S.: Chim. Ind., **50**, 26 (1968)
[6] BIANCHI, G., DE CARLO, L., FAITA, G.: Chim. Ind., **47**, 830 (1965)
[7] BIANCHI, G., LONGHI, P.: Chim. Ind., **46**, 1280 (1964)
[8] SIDHESWARAN, P.: J. Electrochem. Soc. India, **81**, 24 (1975)
[9] INDIRA, C. J., SIDHESWARAN, P.: SAEST, **8**, 103 (1973)
[10] SIDHESWARAN, P.: Ind. J. Chem., **12**, 1077 (1974)
[11] DANIEL-BEK, V. S., VITVITSKAYA, G. V., DANIELENKO, I. F.: Zh. Prikl. Khim., **38**, 806 (1965)
[12] DANIEL-BEK, V. S., VITVITSKAYA, G. V.: Zh. Prikl. Khim., **37**, 1724 (1964)
[13] ATANASIU, I. A., GEANA, D.: Revista de Chimie, **9**, 513 (1971)
[14] HORÁNYI, G., HEGEDŰS, D., RIZMAYER, E. M.: J. Electroanal. Chem., **40**, 393 (1972)
HORÁNYI, G., VÉRTES, G.: J. Electroanal. Chem., **43**, 225 (1973)
HORÁNYI, G., VÉRTES, G., HEGEDŰS, D.: Acta Chim. (Budapest), **79**, 301 (1973)
[15] WEBER, J., VASILEV, YU. B., BAGOTSKII, V. S.: Elektrokhimiya, **2**, 515 (1966)
[16] BESKOROVAINAYA, S. S., KHAZOVA, O. A., VASILEV, YU. B., BAGOTSKII, V. S.: Elektrokhimiya, **2**, 932 (1966)
[17] JOHNSON, J. W., WROBLOWA, H., BOCKRIS, J. O'M.: Electrochim. Acta, **9**, 639 (1964)
[18] JOHNSON, J. W., MUELLER, S. C., JAMES, W. J.: Trans. Faraday Soc., **67**, 2167 (1971)
[19] HORÁNYI, G., SZABÓ, S., SOLT, J., NAGY, F.: Acta Chim. Acad. Sci. Hung., **68**, 206 (1971); **71**, 239 (1972)
[20] HORÁNYI, G., NOVÁK, M.: Z. phys. Chem. N. F., **75**, 323 (1971)
[21] HORÁNYI, G., NOVÁK, M.: Acta Chim. (Budapest), **75**, 369 (1973)
[22] TOMILOV, A. P., MAIRANOVSKII, S. G., FIOSHIN, M. YA., SMIRNOVA, V. A.: Elektrokhimiya organicheskikh soedinenii. Khimiya, Leningrad 1968
[23] DAMASKIN, B. N., PETRII, O. A., BATRAKOV, V. V.: Adsorbtsiya organicheskikh soedinenii na elektrodakh. Nauka, Moskva 1969
[24] BREITER, M. W.: Electrochemical Processes in Fuel Cells. Springer-Verlag, Berlin 1969
[25] KIROWA-EISNER, E., GILEADI, E.: J. Electroanal. Chem., **38**, 191 (1972)
[26] NAGY, F., HORÁNYI, G.: Mechanism of aqueous phase contact catalytic hydrogenation (in Hungarian). Vol. 6. pp. 73—120, Akadémiai Kiadó, Budapest 1971.

György HORÁNYI H-1025 Budapest, Pusztaszeri út 59—67.

György INZELT
Éva SZETEY } H-1088 Budapest, Puskin u. 11—13.

Acta Chimica Academiae Scientiarum Hungaricae, Tomus 97 (3), pp. 327–338 (1978)

MEASUREMENT OF THE HYDROXIDE ION ACTIVITY IN CONCENTRATED ALKALINE SOLUTIONS USING A Hg/HgO ELECTRODE

Z. G. SZABÓ, M. RÓZSAHEGYI-PÁLFALVI and M. ORBÁN

(Department of Inorganic and Analytical Chemistry, Eötvös L. University, Budapest)

Received July 4, 1977

The Hg/HgO electrode, used only as a reference electrode, was modified so that it proved suitable in a broad concentration interval for measurement of the changes in hydroxide ion activity of concentrated alkaline solutions. The hydroxide ion activity in alkaline aluminate solutions was measured with the aid of two such electrodes connected as a galvanic cell. A method of determining the diffusion potential arising in the system was also elaborated. Calculations based on the data thus obtained supported the literature finding that the tetrahydroxoaluminate ion predominates in systems with reasonably low aluminium contents. The formation of dimeric or oligomeric species may be assumed in systems with higher alkali and aluminium contents, but with this experimental method in itself quantitative data were not obtained.

Introduction

The formation of hydroxo complexes can in general be followed by measuring the pH change of the system. This method cannot be employed in concentrated alkaline solutions because of the alkali sensitivity of the customary electrodes. This may be the reason of the many contradictory data in the literature [1–9], for example, in connection with the compositions and structures of the complexes present in aluminate-containing alkaline solutions. In order to solve this problem, we have transformed the mercury–mercuric oxide electrode, previously used exclusively as a reference electrode [9–14], so that it is also suitable for the accurate measurement changes in hydroxide ion activity in concentrated (several molar) alkaline solutions.

The mercury–mercuric oxide indicator electrode

The material of the electrode was prepared from a mixture of metallic mercury of analytical purity, further purified by distillation, and yellow mercuric oxide of analytical purity. The components were ground to a homogeneous paste in small portions in a porcelain mortar, and the resulting paste was packed above a few drops of metallic mercury in the indicated part of the pipe-shaped electrode vessel to be seen in Fig. 1. *Via* the small platinum wire soldered into the glass, the electrode-holding part of the pipe is connected to the mercury contact, and to the millivoltmeter *via* the wire projecting into it.

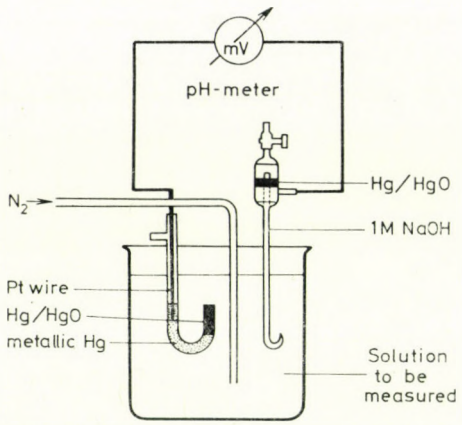

Fig. 1. The scheme of the electrode cell

A study was made on the effect of the mercury–mercuric oxide ratio on the electrode function. A 2 : 1 weight ratio of the two components was found to be optimum. If this ratio is increased, the response time of the electrode is lengthened, but the value of the electrode potential does not change. Decrease of the ratio, on the other hand, results in a too hard, friable paste, which is, therefore, difficult to handle.

The response time of the electrode depends not only on the composition of the paste, but also on the hydroxide ion concentration of the solution into which the electrode is immersed before measurement. If the hydroxide ion concentration of the solution to be measured differs by more than 1 mol/dm^3 from that of the solution with which the electrode was previously in contact, the appropriate potential value of the new solution is established within about 5 min.

The reproducibility of the measurements is ± 0.3 mV, and a Nernst electrode function was found in the concentration interval $10^{-2}-10$ *M*. The slope of the electrode potential *vs.* pOH curve proved to be 59 mV.

As reference electrode, a mercury–mercuric oxide electrode was similarly used. As Fig. 1 shows, this was situated in the tap-containing, pipette-like vessel employed for the calomel reference electrode in potentiometry. In this way, it was simple to ensure a constant ionic strength in the entire system; this was generally maintained at 6 *M*.

If the compositions of the solution to be measured and the solution in the reference electrode are exactly the same, the e. m. f. of the system is 0 or a value differing only very slightly from 0. The difference is constant for a given electrode pair, and hence, it can easily be corrected for. (The difference, which is at most $1-2$ mV, stems from the different geometries of the electrodes.)

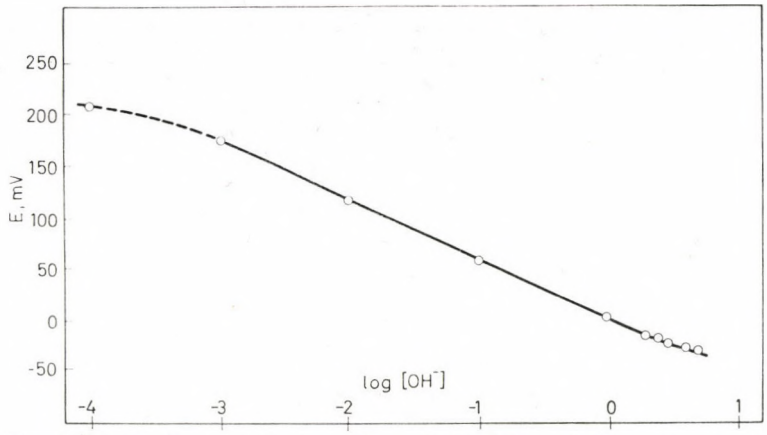

Fig. 2. E.m.f. data *vs.* the logarithm of the hydroxide ion concentration

To present the applicability of the cell for concentration measurement, in Fig. 2 the e. m. f. data on a series of sodium hydroxide solutions adjusted to an ionic strength of 6 *M* with sodium nitrate are plotted as a function of the logarithm of the hydroxide ion concentration. The reference electrode contained 1 *M* sodium hydroxide, naturally, also with an ionic strength of 6 M.

The analytical plot deviates from linearity at low and high hydroxide ion concentrations. The cause of this is the diffusion potential arising because of the different compositions of the solution under study and the solution in the reference electrode.

Study of the diffusion potential

In spite of the constant ionic strength, a diffusion potential arises in the galvanic cell system because of the appreciable difference between the mobilities of the nitrate and hydroxide ions. BARCZA *et al.* [15] demonstrated how the diffusion potential due to hydrogen ion–cation exchange can be taken into account on the basis of conductivity measurements. The diffusion potential due to hydroxide ion–anion exchange in our case was corrected for in an analogous manner. In the knowledge of the concentrations and the equivalent conductivities, the diffusion potential can be expressed as follows [15]:

$$E_d = 59.15 \log \left(1 + [OH^-] \frac{\lambda_{M,\,NaOH} - \lambda_{M,\,NaNO_3}}{M \cdot \lambda_{M,\,NaNO_3}}\right) \qquad (1)$$

At constant ionic strength, the values of the activity and conductivity coefficients are constant, and thus the following simplification may be introduced:

$$k = \frac{\lambda_{M,\,NaOH} - \lambda_{M,\,NaNO_3}}{\lambda_{M,\,NaNO_3}} \tag{2}$$

$$K = \frac{k}{M} \tag{3}$$

Hence, the diffusion potential can be described by the following equation:

$$E_d = E_0 + 59.15 \log (1 + K[OH^-]) \tag{4}$$

The measured electrode potential is comprised of two parts:

$$E_m = E_p + E_d = E_0 + 59.15 \log [OH^-] + E_d \tag{5}$$

By substituting Eq. (4) in place of E_d in relation (5), we obtain the following formula:

$$E_m - E_d = 59.15 \log \frac{[OH^-]}{1 + K[OH^-]} \tag{6}$$

The values of k and K determined in accordance with the above in sodium hydroxide solutions adjusted to ionic strengths of 2, 4 and 6 *M* with sodium nitrate are listed in Table I.

Table I

Data necessary for correction of the diffusion potential

I	$\lambda_{M,\,NaNO_3}$	$\lambda_{M,\,NaOH}$	k	K
2 M	63.7	142.4	1.234	0.617
4 M	44.2	96.2	1.175	0.293
6 M	31.9	62.6	0.963	0.160

The plot of log [OH^-] *vs.* the electrode potential corrected by the diffusion potentials calculated with the above data is presented in Fig. 3, together with the experimental curve. It can be seen that correction for the diffusion potential straightens the curve. The corrected electrode potentials can be utilized for direct equilibrium evaluation purposes.

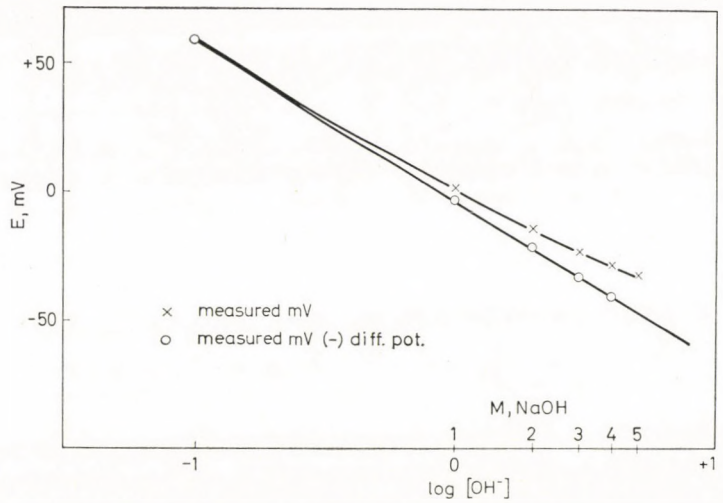

Fig. 3. The measured (-×-) and the corrected (-○-) e.m.f. data vs. the logarithm of the hydroxide ion concentration

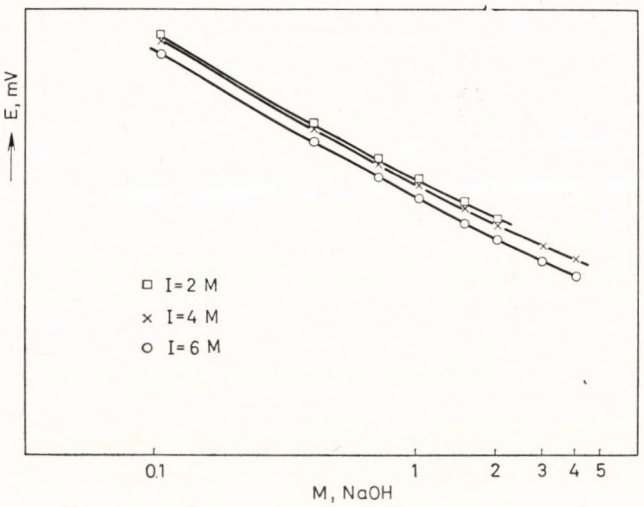

Fig. 4. The dependence of the e.m.f. data on the ionic strength

Study of other factors influencing the measurement

A study was made on how the e. m. f. of the cell depends on the ionic strength. The data measured in systems with ionic strengths of 2, 4 and 6 *M* are presented in Fig. 4.

The calibration curve of the electrode was recorded in solutions thermostated at 25 and at 60 °C. It can be seen in Fig. 5 that elevation of the temper-

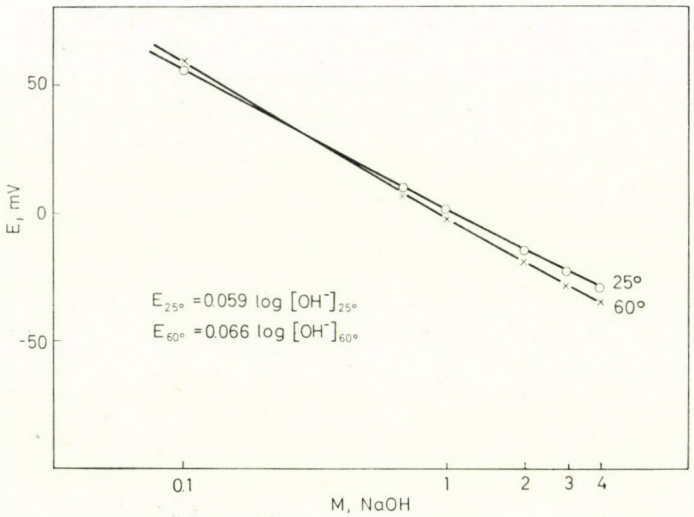

Fig. 5. The temperature dependence of the e.m.f. data

ature changes the electrode potential in accordance with the Nernst relationship, but the functioning of the electrode is not restricted at all. This permits equilibrium studies to be made above room temperature.

The oxygen sensitivity of the cell was also studied. In contrast with mercury–mercury halide electrodes, the present electrode is not sensitive to atmospheric oxygen. In spite of this, the solutions were mixed with oxygen-free nitrogen during the investigations.

After establishment of the electrode potential, its value remains unchanged during several hours. Hence, the electrode is also suitable for kinetic investigations.

Study of hydroxo complexes of aluminium

The electrode system described was employed primarily to study the aluminate complexes present in concentrated alkaline solution. To avoid errors due to the inertness of the aluminium complexes, every solution examined was prepared individually not by dilution from standard solutions.

A weighed quantity of high-purity (99.99 %) aluminium was dissolved in a solution of known concentration of analytical grade sodium hydroxide. After complete dissolution of the metal, the appropriate ionic strength and final volume were adjusted, for equilibration the solutions prepared in this way were kept in a closed plastic vessel in a 100 °C water bath for 60 min.

The concentrations of aluminium and sodium hydroxide were varied in wide intervals, and an effort was made to attain a high aluminium–sodium hydroxide ratio.

On the basis of the calibration curve, the free hydroxide ion concentration was determined from the potentials measured in the aluminium-containing solutions. In the knowledge of the total hydroxide ion and the initial aluminium concentration, it was possible to calculate the average number ($\bar{n}$) of hydroxide ions bound to one aluminium ion. The results of the first series of measurements are listed in Table II.

Table II

Formation data on the aluminium hydroxo complex

Composition (mol/dm³)		$E_{measured}$ (mV)	Equilibrium $[OH]^-$	$[OH^-]$ bound by $Al(OH)_3$	Total bound $[OH^-]$	$\bar{n}$
$[Al]_T$	$[NaOH]_T$					
0.1	0.6	18.3	0.49	0.11	0.41	4.1
0.1	1.1	0.8	1.01	0.09	0.39	3.9
0.1	1.6	−8.7	1.51	0.09	0.39	3.9
0.1	2.1	−15.5	2.04	0.06	0.36	3.6
0.1	3.1	−24.0	3.05	0.05	0.35	3.5
0.2	0.7	17.3	0.51	0.19	0.79	3.95
0.2	1.2	0.0	1.04	0.16	0.76	3.85
0.2	1.7	−9.2	1.58	0.12	0.72	3.60
0.2	2.2	−16.1	2.09	0.11	0.71	3.56
0.2	3.2	−24.1	3.08	0.12	0.72	3.60
0.5	0.9	19.9	0.45	0.45	1.93	3.90
0.5	1.0	11.5	0.57	0.43	1.95	3.85
0.5	1.5	−1.9	1.06	0.44	1.94	3.87
0.5	2.0	−11.2	1.73	0.27	1.77	3.54
0.5	2.5	−17.4	2.27	0.23	1.73	3.45
0.5	3.0	−22.5	2.88	0.18	1.68	3.35
0.5	3.5	−26.0	3.40	0.10	1.60	3.20

Surprisingly, with the increase of the sodium hydroxide concentration, the $\bar{n}$ values decreased, which contradicts with all considerations of coordination chemistry. Analysis of the experimental data revealed that if the measured potential values were increased by a value proportional to the aluminium concentration, then in all cases the calculated $\bar{n}$ values proved to be very close to the value of 4, which corresponds to $[Al(OH)_4]^-$ ion which presumably predominates in the system. It was concluded from this that the $\bar{n}$ values differing from 4 in Table II are caused by the diffusion potential due to aluminium-containing ions.

To clear this assumption, *i.e.* for the experimental determination of the diffusion potential due to the tetrahydroxoaluminate ion, cells were employed

n which the aluminium concentration varied, but the free hydroxide ion concentration was constant at 1.0 *M* in every solution. The results of such series are presented in Table III.

Table III

Diffusion potential caused by the $[Al(OH)_4]^-$ ion

Analytical composition (mol/dm³)		Equilibrium composition (mol/dm³)		Reference electrolyte [NaOH] mol/dm³	$E_{measured}$ (mV)	$E_{asymm.}$ (mV)	$E_{measd.} - E_{asymm.}$
$[Al]_T$	$[NaOH]_T$	$[NaAl(OH)_4]$	[NaOH]				$[Al(OH)_4^-]$
0.3	1.3	0.3	1.0	1.0	4.5	2.5	6.66
0.5	1.5	0.5	1.0	1.0	5.7	2.5	6.4
1.0	2.0	1.0	1.0	1.0	8.0	2.3	5.5
1.5	2.5	1.5	1.0	1.0	10.0	2.5	5.0
2.0	3.0	2.0	1.0	1.0	14.2	2.5	5.85
							average 6 mV

The data indicate that the value of the diffusion potential due to 1 *M* aluminate ion is on average of 6 mV. In the knowledge of this, the diffusion potentials caused by the aluminate ion were corrected for, and the $\bar{n}$ values were recalculated (Table IV).

The data of Table IV show that in the systems examined the number of hydroxide ions bound by one aluminium atom is 4. On the basis of literature data, it may be assumed that with the increase of the aluminium content of the solution and with the decrease of the alkali concentration, dimeric and possibly oligomeric ions [8] may be formed in addition to the monomeric aluminate ion. In the following series, therefore, the aluminium concentration was increased further. The data thus obtained show that corrections for the diffusion potential in these systems, containing higher alkali and aluminium concentrations, do not lead to a linear correlation between the potential difference and the aluminium concentration. This is apparent from the data in Table V and from Fig. 6. This indicates that the aluminium content changes the e. m. f. not only *via* the creation of a diffusion potential, but also by other, presumably coordination chemical means (the formation of dimeric or oligomeric aluminate ions, and possibly other associations).

From the analysis of a large number of experimental data, we have concluded that, merely from measurement of the e. m. f., it is not possible to decide what factors are responsible for the potential difference arising in

Table IV

Corrected n values determined in alkaline aluminate solutions (ionic strength adjusted to 6.0 M with $NaNO_3$)

Solution composition (mol/dm³)		$E_{measured}$ (mV)	$E_{diff.}$ (mV)	$E_{corr.}$ (mV)	Equilibrium [OH⁻] (mol/dm³)	Bound [OH⁻] (mol/dm³)	$\bar{n}$	$\bar{n}_{uncorr.}$
$[Al]_T$	$[NaOH]_T$							
0.1	0.6	18.3		18.9	0.48	0.12	4.2	4.0
0.1	1.1	0.8		1.4	1.00	0.10	4.0	3.9
0.1	1.6	−1.7	0.6	−8.1	1.50	0.10	4.0	3.9
0.1	2.1	−15.5		−14.9	2.00	0.10	4.0	3.4
0.1	3.1	−24.0		−23.4	3.00	0.10	4.0	3.5
0.2	0.7	17.3		18.5	0.49	0.21	4.05	3.95
0.2	1.2	0.0		1.2	1.00	0.20	4.0	3.80
0.2	1.7	−9.2	1.2	−8.0	1.50	0.20	4.0	3.60
0.2	2.2	−16.1		−14.9	2.00	0.20	4.0	3.35
0.2	3.2	−24.1		−2.29	2.96	0.24	4.2	3.6
0.5	0.9	19.9		22.9	0.40	0.50	4.0	3.9
0.5	1.0	14.5		17.5	0.50	0.50	4.0	3.85
0.5	1.5	−1.9		1.1	1.0	0.50	4.0	3.87
0.5	2.0	−11.2	3.0	−8.2	1.50	0.50	4.0	3.54
0.5	2.5	−17.4		−14.7	2.03	0.50	4.0	3.45
0.5	3.0	−22.5		−19.5	2.51	0.49	3.98	3.35
0.5	3.5	−26.0		−23.0	3.00	0.50	4.0	3.20
0.4	1.0	11.6		14.1	0.61	0.39	3.97	3.79
0.4	1.5	−3.6		−1.1	0.98	0.42	4.02	3.68
0.4	2.0	−12.5		−10.0	1.58	0.42	4.02	3.60
0.4	2.5	−18.5	2.5	−16.0	2.05	0.35	3.87	3.50
0.4	3.0	−23.5		−21.0	2.59	0.41	4.01	3.18
0.4	3.5	−27.2		−24.7	3.10	0.40	4.0	3.0
0.6	2.0	−10.5		−6.9	1.39	0.61	4.01	3.64
0.6	2.5	−17.3	3.6	−13.7	1.86	0.64	4.06	3.53
0.6	3.0	−22.4		−18.8	2.35	0.65	4.06	3.37
0.6	3.5	−26.5		−22.9	2.83	0.67	4.1	3.20
0.8	1.5	4.0		8.8	0.75	0.75	3.93	3.73
0.8	3.0	−23.2	4.8	−18.4	2.10	0.90	4.1	3.15
0.8	3.5	−15.9		−21.1	2.56	0.94	4.15	3.25
1.0	2.0	−6.95		−0.95	1.09	0.91	3.91	3.59
1.0	3.0	−21.5	6.0	−15.5	2.0	1.0	4.00	3.35

Table IV (continued)

Solution composition (mol/dm³)		$E_{measured}$ (mV)	$E_{diff.}$ (mV)	$E_{corr.}$ (mV)	Equi-librium $[OH^-]$ (mol/dm³)	Bound $[OH^-]$ (mol/dm³)	$\bar{n}$	$\bar{n}_{uncorr.}$
$[Al]_T$	$[NaOH]_T$							
1.0	3.5	− 26.2		− 20.2	2.5	1.0	4.00	3.13
0.6	1.5	− 3.2		0.4	0.92	0.58	3.97	3.72
0.6	2.2	− 16.0	3.6	− 13.4	1.57	0.63	4.05	3.58
0.6	3.2	− 26.6		− 23.0	2.56	0.64	4.05	3.32
0.6	4.0	− 31.4		− 27.8	3.24	0.76	4.25	3.18
0.8	2.0	− 10.7		− 5.9	1.19	0.81	4.0	3.69
0.8	2.5	− 17.8	4.8	− 13.0	1.63	0.87	4.09	3.60
0.8	3.0	− 23.8		− 19.0	2.12	0.78	4.08	3.44
0.8	4.0	− 31.1		− 26.3	3.09	1.0	3.98	3.26
1.0	2.5	− 16.5		− 16.5	1.45	0.95	3.95	3.61
1.0	3.2	− 24.8	6.0	− 18.8	2.14	1.06	4.06	3.41
1.0	4.0	− 31.4		− 26.4	3.0	1.0	4.0	3.21
1.2	2.5	− 14.2		− 7.0	1.24	1.26	4.05	3.67
1.2	3.0	− 26.0	7.2	− 15.1	1.78	1.22	4.02	3.45
1.2	3.5	− 32.3		− 18.8	2.12	1.38	4.15	3.47
1.4	2.5	− 13.1		− 4.7	1.11	1.39	3.99	3.63
1.4	3.0	− 21.1	8.4	− 12.7	1.60	1.40	4.00	3.49
1.4	3.5	− 26.0		− 16.6	1.93	1.57	4.10	3.39
1.4	4.0	− 29.7		− 21.3	2.48	1.52	4.06	3.32
1.8	3.0	− 21.0		− 10.2	1.42	1.58	3.88	3.38
1.8	3.5	− 26.5	10.8	− 15.7	1.80	1.70	3.94	3.27
1.8	4.0	− 30.4		− 19.6	2.20	1.80	4.00	3.18
1.6	3.5	− 25.5	9.6	− 15.9	1.85	1.65	4.03	3.38
1.6	4.0	− 29.7		− 20.1	2.26	1.74	4.04	3.28

solutions of the same free alkali concentration. There is no doubt that part of the potential difference stems from the diffusion potential caused by the aluminate ions. In addition, the e. m. f. values are changed by all processes accompanied by a change in the hydroxide ion activity, *e.g.* formation of dimeric or oligomeric ions. Thus, it is also conceivable that the change in the e. m. f. due to these processes and the effect of the diffusion potential caused by the aluminate ion feature together in all the experimental data.

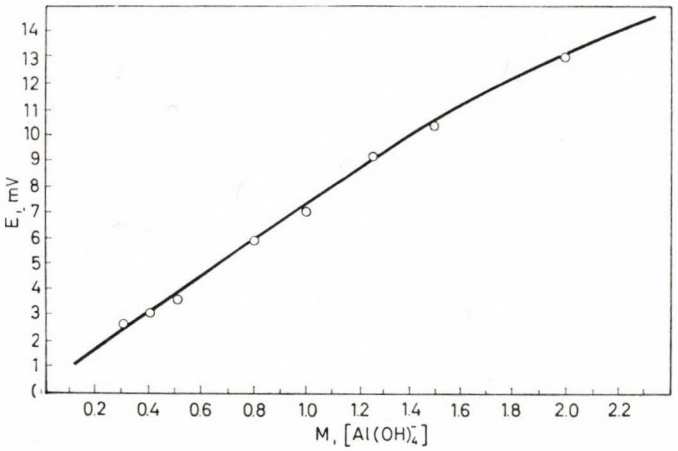

Fig. 6. The corrected e.m.f. data for $Al(OH)_4^-$. Ionic strenght 6 M, free $[OH^-]$ 1.0 M

Table V

Effect of the aluminium content on the e. m. f. measured in alkaline aluminate solutions

Analytical composition (mol/dm³)		Calculated equilibrium composition (mol/dm³)		Reference electrolyte (mol/dm³) [NaOH]	$E_{measured}$ (mV)
$[NaOH]_T$	$[Al]_T$	$[OH^-]$	$[Al(OH)_4^-]$		
3.0	1.0	2.0	1.0	2.0	−21.2
4.0	1.0	3.0	1.0	3.0	−26.8
5.0	1.0	4.0	1.0	4.0	−32.9
6.0	1.0	5.0	1.0	5.0	−42.6
2.5	2.0	0.5	2.0	0.5	+9.2
3.0	2.0	1.0	2.0	1.0	−7.6
4.0	2.0	2.0	2.0	2.0	−20.9
5.0	2.0	3.0	2.0	3.0	−25.5
5.0	3.0	2.0	3.0	2.0	−24.8
6.0	3.0	3.0	3.0	3.0	−30.6

Experimental data suitable for quantitative determination of the extent of aluminate dimer or polymer formation, and for calculation of the equilibrium data describing these, may thus be obtained only if the two above effects can be separated.

Accordingly, we plan in the future to study the hydroxo complexes of aluminium *via* conductometric, viscosity, density and solubility measurements.

REFERENCES

[1] LINDAL, S. L., DHAR, S. R.: Chem. Newslett., 133 (1926)
[2] FUNK, E. P.: Zh. Fiz. Khim., **7**, 899 (1936)
[3] PAZUKHIN, V. P.: Tsvetn. Met., **22**, 159 (1952)
[4] IVEKOVIC, H., VRBASKI, T., PAVLOVIC, D.: Croat. Chem. Acta, **28**, 41 (1956)
[5] KUZNETSOV, S. I.: Nauchn. Dokl. Visshey Shkoli Met., Moskva 1958
[6] KUZNETSOV, S. I., DEREVYANKIN, V. A.: Fizicheskaya khimiya proizvodstva glinozema po sposoby Bayera. Moskva 1964
[7] JAHR, K. F., PERNOLL, L.: Ber. Bunsenges Phys Chem., **69**, 221 (1965)
[8] MOOLENAAR, R. J., EVANS, J. G., MC KEEVER, L. D.: J. Phys. Chem., **74**, 3629 (1970)
[9] SZITA, L., BERECZ, E.: Magy. Kém. Folyóirat, **81**, 383 (1975)
[10] BRIGGS, G. W. D., JONES, E., WYNNE, W. F. K.: Trans. Faraday Soc., **51**, 1433 (1955)
[11] HAMER, W. J., CRAIG, D. N.: J. Electrochem. Soc., **104**, 206 (1957)
[12] EVERY, L. L., BANKS, W. P.: Corrosion, **23**, 151 (1967)
[13] CARE, B., BIGNOLD, G. J.: J. Appl. Electrochem., **1**, 141 (1971)
[14] IVES, D. J. G., JANZ, G. J.: Reference Electrodes, p. 335. Academic Press, London 1961
[15] BARCZA, L., STRÓBL, L., LEHOCZKY, B.: Acta Chim. Acad. Sci. Hung., **63**, 319 (1970)

Zoltán G. SZABÓ
Márta RÓZSAHEGYI-PÁLFALVI
Miklós ORBÁN
H-1088 Budapest, Múzeum krt. 4/B.

Acta Chimica Academiae Scientiarum Hungaricae, Tomus 97 (3), pp. 339–344 (1978)

CONVERSIONS OF TOSYL AND MESYL DERIVATIVES OF THE MORPHINE GROUP, XXI*

C-6 HALOGEN DERIVATIVES OF DIHYDROCODEINE

G. SOMOGYI, S. MAKLEIT and R. BOGNÁR

(Institute of Organic Chemistry, Kossuth Lajos University, Debrecen)

Received December 6, 1976

6-O-Mesyldihydrocodeine was converted into 6-chlorodihydrocodide; also the new compounds 6-fluoro- and 6-bromodihydrocodide have been synthesized. The reaction of 6-O-mesyldihydrocodeine with sodium iodide did not give the 6-iodo derivative, but the product was deoxycodeine-C.

Of the possible C–6 halogen derivatives of dihydrocodeine, only the chloro derivative has been described in the literature; this was prepared by the hydrogenation of α-chlorocodide under controlled conditions or by the treatment of dihydrocodeine with phosphorus pentachloride. The compound has structure **3** (3-methoxy-4,5α-epoxy-6β-chloro-17-methylmorphinan) [1].

On the basis of our earlier results [**2a–f**], 6-O-mesyldihydrocodeine (**1**) was chosen as the starting material in the preparation of halogen derivatives of dihydrocodeine.

The investigations are summarized in Scheme 1 and Table I.

As shown in the Scheme and Table, the chloro derivative (**3**) was prepared from **1** in a new reaction route, and the fluoro (**2**) and bromo (**4**) derivatives unknown up to now have also been synthesized. According to our experiments, the iodo derivative cannot be prepared in this way: conversion occured only under the conditions specified in Experimental, when deoxycodeine-C (**5**) was obtained. The same compound was formed, in addition to the bromo derivative (**4**), at higher temperatures, and this was the only product of the reaction of **1** and bromide anion when the reaction time was prolonged.

Deoxycodeine-C (**5**) can be synthesized from 6-chlorodihydrocodide with sodium methoxide at 140 °C in 24 hrs [3], and this is the only known chemical reaction of chlorodihydrocodide. The resistance of chlorodihydrocodide to take part in reactions has been discussed by STORK [4] with reference to the very slow reactions of β-halogen ethers in S_N1 type processes. According to our experience, the same holds for reactions of S_N2 type, too: no conversion was observed with **3** and azide anion in dimethylformamide, even when applying very long reaction times.

* Part XX: MAKLEIT, S., BERÉNYI, S., BOGNÁR, R., ELEK, S.: Acta Chim. (Budapest) **94**, 161 (1977) and Magyar Kém. Folyóirat **83**, 327 (1977).

Table I

Compound	Solvent	Reaction time, hr.	Temp., °C	Anion	Yield, %	M. p., °C	$[\alpha]_D$	Analysis, % calcd.	Analysis, % found	$J_{5,6}$***
2	CH_3CN	12	b.p.	F^-	8.72	154–6	−108° $CHCl_3$, $c = 0.671$	F 6.28	F 5.77	8 Hz
3	DMF	1	b.p.	Cl^-	75.9*	174–5*	−177° $CHCl_3$, $c = 0.5$*	Cl 11.1	Cl 10.51 10.48	8 Hz
4	DMF	43	100	Br^-	26.1	167–8	−190.4° $CHCl_3$, $c = 0.5$	Br 21.7	Br 21.58 21.51	8 Hz
4	DMF	4	b.p.	Br^-	12.1	Identical with the former				
5	DMF	7	b.p.	I^-	29.2	103–5**	−202.8° $CHCl_3$, $c = 0.5$**	N 4.96	N 5.07 5.02	
5	DMF	4	b.p.	Br^-	63.1	Identical with the former				
5	DMF	7	b.p.	Br^-	48.5	Identical with the former				

* Literature data: yield: 52 %, m. p. 172.5–174 °C, $[\alpha]_D$ −177.8° [1].
** Literature data: m. p. 104–105 °C, $[\alpha]_D$ −199.4° (EtOH, $c = 1.745$) [3].
*** In the PMR spectrum the doublet at 4.6 ppm confirms the C-6 position of the halogen atoms; $J_{5,6} = 8$ Hz substantiates the *trans axial* relation of the C-5 and C-6 protons, *i.e.* the *iso* steric position (C-6 *equatorial)* of the halogen atoms; in compound **5** the two olefinic protons are seen at 5.6 ppm.

Deoxycodeine-C is probably formed from **1** with sodium iodide through the intermediate iodo derivative (which cannot be isolated), although the mesyloxy group and the C–7 proton are in *trans diaxial* position in **1**; this route is indicated by the fact that in the preparation of the bromo derivative the reaction is shifted to give deoxycodeine-C when longer reaction times and higher temperatures are used, furthermore, the bromo derivative isolated can be converted into **5**, whereas **1** remains unchanged in a similar treatment.

Thus as an extension of our earlier results [5], it has been found that the C–6 *axial* tosyloxy and mesyloxy groups are suitable for accomplishing nucleophilic substitution reactions also with halogen anions, unlike the practically non-reactive C–6 *equatorial* chlorine.

The reactions achieved in dipolar aprotic solvent are of S_N2 type, in view of the conditions of the reaction and the structure of the products.

Experimental

M. p.'s were determined in open capillaries; they are uncorrected. The m. p. of 6-fluorodihydrocodide (**2**) was measured on a Koffler apparatus.

Homogeneity of the substances was checked in each case by TLC, using Silica gel G (Merck) adsorbent, benzene–methanol 8 : 2 developing agent and Dragendorff reagent for detection.

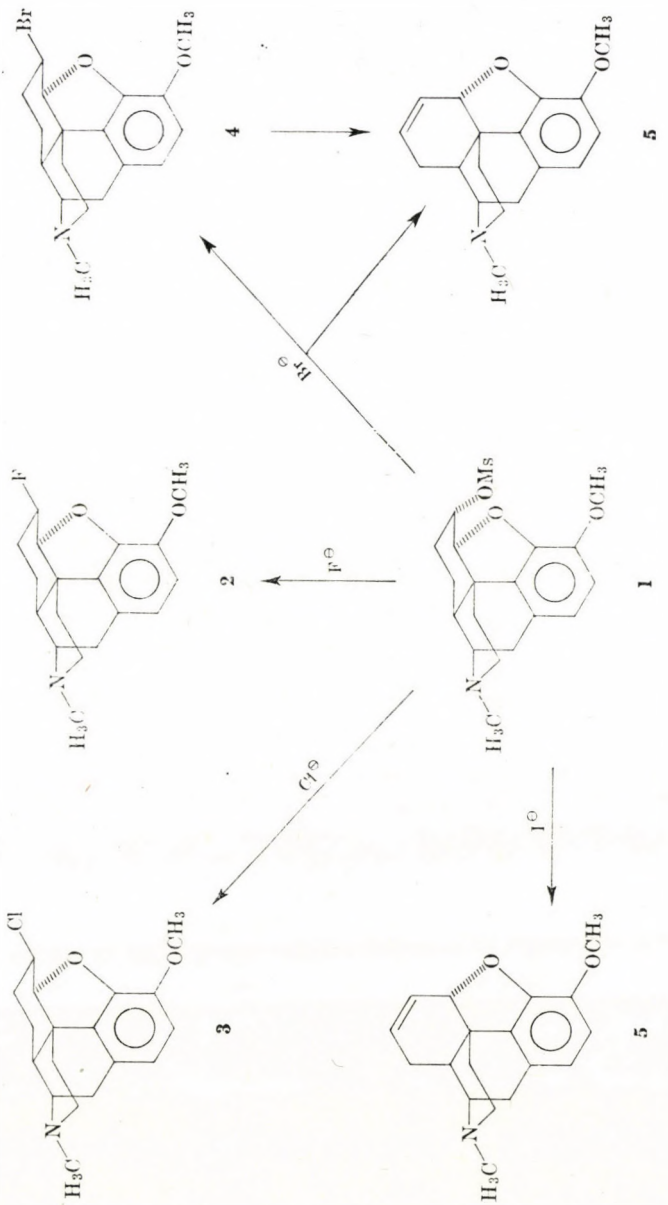
Br
OCH3
O
N
H3C
4
5
Br⊖
F
2
F⊖
OMs
1
Cl⊖
I⊖
Cl
3
5

The PMR spectra were recorded with a Jeol 100 MHz instrument at room temperature in deuterochloroform solution using TMS internal standard.

The IR spectra were recorded with a Unicam SP 200 G spectrophotometer in KBr pellets.

6-O-Mesyldihydrocodeine (1)

The substance was prepared as given in Ref. [5a, b]. $C_{19}H_{25}O_5NS$ (379.47).

6-Fluorodihydrocodide (2)

6-O-Mesyldihydrocodeine (**1**) (0.5 g; 0.00132 mole) and tetrabutylammonium fluoride (3.31 g; 0.018 mole) were dissolved in anhydrous acetonitrile (25 ml). After refluxing the solution for 12 hrs, it was poured into water (70 ml) and extracted with chloroform (3×20 ml). The combined chloroform solution was washed with water (2×15 ml) and dried over magnesium sulfate. After evaporation to dryness a syrupy substance was obtained; this was dissolved in ether (15 ml). The solution was filtered from a small amount of brownish impurity, and the filtrate was evaporated to dryness. The yellow crystals were recrystallized from methanol to obtain white crystals (35 mg; 8.72 %), m. p. 154–156 °C, $[\alpha]_D$ −108° (chloroform, c = 0.671).

$C_{18}H_{22}O_2NF$ (303.37). Calcd. F 6.28. Found F 5.77 %.

6-Chlorodihydrocodide (3)

6-O-Mesyldihydrocodeine (**1**) (1 g; 0.00264 mole) and lithium chloride (1.15 g; 0.0264 mole) were dissolved in anhydrous dimethylformamide (25 ml). After refluxing for 1 hr, the solution was poured into water (80 ml) and extracted with benzene (3×20 ml). The combined benzene solution was washed with water (2×15 ml), dried over magnesium sulfate, filtered and evaporated to dryness in vacuum. The solid product was recrystallized from ethanol to obtain **3** (0.64 g; 75.9 %), m. p. 174–175 °C, $[\alpha]_D$ −177° (chloroform, c = 0.5).

$C_{18}H_{22}O_2NCl$ (319.8). Calcd. Cl 11.1. Found Cl 10.48, 10.51 %.

6-Bromodihydrocodide (4)

(*a*) 6-O-Mesyldihydrocodeine (**1**) (1 g; 0.00264 mole) and lithium bromide (1.06 g 0.0106 mole) were dissolved in anhydrous dimethylformamide (30 ml). The solution was heated at 100 °C for 43 hrs, then poured into water (80 ml) and extracted with benzene (3×20 ml). The combined benzene solution was washed with water (2×15 ml), dried over magnesium sulfate, filtered and evaporated to dryness in vacuum. A sticky brown substance was obtained, which was purified on a chromatographic column (Silica gel H, benzene–methanol, 9 : 1). The combined fractions were concentrated to obtain a solid product; this was recrystallized from ethanol. The pure product (0.25 g; 26.1 %) had m. p. 167–168 °C, $[\alpha]_D$ −190.4° (chloroform, c = 0.5).

$C_{18}H_{22}O_2NBr$ (364.28). Calcd. Br 21.7. Found Br 21.58, 21.51 %.

(*b*) 6-O-Mesyldihydrocodeine (**1**) (1 g; 0.00264 mole) and lithium bromide (2.02 g; 0.021 mole) were dissolved in anhydrous dimethylformamide (30 ml). After refluxing the solution for 4 hrs, it was poured into water (80 ml) and extracted with chloroform (3×20 ml). The combined chloroform solution was washed with water (2×15 ml), dried over magnesium sulfate, filtered and evaporated to dryness in vacuum. A sticky brown product was obtained, which crystallized on standing. The product was recrystallized from ethanol (0.09 g; 12.1 %). The product was identical with that prepared according to (*a*).

Deoxycodeine-C (5)

(*a*) 6-O-Mesyldihydrocodeine (**1**) (3 g; 0.00792 mole) and sodium iodide (12.18 g; 0.0792 mole) were dissolved in anhydrous dimethylformamide (100 ml). After refluxing for 7 hrs, the solution was cooled and poured into water (250 ml), extracted with chloroform (3×60 ml) and the combined chloroform solution was washed with water (2×50 ml), dried over magnesium sulfate, filtered and evaporated to dryness. A sticky brown residue was obtained, which solidified on rubbing with ether. The brown crystalline substance was dissolved in water and made alkaline with 10 % ammonium hydroxide (pH 9 – 10). The solution was extracted with chloroform, washed with water and dried over magnesium sulfate. After filtering of the drying agent, the filtrate was evaporated to dryness in vacuum. A yellow sticky material was obtained which solidified on rubbing with ether (0.65 g; 29.2 %), m. p. 103 – 105 °C, $[\alpha]_D$ – 202.8° (chloroform, $c = 0.5$); the product contained no iodine.

$C_{18}H_{20}O_2N$ (282.35). Calcd. N 4.96. Found N 5.07, 5.02 %.

The substance gave no melting point depression with deoxycodeine-C prepared according to Ref. [3]; the physical constants, PMR and IR spectra were identical.

(*b*) 6-O-Mesyldihydrocodeine (**1**) (1 g; 0.00264 mole) and lithium bromide (2.02 g; 0.021 mole) were dissolved in anhydrous dimethylformamide (30 ml). After refluxing for 4 hrs, the solution was processed as in the case of preparing 6-bromodihydrocodide (*b*). The mother liquor of the chloroform extraction was made alkaline (pH 9 – 10) with 10 % ammonium hydroxide and extracted with chloroform; the combined chloroform solution was washed with water and dried over magnesium sulfate, then evaporated to dryness in vacuum. A yellow sticky material was obtained, which was crystallized from ethanol to give 0.47 g (63.1 %) of **5**.

The product was identical with that obtained according to Ref. [3].

(*c*) 6-O-Mesyldihydrocodeine (**1**) (2 g; 0.00528 mole) and lithium bromide (5.0 g; 0.042 mole) were dissolved in anhydrous dimethylformamide (50 ml). After refluxing the solution for 7 hrs, it was poured into water (140 ml) and extracted with chloroform (3×30 ml). The combined chloroform solution was washed with water (2×20 ml), dried over magnesium sulfate and evaporated to dryness in vacuum to leave a brown sticky material. This was dissolved in water and filtered from a small amount of impurity; the filtrate was made alkaline (pH 9 – 10) with 10 % ammonium hydroxide and extracted with chloroform. The chloroform solution was washed with water, dried over magnesium sulfate and evaporated to dryness in vacuum; the residue was crystallized from ethylacetate. A solid product was obtained, which was identical with the substance (deoxycodeine-C) prepared according to Ref. [3].

The mother liquor of the chloroform extraction step was made alkaline (pH 9 – 10) with 10 % ammonium hydroxide and extracted with chloroform. The combined chloroform solution was washed with water and dried over magnesium sulfate, evaporated to dryness in vacuum and crystallized from ethyl acetate. The product was found to be identical with deoxycodeine-C prepared according to Ref. [3]. Total weight of **5**: 0.722 g (48.5 %).

*

The authors' thanks are due to Department I of Hungarian Academy of Sciences and to the Alkaloid Works, Tiszavasvári, Hungary, for supporting this research.

REFERENCES

[1] Small, L. F.: Chemistry of the Opium Alkaloids. p.223. Government Printing Office, Washington, 1932
Bentley, K. W.: The Chemistry of the Morphine Alkaloids. p. 128. Clarendon Press, Oxford, 1954
Small, L., Faris, B. F., Mallonee, J. L.: Org. Chem. **5**, 334 (1940)

[2] a) Bognár, R., Makleit, S., Radics, L.: Acta Chim. Acad. Sci. Hung. **67**, 63 (1971)
b) Bognár, R., Makleit, S., Radics, L.: Magyar Kém. Folyóirat **76**, 461 (1970)
c) Makleit, S., Radics, L., Bognár, R., Mile, T.: Acta Chim. (Budapest) **74**, 111 (1972)
d) Bognár, R., Makleit, S., Radics, L., Mile, T.: Magyar Kém. Folyóirat **78**, 228 (1972)
e) Makleit, S., Somogyi, G., Bognár, R.: Acta Chim. (Budapest) **89**, 173 (1976)
f) Makleit, S., Somogyi, G., Bognár, R.: Magyar Kém. Folyóirat **81**, 517 (1975)

[3] SMALL, L. F., COHEN, F. L.: J. Am. Chem. Soc. **53,** 2214 (1931)
[4] STORK, G., CLARKE, F. H.: J. Am. Chem. Soc. **78,** 4619 (1956)
[5] a) BOGNÁR, R., MAKLEIT, S.: Acta Chim. Acad. Sci. Hung. **59,** 373 (1969)
b) BOGNÁR, R., MAKLEIT, S.: Magyar Kém. Folyóirat **74,** 523 (1968)
c) MAKLEIT, S., RADICS, L., BOGNÁR, R., MILE, T., OLÁH, É.: Acta Chim. (Budapest) **74,** 99 (1972)
d) MAKLEIT, S., RADICS, L., BOGNÁR, R., MILE, T., OLÁH É.: Magyar Kém. Folyóirat **78,** 223 (1972)

Gábor SOMOGYI
Sándor MAKLEIT
Rezső BOGNÁR
H-4010 Debrecen.

Acta Chimica Academiae Scientiarum Hungaricae, Tomus 97 (3), pp. 345—351 (1978)

SYNTHESIS OF PHENYL 2-DEOXY- AND 3-DEOXY-β-D-GLUCOPYRANOSIDE

L. KISS

(Biochemical Institute, Kossuth Lajos University, Debrecen)

Received March 22, 1977

The synthesis of phenyl 2-deoxy- and -3-deoxy-β-D-glucopyranoside (5) and (10) is reported. The synthesis were performed *via* $LiAlH_4$ reduction of the appropriate *p*-toluenesulfonyl derivatives (4) and (9). Investigations on the conceivable role of epoxid-intermediates have shown that no epoxides are involved in the reductions.

During an investigation of the formation of the enzyme–substrate complex in the case of sweet almond emulsine, phenyl 2-deoxy- and 3-deoxy-β-D--glucopyranoside of high anomer purity were needed.

There are methods for the synthesis of 2-deoxy- [1], [2], [3] and 3-deoxy--D-glucose [1], [4], [5], but when starting from these compounds, it is difficult to attain the desired anomer purity, especially in the case of the 2-deoxy derivative, owing to the lack of a suitable "participating group" at position 2. Furthermore, it is tedious to prepare 2-deoxy- and 3-deoxy-D-glucose, too.

Therefore, the syntheses were performed by an other method, starting from phenyl β-D-glucopyranoside derivatives with high anomer purity.

It is well-known that in the case of the $LiAlH_4$ reduction of tosyloxy groups attached to a secondary hydroxyl group O–S bond cleavage takes place. In some cases [6], [7], [11], [20], however, the deoxy function could be obtained by $LiAlH_4$ reduction of secondary tosyloxy groups.

VIS and KARRER [8] prepared methyl 4,6-O-benzylidene-3-deoxy-β-D-ribo--hexopyranoside by the $LiAlH_4$ reduction of methyl 4,6-O-benzylidene-2,3-di--O-*p*-tolylsulfonyl-β-D-glucopyranoside. ALLERTON and OVEREND [9] obtained methyl 2-deoxy-β-L-erythropentopyranoside by treatment of methyl 2-O-*p*--tolylsulfonyl-β-D-arabinopyranoside with $LiAlH_4$. Methyl 4,6-O-benzylidene-2--deoxy- and -3-deoxy-β-D-glucopyranoside could be synthesized in yield of 30 % by $LiAlH_4$ treatment of methyl 4,6-O-benzylidene-2-O-*p*-tolylsulfonyl- and -3-O-y-tolylsulfonyl-β-D-glucopyranoside, as reported by UMEZAWA *et al.* [10].

Continuing the investigation of the $LiAlH_4$ reduction of secondary tosyloxy derivatives, a method has been evolved for the synthesis of phenyl 2-deoxy-β-D-glucopyranoside and phenyl 3-deoxy-β-D-glucopyranoside in better yields than those obtained by UMEZAWA *et al.* [10]. The reaction routes are summarized in Scheme 1.

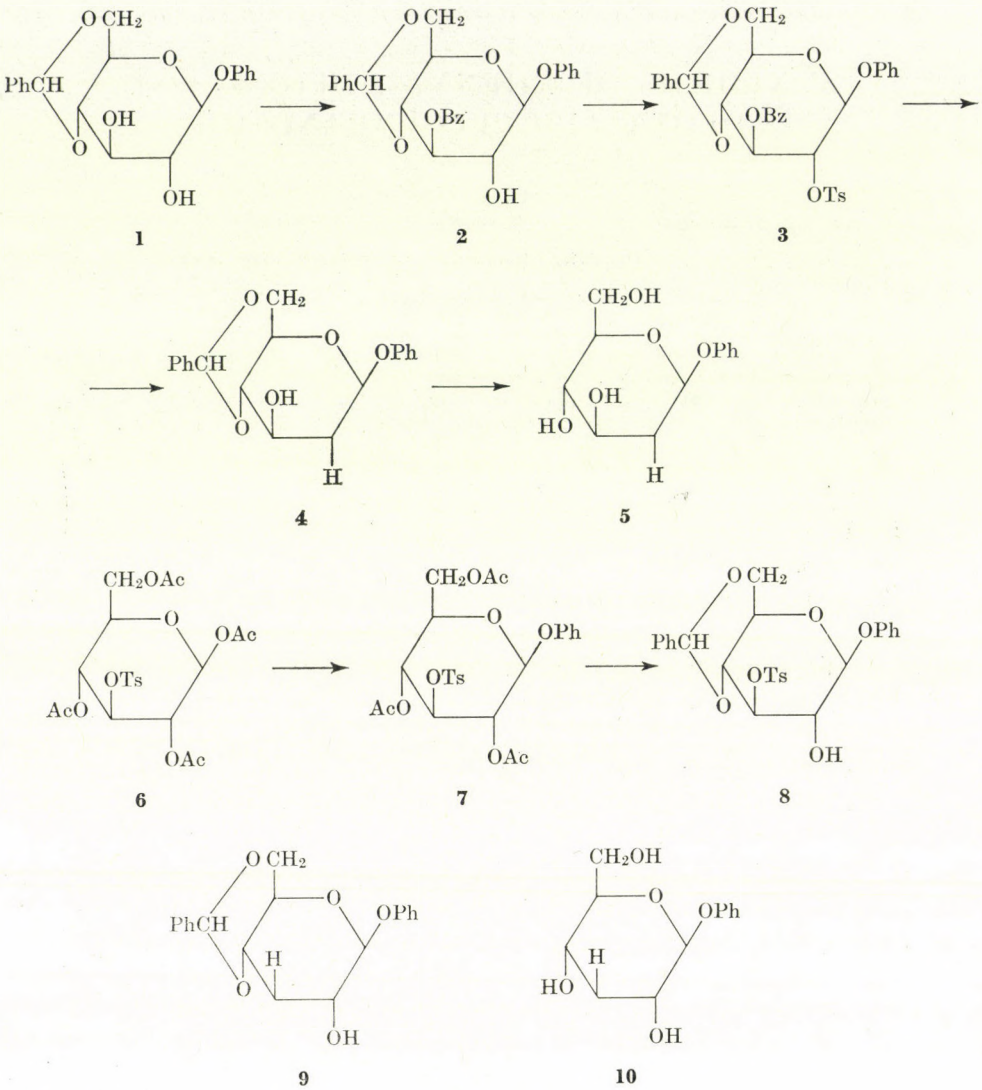

Fig. 1

In the synthesis of phenyl 2-deoxy-β-D-glucopyranoside (**5**) the readily available phenyl 4,6-O-benzylidene-β-D-glucopyranoside (**1**) [12] was used as the starting material; benzoylation of 1 with N-benzoylimidazole according to CHITTENDEN [13] gave predominantly the 3-O-benzoyl-derivative (**2**) as it was shown by TLC; recrystallization from alcohol yielded pure **2**. Treatment of **2** with tosyl chloide in dry pyridine afforded phenyl 4,6-O-benzylidene-3-O--benzoyl-2-O-*p*-tolylsulfonyl-β-D-glucopyranoside (**3**). The reaction was moni-

tored by TLC. Compound **3** was treated with $LiAlH_4$ in boiling anhydrous THF for 20 hrs. to obtain phenyl 4,6-O-benzylidene-2-deoxy-β-D-glucopyranoside (**4**). The structure of **4** was identified by the multiplicity of the NMR signal due to the anomeric proton being coupled with the equatorial and axial proton on C_2 and giving two doublets at 5.2 and 5.3 ppm with the coupling constants of $J_{1,2e} = 2.4$ Hz and $J_{1,2a} = 9.7$ Hz.

In view of the sensitivity of 2-deoxy derivatives to acids, the benzylidene group was eliminated by catalytic hydrogenation to obtain phenyl-2-deoxy--β-D-glucopyranoside (**5**).

1,2,4,6-Tetra-O-acetyl-3-O-*p*-tolylsulfonyl-β-D-glucopyranose (**6**) was the starting material in the synthesis of phenyl-3-deoxy-β-D-glucopyranoside. Phenyl 2,4,6-tri-O-acetyl-3-O-*p*-tolylsulfonyl-β-D-glucopyranoside (**7**) was obtained from **6** according to HELFERICH [14]. Compound **7** was saponified by ZEMPLÉN's method [15], [16] and the product after evaporation without isolation was treated with benzaldehyde and $ZnCl_2$ to obtain **8**. Compound **8** was then treated with $LiAlH_4$ in the same manner as above, to yield **9**. The benzylidene group was eliminated with trifluoroacetic acid to obtain phenyl 3-deoxy-β-D-glucopyranoside (**10**). The structure of **10** was prooved by periodate oxidation; as expected, there was no periodate consumption. The physical constants of **10** were in good agreement with that described in literature [23].

Investigating the mechanism of the $LiAlH_4$ reduction of secondary tosyloxy groups, VIS and KARRER [8] suggested that the reaction proceeded *via* an epoxide intermediate. Later the problem was reinvestigated by OVEREND *et al.* [7]; they proposed that $LiAlH_4$ direct reduction of secondary tosyloxy groups to deoxy function takes place only when there are unsubstituted or acylsubstituted hydroxyl groups in the vicinity of the tosyloxy group. In these cases an alkoxyaluminium hydride derivative can be formed followed by intramolecular hydride displacement of the *p*-tolylsulfonyloxy group [10] (Fig. 2).

In order to decide whether the reaction proceeds *via* the epoxide intermediates, the two possible epoxide derivatives, phenyl 2,3-anhydro-4,6-O--benzylidene-β-D-mannopyranoside (**11**) and phenyl 2,3-anhydro-4,6-O-benzylidene-β-D-allopyranoside (**12**) were prepared [17] and treated with $LiAlH_4$ in the same manner as tosyl derivatives. The reaction mixtures and pure **4** and **9** were investigated by gas chromatography, after acetylation, on a 10 % UCW 982 column. The RT values are summarized in Table I.

It is seen that from **11** only one product was formed which was not identical with **4** on the basis of the RT values; thus, of the two possible deoxy derivatives [18], it is phenyl 4,6-O-benzylidene-3-deoxy-β-D-arabinohexopyranoside [13], [19]; however, in the case of 12 both possible [18] deoxy derivatives, phenyl 4,6-O-benzylidene-2-deoxy-β-D-ribohexopyranoside (**14**) and phenyl 4,6-O-benzylidene-3-deoxy-β-D-ribohexopyranoside (**9**), were formed in ratio of 65 : 33; yet in the $LiAlH_4$ reduction of **8** only **9** was formed.

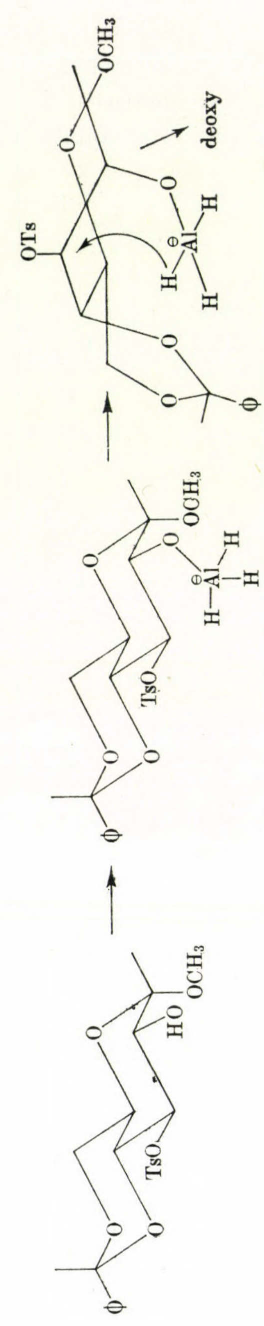

Fig. 2

Table I

	RT
Phenyl 2,3-anhydro-4,6-O-benzylidene-β-D--alloside (**12**)	14.41; 15.78
Phenyl 2,3-anhydro-4,6-O-benzylidene-β-D--mannoside (**11**)	15.51
Phenyl 4,6-O-benzylidene-2-deoxy-β-D--glucoside (**4**)	14.88
Phenyl 4,6-O-benzylidene-3-deoxy-β-D--glucoside (**9**)	15.82

It is obvious from these results that no epoxide intermediate played a part in the $LiAlH_4$ reductions of **3** and **8**.

Experimental

M. p.'s were obtained on a Kofler apparatus and are uncorrected. Optical rotations were measured with a Polamat A (Zeiss) automatic photoelectric polarimeter. NMR spectra were recorded on a Jeol MH-100 instrument in $CDCl_3$ and deuterated DMSO solutions, with TMS internal standard. The reactions were monitored and the purity of the products assessed by TLC on Kieselgel G Merck. Kieselgel G was also used for short column chromatography [21].

Phenyl 4,6-O-benzylidene-β-D-glucopyranoside (1)

This was synthesized according to McCLOSKEY and COLEMAN [12].

Phenyl 3-O-benzoyl-4,6-O-benzylidene-β-D-glucopyranoside (2)

Compound 1 (34.4 g; 0.1 mole) was benzoylated according to CHITTENDEN [13] to obtain pure **2** after crystallization from ethanol–acetone (250 ml); the yield was 19.2 g (42.8 %), m. p. 203 – 206 °C; $[\alpha]_D^{20}$ – 56.8° (c = 1; $CHCl_3$).

$C_{26}H_{24}O_7$ (448.47). Calcd. C 69.63; H 5.39. Found C 69.72; H 5.42 %.

Phenyl 3-O-benzoyl-4,6-O-benzylidene-2-O-p-toluenesulfonyl-β-D--glucopyranoside (3)

Compound **2** (2.6 g; 0.012 mole) was dissolved in dry pyridine (50 ml); 2.8 g (0.015 mole) of *p*-toluenesulfonyl chloride was added and the mixture was kept at 45 – 50 °C for two days, whereafter the reaction was complete as shown by TLC. (solvent : benzene–acetone 9 : 1). The reaction mixture was poured into ice-water and extracted three times with $CHCl_3$ (120 ml). The extract was free from pyridine with 0.5 *N* sulfuric acid and then with water until neutral. After drying over Na_2SO_4, the solvent was evaporated. The residue was crystallized from ethanol (100 ml) to give 3 g (86.3 %) of **3**; m. p. 179 – 180 °C; $[\alpha]_D^{40}$ – 34.5° (c = 1; $CHCl_3$).

$C_{33}H_{30}O_9S$ (602.58). Calcd. C 65.77; H 5.02. Found C 65.68; H 5.0 %.

Phenyl 4,6-O-benzylidene-2-deoxy-β-D-glucopyranoside (4)

$LiAlH_4$ (0.75 g; 19.8 mmoles) was suspended in anhydrous tetrahydrofuran (10 ml) and the mixture was stirred at 65 – 70 °C for 2 hrs. Compound **3** (2 g; 3.3 mmoles) was added in solid form and stirring was continued for 20 hrs. The excess of $LiAlH_4$ was destroyed by

adding 7 ml of ethyl acetate. The mixture was poured into 100 ml of ether, filtered, the filtrate was washed with 10 % solution of potassium sodium tartrate and water. Compound **4** crystallized from the ether, 0.6 g; (55.1 %), m. p. 174 – 176 °C; $[\alpha]_D^{25}$ – 47.6° ($c = 0.2$; pyridine). R.T. 14.88

NMR: δ 7.3 (m, 10 H, aromatic protons); 5.59 (s, 1H, benzylidene proton); 5.31 (dd, 1H, anomeric proton, $J_{1,2e}$ 2.4 Hz, $J_{1,2a}$ 9.7 Hz); 4.3 (dd, 1H, C-4 proton); 3.6 (m, skeleton protons); 2.57 (ddd, 1H $C\text{-}2_e$ proton, $J_{2e,3}$ 6 Hz, $J_{2e,2a}$ 12.87 Hz); 1.94 (ddd, 1H $C\text{-}2_a$ proton, $J_{2a,3}$ 11.2 Hz, $J_{2a,2e}$ 12.87 Hz).

$C_{19}H_{20}O_5$ (328.36), Calcd. C 69.49; H 6.13. Found C 69.58; H 6.21 %.

Phenyl 2-deoxy-β-D-glucopyranoside (5)

Compound **4** (0.4 g) was dissolved with stirring in ethyl acetate (25 ml) and it was hydrogenated in the presence of Pd/C (70 mg). The reaction was monitored by TLC which showed that the elimination of the benzylidene group was complete in 5 hrs. The catalyst was filtered off and the filtrate evaporated to give crystalline **5** in quantitative yield (0.3 g); m. p. 143 – 146 °C; $[\alpha]_D^{25}$ – 75° (c = 0.5; water).

$C_{12}H_{16}O_5$ (240.25). Calcd. C 59.99; H 6.71. Found C 60.21; H 6.68 %.

Phenyl 2,4,6-tri-O-acetyl-3-O-p-toluenesulfonyl-β-D-glucopyranoside (7)

1,2,4,6-Tetra-O-acetyl-3-O-*p*-toluenesulfonyl-β-D-glucopyranose (**6**) (17.5 g; 0.034 mole) [22] was converted according to Helferich [14] to obtain 13 g (67.9 %) of **7**; m. p. 160 – 161 °C; $[\alpha]_D^{20}$ – 50.2° (c = 1; $CHCl_3$).

$C_{25}H_{28}O_{11}S$ (536.56). Calcd. C 55.97; H 5.22. Found C 55.86; H 5.10 %.

Phenyl 4,6-O-benzylidene-3-O-p-toluenesulfonyl-β-D-glucopyranoside (8)

Compound **7** (10 g) was deacetylated according to ZEMPLÉN [15] and the solution was concentrated in vacuum. After two evaporations with benzene, the residual syrup (7.7 g) was shaken with freshly distilled benzaldehyde (25 ml) and freshly fused $ZnCl_2$ (8.5 g) for 18 hrs at room temperature. Water (100 ml) was added, the benzaldehyde layer was separated in a separatory funnel, and petroleum ether was added. The crystalline material was filtered off and recrystallized from ethanol (450 ml) to obtain 7.2 g (82.3 %) of **8**; m. p. 204 – 205 °C; $[\alpha]_D^{20}$ – 87.4° (c = 0.5; $CHCl_3$).

$C_{26}H_{26}O_8S$ (498.56). Calcd. C 6 2.65; H 6.22. Found C 62.5; H 6.2 %.

Phenyl 4,6-O-benzylidene-3-deoxy-β-D-glucopyranoside (9)

$LiAlH_4$ (1.12 g; 32 mmoles) was suspended in dry tetrahydrofuran (20 ml) and the mixture was stirred and refluxed for 2 hrs. Compound **8** (4 g; 8 mmoles) was added, and stirring and refluxing was continued for 20 hrs. The excess of $LiAlH_4$ was decomposed with ethyl acetate (15 ml) and the mixture was poured into ether (200 ml). After filtration the filtrate was washed with 15 % potassium sodium tartrate solution and then with water five times. Crystallization gave 2 g (70 %) of **9**, m. p. 212 – 215 °C; $[\alpha]_D^{25}$ – 76.3° (c = 1; pyridine), R. T. 15.82.

NMR: δ 7.3 (m, 10H, aromatic protons); 5.75 (s, 1H benzylidene proton); 4.98 (d, 1H, anomeric proton, $J_{1,2}$ 8 Hz); 3.6 (m, 4H, skeleton protons); 2.3 (m, 1H C-3 equatorial proton); 1.7 (m, 1H, C-3 axial proton).

$C_{19}H_{20}O_5$ (328.36). Calcd. C 69.49; H 6.13. Found C 69.62; H 6.2 %.

Phenyl 3-deoxy-β-D-glucopyranoside (10)

Compound **9** (2 g) was suspended in chloroform (100 ml) and 10 ml of trifluoroacetic acid containing 1 % water was added. The reaction was monitored by TLC (solvent: benzene–acetone 9 : 1) and when hydrolysis was complete, the mixture was evaporated to dryness. Traces of the trifluoroacetic acid were eliminated by evaporation with toluene. The residue was crystallized from 15 parts of hot water to give 1.2 g (82.2 %) of **10**; m. p. 188 °C (lit. [23] m. p. 183 – 185 °C); $[\alpha]_D^{25}$ – 85° (c = 0.4; water) (Lit. [23] $[\alpha]_D^{25}$ – 94° (c = 0.27; water).

$C_{12}H_{16}O_5$ 240.25. Calcd. C 59.99; H 6.71. Found C 59.9; H 6.64 %.

Treatment of phenyl 2,3-anhydro-4,6-O-benzylidene-β-D-allopyranoside [17] with $LiAlH_4$

The title compound (0.5 g; 0.0015 mole) was treated with $LiAlH_4$ in the same manner as 3. After the usual processing, gas chromatographic examination 10 % UCW 982 column, temp. pr. 180 °C – 220 °C, heating speed 5°/min flamme ionization detector showed the product to consist of two components. One of them was phenyl 4,6-O-benzylidene-2-deoxy-β-D-ribo-hexopyranoside, RT 14.41; the other product was **9**, RT 15.78 see Table I.

Treatment of phenyl 2,3-anhydro-4,6-O-benzylidene-β-D-mannopyranoside [17] with $LiAlH_4$

The epoxide (0.5 g; 0.0015 mole) was treated with $LiAlH_4$ and the reaction mixture processed as described above. Gas chromatographic examination in the same manner as above showed that only one deoxy derivative was formed with RT 15.51, which was not identical with **4**, RT 14.88. According to the literature [19], phenyl 4,6-O-benzylidene-3-deoxy-β-D--arabinohexopyranoside was formed.

REFERENCES

[1] Hanessian, S.: Adv. in Carbohyd. Chem., **21,** 143 (1966)
[2] Stanek, J., Schwarz, V.: Chem. Listy **48,** 879 (1954)
[3] Inglis, G. R., Schwarz, J. C. P., McLaren, L.: J. Chem. Soc., **1962,** 1014
[4] Freudenberg, K., Wolf, A.: Ber., **60,** 232 (1927)
[5] Barton, D. H., McCombie, S. W.: J. Chem. Soc., (C) **16,** 1574 (1975)
[6] Strandtman, M., Puchalski, C., Shavel, J. jr.: J. Org. Chem., **33,** 4015 (1968)
[7] Hedgley, E. J., Mérész, O., Overend, W. G.: J. Chem., Soc., (C) **1967,** 888
[8] Vis, E., Karrer, P.: Chim. Acta **37,** 378 (1954)
[9] Allerton, R., Overend, W. G.: J. Chem. Soc., (C) **1954** 3629
[10] Umezawa, S., Tsuhiya, T., Hineno, H.: Bull. Chem. Soc. Japan **43,** 1212 (1970)
[11] Ekborg, G., Svensson, S.: Acta Chem. Scand., **27,** 1437 (1973)
[12] McCloskey, C. M., Coleman, G. H.: J. Org. Chem., **10,** 184 (1945)
[13] Chittenden, F.: Carbohyd. Res., **15,** 495 (1971)
[14] Helferich, B., Smilz-Hillebrecht, E.: Ber., **66,** 378 (1933)
[15] Zemplén, G.: Ber., **59,** 1254 (1926)
[16] Haworth, W. N., Owen, L. N., Schmith, F.: J. Chem. Soc., **1941** 97
[17] Robertson, J. G., Griffith, C. E.: J. Chem. Soc., **1935,** 1193; Richtmyer, N. K., Hudson, C. S.: J. Am. Chem. Soc., **63,** 1727 (1941)
[18] Fürst, A., Plattner, P.: Abstr. Papers, 12th Inter. Congress of Pure and Applied Chem., New York, 1951, 405
[19] Prins, D. A.: J. Am. Chem. Soc., **70,** 3955, (1948)
[20] Zobácová, A., Hermánková, V., Jary, J.: Coll. Czechoslov. Chem. Commun., **35,** 327 (1970)
[21] Hunt, B. F., Rigby, W.: Chem. Ind. London **1967,** 1868
[22] Freudenberg, K., Ivers, O.: Ber., **55,** 929 (1922)
[23] Pratt, J. W., Richtmyer, N. K.: J. Am. Chem. Soc., **79,** 2597 (1957)

László Kiss, H-4010 Debrecen, Pf. 55.

Acta Chimica Academiae Scientiarum Hungaricae, Tomus 97 (3), pp. 353–357 (1978)

SYNTHESIS OF PHTHALIDEISOQUINOLINE ALKALOIDS BY MEANS OF REISSERT COMPOUNDS, I

A NEW SYNTHESIS OF HYDRASTINE

P. KEREKES, G. HORVÁTH, GY. GAÁL and R. BOGNÁR

(Department of Organic Chemistry, Kossuth Lajos University, Debrecen)

Received June 23, 1977

A new multistep synthesis of (±)-β- and (±)-α-hydrastine has been achieved by the use of 1-cyano-2-benzoyl-6,7-methylenedioxy-1,2-dihydroisoquinoline and methyl opianate.

Several methods are known for the synthesis of phthalideisoquinoline alkaloids [1–12]. These have also been employed in synthesizing hydrastine in various ways [2–5, 10, 12].

The use of Reissert compounds in the total syntheses of isoquinoline alkaloids and related compounds has been summarized in a review published recently [13], which, however, does not mention the preparation of phthalideisoquinoline alkaloids in this way.

In our present work the application of Reissert compounds has been extended to the synthesis of phthalideisoquinoline alkaloids; the other reagents used are the methyl ester of phthalaldehydic acid and its substituted derivatives.

In this paper, the synthesis of (±)-β- and (±)-α-hydrastine is discussed.

1-Cyano-2-benzoyl-6,7-methylenedioxy-1,2-dihydroisoquinoline (**I**) was allowed to react with 2,3-dimethoxy-6-formylbenzoic acid methyl ester (methyl opianate) (**II**) in dimethylformamide, in the presence of sodium hydride. The diester (**III**) obtained in this way was subjected to saponification with potassium hydroxide in aqueous ethanol, and subsequently lactonized by boiling in acid. The product, 1-[1'-(4',5'-dimethoxyphthalidyl)]-6,7-methylenedioxyisoquinoline (**IV**) was hydrogenated at 3 atm. pressure to obtain a mixture of (±)-β- and (±)-α-norhydrastine (**V** and **VI**); the components were then separated by fractional crystallization. N-Methylation of the nor-compounds yielded (±)-β-hydrastine (**VII**) and (±)-α-hydrastine (**VIII**).

The structures of the nor-*erythro*- (**V**) and nor-*threo*- (**VI**) compounds were confirmed, on one hand, by the structures of the β- and α-hydrastine prepared from them by methylation; on the other hand, the structures were established

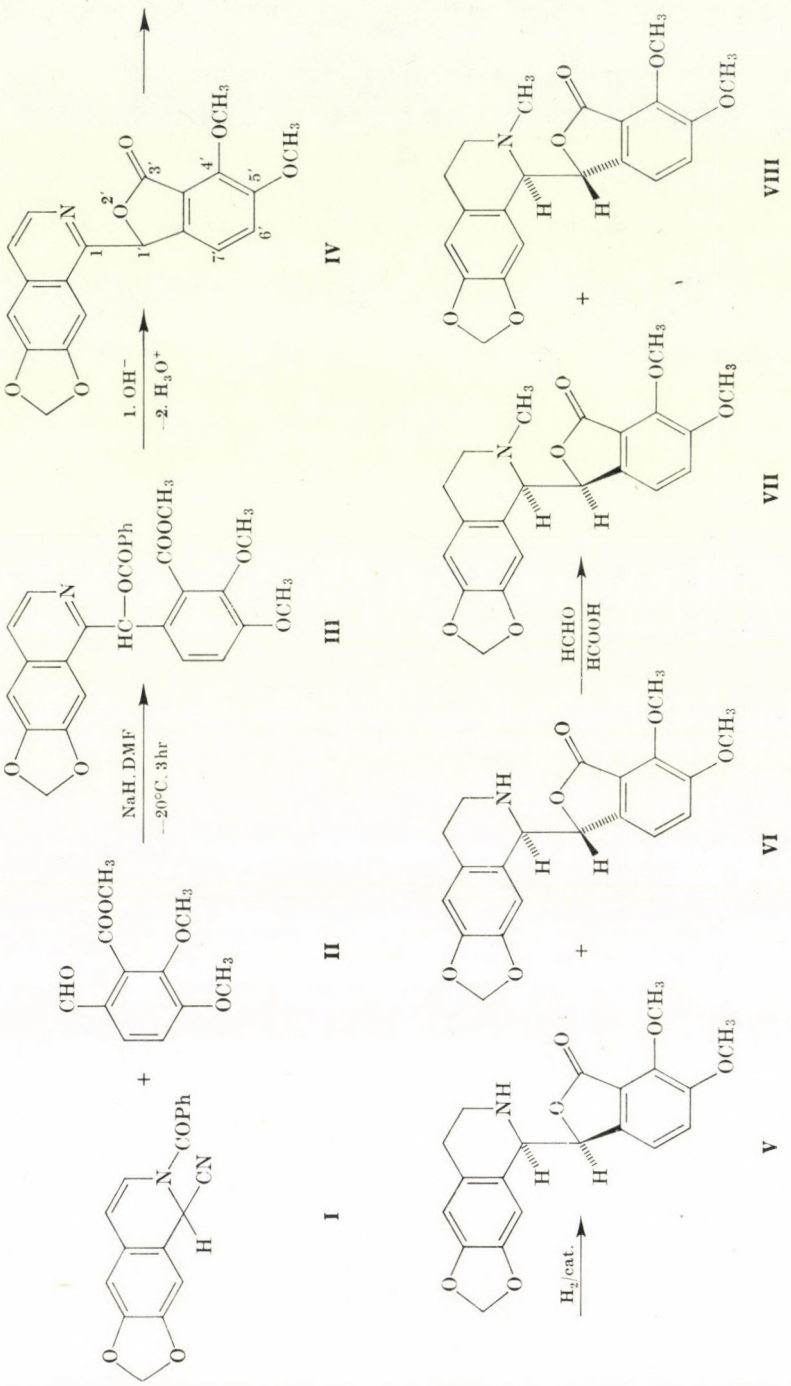
NaH, DMF
−20°C, 3 hr
1. OH⁻
2. H₃O⁺
HCHO
HCOOH
H₂/cat.
I
II
III
IV
V
VI
VII
VIII

unambiguously on the basis of the characteristic chemical shifts of the *ortho* doublets with coupling constant of $J = 8$ Hz, due to the 6',7' aromatic protons of phthalideisoquinoline alkaloids [7, 11, 15].

Synthesis of other natural phthalideisoquinoline alkaloids and related compounds with different substitution patterns are in progress.

Experimental

M. p.'s are uncorrected. The infrared spectra were recorded with a UNICAM SP 200 G instrument in KBr pellets; the PMR spectra were obtained with a JEOL Minimar 100 MHz instrument in deuterochloroform solution. Chemical shift values, referred to TMS internal standard, are given in ppm (δ) units.

1-(α-Benzoyloxy-2-methoxycarbonyl-3,4-dimethoxy-benzyl)-6,7--methylenedioxyisoquinoline (III)

Sodium hydride (0.26 g) was added to a solution of the Reissert compound **I** (3.04 g; 10 mmoles) [14] in dry DMF (40 ml) under a nitrogen atmosphere at −20 °C, with stirring. Stirring was continued for 15 min, then methyl opianate (**II**) (2.46g; 11 mmoles) dissolved in dry DMF (7 ml) was added dropwise. The reaction mixture was stirred further for 3 hrs at −20 °C, then poured into ice-water (200 ml); the raw product was filtered and washed with water until neutral. The substance was dissolved in chloroform (100 ml), and filtered from a small amount of insoluble, yellow-coloured residue. The chloroform solution was washed with water, dried over sodium sulfate and evaporated, the residue was crystallized from ethanol (40 ml). The product was twice recrystallized from ethanol to obtain 2.4 g of the product; processing of the alcoholic mother liquors gave another 0.46 g of **III**. Yield: 2.86 g (57 %), m. p. 169–171 °C.

$C_{28}H_{23}NO_8$ (501.47). Calcd. C 67.06; H 4.62; N 2.79. Found C 67.23; H 4.66; N 2.81 %.
IR: $\nu_{C=O}$ 1725 cm^{-1}.

1-[1'-(4',5'-Dimethoxyphthalidyl)]-6,7-methylenedioxyisoquinoline (IV)

A mixture of the diester **III** (2.26 g; 4.5 mmoles), ethanol (54 ml), KOH (0.77 g) and water (10.8 ml) was refluxed for 5 hrs. Then 10 % HCl (22.5 ml) was added to the mixture and refluxing was continued for 1 hr. Ethanol was removed in vacuum, the residue was diluted with water and basified with dilute NH_4OH. The raw product (1.55 g) was crystallized from CH_2Cl_2-*n*-hexane to obtain 1.46 g (89 %) of **IV**, m. p. 204–207 °C with decomposition.

$C_{20}H_{15}NO_6$ (365.33). Calcd. C 65.75; H 4.14; N 3.83. Found C 66.76; H 4.13; N 3.81 %.
IR: $\nu_{C=O}$ 1765 cm^{-1}.

(±)-β- and (±)-α-Norhydrastine (V and VI)

A solution of the phthalideisoquinoline (**IV**) (2.01 g; 5.5 mmoles) in a mixture of aqueous ethanol (500 ml) and 70 % $HClO_4$ (1.38 ml) was hydrogenated in the presence of PtO_2 (300 mg) under 3 atm initial pressure for 4 hrs. The catalyst was filtered off and the solvent evaporated in vacuum. The residue was diluted with water (100 ml), made alkaline with dilute NH_4OH then extracted with chloroform (3×50 ml). The chloroform solution was washed with water (2×50 ml), dried over $MgSO_4$ and evaporated to dryness. The residue was subjected to fractional crystallization from ethanol. The component less soluble in ethanol is (±)-α-norhydrastine (**VI**). Yield: 0.67 g (32 %): m. p. 202–205 °C.

$C_{20}H_{19}NO_6$ (369.36). Calcd. C 65.03; H 5.19; N 3.79. Found C 65.28; H 5.35; N 3.96 %.
IR: $\nu_{C=O}$ 1761 cm^{-1}.

PMR: 1.56 (1H, s, $-N-H$), 2.4–3.2 (4H, m, C-3 and C-4 H's), 3.9 (3H, s, $-OCH_3$), 4.1 (3H, s, $-OCH_3$), 5.9 (2H, s, $-OCH_2O-$), 4.42 (1H, d, J = 4 Hz, C-1 H), 5.69 (1H, d, J = = 4 Hz, C-1'H), 7.1 (1H, d, J = 8 Hz, C-6'H), 7.21 (1H, d, J = 8 Hz, C-7'H), 6.56 (1H, s, C-8 H), 6.71 (1H, s, C-5 H).

The alcoholic mother liquor was evaporated to dryness and the residue was crystallized from ethanol to obtain (±)-β-norhydrastine (**V**)* (0.54 g; 27 %), m. p. 168–173 °C.

$C_{20}H_{19}NO_6$ (369.36). Calcd. C 65.03; H 5.19; N 3.79. Found C 65.29; H 5.26; N 3.99 %.
IR: $\nu_{C=O}$ 1765 cm^{-1}.

PMR: 1.88 (1H, s, $-N-H$), 2.3–2.8 (4H, m, C-3 and C-4 H's), 3.84 (3H, s, $-OCH_3$), 4,07 (3H, s, $-OCH_3$), 5.95 (2H, s, $-OCH_2O-$), 4.61 (1H, d, J = 4 Hz, C-1 H), 5.62 (1H, d, J = 4 Hz, C-1'H), 6.19 (1H, d, J = 8 Hz, C-7'H), 7.0 (1H, d, J = 8 Hz, C-6'H), 6.59 (1H, s, C-5 H), 6.72 (1H, s, C-8 H).

(±)-β-Hydrastine (VII)

A mixture of the nor-compound (**V**) (0.37 g; 1 mmole), formic acid (0.6 ml) and 35 % formaldehyde (0.8 ml) was refluxed on a water bath for 4 hrs, then evaporated to dryness in vacuum. The residue was dissolved in dilute hydrochloric acid, clarified with decolourizing carbon, filtered and made alkaline with dilute NH_4OH. The crude product (0.35 g) was purified by chromatographic separation on a preparative layer (eluent : chloroform : methanol, 9 : 1) then crystallized from methanol (6.5 ml), to obtain 0.26 g (68 %), of **VII**, m. p. 137–139 °C (lit. [4] m. p. 138–139 °C).

$C_{21}H_{21}NO_6$ (383.39). Calcd. C 65.78; H 5.52; N 3.65. Found C 65.63; H 5.51; N 3.76 %.
IR: $\nu_{C=O}$ 1760 cm^{-1}.

PMR: 2.53 (3H, s, $-NCH_3$), 2.0–3.0 (4H, m, C-3 and C-4 H's), 3.87 (3H, s, $-OCH_3$), 4.04 (3H, s, $-OCH_3$), 5.88 (2H, s, $-OCH_2O-$), 3.95 (1H, d, J = 4 Hz, C-1 H), 5.46 (1H, d, J = 4 Hz, C-1'H), 6.52 (1H, d, J = 8 Hz, C-7'H), 7.09 (1H, d, J = 8 Hz, C-6'H), 6.39 (1H, s, C-8H), 6.57 (1H, s, C-5H).

(±)-α-Hydrastine (VIII)

The nor-compound **VI** (0.37 g; 1 mmole) was methylated as described above. The raw product (0.3 g) was crystallized from methanol (6.5 ml) to give 0.25 g (65 %) of **VIII**, m. p. 148–150 °C (Lit. [4] m. p. 151–152 °C).

$C_{21}H_{21}NO_6$ (383.39). Calcd. C 65.78; H 5.52; N 3.65. Found C 65.59; H 5.39; N 3.65 %.
IR: $\nu_{C=O}$ 1762 cm^{-1}.

PMR: 2.52 (3H, s, $-NCH_3$), 2.2–3.1 (4H, m, C-3 and C-4H's), 3.82 (3H, s, $-OCH_3$), 3.96 (3H, s, $-OCH_3$), 5.76 (2H, ABq, $-OCH_2O-$), 3.97 (1H, d, J = 4 Hz, C-1H), 5.52 (1H, d, J = 4 Hz, C-1'H), 7.31 (1H, d, J = 8 Hz, C-7'H), 7.06 (1H, d, J = 8 Hz, C-6'H), 6.34 (1H, s, C-8H), 6.64 (1H, s, C-5H).

REFERENCES

[1] SHAMMA, M.: The Isoquinoline Alkaloids, pp. 369. Academic Press, New York 1972
[2] HOPE, E., ROBINSON, R.: Proc. Chem. Soc., **28,** 17 (1912)
[3] HOPE, E., PYMAN, F. L., REMFRY, F. G. P., ROBINSON, R.: J. Chem. Soc., **1931,** 236
[4] HAWORTH, R. D., PINDER, A. R.: J. Chem. Soc., **1950,** 1776
[5] HAWORTH, R. D., PINDER, A. R., ROBINSON, R.: Nature **165,** 529 (1950)
[6] KEREKES, P., BOGNÁR, R.: J. prakt. Chem., **313,** 935 (1971)
[7] SMULA, V., CUNDASAWMY, N. E., HOLLAND, H. L., MACLEAN, D. B.: Can. J. Chem., **51,** 3287 (1973)
[8] KAMETANI, T., HIRATA, S., IHARA, M., FUKUMOTO, K.: Heterocycles **3,** 405 (1975)
[9] KAMETANI, T., HONDA, T., INOUE, H., FUKUMOTO, K.: Heterocycles **3,** 1091 (1975)
[10] KAMETANI, T., HONDA, T., INOUE, H., FUKUMOTO, K.: J. Chem. Soc., Perkin I, **1976,** 1221

* On the basis of the TLC of the N-methylated compound, the product is contaminated with some of the α-isomer. The two isomers (**V** and **VI**) have identical R_f values, in the developing agents used (benzene : methanol 8 : 2 and chloroform : methanol 9 : 1).

[11] SHAMMA, M., GEORGIEV, V. ST.: Tetrahedron **32,** 211 (1976)
[12] MONIOT, J. L., SHAMMA, M.: J. Am. Chem. Soc., **98,** 6714 (1976)
[13] POPP, F. D.: Heterocycles **1,** 165 (1973)
[14] BIRCH, A. J., JACKSON, A. H., SHANNON, P. V. R.: J. Chem. Soc., Perkin I, **1974,** 2190
[15] SAFE, S., MOIR, R. Y.: Can. J. Chem., **42,** 160 (1964)

Péter KEREKES
Géza HORVÁTH
György GAÁL
Rezső BOGNÁR

H-4010 Debrecen.

Acta Chimica Academiae Scientiarum Hungaricae, Tomus 97 (3), pp. 359—361 (1978)

THE STEREOCHEMISTRY OF NATURAL 'CIS—ANTHERAXANTHIN'

(PRELIMINARY COMMUNICATION)

Gy. TÓTH,* J. KAJTÁR,** P. MOLNÁR* and J. SZABOLCS*

*(*University Medical School, Pécs, and **Institute of Organic Chemistry, Eötvös L. University, Budapest)*

Received March 20, 1978

'*Cis*-antheraxanthin', the main pigment of the pollen sacs of *Lilium candidum*, which also occurs in *L. regale*, *L. Maxwill*, etc., has long been known as the first natural carotenoid epoxide with a mono-*cis* configuration [1, 2]. The stereochemistry of '*cis*-antheraxanthin', however, has not been established yet. We shall now report some evidence for a tentative configurational assignment.

The mass spectrum confirms the formula $C_{40}H_{56}O_3$ and indicates the presence of two hydroxyl groups and one epoxy group [*m/e* 584.4288 (100%; M), 568 (7%; M—16), 566 (6%; M—18), 221 (85%), etc.] [3]. All-*trans*-antheraxanthin formed by iodine-catalyzed stereomutation [4] of '*cis*-antheraxanthin' (ex *Lilium candidum*) has the same physical and chemical properties, including the CD spectrum, as natural antheraxanthin (**I**). The complete absolute stereochemistry of the chiral centres of '*cis*-antheraxanthin' can therefore, be described, as 3*S*,5*R*,6*S*,3'*R* [5].

Considering the visible light absorption properties of '*cis*-antheraxanthin' [$\lambda_{max}(\varepsilon_{max})$: 483 (97.500), 453 (111.400) and 430 nm (76.900) in benzene; λ_{max} shift = 5 nm, $\varepsilon_{cis-peak} = 9.700$] [4], the *cis* double bond must occupy a peripheral position 9- or 9'. Theoretically, the spatial forms 9- and 9'-*cis* may be supposed to be stable isomers [6] but they have not been isolated separately from the stereoisomeric set of antheraxanthin before. Quite recently, we have succeeded in isolating four mono-*cis* isomers formed by iodine-catalyzed stereomutation of natural antheraxanthin. On a calcium carbonate column, developed with benzene, the zones in the order of decreasing adsorption affinities were as follows: neo A, neo A*, neo B and neo B*. Thus, there are two mono-*cis* isomers of antheraxanthin, neo A and neo A* with the same UV light absorption properties ($Q = 2.1$, λ_{max} shift = 7 nm in benzene) [7], and two others, neo B and neo B* with the same λ_{max} shift (5 nm), but almost without a *cis* peak ($Q = 11$). Evidently, neo B and neo B* represent the peripheral mono-*cis* forms (9 or 9'), and the *cis* double bond occupies a more central position (13 or 13') in neo A and neo A*.

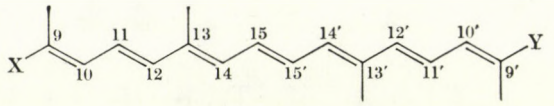

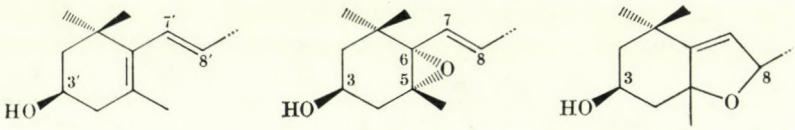

a(3'R) b(3S, 5R, 6S) c

I X = b, Y = a
II X = c, Y = a
III X = b, Y = a (9'-*cis*)
IV X = b, Y = a (9-*cis*)

The difference in behaviour between the neo B and neo B* forms was significant; acid treatment of neo B* gave a furanoid oxide derivative with λ_{max} characteristic of all-*trans*-mutatoxanthin (**II**), whereas neo B yielded *cis*-mutatoxanthin (λ_{max} shift = 5 nm). These findings might be resolved by reasoning that 9-*cis*-antheraxanthin, in which the 5,6-epoxy group and the *cis* 9—10 double bond are in close vicinity, is converted to all-*trans*-mutatoxanthin under acid conditions (owing to simultaneous stereomutation and epoxy-furanoid rearrangement), while 9'-*cis*-antheraxanthin gives 9'-*cis*-mutatoxanthin. So, it can be assumed that neo B is the 9'-*cis* (**III**), and neo B* the 9-*cis* (**IV**) spatial form. No similar wave length difference was observed during acid treatment of neo A and neo A*.

Considering that in a mixed chromatogram '*cis*-antheraxanthin' (ex *Lilium candidum*) proved to be identical with neo-antheraxanthin B* (neo B*), we tenatatively concluded that natural '*cis*-antheraxanthin' has a 9-mono-*cis* geometrical configuration, *i.e.* natural *cis* antheraxanthin is (3*S*,5*R*,6*S*,3'*R*)-9--*cis*-5,6-epoxy-5,6-dihydro-β,β-caroten-3,3'-diol.

The occurrence of 9-*cis*-antheraxanthin in *Lilium candidum* is similar to that of 9-*cis*-violaxanthin [8] in *Viola tricolor* (both in large quantities), which demonstrates the stability of the 9-*cis* type configuration of 5,6-epoxy-carotenoids in nature. Moreover, the absence of 9'-*cis*-antheraxanthin in *Lilium candidum* shows that the production of '*cis*-antheraxanthin' is a stereospecific process.

*

The authors wish to express their thanks to György BUJTÁS (Central Research Institute for Chemistry of the Hungarian Academy of Sciences, Budapest) for the mass spectrum.

REFERENCES

[1] TAPPI, G., KARRER, P.: Helv. Chim. Acta **32,** 50 (1949)
[2] KARRER, P., EUGSTER, C. H., FAUST, M.: Helv. Chim. Acta **33,** 300 (1950)
[3] BALDAS, J., PORTER, Q. N., CHOLNOKY, L., SZABOLCS, J., WEEDON, B. C. L.: Chem. Commun., **1969,** 415
[4] ZECHMEISTER, L.: Cis-trans Isomeric Carotenoids, Vitamins A and Arylpolyenes. Springer, Vienna 1962
[5] BARTLETT, L., KLYNE, W., MOSE, W. P., SCOPES, P. M., GALASKO, P., MALLAMS, A. K., WEEDON, B. C. L., SZABOLCS, J., TÓTH, Gy.: J. Chem. Soc., (C) **1969,** 2527
[6] SZABOLCS, J.: Pure Appl. Chem., **47,** 147 (1976)
[7] INHOFFEN, H. H., BOHLMANN, F., RUMMERT, G.: Liebigs Ann. Chem., **571,** 75 (1951)
[8] SZABOLCS, J., TÓTH, Gy.: Acta Chim. Acad. Sci. Hung., **63,** 229 (1970)

Péter MOLNÁR
Gyula TÓTH
József SZABOLCS — H-7643 Pécs, Szigeti út 12
Judit KAJTÁR — H-1088 Budapest, Múzeum krt. 4/B

RECENSIONES

A. L. TERNAY: *Contemporary Organic Chemistry*

W. B. Saunders Co., Philadelphia – London – Toronto, 1976

Organic chemistry – for a long time regarded as the art of the cooking-pot – has in the last two decades made spectacular advances towards becoming a science with an exact qualitative framework. Teaching organic chemistry must keep level with this development and actually if one compares the accepted organic textbooks of the late fifties with those appearing nowadays, the progress is obvious. TERNAY's book is again an important step forward in this direction.

The material of the book is fundamentally organized according functional groups, the experimental facts and observations are consistently and successfully explained, however, on a theoretical basis. Reaction mechanisms are systematically treated in detail, the electronic structure of molecules is constantly kept in the mind of the reader and the frequent use of energy diagrams significantly helps the understanding of kinetical phenomena. Even FMO theory is used where regarded as necessary.

Three further features of the book deserve appreciation: the systematic discussion of the IR and NMR spectral features of organic molecules (supported by many clear reproductions of spectra), the collection of important terms following each chapter in which these have been treated, and finally, the problems incorporated right into the text thus stimulating the creative application of acquired knowledge immediately (the answers to these questions are compiled at the end of the book).

There are also a lot of problems listed at the end of each chapter, the book does not contain the answer to these, however. Obviously, these are partly meant as a help for the teacher to control his students.

As stated by the author right at the beginning, this book is originally meant mainly for students with biological interests and the selection of material clearly reflects this effort. Accordingly, several topics usually regarded as belonging to biochemistry are treated in detail whereas the industrial applications of organic chemistry are strongly neglected. These two characteristics will probably – and unfortunately – prevent this otherwise excellent book to become a basic text in organic chemistry.

L. MARKÓ

Ion-Selective Electrodes, Second Symposium Held at Mátrafüred, Hungary, 18–21 Oct. 1976. pp. 263

Ed. E. PUNGOR, Akadémiai Kiadó, Budapest 1977

Both theories on the function of ion-selective electrodes have developed and the fields of their application expanded considerably during the past years. For this reason symposia and colloquia are organized more frequently both on national and international levels. The Second Symposium held at Mátrafüred gave a good opportunity for researchers from Hungary and many European countries active on this field to discuss a large variety of theoretical and experimental problems.

The five plenary lectures presented at the Symposium focused the attention to novel results on neutral carrier ion-selective membrane electrodes and their transport properties

(W. SINON, W. E. MORF and A. P. THOMA), on ion-sensing membranes based on PVC matrices (G. J. MOODY and J. D. R. THOMAS), on new methods for automatic analysis with ion-selective electrodes (E. PUNGOR, K. TÓTH, G. NAGY and Zs. FEHÉR) and on the application of ion-selective electrodes to enzymatic analysis (G. JOHANSSON and L. ÖGREN).

The fifteen discussion lectures considered a variety analytical problems solved by the use of ion-selective sensors (*e.g.* analysis of mixtures of gases, and rhenium and gold) the question of sensitivity and selectivity of new types of electrodes, the application of ion-selective electrodes in studying thermodynamical and kinetic problems.

The book contains also the major points discussed during the panel discussion. The four selected topics were as follows:

1. Selectivity coefficients and detection limits in ion-buffered systems.
2. Response time of indicator electrodes and measuring systems.
3. What kind of new sensors are needed?
4. Application of sensors in automatic analysis.

The book can be highly recommanded to analytical chemists working both in research institutes and universities, and in industrial laboratories.

E. KŐRÖS

"*Topics in Current Chemistry*" *Volume* 69. *Inorganic Biochemistry II*

Spinger-Verlag, Berlin, Heidelberg, New York 1977

The 69. volume of "Topics in Current Chemistry" similar to Volume 64 this series includes monographies on some topics of inorganic biochemistry.

The first monography written by K. KUSTIN and G. C. MCLEOD entitled "Metal Ions and Living Organisms in Sea Water" gives an account on the progress that has been made to understand the impact of some heavy metals (V, Cr, Fe, Cu, Pb, and Hg) introduced in the marine environment. Of the metal ions discussed by the authors iron, copper, chromium and vanadium are essential elements for most of the living organisms including mammals; lead and mercury, though not essential, are also accumulated by some marine organisms, enter into the food chain and come ultimately also to human beings. After a brief introduction, the second chapter describes the pathways metal ions are transported to the oceans and how they become available for the biosystems. An important step is the interaction between the various organisms and the environment, which is followed by the entry of metal ions into living systems. The latter includes chelation, ion-exchange and assimilation (regulated removal and transport). The final chapter discusses the impact of metal ions on selected organisms (algae, mollusks, tunicates). The monography is completed with 136 references.

The main significance of the very informative article is that it directs the attention of the reader to a major problem mankind is going to be faced: toxic metal ions are passing upward in the food chain at increasingly higher concentrations and the effects on man ultimately may be hazardous.

The second monography is on "Inorganic Metabolic Gas Exchange in Biochemistry" and written by G. RENGER. The author shows that two gaseous compounds play a central role in the biosystems: O_2 and CO_2. Carbon dioxide either as primary substrate in photosynthesis for the anabolism of organic compounds or as terminal product of their catabolic degradation is the cornerstone of the large variety of bioorganic chemistry in living systems. On the other hand the O_2/H_2O systems provides the molecular basis for the fundamental processes in bioenergetics. The topic discussed by the author is of extreme importance. Firstly he deals briefly with "The Overall Counterbalance Reaction of Autrophic and Heterotropic Organisms", *i.e.*

$$CO_2 + H_2O \underset{\text{heterotroph}}{\overset{\text{autotroph}}{\rightleftharpoons}} - CH_2O - + O_2 \text{ reaction}$$

Then he describes "The Role of Ozone as Atmospheric UV Shield". In the following chapter which is the backbone of the monography "Metabolic Processes in Autotrophic Organisms Involving Gaseous Compounds" are discussed, *i.e.* the reduction of carbon dioxide, in one of the two main regions of the chloroplast, in the stroma region, and the oxygen evolution in the

other, the thylakoid region. "Non-oxygen Evolving Autotrophic Organisms" are also mentioned briefly. – In the next chapter the process of biological dinitrogen fixation is considered and the molecular mechanism of nitrogenase catalyzed dinitrogen-fixation, as far as it is known at present, is described. Finally, the author deals with "Metabolic Processes in Heterotrophic Organisms Involving Gaseous Compounds" considering how biosystems are protected to the toxic attack by oxygen, the oxygen transport systems and the metabolic chemical reactions of oxygen. – 216 references close the monography.

The last monography of this volume written by W. BURGERMEISTER and R. WINKLER-OSWATITSCH is entitled "Complex Formation of Monovalent Cations with Bio-functional Ligands". In biological systems alkali ions play important role in ozmoregulation, and in variety of trigger reactions (*e.g.* nerve conduction). In order to understand the molecular basis of these reactions which are coupled to the selective permeability of biological membranes for these ions, a thorough knowledge as regards their coordination chemistry especially with bioligands is required. – The authors provide an excellently compiled account on the results obtained in this field mainly during the last ten years. They start by considering the selectivity and stability of complex formation and outline the methods which are used to determine the complex stability constants. (The stability constant data are listed through 21 pages). In the next chapter they deal with the kinetics and mechanism of complex formation, and with the methods applied for the determination of rate constants. (The rate constant data are compiled in five tables.) The following chapter is on "Carrier Mediated Ion Transport through Artificial and Biological Membranes", both the carrier mechanism and the channel mechanism are discussed. In the fifth chapter the authors provide detailed information about the chemical composition, structure and conformation of ionophoric ligands and their complexes. This includes depsipeptides, depsides, peptides, nigericin and related open chain compounds, synthetic macrocyclic polyethers, synthetic macrobicyclic and – tricyclic ligands (cryptands), and synthetic non-cyclic ligands. – The last chapter is "Applications of Alkali Cation Selective Ligands." The use of crown polyethers as lipophilizers, the analytical application (in ion-selective electrodes) of some ligands, and their use for studying ion transport and related cell membrane phenomena are mentioned. In the appendix the authors compiled recent publications on biomedical applications of valinomycin. – 327 references are given.

Volume 69. of Topics in Current Chemistry can be highly recommanded to biochemists, organic, inorganic and environmental chemists, biologists and also to undergraduates majoring either in chemistry and biochemistry.

E. KŐRÖS

Richard L. KEITER: *Seminaranleitungen zum Lehrbuch Modellvorstellungen in der Chemie*

Übersetzt und bearbeitet von Hans-Dieter SCHENKE. Walter de Gruyter, Berlin – New York, 1977. 234 Seiten

Das Buch schließt sich eng an das von HAMMOND, OSTERVOUNG, CRAWFORD und GRAY verfaßte Lehrbuch "Modellvorstellungen in der Chemie" (Verlag Walter de Gruyter, Berlin 1976) an. Die Zielsetzung ist, Professoren und Lehrassistenten Weisungen und methodologische Hilfe zur Leitung von Seminaren zu geben, die sich an die einleitenden Chemie Vorlesungen anschließen.

In der Einführung gibt der Verfasser vor allem allgemeine methodologische und pädagogische Ratschläge über den Chemieunterricht. Darauf folgt eine kurze und klare Zusammenfassung der gebräuchlichen physikalischen und chemischen Einheiten. In der Einführung sind auch Ratschläge zu Durchführung eines Seminars angegeben, dessen Thema der Platz der Chemie unter den Naturwissenschaften sowie die Bestimmung ihres Gegenstandes ist. Nach der allgemeinen Einleitung behandelt der Verfasser in 14 Abschnitten den Stoff des genannten Lehrbuches in Seminarform. Die Abschnitte behandeln folgende Themenkreise:

1. Atome und Moleküle. 2. Gase und die Avogadrosche Hypothese. 3. Periodizität und chemische Eigenschaft. 4. Die Bestandteile des Stoffes. 5. Die Elektronenstruktur der Atome. 6. Bindungen in Molekülen. 7. Molekülgeometrie und Molekülorbitale. 8. Flüssigkeiten und feste Stoffe. 9. Lösungen. 10. Chemisches Gleichgewicht. 11. Chemische Reaktionen. 12. Protonsäuren und Basen. 13. Geschwindigkeit und Mechanismus von chemischen Reaktionen. 14. Struktur und Reaktion der Verbindungen von Kohlenstoff und Silicium.

Die Struktur dieser Abschnitte gliedert sich einheitlich und sehr übersichtlich in drei Teile. Der erste Teil befaßt sich jeweils mit den prinzipiellen und praktischen Leitungsfragen des Seminars über den gegebenen Stoff. Dem Stoff des Lehrbuches und der Reihenfolge der Erörterung entsprechend wird auf die im vorangehenden bereits erkannten, grundlegend wichtigen Gesetze und Zusammenhänge hingewiesen, die zum Verständnis der aufgeworfenen Fragen notwendig sind. Dadurch wird ermöglicht, daß der Stoff der Vorlesungen im Seminar kurz wiederholt und zusammengefaßt wird. Zugleich erweitert der Verfasser den vorgetragenen Stoff, indem er auf Einzelheiten eingeht, die in der Vorlesung nicht behandelt werden konnten, jedoch zum Verständnis des gegebenen Themenkreises beitragen. Es werden auch vershiedene Aufgaben und ihre Lösungen behandelt. Der Verfasser lenkt die Aufmerksamkeit des Lehrpersonals auf die Probleme, deren Verständnis – nach seiner langjährigen Erfahrung – den Hörern besonders schwerfällt, und gibt Ratschläge, wie diese Schwierigkeiten überbrückt werden können. Er zählt die Fragen auf, welche die Hörer am häufigsten stellen, und gibt die Antwort dazu an. Er betont, daß das der Seminarstoff den Ansprüchen und dem Niveau des Durchschnittshörers angepaßt werden soll. Es ist falsch, sich mit den durch die hervorragendsten Hörern gestellten Fragen zu befassen, weil dann das Seminar nicht zu dem gestellten Ziel führt, daß sämtliche Hörer sich das nötige Wissen aneignen. Mit solchen überdurchschnittlichen Fragen soll man sich in besonderen Konsultationen befassen.

Der zweite Teil der Abschnitte gibt Literaturhinweise für die jenigen die irgendeinen Teil des gegebenen Themas näher kennenlernen möchten. Der dritte Teil enthält schließlich die verständlich angegebenen, richtigen Lösungen der im Lehrbuch gestellten Fragen und Rechenaufgaben.

Abschließend enthält das Buch im Interesse eines besseren Verständnisses des Lehrstoffes Kontrollfragen und nach der Auswahlmethode die darauf zu gebenden richtigen Antworten.

Obwohl die "Seminaranleitungen" sich eng an das angeführte Lehrbuch anschließen, kann das Buch, wegen seines modernen Stoffes und seiner guten Konzeption, mit Nutzen von all denen gelesen werden, die ähnliche Seminare leiten. Infolge der klaren und übersichtlichen Behandlung des Stoffes und des reichen Beispielmaterials kann das Buch auch all den Hörern empfohlen werden, die ein gründliches Verständnis der einleitenden Chemievorlesungen wünschen.

A. GERGELY

N. D. EPIOTIS, W. R. CHERRY, S. SAIK, R. L. YATES F. BERNARDI: *Structural Theory of Organic Chemistry*, 250 pp.

Springer-Verlag, Berlin – Heidelberg – New York, 1977

The aim of this book is to give a unified, qualitative theory of organic chemistry based on quantum mechanics. Molecules are constructed of small and transferable fragments which interact in a relatively simple manner. These interactions determine molecular properties such as geometry, conformation, reactivity, etc. After an outline of the theory in Part I, non-bonded, geminal and conjugative interactions between molecular fragments are discussed in Parts II, III and IV, respectively. Part V deals with bond ionicity effects. Ample evidence, theoretical and experimental as well, is given to confirm the simplified treatment. Accordingly, 420 references are cited, affording a useful survey of the literature.

Unfortunately, we feel, the book could not achieve its purpose. First, in order to present a qualitative theory which is well understandable to the chemist at the bench, a clear-cut theoretical foundation should be given. Part I does not yield such a theory. The equations, given here, seem to be arbitrary, though the reader may have some idea that they have their origin in quantum chemistry. Further, there are too many effects to be taken into account when experimental trends are explained. For example, in the discussions in Sections 7 and 8, *n*-pi, sigma-pi and pi-pi interactions compete to determine molecular properties. It is not clear in what manner their relative importance can be established. Further, at the bottom of page 54, the following is written: "However, due to the small hydrogen coefficients in these MO's, . . ." From where should the reader know whether the coefficients are really small? A misconception: on page 63, acyclic N_2O_4 is called a "sigma aromatic system". It is known that aromaticity has a meaning in cyclic pi-systems only. A serious drawback is the not always clear presentation; there are some parts of the book which need really hard work to understand.

Despite the above objections, the authors have considerable merits in having developed useful qualitative models of molecular structure. There is a wide variety of interesting ideas and propositions for the specialist working on theoretical organic chemistry or quantum chemistry. However, the book cannot be recommended to non-specialists or to graduate students.

G. NÁRAY-SZABÓ

INDEX

PHYSICAL AND INORGANIC CHEMISTRY

ORGANIC CHEMISTRY

Printed in Hungary

A kiadásért felel az Akadémiai Kiadó igazgatója — Műszaki szerkesztő: Zacsik Annamária

A kézirat nyomdába érkezett: 1978. I. 23. — Terjedelem: 10,15 (A/5) ív, 69 ábra

78.5428 Akadémiai Nyomda, Budapest — Felelős vezető: Bernát György

ACTA CHIMICA

ТОМ 97—ВЫП. 3

РЕЗЮМЕ

Радиолиз водных систем железа(III)-ЭДТУ

М. ВЕБЕР, Г. ФЁЛЬДИАК и Е. КОЧИШ

В интересах того, чтобы в стальных конструкциях атомных хтанций нержавеющую сталь заменить на более дешовую перлитную сталь, были проведены лабораторные исследования γ-радиолиза водных растворов с добавкой железо(III)-ЭДТУ. Было установлено, что между раднолизом железа (III)-ЗДТУ и железа(II)-ЭДТУ устанавливается развновесие. Было исследовано влияние муравыиной кислоты и метанола, как побочных добавок, а также комплексов хрома и никеля стальных сплавов с ЭДТУ. Для системы железо(III)-ЭДТУ полагалось, что между отдельными растворенными веществами и продуктами их радиолиза имеет место конкуренция.

Статистическое приближение электродной функции мембраных электродов с ионной селективностью

С. ЛИТЕАНУ, Е. ХОПИРТЕАН и И. С. ПОПЕСКУ

Статистическая обработка электродной функции позволяет определение следующих фундаментальных параметров: предельную величину области линейности $(\overline{pc})_l$, предел детектирования $(\overline{pc})_d$, предел определимости $(\overline{pc})_D$ и концентрацию фона $(\overline{pc})_b$. Статистическое определение предела детектирования и предела определимости, используя статистическую теорию детектирования сигнала, позволяет использование электродной функции и в налинейной области.

Исследования взаимодействия ион-растворитель в системах спитр — соляная кислота

Ф. РАТКОВИЧ и И-НЕ БАРАТИ

Электродвижущая сила в системе электродов Pt/H_2 газ/HCl спирт/Hg_2Cl_2/Hg была исследована в температурном интервале 20—40°C. Был определен нормальный потенциал спиртового каломельного электрода в метаноле, этаноле, 1-пропаноле и 1-бутаноле. Была исследована концентрационная зависимость средних коэффициентов ионной активности при концентрациях, превышающих область справедливости теории Дебая=Хюкеля, и было установлено, что отклонения от вышеупомянутой теории могут быть объяснены сильными взаимодействиями между ионами и с растворителем. Взаимодействие ионов с растворителем увеличивается с увеличением молекулярного веса последнего. Это объясняет также и то явление, что растворимость хлористого водорода в спирте значительно увеличивается с увеличением молекулярного веса спирта.

Исследование периодических колебаний потенциала на платиновом электроде, погруженном в раствор органических веществ с редокс системами

Возбуждение явлений, подобных осциллированиям гальваностатических потенциалов, наблюдаемым в ходе электроокисления, в случае разомкнутой электрической цепи

ДЬ. ХОРАНИ, ДЬ. ИНЗЕЛЬТ и З-НЕ СЕТЕИ

Экспериментально было подтверждено, что те осциллирующие явления, наблюдаемые на платиновом электроде в ходе гальваностатического электрокисления отдельных органических веществ, могут быть обнаружены и для равновесного потенциала электрода, погруженного в раствор, содержащий органическое вещество и редокс систему. Осциллирование равновесного потенциала было обнаружено в системах, содержащих Ce^{4+}, Fe^{3+} и метанол, формальдегид, муравьиную кислоту, этиленгликоль, гликольальдегид, глиоксаль, изопропанол. Было показано, что для интервала потенциала, соответствующего катодному диффузионному предельному току окисляющего агента, в сущности, справедливы те условия, которые итак обеспечивает гальваностат. Если осциллирование гальваностатического потенциала попадает в эту область, то происходит осциллирование и равновесного потенциала. В случае этиленгликоля сравнивали осциллирование гальваностатического потенциала с осциллированием равновесного потенциала.

Электрохимическое поведение этиленгликоля и его окисленных производных на платиновом электроде, I

Электровосстановление бифункциональных оксосоединений с двумя углеродными атомами

ДЬ. ХОРАНИ, ДЬ. ИНЗЕЛЬТ и Е. СЕТЕИ

Было показано, что в ходе окисления этиленгликоля на электроде платиновой черни в кислой среде образуются такие продукты, которые восстанавливаются со значительной скоростью при потенциалах ненамного более положительных, чем равновесный потенциал водородного электрода. Для объяснения наблюдаемого явления было изучено электрогидрирование и каталитическое гидрирование окисленных производных этиленгликоля ($HOCH_2-CHO$, $OHC-CHO$, $HOCH_2-COOH$, $OHC-COOH$, $HOOC-COOH$) на электроде платинированной платины и катализаторе из платиновой черни, соответственно, в кислых средах. Заметные скорости восстановления наблюдались лишь в случае оксосоединений. Было показано, что реакции гидрирования наблюдаются лишь в случае соблюдения определенной экспериментальной методики. Для скоростей гидрирования и электрогидрирования был найден следующий ряд: $HOCH_2-CHO > OHC-CHO \gg OHC-COOH$. В результате гидрирования и электрогидрирования гликольальдегида и глиоксаля, в основном, образуется этан, вероятно через образование ацетальдегида как промежуточного продукта.

Экспериментальные данные однозначно указывают на то, что в ходе окисления этиленгликоля в значительных количествах образуются гликольальдегид или глиоксаль, или оба соединения.

Применение электрода ртуть-окись ртути для измерения активности гидроксильного иона в концентрированных щелочных растворах

З. Г. САБО, М. ПАЛФАЛВИ-РОЖАХЕДИ и М. ОРБАН

Электрод Hg/HgO, использованный до сих пор как стандартный электрод, оказался пригодным для определения изменений активности гидроксильного иона в концентрированных растворах щелочи натрия. Этот электрод был использован для измерения активности лидроксильных ионов в каустических растворах алюмината. Метод, основанный на измерениях проводимости, был разработан для определения диффузионного потенциала системы.

Расчеты на основе данных, полученных таким путем, подтверждают то заключение в литературе, что в системах с низкой концентрацией алюминия превалирует ион тетрагидроксоалюмината. В системах с более высокой концентрацией алюминия можно полагать образование димерных или олигомерных частиц; однако, данный метод, сам по себе, не дает количественных данных, подтверждающих это предположение.

Исследование тозиловых и мезиловых производных в морфиновом ряду, XXI

С-6-галогенпроизводные дигидрокодеина

Г. ШОМОДИ, Ш. МАКЛЕЙТ и Р. БОГНАР

Исходя из 6-0-мезилдигидрокодеина были получены 6-хлордигидрокодид, а также до сих пор еще не полученные 6-фтор- и 6-бром дигидрокодиды. Реакция 6-0-мезилдигидрокодеина с иодидом натрия не приводит к образованию ожидаемого 6-иодпроизводного, а образуется дезоксикодеин-С.

Синтез фенил 2-деокси- и 3-деокси-β-D-глюкопиранозидов

Л. КИШ

Описывается синтез фенил 2-деокси- и 3-деокси-β-D-глюкопиранозидов (5 и 10). Синтез был осуществлен через восстановление соответствующего п-толуолсульфонилового производного (4 и 9) с помощью $LiAlH_4$ исследовано, происходит ли образование эпоксидного промежуточного продукта в реакции. Оказалось, что в реакции не образуется какой-либо эпоксид.

Синтез алкалоидов со скелетом фталилизосинолина с помощью соединений Рейсерта, I

Новый синтез гидрастина

П. КЕРЕКЕШ, Г. ХОРВАТ, ДЬ. ГААЛ и Р. БОГНАР

Был осуществлен через несколько ступеней новый синтез (±)-β— и (±)-α-гидрастинов с использованием 1-циано-2-бензоил-6,7-метилендиокси-1,2-дигидроизохинолина и метилового эфира опиановой кислоты.

Les Acta Chimica paraissent en français, allemand, anglais et russe et publient des mémoires du domaine des sciences chimiques.

Les Acta Chimica sont publiés sous forme de fascicules. Quatre fascicules seront réunis en un volume (4 volumes par an).

On est prié d'envoyer les manuscrits destinés à la rédaction à l'adresse suivante:

Acta Chimica
H-1521 Budapest, Hongrie

Toute correspondance doit être envoyée à cette même adresse.

La rédaction ne rend pas de manuscrit.

Le prix de l'abonnement: $ 36,00 par volume.

Abonnement en Hongrie à l'Akadémiai Kiadó (1363 Budapest, P. O. B. 24, C. C. B. 215 11488), à l'étranger à l'Entreprise du Commerce Extérieur « Kultura » (H-1389 Budapest 62, P. O. B. 149 Compte-courant No. 218 10990) ou chez représentants à l'étranger.

Die Acta Chimica veröffentlichen Abhandlungen aus dem Bereich der chemischen Wissenschaften in deutscher, englischer, französischer und russischer Sprache.

Die Acta Chimica erscheinen in Heften wechselnden Umfanges. Vier Hefte bilden einen Band. Jährlich erscheinen 4 Bände.

Die zur Veröffentlichung bestimmten Manuskripte sind an folgende Adresse zu senden:

Acta Chimica
H-1521 Budapest, Ungarn

An die gleiche Anschrift ist jede für die Redaktion bestimmte Korrespondenz zu richten.

Manuskripte werden nicht zurückerstattet.

Abonnementspreis pro Band: $ 36,00.

Bestellbar für das Inland bei Akadémiai Kiadó (1363 Budapest, Postfach 24, Bankkonto Nr. 215 11488), für das Ausland bei »Kultura« Außenhandelsunternehmen (H-1389 Budapest 62, P. O. B. 149. Bankkonto Nr. 218 10990) oder seinen Auslandsvertretungen.

«Acta Chimica» издают статьи по химии на русском, английском, французском и немецком языках.

«Acta Chimica» выходит отдельными выпусками разного объекта, 4 выпуска составляют один том и за год выходят 4 тома.

Предназначенные для публикации рукописи следует направлять по адресу:

Acta Chimica
H-1521 Budapest, BHP

Всякую корреспонденцию в редакцию направляйте по этому же адресу.

Редакция рукописей не возвращает.

Подписная цена — $ 36,00 за том.

Отечественные подписчики направляйте свои заявки по адресу Издательства Академии Наук (1363 Budapest, P. O. B. 24, Текущий счет 215 11488), а иностранные подписчики через организацию по внешней торговле «Kultura» (H-1389 Budapest 62, P. O. B. 149. Текущий счет 218 10990) или через ее заграничные представительства и уполномоченных.

Reviews of the Hungarian Academy of Sciences are obtainable at the following addresses:

AUSTRALIA
C.B.D. LIBRARY AND SUBSCRIPTION SERVICE, Box 4886, G.P.O., *Sydney N.S.W. 2001*
COSMOS BOOKSHOP, 145 Ackland Street, *St. Kilda (Melbourne), Victoria 3182*

AUSTRIA
GLOBUS, Höchstädtplatz 3, *1200 Wien XX*

BELGIUM
OFFICE INTERNATIONAL DE LIBRAIRIE, 30 Avenue Marnix, *1050 Bruxelles*
LIBRAIRIE DU MONDE ENTIER, 162 Rue du Midi, *1000 Bruxelles*

BULGARIA
HEMUS, Bulvar Ruszki 6, *Sofia*

CANADA
PANNONIA BOOKS, P.O. Box 1017, Postal Station "B", *Toronto, Ontario M5T 2T8*

CHINA
CNPICOR, Periodical Department, P.O. Box 50, *Peking*

CZECHOSLOVAKIA
MAD'ARSKÁ KULTURA, Národní třida 22, *115 66 Praha*
PNS DOVOZ TISKU, Vinohradská 46, *Praha*
PNS DOVOZ TLAČE, *Bratislava 2*

DENMARK
EJNAR MUNKSGAARD, Norregade 6, *1165 Copenhagen*

FINLAND
AKATEEMINEN KIRJAKAUPPA, P.O. Box 128, *SF-00101 Helsinki 10*

FRANCE
EUROPERIODIQUES S. A., 41 Avenue de Versailles, *78170 La Celle St.-Cloud*
LIBRAIRIE LAVOISIER, 11, rue Lavoisier, *75008 Paris*
OFFICE INTERNATIONAL DE DOCUMENTATION ET LIBRAIRIE, 48, rue Gay-Lussac, *75240 Paris Cedex 05*

GERMAN DEMOCRATIC REPUBLIC
HAUS DER UNGARISCHEN KULTUR, Karl-Liebknecht-Strasse 9, *DDR-102 Berlin*
DEUTSCHE POST ZEITUNGSVERTRIEBSAMT, Strasse der Pariser Kommüne 3—4, *DDR-104 Berlin*

GERMAN FEDERAL REPUBLIC
KUNST UND WISSEN ERICH BIEBER, Postfach 46, *7000 Stuttgart 1*

GREAT BRITAIN
BLACKWELL'S PERIODICALS DIVISION, Hythe Bridge Street, *Oxford OX1 2ET*
BUMPUS, HALDANE AND MAXWELL LTD., Cowper Works, *Olney, Bucks MK46 4BN*
COLLET'S HOLDINGS LTD., Denington Estate, *Wellingborough, Northants NN8 2QT*
W.M. DAWSON AND SONS LTD., Cannon House, *Folkestone, Kent CT19 5EE*
H. K. LEWIS AND CO., 136 Gower Street, *London WC1E 6BS*

GREECE
KOSTARAKIS BROTHERS, International Booksellers, 2 Hippokratous Street, *Athens-143*

HOLLAND
MEULENHOFF-BRUNA B.V., Beulingstraat 2, *Amsterdam*
MARTINUS NIJHOFF B.V., Lange Voorhout 9—11, *Den Haag*
SWETS SUBSCRIPTION SERVICE, 373b Heereweg, *Lisse*

INDIA
ALLIED PUBLISHING PRIVATE LTD., 13/14 Asaf Ali Road, *New Delhi 110001*
150 B-6 Mount Road, *Madras 600002*
INTERNATIONAL BOOK HOUSE PVT. LTD., Madame Cama Road, *Bombay 400039*
THE STATE TRADING CORPORATION OF INDIA LTD., Books Import Division, Chandralok, 36 Janpath, *New Delhi 110001*

ITALY
EUGENIO CARLUCCI, P.O. Box 252, *70100 Bari*
INTERSCIENTIA, Via Mazzé 28, *10149 Torino*
LIBRERIA COMMISSIONARIA SANSONI, Via Lamarmora 45, *50121 Firenze*
SANTO VANASIA, Via M. Macchi 58, *20124 Milano*
D. E. A., Via Lima 28, *00198 Roma*

JAPAN
KINOKUNIYA BOOK-STORE CO. LTD., 17-7 Shinjuku-ku 3 chome, Shinjuku-ku, *Tokyo 160-91*
MARUZEN COMPANY LTD., Book Department, P.O. Boŭ 5056 Tokyo International, *Tokyo 100-31*
NAUKA LTD., IMPORT DEPARTMENT, 2-30-19 Minami Ikebukuro, Toshima-ku, *Tokyo 171*

KOREA
CHULPANMUL, *Phenjan*

NORWAY
TANUM-CAMMERMEYER, Karl Johansgatan 41—43, *1000 Oslo*

POLAND
WĘGIERSKI INSTYTUT KULTURY, Marszałkowska 80, *Warszawa*
CKP I W ul. Towarowa 28 *00-958 Warsaw*

ROMANIA
D. E. P., *Bucureşti*
ROMLIBRI, Str. Biserica Amzei 7, *Bucureşti*

SOVIET UNION
SOJUZPETCHATJ — IMPORT, *Moscow*
and the post offices in each town
MEZHDUNARODNAYA KNIGA, *Moscow G-200*

SPAIN
DIAZ DE SANTOS, Lagasca 95 ,*Madrid 6*

SWEDEN
ALMQVIST AND WIKSELL, Gamla Brogatan 26 *101 20 Stockholm*
GUMPERTS UNIVERSITETSBOKHANDEL AB Box 346, *401 25 Göteborg 1*

SWITZERLAND
KARGER LIBRI AG, Petersgraben 31, *4011 Basel*

USA
ENSCO SUBSCRIPTION SERVICES, P.O. Box 1943, *Birmingham, Alabama 35201*
F. W. FAXON COMPANY, INC., 15 Southwest Park, *Westwood, Mass, 02090*
THE MOORE-COTTRELL SUBSCRIPTION AGENCIES, *North Cohocton, N. Y. 14868*
READ-MORE PUBLICATIONS, INC., 140 Cedar Street, *New York, N. Y. 10006*
STECHERT-MACMILLAN, INC., 7250 Westfield Avenue, *Pennsauken* N. J. 08110

VIETNAM
XUNHASABA, 42, Hai Ba Trung, *Hanoi*

YUGOSLAVIA
JUGOSLAVENSKA KNJIGA, Terazije 27, *Beograd*
FORUM, Vojvode Mišica 1, *21000 Novi Sad*

2. VIII. 1978 HU ISSN 0001—5407 Index: 26.007

ACTA CHIMICA

ACADEMIAE SCIENTIARUM HUNGARICAE

TOMUS 97 FASCICULUS 4

AKADÉMIAI KIADÓ, BUDAPEST

1978

ACTA CHIM. ACAD. SCI. HUNG. ACASA2 97 (4) 369—463 (1978)

ACTA CHIMICA

A MAGYAR TUDOMÁNYOS AKADÉMIA KÉMIAI TUDOMÁNYOK OSZTÁLYÁNAK IDEGEN NYELVŰ KÖZLEMÉNYEI

Acta Chimica is a journal for the publication of papers on all aspects of chemistry, in the English, German, French and Russian languages.

Acta Chimica is published in 4 volumes per year. Each volume consists of 4 issues of varying size.

Manuscripts should be sent to

Acta Chimica
H-1521 Budapest, Hungary

Correspondence with the Editors should be sent to the same address. Manuscripts are not returned to the Authors.

Subscription rate $ 36.00 per volume.

Hungarian subscribers should order from Akadémiai Kiadó, 1363 Budapest, P.O. Box 24. Account No. 215 11488.

Orders from other countries are to be sent to "Kultúra" Foreign Trade Company (H-1389 Budapest 62, P.O. Box 149. Account No. 218 10990) or to its representatives abroad.

Acta Chimica Academiae Scieôtiarum Hungaricae, Tomus 97 (4), pp. 369—374 (1978)

SCHIFF BASE COMPLEXES OF DIOXOURANIUM(VI), V

DIOXOURANIUM(VI) CHLORIDE COMPLEXES WITH DIBASIC TRIDENTATE SCHIFF BASES

R. G. VIJAY and J. P. TANDON

(Chemical Laboratories, University of Rajasthan, Jaipur, India)

Received January 27, 1977

The $UO_2Cl_2(SBH_2)_2$ complexes have been prepared by mixing dioxouranium(VI) chloride in 1:2 mole ratio with the dibasic tridentate Schiff bases (SBH_2) obtained by the condensation of salicylaldehyde, 2-hydroxy-1-naphthaldehyde, *o*-hydroxyacetophenone, 2,4-pentanedione or 1-phenyl-1,3-butanedione with hydroxylalkylamines (such as 2-hydroxyethylamine, 2-hydroxy-1-propylamine and 3-hydroxy-1-propylamine) or 2-hydroxyaniline. The resulting complexes have been characterized by elemental analysis, conductance measurements and infrared spectra.

Introduction

In an earlier publication [1] from these laboratories, reactions of dioxouranium(VI) chloride with monobasic bidentate Schiff bases have been reported and in these the Schiff bases are co-ordinated to the central uranium atom. Such reactions with dibasic tridentate Schiff bases do not seem to have been studied so far. The results of these investigations are discussed in the present paper.

The Schiff bases used in these reactions can be structurally represented as follows (**I** to **IV**):

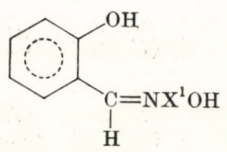

I

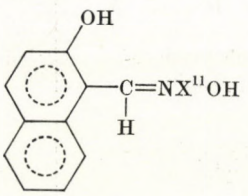

II

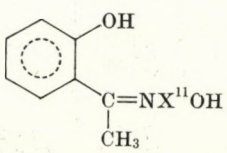

III

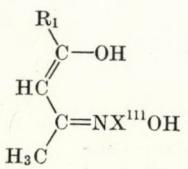

IV

(Where in, **(I)** $X^1 = CH_2CH_2$, CH_2CHCH_3, $CH_2CH_2CH_2$ and *o*-C_6H_4
(II) and **(III)**, $X^{11} = CH_2CH_2$, CH_2CHCH_3 and $CH_2CH_2CH_2$
(IV) when $R_1 = CH_3$, $X^{111} = CH_2CH_2$, CH_2CHCH_3, $CH_2CH_2CH_2$ and *o*-C_6H_4
$R_1 = C_6H_5$, $X^{111} = CH_2CH_2$, CH_2CHCH_3 and $CH_2CH_2CH_2$.)

Experimental

Materials

Absolute ethanol, dimethylformamide and nitrobenzene were dehydrated by chemical methods as reported earlier [2, 3]. Dioxouranium(VI) chloride was used without further purification.

Preparation of Schiff bases

The Schiff bases, 2-hydroxy-1-naphthylidene-2-hydroxyethylamine, 2-hydroxy-1-naphthylidene-2-hydroxy-1-propylamine, 2-hydroxy-1-naphthylidene-3-hydroxy-1-propylamine, 1-phenyl-1,3-butanedione-2-hydroxyethylimine, 1-phenyl-1,3-butanedione-2-hydroxy-1-propylimine and 1-phenyl-1,3-butanedione-3-hydroxy-1-propylimine were prepared by mixing equimolar amounts of aldehyde or β-diketone and desired hydroxyamine in ethanol. These were purified by recrystallization in the same solvent. The analysis and physical characteristics are recorded in Table I.

The synthesis and physical characteristics of the Schiff bases, salicylidene-2-hydroxyethylamine ($C_9H_{11}NO_2$), salicylidene-2-hydroxy-1-propylamine ($C_{10}H_{13}NO_2$), salicylidene-3-hydroxy-1-propylamine ($C_{10}H_{13}NO_2$),* salicylidene(2-hydroxyaniline) ($C_{13}H_{11}NO_2$), *o*-hydroxyacetophenone-2-hydroxyethylinine ($C_{10}H_{13}NO_2$)*, *o*-hydroxyacetophenone-2-hydroxy-1-propylimine ($C_{11}H_{15}NO_2$), *o*-hydroxyacetophenone-3-hydroxy-1-propylimine ($C_{11}H_{15}NO_2$)*, 2,4-pentanedione-2-hydroxyethylimine ($C_7H_{13}NO_2$), 2,4-pentanedione-2-hydroxy-1-propylimine

Table I

Properties and analyses of dibasic tridentate Schiff bases

Schiff base (SBH_2)	Characteristics	M.P. (°C)	Analysis %		
			C Found (Calc.)	H Found (Calc.)	N Found (Calc.)
2-Hydroxy-1-naphthylidene 2-hydroxyethylamine ($C_{13}H_{13}NO_2$)	yellow needles	152 – 5	72.94 (72.55)	6.38 (6.09)	6.76 (6.51)
2-Hydroxy-1-naphthylidene-2-hydroxy-1-propylamine ($C_{14}H_{15}NO_2$)	yellow solid	150 – 51	73.61 (73.38)	6.77 (6.59)	6.08 (6.11)
2-Hydroxy-1-naphthylidene-3-hydroxy-1-propylamine ($C_{14}H_{15}NO_2$)*	yellow solid	120	73.12 (73.38)	6.71 (6.59)	6.15 (6.11)
1-Phenyl-1,3-butanedione 2-hydroxy-ethylamine ($C_{12}H_{15}NO_2$)	pale yellow solid	88	70.39 (70.27)	7.41 (7.37)	6.79 (6.83)
1-Phenyl-1,3-butanedione-2-hydroxy-1-propylimine ($C_{13}H_{17}NO_2$)	pale yellow solid	110 – 12	71.32 (71.20)	7.72 (7.81)	6.48 (6.39)
1-Phenyl- 1,3-butanedione-3-hydroxy-1-propylimine ($C_{13}H_{17}NO_2$)	pale yellow solid	78	71.33 (71.20)	7.84 (7.81)	6.33 (6.39)

* has been used to distinguish between the compounds of the same molecular formula

($C_8H_{15}NO_2$), 2,4-pentanedione-3-hydroxy-1-$_5$propylimine ($C_8H_{15}NO_2$)* and 2,4-pentanedione-2-hydroxyanil ($C_{11}H_{13}NO_2$) have been reported in an earlier paper [3].

Preparation of dioxouranium(VI) complexes

To a solution of dioxouranium(VI) chloride in ethanol was added the ligand solution in the same solvent in 1 : 2 mole ratio under constant stirring. An orange red solution was obtained and in most of the cases an orange red precipitate separated out, which was filtered, washed with ethanol and air dried. The details of these reactions and some important properties of the resulting complexes are reported in Table II.

Table II

Reactions of dioxouranium (VI) chloride with Schiff bases in 1:2 mole ratio and properties of the resulting complexes

UO_2Cl_2 (g)	Schiff base (SBH_2)(g)	Product and characteristics	Analysis %			Molar conductance in (ohm^{-1} $mole^{-1}$ cm^{-1})	
			U Found (Calc.)	N Found (Calc.)	Cl Found (Calc.)	Nitrobenzene	DMF
1	2	3	4	5	6	7	8
2.01	$C_9H_{11}NO_2$ 1.95	$UO_2Cl_2(C_9H_{11}NO_2)_2$ yellow solid	35.53 (35.44)	4.40 (4.17)	10.63 (10.56)	1.59	37.9
1.50	$C_{10}H_{13}NO_2$ 1.58	$UO_2Cl_2(C_{10}H_{13}NO_2)_2$ yellow solid	33.87 (34.04)	4.19 (4.00)	10.02 (10.14)	2.61	36.3
3.22	$C_{10}H_{13}NO_2$* 3.39	$UO_2Cl_2(C_{10}H_{13}NO_2)_2$* orange solid	34.27 (34.04)	3.96 (4.00)	10.03 (10.14)	3.23	42.4
1.13	$C_{13}H_{11}NO_2$ 1.41	$UO_2Cl_2(C_{13}H_{11}NO_2)_2$ red solid	31.60 (31.02)	3.39 (3.65)	9.63 (9.24)	–	41.4
1.66	$C_{13}H_{13}NO_2$ 2.09	$UO_2Cl_2(C_{13}H_{13}NO_2)_2$ yellowish red solid	31.13 (30.86)	3.45 (3.63)	9.43 (9.19)	1.53	37.1
1.80	$C_{14}H_{15}NO_2$ 2.42	$UO_2Cl_2(C_{14}H_{15}NO_2)_2$ yellowish red solid	30.31 (29.78)	3.19 (3.50)	9.03 (8.87)	2.50	41.3
1.57	$C_{14}H_{15}NO_2$* 2.11	$UO_2Cl_2(C_{14}H_{15}NO_2)_2$* yellowish red solid	29.53 (29.78)	3.63 (3.50)	8.60 (8.87)	1.83	45.8
1.41	$C_{10}H_{13}NO_2$* 1.48	$UO_2Cl_2(C_{10}H_{13}NO_2)_2$* yellow solid	34.17 (34.04)	3.99 (4.00)	10.65 (10.14)	–	39.8
1.70	$C_{11}H_{15}NO_2$ 1.93	$UO_2Cl_2(C_{11}H_{15}NO_2)_2$ yellow solid	33.51 (32.72)	3.61 (3.85)	9.99 (9.75)	–	35.4
1.61	$C_{11}H_{15}NO_2$* 1.83	$UO_2Cl_2(C_{11}H_{15}NO_2)_2$* yellow solid	32.73 (32.72)	3.99 (3.85)	9.40 (9.75)	–	42.2
2.17	$C_7H_{13}NO_2$ 1.82	$UO_2Cl_2(C_7H_{13}NO_2)_2$ reddish orange semi-solid	37.39 (37.93)	4.62 (4.46)	11.06 (11.30)	2.71	71.3
1.48	$C_8H_{15}NO_2$ 1.37	$UO_2Cl_2(C_8H_{15}NO_2)_2$ reddish orange-semi-solid	36.64 (36.30)	4.14 (4.27)	10.63 (10.81)	3.44	74.9
1.40	$C_8H_{15}NO_2$* 1.29	$UO_2Cl_2(C_8H_{15}NO_2)_2$* reddish orange-semi-solid	36.40 (36.30)	4.49 (4.27)	10.46 (10.81)	2.82	72.5
1.80	$C_{11}H_{13}NO_2$ 2.02	$UO_2Cl_2(C_{11}H_{13}NO_2)_2$ brownish red solid	32.69 (32.90)	3.92 (3.87)	9.40 (9.80)	1.94	37.6
1.00	$C_{12}H_{15}NO_2$ 1.20	$UO_2Cl_2(C_{12}H_{15}NO_2)_2$ orange solid	31.85 (31.69)	3.63 (3.73)	9.73 (9.44)	3.32	74.8
1.33	$C_{13}H_{17}NO_2$ 1.71	$UO_2Cl_2(C_{13}H_{17}NO_2)_2$ orange solid	30.41 (30.55)	3.67 (3.59)	8.99 (9.10)	2.44	74.8
1.24	$C_{13}H_{17}NO_2$* 1.60	$UO_2Cl_2(C_{13}H_{17}NO_2)_2$* orange solid	30.73 (30.55)	3.45 (3.59)	9.17 (9.10)	2.75	73.6

* has been used to distinguish between the compounds of the same molecular formula.

Analytical methods and physical measurements

Uranium was determined as uranium oxinate [4] nitrogen by Kjeldahl's method, and chlorine gravimetrically as silver chloride.

Molar conductance measurements of the resulting complexes were performed in dimethylformamide and nitrobenzene at 30 ± 1 °C using a Tesla RLC bridge with the cell having a cell constant of 0.74 cm^{-1}. Thermogravimetric analysis was carried out on a Stanton (Mass flow type) Automatic Recording Thermogravimetric Balance.

Infrared spectra of the Schiff bases and their dioxouranium(VI) complexes were recorded in nujol mulls using a Perkin-Elmer 337 grating infrared spectrophotometer with KBr optics. The IR spectra of a few Schiff bases and their complexes were also recorded in the range of 650 – 200 cm^{-1} in nujol mulls using a Beckman IR – 12 infrared spectrophotometer.

Results and discussion

Reactions of dioxouranium(VI) chloride with dibasic tridentate Schiff bases (SBH_2) (i.e. salicylidenehydroxyamines, 2-hydroxy-1-naphthylidenehydroxyamines, *o*-hydroxyacetophenone-hydroxyimines, 2,4-pentanedionehydroxyimines and 1-phenyl-1,3-butanedionehydroxyimines) in 1 : 2 mole ratio can be represented by the following general equation:

$$UO_2Cl_2 + 2SBH_2 \rightarrow UO_2Cl_2(SBH_2)_2$$

All the resulting complexes are stable in light and air, and most of them have been obtained in solid state except the derivatives of the Schiff bases of 2,4-pentanedionehydroxyalkylimines, which are viscous semi-solids. The resulting complexes are soluble in DMF and pyridine, but insoluble in benzene and chloroform.

The Schiff bases used in these reactions are potentially dibasic tridentate in nature, but in the present investigations these behave as neutral bidentate ligands as reported earlier [3]. The possibility of co-ordination through the OH group of the amine residue of the ligand moiety is ruled out by the fact that no reaction has been found to take place between the dioxouranium(VI) chloride and the Schiff bases, benzylidenehydroxylalkylamines. The reason of the inactivity of these Schiff bases is the absence of the OH group in the *ortho* position to the azomethine group as reported by KOVACIC [5] also in the case of bivalent cations.

The behaviour of the alcoholic hydroxy group depends on the central metal ion as well as the nature of the ligand. The crystal structure [6] of bis-(salicylidene-2-hydroxyethylamine)copper(II) shows that the Schiff bases behave as bidentate ligands; the co-ordination takes place through the phenolic oxygen and the nitrogen of the azomethine group. The donating tendency of the alcoholic oxygen is comparatively weak compared to the phenolic oxygen [6] and this is the reason that the alcoholic OH group does not co-ordinate the metal ion in Schiff base complexes.

Conductance measurements

Molar conductance values of these complexes in DMF fall in the range of 35 – 75 ohm^{-1} cm^2 mole^{-1} indicating their partial dissociation in this medium as reported earlier [7], However, the values of molar conductance in nitrobenzene have been found to be below 6 ohm^{-1} cm^2 mole^{-1} indicating that the complexes behave as non-electrolytes [8].

Thermogravimetric analysis

The thermogravimetric analysis of dioxouranium (VI) chloride bis(salicylidene-2-hydroxy-1-propylamine) shows (Fig. 1) that the complex is quite stable up to 160 °C. It loses the two Schiff base molecules up to 475 °C and finally is converted to U_3O_8 at 500 °C.

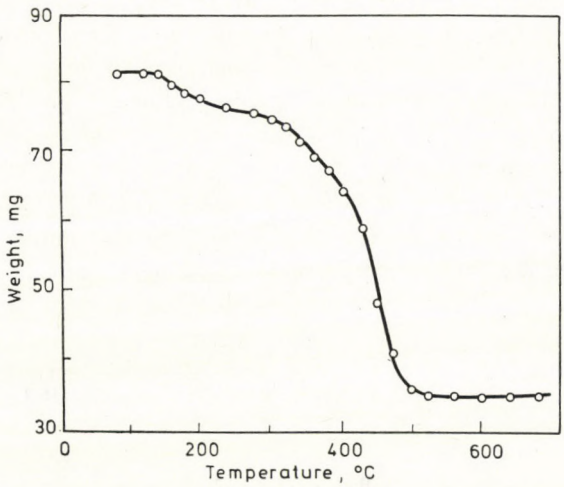

Fig. 1. Thermolysis curve: $UO_2Cl_2(HOC_6H_4CH{:}\,NCH_2CHOHCH_3)_2$ Wt. of the complex = 81 mg, Wt. of the residue = 35 mg, Calcd. Wt. for U_3O_8 = 33 mg

Infrared spectra

The IR spectra of the Schiff bases and their dioxouranium (VI) complexes have been recorded and the important features are as follows.

(i) In the IR spectra of the Schiff bases, weak and broad absorption bonds are observed in the region of 3400 – 3200 cm^{-1}, which are at lower wave numbers than the stretching frequencies of free N–H or O–H group. This can be attributed to the presence of both types of hydrogen bonding, intermolecular (O–H . . . O) as well as intramolecular (O-H . . . N) in these compounds [9, 10]. However, in the resulting complexes, this vibration is shifted by 50

to 250 cm^{-1} toward higher values; this may be attributed to the absorption band of coordinated O–H or N–H vibration.

(ii) Some of these complexes also show absorption band at $\simeq$ 3550 cm^{-1} and this may be due to the free O–H group of the amine residue of the ligand moiety.

(iii) The > C = N-stretching frequency appears in the region of 1625 – 1600 cm^{-1} in the Schiff bases, and this is shifted slightly to the higher wave, numbers in the resulting dioxouranium (VI) complexes. A similar Schift has also been observed in the dioxouranium (VI) complexes by VIDALI *et. al.* [11].

(iv) The dioxouranium (VI) ions exhibit [12] three vibrational frequencies: symmetric (ν_1) and asymmetric (ν_3) stretching and bending (ν_2) frequencies. In the linear dioxouranium(VI) ion, only the asymmetric stretching is easily observed in the normal infrared spectrum, while the bending frequency (ν_2) appears in the lower region. The asymmetric (ν_3) stretching frequency has been observed in the region of 915 – 900 cm^{-1} in the resulting complexes.

In a few derivatives, a weak or medium intensity band appears in the region of 875 – 835 cm^{-1} and this may be assigned to the asymmetric stretching frequency of the dioxouranium(VI) group. Further, another band in the far IR region (*i. e.* 265 – 250 cm^{-1}) has been attributed to the bending vibration (ν_2) of the dioxouranium(VI) ion.

(v) The far IR spectra of a few dioxouranium(VI) chloride complexes of Schiff bases have been recorded to substantiate the bonding of uranium to the chlorine atom. A new band appears at $\simeq$ 225 cm^{-1} and this may be due to the νU-Cl.

*

The authors thank Prof. J. N. GAUR, Head of the Chemistry Department, University of Rajasthan, Jaipur, for Providing Laboratory Facilities. One of us (R. G. V.) is also thankful to the C. S. I. R., New Delhi, for financial support.

REFERENCES

[1] VIJAY, R. G., TANDON, J. P.: J. Inorg. Nucl. Chem., (In press)
[2] VIJAY, R. G., TANDON, J. P.: J. Inorg. Nucl. Chem., **37**, 2326 (1975)
[3] VIJAY, R. G., TANDON, J. P.: Z. Naturforsch., **31b**, 22 (1976)
[4] FRERE, F. J.: J. Amer. Chem. Soc., **55**, 4362 (1933)
[5] KOVACIC, J. E.: Spectrochim. Acta, **23A**, 183 (1967)
[6] IIJIMA, K., OONISHI, I., MUTO, F., NAKAHARA, A., KOMIYAMA, Y.: Bull. Chem. Soc. (Japan), **43**, 1040 (1970)
[7] SAVANT, V. V., PATEL, C. C.: J. Inorg. Nucl. Chem., **31**, 2319 (1969)
[8] WALMSLEY, J. A., TYREE, S. Y.: Inorg. Chem., **2**, 312 (1963)
[9] DAASCH, L. W. HANNINEN, U. E.: J. Amer. Chem. Soc., **72**, 3673 (1950)
[10] BAKER, A. W., SHUGIN, A. T., J. Amer. Chem. Soc., **81**, 1523 (1959)
[11] VIDALI, M., VITAGO, P. A., BANDOLI, G., CLEMENTE, D. A., CASELLATO, U.: Inorg. Chim. Acta, **6**, 671 (1972)
[12] HOEKSTRA, H. R.: Inorg. Chem., **2**, 492 (1963)

R. G. VIJAY, J. P. TANDON } Chemical Laboratories, University of Rajasthan, Jaipur-302004 (India).

Acta Chimica Academiae Scientiarum Hungaricae, Tomus 97 (4), pp. 375—388 (1978)

DIFFUSION IN THE ELEMENTARY CHANNEL SYSTEM OF CLINOPTILOLITE

E. DETREKŐY and D. KALLÓ

(Central Research Institute for Chemistry of the Hungarian Academy of Sciences)

Received February 15, 1977

The diffusion of *cis*- and *trans*-2-butene, methanol and ammonia was studied by infrared spectroscopic and gravimetric methods. The adsorption saturation controlled by diffusion was found to obey BARRER's relation for mass transport in isotropic monocrystals. The relative values of the diffusion coefficients can be correlated with the size of the diffusing molecules, the interactions between molecules and the zeolite pores and with the free pore size.

Zeolites as catalysts and adsorbents have found increasing application in the last 1—2 decades. Unlike in other materials with large surface areas, the pore system of these crystalline aluminosilicates is perfectly regular as a consequence of their crystal structure: cavities of well-defined shape are interconnected by a system of elementary channels.

This pore system is not accessible in natural zeolites because it is filled with exchangeable cations and water, the partial or complete removal of which is necessary to make the pore system permeable for smaller (with a critical diameter of 3—10 Å) molecules. The free cross section of elementary pores in dehydrated zeolites depends on the diameter of the exchangeable cations in the zeolite, it being the largest in the case of H^+-zeolites.

Since the difference between the diameters of the pores and the molecules entering is very small, mass transport in these pores is a particular kind of diffusion: it takes place in crystal and the motion of diffusing material is mainly influenced by the physical and chemical interactions with the wall of the channel.

Such interactions should be taken into account in each practical case, since of interest are only those systems in which there is adsorption (catalytic) interaction between the diffusing molecules and the wall of zeolite pores. The molecules coming to the crystallite pore are thus adsorbed according to the adsorption equilibrium corresponding to the given external concentration. Since the pores are of molecular size, the molecules enclosed within them are located in a chainlike arrangement. The pores are filled gradually by the migration of these molecules. Therefore, the diffusion process can be traced by observing the saturation of the zeolite crystal, which will be termed for simplicity as sorption.

Strictly the process cannot be considered as adsorption since the fluid phase molecules are not bound directly to the internal surface of empty pores.

Instead, the molecules having bound at the pore entrance penetrate deeper into the empty pores. Thus the process is more similar to absorption, its driving force being the concentration difference inside the zeolite crystal.

Let us suppose an isotropic, homogeneous zeolite monocrystal in which the diffusion equation is valid for any spatial direction:

$$\frac{\partial C}{\partial t} = D(\text{div grad})\, C \tag{1}$$

where C is the concentration of the adsorbate (its amount in unit crystal volume) at a certain point of the crystal; D is the phenomenological diffusion coefficient. If sorption takes place at a constant external pressure of the adsorptive on a zeolite consisting of spherical crystallites of radius r_0, in which D is independent of C, the solution of Eq. (1) was given by BARRER [1] using the following boundary conditions:

For any crystallite

$C = C_\infty$ in the external surface layer of the crystallite, if $t > 0$;

$C = C_0$ in the crystallite, if $t = 0$.

If the sorption equilibrium has been reached the amount sorbed in the whole volume of the zeolite crystal is Q_∞, the concentration being uniformly C_∞. At time t after the start of measurement the sorbed amount is Q_t and concentration C in the crystal differs from point to point; Q_0 is the sorbed amount at the start of the measurement.

With these quantities one form of the series solution of Eq. (1) can be given according to [1] as:

$$\frac{Q_t - Q_0}{Q_\infty - Q_0} = 1 - \frac{6}{\pi^2} \sum_{n=1}^{\infty} \frac{1}{n^2} \exp\left(-\frac{Dn^2\pi^2 t}{r_0^2}\right). \tag{2}$$

Since in Eq. (2) only the relative differences of the Q values occur, they can be replaced by the overall sorbed amounts on samples of several spherical zeolite crystals (with radii r_0), which can even be bound together.

At large values of the quantity Dt/r_0^2 all higher terms of the sum of exponentials are negligible compared to the first one [1]:

$$\ln \frac{Q_\infty - Q_t}{Q_\infty - Q_0} = \ln \frac{6}{\pi^2} - \frac{D\pi^2 t}{r_0^2}. \tag{3}$$

Plotting the left-hand side of this equation against t, and using the known value of r_0, D can be determined from the slope of the linear function. Another form of the series solution of Eq. (1) is as follows [2]:

$$\frac{Q_t - Q_0}{Q_\infty - Q_0} = \frac{6(Dt)^{1/2}}{r_0\pi^{1/2}} - \frac{3Dt}{r_0^2} + \frac{12(Dt)^{1/2}}{r_0} \sum_{n=1}^{\infty} \text{ierfc}\, \frac{nr_0}{(Dt)^{1/2}} \tag{4}$$

which, with decreasing $\sqrt{Dt/r_0^2}$, becomes:

$$\frac{Q_t - Q_0}{Q_\infty - Q_0} = 6\left(\frac{Dt}{\pi r_0^2}\right)^{1/2} - \frac{3Dt}{r_0^2} \tag{5}$$

which further simplifies to [1]:

$$\frac{Q_t - Q_0}{Q_\infty - Q_0} = 6\left(\frac{Dt}{\pi r_0^2}\right)^{1/2}. \tag{6}$$

The slope of the left-hand side againts $\sqrt{t}$, in the knowledge of r_0, gives the value of D.

The diffusion measurements were carried out with ammonia for different clinoptilolite derivatives and with *n*-butenes and methanol for H-clinoptilolite. The knowledge of the diffusion process for these materials is important mainly from the point of view of catalytic investigations. In connection with the isomerization of *n*-butenes [13] and the dehydration of methanol [14] it is not clear to what depth of the clinoptilolite crystallite pore system the observed catalytic transformation extends. In the investigation of active centers of zeolite catalysts the observation of ammonia adsorption gives important information [11]. The adsorptive saturation with ammonia is also a diffusion controlled process.

In addition, the above compounds possess those characteristic properties which basically influence the diffusion process in zeolite pores. Our investigations permitted an orientation concerning the effect of molecular size, the role of interaction between the diffusing molecule and the zeolite lattice, and the free size of zeolite pores. Diffusion has been examined by two methods. In the first the weight increase of the sample was followed (upon NH_3 sorption), in the second the concentration of structural hydroxyl groups present in the H-form, interacting with the sorbing molecules, was followed IR spectroscopically (during the sorption of methanol and *n*-butene). As a consequence of these techniques, in the case of ammonia physisorption and chemisorption were measured simultaneously, while in the cases of methanol and the *n*-butene isomers only chemisorption was measured. In the latter case, the decrease of the OH group concentration was recorded, which can be ascribed only to chemical interactions.

Since the internal surface area of clinoptilolite is at least 10 times larger than the external one, the contribution of the latter has been neglected.

Experimental

Clinoptilolites used

In the experiments we used clinoptilolite-containing rocks of Hungarian origin and of American origin, as well (Horseshoe Dam, Maricopa Co., Arizona, USA). The former (NK) contained 60 – 70 % clinoptilolite, while the latter practically 100 %. The Hungarian rock

contained also quartz, tridimite, felspar and volcanic glass. The rocks were powdered and fractionated before the experiments. Their different forms were prepared by ion exchange refluxing with 2 *M* solutions two times, each for three hours. The H-form was prepared by deammoniation of the NH_4-form pumping for 1 hr at 400 °C.

Adsorptives

The three *n*-butene isomers used were Fluka purum products; methanol (Reanal) and ammonia (J. T. Baker) were of analytical grade, the latter with 5 % inert contamination.

Gravimetric measurements

The gravimetric measurements were carried out on Mettler TAl type thermobalance. The sample space could be evacuated and flushed with gas. Its temperature could be varied from 25 to 600 °C, the highest attainable vacuum being 10^{-6} Torr. The sensitivity was 0.01 mg for 50 – 60 mg samples. The change of the sample mass against time during sorption is shown in Fig. 1. (The initial inflection on the curve is due to the non-instantaneous introduction of adsorptive into the adsorbent space.)

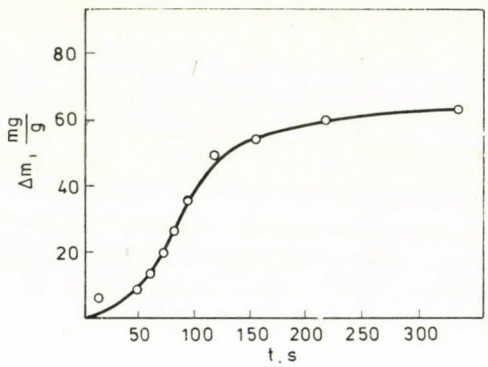

Fig. 1. Mass of sorbed ammonia as a function of time for Hungarian natural clinoptilolite; p_{NH_3} = 760 Torr, T = 25 °C; pretreatment at 10^{-6} Torr and 400 °C for 1 hr

Infrared spectroscopic measurements

The infrared spectroscopic measurements were carried out with a Beckman IR 12 double-beam grating spectrophotometer, producing absorbance *vs.* wave number curves. The sample cell, supplied with a gas inlet, could be evacuated and heated.

The samples investigated were pellets 25 mm in diameter pressed from clinoptilolite powder to a thickness of 10 mg/cm.^{2}

For the quantitative evaluation of spectra, the peak areas from the absorbance *vs.* wave number curves were measured with a planimeter. The area under a band (F) belonging to a given vibration was put into the integrated form of the LAMBERT – BEER law used by HUGHES and WHITE [12]:

$$F = c.e \int \varepsilon_\nu^{(a)} \, d\nu = \int \log (T_0/T)_\nu \, d\nu \qquad (7)$$

where e is the mass per unit pellet surface (g/cm^2), c is the concentration of the given group of atoms or adsorbed molecule in the pellet (meq/g), F is the integrated absorbance for the given band (cm^{-1}), T_0 and T are the transmittances of the adsorbent samples in the absence (C = 0) and in the presence of the given component, respectively, $\int \varepsilon_\nu^{(a)} d\nu$ is the integral adsorption coefficient (cm^{-1}/meq/cm^2). The stretching band of the structural OH groups of zeolite shows a maximum at 3620 cm^{-1}. Evaluation of the measurements shows that the band area

is proportional to the maximum height of the band, thus the latter becomes proportional to the OH group concentration in the sample.

This observation permits to carry out the measurements at a fixed wave length (3620 cm^{-1}). After instantaneous filling of the sample space with gas, the band maximum *vs.* time diagram was recorded. In knowledge of the OH concentration belonging to the maximum peak height, this could be transformed into a concentration *vs.* time diagram (Fig. 2). The decrease of OH concentration was equal to the increase of the concentration of methanol chemisorbed *via* H bonding, and to the increase of *n*-butene concentration during chemisorption in the sample. Consequently, the values of Q_∞ and Q_t are proportional to the decrease of OH concentration (referred to the starting value $C_{OH,0}$) up to time $t = \infty$ and a finite time t, respectively: $Q_\infty \sim (C_{OH,0} - C_{OH,\infty})/C_{OH,0}$ and $Q_t \sim (C_{OH,0} - C_{OH,t})/C_{OH,0}$. (The value of Q_0 was zero in all cases.)

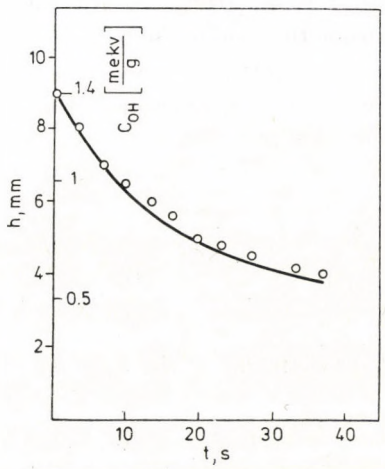

Fig. 2. The decrease of the peak height of the 3620 cm^{-1} band and the corresponding lattice hydroxyl concentration, C_{OH} with time for Hungarian H-clinoptilolite at $p_{CH_3OH} = 6$ Torr and $T = 160$ °C.

Results and discussion

Before a more detailed evaluation of the experimental results let us examine the validity of correlations and approximations derived earlier.

Solution (2) of starting equation (1) is valid if all zeolite crystallites in the sample are spheres of radius r_0, in which the concentration of the diffusing material depends only on the distance measured from the center (spherical symmetry). *i.e.* no diffusion anisotropy exists within the crystallites, and the diffusion coefficient (D) is independent of the concentration of the diffusing material in the zeolite lattice.

It is known, however, that the diffusion properties in clinoptilolite (or in the isostructural heulandite) varies with the direction owing to its structure [3, 4]; the crystallites do not constitute a completely homodisperse system; they are not perfectly spherical, and D is presumably dependent on C.

In the evaluation of our experiments, we neglected these deviations from the ideal case, because we wish to make comparisons only on the basis of rel-

ative values; as regard the absolute values, we are satisfied with an order-of-magnitude agreement.

For small and large Dt values (or if D is fixed, for short and long diffusion times), Eq. (4) simplifies to Eqs (5), (6) and Eq. (70) to (3), respectively [1].

The experimental results were evaluated according to both Eqs (3) and (6). In the first case the values of $\ln (Q_\infty - Q_t)/(Q_\infty - Q_0)$ were plotted against time, in the second the values of $(Q_t - Q_0)/(Q_\infty - Q_0)$ against the square root of time. In both cases the points showed linear correlation with approximately the same error. For *trans*-2-butene, from the first plot we obtained a D value of 14×10^{-13}, whereas from the second plot $D = 3 \times 10^{-13}$ cm^{2}s^{-1}. As for their orders of magnitude, these D values are in fair agreement.

Taking a mean value for D, we examined whether in our case the short or the long time approximation is valid.

Rearranging Eq. (2) to

$$\frac{Q_\infty - Q_t}{Q_\infty - Q_0} = \frac{6}{\pi^2} \sum_{n=1}^{\infty} \frac{1}{n^2} \exp\left(-\frac{Dn^2\pi^2 t}{r_0^2}\right) \tag{2a}$$

and retaining only the first two terms of the right-hand side, one obtains

$$\frac{Q_\infty - Q_t}{Q_\infty - Q_0} = \frac{6}{\pi^2} \exp\left(-\frac{D\pi^2 t}{r_0^2}\right) + \frac{6}{4\pi^2} \exp\left(-\frac{D4\pi^2 t}{r_0^2}\right). \tag{8}$$

For *trans*-2-butene sorption in H-clinoptilolite the value of D is, according to the two types of approximation, 5×10^{-13} cm^{2}s^{-1}; $r_0 = 10^{-5}$ cm and the minimum observation time $t = 6$ s. Upon introduction of these values into Eq. (8), we get

$$\frac{Q_\infty - Q_t}{Q_\infty - Q_0} = \frac{6}{\pi^2}\frac{1}{e^{0,3}} + \frac{6}{4\pi^2}\frac{1}{e^{1,2}} = 6\frac{1}{\pi^2}\left(\frac{1}{e^{0,3}} + \frac{1}{4e^{1,2}}\right) \tag{9}$$

where the first term of the right-hand side equals 0.72, and the second 0.074. Clearly, upon going to longer times, the neglect of the higher terms in the series becomes more and more justified.

Let us now examine expression (5). The starting values are : $D = 5 \times 10^{-13}$ cm^{2}s^{-1}, $r_0 = 10^{-5}$ cm and $t = 200$ s as maximum time. Inserting these values into Eq. (5) the first term of the right-hand side becomes

$$6\left(\frac{Dt}{\pi r_0^2}\right)^{1/2} = 6\left(\frac{5 \times 10^{-13} \times 200}{3.14 \times 10^{-10}}\right)^{1/2} = 3.4$$

beside which the second term

$$-\frac{3Dt}{r_0^2} = \frac{3\times 5\times 10^{-13}\times 200}{10^{-10}} = -3$$

cannot be neglected. Taking $t = 10$ s the first term becomes

$$6\left(\frac{Dt}{\pi r_0^2}\right)^{1/2} = 6\left(\frac{5\times 10^{-13}\times 10}{3.14\times 10^{-10}}\right)^{1/2} = 0.78$$

while the second term

$$-\frac{3Dt}{r_0^2} = \frac{3\times 5\times 10^{-13}\times 10}{10^{-10}} = -0.15$$

is still not negligible.

Summarizing the results of the above calculations it can be concluded that within the range of our experimental conditions expression (3) applies as a satisfactory approximation for the description of diffusion processes.

For the determination of the typical values of $\sim 10^{-13}$ cm^2s^{-1}, the thermogravimetric and infrared spectroscopic methods applied give reproducible, satisfactory results.

The diffusion of small, nonpolar molecules is determined by their critical diameter, the structure of the zeolite crystal lattice, and the interactions arising. For example, the activation energy of helium and neon diffusion in quartz, tridimite and crystobalite [5], and in K-mordenite [6] increases rapidly in the sequence of increasing crystal densities.

The longer the diffusing molecule and the greater its diameter, the smaller is the resulting value for D. In the case of longer, chain-like molecules, the flexibility of the chain and the friction between the molecules and the zeolite assume significance. These effects can be observed mainly for paraffin diffusion [1, 7].

Unlike for nonpolar molecules the diffusion of polar molecules is mainly determined not by dimensional factors, but rather by the interactions between the zeolite lattice (or its particular sites) and the diffusing molecules.

The most typical example is perhaps the diffusion of water. It has been found that diffusing water in a zeolite lattice is bound temporarily to bivalent cations [1]. This manifests itself in the fact that, even if diffusion is sterically unhindered, the energy barriers are higher than those measured in water, but lower than in ice [8].

The binding observed in the case of polar molecules may be so strong that they pratically become fixed to the zeolite lattice, which makes the latter less permeable for other kinds of molecules.

Table I shows the D values determined on the basis of Figs 3–5, according to Eq. (3), for the diffusion of *n*-butene isomers and methanol in H-clinoptilolite.

Table I

Diffusion and sorption of organic molecules in H-clinoptilolite, based on infrared spectroscopic measurements (The uncertainty of D is ± 1 in the second digit)

Adsorptive	$Q_\infty \sim \frac{C_{OH,0} - C_{OH,\infty}}{C_{OH,0}}$	D (cm^2s^{-1})	Conditions of sorption	
			(Torr)	(°C)
Methanol	0.65	11×10^{-13}	6	160
Trans-2-butene	0.15		25	150
Trans-2-butene	0.23		23	125
Trans-2-butene	0.36	14×10^{-13}	24	100
Trans-2-butene	0.40		9	100
Trans-2-butene	0.40		51	100
Cis-2-butene	0.14	3.0×10^{-13}	25	150
Cis-2-butene	0.23	4.3×10^{-13}	30	127
Cis-2-butene	0.36	3.3×10^{-13}	23	100
1-Butene	0.23	*	21	150

* The diffusion coefficient has not been determined

H-clinoptilolite contains four kinds of channels with different diameters [9]. *n*-Butene isomers, having a critical diameter above 5 Å, may only get into the widest (3.5 × 7.9 Å) channels. Owing to the ability of molecules to undergo certain distortions, the critical diameter of the diffusing molecule can be at most 10 % larger than the channel size of the zeolite in the size range considered here. It is interesting to note that when the molecular size approaches the maximum value, the diffusion constant falls off rapidly (Table I): the increase in diameter (0.5 Å) upon going from *trans*-2-butene (5.1 Å) to *cis*-2-butene (5.6 Å) decreases the diffusion coefficient to 1/5 of its original value; the difference of 0.7 Å between the diameters of methanol (4.4. Å) and *trans*-2-butene does not change significantly the diffusion coefficient which even is smaller for methanol than for *trans*-2-butene. In explanining the latter phenomenon it should not be overlooked that, for hindered diffusion, the energy barriers are due not only to steric factors, but also to sorption interactions, which have also a decisive influence upon the value of the diffusion coefficient. Thus in the case of the polar methanol, such adsorption energy barriers may diminish the greater mobility corresponding to the smaller diameter. (Because of its smaller size, methanol may occupy the less accessible active sites of the pores, thus showing enhanced chemisorption.)

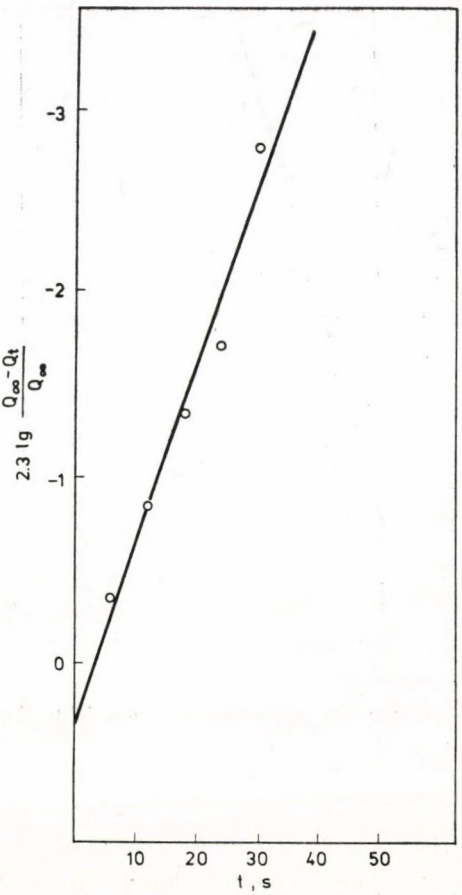

Fig. 3. Sorption of methanol on Hungarian H-clinoptilolite at $p_{CH_3OH} = 6$ Torr and $T = 160$ °C plotted according to Eq (3)

As shown by Fig. 4 the value of D practically does not change with temperature in the case of *trans*-2-butene, which points to a small potential barrier. No pressure dependence was observed either in the range investigated, because diffusion occurs by migration within the pores and if the coverage does not change in the pressure range studied, then diffusion does not change with pressure, even if D depends on the concentration.

In the case of *cis*-2-butene (Fig. 5) D was also shown – within the experimental errors – to be independent of the temperature between 100 – 150 °C.

Since the diffusion of different molecules in zeolites is a process requiring an activation energy [1], the diffusion coefficient should theoretically increase with increasing temperature. In practice, however, in agreement with the data of other authors, the value of D is nearly independent of temperature (see for example the diffusion of propane and butene in Na-mordenite between 25 – 140 °C [10]).

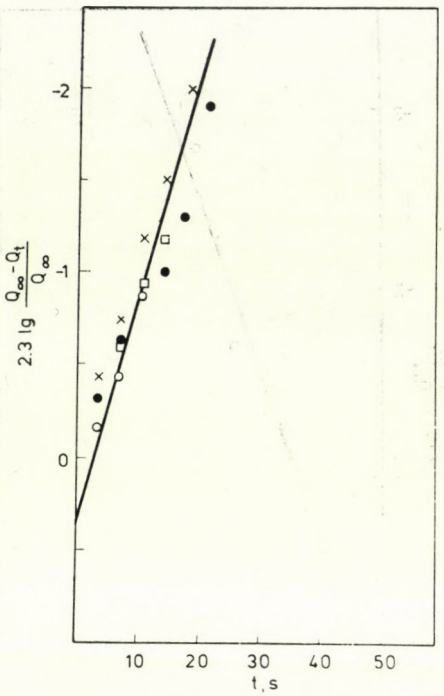

Fig. 4. Sorption of *trans*-2-butene on Hungarian H-clinoptilolite plotted according toEq. (3); ×: 100 °C, 9 Torr; ○ 100 °C, 24 Torr; □ : 125 °C, 23 Torr; ●: 150 ° C, 25 Torr

The reason for the apparent temperature independence is probably that the activation energy is so small that the changes are within the experimental error.

The NH_3 molecule with its critical diameter of 2.86 Å finds enough space in any of the channel types of H-clinoptilolite. The free channel diameter decreases in the substituted derivatives and some channels become nonpermeable for NH_3.

The diffusion or sorption of ammonia in different clinoptilolite derivatives is shown in Figs 6 – 8. The results obtained in our experiments are summarized in Table II.

Comparing the natural clinoptilolites originating from Hungary and the United States (Table II), we find that the ratio of the maximum sorbed amount of NH_3 (Q_∞) is 0.67; this corresponds to the clinoptilolite content of the Hungarian sample determined by other methods, which means that the sorption capacity of the non-zeolite phase is negligible.

The Q_∞ values obtained are 3 – 4 times higher than the amount of chemisorbed ammonia based on the ion exchange capacity, which means that physical and chemical sorption takes place simultaneously.

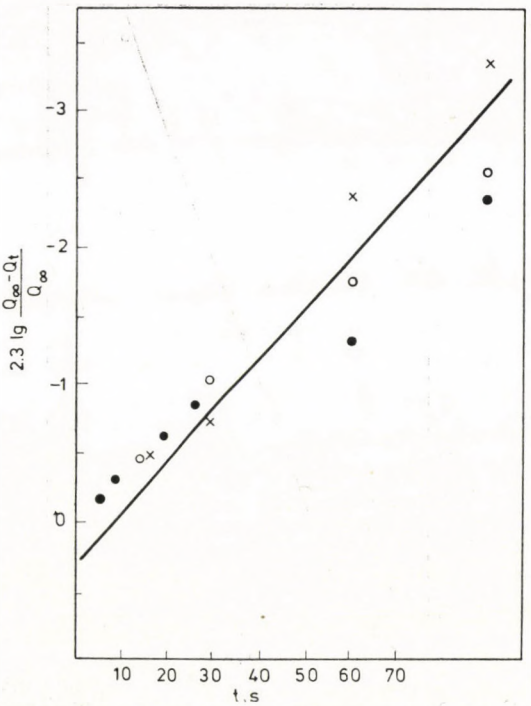

Fig. 5. Sorption of *cis*-2-butene on Hungarian H-clinoptilolite plotted according to Eq. (3); ×: 100 °C, 23 Torr; •: 127 °C, 30 Torr; ○: 150 °C, 25 Torr

Table II

Diffusion and sorption of NH_3 at 25 °C in different clinoptilolite derivatives based on gravimetric measurements

$T = 25$ °C $\qquad p_{NH_3} = 760$ Torr

(The uncertainty of D is ±1 in the second digit)

Zeolite	Temperature of preparation	Q_∞(meq/g)	D (cm^2s^{-1})
Natural clinoptilolite (Hungarian)	400 °C	3.5	2.0×10^{-13}
H-clinoptilolite (Hungarian)	400 °C	4.3	2.0×10^{-13}
H-clinoptilolite, dehydroxylated (Hungarian)	550 °C	3.5	1.9×10^{-13}
Natural clinoptilolite (American)	400 °C	5.2	2.0×10^{-13}
Natural clinoptilolite (American)	600 °C	5.1	2.7×10^{-13}

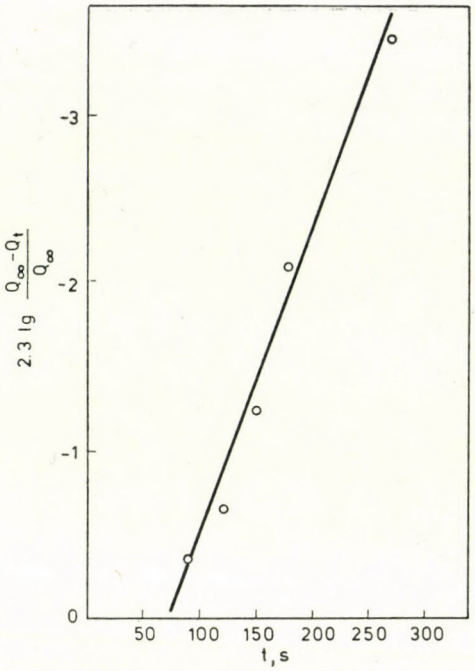

Fig. 6. Sorption of ammonia on Hungarian H-clinoptilolite partially dehydrated at 550 °C, plotted according to Eq. (3); $p_{NH_3} = 760$ Torr, $T = 25$ °C

Since sorption is not uniform, its quantitative evaluation would involve great difficulties. On the basis of our experimental data, however, we may develop certain notions about the interactions in the zeolite pores.

A comparison of the Q_∞ values for partially dehydrated natural clinoptilolite (*cf.* lines 1 and 2 in Table II) shows that the degree of sorption is greater in the H-form. Since the free channel volume is larger in the H-form owing to the absence of metal cations, this phenomenon is not surprising; at the same time, however, the chemisorption of NH_3 on protons may also contribute to the total sorption. The latter assumption seems to be further supported by the observation that dehydroxylation leads to a decrease of Q_∞ (*cf.* lines 2 and 3 in Table II). The difference thus obtained is, however, smaller than expected (0.8 meq/g instead of 1.4 meq/g) but this can be attributed to the uncertainty of determination.

The removal of water bound to cations from natural clinoptilolite at 400—600 °C does not influence the NH_3 sorption capacity as shown by the agreement of the Q_∞ values (*cf.* lines 4 and 5 in Table II).

Experiments with the American natural clinoptilolite prove, as expected, that the decrease of water content (at higher pretreatment temperature) leads to an increase of D (*cf.* 4 and 5 lines in Table II). It is apparent that the D value measured for fully dehydrated natural clinoptilolite (pretreated at 600 °C

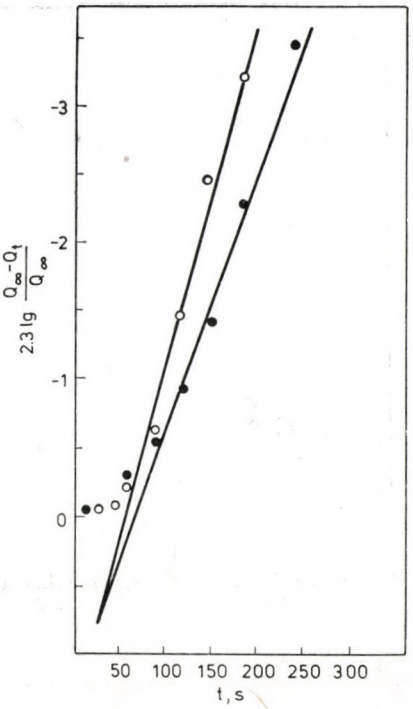

Fig. 7. Sorption of ammonia on American natural clinoptilolite plotted according to Eq. (3). p_{NH_3} = 760 Torr, T = 25 °C, •: pumped off at 400 °C, ○: pumped off at 660 °C

[11]) containing only metal cations, is greater than the D value obtained for the fully dehydrated H-form (pretreated above 300 °C [11]) (*cf.* lines 5 and 2 in Table II). This means that the fully dehydrated exchangeable cations do not exert such hindrance against diffusion as the acidic OH groups, on which ammonia can be chemisorbed. The cations are probably in such positions that the channel diameter does not decrease below 3.0 Å even in the narrowest ones. The cations are located probably either in the widest channels only, or, which is even more likely, they are situated at the boundary of two channels penetrating in both.

From the comparison of Tables I and II it appears that the diffusion coefficient for the NH_3 molecule with a critical diameter of 2.86 Å is smaller than that obtained for *cis*-2-butene, whose critical diameter is 5.6 Å. This phenomenon can be explained by the strong interaction between the NH_3 molecule and the zeolite lattice. The interaction is much weaker in the case of *cis*-2-butene, which is also supported by the observation that the effect of temperature on the value of D is negligible.

*

Our thanks are due to Professor J. B. UYTTERHOEVEN and Dr. P. A. JACOBS University of Leuven, Belgium for their help in performing the IR experiments.

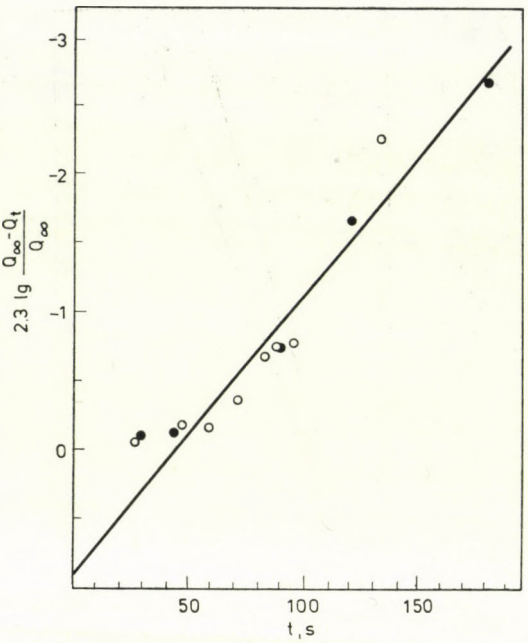

Fig. 8. Sorption of ammonia on Hungarian clinoptilolite derivatives plotted according to Eq. (3). p_{NH_3} = 760 Torr, T = 25 °C; •: natural form pumped off at 400 °C; ○: H-form

REFERENCES

[1] BARRER, R. M.: 2nd International Conference on Molecular Sieves, Worcester, Mass., USA (1970)
[2] CARSLAW, H. S., JAEGER, J. C.: Conduction of Heat in Solids. p. 234. Sec. Ed. Oxford Clarendon Press, 1947
[3] TISELIUS, A.: Z. Phys. Chem. **A 169,** 425 (1934)
[4] TISELIUS, A.: Z. Phys. Chem. **A174,** 401 (1935)
[5] BARRER, R. M., VAUGHAN, D. E. W.: Trans. Faraday Soc. **40,** 207 (1944)
[6] BARRER, R. M., BROOK, D. W.: Trans. Faraday Soc. **49,** 1049 (1953)
[7] BARRER, R. M., IBBITSON, D. A.: Tans. Faraday Soc. **40,** 207 (1944)
[8] DYER, A., MOLYNEUX, A.: J. Inorg. Nucl. Chem., **30,** 829 (1968)
[9] BARRER, R. M., PAPADOPULOS, R., REES, L. V. C.: J. Inorg. Nucl. Chem. **29,** 2047 (1967)
[10] FRABETTI, A. I.: Thesis, M. I. T., Cambridge, Mass., USA, 1965
[11] DETREKŐY, E. J., JACOBS, P. A., KALLÓ, D., UYTTERHOEVEN, J. B.: J. Catal. **32,** 442 (1974)
[12] HUGHES, T. R., WHITE, H. M.: J. Phys. Chem. **71,** 2129 (1967)
[13] KALLÓ, D., DETREKŐY, E., SCHAY, G.: Acta Chim. (Budapest) **94,** 19 (1977)
[14] DETREKŐY, E., KALLÓ, D.: Acta Chim. (Budapest) (In press)

Emil DETREKŐY H-1112 Budapest, Rákó u. 5.
Dénes KALLÓ H-1027 Budapest, Frankel Leó u. 2–4.

Acta Chimica Academiae Scientiarum Hungaricae, Tomus 97 (4), pp. 389—397 (1978)

DISSOLUTION OF ALUMINIUM IN ANHYDROUS ACETIC ACID CONTAINING LITHIUM CHLORIDE

L. KISS, L. SZIRÁKI and M. L. VARSÁNYI

(Department of Physical Chemistry and Radiology, Eötvös Loránd University, Budapest)

Received April 10, 1977

The anodic dissolution of aluminium in a solution of LiCl in anhydrous acetic acid has been studied. Experimental results suggest that the intermediate Al^+ ions, whose formation is supposed on the basis of the apparent charge number, are oxidized by acetic acid molecules or by $CH_3COOH^+_2$ ions to stable Al^{3+} ions. The anodic oxidation of the hydrogen gas formed as a product was detected by voltammetric curves a platinum ring electrode.

A method is described on the basis of which the variation of the effective charge number n_e as a function of the electrode potential may give information on the mechanism of the process. However, in the case discussed in this paper, various changes of the electrode surface and its ohmic resistance preclude the application of this method.

In an earlier communication [1] it has been reported that when aluminium is anodically dissolved in anhydrous acetic acid the apparent charge number of the dissolving ion is less than 3. With a rotating ring-disc electrode in a 0.5 mol/dm^3 solution of lithium perchlorate in acetic acid, the limiting currents for the reduction of ClO_3^- ions and to the oxidation of Cl^- ions have been identified at the platinum ring electrode.

Based on data in the literature [2], we explained this phenomenon by the dissolution of aluminium *via* an Al^+ intermediate, which is oxidized, in the medium mentioned, by ClO_4^- ions to the stable Al^{3+} product. In the reduction of ClO_4^- ions, besides chloride ions, also water is produced, which has been detected and measured.

In preliminary experiments the dissolution of aluminium is anomalous also in solutions of lithium chloride and sodium acetate. In the latter case the formation of an insoluble layer adhering to the surface made further studies impossible. In this paper we discuss some results concerning the anodic dissolution of aluminium in a 0.5 mol/dm^3 solution of lithium chloride in anhydrous acetic acid.

Results and discussion

The disc of the rotating ring-disc electrode was made from 99.999 % aluminium and the ring from pure platinum; the material of the plate electrode was 99.999 % aluminium. The pretreatment of the plate electrode, the purification of acetic acid, the analysis of the water content of the solution have been described in earlier communications [1, 3].

Voltammetric measurements were carried out with a RADELKIS OH-405 type potentiostat suitable for the compensation of ohmic error. The electrode disc was polarized galvanostatically. Potentials were measured against a saturated LiCl acetic acid calomel electrode. Measurements were made at room temperature in an atmosphere of nitrogen or hydrogen. Hydrogen was generated by electrolysis; oxygen and moisture were removed from these gases in the usual way. The water content of the initial solutions was always less than 0.01 mol/dm^3, and this did not change even after long periods of aluminium dissolution.

The apparent charge number n_e determined in the course of galvanostatic dissolution in 0.5 mol/dm^3 LiCl in acetic acid varied between 1.3 and 1.8, in the apparent current density range of $0.5 - 5$ mA/cm^2. Owing to the continuous change of the state of the surface, galvanostatic dissolution occurs at continuously changing true current densities and potentials. At current densities higher than 0.5 mA/cm^2, a gas evoled on the surface of aluminium during dissolution.

By voltammetry on the bright platinum ring electrode, attempts were made to determine the products formed in the anodic dissolution of the aluminium disc electrode using a rotating ring-disc electrode device.

Figure 1 is a voltammetric curve plotted for the platinum ring electrode during the dissolution of the aluminium disc at 2 mA. Above $+0.2$ V on the platinum ring electrode an anodic current is in evidence. The maximum of this anodic current increases (Fig. 2) as a function of the current which polarizes the aluminium.

This current cannot be due to the oxidation of Al^+ ions since, according to the literature [4] on aqueous media, this is to be expected only at much more negative potentials.

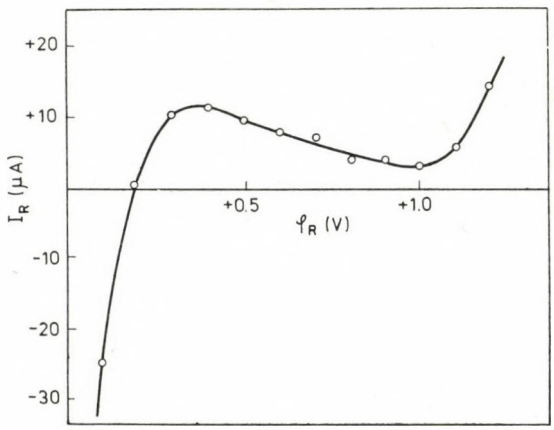

Fig. 1. Voltammetric curve for the platinum ring electrode with the aluminium disc electrode polarized by 2 mA (0.5 mol/dm^3 solution of LiCl in acetic acid). I_R – intensity of current through the ring; φ_R – potential of the ring electrode; speed of rotation $f = 610$ rpm

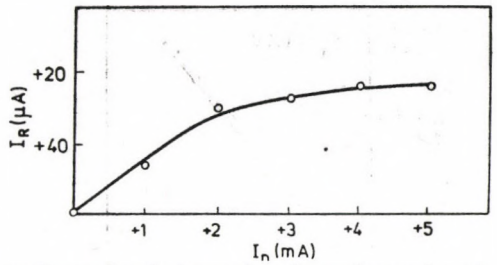

Fig. 2. Limiting current I_R on the platinum ring electrode as a function of the polarizing current I_D through aluminium disc electrode (0.5 mol/dm³ solution of LiCl in acetic acid; $f = 610$ rpm)

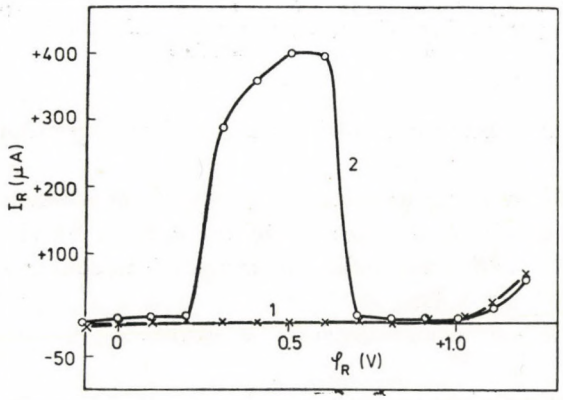

Fig. 3. Voltammetric curve for the platinum ring electrode in a 0.5 mol/dm³ solution of LiC in acetic acid saturated with nitrogen (1) and with hydrogen (2); $f = 610$ rpm

The evolution of a gas on the aluminium electrode was observed during anodic dissolution. At the potentials applied here, the oxidation of the acetate, a possible source of carbon dioxide, could not have occurred [5]. Therefore it may be concluded that the oxidation of Al^+ ions is accomplished by acetic acid in the solution, or by the $CH_3COOH_2^+$ ions produced by the rapid dissociation of acetic acid, consequently, the gas evolved during anodic polarization is hydrogen. Based on this supposition, it seemed obvious to ascribe the anodic current observed from $+0.2$ V to the H_2 formed.

To prove this, voltammetric curves were recorded also with a bright platinum ring electrode, without the aluminium disc, in solutions saturated with hydrogen; such a curve is shown in Fig. 3. The oxidation of hydrogen starts at $+0.2$ V and is represented by a curve abruptly declining right after its maximum at 0.7 V. This slow down of the oxidation of hydrogen is a phenomenon described also in the literature [6] and is due to passivation of the platinum surface against the oxidation of hydrogen.

The diffusional character of the rate of oxidation of hydrogen is shown in Fig. 4; the current recorded for the rotating ring electrode at the potential

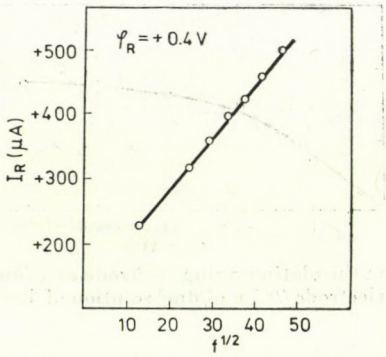

Fig. 4. Limiting current I_R recorded on the platinum ring electrode at $\varphi_R = +400$ mV as a function of the stirring speed, in a 0.5 mol/dm³ solution of LiCl in acetic acid; f – speed of rotation of the electrode (rpm)

corresponding to maximum current increases with the speed of rotation of the ring electrode.

Based on this it seems reasonable to suppose that when the aluminium disc electrode is dissolved, the increase of the current on the platinum ring, incipient at +0.2 V, is due to oxidation current of molecular hydrogen formed in the oxidation of Al^+ ions.

A reaction scheme consistent with the results is

$$Al \underset{k_{k_1}}{\overset{k_{a_1}}{\rightleftarrows}} Al^+ + e \qquad \text{(I)}$$

$$Al^+ \underset{k_{k_2}}{\overset{k_{a_2}}{\rightleftarrows}} Al^{3+} + 2e \qquad \text{(II)}$$

$$Al^+ + 2AcH \xrightarrow{k_3} Al^{3+} + H_2 + 2Ac^- \qquad \text{(III)}$$

where AcH is acetic acid. The concentration of this component at the electrode surface is constant. Accordingly, the product Al^{3+} is the result of an electrochemical reaction (II) and of a homogeneous chemical reaction (III) which proceeds at the surface of the electrode, *via* oxidation of the intermediate Al^+. Since the concentration of AcH at the electrode surfaces is constant, reaction (III) is of the first order.

In a generalized form the reaction sequence (I) – (III) can be written:

$$M \rightleftarrows M^{z_1+} + z_1 e \qquad \text{(Ia)}$$

$$M^{z_1+} \rightleftarrows M^{z_2+} + n_2 e \qquad \text{(IIa)}$$

$$M^+ + n_2 AcH \longrightarrow M^{z_2+} + n_2 Ac^- + \frac{n_2}{2} H_2 \qquad \text{(IIIa)}$$

The rate constants of the electrochemical steps depend on the electrode potential φ as follows [7]

$$k_{a_i} = k'_{a_i} \exp \frac{\alpha_i n_i F \varphi}{RT} \tag{1}$$

$$k_{k_i} = k'_{k_i} \exp \frac{-(1-\alpha_i) n_i F \varphi}{RT} \tag{2}$$

where k'_{a_i} and k'_{k_i} are the rate constants for $\varphi = 0$;

α_i is the transfer coefficient the other symbols have the usual meaning. If the electrode process consists of two steps, $i = 1, 2$; for processes (I) and (II), $n_1 = 1$, $n_2 = 2$, $z_2 = n_1 + n_2 = 3$.

According to this reaction scheme, the effective charge number lower than 3 is due to the occurrence of reaction (III). It is known [8] that conclusions on the mechanism of a stepwise process can be drawn from the way n_e is affected by various parameters.

Let us now examine what kind of information can be obtained from the way n_e is affected by the potential, assuming that the mechanism is that shown by the sequence (I) – (III). As stated, the intermediate will not be removed by diffusion from the surface but will further react electrochemically or will be oxidized, with one of the components of the solution, to the final product. Starting from considerations suggested in the literature [8], in such a case the relationship between n_e and the electrode potential can be constructed as follows.

The current density j from an external source through the electrode is [6]

$$j = n_e F v \tag{3}$$

where n_e is the effective charge number, v is the rate of formation (mol cm^{-2} sec^{-1}) of the product M^{z_2+} ions.
Hence

$$n_e = \frac{j}{Fv} . \tag{4}$$

In the case of reaction (I) – (III), and if the cathodic step of reaction (II) is negligible in comparison with the other steps, then

$$j = k_{a_1} - k_{k_1} c_{10} + k_{a_2} c_{10} \tag{5}$$

and the rate v can be given as

$$v = \frac{k_{a_1} - k_{k_1} c_{10}}{z_1 F} . \tag{6}$$

From Eqs (4)–(6)

$$n_e = z_1 + \frac{z_1 k_{a_1} c_{10}}{k_{a_1} - k_{k_1} c_{10}} . \tag{7}$$

The concentration c_{10} of the intermediate at the electrode surface can be calculated on the assumption that a steady state obtains when the balance of formation and of consumption of M^{z_1+} is zero. Then

$$\frac{k_{a_1}}{z_1} - \frac{k_{k_1} c_{10}}{z_1} - k_3 c_{10} - \frac{k_{a_2} c_{10}}{n_2} = 0 . \tag{8}$$

From this

$$c_{10} = \frac{k_{a_1}}{k_{k_1} + z_1 k_3 + \frac{z_1 k_{a_2}}{n_2}} . \tag{9}$$

From Eqs (7) and (9), after rearrangement, the following expression results

$$\frac{n_e - z_1}{z_2 - n_e} = \frac{k_{a_2}}{n_2 k_3} . \tag{10}$$

Considering the dependence of k_{a_2} on the electrode potential as given by Eq. (1), the following relationship is obtained between n_e and the electrode potential ε

$$\lg \frac{n_e - z_1}{z_2 - n_e} = \lg \frac{k'_{a_2}}{n_2 k_3} + \frac{n_2 \alpha_2 \mathrm{F}}{2.303\ \mathrm{RT}} \varphi . \tag{11}$$

According to Eq. (11), if the value of n_e is determined at various electrode potentials φ, then the term of the left-hand side plotted as a function of φ will give a straight line, whose slope allows the calculation of the transfer coefficient of step (II), and the intercept represents the ratio of the rate constants of the chemical and electrochemical steps. Equation (11) shows that as the electrode potential increases, *i.e.* becomes more and more positive, the value of n_e also increases; when $\varphi \to \infty$, $n_e \simeq z_2$. Also, Eq. (10) shows that if $k_{a_2} \ll k_3$, $n_e \simeq z_1$, and if $k_{a_2} \gg k_3$, $n_e \simeq z_2$. If z_3, $= 3$, $z_1 = 1$ and $\alpha_2 = 0.5$, then, according to Eq. (11) an increase of n_e from 1.1 to 2.9 requires potential more positive by 150 mV.

These qualitative experimental results, *viz.* that the value of n_e is 1.3–1.8 and hydrogen gas is evolved upon anodic polarization, can be explained also on the basis of the negative differential effect [7]. According to this, the anodic dissolution of aluminium activates the metal surface, on which not only anodic but also spontaneous dissolution with hydrogen depolarization occurs. Thus dissolution does not seem to proceed *via* a stepwise mecha-

nism, and the fact that the effective charge number is less than 3 is due to spontaneous dissolution. In such cases the following processes may take place

$$\mathrm{Al} \xrightarrow{k_{a_4}} \mathrm{Al^{3+}} + 3\mathrm{e} \qquad \text{(IV)}$$

$$\mathrm{Al} + 3\mathrm{AcH} \longrightarrow \mathrm{Al^{3+}} + 3\mathrm{Ac^-} + 1\frac{1}{2}\mathrm{H_2}. \qquad \text{(V)}$$

Reaction (IV) is irreversible, reaction (V) consists of two coupled electrochemical steps, *viz.* anodic process (IV) and the evolution of hydrogen gas

$$\mathrm{AcH} + e \xrightarrow{k_{k_5}} \mathrm{Ac^-} + \frac{1}{2}\mathrm{H_2} \qquad \text{(Va)}$$

where k_{a_4} and k_{k_5} stand for the potential-dependent rate constants of processes (IV) and (Va), respectively. The rate of spontaneous dissolution is determined by the rate of H_2 evolution according to Eq. (Va). For the sake of generalization, instead of reaction (IV), we may write

$$\mathrm{M} = \xrightarrow{k_{a_4}} \mathrm{M^{z+}} + ze\,. \qquad \text{(IVa)}$$

Relationships (1) – (4) are valid also here. However, current j from the external source, passing through the electrode is

$$j = k_{a_4} - k_{k_5} \qquad (12)$$

with the proviso that the concentration of AcH at the electrode surface is constant. We have always $k_{a_4} \geq k_{k_5}$, and or $k_{a_4} = k_{k_5}$ if $j = 0$; the case $k_{a_4} < k_{k_5}$ is meaningless. Hence

$$v = \frac{j}{z\mathrm{F}} + \frac{k_{k_5}}{z\mathrm{F}}\,. \qquad (13)$$

From Eqs (4), (12) and (13)

$$\frac{z}{z - n_e} = \frac{k_{a_4}}{k_{k_5}}\,. \qquad (14)$$

According to the potential-dependence of rate constants k_{k_4} and k_{k_5}, *i.e.* Eqs (1) and (2), we have the following relationship between n_e and ε

$$\lg\left(\frac{z}{z - n_e}\right) = \lg\frac{k'_{a_4}}{k'_{k_5}} + \frac{\alpha_4 z + (1 - \alpha_5)\,\mathrm{F}}{2.303\,\mathrm{RT}}\varphi \qquad (15)$$

where α_4 and α_5 stand for the transfer coefficients of the respective electrode reactions. Also expression (14) shows that if $k_{a_4} = k_{k_5}$, then $n_e = 0$, and if $k_{a_4} \gg k_{k_5}$, than $z \simeq n_e$. According to Eq. (15), the increase of n_e from 1.1 to

2.9 requires only a change of $\Delta\varphi \simeq 40$ mV, if $z = 3$, and $\alpha_4 = \alpha_5 = 0.5$. If n_e is changed from 0.1 to 2.9, the $\Delta\varphi$ needed is about 45 mV. According to Eq. (15), the values of n_e at various electrode potentials φ were determined and the left-hand term was plotted as a function of φ. A straight line was obtained, from which the sum of the apparent transfer coefficients of electrode reactions (IV) and (V) was calculated.

It follows from the above considerations that if the dependence of n_e on the electrode potential is determined with sufficient accuracy and the results are treated according to Eqs (11) and (15), it is possible to decide whether a stepwise process or the negative differential effect occurs.

An advantage of this method is that if n_e is measured at a constant potential, the change with time of the true electrode surface does not affect the results. This is also shown by Eq. (4), n_e being a dimensionless number.

Therefore we have determined the n_e values pertaining to given potentials with a potentiostat. In view of the high cell resistance and density current a JATE AFKEL 409/1 type potentiostat with high output voltage was used for the control of the potential; the charge passing was measured with a copper coulometer. Prior to adjustment of the desired potential, the passive surface layer on the aluminium was broken up by heavy anodic current pulses. Around the current-free potential (-600 mV), *viz.* at -500 mV the value for n_e was found to be 1.66 ± 0.05; at $+500$ mV this value was 1.89 ± 0.05.

This finding is in accord with relationships (11) and (15) only so far as the value of n_e increases with the electrode potential, but kinetic parameters cannot be calculated. This is due to the circumstance that the state of the surface changes continuously as dissolution proceeds. These changes consist in separation of the layer formed during pretreatment, formation of a bright or mat deposit (depending on the potential), and at more positive potentials formation, of insoluble precipitate, as well as in etching to a rough surface. Thus the adjusted potential cannot be accepted as the true potential of aluminium since this includes also a large ohmic potential drop. Consequently, under the conditions of these experiments, the n_e values determined do not permit unequivocal conclusions concerning the mechanism of aluminium dissolution. The facts that no value for n_e lower than 1 was ever recorded and that in a rather wide range of potentials this value never reached 3, point to a stepwise mechanism.

REFERENCES

[1] Kiss, L., Varsányi, M. L., Dudás, E.: Magy. Kém. Folyóirat, **79,** 216 (1973)
[2] Epelboin, J., Froment, M.: J. Chim. Phys., Phys. Chim. Biol., **60,** 1301 (1963); 14th Meeting of CITCE, Moscow, 1963
[3] Kiss, L., Do Ngoc Lien, Varsányi M. L.: Ann. Univ. Sci. Budapest. Sect. Chim., **12,** 145 (1971)
[4] Lohonyai, N., Rédey, L.: Periodica Polytechnica, **6,** 121 (1962)

[5] KOLOTYRKIN, Ya. M. Ed: Elektrokhimiya metallov v nevodnykh rastvorakh. Izd. MIR, Moscow (1974)
[6] ERDEY-GRUZ., T.: Elektródfolyamatok kinetikája. Akadémiai Kiadó, Budapest 1969
[7] KISS, L.: Kémiai Közl. **44**, 91 (1975)
[8] KABANOV, B. N., KOKULINA, D. V.: Dokl. Akad. Nauk. SSSR, **120**, 558 (1958); MOLODOV, A. I., MARKOSYAN, G. N., LOSEV, V. V.: Elektrokhimiya, **5**, 918 (1969)

László KISS
Laura SZIRÁKI
L. Magda VARSÁNYI
H-1088 Budapest, Puskin u 11–13.

Acta Chimica Academiae Scientiarum Hungaricae, Tomus 97 (4), pp. 399–406 (1978)

SPONTANEOUS PROCESSES ON METAL SURFACES UNDER THE ACTION OF OWN METALL IONS, II

L. KISS, J. FARKAS, P. KOVÁCS and L. KOZÁRI

(Department of Physical Chemistry and Radiology, Eötvös Loránd University, Budapest)

Received May 19, 1977

The processes occurring in the $Cu/Cu^+/Cu^{2+}$ system in the presence of a high excess of Cu^{2+} ions relative to the equilibrium concentration ($c_{Cu^+} \simeq 0$), has been studied in 1.0 mol/dm³ aqueous HCl (20 °C) and 3.0 mol/dm³ aqueous $HClO_4$ (60 °C) solutions.

It was found that in hydrochloric acid solution the rate of the process is determined by the diffusion of Cu^{2+} ions to the electrode surface. In perchloric acid solution the equilibrium of the system is immediately established at the electrode surface, and the slowest step of the process is the diffusion of the Cu^+ ions formed away from the electrode surface.

The results obtained can be readily interpreted by the relationships described in an earlier communication [1].

In our previous communication [1] relationships were given which permit to draw conclusions on the kinetics of spontaneous processes in the system $M–M^{z_1+}–M^{z_2+}$. For a few characteristic cases, the dependence of the rate of the processes and the steady-state potential of the metal (M) on the concentration of M^{z_1+} and M^{z_2+} ions in the solution has been established: when a rotating disc electrode was used, their dependence on the speed of rotation of the electrode was also studied.

In this communication we report on the investigation of processes proceeding under certain conditions in the Cu–Cu(I)–Cu(II) system. The following two processes may proceed at the copper electrode:

$$Cu \underset{k_{k_1}}{\overset{k_{a_1}}{\rightleftharpoons}} Cu^+ + e \qquad \text{(I)}$$

$$Cu^+ \underset{k_{k_2}}{\overset{k_{a_2}}{\rightleftharpoons}} Cu^{2+} + e \qquad \text{(II)}$$

where k_{a_1}, k_{k_1}, k_{a_2} and k_{k_2} are rate constants depending on the electrode potential.

MOLODOV *et al.* [2] investigated this system in anhydrous methanolic sulfate solutions. They have found that when Cu^{2+} is present in excess over the equilibrium concentration, reverse disproportionation occurs at the copper electrode, proceeding *via* reactions (I) and (II) by an electrochemical mechanism. Their results as already indicated [1], can be interpreted also in terms of the relationships established by us.

PANG *et. al.* [3] investigated the dissolution of copper under the action of copper(II) ions in acetonitrile–water solvent mixture in the presence of sulfuric acid. They have found that under the experimental conditions used the diffusion of copper(II) to the electrode surface is the rate-determining process.

We have studied the processes occurring at the copper electrode in solution containing chloride or perchlorate ions, and excess Cu^{2+} ions relative to the equilibrium copper ion concentration ($c_{Cu^+} \simeq 0$). In this case, process (I) takes place mainly in the direction of the upper, while process (II) in that of the lower arrow.

As described in earlier communications, measurement with the rotating ring-disc electrode may give useful information on the kinetics of spontaneous processes on the copper surface under the action of Cu(II) ions. For this purpose, we should measure the dependence of the steady-state (current-free) potential, ε_{st}, of the copper electrode, and of the limiting current of the Cu (I) ions formed (measurable on the ring electrode) on the Cu^{2+} concentration and on the speed of rotation of the electrode.

Results and discussion

The equipment, methods and materials used in the experiments were the same as those described earlier [4]. The ring electrode of the electrode system was made of platinum. The Cu^{2+} ion concentration of the solution was determined photometrically.

Figures 1–3 show the results obtained at 20 °C in 1 mol/dm^3 hydrochloric acid solution. Figure 1 shows the change of ε_{st}, the steady-state potential, as a function of the logarithm of Cu^{2+} concentration at different speeds of rotation of the electrode. The points lie to a good approximation on a straight

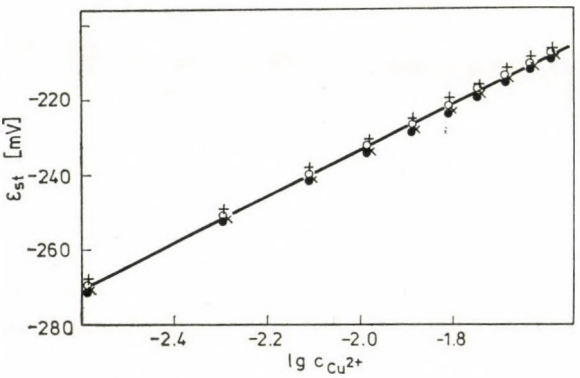

Fig. 1. Dependence of the steady state potential, ε_{st}, of the copper disc electrode on the logarithm of Cu^{2+} concentration ($c_{Cu^{2+}}$) in 1.0 mol/dm^3 HCl background solution at 20 °C, at different speeds of rotation of the electrode. Speed was changed between 275 and 1080 min^{-1} Reference: normal calomel electrode

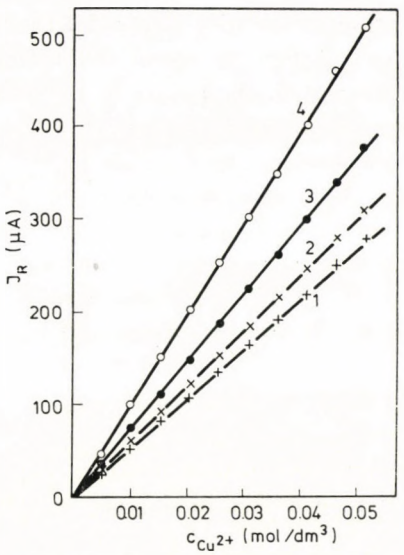

Fig. 2. Limiting current of oxidation (I_R) measurable at the platinum ring electrode as a function of Cu^{2+} concentration ($c_{Cu^{2+}}$) at various speeds of rotation (f) of the electrode, at 20 °C, in 1.0 mol/dm³ HCl. Speed of rotation (min^{-1}); (1) 275; (2) 350; (3) 550; (4) 1080

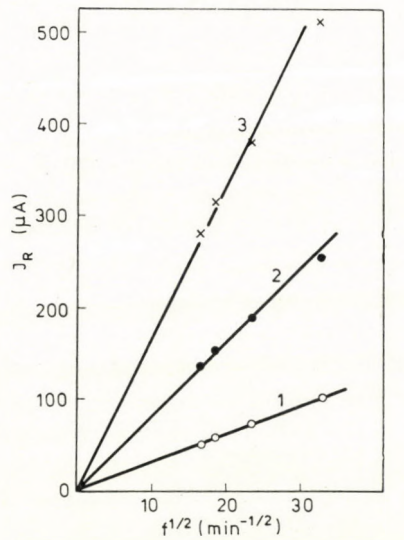

Fig. 3. I_R as a function of the square root of the speed of rotation (f) at 20 °C and various $c_{Cu^{2+}}$ concentrations, in 1.0 mol/dm³ HCl; $c_{Cu^{2+}}$ values (mol/dm³); (1) 5.02×10^{-5}; (2) 1.29×10^{-4}; (3) 2.58×10^{-4}

line, the slope of which is $\simeq$ 62 mV. In this case, the steady-state potential is practically independent of the speed of rotation of the disc.

Figure 2 shows the limiting current (I_R) on the ring electrode due to Cu^+ ions formed at the disc electrode, as a function of Cu^{2+} ion concentration at

different speeds of rotation of the disc electrode. In Fig. 3, the I_R values are plotted against the square root of the speed of rotation (f), for different Cu^{2+} concentrations. As will be noted, the points lie in both cases on straight lines starting from the origin. Thus, the data show that the limiting current of oxidation on the ring is proportional to $c_{Cu^{2+}}$ and $f^{1/2}$.

Thus, data of Figs 1–3 unequivocally show that processes (I) and (II) do take place in HCl solution in the presence of Cu^{2+} and case 1/*d* discussed in the previous communication is realized. Accordingly, the rate constants of Cu^+ and Cu^{2+} diffusion (X_1 and X_2), and the relative values of the rate constants of reactions (I) and (II) are in the following order:

$$X_1 \ll k_{a_2} \ll k_{k_1}; \quad X_2 \ll k_{k_2} \,. \tag{1}$$

According to the previous communication [1], the limiting current of Cu^+ formed at the disc, measurable in this case on the ring electrode, is

$$I_R = \gamma f^{1/2} c_{Cu^{2+}}$$

and

$$\gamma = r_1^2 \pi N \; 0.62 \; D_{Cu^{2+}}^{2/3} \nu^{-1/6} \left(\frac{2\pi}{60}\right)^{1/2} \tag{2}$$

where r_1 is the radius of the copper disc electrode, N the geometrical factor of the rotating ring-disc electrode, $D_{Cu^{2+}}$ the diffusion coefficient of Cu^{2+} ions, ν the kinematic viscosity of the solution, and f the speed of the electrode (min^{-1}).

In Fig. 4, the value of I_R is plotted on the basis of relationship (2) as a function of $c_{Cu^{2+}} f^{1/2}$. As can be seen, in this case too, the values measured fall to a good approximation on a straight line, in accordance with case 1/*d* discussed in our previous communication.

According to the results obtained, in the process occurring under the action of Cu^{2+} ions at the copper electrode in an acidic solution containing excess chloride ions, the slowest steps are the transport of Cu^{2+} ions (of the chloro complex of Cu^{2+}) to the metal surface, and the transport of Cu^+ ions (of the chloro complex of Cu^+) from the surface. It has further been established that in the given medium the exchange current of reaction (I) is much larger than that of step (II) (see inequality(1)).

In the following, results obtained at 60 °C in 3.0 mol/dm^3 $HClO_4$ will be discussed. Figure 5 shows the change of the steady-state potential, ε_{st}, as a function of the logarithm of Cu^{2+} concentration. Measured points belonging to the different speeds of rotation lie also in this case approximately on a straight line. However, the slope of the straight line, 34.0 mV, differs from that obtained in chloride solutions. The slope of the line and its independence

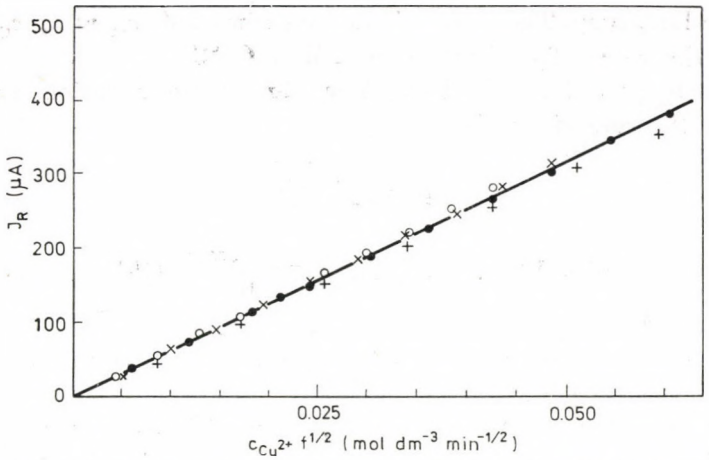

Fig. 4. I_R as a function of the product ($c_{Cu^{2+}} f^{1/2}$) at 20 °C in 1.0 mol/dm³ HCl solution. Points marked with different symbols belong to different speeds of rotation

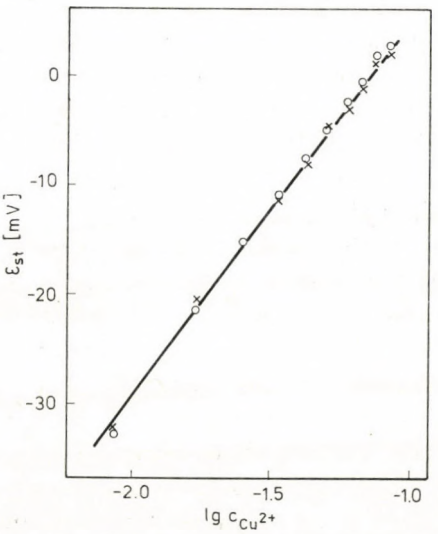

Fig. 5. Dependence of the steady state potential, ε_{st}, of the copper disc electrode on the logarithm of Cu^{2+} concentration at 60 °C in 3.0 mol/dm³ $HClO_4$ background solution at speeds of rotation of 275 and 1080 min^{-1}. Reference: normal calomel electrode

of the speed of rotation indicate that case 1/*e*, discussed in the first communication, is realized. Hence:

$$X_1 \ll k_{k_1} \gg k_{a_2} \quad \text{and} \quad X_2 \gg k_{k_2} . \tag{3}$$

Under these conditions equilibrium concentrations are established at the electrode surface and the dependence of ε_{st} on the Cu^{2+} concentration should obey

Nernst's relationship. The slope of the experimental ε_{st} *vs.* lg $c_{Cu^{2+}}$ agrees well with the value of 32.5 mV, expected at 60 °C.

According to Eq. (25) of the preceeding communication, the limiting current at the ring electrode is:

$$I_R = \gamma' f^{1/2} c_{Cu^{2+}}^{1/2} \tag{4}$$

where

$$\gamma' = 1/2 r_1^2 \pi N \quad 0.62 \, D_{Cu}^{2/3} \nu^{-1/6} \left(\frac{2\pi}{60}\right)^{1/2} K^{1/2}$$

K being the equilibrium constant of the coupled processes (I) and (II), (see Eq. (26) of the preceding communication).

Therefore, in Fig. 6 the relationship I_R *vs.* $f^{1/2}$ has been plotted for different Cu^{2+} concentrations, while in Fig. 7 the relationship I_R *vs.* $c_{Cu^{2+}}^{1/2}$ for different speeds of rotation of the electrode. As can be seen from the Figures, in both cases the respective experimental points give straight lines starting from the origin. However, in Fig. 6 there is a deviation from the straight line at high speeds of rotation in the direction of the abscissa. In Fig. 7 deviations from the straight line are exhibited at low concentrations, experimental points being systematically shifted towards the abscissa. It can be further noted from Fig. 5 that at low Cu^{2+} concentrations ε_{st} is shifted by $1-2$ mV in the negative direction with increasing electrode speed. Figure 8 shows the I_R values as a function of the product $f^{1/2} \, c_{Cu^{2+}}^{1/2}$. Points belonging to low speeds of rotation lie on a straight line starting from the origin. Experimental points belonging to a speed of 1080 min^{-1} considerably deviate from this line.

The systematic deviations from case $1/e$ found are indicative of the fact that in these cases inequality (3) is not completely realized, $X_1 < k_{a_2}$ being obtained instead of $X_1 \ll k_{a_2}$. On increasing the electrode speed and on decreasing the Cu^{2+} concentration (the latter shifts the potential in the negative direction), the condition $X_1 \simeq k_{a_2}$. This means that case $1/e$ approaches case $1/b$ of the preceding communication. The steady-state potential shifts with increasing electrode speed in the negative direction, and the limiting current of Cu^+ oxidation (I_R) measurable at the ring electrode is proportional to the 2/3 power of the Cu^{2+} concentration and to the 1/6 power of the speed of rotation.

The above results show that for electrode processes (I) and (II), occurring at the copper electrode under the action of Cu^{2+} ions at 60 °C in 3.0 mol/dm^3 $HClO_4$, the exchange current of the first process is high, while that of the second lower. Moreover, it can be established that, due to the low rate constant of the cathodic step of process (II) and to the high exchange current of step (I), the equilibrium of the system $Cu/Cu^+/Cu^{2+}$ is approximately established at the electrode surface during the process. In the case investigated, the ratio of

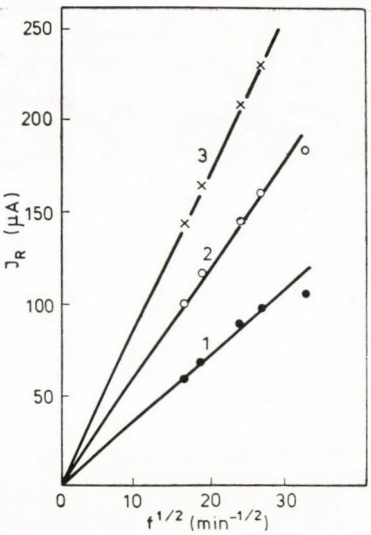

Fig. 6. Relationship between I_R and $f^{1/2}$ at different $c_{Cu^{2+}}$ values in 3.0 mol/dm³ $HClO_4$, at 60 °C. Values of $c_{Cu^{2+}}$ (mol/dm³); (1) 1.69×10^{-2}; (2) 4.22×10^{-2}; (3) 8.44×10^{-2}

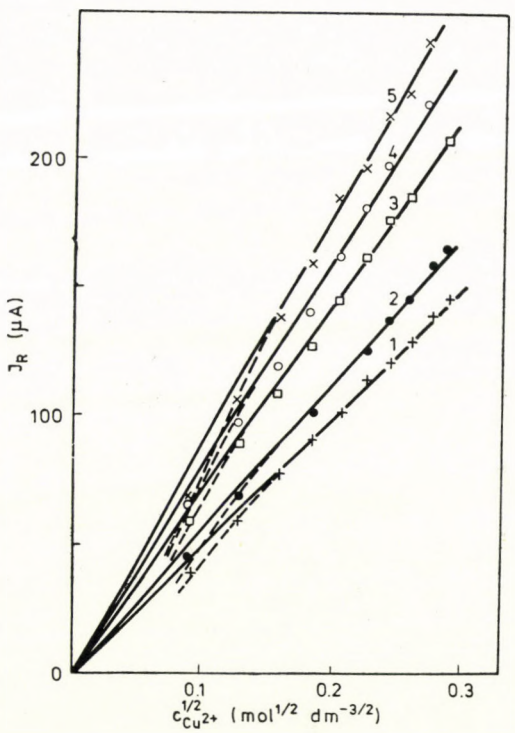

Fig. 7. Relationship between I_R and $c^{1/2}_{Cu^{2+}}$ at different speeds of rotation of the electrode, at 60 C°, in 3.0 mol/dm³ $HClO_4$. Speed of rotation (min^{-1}): (1) 275; (2) 350; (3) 565; (4) 720, (5) 1080

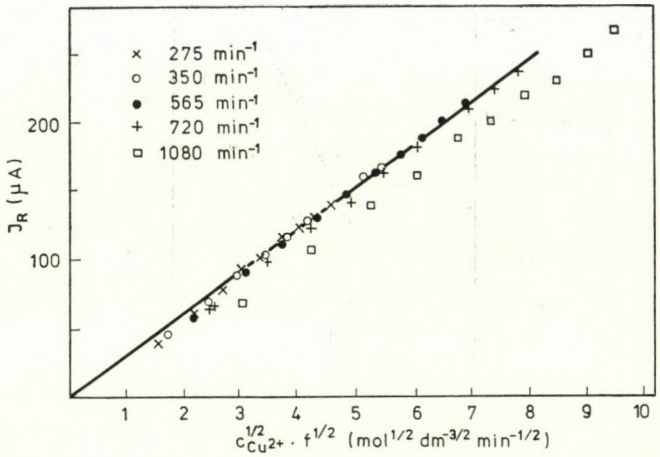

Fig. 8. I_R as a function of $c^{1/2}_{Cu^{2+}} f^{1/2}$ at 60 °C in 3.0 mol/dm³ $HClO_4$

the rate constants of reaction (II) is $k_{k_2} < k_{a_2}$. The slowest step of the process is the diffusion of Cu^+ ions formed away from the electrode surface.

It can be seen that the relationships given in the preceding communication can be used for the interpretation of the processes occurring in the $Cu/Cu^+/Cu^{2+}$ system.

REFERENCES

[1] Kiss, L., Farkas, J.: Magy. Kém Folyóirat **83,** 337 (1977); Acta Chim. (Budapest) (in press)
[2] Molodov, A. I., Yanov, L. A., Losev, V. V.: Elektrokhimiya, **12,** 513 (1976); Zashchita Metallov, **12,** 578 (1976)
[3] Pang, J., Ritchie, J. M., Giles, D. E.: Electrochim. Acta, **20,** 923 (1975)
[4] Kiss, L., Farkas, J., Körösi, A., Mandl, J.: Magy. Kém. Folyóirat **79,** 127 (1973); Acta Chim. (Budapest) **79,** 43 (1973)

László Kiss
József Farkas
Pál Kovács
László Kozári
H-1088 Budapest, Puskin u 11–13.

Acta Chimica Academiae Scientiarum Hungaricae, Tomus 97 (4), pp. 407—412 (1978)

STUDY OF MOLECULAR INTERACTION OF NITROBENZENE IN CARBON TETRACHLORIDE AT MICROWAVE FREQUENCY

ASHOK KUMAR SHARMA

(Department of Physics, Institute of Advanced Studies, Meerut University, Meerut, India)

Received May 30, 1977

The dielectric behaviour of nitrobenzene in carbon tetrachloride solution has been studied at eight concentrations (in the range 0.01 – 0.2 mole fraction) at 9.3 GHz and 1.6 MHz at 27 °C. The molar polarization (P_2) and dipole moment (μ) decrease non-linearly with increasing concentration, while the reduced relaxation time (τ/η) increases. It is suggested that for low concentrations of nitrobenzene in carbon tetrachloride the negative solvent effect is predominant, while at relatively higher concentrations lateral solute–solute interactions prevail.

Introduction

The purpose of the present study is to assess the molecular interactions of nitrobenzene in carbon tetrachloride. Several studies of the solute–solvent interaction based on static dielectric measurements have been reported [1,2,3]. In the present paper the static permittivity and dielectric relaxation behaviour have been investigated. The dielectric relaxation time (τ) of a polar molecule in a nonpolar solvent depends on the temperature, viscosity (η) and the intermolecular (dipole–dipole and solute–solvent) interactions. At low concentrations, where the effect of strong dipole–dipole interaction is suppressed, the reduced relaxation time (τ/η) should be constant and the molar polarization (P_2) should vary linearly with concentration. At relatively higher concentrations, where intermolecular interactions come into play, the τ/η and P_2 values deviate from linearity. The variation of the dipole moment with concentration also reflects the extent of ordering of molecules due to local and intermolecular interactions. Thus, in view of the above, we have measured the relaxation time (τ), molar polarization (P_2) and dipole moment (μ) at constant temperature (27 °C) as a function of the concentration. The distribution parameter (α) for nitrobenzene in a nonpolar solvent [4] as well as in the pure liquid state [5] is zero so that a single frequency can be successfully used for determination of relaxation times.

Experimental

Nitrobenzene was fractionally distilled and the fraction within the boiling range 206–207 °C was collected. The refractive index was found to be 1.547 (27 °C) while the reported value is 1.550 [6] (25 °C). The carbon tetrachloride used was of A. R. grade. Both nitrobenzene and carbon tetrachloride were dried using molecular sieves.

The permittivity (ε') and dielectric loss (ε'') of nitrobenzene in carbon tetrachloride at eight different concentrations were measured at 9.3 GHz. The accuracy of measurement for ε' and ε'' was ± 2 % and ± 5 %, respectively. At low concentrations (0.01 – 0.037 mole fraction) SMYTH's [10] method, while at relatively high concentrations (0.037 – 0.2 mole fraction) POLEY's [8] method was used. The static permittivity (ε_0) at 1.6 MHz, densities, refractive indices and viscosities of these solutions were also measured at 27 °C.

The static permittivity (ε_0) was measured using a type 'B602', 'WAYNE KERR' bridge with an accuracy of ± 1 %.

The viscosity was measured with an Ostwald viscometer, accuracy ± 0.5 %. The densities of solutions were measured by pycnometer, accuracy ± 0.2 %. The refractive indices of solutions were measured by Abbe's refractometer and the values of refractive indices were corrected to the third decimal

Theory

For a system having a single time, $\omega\tau$ is equal to $\varepsilon''/\varepsilon' - \varepsilon_\infty$. When the solvent has no loss, the dispersion equations are identical with those for the pure liquids, provided ε' and ε'' are replaced by the corresponding increments [9] of the permittivity and loss, so that

$$\omega\tau = \frac{\varepsilon''_{12}}{(\varepsilon'_{12} - \varepsilon'_1) - (\varepsilon_{12\infty} - \varepsilon_{1\infty})} \tag{1}$$

The subscripts 12 and 1 refer to solution (with mole fraction x_2 of the polar solute) and solvent, respectively.

The apparent molar polarization (P_2) of the solute is given by the following equation [10, 11] (exactly valid for ideal solutions):

$$P_2 = P_1 + (P_{12} - P_1)/x_2 \tag{2}$$

where $P_1 = [(\varepsilon'_1 - 1)/(\varepsilon'_1 + 2)]\,(M_1/d_1)$, is the molar polarization of the solvent and

$$P_{12} = \left[\frac{(\varepsilon'_{12} - 1)}{(\varepsilon'_{12} + 2)}\right]\left[\frac{M_1x_1 + M_2}{d_{12}}\right] \tag{3}$$

that of the solution. M_1 and M_2 are the molecular weights x_1 and x_2 the mole fractions of the solvent and solute respectively, and d_{12} is the density of the solution.

The dipole moment (μ) has been calculated from ONSAGER'S [12] relation for a dilute solution

$$\varepsilon'_{12} - \varepsilon_{12\infty} = \frac{4\pi N}{3kT}\,\mu^2\left[\frac{\varepsilon'_1(\varepsilon_{2\infty} + 2)}{2\varepsilon'_1 + \varepsilon_{2\infty}}\right]^2 \tag{4}$$

where N is the concentration of the solution in molecules/cm^3 units.

Results and discussion

The variations of P_2, τ/η and μ as functions of x_2 are shown in Figs 1–3. The molar polarization (P_2), as obtained from microwave and static measurements, has been found to decrease nonlinearly with increasing concentration. This indicates intermolecular interactions as the concentration is increased. SRIVASTAVA *et al.* [1] have studied the molecular associations in some substituted anilines in dilute benzene solutions and concluded that the molar polarization changes nonlinearly with increasing concentration. SRIVASTAVA *et al.* [2] have studied various alcohols and halides in dilute benzene and carbon tetrachloride solutions. They have found that in the case of alcohols the P_2 *vs.* X_2 curve is a straight line showing the absence of any interaction. Halides showed no interaction and confirmed the theoretical findings of COOK and SCHUG [13] that benzene invariably reacts with halogen molecules, giving rise to some complexes. SRIVASTAVA *et al.* have also found that in dilute carbon tetrachloride solutions such anomalies disappear. They were unable to give an adequate explanation for the nature of these complexes, but confirmed that at low concentrations, where solute–solute interaction is ineffective, exchange

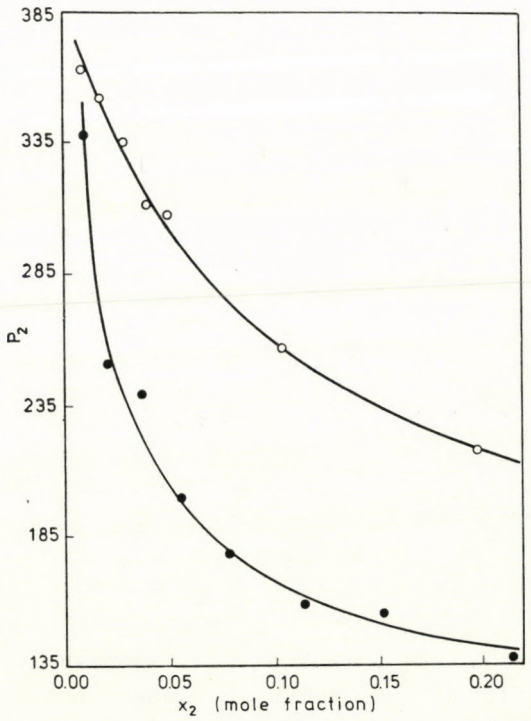

Fig. 1. Variation of the molar polarization (P_2) of nitrobenzene with the mole fraction (x_2) in carbon tetrachloride from microwave ● and static ○ measurements

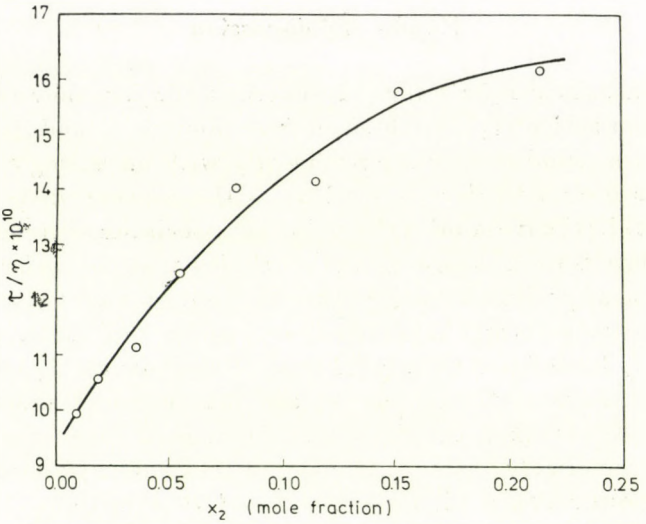

Fig. 2. Variation of the reduced relaxation time (τ/η) with the mole fraction (x_2) of nitrobenzene in carbon tetrachloride

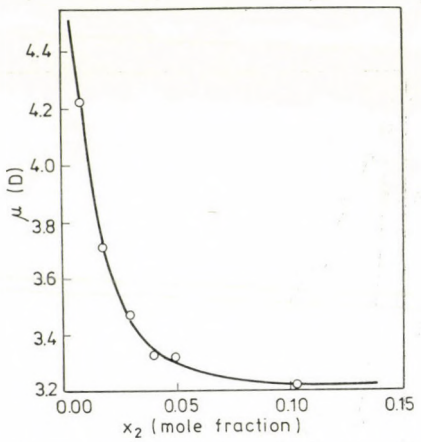

Fig. 3. Variation of the dipole moment (μ) with the mole fraction (x_2) of nitrobenzene in carbon tetrachloride

interaction between benzene and solute molecules will enhance the molar polarization (P_2). Liszi [3] has explained the strong decrease in P_2 by dipolar association with antiparallel arrangements. But this effect will play a dominant role only at relatively higher concentrations, *viz.* 0.1 mole fraction and above. But at low concentrations (0 – 0.1 mole fraction) the strong decrease in P_2 is due to the negative solvent effect [14] as solute–solute interaction is ineffective. Higasi [15, 16] expressed dipole moments in solutions as

$$\mu_s = \mu_{\text{gas}} + \Sigma\mu_i$$

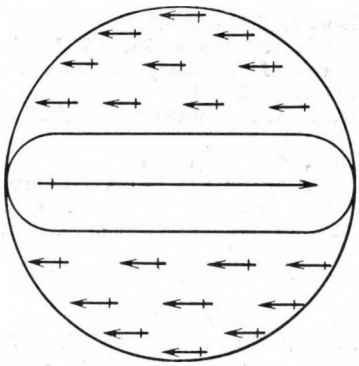

Fig. 4. Negative solvent effect

where $\Sigma\mu_i$ is the sum of the moments induced in the solute molecules. If an ellipsoidal molecule, having its dipole directed along its major axis, is enclosed in a spherical region containing solvent molecules, the induced dipoles outside the sphere cancel and only those produce inside the sphere need be considered. These induced dipoles reduce the effective dipole moment of the solute and produce a negative solvent effect (as shown in Fig. 4). This effect has also been measured in chlorobenzene, acetonitrile, etc.

In concentrated solutions, the solute–solute interactions become important. The molecular dipoles may align head to tail ($\rightarrow\!\!+\!\!\rightarrow$) or laterally ($\begin{smallmatrix}\rightarrow\\+\\\rightarrow\end{smallmatrix}$). The former configuration increases the effective molecular dipole moment and produces solute polarizations which increases with increasing concentration, the latter reduces the effective molecular dipole moment.

In our case the dipole moment decreases nonlinearly with increasing concentration and thus indicates that for low concentrations of nitrobenzene in carbon tetrachloride the negative solvent effect is predominant, while at relatively higher concentrations lateral solute–solute interactions prevail. These facts are also confirmed by the τ/η *vs.* x_2 curves, because with increasing concentration the intermolecular interactions cause hindrance in the orientation of the molecules and thus increase the relaxation time.

*

The author is grateful to Dr. V. K. AGARWAL for this supervision and suggestions in this work, to Prof. S. P. KHARE for his interest in the work and for the facilities, as well as to Dr. ABHAI MANSINGH for many helpful suggestions. Thanks are also due to Mr. V. P. ARORA and Mr. G. K. GUPTA for their co-operation.

REFERENCES

[1] SRIVASTAVA, S. C., PRAKASH, J., MEHROTA, V. K., CHANDRA, S.: J. Chem. Phys., **49,** 964 (1968)
[2] SRIVASTAVA, K. K., NAYAR, R. K., KRISHNA, I.: Indian J. Chem., **9,** 459 (1971)
[3] LISZI, J.: Acta Chim. (Budapest), **84,** 125 (1975)

[4] POLEY, J. P.: Appl. Sci. Res., **4B**, 337 (1955)
[5] FATUZZO, E., MASON, P. R.: J. Appl. Phys., **36**, 427 (1955)
[6] WEAST, R. C. Ed.: Handbook of Chemistry and Physics, 53th edition. The Chemical Rubber Co., Cleveland, Ohio 1972—73
[7] HESTON, Jr. W. H., FRANKLIN, A. D., HENNELLY, E. J., SMYT, C. P.: J. Am. Chem. Soc., **72**, 3443 (1950)
[8] POLEY, J. P.: Appl. Sci. Res., **134**, 337 (1955)
[9] BUCKLEY, F., MURYOTT, A. A.: Tables of Dielectric Dispersion Data for Pure Liquids and Dilute Solutions. National Bureau of Standards Circular, Washington, D. C. 1958
[10] SMYTH, C. P.: Dielectric Behaviour and Molecular Structure. McGraw-Hill Book Co., New York 1955
[11] BOTCHER, C. J. F.: Theory of Electric Polarization. Elsevier Publ. Co. Inc., Amsterdam 1952
[12] ONSAGER, L.: J. Am. Chem. Soc., **58**, 1486 (1936)
[13] COOK, Jr. E. G., SCHUG, J. C.: J. Chem. Phys., **53**, 723 1970
[14] HILL, N. E., VAUGHAN, W. E. PRICE, A. H., DAVIES M.: Dielectric Properties and Molecular Behaviour. Van Nostrand Reinhold Co., London, New York 1969
[15] HIGASI, K.: Bull. Inst. Phys. Chem. Res. Japan, **14**, 146 (1935)
[16] HIGASI, K.: Sci. Pap. Inst. Phys. Chem. Res. Japan, **28**, 284 (1936)

ASHOK KUMAR SHARMA Department of Physics, Institute of Advanced Studies, Meerut University, Meerut-250 001, India.

Acta Chimica Academiae Scientiarum Hungaricae, Tomus 97 (4), pp. 413–428 (1978)

HETEROCYCLIC ANALOGUES OF PROSTAGLANDINS
THIAZOLES, I

G. AMBRUS, I. BARTA, GY. HORVÁTH, ZS. MÉHESFALVI and P. SOHÁR

(Research Institute for Pharmaceutical Chemistry, Budapest)

Received March 14, 1977

The synthesis of *dl*-4-(6-carboxyhexyl)-5-(3-hydroxy-1-*trans*-octenyl)thiazole and its 2-methyl analogue is described. I.r. and ^{1}H-n.m.r. data and the mass spectral behaviour of the new thiazole derivatives are discussed.

Great chemical efforts in the prostaglandin field are directed towards synthesizing compounds which have more specific biological effects and are more resistant to enzymatic inactivation than natural prostaglandins, or those which regulate the prostaglandin biosynthesis and metabolism, or modify the action of endogenous prostaglandins. The synthesis of compounds which contain some of the essential structural parts of natural prostaglandins offers a possibility for studying the structure–activity relationships and may result in finding new therapeutic agents.

In the course of a synthetic approach to heterocyclic prostaglandin analogues, we prepared several compounds in which side chains occurring in natural prostaglandins are connected to a five-membered heteroaromatic ring [1–4]. As several drugs and natural products contain a thiazole ring, we decided to synthesize first thiazoles related to prostaglandins. Of the various side chains occurring in natural prostaglandins, we have chosen the 6-carboxyhexyl and the 3-hydroxy-1-*trans*-octenyl chains. These can only be attached vicinally to a thiazole ring at the carbon atoms 4 and 5. We succeeded in synthesizing compounds with both possible arrangements of these side chains. In the present paper the synthesis and spectroscopical properties of *dl*-4-(6-carboxyhexyl)-5-(3-hydroxy-1-*trans*-octenyl) thiazole and its 2-alkyl derivatives are discussed.

According to the Hantsch synthesis of substituted thiazoles, α-halocarbonyl substances are condensed with thioamides. Employing this favourable procedure we synthesized methyl 4-(6-carbomethoxyhexyl)thiazole-5-carboxylate and its 2-methyl derivative. These compounds were transformed by methods applied previously in the prostaglandin field into *dl*-4-(6-carboxyhexyl)-5-(3-hydroxy-1-*trans*-octenyl)thiazole and its 2-methyl derivative, respectively. The reactions involved are represented in Scheme 1.

The synthesis of dimethyl 2-chloro-3-oxosebacate (**II**), used as the α-halocarbonyl reactant in the formation of the thiazole ring of intermediates **III**, started from ethyl acetoacetate. From the latter compound dimethyl 3-

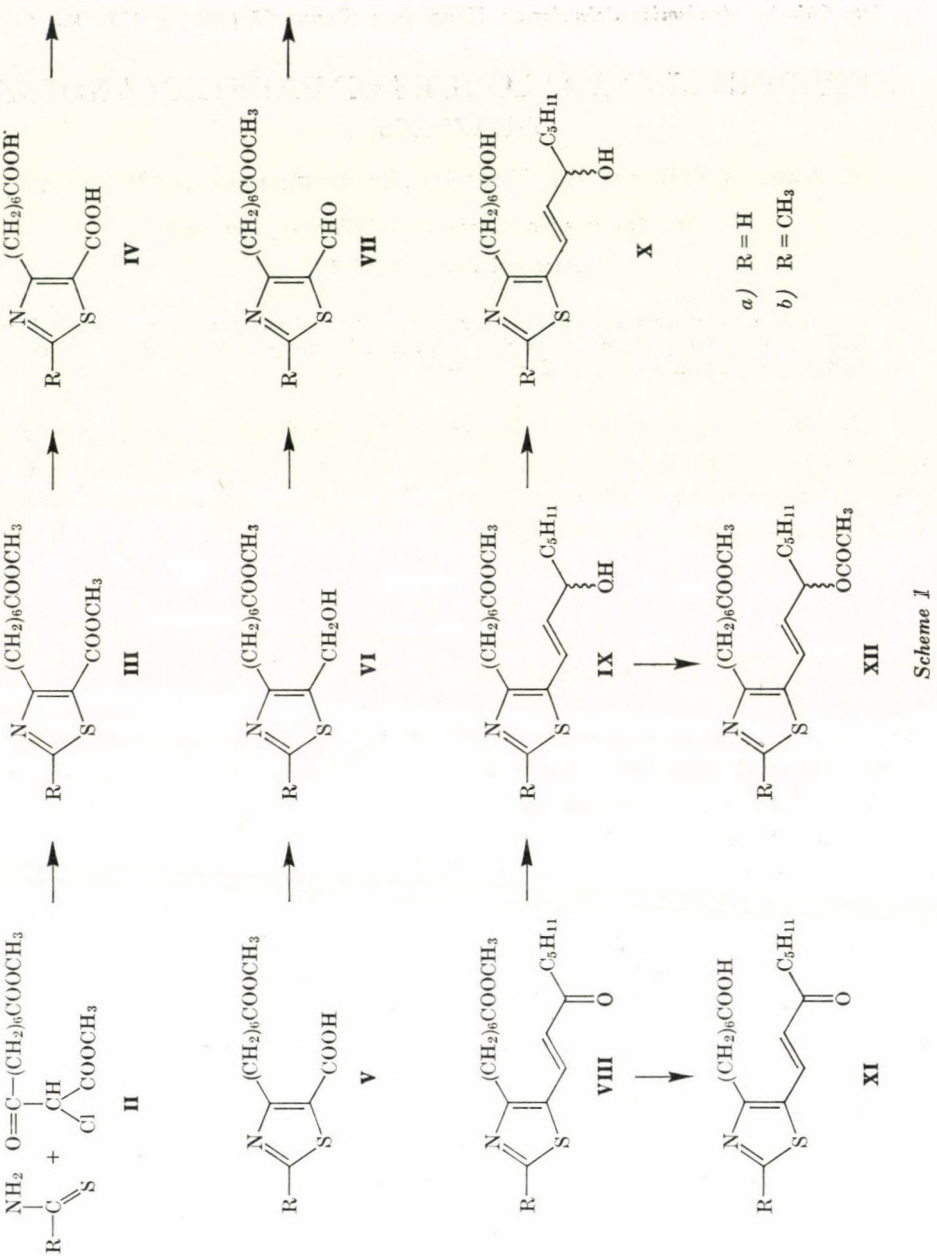

Scheme I

oxosebacate (**I**) was synthesized by using a method described by AROSENIUS *et al.* for the preparation of β-ketoesters [5]. In this synthesis ethyl sodioacetoacetate and 7-carbomethoxyheptanoyl chloride [6] were condensed in benzene to give ethyl 2-(7-carbomethoxyheptanoyl)-acetoacetate, which was treated with sodium methoxide in methanol, yielding dimethyl 3-oxosebacate, since besides the removal of the acetyl group, transesterification of the carboethoxyl group also occurred. Chlorination of dimethyl 3-oxosebacate at C-2 was effected with SO_2Cl_2 in carbon tetrachloride.

Methyl 4-(6-carbomethoxyhexyl)thiazole-5-carboxylate and its 2-methyl derivative (**IIIa, IIIb**) were readily formed when dimethyl 2-chloro-3-oxosebacate was allowed to react with 1 – 1.2 mole of thioformamide or thioacetamide, respectively, in methanol, at boiling temperature.

As regards the further reactions starting from **IIIa**, it was hydrolyzed by refluxing with ethanolic sodium hydroxide. The carboxyl group in the side chain of the resulting 4-(6-carboxyhexyl)thiazole-5-carboxylic acid (**IVa**) was selectively esterified with methanol in the presence of *p*-toluenesulfonic acid at room temperature. The 4-(6-carbomethoxyhexyl)thiazole-5-carboxylic acid (**Va**) was transformed into the acid chloride, which was reduced by sodium borohydride in dioxane affording 4-(6-carbomethoxyhexyl)-5-hydroxymethylthiazole (**VIa**). Compound **VIa** was oxidized with COLLINS reagent [7] in CH_2Cl_2 to give 4-(6-carbomethoxyhexyl)-5-formylthiazole (**VIIa**). Wittig reaction of **VIIa** with hexanoylmethylene triphenylphosphorane [8, 9] in CCl_4 afforded 4-(6-carbomethoxyhexyl)-5-(3-oxo-1-*trans*-octenyl)thiazole (**VIIIa**). This compound can also be prepared using the sodium derivative of dimethyl 2-oxoheptylphosphonate as reagent in 1,2-dimethoxyethane [10]. The oxo group in the side chain of compound **VIIIa** was reduced to hydroxyl group by sodium borohydride in aqueous isopropanol. The best procedure for the removal of the ester group of **IXa** proved to be a hydrolysis catalyzed by the lipase enzyme of *Rhizopus oryzae* [11] resulting in *dl*-4-(6-carboxyhexyl)-5-(3-hydroxy-1-*trans*-octenyl)thiazole (**Xa**). In the case of alkaline hydrolysis a partial decomposition was observed. Compound **Xb** was prepared from **IIIb** by a similar synthetic route.

In order to perform a more extensive study of the spectroscopic properties, we prepared some additional derivatives. Enzymatic hydrolysis of **VIIIa** and **VIIIb** afforded 4-(6-carboxyhexyl)-5-(3-oxo-1-*trans*-octenyl)thiazole (**XIa**) and its 2-methyl derivative (**XIb**), respectively. Acetylation of **IXa** and **IXb** with acetic anhydride in pyridine gave *dl*-4-(6-carbomethoxyhexyl)-5-(3-acetoxy-1-*trans*-octenyl)thiazole (**XIIa**) and its 2-methyl derivative (**XIIb**), respectively. The *O*-deutero analogue (**XIII**) of compound **Xa** was prepared by direct deuteration. Reduction of **VIIIa** with sodium borodeuteride in dioxane resulted in *dl*-4-(6-carbomethoxyhexyl)-5-(3-hydroxy-3-deutero-1-*trans*-octenyl)thiazole (**XIV**).

Data and assignments of the i.r. and ^{1}H-n.m.r. spectra of compounds **III**–**XII** are given in Tables I and II, respectively.

In general, these spectra furnish evidence for the presence of the appropriate structural parts in all of these molecules. Nevertheless, some spectral features deserve particular attention.

In the i.r. spectra of compounds **IV** and **V** the bands νN^+H and $\nu_{as}COO^-$ (at $\sim$ 1600 cm^{-1}) indicate that a minor part of the molecules has a zwitterionic structure under the conditions applied [12].

In the ^{1}H-n.m.r. spectra of **IIIa** and **IIIb** two separate ester-methoxy singulets appear at 3.85, 3.60 and 3.82, 3.60 ppm, respectively. The signal being at lower field can be assigned to the methoxycarbonyl group attached to the thiazole ring. In accordance with this assignment, in the monoesters **Va** and **Vb** the respective signal appears at 3.65 ppm. As shown in Table II, the signal of the methylene group attached to C-4 of the thiazole ring is shifted paramagnetically in compounds **III**, **IV**, **V** and **VII** as compared with the respective signal of compounds **VI**. This fact can be explained by the $-I$ effect of the carbonyl function in the C-5 substituents of the former compounds.

As regards the spectra of compounds containing a substituted 1-*trans*-octenyl side chain, the following comments are made. In the i.r. spectra of **VIIIa** and **VIIIb** the ketone band is split and appears at 1660 and 1685 cm^{-1}. This is assumed to be due to the presence of s-*cis* and s-*trans* conformers [13]. In the i.r. spectra of **VIII**–**XII** a strong absorption appears at about 960 cm^{-1} corresponding to the $\gamma(=CH)$ band of the *trans* olefinic hydrogens. In the ^{1}H-n.m.r. spectra of compounds **VIII** and **XI**, the olefinic hydrogens of the 1,2-disubstituted, isolated ethylene group appear as an AB multiplet with a coupling constant of 15.5 Hz, characteristic of *trans* configuration. The considerable difference between the chemical shifts of olefinic protons (7.5 and 6.3 ppm, respectively) is due to the charge distribution of enones in which the olefinic carbon being attached to the thiazole ring possesses a positive polarity, and hence the signal of the corresponding hydrogen atom is shifted downfield [14]. Accordingly, the chemical shift difference of the olefinic protons in the spectra of **IX**, **X**, and **XII** is smaller. The signal being at higher field in the spectra of these compounds is split into a double doublet in consequence of coupling with the vicinal carbinol hydrogen (J = 6 Hz).

When comparing the ^{1}H-n.m.r. data of the 2-H and 2-methylthiazole series (Table II), a systematic diamagnetic shift occurs in the signals of protons attached to carbon atoms directly coupled with the thiazole ring in the case of the 2-methyl compounds, which can be explained by the $+I$ effect of the methyl group.

The mass spectral behaviour of some heterocyclic prostaglandin analogues has been studied in detail previously [15]. The mass spectral data of the compounds discussed are given in Table III.

Table I

I.r. data of compounds **IIIa,b – XIIa,b** (cm^{-1})

Compound	νOH band	νN⁺H band	ν(=CH) band (sharp)	νC = O band			Group vibrations of νC=N and νC=C character of the thiazole ring and the conjugated double bond in the side chain			γ(=CH) band
				ester	carboxylic acid	other				
IIIa	–	–	–	1740x■ 1715*■	–	–	1520	1435		–
IIIb	–	–	–	1735x 1720*	–	–	1525	1435		–
IVa	~3320□xo ~2400□*o	~1850	3080	–	1720x 1700*	–	1525	1435		–
IVb	3300 – 2200*xo	~1830	–	–	1685x*	–	1530	1435		–
Va	~2480*o	~1850	3090	1730x	1705*	–	1525	1440		–
Vb	~2450*o	~1840	–	1735x	1695*	–	1540	1435		–
VIa	3600 – 3000*●	–	–	1735x	–	–	1540	1440		–
VIb	3600 – 3000*●	–	–	1735x	–	–	1545	1435		–
VIIa	–	–	3090	1730x	–	1660*▽	1515	1440		–
VIIb	–	–	–	1730x	–	1660*▽	1520	1435		–
VIIIa	–	–	–	1735x	–	1685*▼ 1660*▼	1595	1505	1435	970
VIIIb	–	–	–	1735x	–	1685*▼ 1660*▼	1592	1515	1435	965
IXa	3600 – 3000*●	–	–	1735x	–	–	1640+	1510	1435	955
IXb	3600 – 3000*●	–	–	1740x	–	–	1640	1530	1440	955
Xa	3500 – 2300x*o●	–	–	–	1710x	–	1635+	1510	1410	955
Xb	3500 – 2300x*o●	–	–	–	1710x	–	1640+	1525	1435	955
XIa	~2600□xo	1850+	3095	–	1713x	1690*▼	1590	1510	1400	985
XIb	3500 – 2400xo	–	–	–	1720x	1685*▼	1590	1510	1435	970
XIIa	–	–	–	1735x*	–	–	1642+	1510	1435	955
XIIb	–	–	–	1735x*	–	–	1640	1520	1435	950

x in the side chain attached to C-4 of the thiazole ring
* in the side chain or in the substituent attached to C-5 of the thiazole ring
o carboxylic acid
● alcohol
▽ aldehyde
▼ ketone
□ maximum of a diffuse absorption
■ overlapping band
+ very weak band

Table II

^1H-n.m.r. data of compounds **IIIa,b – XIIa,b** ($\delta_{TMS} = 0 ppm$)

Compound	δCH_3^* *t* (3H)	δCH_3 (at C-2 of ring) *s* (3H)	δOCH_3 *s* (3H)	$\delta COCH_2$ *t* (2H)	$\delta C_{Ar}CH_2^{*x}$ *t* (2H)	δH-2 (in ring) *s* (1H)	$\delta CH(OR)^*$ (R=H or Ac) *m* (1H)	$\delta(=CH)^{*\triangle}$ (1H)	$\delta C_{Ar}(=CH)^*$ (1H)	δOH *s* (broad)	Other signals
IIIa	–	–	3.60[x] 3.85*	2.25[x]	3.15	8.70	–	–	–	–	
IIIb	–	2.65	3.60[x] 3.82*	2.25[x]	3.05	–	–	–	–	–	
IVa	–	–	–	2.25[x]	3.20	8.85	–	–	–	~8.65° (2H)	
IVb	–	2.65	–	2.25[x]	3.08	–	–	–	–	~9.0° (2H)	
Va	–	–	3.65[x]	2.30[x]	3.25	9.00	–	–	–	11.45° (1H)	
Vb	–	2.75	3.65[x]	2.25[x]	3.20	–	–	–	–	11.45° (1H)	
VIa	–	–	3.60[x]	2.22[x]	2.65	8.50	–	–	–	4.35● (1H)	4.72▽
VIb	–	2.60+	3.62[x]	2.25[x]	2.60+	–	–	–	–	~4.2● (1H)	4.62▽
VIIa	–	–	3.65[x]	2.35[x]	3.20	9.05	–	–	–	–	10.20▼
VIIb	–	2.70	3.60[x]	2.25[x]	3.00	–	–	–	–	–	10.05▼
VIIIa	0.90	–	3.55[x]	2.20[x] 2.50*	2.85	8.55	–	6.30▲	7.54▲	–	
VIIIb	0.95	2.63+	3.60[x]	2.25[x] 2.50*+	2.78	–	–	6.22▲	7.52▲	–	
IXa	0.90	–	3.60[x]	2.25[x]	2.75	8.50	4.20	5.97□	6.67■	3.1● (1H)	
IXb	0.90	2.58+	3.55[x]	2.22[x]	2.60+	–	4.16	5.70□	6.50■	3.0● (1H)	

Xa	0.87	–	–	2.28[x]	2.75	8.55	4.22	5.90□	6.65■ +	6.65°● + (2H)	
Xb	0.90	2.62+	–	2.28[x]	2.66+	–	4.20	5.78□	6.55■	7.15°● (2H)	
XIa	0.88	–	–	2.32[x] 2.65*	2.90	8.80	–	6.52▲	7.72▲	10.9° (1H)	
XIb	0.90	2.65+	–	2.25[x] 2.45*	2.75+	–	–	6.18▲	7.45▲	10.4° (1H)	
XIIa	0.90	–	3.60[x]	2.25[x]	2.75	8.45	5.35	5.76□	6.70■	–	2.00⌀
XIIb	0.90	2.60+	3.60[x]	2.30[x]	2.65+	–	5.30	5.60□	6.55■	–	2.05⌀

[x] in the side chain attached to C-4 of the thiazole ring
* in the side chain or in the substituent attached to C-5 of the thiazole ring
△ vicinal to the ketone or to the carbinol group

° carboxylic acid
● alcohol
▽ $CH_2(OH)$*, *s* (2H)
▼ CH (aldehyde)*, *s* (1H)
⌀ $COCH_3$, *s* (3H)
▲ *d* (AB multiplet), $J = 15.5$ Hz
□ 2x*d* (AMX multiplet), $J = 6$ and 15.5 Hz

■ *d* (AMX multiplet), $J = 15.5$ Hz
+ overlapping signals
s singulet
d doublet
t triplet
m multiplet

H-rearrangement
[M]+·
M1
M2
[1,2] H-shift
a
b
c
d
e
f
g
Scheme 2

The mass spectral fragmentation of compounds **IXa, IXb, Xa** and **Xb**, shown in Scheme 2, is governed by two main types of process: one being initiated by the interaction of the COOQ group with the hydroxyl group in the octenyl side chain, which yields the rearranged molecular ion M_1; the other resulting from the interaction of the thiazole ring with the carboxy- (or carbalkoxy)

Table III

Selected mass spectral data of compounds discussed in Schemes 2 to 4

Compound	Data*	M+•	Ion symbols								Other ions
			a	*b*	*c*	*d*	*e*	*f*	*g*	*h*	
IXa	*m/e*	353	282	250	254	222	280	238	225	324	322
	R.I.	26	14	11	100	15	5	8	3	4	8
IXb	*m/e*	367	296	264	268	236	294	252	239	338	336
	R.I.	33	34	17	100	10	14	17	12	3	15
Xa	*m/e*	339	268	250	240	222	280	238	225	310	321
	R.I.	22	20	32	100	38	20	23	12	3	7
Xb	*m/e*	353	282	264	254	236	294	252	239	324	335
	R.I	38	43	57	100	24	37	28	38	3	15
XIV	*m/e*	354	283	251	255	223	281	239	226	324	323
	R.I.	21	23	17	100	16	6	10	4	7	10
		M+•	*e'*	*f'*	*g'*	*i*	*j*	*k*	*l*	Other ions	
VIIIa	*m/e*	351	278	236	223	295	280	252	208	320	222
	R.I.	100	16	32	12	28	53	60	48	25	20
VIIIb	*m/e*	365	292	250	237	309	294	266	222	334	236
	R.I.	81	18	32	17	19	67	59	100	27	22
XIa	*m/e*	337	278	236	223	281	266	238	208		
	R.I.	39	21	27	23	50	90	67	100		
XIb	*m/e*	351	292	250	237	295	280	252	222		
	R.I.	75	9	15	12	16	58	34	100		

* R.I. = relative intensities in per cent

hexyl side chain. The separated radical site in ion M_1 can cause the cleavage of the adjacent bond, leading to the formation of ion *a* which can lose QOH to give ion *b***. On the other hand, it may interact with the adjacent π-electron system whereby the rearranged molecular ion M_2 is formed. A [1,2]-hydrogen migration can occur in ion M_2, followed by the loss of the $^{\cdot}COC_5H_{11}$ radical, yielding ion *c*, which gives rise to the base peak in all these spectra. Ion *c* can lose QOH to give ion *d* which can also be formed from ion *b* by the loss of CO [16]. The prominent ions *e*, *f* and *g* arise from the interaction of the thiazole ring with the carboxyhexyl side chain. The formation of both ions *e* and *f* can be rationalized as being a synchronous cyclization and bond fission effected by the nitrogen atom of the thiazole ring.

** In the spectrum of the *O*-deutero compound **XIII** only D_2O is lost in this process, supporting the mechanism proposed for the formation of ion M_1.

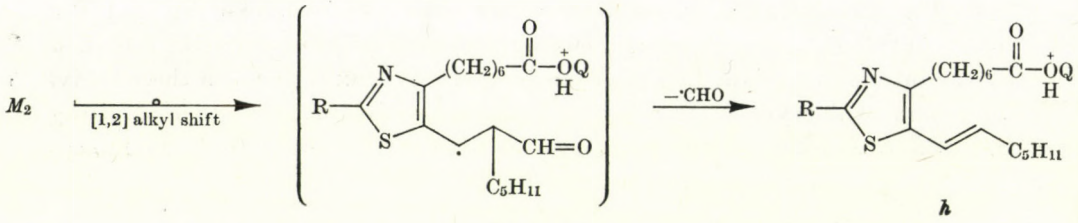

Scheme 3

An interesting mass spectral process was observed in the case of compounds **IXa**, **IXb**, **Xa** and **Xb**, which results in the loss of ·CHO radical from their molecular ions. The mechanism proposed for this process is depicted in Scheme 3. The formation of ion *h* is assumed to start with a [1,2]-alkyl migration in the rearranged molecular ion M_2. Provable [1,2]-alkyl shifts have seldom been observed in radical cations [17] and they were stated not at all to occur in simple radicals [18]. Our assumption is based on the following evidence: (i) according to high resolution mass measurements ion *h* of compounds **IXa** and **Xa** possesses elemental compositions $C_{18}H_{30}NO_2S$ (2.1 ppm)* and $C_{17}H_{28}NO_2S$ (2 ppm), respectively, indicating the loss of CHO from the molecular ions; (ii) in the case of compound **XIV**, the *C*-deutero analogue of **IXa**, a complete loss of the deuterium label occurs in this process. The high rate of formation of ion M_2, reflected in the high abundance of ion *c*, is also of importance in making possible the observation of ion *h* which, of course, is much less abundant (Table III).

The mechanisms proposed for the prominent fragmentation processes of compounds **VIIIa**, **VIIIb**, **XIa** and **XIb** are depicted in Scheme 4. A McLafferty rearrangement leads to the formation of ion *i*. The loss of $^{\cdot}C_5H_{11}$ radical from the molecular ions involves partly a direct cleavage at the carbonyl group, yielding ion *j*. It can also proceed, however, in part after a cyclization step. Analysis of the mass spectral data obtained for the process $[M]^{+\cdot} \rightarrow k$ has revealed that this involves a ring closure as shown in Scheme 4. Ion *k* can also be formed from ion *j* by elimination of CO. One of the most abundant ions in the spectra of **VIIIa**, **VIIIb**, **XIa** and **XIb** is formed by the loss of the carboxyhexyl side chain. We assume this process to involve a mesomeric structure of the molecular ion, shown in Scheme 4, which can preferably exist in these thiazoles. In this intermediate state a radical attack at C-4 can take place, leading to the formation of ion *l*. Similarly to the corresponding hydroxy derivatives, ions arising from the interaction of the thiazole ring with the carboxyhexyl side chain also occur in the spectra of **VIIIa**, **VIIIb**, **XIa** and **XIb** (these are denoted with a prime in Table III).

* To resolve the $H_2{}^{32}S/{}^{34}S$ doublet, a resolution of 16,500 was applied.

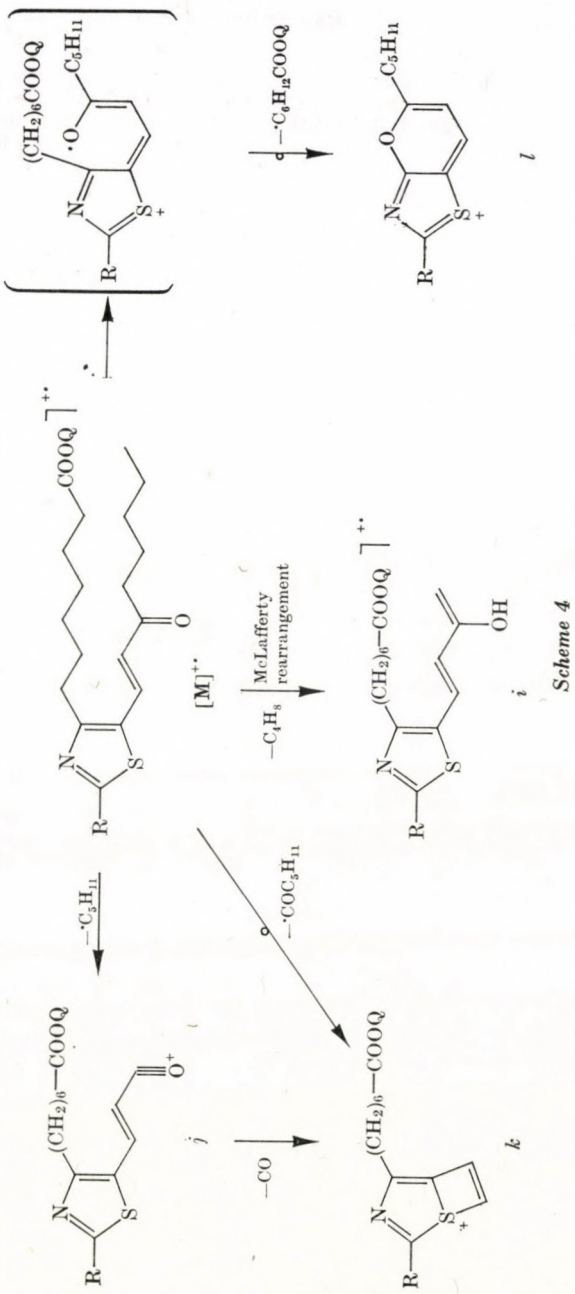
(CH2)6COOQ
C5H11
R
-·C6H12COOQ
l
COOQ
[M]+·
-C4H8
McLafferty rearrangement
(CH2)6—COOQ
OH
i
-·C5H11
-·COC5H11
(CH2)6—COOQ
j
-CO
(CH2)6—COOQ
k

Scheme 4

Experimental

M.p.'s were measured with a Kofler hot stage apparatus. I.r. spectra were taken with a Perkin Elmer 475 instrument in liquid films (**IIIa,b**, **VIa,b**, **VIIb**, **VIIIa,b**, **IXa,b**, **Xa,b**, **XIb**, and **XIIa,b**) and in KBr pellets (**IVa,b**, **Va,b**, **VIIa** and **XIa**). ^{1}H-n.m.r. spectra were recorded on a JEOL C-60 HL spectrometer. The following solvents were used: CCl_4 for compounds **IIIa,b**, **VIa,b**, **VIIb**, **VIIIa,b**, **IXa,b**, and **XIb**; $CDCl_3$ for compounds **Va,b**, **VIIa**, **Xa,b**, **XIIa,b**, **XIa**; DMSO-d_6 for compounds **IVa,b**. Mass spectra were taken on a Varian MAT SM-1 instrument.

In preparative thin-layer chromatography a 2 : 1 mixture of Kieselgel G, Typ 60 (Merck) and Kieselgel $HF_{254-366}$, Typ 60 (Merck) was used as the adsorbent.

In enzymatic hydrolyses we applied a lipase enzyme (purity: 40 units), which was prepared from the fermentation beer of *Rhizopus oryzae* (MNG 135) by using the method of SZABÓ *et al.* [19].

Dimethyl 3-oxosebacate (I)

To a stirred solution of ethyl acetoacetate (13 g) in dry benzene (170 ml) sodium (2.3 g) was added in small portions. After stirring for 4 hrs 7-carbomethoxyheptanoyl chloride (20.6 g) was added dropwise to the suspension, which was then refluxed for 15 min. The mixture was allowed to cool to ambient temperature and poured into ice and excess 10 % sulfuric acid. The aqueous phase was separated. The benzene phase was washed with water, dried over anhydrous sodium sulfate and evaporated *in vacuo* to give a residue containing ethyl 2-(7-carbomethoxyheptanoyl)acetoacetate. A solution of sodium (2.3 g) in anhydrous methanol (65 ml) was added to this residue and the mixture was allowed to stand at ambient temperature for 16 hrs, and then poured into ice and excess 10 % sulfuric acid. The resulting mixture was extracted with ether. The ether extract was washed with water, dried over anhydrous Na_2SO_4 and evaporated *in vacuo*. The residue was distilled under reduced pressure to give **I** (14.9 g; b.p. 160 °C/0.4 mm).
I.r. (film); νC=O 1732 cm^{-1}.
^{1}H-n.m.r., (CCl_4): δOCH_3 3.70 (3H, s), 3.62 (3H, s), $\delta COCH_2$ 3.35 (2H, s), 2.6 – 2.0 (4H, m) ppm.

Dimethyl 2-chloro-3-oxosebacate (II)

To a stirred solution of **I** (14.6 g) in carbon tetrachloride (15 ml) cooled to – 5 °C was added dropwise a solution of sulfuryl chloride (8 g) in carbon tetrachloride (12 ml). The mixture was stirred for 1 hr at ambient temperature, then for 30 min at 40 °C. After cooling to ambient temperature the solution was diluted with carbon tetrachloride, washed with water, then with 5 % sodium carbonate and with water again; after drying over anhydrous Na_2SO_4 it was evaporated *in vacuo*. The residue was distilled under reduced pressure to give **II** (11.4 g; b.p. 155°C/0.3 mm).
I.r. (film): νC=O 1735 cm^{-1}.
^{1}H-n.m.r. (CCl_4): δCH(Cl) 4.70 (1H, s), δOCH_3 3.8 (3H, s), 3.6 (3H, s), $\delta COCH_2$ 2.68 (2H, t), 2.25 (2H, t) ppm.

Methyl 4-(6-carbomethoxyhexyl)thiazole-5-carboxylate (IIIa)

Compound **II** (10.9 g) and thioformamide(2.9 g) were refluxed in methanol (60 ml) for 1 hr; the solvent was then evaporated *in vacuo*. The residue was taken up in water. The mixture was neutralized with 5 % Na_2CO_3 solution and thoroughly extracted with ether. The ether extract was dried over anhydrous Na_2SO_4 and evaporated *in vacuo* to leave a residue (10.3 g) containing the crude **IIIa**. An analytical sample of **IIIa** (oil) was obtained by preparative TLC (solvent: ethyl acetate–*n*-heptane, 6 : 4).

Methyl 2-methyl-4-(6-carbomethoxyhexyl)thiazole-5-carboxylate (IIIb)

A crude product of **IIIb** (9.8 g) was similarly obtained from **II** (10.9 g) and thioacetamide (3.23 g), as described for **IIIa**. An analytical sample of **IIIb** (oil) was prepared by preparative TLC using the same solvent mixture as applied in the purification of **IIIa**.

4-(6-Carboxyhexyl)thiazole-5-carboxylic acid (IVa)

Crude **IIIa** (10 g), obtained as an oily residue in the former reaction, was dissolved in ethanol (30 ml) and refluxed with 10% aqueous NaOH solution (50 ml) for 30 min. After cooling in ice-water, the mixture was acidified with dilute H_2SO_4, and then thoroughly extracted with ethyl acetate. The ethyl acetate extract was washed with water, dried over anhydrous Na_2SO_4 and evaporated *in vacuo*. The residue was recrystallized from acetone to give **IVa** (5.9 g; m.p. 151 – 153 °C).

2-Methyl-4-(6-carboxyhexyl)thiazole-5-carboxylic acid (IVb)

Crude **IIIb** (9.5 g), obtained as an oily residue in the former reaction, was similarly hydrolyzed as described in the preparation of **IVa** to give, after recrystallization from acetone, **IVb** (6.2 g; m.p. 147 – 149 °C).

4-(6-Carbomethoxyhexyl)thiazole-5-carboxylic acid (Va)

A solution of **IVa** (5.8 g) and *p*-toluenesulfonic acid monohydrate (6.4 g) in methanol (250 ml) was stirred at ambient temperature for 3 hrs, then diluted with water (650 ml). The resulting solution was saturated with ammonium sulfate and extracted with ethyl acetate (three 250-ml portions). The organic extracts were combined, washed with water, dried over anhydrous Na_2SO_4 and evaporated *in vacuo*. The residue was recrystallized from ether–*n*-hexane to give **Va** (4.95 g; m.p. 113 – 114 °C).

2-Methyl-4-(6-carbomethoxyhexyl)thiazole-5-carboxylic acid (Vb)

Compound **IVb** (5.8 g) was similarly esterified as described in the preparation of **Va** to give **Vb** (4.9 g; m.p. 106 – 107 °C) after recrystallization from ether–*n*-hexane.

4-(6-Carbomethoxyhexyl)-5-hydroxymethylthiazole (VIa)

Oxalyl chloride (5 ml) was added dropwise to a solution of **Va** (4.7 g) in dry benzene (60 ml). The resulting mixture was allowed to stand at ambient temperature for 16 hrs, then benzene and the excess of oxalyl chloride were evaporated *in vacuo*. The residue containing 4-(6-carbomethoxyhexyl)thiazole-5-carboxylic acid chloride was dissolved in anhydrous dioxane (12 ml). This solution was added to a stirred suspension of sodium borohydride (1.3 g) in anhydrous dioxane (24 ml). The mixture was stirred at ambient temperature for 30 min, then for additional 30 min at 80 °C. After cooling in ice-water, water (40 ml) was added dropwise. The aqueous mixture was stirred at ambient temperature for 2 hrs, and then extracted with ethyl acetate. The ethyl acetate extract was washed with water, dried over anhydrous Na_2SO_4 and evaporated *in vacuo* to give a residue (3.85 g) containing impure **VIa**. An analytical sample of **VIa** (oil) was obtained by preparative TLC (solvent: ethyl acetate–*n*-heptane, 7 : 3).

2-Methyl-4-(6-carbomethoxyhexyl)-5-hydroxymethylthiazole (VIb)

Transformation of **Vb** (4.8 g) by the method described in the preparation of **VIa** gave an oily residue (3.55 g) containing impure **VIb**. An analytical sample of **VIb** (oil) was obtained by preparative TLC using the solvent applied in the purification of **VIa**.

4-(6-Carbomethoxyhexyl)-5-formylthiazole (VIIa)

To a stirred solution of chromium trioxide dipyridine complex (22.3 g) prepared according to COLLINS *et al.* [7] in dichloromethane (460 ml), was added dropwise a solution of crude **VIa** (3.7 g) in dichloromethane (40 ml). The mixture was stirred at ambient temperature for 30 min and then filtered. The filtrate was evaporated *in vacuo*. The residue was chromatographed by preparative TLC (solvent: ethyl acetate–*n*-heptane, 1 : 1) to give homogeneous **VIIa** (2.45 g). An analytical sample of **VIIa** (m.p. 60 – 62 °C) was obtained by recrystallization from ether.

2-Methyl-4-(6-carbomethoxyhexyl)-5-formylthiazole (VIIb)

Oxidation of crude **VIb** (3.4 g), carried out by the method described in the preparation of **VIIa**, resulted in an impure **VIIb**, which was chromatographed by preparative TLC using the solvent applied in the purification of **VIIa** to give homogeneous **VIIb** (2.4 g, oil).

4-(6-Carbomethoxyhexyl)-5-(3-oxo-1-*trans*-octenyl)thiazole (VIIIa)

A solution of **VIIa** (2.3g) and hexanoylmethylene triphenylphosphorane (6.75 g) in carbon tetrachloride (15 ml) was stirred under nitrogen at ambient temperature for 16 hrs and then evaporated *in vacuo*. The residue was chromatographed on silicic acid (120 g) eluting with 250 ml each of 5, 10, 15, 20, 25 and 30 % ethyl acetate–*n*-heptane, collecting 50 ml fractions. From the 25 % ethyl acetate–*n*-heptane fractions pure **VIIIa** (2.5 g, oil) was obtained.

2-Methyl-4-(6-carbomethoxyhexyl)-5-(3-oxo-1-*trans*-octenyl)thiazole (VIIIb)

A solution of dimethyl 2-oxoheptylphosphonate (5.57 g) in 1,2-dimethoxyethane (25 ml) was added to a stirred suspension of sodium hydride (0.6 g) in anhydrous 1,2-dimethoxyethane (8 ml) cooled to −15 °C. After stirring for 1 hr at −15 °C, the temperature of the mixture was raised to 0 °C and a solution of **VIIb** (2.25 g) in 1,2-dimethoxyethane (25 ml) was added dropwise. The resulting mixture was stirred for 1 hr at 0 °C and for 4 hrs at ambient temperature and then, after cooling in ice-water, it was diluted with water (75 ml). The aqueous solution was exhaustively extracted with ether. The ether extract was dried over anhydrous Na_2SO_4 and evaporated *in vacuo*. The residue was purified by preparative TLC (solvent: ethyl acetate–*n*-heptane, 4 : 6) to give pure **VIIIb** (1.9 g, oil).

***dl*-4-(6-Carbomethoxyhexyl)-5-(3-hydroxy-1-*trans*-octenyl)thiazole (IXa)**

A solution of **VIIIa** (1.6 g) in isopropanol (25 ml) was prepared and sodium borohydride (107 mg) in water (25 ml) was added. After stirring at ambient temperature for 2 hrs, the solution was diluted with water and extracted exhaustively with ethyl acetate. The ethyl acetate extract was washed with water, dried over anhydrous Na_2SO_4 and evaporated *in vacuo*. The residue was chromatographed on silicic acid (80 g) with 200 ml each of 5, 10, 15, 20, 25, 30 and 35 % ethyl acetate–*n*-heptane, collecting 25 ml fractions. From the 30 % ethyl acetate–*n*-heptane fractions pure **IXa** (1.25 g, oil) was obtained.

***dl*-2-Methyl-4-(6-carbomethoxyhexyl)-5-(3-hydroxy-1-*trans*-octenyl)thiazole (IXb)**

Compound **VIIIb** (1.0 g) was reduced as described in the preparation of **IXa**. The crude product was chromatographed by preparative TLC (solvent: ethyl acetate–*n*-heptane, 1 : 1) to give pure **IXb** (0.76 g, oil).

***dl*-4-(6-Carboxyhexyl)-5-(3-hydroxy-1-*trans*-octenyl)thiazole (Xa)**

To a suspension of **IXa** (0.8 g) in 0.2*M* phosphate buffer of pH 7.5 (40 ml) were added *Rhizopus oryzae* lipase (0.2 g), sodium taurocholate (20 mg) and gum arabic (0.4 g) in water (10 ml). The mixture was shaken at 28 °C on a rotary shaker for 16 hrs, then diluted with water (50 ml), acidified with citric acid and extracted exhaustively with ethyl acetate. The ethyl acetate extract was dried over anhydrous Na_2SO_4 and evaporated *in vacuo*. The residue was chromatographed on silicic acid (40 g) with 100 ml each of 10, 20, 30, 40, 50, 60, 70 and 80 % ethyl acetate–*n*-heptane, collecting 20-ml fractions. The residue obtained on evaporation of the 70 % ethyl acetate–*n*-heptane fractions was recrystallized from ether–*n*-hexane to give pure **Xa** (0.6 g; m.p. 73 – 74 °C).

***dl*-2-Methyl-4-(6-carboxyhexyl)-5-(3-hydroxy-1-*trans*-octenyl)thiazole (Xb)**

Compound **IXb** (0.4 g) was hydrolyzed by the method applied in the preparation of **Xa**. The crude product was purified by preparative TLC (solvent: upper phase of the following mixture: ethyl acetate–*n*-heptane–water–acetic acid, 11 : 5 : 10 : 2) to give pure **Xb** (0.28 g, oil).

4-(6-Carboxyhexyl)-5-(3-oxo-1-*trans*-octenyl)thiazole (XIa)

Compound **VIIIa** (0.8 g) was hydrolyzed by the method described in the preparation of **Xa**. The crude product was chromatographed on silicic acid (50 g) with 100 ml each of 10, 20, 30, 40, 50, 60, 70 and 80 % ethyl acetate–*n*-heptane, collecting 20-ml fractions. The residue obtained by evaporation of the 60 % ethyl acetate–*n*-heptane fractions was recrystallized from acetone to give pure **XIa** (0.54 g; m.p. 67 – 68 °C).

2-Methyl-4-(6-carboxyhexyl)-5-(3-oxo-1-*trans*-octenyl)thiazole (XIb)

Compound **VIIIb** (0.75 g) was hydrolyzed by the method described in the preparation of **Xa**. The crude product was purified by preparative TLC, using the solvent applied in the purification of **Xb**, to give pure **XIb** (0.51 g, oil).

dl-4-(6-Carbomethoxyhexyl)-5-(3-acetoxy-1-*trans*-octenyl)thiazole (XIIa)

A solution of **IXa** (350 mg) in anhydrous pyridine (4 ml) was mixed with acetic anhydride (1 ml). The resulting solution was allowed to stand for 24 hrs at ambient temperature, then diluted with water (50 ml) and thoroughly extracted with ethyl acetate. The ethyl acetate extract was dried over anhydrous Na_2SO_4 and evaporated *in vacuo*. The residue was chromatographed by preparative TLC (solvent: ethyl acetate–*n*-heptane, 4 : 6) to give pure **XIIa** (280 mg, oil).

dl-2-Methyl-4-(6-carbomethoxyhexyl)-5-(3-acetoxy-1-*trans*-octenyl)thiazole (XIIb)

Compound **IXb** (350 mg) was acetylated by the method described in the preparation of **XIIa**. The crude product was chromatographed by preparative TLC using the solvent applied in the purification of **XIIa** to give **XIIb** (285 mg, oil).

O-Deuteration of compound Xa

Compound **Xa** (2 mg) was dissolved in a mixture of CH_3OD (1 ml) and D_2O (0.5 ml). The solution was kept for 48 hrs at room temperature. The *O*-dideutero analogue **XIII** was obtained on evaporation of the solvent. To reduce back-exchange, D_2O was introduced with the sample of **XIII** into the mass spectrometer.

dl-4-(6-Carbomethoxyhexyl)-5-(3-hydroxy-3-deutero-1-*trans*-octenyl)thiazole (XIV)

A solution of **VIIIa** (70 mg) and sodium borodeuteride (4.2 mg) in dioxane (5 ml) was stirred at ambient temperature for 2 hrs, then diluted with water (30 ml) and thoroughly extracted with ethyl acetate. The organic extract was washed with water, dried over anhydrous Na_2SO_4 and evaporated *in vacuo*. The residue was purified by preparative TLC (solvent: ethyl acetate–*n*-heptane, 4 : 6) to give homogeneous **XIV** (32 mg, oil).

*

The authors are indebted to E. Mező and É. Ilkőy for technical assistance.

REFERENCES

[1] Ambrus, G., Barta, I., Méhesfalvi, Zs., Horváth, Gy.: Hung. Pat. 169,072 (May 14, 1974)
[2] Ambrus, G., Barta, I., Cseh, G., Tolnay, P., Méhesfalvi, Zs.: Hung. Pat. 169,320 (Oct. 28, 1974)
[3] Ambrus, G., Barta, I.: International Conference on Prostaglandins, Florence, May 26—30, 1975. Abstracts book, p. 66.
[4] Ambrus, G., Barta, I.: Prostaglandins **10**, 661 (1975)
[5] Arosenius, K. E., Ställberg, G., Stenhagen, E., Tägström-Eketorp, B.: Arkiv Kemi, Mineral Geol. **26A** (19), 1 (1948)

[6] RAPOPORT, H., VOLCHECK, E. J.: J. Am. Chem. Soc. **78,** 2451 (1956)
[7] COLLINS, J. C., HESS, W. W., FRANK, F. J.: Tetrahedron Letters **1968,** 3363
[8] BEAL III, P. F., LINCOLN, F. H., BABCOCK, J. C.: U. S. Pat. 3,505,387 (Apr. 11, 1966)
[9] CATON, M. P. L., COFFEE, E. C. J., WATKINS, G. L.: Tetrahedron Letters **1972,** 773
[10] COREY, E. J., VLATTAS, I., ANDERSEN, N. H., HARDING, K.: J. Am. Chem. Soc. **90,** 3247 (1968)
[11] SIH, C. J., HEATHER, J. B., PERUZZOTTI, G. P., PRICE, P., SOOD, R., LEE, L. F. H.: J. Am. Chem. Soc. **95,** 1676 (1973)
[12] HOLLY, S., SOHÁR, P.: Infrared Spectroscopy (In Hungarian), p. 79. Műszaki Kiadó, Budapest, 1968
[13] COREY, E. J., BECKER, K. B., VARMA, R. K.: J. Am. Chem. Soc. **94,** 8616 (1972)
[14] SOHÁR, P.: Nuclear Magnetic Resonance Spectroscopy (In Hungarian), Vol. 1, p. 215. Akadémiai Kiadó, Budapest, 1976
[15] HORVÁTH, GY., AMBRUS, G.: in Advances in Mass Spectrometry in Biochemistry and Medicine (Frigerio, A., ed.), Vol. II. Spectrum Publications, New York 1976
[16] For a discussion of similar processes, see: HORVÁTH, GY.: Biomed. Mass Spectrom. **2,** 190 (1975)
[17] BROWN, P., DJERASSI, C.: Angew. Chem. **79,** 481 (1967)
[18] *Cf.:* WILT, J. W.: in Free Radicals (Kochi, J. K., ed.) Vol. 1, pp. 340—344. Wiley, New York 1973
[19] SZABÓ, I. K., CSEH, GY., KELEMEN, Á., SZÉLL, V., HORVÁTH, I., RICHTER, J., TÖLGYESI, L., MONOSTORI, L.: Hung. Pat. 160,109 (June 3, 1970)

Gábor AMBRUS
István BARTA
Gyula HORVÁTH
Zsuzsa MÉHESFALVI
Pál SOHÁR

H-1045 Budapest, Szabadságharcosok útja 47—49.

Acta Chimica Academiae Scientiarum Hungaricae, Tomus 97 (4), pp. 429—438 (1978)

SYNTHESIS OF VINCA ALKALOIDS AND RELATED COMPOUNDS, V*

SYNTHESIS OF ETHYL (±)-APOVINCAMINATE

GY. KALAUS, P. GYŐRY, L. SZABÓ and CS. SZÁNTAY

(Institute of Organic Chemistry, Technical University, and Central Research Institute for Chemistry, Hungarian Academy of Sciences, Budapest)

Received March 21, 1977

Starting from tryptamine, a four-step synthesis resulted in the enamine of structure **7a**. On addition of ethyl α-acetoxyacrylate to this enamine, the derivative **8a** was obtained whose reduction gave two stereoisomeric products (**9** and **10**), their ratio being dependent on the reaction conditions. The racemic ethyl apovincaminate (**1**) can be obtained by oxidation of the derivative **9b**, followed by dehydration.

The dextrorotatory enantiomer of ethyl apovincaminate (**1**) is commercially available under the name Cavinton, an excellent vasodilator drug.

It was earlier prepared from natural vincamine by hydrolysis to vincaminic acid (**2a**) followed by dehydration and esterification of the resulting apovincaminic acid with ethanol [2].

We intended to carry out the preparation of Cavinton (**1**) on the analogy of our earlier vincamine synthesis [3].

The enamine of structure **7a** was used again as the key intermediate; the possibility of preparing this compound in a way differing from the earlier synthesis was also investigated.

Synthesis of the enamine 7a

The reaction of tryptamine and butyric acid gave first the salt **3a** from which the acid amide **3b** was formed on heating. On cyclizing **3b** with phosphoryl chloride in benzene and liberating the base, the β-carboline derivative **4** was obtained.

We desired to build up the fourth ring similarly to the reaction carried out by ATTA-UR-RAHMAN [4], with 1-methyl-3,4-dihydro-7-methoxy-β-carboline. Therefore compound **4** was allowed to react with methyl acrylate. The reaction was carried out in a mixture of benzene and methanol under the exclusion of light and atmospheric oxygen. The ketone of structure **5** precipitated from the reaction mixture in a poor yield (12.5%), and on acidifying the mother liquor with perchloric acid, the quaternary salt **6b** could be isolated.

* For Part IV, see Ref. [1]

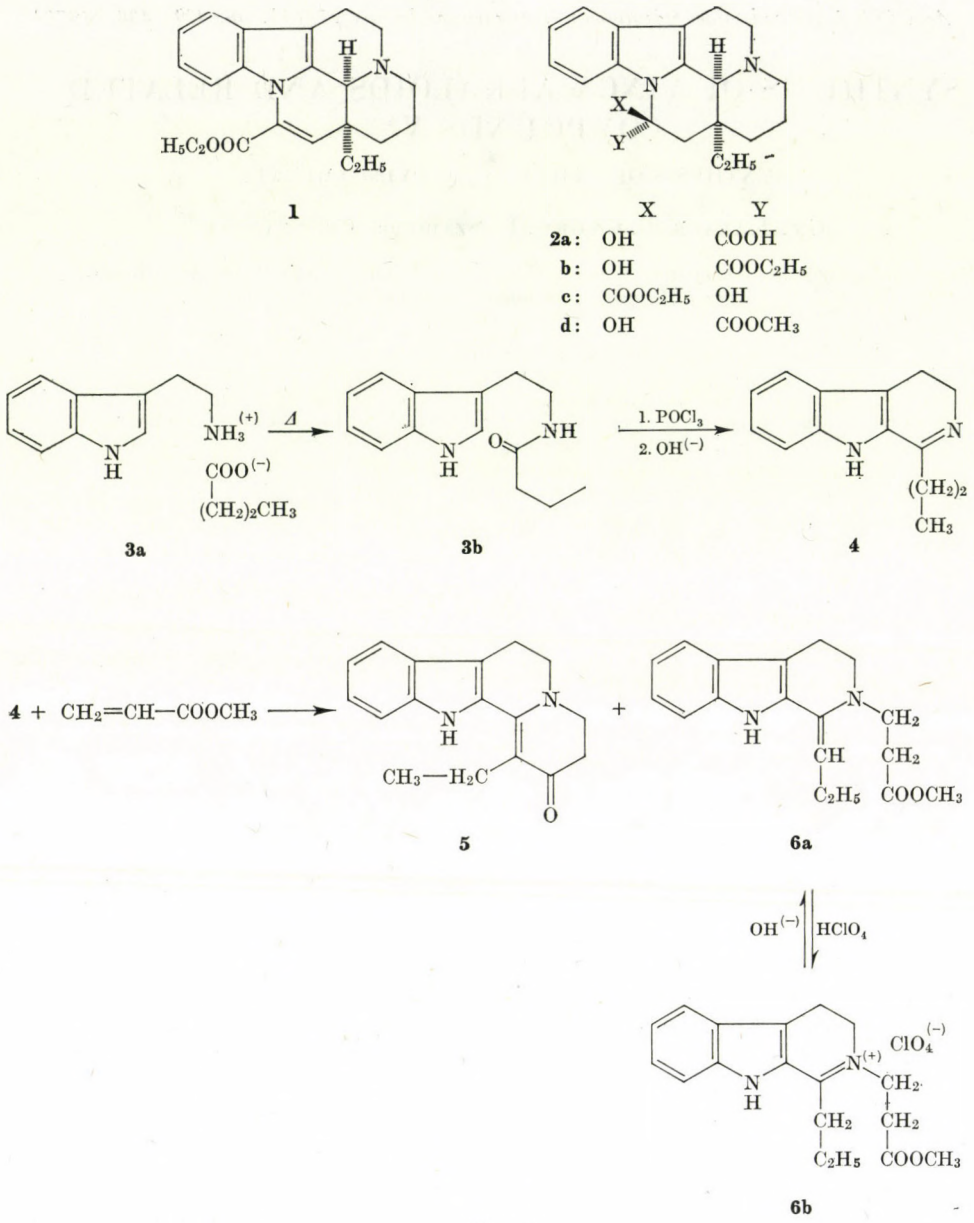

Fig. 1

The presumption appeared to be obvious that further boiling of the base **6a**, liberated from the salt **6b**, in a mixture of benzene and methanol would similarly lead to the ketone **5**. However, even after prologed boiling under these conditions no traces of the tetracycle **5** could be detected by chromatography in the reaction mixture.

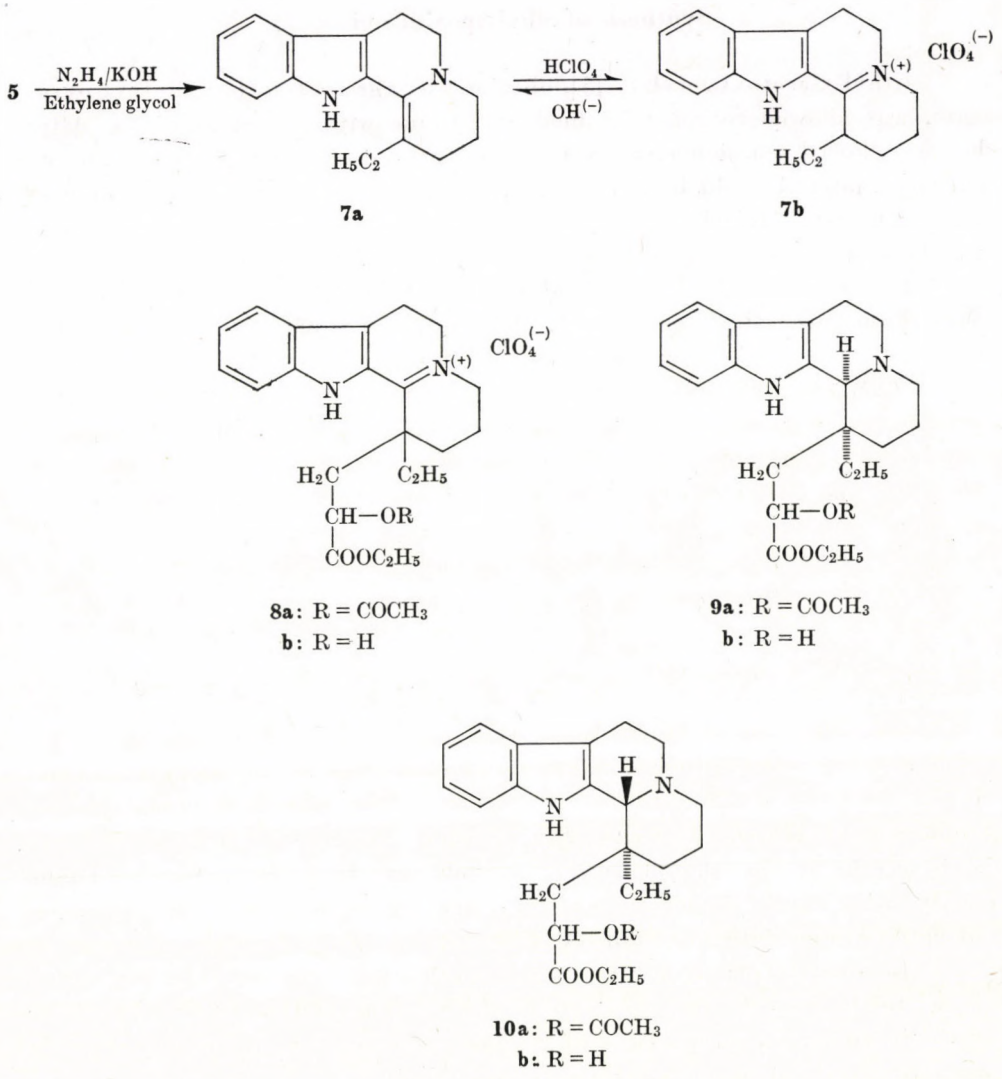

Fig. 2

However, the conversion **6** → **5** could be readily effected in benzene, by means of potassium *t*-butoxide. The product obtained in this way was completely identical in all respects with the substance formed directly in the reaction of the tetracycle **4** with methyl acrylate.

The unsaturated ketone **5** could be reduced in a Wolf-Kizhner reaction to the desired enamine (**7a**) which was isolated as the perchlorate salt (**7b**). Though this newly investigated route of reaction could not technically compete, owing to the poor yields, with the procedure described earlier [3], interest may be attached to it from the chemical aspect.

Synthesis of ethyl apovincaminate

Ethyl α-acetoxyacrylate [5], obtained by the acetylation of ethyl pyruvate, was allowed to react in dichloromethane with the enamine **7a**. After having allowed reaction mixture to stand two days at room temperature, no starting material could be detected. The addition product **8a** was isolated as the perchlorate salt, which crystallized very readily from ethanol but the yield was lower than in the case of the corresponding methyl ester.

Reduction of the hexahydroindoloquinolizine **8a** either catalytically or by sodium borohydride gave practically one single isolable epimer, **9a**, which afforded on deacetylation the readily crystallizing **9b**.

When the hydrolysis of the acetoxy group of the ester **9a** was effected prior to the reduction, the stereoselectivity of the catalytic reduction changed only slightly, but reduction with sodium borohydride gave the *cis* compound **9b** as the sole *trans* derivative **10b** appeared in a readily isolable amount even at room temperature. The ethyl ester of type **8** could thus be reduced with a higher stereoselectivity than the corresponding methyl ester [3].

All these observations support our earlier experience that the higher the space requirement of the substituents attached to C-1 of the indolo[2,3-a]-quinolizidine ring, the higher the stereoselectivity in favour of the *cis* product in the catalytic or sodium borohydride reduction of the C=N bond.

When the alcohol **9b** was made to react with Fétizon reagent, according to our earlier observations, oxidation and epimerisation took place; accordingly two products (**2b** and **2c**) were formed. The relation between the two epimers is elucidated also by the epimerisation experiments. When boiled with sodium ethoxide in ethanol, **2c** is completely converied into the thermodynamically more stable **2b**, similarly to the observations [3] made in the conversion of epivincamine into vincamine.

In order to prove the structure unequivocally, the ester **2b** was hydrolyzed to the acid **2a** and then esterified with diazomethane, affording thus racemic vincamine prepared earlier. These reactions unambiquously confirm also the steric structures previously suggested.

The fact that the compounds are epimers has been proved by a simple dehydration reaction. Either **2b** or **2c** lost water when treated with acetic anhydride, to give racemic ethyl apovincamate (**1**), the target compound of the work.

Experimental

The infrared spectra were recorded in KBr pills or as liquid films with a Spektromom 2000 spectrophotometer; the NMR spectra were taken on a Perkin-Elmer R12 (60 MHz) spectrophotometer, and the UV spectra on a Unicam SP 800 spectrophotometer.

Tryptamine butyrate (3a)

Tryptamine (16.00 g; 100 mmoles) was dissolved in 320 ml of ethyl acetate and 9.50 ml (103 mmoles) of *n*-butyric acid was dropwise added. The precipitation of crystals started instantaneously and continued when the reaction mixture was allowed to stand in a refrigerator. Separation of the crystalline product gave 24.5 g (98.8 %) of the salt **3a**, m.p. 151 – 153 °C. Recrystallization from ethyl acetate raised the m.p. to 152 – 153 °C.

$C_{14}H_{20}N_2O_2$ (248.32). Calcd. C 67.71; H 8.12; N 11.28. Found C 67.64; H 8.16; N 11.12 %.

IR(KBr): ν_{max} 3240 cm^{-1} (indole-NH), broad band 1520 – 1565 cm^{-1} ($>C=O$ and $-NH_3^+$).

1-*n*-Propyl-3,4-dihydro-β-carboline (4)

Tryptamine butyrate (**3a**) (11.55 g; 46.5 mmoles) was melted, the melt was slowly heated to 190 – 200 °C and kept for 45 min at this temperature. (Water formed during the reaction was removed.) The melt after cooling was mixed with 120 ml of anhydrous benzene, 22 ml (242 mmoles) of freshly distilled phosphoryl chloride was added and the reaction mixture refluxed for 4 hrs. The dark solution was evaporated in vacuum and the residual dark oil mixed with a 20 % solution of acetic acid (100, 80, 50 ml). The solid was filtered off, and the aqueous solution neutralized to pH 7 with conc. ammonium hydroxide solution under cooling. After shaking with 80 ml of dichloromethane, the organic phase was discarded, and the aqueous phase made was alkaline (pH 11) with conc. ammonium hydroxide and shaken again with dichloromethane (80, 50, 30 ml). The combined organic phases were dried over magnesium sulfate, the drying agent was filtered off, and the filtrate evaporated in an inert atmosphere to leave 3.80 g (38.7 %) of a yellow crystalline substance (**4**), m.p. 162 – 165 °C.

The base **4** (1.00 g) was dissolved in 3 ml of methanol and a 70 % aqueous solution of perchloric acid was added (up to pH 5). Crystallization started on scratching. Filtration with suction gave 1.05 of a crystalline powder (**4**.$HClO_4$), m.p. 183 – 185 °C. Recrystallization from water raised the m.p. to 184 – 186 °C.

$C_{14}H_{17}N_2\ ClO_4$ (312.75). Calcd. C 53.76; H 5.49; N 8.97. Found C 54.03; H 5.54; N 8.94%.

IR(KBr): ν_{max} 1640 cm^{-1} ($>C=\overset{(+)}{N}H$).

1-*n*-Propyl-2-(methoxycarbonylethyl)-3,4-dihydro-β-carboline perchlorate (6b)

1-*n*-Propyl-3,4-dihydro-β-carboline (**4**) (5.75 g; 27.2 mmoles) was dissolved in a mixture f 20 ml of anhydrous methanol and 20 ml of anhydrous benzene; 2.70 ml (29.8 mmoles) of methyl acrylate was added and the mixture refluxed for 37 hrs in a stream of nitrogen. After refluxing for 11 hrs 0.50 ml (5.52 mmoles) of methyl acrylate and after 21 hrs again 0.50 ml (5.52 mmoles) of methyl acrylate was added; the mixture thus contained a total of 40.84 mmoles of methyl acrylate.

The reaction mixture was evaporated in vacuum, the residual oil dissolved in 8 ml of methanol and acidified with a 70 % perchloric acid to pH 6. In a refrigerator deposited 2.20 g (20.3 %) of a yellow crystalline substance, m.p. 134 – 136 °C.

Recrystallization of 0.35 g of the perchlorate salt from a mixture of 2 ml of anhydrous methanol and 6 ml of dry ether gave 0.30 g of the analytically pure product, m.p.135 – 137 °C.

$C_{18}H_{23}N_2ClO_6$ (398.83). Calcd. C 54.20; H 5.81; N 7.02. Found C 54.18; H 6.01; N 6.95 %.

IR(KBr): ν_{max} 1728 cm^{-1} ($>C=O$), 1624 cm^{-1} ($>\overset{(+)}{C}=N<$).

1-Ethyl-2,3,4,5,6,7-hexahydro-12H-indolo[2,3-a]quinolizin-2-one (5)

(a) 6,70g (31,7 mmoles) 1-*n*-Propyl-3,4-dihydro-β-carboline (**4**) was dissolved in a mixture of 40 ml of anhydrous methanol and 40 ml of anhydrous benzene: 3.70 ml (41 mmoles) of methyl acrylate was added and the mixture refluxed for 96 hrs in a stream of nitrogen. (The flask and the condenser were coated with aluminium foils.) After refluxing for 40 hrs, further 3.70 ml (41 mmoles) of methyl acrylate was added and the refluxing continued. At the end of reaction the solution was evaporated in vacuum, the residual oil dissolved in 6 ml of methanol and the solution allowed to stand in a refrigerator to yield 1.05 g (12.6 %) of a

white crystalline powder, m.p. 240 – 243 °C. Recrystallization from methanol gave m.p. 242 – 243 °C.

$C_{17}H_{18}N_2O$ (266.33). Calcd. C 76.66; H 6.81; N 10.52. Found C 76.80; H 7.10; N 10.51 %.

IR(KBr): ν_{max} 3310 cm^{-1} (indole-NH), broad band of 1620 – 1668 cm^{-1} (>C=O and >C=C<).

NMR (in deuterochloroform); δ 8.38 (s, 1H, indole-H); δ 7.58 – 6.96 (m, 4H, aromatic H); δ 4.05 (t, 2H, $-C(=O)-CH_2-$); δ 1.25 (t, 3H, $-CH_3$).

Aqueous 70 % perchloric acid was added (to adjust pH 6) to about 6 – 7 ml of the methanolic mother liquor of the first crystallization, and the mixture was allowed to stand in a refrigerator to yield 1.25 g (9.9 %) of a yellow crystalline salt (**6b**), m.p. 135 – 137 °C. The product was in all respects identical with compound described previously.

(b) Potassium *t*-butoxide (1.40 g; 12.5 mmoles) was added into 60 ml of anhydrous benzene; part of the benzene was then evaporated to obtain a solution of a volume of 20 ml. A solution of 1.80 g (6.02 mmoles) of methyl 3-(1-propylidene-1,2,3,4-tetrahydro-2-β-carbolinyl) propionate (**6a**) in 20 ml of anhydrous benzene was added and the reaction mixture refluxed for 10 hrs in a stream of nitrogen. The reaction mixture was allowed to cool and 0.75 ml (12.9 mmoles) of glacial acetic acid (pH 6.5) and 100 ml of distilled water were added. The mixture was made strongly alkaline with conc. ammonium hydroxide solution (pH 11), and the phases were separated. The benzene solution was dried over magnesium sulfate and evaporated in vacuum to leave 1.25 g of an oil. Crystallization from methanol gave 0.95 g (59.2 %) of a crystalline powder, m.p. 240 – 243 °C. The product was in all respects identical with the compound described above.

1-Ethyl-1,2,3,4,6,7-hexahydro-12H-indolo[2,3-a]quinolizin-5-ium perchlorate (7b)

1-Ethyl-2,3,4,5,6,7-hexahydro-12H-indolo[2,3-a]quinolizin-2-one (**5**) (0.35 g; 1.32 mmole) was suspended in 20 ml of ethylene glycol, then 2.0 g (35.7 mmoles) of finely powdered potassium hydroxide and 1.50 ml 98 – 99 % hydrazine hydrate were added.

The mixture was refluxed for 9 hrs in nitrogen atmosphere at 205 – 210 °C bath temperature. The reaction mixture was then evaporated in vacuum, 10 ml of distilled water was added and shaken with dichloromethane (10, 5, 5 ml). The organic phase was dried over magnesium sulfate, filtered, and the filtrate evaporated in vacuum to leave 0.25 g of a red oil. It was dissolved in some methanol and slightly acidified (to pH 5) with a 70 % aqueous solution of perchloric acid. On scratching 0.15 g (32.6 %) of the perchlorate salt separated as yellow crystals, m.p. 175 – 177 °C. Recrystallization from methanol raised the m.p. to 177 – 178 °C.

$C_{17}H_{21}N_2O_4Cl$ (352.82). Calcd. C 57.87; H 6.00; N 7.94. Found C 57.58; H 6.20; N 8.00 %.

IR(KBr): ν_{max} 3280 cm^{-1} (indole-NH), 1622 cm^{-1} ($>C=\overset{(+)}{N}<$).

UV(in methanol): λ_{max} 363 nm (log ε 4.2095).

1-Ethyl-1-{[2-(acetyloxy)]-(ethoxycarbonylethyl)}-1,2,3,4,6,7-hexahydro-12H-indolo-[2,3-a]quinolizin-5-ium perchlorate (8a)

1-Ethyl-1,2,3,4,6,7-hexahydro-12H-indolo[2,3-a]quinolizin-5-ium perchlorate (**7b**) (10.0 g; 28.4 mmoles) was suspended in 100 ml of dichloromethane, and 75 ml distilled water and 20 ml of a 2 *N* NaOH solution were added. After stirring for 10 min in argon atmosphere, the organic phase was separated. The aqueous solution was extracted with 20 ml of dichloromethane, and the combined organic solutions dried over magnesium sulfate. The drying agent was filtered off and 10.0 ml of freshly distilled ethyl [2-(acetoxy)]-acrylate was added to the filtrate; the reaction mixture was flushed with argon gas, sealed, and allowed to stand for 2 days at room temperature. Evaporation of the solvent in vacuum left a dark red oil, which was rubbed with 3 × 50 ml of petroleum ether. The solidifying yellowish red substance was dissolved in 30 ml of hot ethanol and slightly acidified (pH 6) with a 70 % aqueous solution of perchloric acid. On scratching, the precipitation of crystals started; their deposition could be promoted by allowing the mixture to stand at room temperature. The yellow substance was filtered off with suction and washed with some ethanol to obtain 6.20 g (42.8 %) of the perchlorate salt, m.p. 178 – 179 °C

$C_{24}H_{31}N_2ClO_8$ (510.96). Calcd. C 56.41; H 6.11; N 5.48. Found C 56.55; H 6.19; N 5.42 %.
IR(KBr): ν_{max} 3330 cm^{-1} (indole-NH), 1745 – 1760 cm^{-1} (>C=O), 1630 cm^{-1} (>C=$\overset{(+)}{N}$<).

1-Ethyl-1-[2-hydroxy-(ethoxycarbonylethyl)]-1,2,3,4,6,7-hexahydro-12H-indolo[2,3a]-quinolizin-5-ium perchlorate (8b)

The salt **8a** (3.00 g; 5.88 mmoles) was dissolved in 100 ml of ethanol which had been saturated at 0 °C with gaseous hydrochloric acid. The solution was refluxed for 3 hrs, then evaporated in vacuum. The solid residue was dissolved in hot water and mixed with a 70 % aqueous solution of perchloric acid. On allowing the solution to stand, crystallization started to give 2.35 g of a yellow salt, m.p. 208 – 211 °C. Recrystallization from ethanol yielded 2.05 g (74.7 %) of the pure crystalline product, m.p. 214 – 215 °C.

$C_{22}H_{29}N_2ClO_7$ (468.93). Calcd. C 56.34, H 6.23; N 5.98. Found C 56.52; H 6.18; N 5.91 %.
IR(KBr): ν_{max} 3380 cm^{-1} (indole-NH), 1738 cm^{-1} (>C=O), 1630 cm^{-1} (>C=$\overset{(+)}{N}$<), 1608 cm^{-1} (>C=$\overset{(+)}{N}$<).

1α-Ethyl-1-{[2-(acetyloxy)]-(ethyloxycarbonylethyl)}-1,2,3,4,6,7,12,12bα--octahydroindolo[2,3-a]quinolizine (9a)

(a) About 1.5 g of 5 % palladium-on-carbon was prehydrogenated in some ethanol, then a solution of 2.55 g (5.00 mmoles) of the perchlorate salt **8a** in 120 ml of ethanol was added and hydrogenation was effected at room temperature and atmospheric pressure. After the absorption of the calculated amount (120 ml) of hydrogen (about 2 hrs), the catalyst was filtered off and the filtrate evaporated in vacuum. The residual solid was dissolved in 60 ml of acetone, made alkaline (pH 10) with conc. ammonium hydroxide solution and evaporated in vacuum. The residual oil was mixed with distilled water and extracted with dichlormethane (50, 30 ml). The organic phase was dried over magnesium sulfate and evaporated in vacuum. The residual oil was crystallized from ethanol to yield 1.55 g (75.6 %) of a white crystalline powder, m.p. 147 – 149 °C.

$C_{24}H_{32}N_2O_4$ (412.51). Calcd. C 69.88; H 7.82; N 6.79. Found C 69.63; H 7.70; N 6.88 %.
IR(KBr): ν_{max} 3420 cm^{-1} (indole-NH), 1750 cm^{-1}, 1738 cm^{-1} (>C=O).
NMR(in deuterochloroform): δ 7.87 (s, 1H, indole-H); δ 7.68 – 7.02 (m, 4H, aromatic H); δ 4.95 (q, 1H, $-CH_2-\underset{|}{CH}-COOC_2H_5$); δ 4.08 (q, 2H, $-\overset{O}{\overset{\|}{C}}-O-\mathbf{CH_2}-CH_3$); δ 3.40 (s, 1H, annellation-H); δ 2.04 (s, 3H, $-\overset{O}{\overset{\|}{C}}-CH_3$).

(b) The perchlorate salt **8a** (2.00 g; 3.92 mmoles) was suspended in 100 ml of methanol, cooled to 0 °C with continuous stirring, and 1.40 g (37.2 mmoles) of sodium borohydride was added in small portions. After the addition had been completed, stirring was continued for 1 hr, then the solution acidified to pH 5 with glacial acetic acid, evaporated in vacuum and the residue suspended in a 5 % solution of sodium hydrogen carbonate and extracted by shaking with dichloromethane (30, 20, 10 ml). The organic phase was dried over magnesium sulfate, the drying agent filtered off, the filtrate evaporated in vacuum, and the residual oil crystallized from ethanol to obtain 1.10 g (68.2 %) of a crystalline product, m.p. 147 – 149 °C.

This substance was identical in all respects with the product prepared according to (a).

1α-Ethyl-1-[2-hydroxy-(ethoxycarbonylethyl)]-1,2,3,4,6,7,12,12bα-octahydroindolo[2,3-a]-quinolizine (9b)

(a) About 1.5 g of 5 % palladium-on-carbon was prehydrogenated in ethanol or acetone, then a solution of 2.55 g (5.00 mmoles) of the perchlorate salt **8a** in 120 ml of ethanol (or in 50 ml of acetone) was added. Hydrogenation was carried out at room temperature and atmospheric pressure. After the absorption of the calculated amount of hydrogen (120 ml) (about 2 hrs) the catalyst was filtered off and the solution evaporated in vacuum. The residual solid salt mixture was dissolved in 50 ml of ethanol which had been saturated at 0 °C with hydrogen chloride, and the solution was refluxed for 3 hrs. The acid solution was evaporated in vacuum, the residue rubbed with 5 ml of ethanol and filtered off with suction to obtain 1.70 g of the product. It was dissolved in 70 ml of a 1 : 1 mixture of acetone and water and the solution was

made alkaline (pH 10) with a saturated solution of sodium carbonate. The resulting white precipitate was filtered off with suction and washed with distilled water to yield 1.20g (64.9 %) of **9b**, m.p. 242 – 244 °C. Recrystallization from ethanol gave m.p. 243 – 244 °C.

$C_{22}H_{30}N_2O_3$ (370.48). Calcd. C 71.32; H 8.16; N 7.56. Found C 71.18; H 8.09; N 7.90 %.

IR(KBr): ν_{max} 3220 cm^{-1} (indole-NH), 1742 cm^{-1} (>C=O).

NMR(in deuterochloroform): δ7.72 (s, 1H, indole-H); δ 7.58 – 6.92 (m, 4H, aromatic H); δ 4.17 (q, 2H, $-C(=O)-\mathbf{OCH_2}-CH_3$).

(b) 1α-Ethyl-1-{[2-(acetoxy)]-(ethoxycarbonylethyl)}-1,2,3,4,6,7,12,12bα-octahydroindolo[2,3-a]quinolizine (**9a**) (0.55 g; 1.33 mmole) was dissolved in 20 ml of ethanol, and 0.05 g (0.92 mmole) of sodium ethoxide was added. The mixture was refluxed for 1 hr, cooled, acidified to pH 6 with glacial acetic acid, and evaporated in vacuum. The residue was suspended in a 5 % solution of sodium hydrogen carbonate and extracted with dichloromethane (30, 20, 10 ml). The solution was dried over magnesium sulfate and evaporated to yield 0.45 g (91.8 %) of a white crystalline substance, m.p. 242 – 244 °C.

The product was in all respects identical with the substance prepared according to (a).

(c) 1α-Ethyl-1-[2-hydroxy-(ethoxycarbonylethyl)]-1,2,3,4,6,7-hexahydro-12H-indolo [2,3-a]quinolizin-5-ium perchlorate (**8b**) (1.50 g; 3.20 mmoles) was suspended in 150 ml of methanol and cooled to 0 °C under continuous stirring. Sodium borohydride (1.00 g; 26.4 mmoles) was added in small portions, and stirring was continued for 1 hr. The solution was then acidified (pH 5) with glacial acetic acid and evaporated in vacuum. The residue was suspended in a 5 % solution of sodium hydrogen carbonate and shaken with dichloromethane (30, 20, 10 ml). After drying the organic phase over magnesium sulfate, the solution was evaporated and the residual solid crystallized from methanol to obtain 1.05 g (88.9 %) of a crystalline powder, m.p. 241 – 243 °C.

The product was in all respects identical with that described under (a).

(d) 1α-Ethyl-1-[2-hydroxy-(ethoxycarbonylethyl)]-1,2,3,4,6,7-hexahydro-12H-indolo [2,3-a]quinolizin-5-ium perchlorate (**8b**) (1.0 g; 2.13 mmoles) was dissolved in 60 ml of acetone, and the solution added to a prehydrogenated suspension of about 1.5 g of 5 % palladium-on-carbon. Hydrogenation was effected at room temperature and atmospheric pressure. After absorption of the calculated amount of hydrogen (52 ml) (in about 1 hr), the catalyst was filtered off, and the solution evaporated in vacuum. The residual salt was dissolved in a mixture of 7 ml of acetone and 7 ml of distilled water, and the solution made alkaline (pH 10) with a saturated solution of sodium carbonate. The resulting white precipitate was filtered off with suction and washed with water to obtain 0.70 g of the product. Recrystallization from ethanol gave 0.65 g (82.8 %) of a crystalline substance m.p. 242 – 244 °C.

The product was in all respects identical with that prepared according to (a).

1α-Ethyl-1-[2-hydroxy-(ethoxycarbonylethyl)]-1,2,3,4,6,7,12,12bβ-octahydroindolo[2,-3a]-quinolizine (10b)

Compound **8a** (1.5 g; 3.2 mmoles) was suspended in 150 ml of ethanol and 1.0 g (26.4 mmoles) of sodium borohydride was added at 25 – 30 °C in small portions, under continuous stirring. After the addition had been completed (in about 30 min), stirring was continued for 1 hr at the same temperature, then the mixture was refluxed for 30 min. The solution was cooled and acidified to pH 5 with glacial acetic acid and evaporated in vacuum. The residue was suspended in a 5 % solution of sodium hydrogen carbonate and extracted with dichloromethane (30, 20, 10 ml). The organic phase was dried over magnesium sulfate, filtered, and the filtrate evaporated in vacuum. The residual solidifying product was subjected to fractional crystallization from ethanol. At first 0.20 g (16.8 %) of **9b**, m.p. 239 – 242 °C, crystallized from the hot ethanolic solution. Recrystallization from ethanol gave m.p. 242 – 243 °C. On concentrating the mother liquor of the previous crystallization, 0.70 g (59.0 %) of a previous crystallization, 0.70 g (59.0 %) of a crystalline powder (**10b**), m.p. 133 – 135 °C was obtained; m.p. 136 – 137 °C after recrystallization from ethanol.

$C_{22}H_{30}N_2O_3$ (370.48). Calcd. C 71.32; H 8.16; N 7.56. Found C 71.39; H 8.19; N 7.83 %.

IR(KBr): ν_{max} 3500 cm^{-1}, 3360 cm^{-1} (indole-NH, OH), 1738 cm^{-1} (>C=O).

NMR(in deuterochloroform): δ 9.44 (s, 1H, indole-NH); δ 6.92 – 7.52 (, 4H, aromatic H); δ 4.36 (q, 2H, $-C(=O)-O-\mathbf{CH_2}-CH_3$); δ 1.32 (t, 3H, $-C(=O)-O-CH_2-\mathbf{CH_3}$); δ0.63 (t, 3H, $-CH_2-\mathbf{CH_3}$).

Ethyl (±)-vincaminate (2b)

(a) 1α-Ethyl-1-[2-hydroxy-(ethoxycarbonylethyl)]-1,2,3,4,6,7,12,12bα-octahydroindolo [2,3-a]quinolizine (**9b**) (1.00 g; 2.71 mmoles) was dissolved in 50 ml of hot anhydrous xylene, 5.00 g of Fétizon reagent was added and the suspension refluxed for 7 hrs, with stirring. Oxidation was completed in 2 – 3 hrs. Further heating caused epimerization of the primary product **2c** into **2b**. The progress of the reaction was followed by thin-layer chromatography. (Alumina 60 F 254 (Merck) absorbent; solvent system consisting of 10 ml of dichloromethane and 0.05 ml of methanol; detection with iodine vapour.) After 7 hrs which proved to be the optimum reaction time, ethyl (±)-14-epivincaminate (**2c**) was hardly detectable in the reaction mixture. The solid was filtered off hot from the suspension, and the xylene solution was allowed to stand first at room temperature then in a refrigerator to obtain 0.70 g (70.2 %) of chromatographically homogeneous ethyl (±)-vincaminate, m.p.249 – 251 °C. On recrystallization from xylene, the m.p. rose to 252 – 253 °C.

$C_{22}H_{28}N_2O_3$ (368.46). Calcd. C 71.71; H 7.66; N 7.60. Found C 71.50; H 7.48; N 7.75 %.
IR(KBr): ν_{max} 1740 cm^{-1} (>C=O).

(b) Ethyl (±)-14-epivincaminate (**2c**) (0.15 g; 0.40 mmole) was mixed with 20 ml of a solution sodium ethoxide in ethanol, the sodium ethoxide content being 0.17 mmole. The starting material dissolved, then the precipitation of crystals started from the solution. The reaction mixture was refluxed for 5 hrs under conditions excluding moisture. The suspension was then evaporated in vacuum and the residue rubbed with distilled water. The solution was filtered off with suction and washed with ethanol to obtain 0.12 g (80.0 %) of a crystalline product, m.p. 250 – 252 °C.

The product was in all respects identical with the substance prepared according to (a).

Ethyl (±)-14-epivincaminate (2c)

The base **9b** (1.00 g; 2.71 mmoles) was suspended in 80 ml of anhydrous benzene, 5.00 g of Fétizon reagent was added, and the mixture was refluxed for 38 hrs, with stirring. (The progress of the reaction may be followed by chromatography, using the conditions specified in the description of ethyl (±)-vincaminate). The solid was filtered off, and the filtrate allowed to stand at room temperature, when 0.70 g (70.2 %) of a crystalline substance, m.p. 224 – 226°C, precipitated. Recrystallization from benzene gave m.p. 233 – 235 °C.

$C_{22}H_{28}N_2O_3$ (368.46). Calcd. C 71.71; H 7.66; N 7.60. Found C 71.91; H 7.66; N 7.42 %.
IR(KBr): ν_{max} 1742 cm^{-1} (>C=O).

Ethyl (±)-apovincaminate (1)

Ethyl (±)-vincaminate (**2b**) or ethyl (±)-14-epivincaminate (**2c**) (1.85 g; 5.00 mmoles) was dissolved in 70 ml of acetic anhydride and the mixture refluxed for 24 hrs. The dark-coloured solution was evaporated in vacuum, the residual oil dissolved in 150 ml of distilled water and the solution made alkaline (pH 10) with 40 % NaOH solution. It was extracted with ether (50, 40, 30 ml), the organic solutions were combined and dried over magnesium sulfate. Filtration followed by evaporation left 1.70 g of a light yellow oil, which was crystallized from ethanol to give 1.25 g (71.7 %) of a white crystalline product, m.p. 130 – 132 °C. Recrystallization from ethanol raised the m.p. to 132 – 134 °C.

$C_{22}H_{26}N_2O_2$ (350.44). Calcd. C 75.40; H 7.48; N 7.99. Found C 75.47; H 7.52; N 7.99 %.
IR(KBr): ν_{max} 1720 cm^{-1} (>C=O), 1656 cm^{-1}, 1610 cm^{-1} (>C=C<).
NMR(in deuterochloroform): δ 7.65 – 6.97 (m, 4H, aromatic H); δ 6.11 (s, 1H, >C=**CH**-); δ 4.42 (q, 2H, $-C(=O)-O-\mathbf{CH_2}-CH_3$); δ 1.02 (t, 3H, $-CH_2-\mathbf{CH_3}$).

(±)-Vincamine (2d)

Ethyl (±)-vincaminate (**2b**) (0.45 g; 1.22 mmole) was dissolved in 10 ml of 95 % ethanol, a solution of 0.12 g (3.00 mmoles) of sodium hydroxide in 1 ml of distilled water was added, and the mixture refluxed for 5 hrs. At the end of the reaction the solvent was evaporated in vacuum, the residual oily substance dissolved in 10 ml of distilled water and the solution adjusted to a pH value between 7.0 and 7.5 with 20 % acetic acid. On scratching, 0.35 g (84.8 %) of a white crystalline powder precipitated (**2a**), m.p. 265 – 267 °C ((±) – vincaminic acid).

0.35 g of (±)-vincaminic acid was dissolved in 35 ml of dioxan and an etheral diazomethane solution was added, with shaking, until a permanent yellow colour was obtained. The mixture was allowed to stand for 24 hrs at room temperature, then glacial acetic acid was added until the solution became colourless (pH 5). Evaporation in vacuum left an oily substance which was mixed with distilled water and made alkaline (pH 10 – 11) with 2*N* NaOH solution. The solution was extracted with dichlormethane (50, 30, 20, 10 ml), the combined organic solutions were dried over magnesium sulfate and then filtered from the drying agent. Evaporation of the filtrate afforded a solid substance which on crystallization from xylene afforded 0.32 g (74.2) % of a crystalline powder, m.p. 230 – 232 °C.

The product was in all respects identical with the substance prepared as described in the literature (*e. g.* [3]).

The authors' thanks are expressed to the Chemical Works of Gedeon Richter Ltd. for supporting our studies.

REFERENCES

[1] For Part IV see: KALAUS, GY., GYŐRY, P., SZABÓ, L., SZÁNTAY, Cs., Acta Chim. Acad. Sci. Hung. **96** (4), 385 – 391 (1978)
[2] LŐRINCZ, Cs., KÁRPÁTI, E., SZPORNY, L., SZÁSZ, K., KISFALUDY, L.: Hungarian Pat. 163 434; C. A. **79**, 42 726 c (1973)
[3] SZÁNTAY, Cs., SZABÓ, L., KALAUS, GY.: Tetrahedron **33**, 1803 (1977)
[4] ATTA-UR-RAHMAN: J. Chem. Soc. Perkin I **1972**, 731
[5] CANTELLO, B.C. C., MELLER, J. M.: Tetrahedron Letters **1968**, 5179

György KALAUS
Péter GYŐRY
Lajos SZABÓ
Csaba SZÁNTAY

H-1521 Budapest, Gellért tér 4.

Acta Chimica Academiae Scientiarum Hungaricae, Tomus 97 (4), pp. 439–449 (1978)

PLATINUM CATALYZED TRANSFORMATIONS OF CYCLOHEXANOL, I

I. MANNINGER, Z. PAÁL and P. TÉTÉNYI

(Institute of Isotopes of the Hungarian Academy of Sciences)

Received May 31, 1977

Radiotracer studies demonstrated that the dehydrogenation of cyclohexanol to phenol takes place *via* cyclohexanone as well as *via* a direct pathway. Hydrocarbons are produced mainly by the dehydroxylation of phenol. The temperature, catalyst activity and hydrogen supply will determine how the product composition in the two triangular systems including cyclohexanol, cyclohexanone, phenol and cyclohexane, cyclohexene, benzene, respectively, will be shifted. This is also influenced by the ability of the catalysts to retain hydrogen, which, in turn, is a function of the pretreatment temperature.

Introduction

The several different reaction possibilities of cyclohexanol make it an attractive model compound for the investigation of catalyst selectivity [1]. At the same time, the comparison of its reactions with those of cyclohexane may reveal how the introduction of an oxygen atom into the six-membered ring affects its reactivity.

The main reaction of cyclohexanol over metal catalysts is dehydrogenation into cyclohexanone [2 3], this reaction having also an industrial importance. Copper, zinc, iron and nickel or their alloys are used most generally as industrial catalysts for this reaction. Some kinetic parameters including the activation energy and the adsorption parameters of the product and the reagent have been determined on these metals [4, 5].

Phenol can often be observed among the products. Presumably it involves cyclohexanone as an intermediate* and the reaction takes place *via* its enolic form. SWIFT and BOZIK [6] suggested that the considerable increase of phenol yield with increasing amounts of tin in different Sn–Ni/silicagel catalysts was due to basic surface sites of tin oxide which promoted enolization and stabilized the enolic form.

Over nickel and copper catalysts, phenol formation takes place only *via* this consecutive pathway, as has been shown by radioactive tracer studies [7,8]. On the other hand, on a platinum catalyst, phenol formation *via* direct dehydrogenation of the C_6 ring has actually been observed [8].

* The term intermediate refers to a fully desorbed species. The isotopic tracer method does not permit the detection of surface intermediates.

RICHARDSON and LU [9] suggested the participation of an 'edgewise' adsorbed intermediate in direct phenol formation.

Yields up to 50 % of benzene were observed when phenol was converted over an Al–Cu–Mo catalyst at 50 atm pressure of hydrogen at 623 K [11]. This hydrogenolytic splitting of the phenolic OH group has been observed at atmospheric pressure over a Ni catalysts [7].

RICHARDSON and LU [9] interpreted cyclohexane formation over Pt/Al_2O_3 and Pt/C in terms of the hydrogenolytic splitting of an OH group from cyclohexanol. This explanation is, however, not quite convincing; it is more likely that dehydration into cyclohexene over the alumina and charcoal supports occurs and is followed by hydrogenation into cyclohexane over platinum [12]. Alumina is a good catalyst for dehydration [13, 14], being always acidic to some extent; dehydration has been observed over charcoal, too [12]. Dehydration has been reported over unsupported metals as well [15].

The separation of various pathways of hydrocarbon formation is very difficult because the reaction products may transform into each other. Radioactive tracers may be helpful in this respect [8].

The purpose of the present investigations was to elucidate the different reaction possibilities of cyclohexanol in the presence of a well-known catalyst metal, platinum. This may facilitate the better understanding of its catalytic activity and, at the same time, may throw light on the mechanisms of various transformations of cyclohexanol. The present paper will deal with reactions in which the cyclic-C_6 skeleton of the molecule remains unchanged (they include dehydrogenation and dehydroxylation processes); a forthcoming paper will describe degradation reactions.

Experimental

Apparatus

The experiments were carried out in a pulse-microcatalytic reactor. 1 μl pulses of cyclohexanol were injected into a nitrogen (40 ml/min) or hydrogen (80 ml/min) carrier gas stream. The temperature of the tubular reactor (100 mm long, 3.5 mm in diameter) was controlled to within $\pm$ 0.5 °C and measured by a thermocouple at the external surface of the reactor. The column of a Packard-Becker 419 gas chromatograph was connected directly downstream to the reactor.

For radio gaschromatographic measurements the column outlet stream was split into two parts, one of them being connected to the FID, the other passing over copper oxide heated to red glow to burn organic compounds; after the absorption of water methane was admixed to the carrier gas and, the CO_2 was led into a flow-through proportional counter.

Analysis

A temperature program (25 °C → 120 °C) permitted the GLC analysis of the reaction products (between pentane and phenol) in a single run. The mechanical mixture of 1 part of 16 % bis-2-ethylhexyl-sebacinate and 4 parts of 10 % diglycerol on Chromosorb W was used as the column packing.

The specific radioactivity of the components was expressed by calculating the percentages of radioactivity counts in individual fractions and dividing these values by the corresponding mole per cents measured by the FID [7].

Catalyst

The platinum catalyst was reduced from H_2PtCl_6 with formaldehyde in KOH at 293–298 K [16]. The metal was submitted to a standard thermal treatment at 473 K and 633 K, respectively; thus catalysts with different crystallite sizes were produced [17]. The specific surfaces of the samples were 8.2 m^2/g and 4.1 m^2/g, respectively (BET/N_2).

The catalysts were regenerated at 543 K with 5 × 10 ml air pulses followed by a hydrogen stream (70 ml/min) for 5 min [20], a similar treatment having been found effective for restoring of platinum activity lost in hydrocarbon reactions [18].

Results

Medium amounts of cyclohexanone, large amounts of phenol and benzene and small amounts of cyclohexane and cracked products were formed from cyclohexanol over platinum. Results obtained in the presence of N_2 and H_2 are shown in Table I, as a function of temperature. The conversion was much lower in H_2 than in N_2 at low temperatures but above 573 K this was reversed.

Cyclohexanone may give phenol apart from its hydrogenation into cyclohexanol (Table II).

Table I

Transformation of cyclohexanol in nitrogen and hydrogen atmosphere over Pt black

T (K)	Carrier gas	Composition (mol%)								
		$<C_6$	C_6H_{12}	C_6H_{10}	C_6H_6	$C_6H_{10}O$	$C_6H_{11}OH$	C_6H_5OH	Others*	$\frac{C_6H_6}{C_6H_5OH}$
483	N_2	0.12	0.045	0.0008	7.47	18.03	62.03	11.68	0	0.64
	H_2	0.004	0.068	0	0.01	8.71	91.21	0	0	–
513	N_2	0.39	0.013	–	13.35	8.81	47.45	29.98	0	0.44
	H_2	0.03	0.27	0	0.58	17.89	80.05	1.38	0	0.427
543	N_2	0.451	0.019	–	17.32	6.80	29.03	46.38	0.026	0.37
	H_2	0.53	0.78	0	8.26	28.94	46.48	14.67	0.333	0.56
573	N_2	1.57	0.015	0.0025	13.44	4.30	16.72	63.85	0.081	0.21
	H_2	2.18	0.56	0	28.39	16.19	12.83	38.69	1.147	0.73
603	N_2	4.76	0.011	0.0036	9.72	2.22	9.31	73.75	0.314	0.13
	H_2	4.38	0.23	0	23.65	5.57	8.58	56.42	1.070	0.42
633	N_2	5.67	0.012	0.0071	10.07	2.05	6.48	75.20	0.498	0.13
	H_2	14.25	0.065	0	22.02	1.68	2.05	55.63	1.721	0.40

Catalyst 0.4 g Pt; pretreated at 633 K; carrier gas 30 ml/min N_2; 80 ml/min H_2; reagent 1 μl cyclohexanol

* 0–8 unidentified products

Table II

Transformation of cyclohexanone over Pt black

T(K)	Composition (mol%)						
	$<C_6$	C_6H_{12}	C_6H_6	$C_6H_{10}O$	$C_6H_{11}OH$	C_6H_5OH	Others*
423	0.020	0.028	2.06	75.97	7.69	14.24	0
453	0.032	0.057	7.64	52.55	5.12	34.55	0
483	0.12	0.046	16.27	33.09	3.12	47.34	0
513	0.24	0.036	20.29	16.97	2.13	60.28	0.014
543	0.48	0.010	19.35	5.76	0.38	73.97	0.043
573	1.89	0.006	18.22	1.74	0.22	78.47	0.437
603	2.81	–	9.40	0.99	0.12	85.39	1.29
633	3.35	0.004	5.64	0.58	0.18	89.39	0.84

Catalyst 0.4 g Pt; pretreated at 633 K; carrier gas 30 ml/min N_2; reagent 1 μl cyclohexanone
* 0 – 6 unidentified productst

Table III

Transformation of a mixture of cyclohexanol-[^{14}C] and inactive cyclohexanone

T (K)	Composition (mol%)					Specific radioactivity (r%/			
	$<C_6$	C_6H_6	C_6H_5OH	$C_6H_{10}O$	$C_6H_{11}OH$	C_6H_6	C_6H_5OH	$C_6H_{10}O$	$C_6H_{11}OH$
483	0.1	6.9	2.0	38.6	52.4	0.46	0.41	0.23	1.56
513	0.1	19.8	6.6	30.2	43.3	0.49	0.63	0.34	1.66
543	0.2	24.3	11.1	23.9	40.5	0.60	0.67	0.37	1.60
573	0.1	11.4	16.3	32.4	39.8	0.64	0.72	0.27	1.69
603	0.3	4.1	20.5	33.1	42.0	0.86	0.70	0.28	1.60
Reagent	–	–	–	47.6	52.4	0	0	0.16	1.74

Catalyst 0.1 g Pt; pretreated at 633 K; carrier gas 30 ml/min N_2

The measurements with mixtures of radioactive cyclohexanol and inactive cyclohexanone (Table III) have confirmed earlier results [8] that phenol is formed not only *via* cyclohexanone but also directly from cyclohexanol on Pt catalysts, as the specific radioactivity of phenol formed during the reaction was in all cases higher than that of cyclohexanone.

The catalysts were strongly deactivated during the reactions (Figs 1 and 2). The amount of benzene decreased and this was accompanied by an increase of the amount of phenol with a practically unchanged overall conversion. This behaviour is characteristic of the intermediates and products of consecutive reactions [18]. Consequently, benzene must have formed mainly *via* phenol.

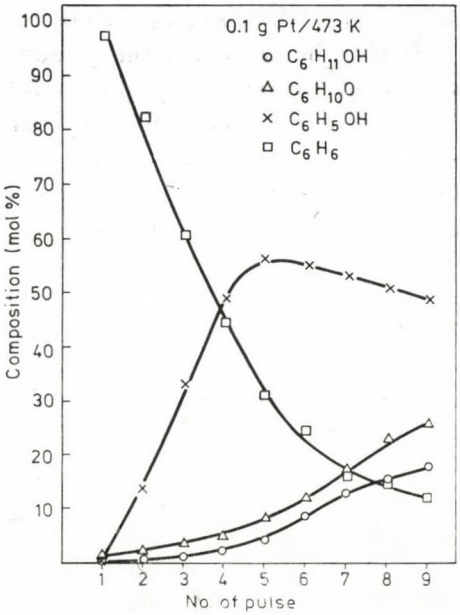

Fig. 1. **Product composition obtained from subsequent pulses introduced without regeneration onto a platinum catalyst pretreated at 473 K**

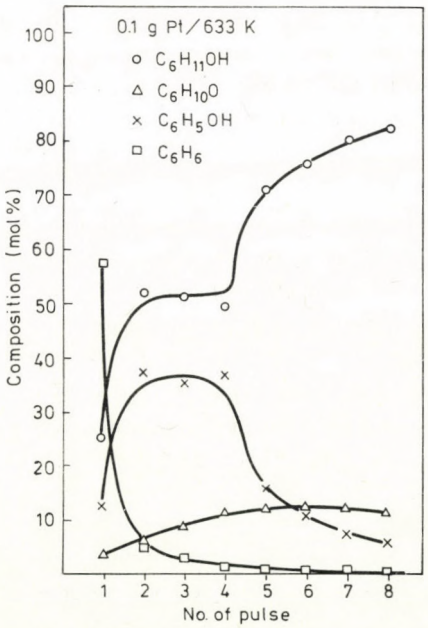

Fig. 2. **Product composition obtained from subsequent pulses introduced without regeneration onto a platinum catalyst pretreated at 633 K**

Very small amounts of cyclohexane and cyclohexene have been observed among the products. It may be (although this is not very likely) that they are very reactive intermediates being rapidly converted to benzene or, alternatively, their direct formation *via* cyclohexanol dehydration or hydrogenolysis, respectively, may be negligible. To elucidate this point, measurements were carried out with mixtures of radioactive cyclohexanol plus inactive cyclohexane and radioactive cyclohexanol plus inactive cyclohexene, respectively (Table IV). The radioactivity of the fractions corresponding to the added hydrocarbons was practically equal to the background in both cases, indicating that these compounds in fact were not formed in significant amounts from radioactive cyclohexanol.

The concentration of oxygenated components (as judged from their radioactivites) increased in the effluent with respect to the starting mixture. This may have been due to their formation from hydrocarbons*. Special experiments with a mixture of labelled benzene and inactive cyclohexanol indicate that this is not the case. Thus, this apparent contradiction must be attributed to the partial retention of hydrocarbons by the catalyst as carbonaceous residues. This fact, together with the formation of carbon dioxide (to be discussed in Part II), may lead to an incomplete material balance which, however, does not influence the conclusions drawn on the basis of the comparison of *relative* specific radioactivities.

Measurements with a mixture of radioactive cyclohexanol plus inactive phenol (Table V) indicate that the radioactivity of benzene is higher than that of phenol, *i.e.* a pathway of its formation bypassing phenol should exist [23].

Since the reactions involving cyclohexane and cyclohexene as intermediates have been excluded, part of the benzene must have formed directly from cyclohexanol without desorption of phenol. The actual specific radioactivity of benzene in Table IV indicates to what extent it was formed from cyclohexanol and the added hydrocarbon. Whereas the rate of cyclohexane dehydrogenation was negligible as compared with cyclohexanol, cyclohexene gave much more benzene than the oxygenated compound.

Comparing the product distribution over two Pt catalysts pretreated at 473 and 633 K (Table VI), we can see that not only a higher overall conversion was produced by the Pt with higher specific surface but also much higher amounts of benzene appeared. Its deactivation took place much slower than that of Pt pretreated at 633 K (Figs 1 and 2).

* We thank one of the referees for this suggestion.

Table IV

Transformation of cyclohexanol-[^{14}C]-cyclohexene, cyclohexanol-[^{14}C]-cyclohexane and cyclohexanol-[^{14}C]-benzene mixtures

	Composition (mol%)					
	C_6H_{12}	C_6H_{10}	C_6H_6	$C_6H_{10}O$	$C_6H_{11}OH$	C_6H_5OH
I Reagent	0.03	72.3	–	0.3	27.40	–
Product	3.0	20.05	46.25	2.0	25.1	3.3
II Reagent	27.8	–	–	0.07	72.1	–
Product	21.3	–	54.1	2.0	7.0	15.2
III Reagent	–	–	59.8	–	40.2	–
Product	–	–	63.8	4.5	19.0	12.7
Product*	–	–	63.9	3.6	14.3	18.2

	Specific radioactivity (r%/mol%)					
	C_6H_{12}	C_6H_{10}	C_6H_6	$C_6H_{10}O$	$C_6H_{11}OH$	C_6H_5OH
I Reagent	–	–	–	11.4	3.7	–
Product	–	–	0.25	4.8	2.5	2.7
II Reagent	–	–	–	0.12	1.38	–
Product	–	–	1.11	0.54	0.94	1.15
III Reagent	–	–	1.67	–	–	–
Product	–	–	1.57	–	–	–
Product*	–	–	1.57	–	–	–

Temperature 543 K, catalyst 0.1 g Pt; pretreated at 633 K; carrier gas 30 ml/min N_2
* T = 573 K

Table V

Transformation of a mixture of cyclohexanol-[^{14}C] and non-radioactive phenol

T (K)	Composition (mol%)				Specific radioactivity (r% mol%)				
	C_6H_6	$C_6H_{10}O$	$C_6H_{11}OH$	C_6H_5OH	C_6H_6	$C_6H_{10}O$	$C_6H_{11}OH$	C_6H_5OH	$\frac{C_6H_6}{C_6H_5OH}$
Reagent	–	0.8	65.3	33.9	–	8.97	1.48	–	
483	2.5	3.85	59.7	33.9	0.22	1.96	1.38	0.13	1.7
513	4.45	4.5	55.5	35.4	0.32	2.10	1.40	0.18	1.8
543	11.3	6.6	42.6	39.2	0.56	1.41	1.44	0.44	1.3
543*	0.2	2.9	63.5	33.3	1.140	1.98	1.38	0.025	45.6
573	6.05	6.3	41.8	45.5	0.50	1.34	1.45	0.44	1.2
603	1.8	4.3	49.5	43.3	0.91	3.10	1.27	0.31	2.9
633	2.3	3.25	51.6	42.6	0.74	1.08	1.46	0.28	2.6

Catalyst 0.1 g Pt; pretreated at 633 K; carrier gas 30 ml/min N_2
* Deactivated catalyst

Table VI

Comparison of cyclohexanol transformation over Pt black catalysts pretreated at 473 and 633 K

T (K)	Catalyst pretreatment (K)	Composition (mol%)							
		$<C_6$	C_6H_{12}	C_6H_{10}	C_6H_6	$C_6H_{10}O$	$C_6H_{11}OH$	C_6H_5OH	Others*
453	473	0.10	0.40	0	45.5	14.6	36.8	2.6	0
	633	0.055	0.02	0	5.8	8.3	81.6	4.2	0
513	473	0.40	0.24	0	73.9	8.4	11.9	5.1	0
	633	0.10	0.01	0.0003	3.1	7.1	72.6	17.0	0.114
573	473	1.27	0.03	0	85.3	1.9	3.2	8.2	0.18
	633	0.48	0.01	0.001	5.0	5.0	41.5	48.0	0.08
603	473	1.81	0.01	0	42.1	3.3	6.8	45.4	0.62
	633	0.56	0.004	–	2.8	4.8	40.7	51.0	0.11
633	473	0.83	0.01	0.0001	10.7	5.0	17.3	65.7	0.44
	633	0.99	0.01	0.003	4.4	4.0	31.9	58.4	0.29

Catalyst 0.1 g; carrier gas 30 ml/min N_2; reagent 1 μl cyclohexanol
* 0–8 unidentified products

Discussion

The main pathways of cyclohexanol reactions on platinum catalysts deduced from the enumerated radiotracer and other studies are depicted in Fig. 3.

This scheme consists of three triangular reactions. Two of them involves hydrogenation–dehydrogenation processes between aromatic and saturated C_6 rings (with or without an OH group) with a double bonded intermediate in both cases (cyclohexene and cyclohexanone, respectively; the latter eventually in its enolic form). The six reactions of these two triangles have been found to be reversible. The two irreversible reactions shown in the scheme represent

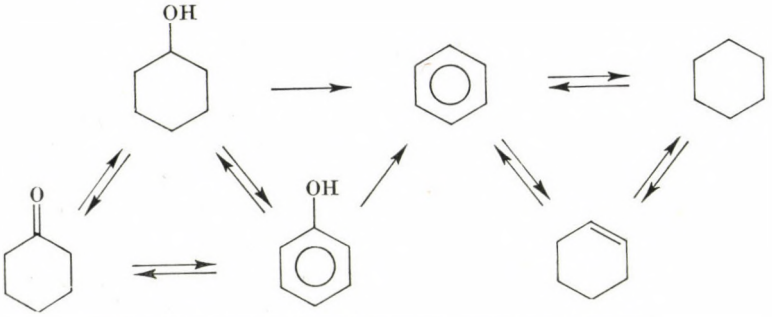

Fig. 3. Scheme of possible reactions of cyclohexanol

the formation of hydrocarbons from the oxygenated compounds: they both lead to benzene. The other two possible hydrocarbon producing reactions mentioned in the introduction have been found to be negligible under the conditions applied.

The peculiarity of platinum as compared with nickel and copper [7,8] is 'direct' phenol formation, that is, it can interact also with the six-membered ring and not only with the polar OH group. It is likely, therefore, that the adsorption of the reactant takes place in a 'planar' way (Fig. 4) [12].*

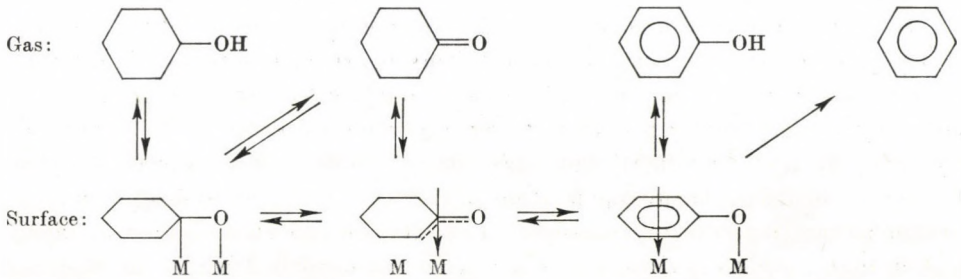

Fig. 4. Possible surface intermediates in dehydrogenation and dehydroxylation of cyclohexanol

The participation of the polar O-atom in the formation of the reactive surface species should be favourable (although not necessary, as shown by the rather large contribution of the stepwise dehydrogenation reaction *via* cyclohexanone).

This is supported also by the fact that the radioactivity of benzene was nearly equal to that of phenol in those cases, too, when the initial mixture contained cyclohexane (Table IV), consequently, the dehydrogenation (and subsequent dehydroxylation) of cyclohexanol into benzene is much faster than the dehydrogenation of (inactive) cyclohexane.

One of the reasons why the presence of the oxygen atom facilitates dehydrogenation may be that it promotes the $sp^3 \longrightarrow sp^2$ rehybridization of the carbon atom to which it is linked. Once this transformation has taken place with one of the carbon atoms, further dehydrogenation may proceed rather rapidly. This is shown by the data in Table IV indicating that the dehydrogenation of cyclohexene (with 'ready' sp^2 C-atoms in the molecule) is faster than that of cyclohexanol, whereas the latter exhibits much higher reactivity than cyclohexane. The appearance of a π-bond in the molecule (*cf.* Fig. 4) weakens its other C–H bonds, too.

* We cannot be sure whether the species shown is the only possible structure for adsorbed cyclohexanol.

The surface intermediate of dehydrogenation of the OH-substituted C_6-ring presumably involves a species adsorbed with participation of the oxygen atom. According to the scheme, 'direct' phenol and benzene formation involve the same surface intermediates as the 'stepwise' reactions but they do not desorb (Fig. 4).

In a preliminary paper [12], it has been suggested that the assumption of a planar surface complex explains all the reactions shown in Fig. 3. This, however, may be true only if we assume that hydrogen 'economy' is an important factor influencing product composition. It must be remembered that the formation of cyclohexanone and phenol involves hydrogen liberation, whereas the formation of benzene *via* hydrogenolytic splitting of the phenolic OH group consumes hydrogen; the resulting benzene, in turn, can be hydrogenated into cyclohexane. Several factors should be considered here: the presence of *gaseous hydrogen* promotes C_6 hydrocarbon formation; it is determined by (temperature dependent) *thermodynamics* whether they appear as cyclohexane or benzene. In nitrogen atmosphere, two types of hydrogen may be present: that from the pretreatment in hydrogen and that formed upon dehydrogenation; both of them may exist in various adsorbed [19,20] or absorbed [21] forms. Their availability for secondary reactions depends on the hydrogen retention ability of the catalyst. This, in turn, is the function of the *temperature*, the catalyst *activity level* and – apparently – of its *pretreatment*.

In terms of these '*primary*' and '*secondary*' hydrogen effects, [22] the decreasing benzene formation at higher temperatures and with catalyst deactivation can be explained satisfactorily. Since the aromatic ring has a tendency to be adsorbed dissociatively and this species can be removed by hydrogen treatment from the surface, it is not surprising that 'direct' benzene formation from cyclohexanol increases over deactivating catalysts, *i.e.* the desorption of the surface phenol intermediate is not favoured under these conditions [23]*.

Whereas the relative order of rates of various reactions (except for phenol hydrogenolysis) is approximately the same with the two types of platinum catalysts, the large differences in benzene formation and its behaviour under the conditions of catalyst deactivation (*cf.* Figs 1 and 2) clearly show that the hydrogen retention ability of these two catalysts is not the same. Although the underlying reasons may not be quite clear at present, this gives evidence that different temperatures of platinum pretreatment lead not only to different crystallite sizes [17] (and consequently, to different specific surfaces) but also to different sorption and catalytic properties (including resistance against deactivation).

* Since the specific activity of benzene is lower than those of phenol and cyclohexanol, inactive cyclohexanone must also participate in benzene formation. This can be visualized *via* adsorbed surface species as depicted in Figure 4.

Benzene formation (as the most sensitive reaction with respect to hydrogen) shows a definite drop above about 573 K. This indicates that its formation must be connected with the presence of a particular type of adsorbed hydrogen (δ [19] or ε [20]), which is not present at higher temperatures. Further studies are necessary to identify this active type of hydrogen.

[1] LYUBARSKII, G. D., STRELETS, M. M.: Khim. Prom., **43,** 481 (1967)
[2] SAITO, Y., HIRAMATSU, N., KAWANAMI, N.: Bull. Jap. Petrol. Inst., **14,** 164 (1972)
[3] FREIDLIN, L. K., SHARF V. Z., SMOLYAN, Z. S.: Zh. Prikl. Khim., **32,** 901 (1959)
[4] BALANDIN, A. A., TÉTÉNYI, P.: MTA Kém. Tud. Oszt. Közl., **2,** 299 (1959)
[5] CUBBERLEY, A. H., MÜLLER, M. B.: J. Am. Chem. Soc., **69,** 1535 (1947)
[6] SWIFT, W. E., BOZIK, J. E.: J. Catal., **12,** 5 (1968)
[7] PAÁL, Z., PÉTER, A., TÉTÉNYI, P.: Z. Phys. Chem. N. F., **91,** 54 (1974)
[8] PAÁL, Z., PÉTER, A., TÉTÉNYI, P.: React. Kinet. Catal. Lett., **1,** 121 (1974)
[9] RICHARDSON, J. R., LU, W. C.: J. Catal., **42,** 274 (1976)
[10] TÉTÉNYI, P., PAÁL, Z., DOBROVOLSZKY, M.: Z. Phys. Chem. (Frankfurt), **102,** 267 (1967)
[11] VOL-EPSTEIN,, A. B., ZHOROVA, M. N., BORENTS, A. D.: Neftekhimiya, **6,** 817 (1966
[12] MANNINGER, I., PAÁL, Z., TÉTÉNYI, P.: J. Catal., **48,** 344 (1977)
[13] GUERRIER, E., POLITZER, M., GUILLAUME, R.: Bull. Soc. Chim. Fr., 2882 (1970)
[14] ANTIPINA, T. V., KIRINA, O. F.: Dokl. Akad. Nauk SSR, **207,** 121 (1972)
[15] TÉTÉNYI, P., SCHÄCHTER, K.: Acta Chim. Acad. Sci. Hung., **65,** 253 (1970)
[16] TÉTÉNYI, P., BABERNICS, L.: Acta Chim. Acad. Sci. Hung., **35,** 419 (1963)
[17] BAIRD, T., PAÁL, Z., THOMSON, S. J.: J.C.S. Faraday I, **69,** 1237 (1973)
[18] PAÁL, Z., TÉTÉNYI, P.: Acta Chim. Acad. Sci. Hung., **53,** 193 (1967)
[19] TSUCHIYA, S., AMENOMIYA, Y., CVETANOVIC, R. J.: J. Catal., **19,** 245 1(970)
[20] MÓGER, D., HEGEDÜS, M., BESENYEI, G., NAGY, F.: React. Kinet. Catal. Lett., **5,** 73 (1976)
[21] PAÁL, Z., THOMSON, S. J.: J. Catal., **30,** 96 (1973)
[22] BRAGIN, O. V., KARPINSKI, Z., MATUSEK, K., PAÁL, Z., TÉTÉNYI, P.: to be published
[23] MANNINGER, I., PAÁL, Z., TÉTÉNYI, P.: Magyar Kém. Foly., **82,** 267 (1976)

István MANNINGER
Zoltán PAÁL
Pál TÉTÉNYI
H-1525 Budapest, P.O. Box 77.

Acta Chimica Academiae Scientiarum Hungaricae, Tomus 97 (4), pp. 451—458 (1978)

CLEAVAGE OF THE HETEROCYCLIC RING OF ISOFLAVONOIDS BY NUCLEOPHILIC REAGENTS, VI

STABILITY OF THE HETERO RING OF MONOSUBSTITUTED ISOFLAVONES

V. SZABÓ and M. ZSUGA

(Institute of Applied Chemistry, Kossuth Lajos University, Debrecen)

Received July, 4, 1977

On the basis of kinetic examinations it is concluded that the substituents attached to isoflavone modify the stability to bases of the parent compound **Ia** in accordance with their nature and position, and their action is determined by the strength of their influence on the electron density at the C-2 atom of the molecule. Steric effects of the substituents are less crucial.

In our previous papers [1–3], the ring cleavage reaction and decomposition of unsubstituted isoflavone were discussed. It was established that the two reactions are kinetically independent. The first one is reversible and the rate-determining step is a bimolecular AN_2 addition, while the other is a hydrolysis reaction being by several orders of magnitude slower than the former [4]. A correlation between the sensitivity of the isoflavone molecule towards nucleophilic reagents and its structure has been indicated by some researchers earlier [5], however, there are no investigations published which provide a quantitative evalution of the ring stability of the isoflavone molecule. Since the rate of the AN_2 reaction at the C-2 atom (**I** → **II**) depends evidently on the charge density on this atom, that is, on the substitution conditions of the isoflavone molecule, the rate constant of this reaction may be characteristic of the nucleophilic reactivity or stability of the molecule.

In the present paper, the correlation between the stability of the ring of monosubstituted isoflavones (their nucleophilic reactivity) and the substitution conditions is discussed.

Experimental

Kinetic measurements and evaluation of the results were carried out as described in an earlier paper [1] under the conditions given for pseudofirst-order reactions, and the apparent rate constants were calculated from the relationship

$$k_b = 1/t \cdot \ln \frac{E_\infty^\lambda - E_t^\lambda}{E_\infty^\lambda - E_0^\lambda},$$

where E_t^λ is the light adsorption of the solution at time t; this was measured at $\lambda = 290$ nm when the substituent was MeO, and at 310 nm, when C-2 alkyl or –COOH substituents were present.

The ring cleavage rate constants (k_1) were calculated on the basis of the correlation

$$k_b = k_1[OH^-] \ .$$

In both cases, the accuracy of the constants was checked by back-calculating.

Results and discussion

The MeO-substituted isoflavones (**Ib-e**) show spectral changes in alkaline medium identical with those exhibited by the unsubstituted isoflavone, *i.e.* a broad, intense band appears at about 290 nm, which has a constant intensity for a relatively long time (Fig. 1), then slowly weakens and the spectrum tends to that of the corresponding 2-hydroxydeoxybenzoin in alkaline medium.

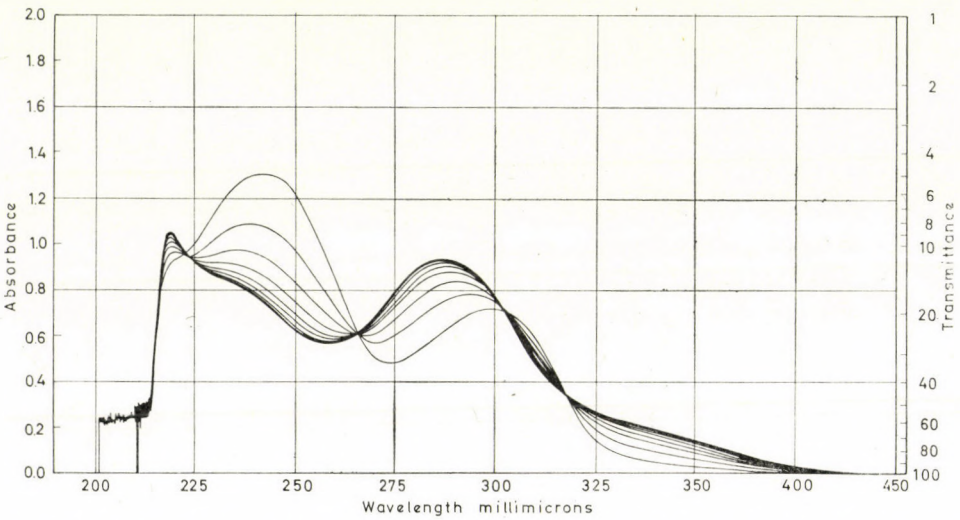

Fig. 1. Change of the spectrum of 7-MeO-isoflavone at 20 °C, $C_{IF} = 5 \cdot 10^{-5} M$, $[OH^-] = 0.1\ M$, $\Delta t = 3$ min

In our previous paper [1], this spectral change with time was attributed to the development or disappearance of the equilibrium system **III** $\rightleftharpoons$ **IV**, *i.e.* to the hydrolysis of **III** into **V**.

The rate of the conversion **I** → (**II**) → **III** → **IV** (in which the rate-determining step is **I** → **II** in the given group of monosubstituted isoflavones, too) seems to be much higher than that of the hydrolysis step **III** → **V**, also on the basis of a qualitative evaluation of the spectral change, therefore the rate of the ring cleavage reaction could be examined in the same way as in the case of unsubstituted isoflavone [1].

Ia: $R_1 = R_2 = R_3 = H$

Ib: $R_1 = R_3 = H$; $R_2 = 2'$-MeO

Ic: $R_1 = R_3 = H$; $R_2 = 4'$-MeO

Id: $R_2 = R_3 = H$; $R_1 = 6$-MeO

Ie: $R_2 = R_3 = H$; $R_1 = 7$-MeO

If: $R_1 = R_2 = H$; $R_3 = COOH$

Ig: $R_1 = R_2 = H$; $R_3 = Me$

Ih: $R_1 = R_2 = H$; $R_3 = Et$

Ii: $R_1 = R_2 = H$; $R_3 = CF_3$

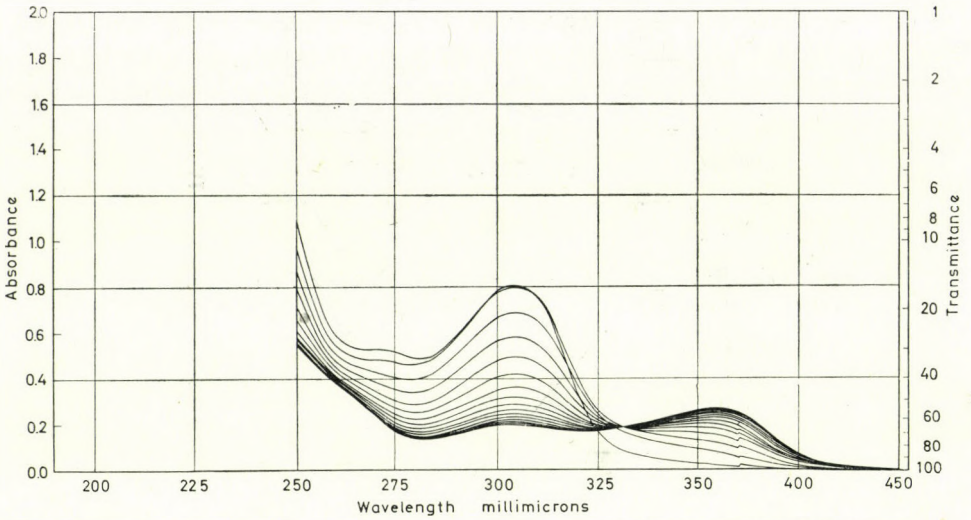

Fig. 2. Change of the spectrum of 2-Me-isoflavone at 30 °C, $C_{IF} = 10^{-4}M$, $[OH^-] = 0.6\ M$, $\Delta t = 3$ min

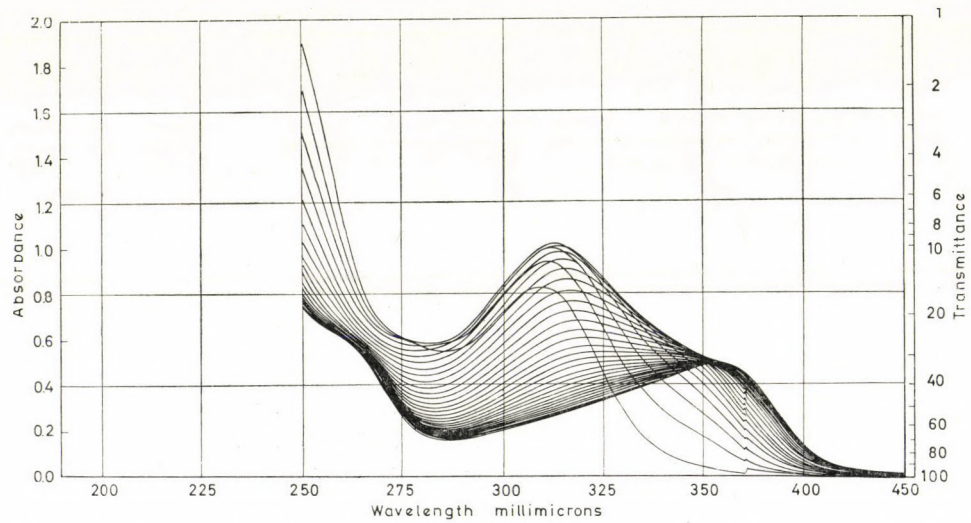

Fig. 3. Change of the spectrum of 2-COOH-isoflavone at 30 °C, $C_{IF} = 10^{-4}M$, $[OH^-] = 0.8M$, $\Delta t = 5$ min

In C-2 substituted isoflavones (**If-i**), the spectral situation and the rate relations of the two part-reactions differ significantly from the previous picture. In **Ig, h, i** the spectra show a **I** → **V** transition (Fig. 2), thus the rate of the ring cleavage reaction is lower than that of the formation of 2-hydroxydeoxybenzoin, while the spectral change in **If** (Fig. 3) indicates commensurable rates of the two part processes mentioned.

Since isoflavones **Ib-e** yield formic acid, compounds **If-i** are converted into the corresponding alkanecarboxylic acid and 2-hydroxydeoxybenzoin on decomposition, furthermore, the character of the changes of the spectra (except for **Ig, h, i**) is identical with those obtained with unsubstituted isoflavone, it can be stated that the mechanism of the ring cleavage and decomposition of substituted isoflavones must be identical with that observed for the unsubstituted compound. The deviation of the kinetic constant (k_1) of ring cleavage from that of isoflavone is a measure of the modification of the hetero ring on the effect of the substituent, this it affords information on the stabilizing action of the substituent.

This substituent effect is demonstrated by the dependence of the apparent reaction rate constants (k_b) on the hydroxide ion concentration (Fig. 4). The slopes of the straight lines in Fig. 4 give the rate constant of ring cleavage (k_1) [1].

Since the ring cleavage proceeds by the same mechanism in all substituted isoflavones examined, the effect of substituents can be expressed most simply by the rate constant of the ring cleavage related to that of isoflavone:

$$\gamma' = \frac{k_1 \mathrm{H}}{k_1 \text{ subst.}} .$$

The data in Table I and in Fig. 4 show that, except for **Ii**, the substituents increase the relative rate constant of ring cleavage, that is, the ring stability of isoflavone, to an extent depending on their character and position. The extent of the stabilizing action of the substituents is evidently dependent on their electron-donating activity at C-2as compared with the case of isoflavone (**Ia**). This effect which can also be expressed quantitatively by γ', can be explained by the mesomeric forms **VI** ↔ **X**. Comparison of the mesomeric forms and the rate constants, k_1, allow to assume that the stability of the ring is increased by those substituents which hinder the development of structures **X** and **VII**, **VIII** by their electron-donating action. This statement is in accordance with the nucleophilic sensitivity of the pyrylium cation described in the literature [6] and with our earlier suggestion regarding the mechanism of ring cleavage [1–3].

In support of this assumption, a value regarding the stability of chromone must be given first here, which will be discussed in detail only later. The constant for the ring cleavage of chromone is $k_1 = 0.476$ $\mathrm{min^{-1}mole^{-1}}$, thus chromone is more stable by one order of magnitude than 3-phenylchromone (isoflavone, **Ia**). The 3-phenyl group is involved in a conjugative relationship with the $C_2 = C_3$ double bond and, as shown by the limiting form **VIII**, it reduces the charge density at the C-2 atom thus increasing the nucleophilic reactivity at this site. The presence of electron-donating groups in the phenyl group

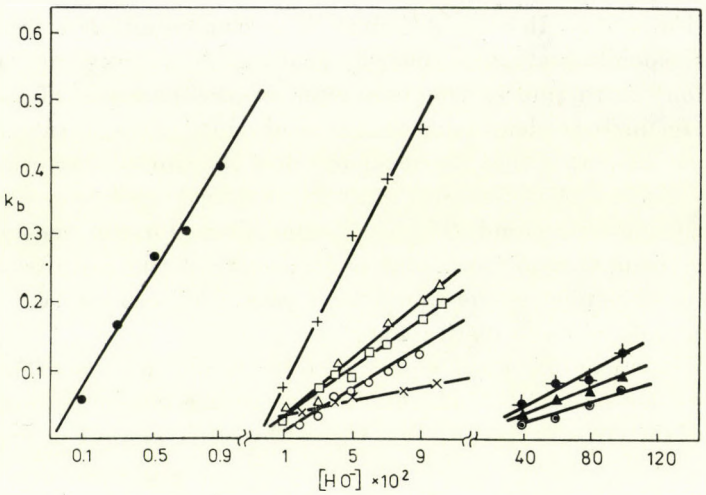

Fig. 4. Dependence of the apparent rate constants of the ring cleavage reaction of isoflavone derivatives on the hydroxyl ion concentration at 25 °C; – . – . – Ii; – + – + – Ia; – Δ – Δ – Δ – Ib; – □ – □ – Id; – ○ – ○ – Ic; – × – × – Ie; – ⊠ – ⊠ – If; – ▲ – ▲ – Ih; – ⊙ – ⊙ – Ig

Table I

Rate constants (k_1) of ring cleavage of substituted isoflavone derivatives at 25 °C

Substituent	k_1(mole^{-1}min^{-1})	Intersect	$\gamma = k_{1H}/k_1$ subst.
Ia H	5.21 ±0.23	0.006 ±0.051	1.00
Ib 2'-MeO	1.95 ±0.23	0.043 ±0.055	2.67
Ic 4'-MeO	1.31 ±0.1	0.0016±0.025	3.98
Id 6-MeO	1.41 ±0.011	0.013 ±0.028	3.70
Ie 7-MeO	0.45 ±0.05	0.031 ±0.025	11.58
If 2-COOH	0.115 ±0.03	0.006 ±0.03	45.30
Ig 2-Me	0.0475±0.005	0.018 ±0.024	109.6
Ih 2-Et	0.0976±0.004	0.006 ±0.003	53.4
Ii 2-CF_3	41.81 ±3.5	0.027 ±0.25	0.12

in *o*- and *p*-position to the linkage counteracts this effect, resulting in the higher (increasing) stability of the C_2' and C_4'-MeO-isoflavones (**Ib**, **Ic**), as compared with **Ia**.

The C_7-MeO group which has the largest stabilizing action is in conjugative interaction with the CO group having a large -*M* effect. The groups are coplanar and the interaction is 'undisturbed'. This will indirectly increase the electron density at the C-2 atom, since it hinders the development of the benzopyrylium structure (**X**).

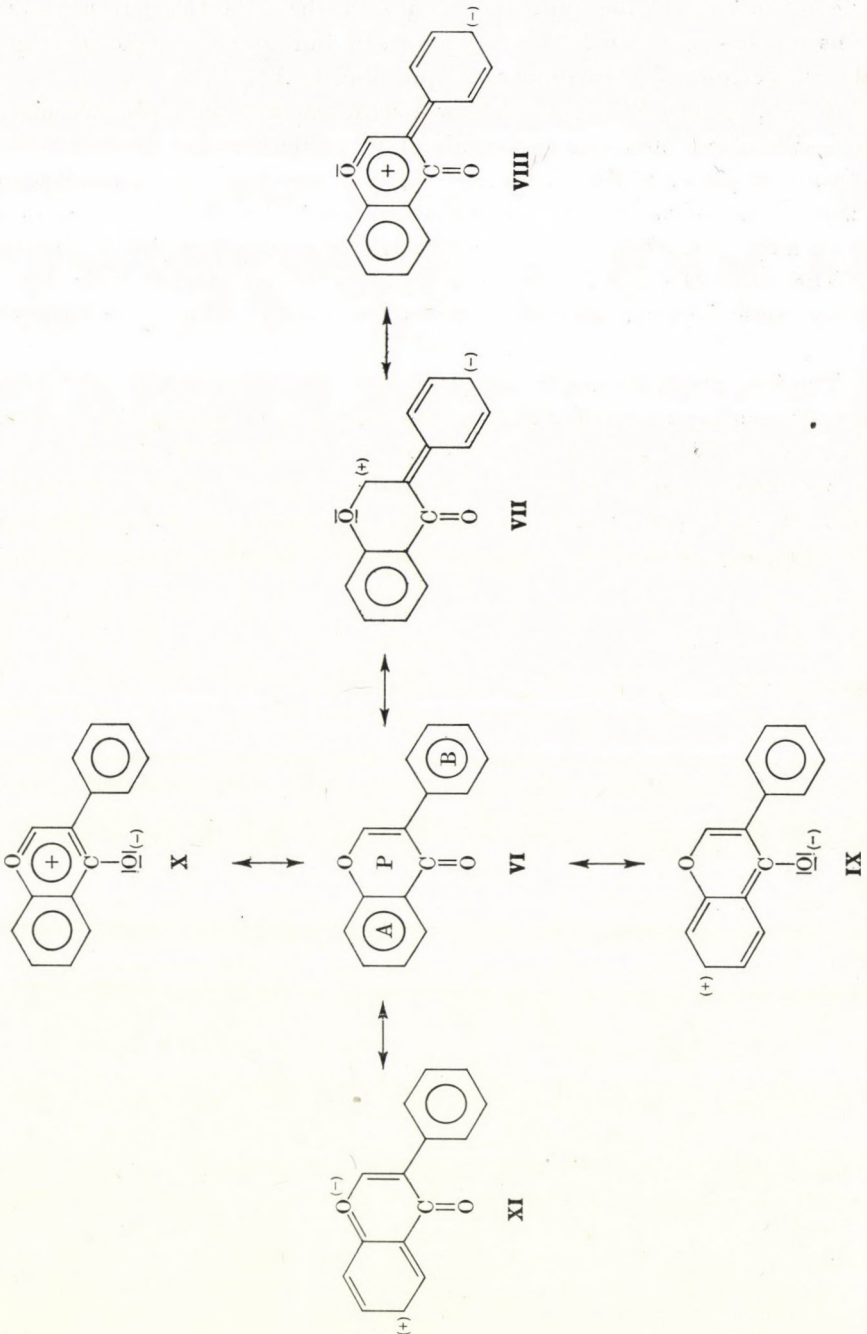
VIII
VII
X
VI
IX
XI
A
P
B

On the basis of the limiting formula **XI**, the C_6-MeO group will increase the charge density at the hetero oxygen atom thus hindering the development of the π-electron delocalization corresponding to **X**.

The C_4'- and C_2'-MeO groups show a significantly lower effect as compared with C_7-MeO, and this can be explained by steric reasons. Ring B will turn out from the plane of the chromone ring [7], therefore, the delocalization of the π-electrons of the $C_2 = C_3$ bond and of ring B will be less pronounced, consequently, the effect of the electron donor substituent will be weakened.

The effect of the C-2 substituents can be better explained by electronic than by steric factors, since the highest stabilizing action is exerted by the methyl group having the lowest spa.ce requirement.

The CF_3 group having the largest space requirement makes the molecule definitely unstable, therefore, by comparing the γ' values for compounds **Ig, h, i**, it can be assumed that the isoflavone molecule is stabilized by the hyperconjugation effect of the methyl and ethyl groups, while the significant **-I** effect of the CF_3 group makes it strikingly unstable. These data also support our assumptions discussed above, regarding the pyrylium character and the stability.

REFERENCES

[1] SZABÓ, V., ZSUGA, M.: Acta Chim. (Budapest) **85,** 179 (1975)
[2] SZABÓ, V., ZSUGA, M.: Acta Chim. (Budapest) **85,** 191 (1975)
[3] SZABÓ, V., ZSUGA, M.: Acta Chim. (Budapest) **88,** 27 (1976)
[4] SZABÓ, V., ZSUGA, M.: Reaction Kinetics and Catal. Letters **5,** 229 (1976)
[5] SZABÓ, V.: Candidate Thesis, Debrecen, 1958; WALZ, E.: Ann. **489,** 118 (1931); ELDERFIELD: Heterocyclic Compounds vol: II, p. 257. New York 1951; SANNIE, Ch., SAUVAIN, H.: Les couleurs des fleurs et des fruits. Paris, 1952; INOUE, N.: The Sci. Rep. Tohoku Univ. Ser. I **XLV (2),** 73 (1961)
[6] LEMPERT, K.: Szerves Kémia, Műszaki Könyvkiadó, Budapest 762 (1976)
[7] DINYA, Z.: Private communication

Vince SZABÓ
Miklós ZSUGA
H-4010 Debrecen 10.

RECENSIONES

Reviews on Analytical Chemistry

Ed. W. FRESENIUS Joint edition of Akadémiai Kiadó, Budapest and Masson S. A. Paris 1977. 253 p.

The book contains the opening and plenary lectures of the 2nd Euroanalysis Conference August 1975, Budapest, and gives an excellent cross section on the present state of the analytical fields of greatest interest in our days. The authors of the book are highly competent experts of their subject and thus the chapters truly summa rize the most important results and trends of the selected branches of science in an authentic and clear-cut form, with extensive bibliographies.

The book, a publication of the conference of the Analytical Working Committy of the Federation of European Chemical Societies (FECS), is one of the first important and representative documents of the collaboration of European analytical chemist. The cover features the stylized emblem of FECS.

It is rather regrettable that papers presented in 1975 are published only two years later, in 1977. In spite of this delay, the chapters are still fresh, and probably will be useful for furher 5 – 10 years for analysts who wish to keep abreast of advances in their field.

The first part of the book contains the opening lectures. The papers discuss and evaluate the past development of analytical chemistry and indicate trends for the future. The paper of W. FRESENIUS summarizes the most important events of the last 20 years, the paper of F. SZABADVÁRY gives the history of analytical chemistry in Hungary, and the paper of E. PUNGOR surveysthe present state of analytical sciences in Hungary. The paper of A. DIJKSTRA outlines the future of analytical sciences.

The first of the series of plenary lectures is the paper of J. T. CLERC on the importance of modern instrumental methods of organic analysis, and their significance in teaching. The study of Z. GALLUS gives a survey on the present state of voltammetric methods.

Problems of the basic processes of stripping voltammetry and the very good detection limits ($\sim 10^{-11}M$) of modern techniques are discussed in detail. R. E. KAISER reports on a new technique, high performance thin-layer chromatography, and the remarkably high attainable efficiency (separation of 11 different substances over a distance of 24 mm in 1 min). The paper of H. MALISSA deals with the role of analytical chemistry in environmental protection. The detailed study, discusses from the theory of systems associated with technical problems of the protection of the biosphere. In the extensive tables a great number of important data are condensed on the composition of the tropo-, hydro- and lithosphere. Finally, a strict critical discussion and evaluation is given on the applicable analytical methods.

D. L. MASSART, H. De CLERCQ and R. SMITS are co-authors of a review discussing and evaluating mathematical methods for the design and optimization of analytical methods. The paper describes the application of information theory in the selection of the appropriate chromatographic method, and evaluates on hand of examples the method of steepest descent, introduced by BOX and WILSON, the simplex method, etc. in the determination of the most suitable experimental parameters.

H. R. OSWALD and E. DUBLER discuss thoroughly and extensively, with many references, the possible applications of thermoanalytical methods in quantitative analysis.

The paper of F. PELLERIN and J. E. LETAVERNIER deals with one of the most important problems of contemporary biochemistry, the analysis of drug metabolites. In the investigation

of drug metabolites, analytical chemistry has a very important and decisive role. Of these methods, primarily chromatography has an outstanding role. Electrochemical (polarographic), photometric, fluorometric and enzymatic methods, too, proved to be very useful. The subject of the review of E. PUNGOR and K. TÓTH is the present state of research on ion-selective electrodes. After a description of novel (enzyme) electrodes, problems in conjunction with the standardization and calibration of electrodes, and finally their application in continuous analysis are discussed, with many references. E. ZIEGLER surveyed the most important fields and aspects of the analytical application of computers. In addition to new methods developed with the aid of the computer (Fourier spectroscopy), the application of computers greatly improved the efficiency of X-ray diffraction and mass spectrometric methods, and increased the speed of determination of structure.

The subjects of the plenary lectures actually comprise the most important results of the fields mentioned, with an evaluation and references. Thus, it will give reliable information and good orientation for the readers.

Orientation is facilitated by a subject index. The book of nice presentation, a credit to the work of Akadémiai Kiadó, will be a useful and enjoyable reading to chemists interested in the advances of their own branch of science, and willingly contributing with their work to the development of analytical chemical sciences.

J. INCZÉDY

B. RÅNBY, J. F. RABEK: *ESR Spectroscopy in Polymer Research*

Springer-Verlag, Berlin—Heidelberg—New York, 1977. 410 pages, 365 figures.

The book continues the series "Chemie, Physik und Technologie der Kunststoffe in Einzeldarstellungen", entitled now "Polymers, Properties and Applications". It contains 13 chapters very accurately subdivided to numerous sections and subsections. In the first three chapters the basic principles of free radical chemistry and ESR technique are discussed very briefly in 53 pages. The next chapter deals with ESR study of polymerization processes in 111 pages outlining rather thoroughly the main experimental results. In chapter 5 the ESR study of degradation processes in polymers is discussed in 74 pages with special emphasis on radiation and photo-degradation processes. Chapter 6 deals with the effect of reactive gases on polymers as studied by ESR spectroscopy; it is a very short chapter of 5 pages followed by a 13-page one discussing oxidation of polymers. The subsequent chapters deal with molecular fracture (mechanochemistry), grafting and crosslinking (chapters 8, 9 and 10, respectively).

In chapter 11 the spin-probe and spin-labelling techniques of studying molecular mobilities in polymers are discussed in 11 pages, followed by a 33-page chapter dealing with ESR spectroscopy of stable polymer radicals and their low molecular analogues. In the last, short (1/2 pages) chapter some results on ion-exchange resins are demonstrated.

In the last 2 decades the ESR technique has become one of the basic tools in polymer chemistry especially in studying radical reactions. Quite a number of books have been published about the application of the ESR technique in chemistry including chemistry of polymers. The work of RÅNBY and RABEK is, however, the first, which tries to collect comprehensively the ESR-data available particularly in polymer research. In the last 15 – 20 years quite a lot of work has been done in this field in several laboratories all over the world and the author's effort to review it came quite in time. The number of references cited in the book is 2519 which, itself, shows how difficult is to treat them in a legible coherent way. The authors, apparently, wanted to present the experimental results without caring too much for theoretical interpretation.

As a result the book is indeed a very valuable source of information for specialists who want to study a particular polymer system and would like to know what has been done in this particular field so far. In this respect chapter 4: "ESR study of polymerization processes" and chapter 5: "ESR study of degradation processes in polymers" are especially valuable. It seems doubtful, however, why graft copolymerization has been separated from polymerization and also why oxidation and mechanical fracture of polymers are separated from degradation. To the reviewer it seems that a guiding theoretical conception is missing in the structure of the book, which would help the reader to form a uniform picture of the processes discussed. Evidently the authors tried to present the experimental facts only without further interpretation leaving this job to the readers. Although experimental polymer chemists are not especially enthusiastic in using concepts of quantum chemistry, the structure of free radicals and the corresponding ESR spectra are hardly understandable without them. At least determination

of spin densities from the experimental spectra should have been included. By using quantum aspects the apparently wide and scattered field of polymer chemistry covered by the book could have been presented probably in a more coherent way.

The apparent impartiality of the authors in discussing particular problems is also somewhat embarrassing. The authors are known as outstanding specialists of many fields covered by the book: one would be interested in learning their opinion about certain questions discussed heavily in the literature. This would, evidently, lenghthen the volume considerably but the theoretical and practical importance of the subject should verify it.

Nevertheless, the book even in its present form, will most likely become one of the basic sources of information about experimental facts in free radical polymer chemistry in the next decade, especially when used together with the available textbooks and monographs dealing with the theoretical aspects. For beginners in ESR work simultaneous use of additional textbooks of basic theory and technique of ESR spectroscopy is recommended.

P. HEDVIG

H. HAKEN: *Synergetics*

Springer-Verlag, Berlin–Heidelberg–New York, 1977, 323 pages, 125 figures

Many scientists who were raised on the good old thermodynamics – or thermostatics, as it has been renamed in the recent years – have witnessed a growth in the number of experimental evidences which proved that some chemical processes take place periodically in time and/or space. These complicated reactions were so much unusual and unexpectable on the grounds of classical thermodynamics that some scientists even voiced their doubts in its fundamental laws, while others considered the oscillatory phenomena as experimental artifacts. However, what seemed to be unique in chemistry is quite common in many other branches of science. From the spacial periodicity of fleecy clouds to swirls in turbulent flows to the circadien, monthly, and yearly periodicity of living creatures, nature provides countless examples of oscillatory phenomena. To explain all this, statistical physicists had to look for initial and boundary conditions which direct the solution of the equations of motion in such a way that the results would describe the periodicity in time or space.

HAKEN's is a very good introductory textbook to this new branch of science (so far finding most of its applications in theoretical physical chemistry) specified by the subtitle as "*non-equilibrium phase transitions and self-organization in physics, chemistry, and biology*". The outline of this topic is, perhaps, best represented by the list of the chapter titles and the short-sentence mottos attached to them: 1. Goal – Why you might read this book, 2. Probability – What we can learn from gambling, 3. Information – How to be unbiased, 4. Chance – How far a drunken man can walk, 5. Necessity – Old structures give way to new structures, 6. Chance and necessity – Reality needs both, 7. Self-organization – Long-living systems slave short-living systems, 8. Physical systems, 9. Chemical and biochemical systems, 10. Applications to biology, 11. Sociology: a stochastic model for the formation of public opinion.

The introductory chapters (1 to 5) give all the necessary mathematical and statistical physical tools to the reader to understand what is going on in the next chapters. Of course, as it is usual with books aimed to be self-sufficient, this part is rather a short and elegant recapitulation of the mathematics and physics the reader already knows than a replacement of necessary basic textbooks. In Chapter 6 the Fokker-Planck equation is treated and solved for stationary and time-dependent cases. Chapter 7 gives some further solutions of the Fokker-Planck equation and the master equation with results explaining the essential features of self-organization, and non-equilibrium phase transitions are handled with the use of the Ginzburg-Landau equation. The different laser phenomena and fluid dinamics are treated in Chapter 8. As chemical oscillatory systems, the so-called Brusselator and Oregonator are described in Chapter 9 as well as some basic biological processes showing periodicity in time. In the next chapter some typical biological applications are discussed such as population dynamics, the predator–prey system, evolution, and morphogenesis. Rather a perspective than a real discussion of sociological problems is given in Chapter 12. Finally the author circumscribes the subject of the new discipline *synergetics* – the science studying the laws by which the co-operation of the subsystems of a system is governed to organize it for a given performance – and its possible future applications.

The reviewer cannot but recommend this clearly written, logically structured, fascinating book to students and scientists interested in physical or quantitative social sciences.

I. RUFF

Advances in Chemistry Vol. 35.

Vol. 35.
Ed. B. CSÁKVÁRI. Akadémiai Kiadó, Budapest 1977. 218 pp.

Volume 35 comprises three longer studies, which are not closely connected with one another.

The first study is by Tibor ERDEY-GRÚZ and Sándor LENGYEL: "Proton transfer in solution", a 69-page summary on the fundamental mechanism of the anomalous electric conductivity of solutions. This phenomenon is of particular importance in aqueous solutions. The authors investigate extensively the anomalous mobility of the ions of solvent molecules and the effect of the change in liquid structure on the conductivity by proton transfer. They give a very good summary on earlier and recent results pertinent to anomalous conductivity, discussing semi-empirical explanations and quantum-mechanical theories, mentioning even views contesting the conduction mechanism by proton transfer. They mention in their discussion the contribution of the given exchange reactions to transport processes (when meeting appropriate particles, the proton exchange water molecules), and give a modern theoretical approach on how, besides proton transfer, the hydrodynamical migration of H_3O^+ ions participates in the conduction of electricity by hydrogen ions.

As a final conclusion, the authors consider it as proved that H_3O^+ and OH^- ions of relatively long life are present in aqueous solution, strongly interacting with the solvent, and that proton transfer in succession between the respective ions and molecules along the hydrogen bond is possible only in liquids of a structure, in which aggregates connected by hydrogen bonds are present. The authors indicate that research in conjunction with anomalous conductivity is neither closed not free of contradictions even in the case of aqueous solutions, and that further experimental and theoretical investigations are needed to obtain reliable knowledge on the parameters of the steps of anomalous conduction. A list of 144 references closes the chapter.

Dénes BERÉNYI: "Fundamentals and recent results of the ESCA method". The study 100 p.) presents one of the new, very useful and promising methods of structural investigation, and is the first survey in Hungarian, written on this subject. The author discusses fundamentals, origin, theoretical basis, possible applications, results obtained and experimental techniques of the ESCA method (electron spectroscopy for chemical applications, or in other wording, electron spectroscopy concerned with applications). The main fields of application of the method are: chemical structural investigations, measurement of molecular orbitals, surface research, research of the band system of solids, and solving of certain qualitative and quantitative analytical problems, but there are also other, at present less frequented, promising fields of application.

As concerns research technique, the author discusses quantities measurable with the method, the electron spectrometer proper, relevant methods of preparation, irradiation, calibration, detection and data processing, and ESCA instruments available on the market.

The final conclusion of the author is that the ESCA method surpasses some of the very modern methods of chemical structural analysis, such as Mössbauer spectroscopy, NMR and infrared spectroscopy and mass spectroscopy, not with respect to resolution power, but by its more general applicability. Indeed, it is virtually suitable for all elements, and solid, liquid and gaseous samples alike can be investigated, generally in non-destructive tests.

The chapter includes an extensive bibliography of 349 references.

Tibor ERDEY-GRUZ, György HORÁNYI and Mrs. Zoltán SZETEY: "The state of platinum anode surfaces and kinetics of the oxygen electrode". The study (40 p.) deals with the mode of operation of the oxygen electrode, an electrochemical system relatively less investigated and known, but very important from the practical point of view, and discusses results attained so far. This is the more important and interesting, because actually unequivocal experimental conditions are more difficult to realize in the case of the oxygen electrode, than in that of the hydrogen electrode, so that the measurements and conclusions of the various authors must be evaluated also from this aspect. The authors investigate the problems of the equilibrium potential, rest potential and of platinum–oxygen interaction, the formation and properties of the oxide surface layer, the kinetics of the electrode and the reaction mechanism of anodic oxygen evolution.

The conclusion of the authors is that even today we are far from knowing the mechanism of anodic oxygen evolution, and further intensive work is needed to obtain from every aspect an overall picture of the processes. Particularly, the role of the oxide layer needs further elucidation, which, on the one hand, is a difficult experimental task, because this is a partial phenomenon difficult to investigate, while on the other hand, theoretical apparatus needed for its interpretation is still insufficient. This relatively shorter chapter closes with 69 references.

It should be mentioned that in the case of this study the actual title in the text and the title on the cover are not identical, and the latter is not even an abbreviation of the former, but concerns only one subject discussed in the chapter.

In summary, all three subjects of Volume 35 discuss very actual problems. The authors, known as the best experts of the subjects and successfully active in the field concerned, gave a very good survey of the results obtained so far in their branch of science and on further perectives.

With its clear style and good organization, the volume can be recommended to researchers and industrial chemists who wish to keep abreast of advances in their subject.

E. BERECZ

INDEX

PHYSICAL AND INORGANIC CHEMISTRY

ORGANIC CHEMISTRY

Printed in Hungary

A kiadásért felel az Akadémiai Kiadó igazgatója — Műszaki szerkesztő: Zacsik Annamária

A kézirat nyomdába érkezett: 1978. II. 2. — Terjedelem: 8,75 (A/5) ív, 42 ábra

78.5479 Akadémiai Nyomda, Budapest — Felelős vezető: Bernát György

ACTA CHIMICA

ТОМ 97 — ВЫП. 4

РЕЗЮМЕ

Комплексы шиффовых оснований с соединениями двуокиси урана (VI). V.

Комплексы дихлородвуокиси урана (VI) с двуосновными тридентатными основаниями Шиффа

Р. Г. ВИДЖЭЙ и ДЖ. Л. ТАНДОН

Описывается синтез производных типа $UO_2Cl_2(SBH_2)_2$. Они были получены на основе реакции 1 : 2 молярных количеств дихлородвуокиси урана(VI) с двуосновными тридентатными основаниями Шиффа (SBH_2), полученными конденсацией салицилальдегида, 2-гидрокси-1-нафтальдегида, о-гидроксиацетофенона, 2,4-пентандиона или 1-фенил-1,3-бутандиона с гидроксиалкиламинами (такими как 2-гидроксиэтиламин, 2-гидрокси-1-пропиламин и 3-гидрокси-1-пропиламин) или 2-гидроксианилином. Полученные комплексы были охарактеризованы на основе данных элементарного анализа, измерений проводимости и их ИК спектров.

Диффузия в системе елементарных каналов клиноптилолита

Э. ДЕТРЕКЁИ и Д. КАЛЛО

Исследуя диффузию молекул различных типов в системе элементарных каналов клиноптилолита с помощью ИК спектроскопии и гравиметрическим методом, было найдено что зависимость Баррера для масспереноси в изотропном монокристалле применима и для масспереноси в системе элементарных каналов клиноптилолита. На основе измеренных величин коэффициентов диффузии были сделаны заключения относительно природы и силы взаимодействий между адсорбтивом и атомами или функциональными группами стенок каналов в различных модификациях клиноптилолита, а также относительно структуры последних.

Анодное растворение алюминия в безводном умсуснокислом растворе хлористого лития

Л. КИШ, Л. СИРАКИ, Л. и М. ВАРШАНИ

Было изучено анодное растворение алюминия в безводном уксуснокислом растворе хлористого лития. Экспериментальные результаты указывают на то, что предполагаемый промежуточный продукт Al^+ окисляется молекулами уксусной кислоты или ионами $CH_3COOH_2^+$ до стабильных ионов Al^{3+}. Образующиеся при этом молекулы H_2 были идентифицированы с помощью алюминиевого диска и платинового кольца.

Нами описан метод, с помощью которого по зависимости эффективной валентности от потенциала электрода можно судить о механизме процесса. Этот метод в нашем случае неприменим, так как поверхность электрода имела большое омическое сопротивление.

О спонтанных процессах, происходящих на поверхности металлов, под влиянием собственных ионов, II

Л. КИШ, Й. ФАРКАШ, П. КОВАЧ и Л. КОЗАРИ

Были изучены процессы, происходящие в системе Cu/Cu(I)/Cu(II), при большом избытке ионов Cu^{+2} относительно равновесной концентрации, в водных растворах с 1,0 моль/дм³ HCl (20°C) и с 3,0 моль/дм³$HClO_4$ (60°C).

Установлено, что в растворе HCl скорость процесса определяется скоростью диффузии ионов Cu^{+2} к поверхности электрода. В растворе $HClO_4$ на поверхности электрода быстро устанавливается равновесие и ступенью, лимитирующей скорость процесса, является диффузия образующихся ионов Cu^{+} с поверхности электрода в глубину раствора.

Полученные результаты подчиняются уравнениям, выведенным нами ранее [1].

Исследование молекулярных взаимодействий нитробензола в четыреххлористом углероде при микроволных частотах

А. К. ШАРМА

Диэлектрическое поведение нитробензола в растворе четыреххлористого углерода было исследовано при восьми концентрациях (в интервале мольных долей 0,01—0,2), при 9,3 ГГц и 1,6 МГц и при 27°C. Молярная поляризация (P_2) и дипольный момент (μ) уменьшаются нелинейно с увеличением концентрации, в то время как относительное время релаксации (τ/τ) увеличивается. Полагается, что при низких концентрациях нитробензола в CCl_4 доминирует отрицательный эффект растворителя, в то время как при относительно высоких концентрациях побочные взаимодействия между растворенным веществом доминируют.

Ситез алкалоидов виика и родсвеииых им соедиеиий , V

Синтез стилового змира (±)-аповинкаминовой кислоты

ДЬ. КАЛАУШ, П. ДЬЁРИ, Л. САБО и Ч. САНТАИ

Исходя из триптамина, в результате четырехступенчатого ситеза был получен энамин со строением *7a*, присоединяя к которому этилорый эфир α-ацетоксиакриловой кислоты, было получёно производное *8a*. Восстановлеие соединения *8a* пруводит к двум стереоизомерным продуктам (*9* и *10*), весовия доля которых зависит от условий реакции.

Окисление производного *9b* с дальнейшим отщеплением воды приводит к рацемату зтилового зфира аповинкаминовой кислоты.

Гетероциклические аналоги простагландинов, тиазоли I

Г. АМБРУШ, И. БАРТА, ДЬ. ХОРВАТ, Ж. МЕХЕШФАЛВИ и П. ШОХАР

Описывается синтез dl-4-(6-карбоксигексил)-5-(3-гидрокси-1-*транс*-октенил)-тиазола и его 2-метильных аналогов. Приводятся и обсуждаются ИК и H^1—ЯМР данные, а также массспектроскопическое поведение новых производных тиазола.

Превращения циклогексанола, катализированные платиной, I

Процессы дегидрирования и дегидроксилирования

И. МАННИНГЕР З. ПААЛ и П. ТЕТЕНИ

Исследования с меченными молекулами указывают на то, что дегидрирование циклогексанола протекает как через образование циклогексанона, а также по «прямому» пути к фенолу. Углеводороды получаются в основном дегидроксилированием фенола. Температура, активность катализатора и подача водорода определяют состав продуктов и его сдвиги в двух трехугольных системах, включающих циклогексанол, циклогексанон и фенол, а также циклогексан, циклогексен и бензол, соответственно. Способность катализатора задерживать водород, которая, в свою очередь является функцией температуры предварительной обработки, также оказывает эффект.

Расщепление гетерокольца изофлавонов с помощью нуклеофильных реагетов, VI

Стабилизация гетерокольца монозамещенних изофлавонов

В. САБО и М. ЖУГА

Исходя из кинетических исследований, было заключено, что заместители молекулы изофлавона, соответственно их природе и расположению, так изменяют стабильность основного соединения (Ia) по отношению к основаниям, насколько увеличивают или уменьшают электронную плотность на атоме C_2 молекулы. Стерическое влияние заместителей сказывается в меньшей степени.

Les Acta Chimica paraissent en français, allemand, anglais et russe et publient des mémoires du domaine des sciences chimiques.

Les Acta Chimica sont publiés sous forme de fascicules. Quatre fascicules seront réunis en un volume (4 volumes par an).

On est prié d'envoyer les manuscrits destinés à la rédaction l'adresse suivante:

Acta Chimica
H-1521 Budapest, Hongrie

Toute correspondance doit être envoyée à cette même adresse.

La rédaction ne rend pas de manuscript.

Le prix de l'abonnement est de $ 36,00 par volume.

Abonnement — en Hongrie l'Akadémiai Kiadó l'Entreprise pour le Commerce Extérieur « Kultúra » (1389 H-Budapest 62, P.O.B. 149 Compte-courant No. 218 10990) ou à l'étranger chez tous les représentants ou dépositaires.

Die Acta Chimica veröffentlichen Abhandlungen aus dem Bereich der chemischen Wissenschaften in deutscher, englischer, französischer und russischer Sprache.

Die Acta Chimica erscheinen in Heften wechselnden Umfanges. Vier Hefte bilden einen Band. Jährlich erscheinen 4 Bände.

Die zur Veröffentlichung bestimmten Manuskripte sind an folgende Adresse zu senden:

Acta Chimica
H-1521 Budapest, Ungarn

An die gleiche Anschrift ist auch jede für die Redaktion bestimmte Korrespondenz zu richten.

Manuskripte werden nicht zurückerstattet.

Abonnementpreis pro Band: $ 36,00.

Bestellbar für das Inland bei Akadémiai Kiadó (1363 Budapest, Postfach 24, Bankkonto Nr. 215 11488), für das Ausland Außenhandels-Unternehmen » Kultúra « (1389 Budapest 62, P.O.B. 149. Bankkonto Nr. 218 10990) oder bei seinen Auslandsvertretungen und Kommissionären.

«Acta Chimica» издает статьи по химии на русском, французском, английском и немецком языках.

«Acta Chimica» выходит отдельными выпусками разного объема, 4 выпуска составляют один том и за год выходит 4 тома.

Предназначенные для публикации рукописи следует направлять по адресу:

Acta Chimica
H-1521 Budapest, ВНР

Всякую корреспонденцию в редакцию направляйте по этому же адресу.

Редакция рукописей не возвращает.

Подписная цена — $ 36,00 за том.

Отечественные подписчики направляйте свои заявки по адресу Издательства Академии Наук (1363 Budapest, P.O.B. 24, Текущий счет 215 11488), а иностранные подписчики через организацию по3 внешней торговле «Kultúra» (H-1389 Budapest 62, P.O.B. 149. Текущий кчет 218 10990) или через ее заграничные представительства и уполномоченных.

Reviews of the Hungarian Academy of Sciences are obtainable at the following addresses:

AUSTRALIA
C.B.D. LIBRARY AND SUBSCRIPTION SERVICE, Box 4886, G.P.O., *Sydney N.S.W. 2001*
COSMOS BOOKSHOP, 145 Ackland Street, *St. Kilda (Melbourne), Victoria 3182*

AUSTRIA
GLOBUS, Höchstädtplatz 3, *1200 Wien XX*

BELGIUM
OFFICE INTERNATIONAL DE LIBRAIRIE, 30 Avenue Marnix, *1050 Bruxelles*
LIBRAIRIE DU MONDE ENTIER, 162 Rue du Midi, *1000 Bruxelles*

BULGARIA
HEMUS, Bulvar Ruszki 6, *Sofia*

CANADA
PANNONIA BOOKS, P.O. Box 1017, Postal Station "B", *Toronto, Ontario M5T 2T8*

CHINA
CNPICOR, Periodical Department, P.O. Box 50, *Peking*

CZECHOSLOVAKIA
MAD'ARSKÁ KULTURA, Národní třida 22, *115 66 Praha*
PNS DOVOZ TISKU, Vinohradská 46, *Praha 2*
PNS DOVOZ TLAČE, *Bratislava 2*

DENMARK
EJNAR MUNKSGAARD, Norregade 6, *1165 Copenhagen*

FINLAND
AKATEEMINEN KIRJAKAUPPA, P.O. Box 128, *SF-00101 Helsinki 10*

FRANCE
EUROPERIODIQUES S. A., 41 Avenue de Versailles, *78170 La Celle St.-Cloud*
LIBRAIRIE LAVOISIER, 11, rue Lavoisier, *75008 Paris*
OFFICE INTERNATIONAL DE DOCUMENTATION ET LIBRAIRIE, 48, rue Gay-Lussac, *75240 Paris Cedex 05*

GERMAN DEMOCRATIC REPUBLIC
HAUS DER UNGARISCHEN KULTUR, Karl-Liebknecht-Strasse 9, *DDR-102 Berlin*
DEUTSCHE POST ZEITUNGSVERTRIEBSAMT, Strasse der Pariser Kommüne 3—4, *DDR-104 Berlin*

GERMAN FEDERAL REPUBLIC
KUNST UND WISSEN ERICH BIEBER, Postfach 46, *7000 Stuttgart 1*

GREAT BRITAIN
BLACKWELL'S PERIODICALS DIVISION, Hythe Bridge Street, *Oxford OX1 2ET*
BUMPUS, HALDANE AND MAXWELL LTD., Cowper Works, *Olney, Bucks MK46 4BN*
COLLET'S HOLDINGS LTD., Denington Estate, *Wellingborough, Northants NN8 2QT*
W.M. DAWSON AND SONS LTD., Cannon House, *Folkestone, Kent CT19 5EE*
H. K. LEWIS AND CO., 146 Gower Street, *London WC1E 6BS*

GREECE
KOSTARAKIS BROTHERS, International Booksellers, 2 Hippokratous Street, *Athens-143*

HOLLAND
MEULENHOFF-BRUNA B.V., Beulingstraat 2, *Amsterdam*
MARTINUS NIJHOFF B.V., Lange Voorhout 9—11, *Den Haag*
SWETS SUBSCRIPTION SERVICE, 347b Heereweg, *Lisse*

INDIA
ALLIED PUBLISHING PRIVATE LTD., 13/14 Asaf Ali Road, *New Delhi 110001*
150 B-6 Mount Road, *Madras 600002*
INTERNATIONAL BOOK HOUSE PVT. LTD., Madame Cama Road, *Bombay 400039*
THE STATE TRADING CORPORATION OF INDIA LTD., Books Import Division, Chandralok, 36 Janpath, *New Delhi 110001*

ITALY
EUGENIO CARLUCCI, P.O. Box 252, *70100 Bari*
INTERSCIENTIA, Via Mazzé 28, *10149 Torino*
LIBRERIA COMMISSIONARIA SANSONI, Via Lamarmora 45, *50121 Firenze*
SANTO VANASIA, Via M. Macchi 58, *20124 Milano*
D. E. A., Via Lima 28, *00198 Roma*

JAPAN
KINOKUNIYA BOOK-STORE CO. LTD., 17-7 Shinjuku-ku 3 chome, Shinjuku-ku, *Tokyo 160-91*
MARUZEN COMPANY LTD., Book Department, P.O. Boü 5056 Tokyo International, *Tokyo 100-31*
NAUKA LTD., IMPORT DEPARTMENT, 2-30-19 Minami Ikebukuro, Toshima-ku, *Tokyo 171*

KOREA
CHULPANMUL, *Phenjan*

NORWAY
TANUM-CAMMERMEYER, Karl Johansgatan 41—43, *1000 Oslo*

POLAND
WĘGIERSKI INSTYTUT KULTURY, Marszałkowska 80, *Warszawa*
CKP I W ul. Towarowa 28 *00-958 Warsaw*

ROMANIA
D. E. P., *Bucureşti*
ROMLIBRI, Str. Biserica Amzei 7, *Bucureşti*

SOVIET UNION
SOJUZPETCHATJ — IMPORT, *Moscow*
and the post offices in each town
MEZHDUNARODNAYA KNIGA, *Moscow G-200*

SPAIN
DIAZ DE SANTOS, Lagasca 95, *Madrid 3*

SWEDEN
ALMQVIST AND WIKSELL, Gamla Brogatan 26 *101 20 Stockholm*
GUMPERTS UNIVERSITETSBOKHANDEL AB Box 346, *401 25 Göteborg 1*

SWITZERLAND
KARGER LIBRI AG, Petersgraben 41, *4011 Basel*

USA
ENSCO SUBSCRIPTION SERVICES, P.O. Box 1943, *Birmingham, Alabama 35201*
F. W. FAXON COMPANY, INC., 15 Southwest Park, *Westwood, Mass, 02090*
THE MOORE-COTTRELL SUBSCRIPTION AGENCIES, *North Cohocton, N. Y. 14868*
READ-MORE PUBLICATIONS, INC., 140 Cedar Street, *New York, N. Y. 10006*
STECHERT-MACMILLAN, INC., 7250 Westfield Avenue, *Pennsauken* N. J. 08110

VIETNAM
XUNHASABA, 42, Hai Ba Trung, *Hanoi*

YUGOSLAVIA
JUGOSLAVENSKA KNJIGA, Terazije 27, *Beograd*
FORUM, Vojvode Mišica 1, *21000 Novi Sad*

31. VIII. 1978 HU ISSN 0001—5407 Index: 26.007